Draft Title 40 CFR 191
Compliance Certification
Application
for the
Waste Isolation Pilot Plant

Volume VII

Appendix
GCR Vol. II

March 31, 1995

United States Department of Energy
Waste Isolation Pilot Plant

Carlsbad Area Office
Carlsbad, New Mexico

Geological Characterization Report, Waste Isolation Pilot Plant (WIPP) Site, Southeastern New Mexico

Volume II

August 1978

Dennis W. Powers, Steven J. Lambert, Sue-Ellen Shaffer,
Leslie R. Hill, Wendell D. Weart, Editors

Sandia Laboratories

MASTER

DISTRIBUTION OF THIS DOCUMENT IS UNLIMITED

DISCLAIMER

Portions of this document may be illegible in electronic image products. Images are produced from the best available original document.

GEOLOGICAL CHARACTERIZATION REPORT
WASTE ISOLATION PILOT PLANT (WIPP) SITE,
SOUTHEASTERN NEW MEXICO

SAND78-1596

VOLUME II

Dennis W. Powers, Steven J. Lambert, Sue-Ellen Shaffer,
Leslie R. Hill, Wendell D. Weart, Editors

Department 4510
Waste Management Technology
Sandia Laboratories
Albuquerque, New Mexico 87185

AUGUST, 1978
PRINTED DECEMBER, 1978

GEOLOGICAL CHARACTERIZATION REPORT
TABLE OF CONTENTS
VOLUME II

APPENDICES

6.1   INTRODUCTION

The location of the proposed WIPP site is within the surface water boundaries of the Rio Grande Water Resources Region and the groundwater boundaries of the Unglaciated Central region of the Permian Basin. In addition, the site lies within the boundaries of the Delaware Basin, a portion of the Unglaciated Central region that includes some of the least productive aquifers in the United States. The Delaware Basin is characterized by a semiarid climate with low rainfall and runoff, high evaporation, and frequent strong winds. The proposed site contains neither perennial streams nor surface water impoundment, and the water bearing strata beneath the site do not yield large quantities of water to wells. Shallow wells in the local area are generally used only for watering livestock and typically produce non-potable groundwater with total dissolved solids (TDS) concentrations in excess of 3,000 parts per million (ppm).

Hydrologic studies of the water resources surrounding the site have been supported by universities and state and federal agencies since the late 1930's (Robinson and Lang, 1938; Theis and Sayre, 1942; Hendrickson and Jones, 1952; Bjorklund and Motts, 1959; Nicholson and Clebsch, 1961; Brokaw et al., 1972; Hiss, 1975a). The early studies were primarily concerned with the control of water quality in the Pecos River for agricultural usage downstream from the brine discharge at Malaga Bend (Robinson and Lang, 1938; Hale et al., 1954). The first investigations of hydrogeologic parameters describing the occurrence and flow of groundwater in close proximity to the proposed WIPP location began in the late 1950's with Project Gnome (Cooper, 1962; Gard, 1968; Cooper, 1971).

Hydrologic studies at the site and adjacent site areas have concentrated on defining the hydrogeology and associated salt dissolution phenomena (Griswold, 1977; Lambert and Mercer, 1977; Mercer and Orr, 1977; Mercer and Orr, 1978; Anderson, 1978). These investigations are directed toward a more quantitative evaluation of the salt dissolution process, the

hydrogeologic parameters affecting groundwater movement, and the major elements of surface and groundwater quality affecting water resource use and local ecology. The collection of hydrologic data is projected to continue for several years to provide site-specific information for a detailed safety analysis of the WIPP.

Hydrologic test results to date have been used to make bounding calculations of hypothetical occurrences based upon simplifying assumptions of the physical system. Future measurements obtained from the experimental programs and analysis of the test data will be used to refine the initial bounding calculations and to provide a more detailed description of the physical system and system dynamics. The use of computer models as predictive tools is expected to be closely coordinated with current test results from an established monitoring network. Compatible chemical tracers will be injected directly into the groundwater system as a test of the predictive computer results. Also, the use of chemical tracers during construction phases of the WIPP may provide an early indication of leaky borehole plugs or faulty repository seals, if any, far in advance of radionuclide concentrations in the groundwater system.

6.2   SURFACE WATER HYDROLOGY

The area proposed for the Waste Isolation Pilot Plant (WIPP), located in southeastern Eddy County, New Mexico, lies at an average elevation of 3410 feet above mean sea level (MSL) in the Northern Chihuahuan Desert. Although the area belongs to the drainage basin of the Pecos River, surface drainage patterns at the site are not well defined. Preliminary studies indicated that areal requirements for the surface facilities, underground storage, and safety considerations during the operation of the repository would be as shown in Table 6.2-1 (see also Table 2.1).

6.2.1 Surface Water Features

The Rio Grande Water Resources Region, which includes the Pecos River basin, is an area of 88,968 square miles. The Pecos River basin has a

total drainage area of about 44,535 square miles (approximately 20,500 square miles of which do not contribute to river flow), a maximum basin width of about 130 miles, and an overall length of about 500 miles before combining with the Rio Grande River. The Pecos is generally perennial, except in the reach below Anton Chico and in the reach between Fort Sumner and Roswell, where the low flows percolate into the stream bed. About 60 percent of the annual flow occurs between April and September.

The Pecos River is located west of the site and flows southeast through Carlsbad. At the closest point (river mile 430), the Pecos River is approximately 14 miles west of the WIPP site center. The total drainage area of the river at this location is 19,000 sq. miles. A few small unnamed creeks and draws constitute all tributaries flowing westward of the Pecos River within 20 miles north or south of the site. From the west, the Black River (drainage area of 400 square miles) joins the Pecos at a point approximately 16 miles southwest of the site near river mile 436. The Delaware River (drainage area of 700 square miles) joins the Pecos near river mile 446, and a number of small unnamed creeks and draws join at various points along this reach. Pecos River flow in this reach is regulated by storage in Lake Sumner (river mile 401.9), Lake McMillan (river mile 404.2), Lake Avalon (river mile 407.2) and several other smaller upstream dams that divert water for irrigation. The salient features of the five existing dams on the Pecos River in a reach extending 25 miles upstream and 25 miles downstream of the WIPP site are listed in Table 6.2-2. The approximate slope of the Pecos riverbed in the vicinity of the WIPP site is 4.5 ft/mile (U.S.G.S. Topographic Maps NI 13-11 & NI 13-12).

There are no major lakes or ponds within 10 miles of the WIPP site center. Laguna Gatuna, Laguna Tonto, Laguna Plata and Laguna Toston are lakes located to the north more than 10 miles from the site. All these lakes are at or above elevation 3,450 feet. Therefore, surface runoff from the site would not flow toward any of the lakes to the north. To the west and northwest, Red Lake, Lindsey Lake, Salt Lake, and a few unnamed ponds are located more than 10 miles from the site, between elevations 3,000 and 3,300 feet (U.S.G.S. Topo. Maps, 1:250,000).

Surface water and groundwater withdrawals in the Pecos River basin are listed in Table 6.2-3.

6.2.2 Precipitation Patterns

The nearest station to the WIPP site for which climatological records are available is located at Carlsbad, about 26 miles west of the site, at an elevation of 3,120 feet MSL (U.S. Weather Bureau, 1961). Over a period of more than 71 years (NOAA, 1977), the annual precipitation at Carlsbad ranged from 2.95 inches to 33.94 inches. The average annual precipitation over a period of 30 years (1931-1960) was 12.43 inches (U.S. Weather Bureau, 1961). The average annual precipitation from 1951 to 1974 was 9.78 inches at Artesia (elevation 3320 feet), which is about 48 miles northwest of the WIPP site. At Hobbs (elevation 3615 feet), which is about 44 miles northeast of the site, the average annual precipitation for the period 1951-1974 was 14.29 inches. Interpolation of precipitation data for Carlsbad, Artesia and Hobbs indicates that the average annual precipitation at the site should be approximately 12 inches, which is nearly equal to the average annual precipitation at Carlsbad. Therefore, the precipitation patterns at Carlsbad are assumed to be representative of the conditions at the WIPP site.

Maximum, average, and minimum monthly precipitation at Carlsbad over a period of 30 years (1931-1960) are given in Table 6.2-4. The maximum monthly precipitation, 12.28 inches, occurred in May. With the exception of May and August, when the record minimum monthly precipitation were 0.18 and 0.01 inch, respectively, the record minimum precipitation for all other months has been 0.00 inch. The maximum daily precipitation since 1905 occurred in August, 1916, and was 5.12 inches.

The maximum daily and monthly snowfalls at Carlsbad since 1905 have been 10 inches (December, 1923) and 17.8 inches (February, 1905), respectively (U.S. Weather Bureau, 1961).

In general, summer rain is more abundant than that of other seasons and is caused by thunderstorms generated by the southeasterly circulation of moist air from the Gulf of Mexico. Approximately 75 percent of the total annual precipitation occurs from April through September. Winter rainfall is least abundant and is caused mainly by frontal activity associated with the movement of the Pacific storms across the country from west to east (NOAA, 1977).

6.2.3 Drainage

The site is located between elevations 3,250 and 3,570 feet MSL (Griswold, 1977). General ground slope in the vicinity is approximately 39 feet/mile from the northeast to southwest. Average ground slope from north to south is approximately 13 feet/mile. A topographic and surface water divide (Antelope Ridge) exists approximately 8 miles east of the site center and 4 miles from the exterior boundary of Zone IV (Refer to Table 6.2-1).

In general, the surface in the site vicinity is hummocky and covered by sand dunes. The local slope is poorly defined, and rain collects in pools between sand dunes and evaporates, is transpired, or sinks into the sand. Surface runoff from an area of about 10 sq. miles to the northeast, along with that from the site area, drains through a number of small draws which terminate in unnamed ponds to the southwest. Runoff is typically 0.1 to 0.2 inches annually.

6.2.4 Floods

Historically, floods for the Pecos River are reported to have occurred in 1904, 1905, 1915, 1916, 1919, 1937, 1941, 1942, and 1966 (NOAA, 1977). The earliest flood for which discharge information is available occurred on October 2, 1904, following the failure of Avalon Dam. During this flood, the flow at Avalon gaging station (river mile 406.3) exceeded 90,000 cfs. The corresponding river stage is not available. The river stage at Red Bluff (river mile 459.8) is reported to have reached 28 feet

(gage datum of 2850.05 feet) during this flood. Another major flood occurred on August 7, 1916, when the discharge at Carlsbad Station (river mile 419.1) reached 70,000 cfs.

A third major flood occurred in September, 1919, when the river stage at Malaga gaging station (river mile 432.2) was recorded as 29.4 feet (gage datum of 2895.64 feet). The corresponding discharge was 40,400 cfs. The highest flood of record (through 1976) for the Pecos River occurred on August 23, 1966, when the discharge and stage at Malaga were 120,000 cfs and 42.1 feet, respectively (U.S. Geological Survey, 1976). The minimum surface elevation of the site is more than 310 feet above this maximum historic flood level.

6.2.5 Evaporation and Transpiration

In New Mexico, potential evaporation is much greater than the average annual precipitation. In the southeastern valleys, evaporation from a class A pan is on the order of 110 inches per year. During the warm months, May through October, evaporation in the southeast portion of the state is approximately 73 inches.

The record high temperature at Carlsbad is $112^{O}F$ (June, 1902). The record low temperature at this station is $7^{O}F$ (January, 1911). The maximum, average and minimum monthly temperatures at this station over a period of 30 years (1931-1960) are given in Table 6.2-5 (U.S. Weather Bureau, 1961). June, July and August are the warmest (average temperature of $80.7^{O}F$) while December and January are the coldest months of the year (average temperature of $44.3^{O}F$).

In this type of desert climate, more than 90 percent of all infiltrated water evaporates or transpires. The high rate of evapotranspiration is aided by the frequent winds, the low relative humidity (typically 36 percent during daylight hours), and the high mean annual temperature $(61^{O}F)$.

6.2.6 Infiltration

Soils at the site are generally comprised of sands extending to a depth of as much as 25 feet. Actual sand dunes cover a good portion of the site area. With pervious sand on the surface, infiltration rates are high and probably similar to the 1.6 inch-per-hour intake rate of Harkey Sand Loam (75 percent sand) near Carlsbad (Blaney and Hanson, 1965). Groundwater in the area of the site is more than 50 feet below surface elevations. Because the surface sands are underlain by a caliche layer about 2 to 8 feet thick, percolation of rainfall through the sands to the nearest groundwater would be only a portion of the total infiltration. Most infiltration will return to the atmosphere by evapotranspiration.

6.2.7 Surface Water Quality

Water quality in the Pecos River basin is affected by mineral pollution from natural sources and from irrigation return flows. Springs near the headwaters of the basin below Colonias, New Mexico, are estimated to discharge approximately 707 tons per day of dissolved solids into the Pecos River. Below Lake McMillan, springs flowing into the river are usually submerged and difficult to sample; however, dissolved solids concentrations between 3350 and 4000 ppm have been measured in springs that could be sampled. The chemical quality of these mineral discharges indicates the nonpotable character of the ground water in contributing source beds. Inflow of concentrated brine solutions at Malaga Bend increases the chloride content of the Pecos River by an estimated 370 tons per day (see account by Swenson in Bachman and Johnson, 1973). Time-weighted averages of water quality parameters for three sampling stations on the Pecos River between Carlsbad and Malaga Bend are shown in Table 6.2-6. In general, natural spring flows and irrigation return flows progressively concentrate salts downstream. Further downstream at Red Bluff Reservoir, the water is useable occasionally during high flow periods.

·6.3 GROUND WATER HYDROLOGY

Detailed investigations of ground water conditions at the proposed site
are being conducted to identify the presence of ground water, to measure
ground water quality, and to determine hydraulic conductivity and other
characteristics of the stratified rocks. The data will provide a basis
for assessment of the continued isolation of the proposed repository from
ground water circulation. The thick halite beds of the Salado Formation
at the WIPP site are isolated from circulating ground water by beds of
low hydraulic conductivity, both above and below the formation. In the
vicinity of the proposed site, fresh or potable ground water is not
present except in small, isolated, near-surface perched bodies.

Investigations to evaluate the transport of radionuclides by ground water
flow in the southeastern New Mexico portion of the Delaware Basin were
made by the Water Resources Division of the U.S. Geological Survey for
Project Gnome in the late 1950's. Since that time, several studies have
been carried out by individual consultants, the U.S. Geological Survey,
Oak Ridge National Laboratories, and Sandia Laboratories. These studies
have been directed to the specific task of providing a better
understanding of the relationship between the proposed waste repository
and ground water movement. The following is a description of ground
water occurrence and flow as understood from the studies completed to
date. Ground water is first described on a regional basis, then the
results of site specific studies are reviewed, and, finally, dissolution
of salt evaporites is discussed.

6.3.1 Regional Ground Water Conditions

Ground water within the Delaware Basin is predominantly of poor quality,
with total dissolved solids concentrations in excess of 3,000 ppm. The
only large quantities of potable ground water are found in aquifers west
of and along the Pecos River. To the west in the Guadalupe Mountains,
many rock units of the basin crop out, and the soluble salts have been
leached from the Ochoan evaporites.

Important aquifers of the region are the San Andres Limestone and the Capitan Limestone and related reef limestones. The San Andres is a major source for irrigation waters in the Roswell basin, and other areas to the north and northwest of the site. The Capitan aquifer southwest of the community of Carlsbad is the primary source of municipal water. An important aquifer in the region east of the proposed site is the Ogallala Formation. Unconsolidated alluvium along the Pecos River yields large amounts of relatively fresh ground water in some areas, although it is commonly of marginal quality for drinking purposes.

From the outcrop areas west of the Pecos River, ground water moves eastward. The shallow aquifers, those cut by the Pecos River, discharge to the river, either directly or to alluvium of the river channel. The Capitan aquifer is the oldest permeable formation that may have contact with the river. Ground water in permeable formations older than the Capitan is not directly affected by the river, is present under confined conditions, and migrates eastward into the Delaware Basin.

East of the Pecos River, thick beds of evaporites are present at depth, and brines are common in the underlying permeable formations. Ground water in any of the rock units east of the river in Eddy County is of brackish quality, at best. Fresh meteorically-derived ground water does not flush out the poor quality waters in these aquifers. Consequently, the major utilization of ground water in the central and eastern Delaware Basin is for oil-field flooding. The predominant source of the ground water is the Capitan aquifer.

The shallow aquifers east of the Pecos River are limited in extent, are low yielding, and usually contain water of poor quality. Recharge to these shallow aquifers is presumed to be from precipitation on outcrop areas or from overlying formations, and migration of the water generally follows surface drainage patterns, eventually reaching the Pecos River.

In discussing ground water occurrences in relation to the proposed repository, it is convenient to relate them to the Salado Formation because the Salado and its associated evaporite formations have very low hydraulic conductivities and form a barrier to vertical flow (see Table 9.2.3-1). Aquifers stratigraphically below the Salado are widespread and contain large quantities of brine under confined conditions. Aquifers present above the Salado in the proposed site area are either limited in extent or very low-yielding. This upper ground water is of poor quality (TDS concentrations greater than 3,000 ppm) and occurs under unconfined, as well as confined, conditions.

6.3.2 Hydrology of Rocks Underlying the Salado Formation

The halite beds of the Salado Formation that are proposed for the repository are underlain by thick anhydrite and salt beds of the Castile Formation. They act as an aquiclude, separating the Salado from the underlying sandstones of the Delaware Mountain Group. The sandstones are present at a depth of about 4,200 feet in the site area. The hydraulic conductivity of the sandstones of the Delaware Mountain Group, associated with the relatively high hydraulic conductivity of the shelf-margin facies (the Capitan Limestone) and the shelf facies (which includes the San Andres Limestone) make this group the most important hydrologic system underlying the Salado. The hydrology of these Guadalupian-age rocks has been investigated in detail by Hiss (1975a).

Considerable information derived from hydrocarbon exploration in the basin is available on the hydrologic properties of the formations underlying the Permian evaporites. As reported by Lambert and Mercer (1977), the Delaware Mountain Group is the uppermost of the oil- and gas-producing horizons, which extend to the Ellenburger Group at a depth of about 18,000 feet. Several zones are encountered that contain water, oil, and/or gas that are under sufficient pressure to maintain a potentiometric surface at an elevation above that of the Salado Formation. Some of the zones have sufficient hydraulic conductivity to allow flow rates of several hundred barrels per day. In addition to the

Delaware Mountain Group, the Atoka zone at a depth of about 13,150 feet, and the Strawn (Desmoinesian) zone at about 12,900 feet are other oil and gas production zones that are considered deep aquifers by Lambert and Mercer (1977).

Deep Hydrologic Units. The hydrologic parameters of pre-Guadalupian zones are not as well defined, nor are they as hydrologically significant to the proposed repository as the Guadalupian-age rocks. Nevertheless, a review of them is presented, based primarily on McNeal's (1965) analysis of hydrodynamics of the Permian Basin. He described the potentiometric surfaces of seven zones, using elevations of outcrops where cut by a stream or body of water, static water levels in cable tool holes or water wells, and formation pressures converted to potentiometric surface elevations. McNeal prepared maps showing the regional potentiometric surfaces in terms of fresh water, using density differences of the various brine concentrations and depths of the nearby wells. The three deep hydrologic units reviewed are the Ellenburger Group, the Devonian zone, and the Mississippian- Pennsylvanian zone.

1) **Ellenburger Group.** The Ellenburger Group consists mainly of chert-bearing limestones and dolomites. It is a widespread unit, covering some 100,000 square miles in southeastern New Mexico and northwestern Texas (McNeal, 1965, Figure 1). The unit is estimated to be 350 feet thick at the proposed site (Lambert and Mercer, 1977) and as much as 1000 feet thick elsewhere in the region. The potentiometric surface compiled by McNeal for the Ellenburger indicates an altitude range from 4,200 feet MSL southwest of the site to less than 1,400 feet MSL in central Texas. In the vicinity of the WIPP site, the ground surface elevation is about 3200 feet MSL. The average gradient of the potentiometric surface is about 8 feet per mile in an easterly direction. Water in the Ellenburger is a brine solution, with a dissolved solids range of 50,000 ppm to more than 200,000 ppm. No water production data are available for this group.

2) <u>Devonian Zone</u>. McNeal's potentiometric surface for the Devonian hydrodynamic zone ranges in altitude from 4,000 feet MSL in the vicinity of the Glass Mountains to 3,200 MSL feet along the Lea County – Texas line. In the Midland Basin, there are nearly hydrostatic conditions at an elevation range of 2,800 to 3,200 feet MSL. A high potentiometric nose extending across southeast Eddy County indicates a potentiometric surface at the proposed site of about 3,700 feet MSL. Salinity of the formation water is less than 50,000 ppm in most of southeast New Mexico. In west Texas, salinity reaches 200,000 ppm in one area.

The Devonian, as inferred from McNeal's potentiometric map, extends throughout southeast New Mexico and northwest Texas. He has included Silurian data in the eastern (Texas) subcrop area. The potentiometric surface generally slopes to the east, and the average gradient appears to be about 7 feet per mile.

3) <u>Mississippian-Pennsylvanian Zone</u>. Mississippian rocks are thin and few data are available on the occurrence of fluids under the Delaware Basin. McNeal (1965) delineated a potentiometric surface for the Mississippian zone of West Texas, but has not extended it into New Mexico.

There are three water-bearing zones in Pennsylvanian age rocks. In ascending order they are the Morrow, the Atoka, and the Strawn (Desmoinesian). Lambert and Mercer (1977, p. III-2) report that the Morrow may be a high pressure, low capacity reservoir with water-production rates ranging from 10 to 20 barrels per day. The Atoka also may be an overpressured reservoir with enough head to yield fluid columns of 3375 to 6552 feet MSL at gradients of 0.47 psi per foot. The water is produced from gas wells at rates ranging from 21.6 barrels per day to as much as 214.4 barrels per day (Texas American's Todd Federal Well No. 1).

Lambert and Mercer (1977) report that several wells have been drill stem tested in the Desmoinesian age Strawn zone and several others have been completed as oil wells. On five drill stem tests, the calculated heads

ranged from 3350 to 6203 feet MSL. Water production was reported to be as much as 416 barrels per day in one drill-stem test, and one well (Phillip's James "E" No. 1) produced an average of 106 barrels per day. A potentiometric surface of the Strawn zone is presented by McNeal (1964, Figure 4), but the only area in the Delaware Basin for which data were available was in the southwestern part of Eddy County. Elevation of levels in that area range from 3,200 feet to 3,800 feet MSL. The gradient is easterly at about 20 feet per mile.

Bone Spring Formation. According to Lambert and Mercer (1977), the Bone Spring Formation (Leonardian Series) can be considered an aquiclude. They report that bottom-hole pressure data from the majority of seven wells tested had insufficient heads to prevent downward movement of shallower water. They suggest the pressure data indicate the formation has a low capacity and contains reservoirs of limited volume.

Guadalupian Age Rocks. The most important aquifers of the Delaware Basin are part of a hydrologic system that incorporates rocks of Guadalupian age. The system comprises three interconnected aquifer groups; the shelf aquifers (including the San Andres Limestone and the Artesia Group), the Capitan aquifer (including primarily the reef deposits - Capitan and Goat Seep Limestones), and the basin aquifers (sands of the Delaware Mountain Group). These aquifers are depositionally juxtaposed, but are distinguished in most areas by contrasting hydraulic conductivities, water salinities, and potentiometric levels. Along the north and northwest interface, hydraulic conductivity of the shelf aquifer, although lower, is near the hydraulic conductivity of the Capitan aquifer. The basin aquifers have the lowest values of hydraulic conductivity, and the Capitan is a discharge point for ground water flows in them. Recharge to these basin aquifers probably occurs in outcrop areas along the west flank of the Delaware Basin. Ground water then moves generally eastward, downdip in the tilted beds. Data on aquifer characteristics, compiled by Hiss (1975a), are summarized in Table 6.3-1. Hydrologic, lithologic, and physical properties of the formations in which these aquifers occur are discussed below.

1) <u>Delaware Mountain Group Aquifer.</u> The Delaware Mountain Group includes, in ascending order, the Brushy Canyon, Cherry Canyon, and Bell Canyon Formations and comprises the basin facies of the system. The combined thickness of these formations ranges from less than 2,000 feet in the southern part of the Delaware Basin to more than 4,000 feet in southwestern Lea and eastern Eddy Counties, New Mexico (Hiss, 1975a).

The Brushy Canyon Formation is as much as 1,000 feet thick and consists chiefly of sandstone with limestone lenses and occasional conglomerate at the base. No wells are known to be extracting water from this formation in Eddy County (Hendrickson and Jones, 1952).

The Cherry Canyon Formation is also as much as 1,000 feet thick and consists of thin-bedded, fine-grained sandstone and some persistent limestone beds. The lower one-fourth of the formation persists as a sandstone tongue striking northwestward into the Guadalupe Mountains which may yield water to some wells and springs in that area (Hendrickson and Jones, 1952).

The Bell Canyon Formation ranges in thickness from 670 to 1,040 feet and consists mainly of sandstone and thin beds of limestone (King, 1948). The formation interfingers to the northwest with the reef limestone of the Capitan Formation, providing the potential hydrologic interconnection of the Guadalupian Age rocks. Large springs near the base of the reef escarpment west of the Pecos River are probably supplied by ground water moving through the upper beds of the Bell Canyon Formation (Hendrickson and Jones, 1952).

An average hydraulic conductivity of 0.016 ft/d (feet per day) and a porosity of 15.65 percent were determined by Hiss (1975a) from analyses of approximately 4,500 samples of rock core cut from the Delaware Mountain Group in Eddy and Lea Counties, New Mexico, and Ward and Winkler Counties, Texas. Hiss also computed a similar hydraulic conductivity from productivity indexes (approximately equivalent to specific

capacities) obtained from an oil company for two wells in the El Mar field located on the boundary between Lea County, New Mexico, and Loving County, Texas.

Hiss (1975a) indicated that similar values of hydraulic conductivity were reported by earlier writers for much of the same part of the Delaware Basin.

Hiss compiled a potentiometric surface map of the Delaware Mountain Group, of which the northern Delaware Basin portion is shown in Figure 6.3-1. The data used by Hiss in compiling the map were taken at different times over a period of about 25 years between the late 1940's and early 1970's. However, he believes the contours are representative of conditions during the period 1960 and 1970. Although some local changes to the potentiometric surface are due to oil and water withdrawals during that period, no data suggest that the regional directional trend has changed. The potentiometric surface data for the brines have been corrected to "fresh-water" density, indicating a potentiometric elevation of 3350 feet MSL in the vicinity of the proposed WIPP site. The hydraulic gradient in the northern portion of the basin dips northeasterly at approximately 15 feet per mile.

Quality of the water in the Delaware Mountain Group is generally poor. An isochlor map compiled by Hiss (1975a, Figure 26) shows a chloride-ion concentration range from 50,000 to 150,000 ppm in the east half of the Delaware Basin. Concentration diminishes to approximately 1,000 ppm southward in the vicinity of the Glass Mountains and northwestward in the vicinity of the Guadalupe Mountains. These are outcrop areas where the Guadalupian Age rocks probably have been recharged by precipitation. However, analyses of water samples taken from the hydrologic system in the vicinity of the repository site indicate that the brine solutions do not contain oxygen and hydrogen isotopes in ratios characteristic of meteoric waters. The relative proportions of $O18/O16$, and deuterium/ hydrogen ratios have probably been altered through interaction with the rock of the formation (Lambert, 1978; see also Chapter 7 of this report).

According to Hiss, recharge to the basin aquifers is through precipitation on the outcrops in the Guadalupe, Delaware, Apache, and Glass Mountains, and from downward leakage through the younger rocks in areas where the overlying soluble Ochoan evaporites have been removed. The potentiometric surface (Figure 6.3-1) indicates water moves north and northeastward, and discharge is to the overlying Capitan and shelf aquifers.

2) Capitan Aquifer. The Capitan Limestone and the underlying Goat Seep Limestone constitute the main body of the Capitan aquifer, which is the reef facies of the Guadalupian rocks. Hiss (1975a) describes the aquifer as a long continuous unit that extends in an arcuate strip along the north and east margins of the basin, with exposures in the Guadalupe and Glass Mountains, as well as the Delaware and Apache Mountains. The thickness of the aquifer ranges from a few hundred to more than 2,000 feet, and the average width is approximately 10 miles (Hiss, 1975a, Figure 11). It is one of the most important aquifers of the region and is a major control in the hydrologic system (Mercer and Orr, 1977).

Relatively few aquifer tests have been performed to measure the hydraulic conductivity of the Capitan aquifer. The data compiled by Hiss (1975a) are summarized in Table 6.3-1. Hiss calculated that the hydraulic conductivity of the Capitan aquifer along the western margin of the Central Basin Platform in Texas and New Mexico ranges from 1 to 25 ft/d and estimated that for most of southern Lea County and for about 15 miles east of the Pecos River valley from Carlsbad it is about 5.0 ft/d. Although Hiss was unable to conduct any aquifer tests in the area west of the Pecos River, he concluded that high production wells, the presence of caverns, and high porosity suggest that the hydraulic conductivity of the Capitan is higher west of the river than east of the river. The hydraulic conductivity is probably very high, as well, in the Glass Mountains, because of numerous small caverns (Hiss, 1975a). The coefficient of transmissivity of the Capitan aquifer along the northern and eastern margins of the Delaware Basin is estimated by Hiss to range from 10,000 ft^2/d (square feet per day) in thick sections to less than 500 ft^2/d in the vicinity of eroded, thin sections of the reef.

The Capitan aquifer receives some recharge by direct infiltration on outcrops in the Guadalupe and Glass Mountains, and probably more by percolation of discharge from the basin and shelf aquifers along the north and east margins of the basin. Water-table conditions exist in the aquifer west of the Pecos River and in the Glass Mountains, but to the north of the Glass Mountains and east of Carlsbad water in the aquifer is confined. Hiss believes that water entering the Capitan aquifer in the Guadalupe Mountains moves northeastward toward Carlsbad where most of the water discharges into the Pecos and Carlsbad Springs. The Pecos River controls the movement of ground water in the Capitan aquifer in the vicinity of Carlsbad, and east to the ground-water divide near the Eddy-Lea County line (figure 6.3-1).

Hiss (1975a) believes that a deep submarine canyon cut into the Capitan Limestone is present near the Eddy-Lea county line, and a hydraulic restriction is formed to constrain the eastward movement of water in the aquifer from the vicinity of the Pecos River. Apparently there is little movement of water between the Pecos River and the Eddy – Lea County line. East of the hydraulic restriction, the potentiometric surface declines with an eastward gradient. Hydrographs of observation wells, established by the U. S. Geological survey in the Capitan aquifer from Carlsbad east and south to the Texas – New Mexico state line have recorded these water level differences. Water levels during the years 1967 through 1972 indicate that from Carlsbad eastward to near the Eddy – Lea County line, the potentiometric surface has remained nearly constant, responding to minor fluctuations of the Pecos River. East of the county line, water levels declined more than 100 feet, at a constant rate, during those 6 years (Hiss, 1975a, Figure 24). The eastward gradient and decline in potentiometric surface are caused primarily by the large withdrawals of water for oil-field water flooding in eastern New Mexico and western Texas (Mercer and Orr, 1977). These withdrawals are apparently the primary discharge from the aquifer at the present time. The similar potentiometric heads and directions of movement of the Capitan and shelf aquifers along the northeast and east sides of the basin (Figure 6.3-1) suggest some discharge from the shelf aquifer also

occurs. In analyzing potentiometric data prior to 1950, when large extractions of water from the Capitan had not developed, Hiss (1975a), concluded that discharge at the time was east, into the shelf aquifers.

Water of good quality, although hard, is available in the Capitan aquifer in the area west of Carlsbad (Hendrickson and Jones, 1952), and apparently in the Glass Mountains. However, in the major portion of the aquifer, east of the Pecos River, quality is poor. Chloride-ion concentration increases from 200 ppm just west of Carlsbad to as much as 23,000 ppm east of the community. Along the east flank of the basin, salinity of Capitan water is significantly lower than that in the adjacent shelf and basin aquifers, ranging from about 1,100 to 5,000 ppm in most wells (Hiss, 1975a, Figure 26).

3) Shelf Aquifers.

The shelf aquifers do not have a direct impact on hydrologic conditions underlying the proposed site because the Capitan aquifer is a hydrologic boundary. Nevertheless, they are in close hydraulic connection with that aquifer, and would apparently accept some discharge from the Capitan, should the extensive pumping from the Capitan be discontinued.

The lowermost unit of the Guadalupian age shelf or "back-reef" facies, known as the San Andres Limestone, extends over much of southeast New Mexico and into northwest Texas. The average thickness of the unit is about 1500 feet. Overlying the San Andres are formations of the Artesia Group. Strata in these formations that yield significant quantities of water are the shelf aquifers. The contact between the Capitan and shelf aquifers is gradational and difficult to differentiate in some areas. In the Pecos River Valley between Carlsbad and Roswell, and to the west of that area, the shelf aquifers are quite porous and yield large quantities of potable water to wells (Hendrickson and Jones 1952). The hydraulic conductivity of the aquifers east of the river and in the Central Basin Platform are significantly less than those to the west, and water quality is poor (Hiss, 1975a).

Measurements of hydraulic conductivity and porosity of core samples of the shelf aquifers were collected by Hiss (1975a) and the data are summarized in Table 6.3-1. It can be seen that the hydraulic conductivities in this area are at least one order of magnitude less than hydraulic conductivities of the Capitan aquifer. Potentiometric levels of the shelf aquifer, shown on Figure 6.3-1, are similar to those of the Capitan aquifer along the east side of the Delaware Basin. In the vicinity of Carlsbad, however, the levels are as much as 200 feet higher than those of the Capitan, suggesting poor interconnection between aquifers in that area.

The major areas of recharge to the shelf aquifers are probably north and west of Carlsbad in the Guadalupe mountains and areas west of the Roswell basin. Water in the shelf aquifers to the north moves either southwestward to the Pecos River, or southeastward onto the Central Basin Platform. Water quality in the shelf aquifers varies considerably from one area to another, but is generally poor east of the Pecos River. Chloride-ion concentrations in excess of 150,000 ppm are indicated by Hiss (1975a, Figure 26) north of the Capitan aquifer and along the east flank of the Delaware Basin. However, a narrow band of better quality water (salinity less than 10,000 ppm) in the San Andres Limestone is indicated to the northeast, between the shelf and the Central Basin Platform.

Castile Formation. The Castile Formation overlies the Delaware Mountain Group and consists predominantly of anhydrite with halite interbeds, and subordinate limestone. Its thickness ranges from 1,300 to 2,000 feet over most of the Delaware Basin. In most of the basin hydraulic conductivity of the Castile is very low so that this formation acts as a confining layer for the underlying Delaware Mountain Group (Mercer and Orr, 1977). However, west of the Pecos River, the salt beds have been removed, hydraulic conductivity of the residuum is higher and water is available to wells (Bjorklund and Motts, 1959).

In the central Delaware Basin, isolated pockets of brine and associated hydrogen-sulfide gas have been encountered by various·oil companies in

the Castile, and also in the Sandia Laboratories exploratory hole, ERDA-6 (Mercer and Orr, 1977). High-pressured brines encountered in three oil wells east of the proposed site reportedly have had flow rates as high as 20,000 barrels per day. These brines are present near the top of the formation, suggesting a brine zone, but since no other wells have encountered brines, the zone is apparently not continuous (Rose, 1977). Brine from ERDA-6 further suggests a long isolation time on the order of one million years for that pocket (Barr, Lambert and Carter, 1978).

Salado Formation. Massive beds of halite of the Salado Formation are the intended host rock for the WIPP repository. The formation extends more than 100 miles both north and east of the Delaware Basin and underlies an area of approximately 25,000 square miles (Pierce and Rich, 1962). Formation thickness in the Los Medanos area is 1,976 feet, as measured at ERDA-9, and the depth to the top is 848 feet.

Porosity of the halite is very low and interconnected pores are virtually non-existent. Lack of open fractures is assured because of the high plasticity of the material. As a result, hydraulic conductivity of the beds is effectively zero. As reported by C. L. Jones (1973), microscopic to very small angular cavities in grains of halite contain very minor amounts of brine and gas. Less common are much larger cavities or pockets in the halite beds that contain halite-saturated brine and nitrogenous gas confined under pressure sufficient to produce a "blow-out" when encountered during drilling. Nevertheless, the brine pockets do not appear to be interconnected, but seem to be isolated fluid bodies within the rock.

Because halite is quite soluble, it would readily dissolve if the beds came in contact with circulating, unsaturated solutions. West of the proposed site, where the Salado rises to the surface, progressively less halite is present as a result of leaching by percolating ground water. Where exposures existed, all of the salt has been removed (see Section 4.3.2.).

As discussed in Section 4.3.2., removal of salt from the Salado Formation
in the western portion of the basin where it is exposed, or near the
surface, has formed a residuum of clay, gypsum and sand. In the Carlsbad
area along the Pecos River and to the west, Bjorklund and Motts (1959)
report that these clays are dense, and are referred to as "red beds".
They suggested that the residue has slowed ground-water infiltration and
subsequent salt removal.

Underlying Nash Draw, a salt dissolution zone is present in the residuum
at the contact between the Salado and the overlying Rustler Formation.
As reported by Mercer and Orr (1977), the dissolution zone extends from
the recharge area north of Nash Draw to its termination in the vicinity
of Malaga Bend. Water penetrates the overlying units through fractures
and solution zones in the recharge area and moves southward along the top
salt, and discharges into the Pecos River at Malaga Bend (Figure 6.3-2).
The dissolved solids content of the brine at the river has been reported
to be in excess of 300,000 ppm. Theis and Sayre (1942) calculated the
discharge from the brine aquifer into the Pecos River at Malaga Bend to
be about 200 gpm. Hale (in Hale, Hughes, and Cox, 1954) calculated a
value of transmissivity of 8,000 ft^2/d from aquifer tests in the area
between Malaga Bend and Laguna Grande de la Sal. Apparently, as salt has
been progressively leached from the overlying beds, the residuum has
developed a base of low hydraulic conductivity, preventing further
downward leaching, and the dissolution zone has developed along the same
structural control as Nash Draw (Robinson and Lang, 1938).

6.3.3 Hydrology of Rocks Overlying the Salado Formation

Nearly all of the water bearing formations overlying the Salado in the
Delaware Basin are of materials with low hydraulic conductivity and which
contain limited amounts of poor-quality water. The major hydrologic unit
in the area that yields moderate quantities of marginal-quality water to
wells is the alluvium of the Pecos River valley. Information on the
hydraulic characteristics of these water bearing formations is limited,
and only regional descriptions of potentiometric levels and hydraulic
conductivity can be established.

Rustler Formation The Rustler Formation extends laterally beyond the limits of the Salado Formation and consists of interbedded anhydrite, dolomite, siltstones, clays, and halite. Two dolomite beds in the formation are water-bearing units, other than the Rustler-Salado contact, discussed above. The thickness of the dolomite beds ranges from 20 to 30 feet; these beds are areally extensive. The Magenta Dolomite is a finely crystalline, dense dolomite, and the Culebra Dolomite is vuggy and commonly associated with some anhydrite. The Magenta transmits only minor amounts of water and is not considered an important aquifer (Lambert and Mercer, 1977).

Although the Culebra Dolomite is areally persistent, yields of water vary considerably from place to place. Cooper and Glanzman (1971) suggested that the variability of yields is related to the size and number of fractures and openings in the dolomite, which in turn, could be related to its depth. In the northern part of Nash Draw, the dolomite is near the surface and is reported to yield as much as 700 gpm. East of Nash Draw, where the dolomite is covered with Triassic and younger rocks, yields are typically at least two orders of magnitude less.

Measurements of the hydraulic properties of the Culebra in the region are scarce, primarily originating from studies related to Project Gnome investigations (Cooper and Glanzman, 1971). Aquifer-performance tests in holes drilled for Project Gnome studies indicate a transmissivity of 460 ft^2/d, an average hydraulic conductivity of 16 ft/d, a storage coefficient of about 10^{-4}, and an average effective porosity of 10 percent.

Mercer and Orr (1977) prepared a map of the potentiometric surface from water levels measured in wells open to the Rustler Formation in the north portion of the Delaware Basin (Figure 6.3-2). The data were taken from several sources and represent a composite of the Culebra and Magenta dolomites, or other zones. However, it is believed that most wells are open to the Culebra dolomite bed because it is the most consistently producing rock in the vicinity.

These data indicate that water in the Rustler Formation moves west and southwestward across the Lea – Eddy County line, and southeastward from the community of Carlsbad toward Nash Draw, and the Pecos River to the south. Only the Magenta is exposed locally on the flanks of Nash Draw, and both the Culebra and the Magenta form the floor of wide sections of Nash Draw in the vicinity of Laguna Grande de la Sal.

A single water well in Lea County is reportedly deep enough to have reached Permian beds (Nicholson and Clebsch, 1961); otherwise no additional information is available on occurrence of water in the Rustler Formation in the area.

The Dewey Lake Redbeds. The youngest formation in the Ochoan Series, the Dewey Lake Redbeds, consists of orange-red siltstone with some mudstone and sandstone. This formation has been removed from the western and southern parts of the Delaware Basin by post-Permian erosion but is present in the subsurface throughout most of the site area. The thickness of the formation varies from about 200 feet to as much as 600 feet (Hiss, 1975a).

The Dewey Lake Redbeds are not an aquifer, although some permeable sand lenses are present and yield small quantities of water to a few wells. Regionally, the beds act as an aquiclude, restricting water at the surface from percolating downward to more permeable units in the underlying Rustler Formation.

Dockum Group. The Dockum Group consists of three formations. In ascending order, they are, 1) the Tecovas Formation, which consists of up to 300 feet of red shale, siltstone, and fine-grained sandstone, 2) the Santa Rosa Sandstone, which is composed of 100 to 650 feet of red, brown, and gray sandstone, and 3) the Chinle Formation equivalent, which consists of up to 1,300 feet of red, maroon, and purple shales and siltstones with lenses of fine-grained red-to-gray sandstone (Hiss, 1975a). The group is present only as a thin wedge in Eddy County, thickening to the east in Lea County and in Texas.

Both the Chinle Formation equilvalent and the Tecovas Formation are present only as thin, isolated remnants in southeastern New Mexico, primarily in Lea County. The few wells drilled into these formations yield small quantities of poor-quality water (Hiss, 1975a). In contrast, the Tecovas and Chinle are not considered aquifers in the Delaware Basin. The Santa Rosa Sandstone is a principal aquifer in several areas, particularly in Winkler and Ward Counties, Texas (Hiss, 1975a). It produces both fresh and saline water, depending on location. The westernmost extent of the Santa Rosa Sandstone is just into Eddy County, as shown in Figure 6.3-3. Water levels in wells open to the Santa Rosa Sandstone, reported by several sources, are the basis of the potentiometric surface by Mercer and Orr (1977) shown in Figure 6.3-3. Wells completed in the Santa Rosa Sandstone have low yields with specific capacities of 0.14-0.2 gpm per foot of drawdown (Nicholson and Clebsch, 1961); the formation porosity is about 13 percent.

Ground water recharge to the Santa Rosa Formation is from precipitation on the outcrop and percolation through sand dunes and the overlying Ogallala Formation to the east (Nicholson and Clebsch, 1961). Movement is generally southwest, but additional recharge apparently occurs along the potentiometric high that trends southwest along the eastern side of Eddy County. Discharge is to underlying formations at the edge of outcrops and reportedly downward through collapse zones such as San Simon Swale.

Ogallala Formation. The High Plains (Llano Estacado) region south of the Canadian River is mantled by the Ogallala Formation, which consists of Pleistocene sediments from 0 to 500 feet thick. South of Mescalero Ridge in Lea County the formation becomes discontinuous, and there are no definite remnants of the Ogallala west of easternmost Eddy County. Recharge to the Ogallala is by direct precipitation on the outcrop and by percolation through overlying sand dunes and alluvium. Nicholson and Clebsch (1961) reported that the saturated thickness of the Ogallala ranges from 25 to 175 feet. This variability can be attributed to the very irregular Triassic surface that underlies it. Movement of water in

the Ogallala is controlled to a great extent by the generally southeastward slope of the underlying Triassic red beds (Mercer and Orr, 1977).

Quaternary Deposits The Gatuna Formation is the oldest known Quaternary formation in the area and fills channels and steep-walled valleys cut primarily into the Dewey Lake red beds and Rustler Formation. In the type section and in the vicinity of Nash Draw where the Gatuna is readily recognizable, it is overlain by an extensive caliche zone that marks the Mescalero surface (Bachman, 1974). East of Nash Draw, there are few outcrops of the formation.

The Gatuna Formation yields limited amounts of water to wells where the water is in isolated gravel and sand lenses. Yields of one to five gpm are small but are usually sufficient for stock and domestic use. Ground water from the Gatuna probably percolates downward into Triassic sandstone or the Rustler Formation (Mercer and Orr, 1977).

Younger quaternary deposits are represented by alluvium. The most extensive alluvial deposits are along the west side of the Pecos River north of Malaga. Isolated patches of alluvium, however, occur along the Pecos to the south. In some areas the thickness is nearly 300 feet, and yields are reported to be as much as 3,000 gpm (Hendrickson and Jones, 1952). The source of water is primarily underflow from west of the Pecos River augmented by leakage from canals and from irrigation return flow.

Alluvium east of the Pecos River is restricted to relatively small closed depressions. Nash Draw and Clayton Basin contain Quaternary alluvium, and, in places such as Laguna Grande de la Sal, contain lake or playa deposits. The thickest alluvial deposits occur within San Simon Swale where they are in excess of 500 feet. Ground water present in the San Simon alluvium may be derived from discharge from the Santa Rosa Sandstone (Mercer and Orr, 1977). The lake and playa deposits often yield some water, although it is generally highly mineralized.

6.3.4 Regional Ground Water Use

Ground water is used in the region for irrigation, municipal supplies, rural domestic supplies, stock watering, a few industrial purposes, and for secondary oil recovery (usually referred to as "oil field flooding"). In southeastern New Mexico and western Texas almost all the ground water produced is used for this latter category. The Capitan aquifer is the largest source, but supplies are also taken from the Santa Rosa Sandstone and the Rustler Formation (Hiss, 1975a).

Demand for water throughout the region has increased steadily over the past three decades and is expected to continue into the 1980's. Production from the Capitan aquifer alone increased from approximately 80,000 acre-feet in 1950 to about 700,000 acre-feet in 1970 (Hiss, 1975a, Figure 38). The increase has been fairly linear over the 20 year period. Most of the increased demand has been for oil-field flooding which began in the early 1950's. The largest amount of pumping for this purpose is in Ward and Winkler Counties, Texas, and is primarily extracted from the Capitan aquifer. The other major source is the San Andres Limestone. According to Hiss (1975a), the cumulative total of water produced from these aquifers for the period 1920-1969, in thousands of acre-feet, is as follows:

	Eddy County	Lea County	West Texas	Total
Industrial	65.4	–	–	65.4
Irrigation	151.0	–	223.7	374.7
Municipal	162.0	–	–	162.0
Secondary Recovery	0.6	2.8	293.0	296.4
TOTAL	379.0	2.8	516.7	898.5

Listed below (in acre-feet) is a summary of usage in Eddy County for the year 1949 (Hendrikson and Jones, 1952) and in Lea County for the year 1954 (Nicholson and Clebsch, 1961). It is reasonable to assume that the quantities reported for industrial, irrigation, municipal, and rural use

have increased a moderate amount. The quantity listed for secondary recovery has increased moderately in southeastern New Mexico and dramatically in west Texas, as noted above.

	Eddy County (1949)	Lea County (1954)
Industrial	4,000	2,710
Irrigation	130,000	2,600
Secondary Recovery	0	40
Rural Domestic/Stock	2,000	450
TOTAL	141,000	6,350

Occurrence of large quantities of potable ground water is restricted to west of the Pecos River, and most of this water is extracted from the Capitan aquifer. Hiss (1975a) reported that the municipal water supplies for the communities of Carlsbad and White's City are obtained from wells completed in the Capitan aquifer. Hiss also reported that water pumped from the Capitan aquifer is used to irrigate about 2,300 acres of farmland in the Pecos River valley, the immediate vicinity of Carlsbad.

In addition, water pumped from the Capitan aquifer at Carlsbad is transported by pipeline to a potash refining plant located about 18 miles east of Carlsbad. Approximately 3,740 acre-feet of water per year was used to refine potash ore during the period 1965-1969.

Oil Field Secondary Recovery. In the early 1950's, the petroleum companies operating in the region initiated a process to recover crude oil that could no longer move to wells under existing reservoir pressure. This secondary recovery technique is one in which water is injected under pressure into the oil-bearing formation to drive the residual oil to the pumping wells. Injection may be into existing depleted wells or into wells constructed specifically for this purpose.

According to Hiss (1975a, Table 15), a cumulative total of nearly 300,000 acre-feet of water has been produced from the Capitan aquifer for

secondary recovery versus a total of about 725,000 acre-feet actually used in the flooding process. The difference of 425,000 acre-feet has been supplied from other sources including the San Andres Limestone and the Ogallala and Rustler Formations. The major areas of extraction for this use are in Ward and Winkler Counties, Texas.

Ground Water Utilization East of the Pecos River, Southeast New Mexico. In this area, small amounts of ground water are used for rural domestic supplies, stock watering, gasoline plants, and gas stripping. The Rustler Formation, the Santa Rosa Sandstone, and the Artesia Group are the principal hydrologic units pumped for those purposes. In the Nash Draw area, relatively large quantities of ground water have been taken from the Rustler Formation for use in potash refining. In the past, considerable amounts were pumped for irrigation in Lea County, but this has apparently been discontinued (Nicholson and Clebsch, 1961).

Gasoline plants use a considerable amount of water for their cooling and boiler systems. Nicholson and Clebsch (1961) report that in Lea County a total of 2400 acre-feet of ground water was used for this purpose in 1959. Gas stripping plants in the area also use water for extracting hydrogen sulfide and carbon dioxide from residual gas. Nicholson and Clebsch (1961) estimated that 150 acre-feet per year is used for this purpose.

In 1972, Cooley (1973, Table 4) inventoried the existing and abandoned wells in a nine-township block in east-central Eddy and west-central Lea Counties, New Mexico. Most of these wells are of low yields and are used mainly for domestic supplies and stock watering. Table 6.3-2 is extracted from the Cooley survey; well locations are shown on Figure 6.3-4.

6.3.5 Ground-Water Occurrence at the Proposed Site

The wells in the vicinity of the site (Figure 6.3-4) indicate that ground water above the Salado Formation is found only in limited quantities, and

is commonly of such poor quality, that it is not usable. Where the quality is marginal, it is utilized for watering stock, and is considered a valuable resource (Nicholson and Clebsch, 1961). Below the Castile Formation, at considerable depth, the Bell Canyon Formation might yield large quantities of water, but it would be brine. Although these units are technically regarded as aquifers, in the following discussion, only the hydrologic characteristics of fluid-bearing zones underlying the proposed site will be described. These zones are not identified as aquifers because an aquifer readily yields good quality water to wells.

Fluid-bearing Zones. The hydrologic exploration at the proposed site performed by the U. S. Geological Survey to date has been directed primarily to the fluid-bearing rocks of the Rustler Formation, and to the Rustler-Salado contact zone. They directly overlie the Salado salt and furnish a potential, although remote avenue for salt dissolution and radionuclide transport (Mercer and Orr, 1978). Additionally, brines in the sands of the underlying Bell Canyon Formation have been tested. These fluids are under sufficient head to allow them to reach the Salado salt. Because the brines are undersaturated, they could dissolve the salt. However, to reach the Salado, these fluids would have to first penetrate the Castile Formation. Permeabilities (or lack of permeability) of the Castile and Salado Formations at the site have been determined by drill-stem tests in two exploratory holes: ERDA No. 9 and AEC No. 8. The tests, summarized by Lambert and Mercer, 1977, Tables 1 and 2, indicate that the two formations are extremely tight. The tests gave no indication of fluid content in either formation.

Other zones that were briefly tested include zones in the Dewey Lake red beds where circulation was lost during drilling, or where hydraulic conductivity was believed to be measurable. However, no appreciable amounts of fluid were encountered (Mercer and Orr, 1978).

When the exploration and testing were completed, Mercer and Orr (1978) made several conclusions concerning the occurrence of fluids in the rocks. These include the following:

Monitoring of fluid-bearing zones in the Rustler Formation indicate
that stabilized heads decrease with depth; consequently, potential
fluid movement would be downward in rocks above the salt. However,
the large head differences between fluid-bearing units within the
Rustler indicate little or no vertical connection.

Head distribution determined for the Culebra dolomite indicates
fluid movement to the southeast across the site. Gradients range
from 7 to 120 ft/mi and vary as a function of hydraulic conductivity.

Head distribution within the Magenta dolomite has been determined
only in three holes and indicates fluid movement to the southwest.
The hydraulic gradient is 50 ft/mi.

Fluids in the Culebra and Magenta are expected to move primarily
along fracture systems, and measurements of the effective porosities
and hydraulic conductivities in low-yielding fractured rocks are
very difficult to obtain.

Brines were found at some locations along the Rustler-Salado
contact, but extremely low yields were measured.

Although evaluation of the testing of Bell Canyon sands is not
complete, preliminary results at AEC-8 indicate the potentiometric
surface, corrected to fresh-water density, is higher than similarily
corrected levels of fluid zones in the Rustler Formation.

Hydrologic Testing. The geologic and geophysical exploration performed
at the site provides a detailed understanding of the stratigraphy and
structure of the underlying formations. This work was described in
previous sections. In coordination with the exploratory drilling, a
program of hydrologic testing and monitoring was established. As a
result, considerable data on the occurrence of ground water have been
collected. The ground-water studies are continuing and the data
collected will further our understanding of the site conditions.

In addition to continued monitoring of the existing observation wells, long-term pumping tests to measure vertical connection between zones, and other tests have been planned. Also, some hydrologic information is available from the recently completed ERDA 10 test hole, located approximately 8.5 miles southwest of the proposed site.

One of the major problems faced in this program is the difficulty of measuring hydrologic parameters in materials of extremely low hydraulic conductivity in the field. Thorough testing of even the more permeable zones, such as the Culebra Dolomite, requires long periods of time, as well as close control of the interval being tested. To collect a sufficient quantity of water from these materials for proper water quality sampling requires long periods of time. Recovery of water levels in observation wells to static conditions is very slow; levels in some of the wells on site had not stabilized after more than 12 months of monitoring. Nevertheless, the data collected are sufficient to provide a good measure of the hydraulic characteristics and an understanding of ground-water occurrence at the proposed site. Hydrologic test data as of August, 1978, are available from 9 exploratory holes within the proposed land withdrawal boundary, and from the hole designated AEC 8, which is just outside the boundary, as shown on Figure 6.3-5. The U. S. Geological Survey Water Resources Division has been directing the testing program. A summary of drilling and testing operations is given for each hole in Section 6.4. A full description of the testing program and the data collected is presented in Mercer and Orr, 1978. The following discussion is extracted from that report.

The objectives of the program have been to determine the static head or reservoir pressure, the water-yielding potential (i.e., hydraulic conductivity and transmissivity) of the rock strata, and the chemistry of formation waters. These hydrologic tests are made in the exploratory test holes both during drilling and after the hole has been drilled to total depth.

Five of the test holes were specifically designed for hydrologic testing (H-1, H-2 complex, and H-3); the others were drilled for other purposes as well (potash mineral evaluation and/or geologic exploration) but were adapted for hydrologic testing. After drilling and testing wells H-1 and H-3, triangular arrays H-4, H-5, and H-6 complexes were designed similar to the H-2 complex but with a 100-foot well spacing. The additional sets of triangular arrays (H-4, H-5, and H-6) have been completed recently and testing has started.

The H-series test holes were drilled with air and detergent to avoid the undesirable mudcake that occurs when drilling with gel. This method also allows detection of fluid-producing zones that are encountered during drilling. When detected, some of these zones were tested before completion of drilling for a preliminary estimate of yield. On completion of drilling, geophysical logging was performed in all holes. These logs provided detailed information on lithologic changes, formational characterstics, potential zones of water yield, and borehole diameter changes. These data are used to select intervals to be tested, as well as provide information on hole conditions in the selection of packer seats.

Following logging, each potential zone of water yield was isolated with packers, and a drill-stem test (DST) was conducted. The DST is a temporary well completion designed to furnish hydrologic data, such as representative samples of formation fluid, undisturbed formation pressures, and indications of the formation permeablity, and/or transmissivity. The standard DST, as used in oil-field exploration, was run in test holes AEC 8 and ERDA 9, but in the other tests the procedures were modified. The modification most commonly made was in the method of recording formation pressures. In the standard DST, pressures are recorded throughout the test by a Bourdon-tube pressure recording gage (pressure bomb) located near the bottom of the drill string. Data from this pressure bomb cannot be retrieved until after completion of the test. In the modification DST used in these investigations, the fluid was initially removed from the tubing, and the stabilizing fluid levels

were measured in the drill string. This modification allowed for continuous monitoring throughout the test. Additionally, pressure-monitoring devices were placed above and below packers to determine the degree of isolation of the zone from the rest of the borehole.

The test zones were bailed or swabbed until temperature, conductivity, and density of fluid in the casing stabilized to assure that the fluid was representative of formation fluid. Samples were then collected, treated according to standard U. S. Geological Survey techniques, and chemically analyzed for the major and trace elements and for radiochemistry. Results of these analyses are listed in Table 6.3-3. The geochemistry of these fluids is discussed in Chapter 7.

During the bailing, the volume and rate of fluid withdrawal were monitored. The rate of recovery following withdrawal was measured, and yields from test zones were then calculated. The results of these tests are summarized in Table 6.3-4.

After all potential water zones were tested in the open hole, casing was installed and grouted in all holes except ERDA 9. Selected intervals were perforated for monitoring potentiometric levels, and provision was made for long-term hydrologic testing. Radioactive tracer tests were conducted in some of the holes after they had been cased and perforated to examine the cement-bond for leaks between casing and the borehole wall. These tests also yielded some information on vertical distribution of permeability across the test interval. The perforated zones were then tested for yield by bailing or swabbing, as was done in the open hole, and results are summarized in Table 6.3-4.

When the testing of the cased holes was completed, the holes were prepared as multiple observation wells. The holes are used to monitor potentiometric levels of two separate zones with the use of packers and inner tubing. In some wells, a third zone was perforated, but a bridge plug was set above it, and the zone is not available for periodic

monitoring. Figure 6.3-6 illustrates the method of completing the wells, and Table 6.3-5 indicates the zones monitored at each observation well.

Periodic monitoring of the fluid levels in the wells began after completion of testing. Because of the low yield of the zones tested, considerable time is required after bailing for the recovery of fluid to reach a stabilized level. Most levels had stabilized by October 1977, as indicated in Table 6.3-6. These levels provide a measure of the potentiometric surfaces of the monitored zones, and an indication of hydraulic gradients.

Bell Canyon Formation. During the WIPP hydrologic testing program, cores were taken in the Bell Canyon Formation in exploratory hole AEC 8. Analyses of these cores indicated the presence of two sandstone units whose permeabilities were higher than those of the surrounding rocks. These units are referred to as the lower sand and upper sand; their depths are, respectively, 4,844 to 4,860 feet, and 4,821 to 4,827 feet.

Hydrologic testing of the two sand units was made only in cased, perforated zones. There was no open-hole testing. These tests included formation pressure testing, fluid level monitoring, aquifer yields, recovery rates, water sampling, and geophysical logs. Radioactive tracer logs were also run on this hole. Analysis of the data had not been completed at the time of the report by Mercer and Orr (1978).

After the fluid in the casing had been removed by swabbing to a depth of approximately 4,200 feet, the lower sand yielded 31 gallons of fluid in 166 minutes (average 0.2 gpm), recovering to a depth of 4,095 feet. The zone was then shut-in, and a static formation pressure of 2,037 lbs/in^2 was reached in 44-1/2 hrs. The upper sand was not tested for yield. Static formation pressure was 2,044 lbs/in^2 after 57 hours.

Samples collected from the two sand units indicate that these units contain dense brines. For example, the upper sand contains 189,000 ppm of total dissolved solids, 175,000 ppm of which is sodium chloride

(Mercer and Orr, 1978, p. 80). The major constituents from the analyses are listed in Table 6.3-3. Density of the brines of each zone was determined to be 1.11 gm/cm^3 for the upper sand, and 1.12 gm/cm^3 for the lower sand. These values were used to correct static heads to fresh-water equivalents (Table 6.3-6).

Rustler-Salado Contact. The contact zone between the Rustler and Salado Formations was tested in holes H-1, H-2c, H-3, P-14, P-15, P-17, and P-18.

Both open-hole and cased-hole tests were run on the Rustler-Salado contact in H-1 and H-3, and cased hole tests were run in H-2c, P-14, P-15, P-17, and P-18. Without exception, all tests showed very low yields, typically producing a few gallons per day in the cased holes and only slightly more in the open holes (Table 6.3-4). A yield of 9.1 gallons in a 20-hour period (in H-1) was the highest yield recorded. Based on the collected data, Mercer and Orr (1978, p. 83) calculated transmissivities from the yield data, ranging from 10^{-1} ft^2/day (in P-14) to 10^{-4} ft^2/day (in P-18). Recovery rates in the monitoring wells are so slow that the level had not stabilized in P-18, after 4 months (Table 6.3-6).

Samples were taken from all of the test wells except P-18. Analyses of these samples show that the fluid in the Rustler-Salado contact zone is a saturated brine containing more than 300,000 ppm total dissolved solids (Table 6.3-3).

Culebra Dolomite. The Culebra dolomite was tested in holes H-1, H-2b, H-2c, H-3, P-14, P-15, P-17, and P-18. Logs of these holes indicate that the thickness of this unit is about 28 feet and that its depth ranges from 410 to 940 feet below ground level.

Both open-hole and cased-hole tests were run in the Culebra in H-1 and H-3, and cased hole tests were run in H-2c, P-14, P-15, P-17, and P-18. Yields varied considerably. At P-14, 720 gallons of fluid were bailed with no noticable drawdown, while P-18 produced only 16 gallons of fluid

in 33 days of monitoring. Preliminary transmissivity values calculated by Mercer and Orr (1978) also reflect the variability with values of 140 ft^2/day at P-14, 10^{-1} ft^2/day at H-1, and 10^{-4} ft^2/day at P-18.

Mercer and Orr (1978) reported that fluids in the Culebra have a total dissolved solid range of 23,700 to 118,300 ppm, and a sodium chloride range of 17,900 to 89,200 ppm. The major constituents of samples taken from the Culebra are listed in Table 6.3-3.

Magenta Dolomite. The Magenta Dolomite was tested only in H-1, H-2a, and H-3. In these holes the Magenta is 25 feet thick and the top of the unit is 502 feet below ground level.

Both open-hole and cased-hole modified drill stem tests were run on the Magenta in H-1 and H-3; well number H-2a was constructed as an observation well for the Magenta. The open-hole drill-stem test on the Magenta in H-1 produced only 13 gallons of fluid in 13 hours. A subsequent swabbing of the permeable zone produced 107 gallons of fluid, which indicated higher productivity than the DST displayed. In the cased-hole test, the Magenta zone was bailed constantly until a pumping level of 424 feet (depth) was attained. After bailing was stopped, the fluid level recovered to a depth of 340 feet in 33 days. In H-3, an open hole drill-stem test produced 23 gallons of fluid in 38 hours, but 442 gallons were swabbed from the hole after the DST was discontinued. In the cased hole test, 1 hour of bailing produced 6 feet of drawdown, and recovery was from 405 to 401 feet in 33 days of monitoring. Preliminary transmissivity values computed by Mercer and Orr (1978) range from 40 ft^2/d to less than 1 ft^2/d.

The quality of the Magenta fluids is poor (Table 6.3-3), with a total dissolved solids range of 10,300 to 29,700 ppm. The sodium chloride range is from 6800 to 24,300 ppm.

Salt-Residue Zone. Rocks of the Rustler Formation in which halite beds have been removed by leaching--salt-residue zones--were considered to be

areas for possible fluid retention. A potential zone was identified from geophysical logging and drill stem tests performed in H-1 and H-3. Results show that very little fluid now exists in those zones. In H-1, the suspected zone yielded 11.2 gallons of fluid in 12 hours of monitoring.

6.3.6   Dissolution of Salt in the Permian Evaporites

Features apparently caused by solution and/or subsidence are common in southeastern New Mexico. The extensive karst plain of the Llano Estacado (the High Plains or Caprock region) indicate the prominence or rock solution as a geologic process. Depressions near the WIPP site range from small features no more than a few meters in diameter to large features such as Laguna Grande de la Sal (Salt Lake), 11 miles to the west-southwest of the WIPP site, and Laguna Plata and Laguna Gatuna, 14 miles to the north. Not all depressions in the region, however, have been formed by solution and collapse. Some have been formed by wind action, and others are the result of solution or etching of the caliche. Salt Lake does appear to occupy an area of coalesced collapse dissolution sinks, but Laguna Plata and Laguna Gatuna appear to have formed as solution blowouts in windborne sand deposits.

A report to Sandia Laboratories by R. Y. Anderson was prepared in early 1978. This report served to assemble and summarize available data regarding the dissolution of evaporites in the Delaware Basin. The Anderson (1978) report also proposed a set of working hypotheses for the origin of various dissolution features, in order to guide future Sandia investigations of evaporite dissolution relevant to the potential integrity of the WIPP horizons and adjacent evaporites. In the text that follows, an attempt is made to distinguish available data from working hypothesis, whenever Anderson (1978) is cited.

It has been estimated that as much as 50 percent of the original salt of the Delaware Basin evaporites has been removed (Anderson, 1978) either by surface erosion or by subsurface dissolution and transport by ground

·water. These processes have been in progress intermittently through more than 100 million years (Bachman, 1974). At least four erosional periods, in which the removal of salt could have been accomplished, can be recognized. These include: 1) Early Triassic time, 2) Jurassic through Early Cretaceous time, 3) a Late Cretaceous through mid-Tertiary period, and 4) post-Ogallala uplift and erosion.

Of the processes which accomplished the removal, two types of salt dissolution have been recognized in the Delaware Basin. The more familiar dissolution is the removal of salt by waters percolating downward from above (primarily from precipitation falling directly on the ground surface above the salt). The percolating water removes soluble salts, leaving behind a residuum of insoluble material that is referred to as a leached zone (Vine, 1963). The shallow dissolution beneath Nash Draw is such a zone and is apparently the route of lateral migration of the leached salts that discharge into the Pecos River.

A second type of salt dissolution has been recognized as having dissolved salt from somewhere within the body of evaporites, generally resulting in the collapse and lowering of the overlying stratigraphic units. Anderson (1978) recognized the resulting insoluble residue as a blanket dissolution breccia which occurs to the west of the present salt edge in the basin. In addition, deep dissolution phenomena within the evaporites may have developed more localized collapse features that have been recognized around the margin of the basin and within the basin (Maley and Huffington, 1953). The origin of these deep dissolution features and breccias is more problematical than the origin of surface dissolution and the rates of dissolution more difficult to assess. Source of the water to dissolve the salt is hypothetically assumed to be aquifers underlying the salt beds, communicating through fracture systems in the intervening anhydrite beds.

Shallow Dissolution. The depth of shallow dissolution in the evaporites (base of leached zone) is highly irregular, but is usually less than 300 feet in the vicinity of the proposed site (see Section 4.3.2). It is

developed in the western part of the Delaware Basin where the evaporites are exposed, or near the surface. For example, in Nash Draw, where the Rustler Formation is exposed, leaching extends into the Salado, and the permeable residuum contains brine (Vine, 1963). It appears that percolating ground waters move laterally toward Nash Draw, eventually discharging to the Pecos River after becoming saturated with salt.

East of Nash Draw, down dip into the basin, the evaporite formations become progressively deeper, and the present-day top of salt becomes progressively higher in the stratigraphic section. The top of salt is at the top of the Salado Formation about 2 miles west of the center of the proposed site, and becomes progressively higher in the Rustler Formation across the site (Figure 6.3-7, also see Figure 2-6).

Jones (1972) reported the solution front in the Salado Formation to be between 2 and 3 miles west of the center of the site. Bachman (1974) described a thinning of the upper member of the Salado Formation to the west and north that he attributed to a combination of thinning inherent in the original deposition processes and thinning due to subrosion "during the middle and late Cenozoic. West of the line marked "edge of Salado salt" in Figure 6.3-8, there is almost a fourfold reduction in thickness of the upper member of the Salado Formation to as little as 150-170 feet in some places. This is the residue of a 500-foot thick section from which the soluble portions have been leached by circulating ground water. Wherever the upper member of the Salado has been thinned by dissolution, the section of rock between the upper surface of the remaining salt and the top of the formation consists of clay with crudely interlayered seams of broken gypsum (from rehydration of anhydrite) and fine-grained sandstone.

As dissolution progresses and the salts are carried away, voids develop and the residual layer is weakened until it is no longer able to support the overlying material. Slumping of the residue and the associated collapse of the roof can extend to surface elevations, resulting in a

topographic sink. The distinctive pitted topography that results is
termed karst. Such topography, in which surface drainage is poorly
defined, is extensive in southeastern New Mexico.

Bachman (1974) reported that dolines (that are believed to develop into
shallow sinks on the rock surface beneath the soil mantle) are very
common, and suggested that the course of the Pecos River southward from
Carlsbad to the proximity of the New Mexico-Texas state line lies in a
major belt of collapsed sinks. For example, along the east side of the
Pecos River, southeast of Carlsbad at Malaga Bend, a linear scarp is
believed to have formed along a collapse structure that is now occupied
by the river. Other major collapse features mentioned by Bachman include
Clayton Basin and Nash Draw. Bachman believes that these features formed
as coalescing sinks, probably during Pleistocene time.

Another large depression cited by Bachman is San Simon Sink, located 22
miles east of the proposed site. Shallow dissolution is a factor in the
development of this sink, which is apparently still in process. The last
recorded collapse in San Simon Sink occurred approximately 40 years ago
(Nicholson and Clebsch, 1961). Many sinks along the Pecos River Valley
have collapsed in historic time (Bachman, 1974). As recently as 1973 a
small collapse sink formed at Lake Arthur, N.M., about 50 miles (80 km)
north of Carlsbad.

Deep Dissolution. Large, deep dissolution features filled with Cenozoic
sediments overlying the inner margin of the Capitan reef (Figure 6.3-8)
were recognized by some of the first geologists working in the Delaware
Basin (Maley and Huffington, 1953). The source of water to dissolve the
salt was assumed to be the Capitan aquifer.

The extent of large-scale dissolution structures is shown on Figure
6.3-8. The dissolution wedges were identified through varve correlation
across the basin in the Castile Formation and recognition of dissolution
breccia beds in the western part of the basin (Anderson et al., 1972).
These studies suggest that deep dissolution wedges in the Castile

Formation occurred in the lower Salado and upper Castile salt beds
(Anderson, 1978). The position of the eastern margin of the western
wedge coincides with the location of dissolution features containing deep
Cenozoic fill (Figure 6.3-8). The development of these features and the
wedge was apparently a complex process. It probably included initial
wedge development adjacent to the reef, similar to that seen in the
eastern wedge (Anderson 1978), and later combined with shallow
dissolution.

The most prominent small-scale, (less than 1 mile across) dissolution
features in the vicinity of the Delaware Basin have been described by
Vine (1960) as "domal karst features". The subsurface projection of one
of these (dome "C") was encountered at the level of the McNutt potash
zone by Mississippi Chemical Corporation. It was found to be a chimney
in the Salado Formation filled with clay-cemented brecciated rock
belonging to strata above the 7th ore zone. There are other
erosion-breached domes similar to Vine's dome "C" in the vicinity of Nash
Draw. The subsurface expression of the domes, if any, is virtually
unknown. A chimney containing cemented rubble (incorrectly termed a
"breccia pipe") was encountered in commercial exploratory drilling within
the proximity of a low circular hill near the Wills-Weaver Mine, but this
chimney was not associated with a breached-dome at the surface. Recent
geophysical surveys of the region have revealed that some of these hills,
including the "Weaver Pipe" and dome "C", are associated with resistivity
lows. Both Vine (1960) and Anderson (1978) have proposed mechanisms for
origin of these features, all of which remain to be tested by field
investigations of their subsurface structure and composition (see Chapter
10). These mechanisms involve various combinations of differential
solution, hydration of anhydrite to gypsum, and salt intrusion. An
attempt to reconcile these mechanisms and apply them to the origin of
domes near Queen Lake southwest of Nash Draw was made by Reddy (1961).

Anderson believes that the dissolution giving rise to these features is
an ongoing process. The proposed site is in an area of the Delaware
Basin that is free of regional deep dissolution, but localized features

are present in the vicinity. Nevertheless, the extensive investigation
carried out at and near the proposed site, including exploratory holes,
ERDA-10, ERDA-11, ERDA-9, and AEC-8, indicate that deep dissolution is
not taking place there. ERDA 10 was located and drilled specifically to
evaluate the suggestion of Anderson that the absence of Halite III in the
Castile south of the WIPP site was due to deep dissolution. Examination
of the core revealed no apparent solution residue or collapse breccia;
the recently collected data indicate nondeposition rather than
dissolution since this was the nearest probable location of regional deep
dissolution, its absence implies a lack of threat to the WIPP site from
this phenomenon.

Rates of Dissolution. It is evident that dissolution is an active
process, and can be expected to continue in the future. The potential
hazard to the proposed site by continued dissolution in nearby places
such as Nash Draw, 7 to 8 miles west of the site, can be evaluated if the
rates of dissolution are known. In relation to human activity, the rate
of dissolution is almost immeasureably slow. However, in terms of
geologic processes, an attempt to estimate the rate is not altogether
impractical. As stated by Bachman (1974): "Active geologic processes
have not changed since the close of Tertiary Ogallala time, about 3-4
m.y. (million years) ago. However, the rates of these processes have
varied considerably. It is assumed that the rates of these processes
will continue to vary and that prediction of future events can be made by
assuming that the extremes of past conditions will not be exceeded in the
future."

With this in mind, Bachman analyzed the rate of dissolution in Nash Draw
since the development of the Mescalero caliche, estimated to be 600,000
years ago. The following summarizes his analysis (Bachman, 1974):

Collapse of the Mescalero caliche along the margins of Nash Draw
indicates that this depression has formed, at least in part, since the
deposition of the caliche.

Along Livingstone Ridge on the east side of Nash Draw, the Mescalero caliche is undeformed at elevations above 3,300 feet. It dips steeply into the depression along the ridge and occurs at elevations of 3,200 feet, and less, within the depression. Along Quahada Ridge on the west side of Nash Draw the Mescalero is likewise undeformed at elevations about 3,300 feet, but it dips steeply into Nash Draw and occurs as collapsed fractured masses within the depression (NE 1/4 sec. 1, T. 22 S., R. 29 E.).

A cross section through potash exploratory holes in Nash Draw indicates the approximate extent of salt dissolution in the Salado Formation since Mescalero time (Figure 6.3-9).

Nash Draw appears to have subsided between Livingstone and Quahada Ridges as much as 180 feet since Mescalero time. At one locality the surface of Nash Draw is 180 feet below the projected altitude of the Mescalero caliche (See figure 6.3-9). However, the interval between the top of the Salado Formation and the top of marker bed 124 at the same location is 420 feet, or 330 feet less than at Livingston Ridge where relatively little Salado salt has been removed. It is therefore interpreted that about 150 feet of Salado salt was removed before Mescalero time and about 180 feet has been removed since Mescalero time. At another locality, Nash Draw subsided approximatley 160 feet below the projected elevation of the Mescalero caliche while about 120 feet of Salado salt was being removed. There is a discrepancy here of about 40 feet that could be explained by surficial erosion.

Thus, in the area of Nash Draw that subsided 180 feet, the average rate of vertical dissolution over the 600,000 years was about 0.33 feet per 1000 years (Bachman, 1974).

These conclusions are based on the available geologic evidence, but the assumption should not be made that this rate of dissolution is a constant for the region. At least two other factors must be considered in this interpretation, but geologic information is not currently available to permit evaluation of them. The factors are:

Dissolution and subsidence rates probably have not been constant in Nash Draw during the past 600,000 years. A major part of this subsidence may have occurred during periods of high humidity in late Pleistocene (Wisconsin time).

The subsidence in Nash Draw, whenever it occurred in the Pleistocene, is not an average rate for the region. In the area of "the Divide," between Antelope and Livingstone Ridges, the Mescalero caliche is relatively undisturbed and probably no dissolution has occurred there since Mescalero time.

Calculations have also been made of the removal of salt from the Rustler and Salado Formations in Nash Draw based on the rates of discharge of dissolved sodium chloride and calcium sulfate into the Pecos River by brine seeps at Malaga Bend. Active dissolution of halite from the upper part of the Salado Formation occurs in the solution breccia zone at the base of the Rustler Formation in Nash Draw (Brokaw et al. 1972). The brine solution is believed to be recharged by aquifers in the Rustler and above, and its discharge is thought to be primarily at the Malaga Bend brine seeps and the salt lakes in Nash Draw. Piper (1973) calculated that the salts discharged into the Pecos River between Malaga Bend and a point 6 miles (10 km) downstream amount to 310,000 tons (2.8×10^8 kg) of NaCl and 170 tons (1.5×10^8 kg) of $CaSO_4$ each year. This is equivalent to a loss of 0.16 vertical feet of salt section per thousand years, a rate of the same order of magnitude as that calculated from the subsidence of Nash Draw.

An alternative approach of estimating vertical dissolution was used by F.A. Swenson (Bachman and Johnson 1973). He investigated the tonnage of salt dissolved and discharged by springs and streams along the east flank of the basin and found the maximum tonnage for the many subbasins to be 955 tons per square mile of drainage area each year. If the discharge continued at that rate it would mean a vertical dissolution of about 0.5 foot of salt in 1,000 years, provided the dissolution was distributed evenly over the area drained.

A rate of lateral shallow dissolution of salt in the western part of the Delaware Basin has been estimated to be about 6 to 8 miles per million years horizontally (Bachman and Johnson 1973). These estimates were based on the assumption that the salt-bearing Salado Formation extended to the Capitan reef escarpment on the western edge of the basin at the end of Ogallala time. It is now recognized that dissolution of this salt could have occurred at previous times in the past, and the average rate of salt removal by shallow dissolution is believed to be much slower than those estimates which establish an upper bound.

As stated previously, it is estimated that about 50 percent of the original volume of salt has been removed from the Basin. In considering the rate at which the salt was removed, it is generally recognized that much of the erosion and dissolution probably occurred since the beginning of Cenozoic time. This is a period of major uplift and erosion. Anderson pointed out (1978) that the dissolution features are closely associated with Cenozoic and postuplift hydrologic and structural controls. Nevertheless, as early as Jurassic time the basin was tilted and the western portion shown on Figure 6.3-8 was exposed and subject to erosion (Bachman, 1976). The hydrologic and structural conditions were apparently similar at that time to those of the Cenozoic, and the Jurassic climate is recognized to have been wet. Thus, it seems quite likely that the deep dissolution and erosional processes of salt removal could have been significantly accelerated during the Jurassic period.

The rate of deep dissolution is difficult to assess, and Anderson (1978) does not believe that estimates can be made with any degree of confidence, considering the available data. He suggests that if it is assumed that 1) deep dissolution progresses at a constant rate, and 2) that significant dissolution did not begin until after stripping of the Ogallala Formation from the basin (3-4 million years ago), projection of that rate would imply all of the lower Salado salt would be removed in about another million years. However, he does not believe the assumptions are valid.

Deep dissolution, as hypothesized by Anderson, would seem to have been a significant geologic process in Jurassic time, as well as in the Cenozoic. It is apparent that further study of these factors is needed to fully assess the impact on the proposed site. Sandia Laboratories and the U.S. Geological Survey are currently performing studies to provide data which should aid in this evaluation (see Chapter 10).

6.4 HYDROLOGY DRILLING AND TESTING SUMMARY

6.4.1 HOLE NO. H-1

LOCATION: T.22 S., R.31 E., Sec. 29

ELEVATION: 3,403.2 feet (ground level)

DEPTH DRILLED: 848 feet

DATE COMPLETED: June 9, 1976

DRILLING CONTRACTOR: Sonora Drilling Co., Carlsbad, N. Mexico

DRILLING METHOD: Auger 18 inch hole (0-40 feet)
Rotary 7.88 inch hole with air-air/mist (40-731 feet)
Core 4.75 inch hole with air mist (731-842 feet)
Ream 9.88 inch hole (40-848 feet)

CASING RECORD: 10.75 inch O.D. steel surface pipe, (0-40 feet) cemented to surface
7 inch O.D. steel casing (0-848 feet), cemented to surface (cement plug to 797 feet, drilled to 831 feet)

GEOPHYSICAL LOGS: Differential Temperatures
BHC Acoustic
Compensated Densilog
Dual-Laterolog

Micro-Laterolog

Compensated Neutron-Gamma

Sperry-Sun Magnetic Survey

HYDROLOGIC TESTING (OPEN HOLE):

A. 699-842 feet: DST, of Rustler-Salado Contact, 9.1 gallons of water in 20 hours

B. 667-699 feet: DST of Culebra Dolomite, 10.6 gallons of water in 11.5 hours

C. 626-667 feet: DST, of suspected salt residue, 11.2 gallons of water in 12 hours.

D. 562-592: DST of Magenta Dolomite, 13 gallons of water in 13.5 hours; after hole was drilled to 592 feet inflow of 490 gpd was observed.

HYDROLOGIC TESTING (CASED HOLE):

E. 803-837 feet: Perforated zone, Rustler-Salado contact, water level rose from 826.5 to 811 (25 gallons) in 33 days.

F. 675-703 feet: Perforated zone, Culebra Dolomite, fluid level rose from 665 to 406 (416 gallons) in nine days.

G. Tracer, ^{131}I, no annulus leaks, no flow in 694-703 interval, major loss in 675-694 interval, tracer injection rate of 8 gpm, total 1634 gal. injected.

H. 562-590 feet: Perforated zone, Magenta Dolomite, after bailing, water rose from 424.5 to 340.7 feet in 33 days (53 gallons), could not bail below 424 feet.

I. Culebra water level stable at 390 feet depth. (October 1977)

J. Magenta water level stable at 249 feet depth. (October 1977)

DRILLING & TESTING SUMMARY

6.4.2 HOLE NO. H-2a

LOCATION: T.22 S., R.31, E., Sec. 29

ELEVATION: 3,377.1 feet (ground level)

DEPTH DRILLED: 563 feet

DATE COMPLETED: February 19, 1977

DRILLING CONTRACTOR: Pennsylvania drilling Co., Carlsbad, N. Mexico

DRILLING METHOD: Auger 18 inch hole (0-33 feet)
Rotary 8.75 inch hole with air-air/mist (33-513 feet)
Core 4.75 inch hole with air/mist (513-563 feet)
(cut 2.25 inch diameter core)

CASING RECORD: 10.75 inch O.D. steel casing (C-33 feet) cemented to surface
6.63 inch O.D. steel casing, (0-511 feet), cemented to surface

Geophysical Logs: None. Available from H2C, 90 feet away.

HYDROLOGIC TESTING:

A. 0-188 feet: Stopped drilling after encountering wet zone at 185 feet; interval produced no appreciable fluid in 5 hours

B.   513-563 feet: Open hole, Magenta Dolomite, water rose from 556.8 to 538.7 in one day (22 gallons).

C. Magenta static level at 249 feet, October, 1977

DRILLING & TESTING SUMMARY

6.4.3 HOLE NO. H-2b

LOCATION: T.22 S., R. 31 E., Sec 29

ELEVATION: 3,377.1 feet (ground level)

DEPTH DRILLED: 661 feet

DATE COMPLETED: February 12, 1977

DRILLING CONTRACTOR: Pennsylvania Drilling Co., Carlsbad, N. Mexico

DRILLING METHOD: Auger 18 inch hole (0-33 feet)
Rotary 8.75 feet hole with air-air/mist (33-611 feet)
Core 4.75 inch hole with air/mist (611-661 feet) (cut 2.25 inch diameter core)

CASING RECORD: 10.75 inch O.D. steel casing (0-33 feet) cemented to surface
6.63 inch O.D. steel casing, (0-609 feet)., cemented to surface

Geophysical Logs: None. Available from H2C, 75 feet away.

HYDROLOGIC TESTING:

A.   611-661 feet: Open hole, Culebra cored interval, water rose from 636.9 to 458.0 feet in one day (260 gallons). Level stable at 352 feet (February 1977)

B.   Hole # H-2c was bailed from the Culebra while monitoring H-2b in the Culebra. First response in H2b was detected 50 minutes after bailing of H2C started.

C.   510-538 feet: Perforated zone, Magenta Dolomite, water rose from 560 to 420 feet in one day (210 gallons).

D. Well constructed for monitoring at Culebra Dolomite via tubing and Magenta via annulus. Culebra static level at 351 feet, Magenta static level at 292 feet (perforations may be blocked).

DRILLING & TESTING SUMMARY

6.4.4 HOLE NO. H-2c

LOCATION: T.22 S., R.31 E., Sec 29

ELEVATION: 3,377.1 feet (ground level)

DEPTH DRILLED: 795 feet

DATE COMPLETED: February 5, 1977

DRILLING METHOD: Auger 18 inch hole (0-33 feet)
Rotary 8.75 inch hole with air/mist (33-743 feet)
Core 4.75 inch hole with air/mist (743-795 feet)
(cut 2.25 inch diameter core)

CASING RECORD: 10.75 inch steel casing (0-33 feet) cemented to surface
6.63 inch O.D. steel casing, (0-742 feet), cemented to surface.

Geophysical Logs: Compensated Densilog
Dual-Laterolog
BHC Acoustilog
Micro-Laterolog

Compensated Neutron-Gamma

4-Arm Caliper

USGS Lithologic-log

HYDROLOGIC TESTING:

A.   743-795 feet: Open hole, Rustler-Salado cored interval produced 14 gallons in 18 days.

B.   624-652 feet: Culebra perforated zone, water rose from 656.4 to 446.6 in one day (310 gallons). Static level at 352 feet. (March 1977)

C. Tracer ^{131}I, no flow below 642 in casing, fluid loss zone was between 631 and 644, especially 640-644 where core indicates pitted and fractured dolomite, tracer injection rate was 8 gpm, total 697 gal. injected.

D. Dual completion monitoring (Rustler-Salado via tubing and Culebra via annulus) shows Culebra stable at 355 feet (October 1977) and Rustler-Salado still recovering at 34 feet per month. (June 1978)

DRILLING AND TESTING SUMMARY

6.4.5 HOLE NO. H-3

LOCATION: T.22 S., R.31 E., Sec. 29

ELEVATION: 3,388.7 feet (ground level)

DEPTH DRILLED: 894 feet

DATE COMPLETED: August 12, 1976

DRILLING CONTRACTOR: Pennsylvania Drilling Co., Carlsbad, New Mexico

DRILLING METHOD: Auger 18 inch hole (0-38 feet)

Rotary 7.88 inch hole with air-air/mist (38-894 feet)

Ream 8.75 inch hole (38-894 feet)

CASING RECORD: 10.75 inch O.D. steel surface pipe (0-38 feet) cemented to surface.
6.63 inch O.D. steel casing, (0-891 feet), cemented to surface (cement plug to 804 feet drilled to 864 feet)

Geophysical Logs: Compensated Densilog
Micro-Laterolog
Dual-Laterolog
BHC Acoustilog
Compensated Neutron-Gamma
Differential Temperature

HYDROLOGIC TESTING (OPEN HOLE)

A.   800-868 feet: DST, Rustler-Salado contact, produced 1.8 gallons of water in 16.5 hours;

B.   672-703 feet: DST, Culebra, produced 2.1 gallons of water in 21.5 hours.

C.   703-780 feet: DST, salt residue, 2 gallons of water in 26 hours.

D.   558-608 feet: DST, Magenta, 23 gallons after 37.5 hours. after developing operation via swabbing.

HYDROLOGIC TESTING (CASED HOLE)

E.   813-837 feet: Perforated Rustler-Salado contact; produced 37 gallons in 32 days.

F. 675-703 feet: Perforated Culebra, bailed hole and monitored, recovery was up to 410 from an initial level of 550 feet (200 gallons in 8 days).

G. Tracer ^{131}I, showed no flow below 696 feet; major fluid losses in intervals 684-692 and 692-695; tracer injection rate was 8 gpm, total injected 450 gal.

H. 562-590 feet: Perforated Magenta, bailed 360 gallons in one hour with 6 feet of drawdown.

I. Dual-completion monitoring (Culebra via tubing and Magenta via annulus) indicate Culebra static level at 404.5 and Magenta static level at 245.1 as of October 1977.

DRILLING & TESTING SUMMARY

6.4.6 HOLE NO. P-14

LOCATION: T.22 S., R.30 E., Sec. 24

ELEVATION: 3,358.1 feet (ground level)

DEPTH DRILLED: 1,545 feet.

DATE COMPLETED: October 3, 1976

DRILLING CONTRACTOR: Boyles Brothers Drilling Co., Las Cruces, New Mexico

DRILLING METHOD: Rotary 8.75 inch hole with air (0-20 feet)
Rotary 7.88 inch hole with air-air/mist (20-784 feet)
Rotary with air/mist (784-1,168 feet)
Core with brine mud (1,168-1,545 feet)

CASING RECORD: 8.63 inch O.D. steel casing (0-20 feet)
4.50 inch O.D. steel casing, (0-775 feet) cemented to surface, hole
plugged back from 1,345 feet to 759 feet with cement.

Geophysical Logs: Gamma

Gamma-Gamma

Neutron

Caliper

HYDROLOGIC TESTING (CASED HOLE)

A.   676-700 feet: Perforated Rustler-Salado, fluid level rose from 730
to 620 feet in one day (75 gallons).

B.   573-601 feet: Perforated Culebra, bailed 720 gallons of water in
three hours with no drawdown.

C.   Tracer ^{131}I, showed 63 percent fluid loss in interval 583-590,
remaining loss in interval 573-583; no loss below 590 feet.   Injection
rate 7 gpm.   Total injected 1634 gal.

D.   Dual-completion monitoring (Rustler-Salado via tubing and Culebra via
annulus); Rustler-Salado stabilized at 386 feet, Culebra stabilized at
324 feet (October 1977)

DRILLING & TESTING SUMMARY

6.4.7   HOLE NO. P-15

LOCATION: T.22 S., R.31 E., Sec. 31

ELEVATION: 3,309.7 feet (ground level)

DEPTH DRILLED: 1,465 feet

DATE COMPLETED: October 14, 1976

DRILLING CONTRACTOR: Boyles Brothers Drilling Co., Las Cruces, New Mexico.

DRILLING METHOD: Rotary 8.75 inch hole with air (0-20 feet)
Rotary 7.88 inch hole with air-air/mist (20-515 feet)
Core 4.75 inch hole with air/mist (515-600 feet) (cut 2.25 inch diameter core)
Ream 7.88 inch hole with air/mist (515-637 feet)
Rotary 5 inch hole with air/mist (637-1,038 feet)
Core with brine mud (1,038-1,465 feet)

CASING RECORD: 8.63 inch O.D. steel casing (0-20 feet)
4.50 inch O.D. steel casing, (0-635 feet), cemented to surface, hole plugged back from 1,465 to 600 feet with cement, cement drilled out to 620 feet.

Geophysical Logs: Gamma
Gamma-Gamma
Neutron
Caliper
Spectralog

HYDROLOGIC TESTING:

A. 532-556 feet: Perforated Rustler-Salado contact, fluid rise from 618 to 497 in 42 days (81 gallons).

B. 410-438 feet: perforated Culebra, fluid rose from 496 to 420 feet in one day (50 gallons); 125 gallons in 33 days

C. Dual Completion monitoring (Rustler-Salado via tubing and Culebra via annulus) shows Rustler-Salado static level at 324 feet and Culebra at 308 feet as of October, 1977.

DRILLING AND TESTING SUMMARY

6.4.8 HOLE NO. P-17

LOCATION: T.23 S., R.31 E., Sec. 4

ELEVATION: 3,339.5 feet (ground level)

DEPTH DRILLED: 1,660 feet

DATE COMPLETED: October 26, 1976

DRILLING CONTRACTOR: Boyles Brothers Drilling Co., Las Cruces, New Mexico.

DRILLING METHOD: Rotary 8.75 inch hole with air (0-20 feet)
Rotary 7.88 inch hole with air-air/mist (20-755 feet)
Rotary with air/mist (755-1,220 feet)
Core with brine mud (1,220-1,660 feet)

CASING: 8.63 inch O.D. steel casing (0-20 feet)
4.50 inch O.D. steel casing, (0-751 feet), cemented to surface, hole plugged back from 1,660 feet to 720 feet with cement, cement drilled out to 731 feet.

Geophysical Logs: Gamma
Gamma-Gamma
Neutron
Caliper

HYDROLOGIC TESTING (CASED HOLE)

A. 702-726 feet: Perforated Rustler-Salado contact; fluid rose from 726 to 622 feet (71 gallons in 73 days).

B.   558-586 feet: Perforated Culebra, single packer set at 683 feet, bailed and monitored for 29 days with fluid rise from 622 to 372 feet.

C.   Dual Completion monitoring (Rustler-Salado via tubing and Culebra via annulus) indicates fluctuating levels; problem could be leaking bridge packer or communication in cemented annulus.

DRILLING & TESTING SUMMARY

6.4.9 HOLE NO. P-18

LOCATION: T.22 S., R.31 E., Sec. 26

ELEVATON: 3,478.7 feet (ground level)   .

DEPTH DRILLED: 1,998 feet

DATE COMPLETED: November 5, 1976

DRILLING CONTRACTOR: Pennylsvania Drilling Co., Carlsbad, New Mexico.

DRILLING METHOD: Rotary 8.75 inch hole with brine mud (0-18 feet)
Rotary 7.88 inch hole with brine mud (18-1139 feet) to casing depth.
Rotary with brine mud (1,139-1,630 feet)
Core with brine mud (1,630-1,998 feet)

CASING RECORD: 8.63 inch O.D. steel casing (0-18 feet)
4.50 inch O.D. steel casing, (0-1, 138 feet), cemented to surface, hole plugged back from 1,998 feet to 1,125 feet with cement.

Geophysical Logs: Gamma
Gamma-Gamma
Neutron
Caliper

HYDROLOGIC TESTING (CASED HOLE)

A. 1076-1100 feet: Perforated Rustler-Salado contact, fluid rise from 1123 to 1073 feet in 73 days (34 gallons)

B. 912-940 feet: Perforated Culebra, bailed and monitored recovery for 33 days with fluid rise from 1045 to 1022 feet (16 gallons).

C. Dual completion (Rustler-Salado via tubing, Culebra via annulus) indicated Rustler-Salado at 755 feet and still recovering as of October, 1977.

DRILLING & TESTING SUMMARY

6.4.10 HOLE NO. AEC-8

LOCATION: T.22 S., R.31 E., Sec. 11

ELEVATION: 3,531.9 feet (ground level)

DEPTH DRILLED: 3,019 feet (1974), deepened to 4,910 feet (1976)

DATE COMPLETED: August 5, 1976

DRILLING CONTRACTOR: Sonora Drilling Co., Carlsbad, New Mexico

DRILLING METHOD: Core, ream, rotary 7.88 inch hole with brine mud (31-3,019 feet)
Core, ream, rotary 7.88 inch hole with brine mud (3,018.5-4,910.5 feet)

CASING RECORD: 8.63 feet O.D. steel casing (0-874 feet), cemented to surface.
5.50 inch O.D. steel casing, (0-4,907 feet), cemented to 880 feet.

Geophysical Logs;   Compensated Neutron

Micro-Laterlog

Dual-Laterolog

Gamma

HYDROLOGIC TESTING (CASED HOLE)

A. 4,844-4,860 feet: Perforated lower sand lense of Bell Canyon
Formation; fluid level rose from 4126 feet to 4095 feet in 166 minutes
(31 gallons).

B. 4,832 - 4,910 feet: Production packer with sentry monitoring device
showed formational pressure of 2037 lbs/ in^2 reached in 44.5 hours;
fluid density was 1.11 g/cm^3.

C. Tracer ^{131}I, along with temperature logs, indicated major fluid
loss in interval 4839 to 4860 feet; minor communication down casing to
4870 feet; tracer injection rate was 14 gpm. Total injected 2289 gal.

D. 4,821-4,827 feet: Perforated upper sand lense of Bell Canyon
Formation; single packer set at 4835 feet; swabbed fluid to 2600 feet;
pressure monitor installed at 4805 feet; shut-in pressure recovered to
2037 lbs/in^2 in 57 hours, fluid density was 1.12 gm/cm^3,

E. Tracer ^{131}I, showed no upward or downward communication; injection
rate at tracer was 11 gpm. Total injected 300 gal. Injection was
occurring uniformly in the lower 4 feet of perforations.

F. Dual completion monitoring (lowering sand via tubing and upper sand
via annulus) indicate lower sand stablized at 615 feet and upper sand at
560 feet as of November, 1977.

6.5 SUMMARY

The proposed site contains neither perennial streams nor surface water impoundment, and the water bearing strata above and below the evaporite section do not yield large quantities of water to wells. At its closest point, the Pecos River is approximately 14 miles southwest of the WIPP site. Water bearing strata in the local site area at stratigraphic horizons above the proposed repository include the Santa Rosa Sandstone and the Culebra and Magenta members of the Rustler Formation. Hydrologic units below the repository horizons include the Bell Canyon Formation of the Delaware Mountain Group. Ground water velocities vary with porosity, hydraulic conductivity, and head gradient but are typically 0.3 ft/d in the Santa Rosa Sandstone, 0.5 ft/d in the Rustler Formation, and 0.0006 ft/d in the Bell Canyon Formation. Shallow wells in the local area are generally used only for watering livestock and typically produce nonpotable ground water with total solute concentrations in excess of 3,000 ppm.

Natural potentiometric levels of fluids from rocks above and below the evaporites at the WIPP site (from the Rustler and Bell Canyon Formations, respectively) are comparable (about 2950 to 3050 above mean sea level). The head differential between upper and lower units varies within about 200 feet on the periphery of the site, the sign and magnitude of the differential depending upon precise geographic location.

Gentle eastward tilting of the Delaware Basin resulting in the exposure of the Salado Formation to near-surface waters has given rise to the removal of a wedge-shaped mass of soluble salts between the Guadalupe escarpment (30 miles due west of the site), where there remains no rock salt, and a point about 3 miles due west of the site center, where the Salado Formation is intact.

The proposed site is in an area of the Delaware Basin that is free of regional deep dissolution, but localized shallow features are present in the vicinity. A shallow salt dissolution zone (called the "brine aquifer") occurs in Nash Draw at the contact between the Salado and

Rustler Formations. This local shallow dissolution area ranges in width from 2 to 10 miles and has a length of approximately 30 miles. The brine solution flows southwesterly at a rate of about 0.2 ft/d and discharges into the Pecos River at Malaga Bend. The average rate of vertical dissolution has been estimated to be between 0.33 and 0.5 feet per 1,000 years, and the average rate for lateral dissolution has been estimated to be between 6 and 8 miles per million years.

Climatological records show that mean annual precipitation of the site is approximately 12 inches per year. Aided by the low relative humidity (typically 36% during daylight hours) and high mean annual temperature (61°F), most of the annual precipitation returns to the atmosphere through evaporation and transpiration. Runoff is typically 0.1 to 0.2 inches annually.

6.6 REFERENCES

Anderson, R.Y., Dean, W.E., Kirkland, D.N., and Snider, H.I., 1972, Permian Castile varved evaporite sequence West Texas and New Mexico: Geol. Soc. Amer. Bull. v. 83, p. 59-86.

Anderson, R. Y., 1978, Report to Sandia Laboratories on deep dissolution of salt, northern Delaware Basin, New Mexico, January 1978, 98pp.

Anderson, R.Y., and Powers, D. W. (in press). Salt anticlines in the Castile-Salado evaporite sequence, Northern Delaware Basin, New Mexico, Symposium on the Ochoan rocks of southeastern New Mexico and West Texas, Cir. 159, New Mexico Bureau of Mines and Mineral Resources.

Bachman, G.O., and Johnson, R., 1973, Stability of salt in the Permian Salt Basin of Kansa, Oklahoma, Texas and New Mexico: U.S. Geol. Survey Open-file report 4339-4.

Bachman, G.O., 1974, Geologic processes and Cenozoic history related to salt dissolution in southeastern New Mexico: U.S. Geol. Survey Open-file report 74-194.

Bachman, G. O., 1976, Cenozoic deposits of southeastern New Mexico and an outline of the history of evaporite dissolution: U.S. Geol. Survey, Jour. Research v. 4, No. 2, p. 135-149.

Barr, G.E., Lambert, S.J., and Carter, J.A., 1978, Uranium isotope disequilibrium in groundwaters of southeastern New Mexico and implications regarding age-dating of waters. SAND77-1779. IAEA-SM-228/32, Sandia Laboratories, Albuquerque, New Mexico.

Bjorklund, L. J. and Motts, W. S., 1959, Geology and water resources of Carlsbad area, New Mexico: U.S. Geol. Survey Open-file report 59-9.

Blaney, H.F., and Hanson, E.G., 1965, Consumptive use and water requirements in New Mexico: New Mexico state engineer, technical report 32.

Brokaw, Arnold L., Jones, C.L., Cooley, M.E., and Hays, W.H., 1972, Geology and hydrology of the Carlsbad potash area, Eddy and Lea Counties, New Mexico: U.S. Geol. Survey Open-file report 4339-1.

Cooper, J.B., 1962, Ground-water investigations of the Project Gnome area, Eddy and Lea Counties, New Mexico: U.S. Geol. Survey Report REI-802.

Cooper, J. B., and Glanzman, V. M., 1971, Geohydrology of project Gnome site, Eddy County, New Mexico: U.S. Geol. Survey, Prof. Paper 712-A, 24 p.

Gard, L.M., Jr., 1968, Geologic studies, Project Gnome, Eddy County, New Mexico: U.S. Geol. Survey Prof. Paper 589.

Griswold, G. B., 1977, Site selection and valuation studies of the Waste Isolation Pilot Plant (WIPP), Los Medanos, Eddy County, New Mexico: SAND77-0946 Sandia Laboratories, Albuquerque, New Mexico.

Hale, W. E., Hughes, L.S., and Cox, E.R., 1954, Possible improvement of quality of water of the Pecos River by diversion of brine of Malaga Bend, Eddy County, New Mexico: Report of the Pecos River Commission, New Mexico and Texas with U.S. Geol. Survey Water Resources Division.

Hendrickson, G. E., and Jones, R. J., 1952, Geology and ground water resources of Eddy County, New Mexico: New Mexico Bureau of Mines and Mineral Resources, Ground-Water Report 3.

Hiss, W.L., 1975a, Stratigraphy and ground-water hydrology of the Capitan Aquifer, southeastern New Mexico and western Texas, unpublished Ph.D. thesis, University of Colorado, Boulder, Colorado.

Hiss, W.L., 1975b, Thickness of the Permian Guadalupian Capitan aquifer, southeast New Mexico and west Texas: New Mexico Bureau of Mines and Mineral Resources, Resource Map 5.

Hiss, W.L., 1975c, Chloride-ion concentration in ground water in Permian Guadalupian rocks, southeast New Mexico and west Texas: New Mexico Bureau of Mines and Mineral Resources, Resource Map 5.

Hiss, W. L., 1976a, Structure of the Permian Ochoan Rustler Formation, southeast New Mexico and West Texas: New Mexico Bureau of Mines and Mineral Resources, Resource Map 7, 1976.

Hiss, W.L., 1976b, Structure of the Permian Guadalupian Capitan Aquifer southeast New Mexico and west Texas: New Mexico Bureau of Mines and Mineral Resources, Resource Map 6.

Jones, C. L., Cooley, M.E., and Bachman, G.O., 1973, Salt deposits of Los Medanos area, Eddy and Lea Counties, New Mexico, U.S. Geol. Survey Open-file report 4339-7.

Kelley, V.C., 1971, Geology of the Pecos country, southeastern New Mexico New Mexico Bureau of Mines and Mineral Resources, Memoir 24.

King, P. B., 1948, Geology of the southern Guadalupe Mountains, Texas: U.S. Geol. Survey Prof. Paper 215.

Lambert, S.J., 1977, The geochemistry of Delaware Basin groundwaters, Sandia Laboratories Report, Albuquerque, New Mexico, SAND77-0420. Report also in New Mexico Bureau of Mines and Mineral Resources, Circ. 159 (1978 - in press).

Lambert, S. J. and Mercer, J. W., 1977, Hydrologic investigations of the Los Medanos area, southeastern New Mexico, 1977: SAND77-1401, Sandia Laboratories, Albuquerque, New Mexico.

Lohman, S.W., 1972, Definitions of selected ground-water terms--revisions and conceptual refinements: U.S. Geol. Survey Water Supply Paper 1988.

Maley, V. C., and Huffington, R. M., 1953, Cenozic fill and evaporite solution in the Delaware Basin, Texas and New Mexico: Geol. Soc. Amer. Bull. v. 64, pp 539-546..

McNeal, R. P., 1965, Hydrodynamics of the Permian Basin Fluids, in subsurface environments symposium: Amer. Assoc. of Petrol. Geologists Memoir No. 4, p. 308-326.

Mercer, J.W., (to be published), Hydrologic tests and observations in the potash-hydro holes P-14, P-15, P-17, and P-18, U.S. Geol. Survey.

Mercer, J.W., and Orr, B. R., 1977, Review and analysis of hydrogeologic conditions near the site of a potential nuclear waste laboratory, Eddy and Lee Counties, New Mexico, U.S. Geol. Survey Open-file report 77-123.

Mercer, J. W., and Orr. B. R., 1978, Geohydrology of the proposed Waste Isolation Pilot Plant, southeastern New Mexico: U.S. Geol. Survey report submitted to DOE (preliminary).

Motts, W.S., 1957, Geology and ground water resources of the Carlsbad area, New Mexico, unpublished Ph.D. Thesis, University of Illinois (Urbana).

Nicholson, Alexander, Jr., and Clebsch, A., Jr., 1961, Geology and ground-water conditions in southern Lea County, New Mexico: Ground-water Report 6, New Mexico Bureau of Mines and Mineral Resources.

NOAA Environmental Data Service, 1977, Climatography of the United States, No. 60, Climate of New Mexico: U.S. Dept. of Commerce, March 1977.

Pettigrew, Richard R. and Assoc., 1977, WIPP conceptual design report (soils and foundation investigation): Prepared for Sandia Laboratories Albuquerque, New Mexico.

Pierce, W. G. and Rich, E. I., 1962, Summary of rock salt deposits in the United States as possible storage sites for radioactive waste materials: U.S. Geol. Survey Bull. 1148, 33-35P.

Piper, A.M., 1973. Subrosion in and about the four-township study area near Carlsbad, New Mexico, ORNL subcontract 3745, Oak Ridge National Laboratory, Oak Ridge, TN.

Reddy, G. R., 1961, Geology of the Queen Lake domes near Malaga, Eddy County, New Mexico: unpublished M.S. Thesis, Univ. of New Mexico.

Robinson, T. W., and Lang, W. G., 1938, Geology and ground water conditions of the Pecos River Valley in the vicinity of Laguna Grande de la Sal, New Mexico, with special reference to the salt content of the river water. N. Mex. State Engineer 12th and 13th Bienn. Repts., p. 77-100.

Rose, Walter, 1977, Development of a conceptual model to explain brine flowage into wells drilled thru the Salado-Castile Formation. Contact in locations such as the ERDA #6 site near Carlsbad in southeastern New Mexico: Report to Sandia Laboratories.

Theis, C.V., and Sayre, A.N., 1942, Geology and ground water, in (U.S.) National Resources Planning Board, 1942, Pecos River Joint Investigation-Reports of the participating agencies: Washington, U.S. Govt. Printing Office, P. 27-38.

U.S. Department of Agriculture, Soil Conservation Service, 1971, Soil survey of Eddy area, New Mexico, U.S. Government Printing Office, Washington, D.C.

U.S. Department of Agriculture, Soil Conservation Service, 1974, Soil survey of Lea area, New Mexico, U.S. Government Printing Office, Washington, D.C.

U.S. Department of Commerce, Weather Bureau, 1952, Mean number of thunderstorm days in the United States, Technical paper No. 19.

U.S. Department of Commerce, Weather Bureau, 1955, Rainfall intensity-duration-frequency curves. Technical paper No. 25.

U. S. Department of Commerce, Weather Bureau, 1969, Severe local storm occurrences, 1955-1967. Technical Memorandum WBTM FCST 12.

U.S. Department of Commerce, Weather Bureau, 1961, Climatological Survey Station, Carlsbad, New Mexico.

U.S. Department of Commerce and U.S. Department of Army, Weather Bureau and corps of Engineers, 1976, Hydrometeorological report No. 33, seasonal variation of the probable maximum precipitation east of the 105th meridian.

U.S. Department of the Interior, 1975, Preliminary regional environmental analysis record potash leasing in southeastern New Mexico: Bureau of Land Management, New Mexico State Office.

U.S. Geological Survey, 1976, Water resources data for New Mexico, water year 1976: U.S. Geol. Survey Water-Data Report NM-76-1.

U.S. Geological Survey Topographic maps, 15 minute series (1:62,500) for Nash Draw and Hat Mesa, New Mexico.

U. S. Geological Survey Topographic Maps, (1:250,000), NI 13-11 (Carlsbad) and NI 13-12 (Hobbs), New Mexico.

Vine, J. D., 1960, Recent domal structures in southeastern New Mexico:
Amer. Assoc. Petrol. Geol. Bull., v. 44, no. 12, p. 1903-1911.

Vine, J. D., 1963, Surface geology of the Nash Draw quadrangle, Eddy
County, New Mexico: U.S. Geol. Survey Bull. 1141-B.

Wolfe, H.G., editor, 1977a. An environmental baseline study of the Los
Medanos Waste Isolation Pilot Plant (WIPP) project area of New Mexico: a
progress report: SAND77-7017, Sandia Laboratories, Albuquerque, New
Mexico.

Wolfe, H.G., editor, 1977b. An environmental baseline study of the Los
Medanos Waste Isolation Pilot Plant (WIPP) project area of New Mexico: a
progress report. An addendum: SAND77-7018, Sandia Laboratories,
Albuquerque, New Mexico.

104°30' 104°00'

CHAVES CO
EDDY CO

24 25 26 27 28 29 30 31

T
16
S

17

ARTESIA

18

19

LAKE McMILLAN

20

3000 3400 3300 3200

32°30'

24 25 26 27 28 29 30

LAKE AVALON

21

CARLSBAD

22

PECOS RIVER

SITE

23

LOVING

24

WHITES CITY

25

3900 3800 3700

26

32°00'

23 24 25 26 27 28 30 NEW M
TEX

RED BLUFF RESERVOIR

3600

PECOS REEVES CO

CULBERSON CO
REEVES CO

31°30'

104°30' 104°00'
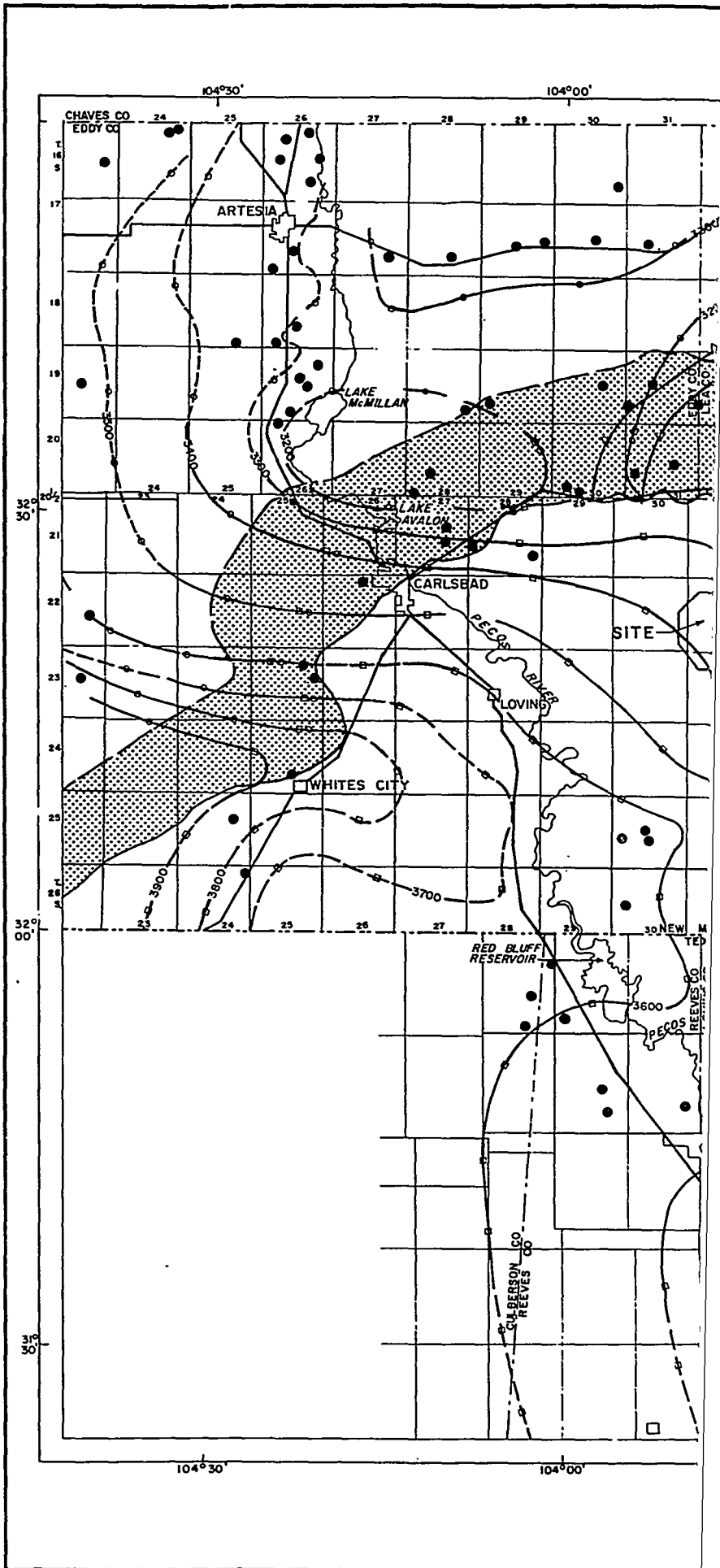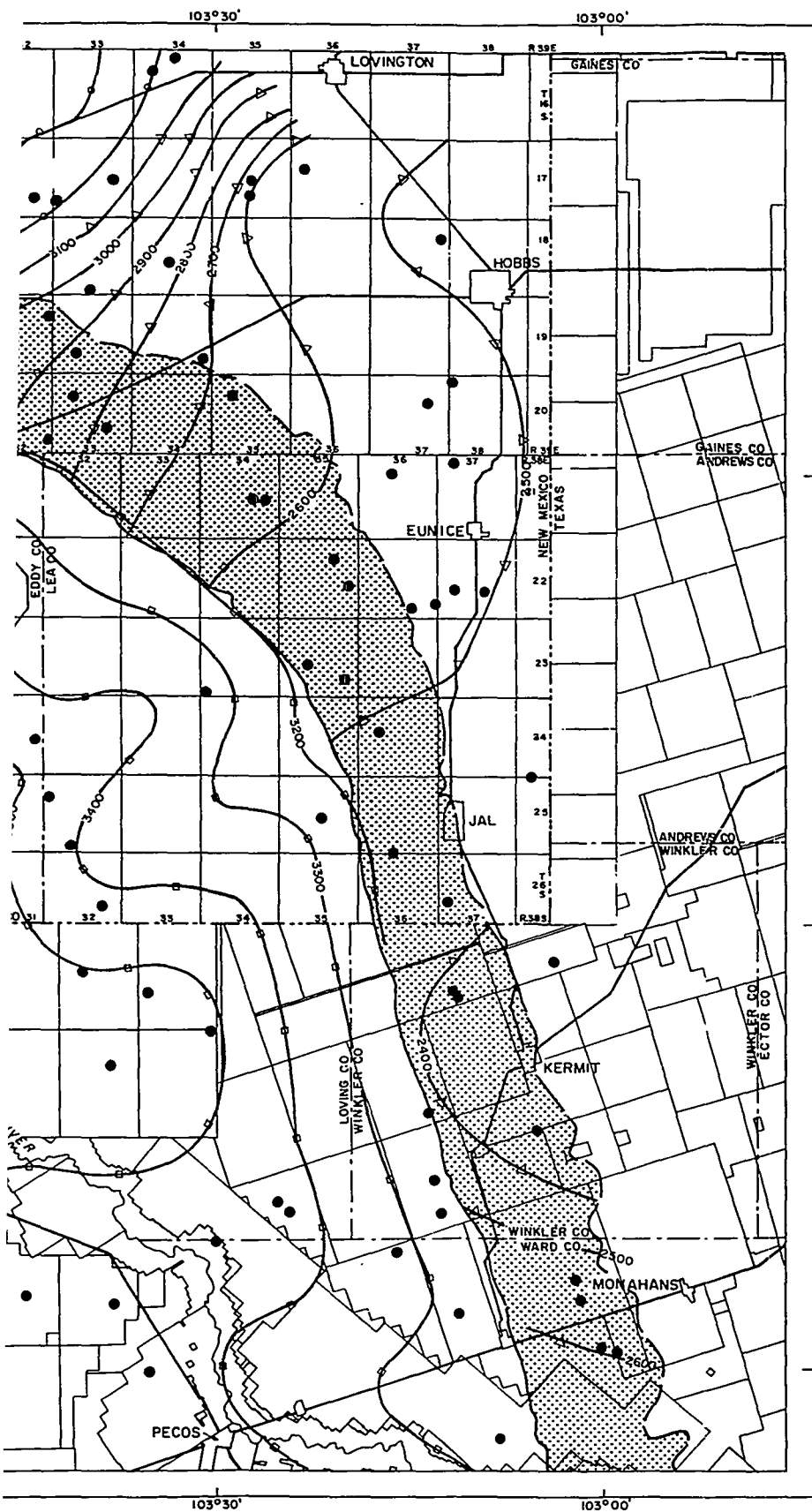
EXPLANATION

Position of
Capitan
aquifer

Approximate position
of extreme shelf-
ward edge

Basinal edge

CONTOURS OF HEAD (in feet above sea level).
Values of head are expressed as water with
specific gravity of 1.00. Contours are dashed
wherever data are sparse or of doubtful
reliability.

Head measured in shelf aquifer system
where the hydraulic communication
with the Capitan aquifer is relatively
poor.

Head measured in the Capitan aquifer
system where the hydraulic communica-
tion between the two aquifers is
relatively good.

Head measured in basin aquifer
system where the hydraulic
communication with the Capitan
aquifer is relatively poor

The contours express a generalized regional
head considered to be reresentative for basin
and shelf aquifers during the period 1960 to
1970. Similarly, contours in the Capitan
aquifer are an interpretation of the head
representative for the latter part of 1972.

Considerable subjective judgment was used
in contouring the data points. In general
two factors were weighed in considering each
data point-

(1) The year in which the head was
measured This is important because
prior fluid withdrawl from the oil
and water fields causes a decline
in head in nearby areas.

(2) The reliability of the data: In
general the data were ranked
according to reliability in the
following order: fluid level in
water wells, initial oil field
bottom-hole pressures, and analysis
of pressures from drill-stem tests.

Well penetrating sediments of
Permian, Ochoan, Guadalupian,
or Leonardian age in which
pressure or water level was measured

Reference: Fig 22 Hiss, W L., 1975

5   0   5   10 MILES
5   0   5   10   15 KILOMETERS
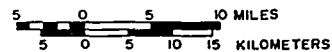
POTENTIOMETRIC SURFACE
OF THE GUADALUPIAN
AQUIFER SYSTEM

FIGURE 6.3-1

Map labels: LOVINGTON, GAINES CO, HOBBS, EUNICE, JAL, KERMIT, MONAHANS, PECOS, GAINES CO / ANDREWS CO, ANDREWS CO / WINKLER CO, WINKLER CO / WARD CO, NEW MEXICO / TEXAS, EDDY CO / LEA CO, LOVING CO / WINKLER CO, WINKLER CO / ECTOR CO
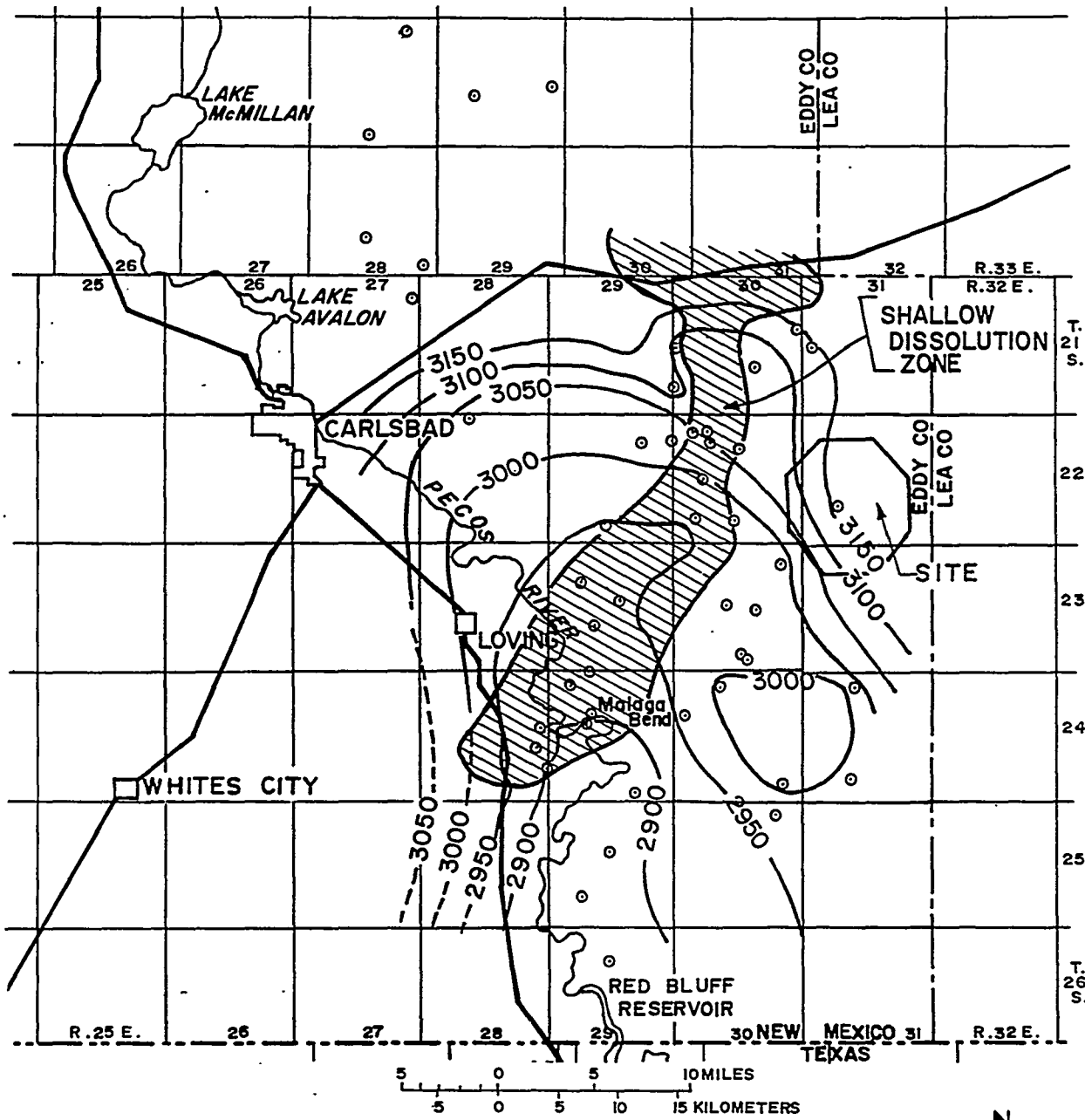
EXPLANATION

⊙   Well or exploratory hole open to the Rustler Formation

3000 ―― Potentiometric elevation contour based on water levels measured
in wells, 1952–1973. Dashed where approximately located.
Datum is mean sea level.

Reference: Figures 5 & 6, U.S.G.S. Open File Rpt. 77-123, 1977

POTENTIOMETRIC SURFACE
RUSTLER FORMATION AND AREAL
EXTENT OF SHALLOW DISSOLUTION ZONE

FIGURE 6.3-2

Map labels: T. 18 S., 19, 20, 21, 22, 23, 24, 25, T. 26 S.

Llano Estacado, EDGE OF OGALLALA OUTCROP

3200, 3300, 3400, 3500, 3600

EDDY CO, LEA CO

Laguna Tonte, Laguna Gatuna, Laguna Plata, Laguna Toston

Clayton Basin

3400

R. 35 E., R. 34 E.

29, 30, 31, 32, 33, 34

3400, 3500, 33

Ouahada Ridge, Nash Draw, Livingston Ridge, "The Divide", San Simon Swale

3300, 3200

3400, 3200, 3300, 3400

LAGUNA GRANDE DE LA SAL, SITE, 3300, 3200

PECOS, Malaga Bend, WESTERN LIMIT OF SANTA ROSA

3200

RIVER, 3200

3100, 3000

RED BLUFF RESERVOIR

R. 28 E., 29, 30 NEW MEXICO 31, 32, 33, R. 34 E.
TEXAS

| 5 | 0 | 5 | 10 MILES |
| 5 | 0 | 5 | 10 | 15 KILOMETERS |

EXPLANATION

◎ Well open to Triassic rocks

⌐ Potentiometric elevation contour, based on water levels
measuerd in wells, 1952 –1973. Dashed where approximately
located. Datum is mean sea level.

POTENTIOMETRIC SURFACE
SANTÁ ROSA SANDSTONE

Reference:

   Mercer and Orr, 1977, figure 7.

FIGURE 6.3-3

R.31E.   R.32E.   R.33E.   R

Wells completed in Capitan aquifer

T.19 S.

T. 20 S.

LAGUNA PLATA

LAGUNA GATUNA

R.30E.   R.31E.   R.32E.   R.33

T.21 S.

Site Boundary

WESTERN LIMIT OF SANTA ROSA SANDSTONE

T.22 S.

T.23 S.

SECTIONS WITHIN A TOWNSHIP   TRACTS WITHIN A SECTION

R.35E.   Sec.31

6	5	4	3	2	1
7	8	9	10	11	12
18	17	16	15	14	13
19	20	21	22	23	24
30 well	29	28	27	26	25
31	32	33	34	35	36

T. 20 S.

4 E.

N

well

6 miles

1 mile

Well 20.35.31.113

WELL-NUMBERING SYSTEM

The well number consists of four parts separated by periods. The first part is the township number, the second part is the range number, and the third part is the section number. The fourth part of the number consists of three digits which denote the particular 10-acre tract within the section in which the well is located.

EXPLANATION

⌐——⌐ Approximate western limit of occurrence of ground water in the Santa Rosa Sandstone.

○   Water well completed in surficial deposits or upper sandstone beds of the Chinle Formation.

●   Water well completed in lower sandstone beds of the Chinle Formation, Santa Rosa Sandstone, Dewey Lake Redbeds, or Rustler Formation.

NOTE:
See Table 6.3—2 for descriptions of wells.

Reference: USGS Open File Report 4339-7, Jones, C.L., et al, 1973

```
0   1   2   3   4   5
SCALE IN MILES
```

N

WATER WELL SURVEY

FIGURE 6.3-4
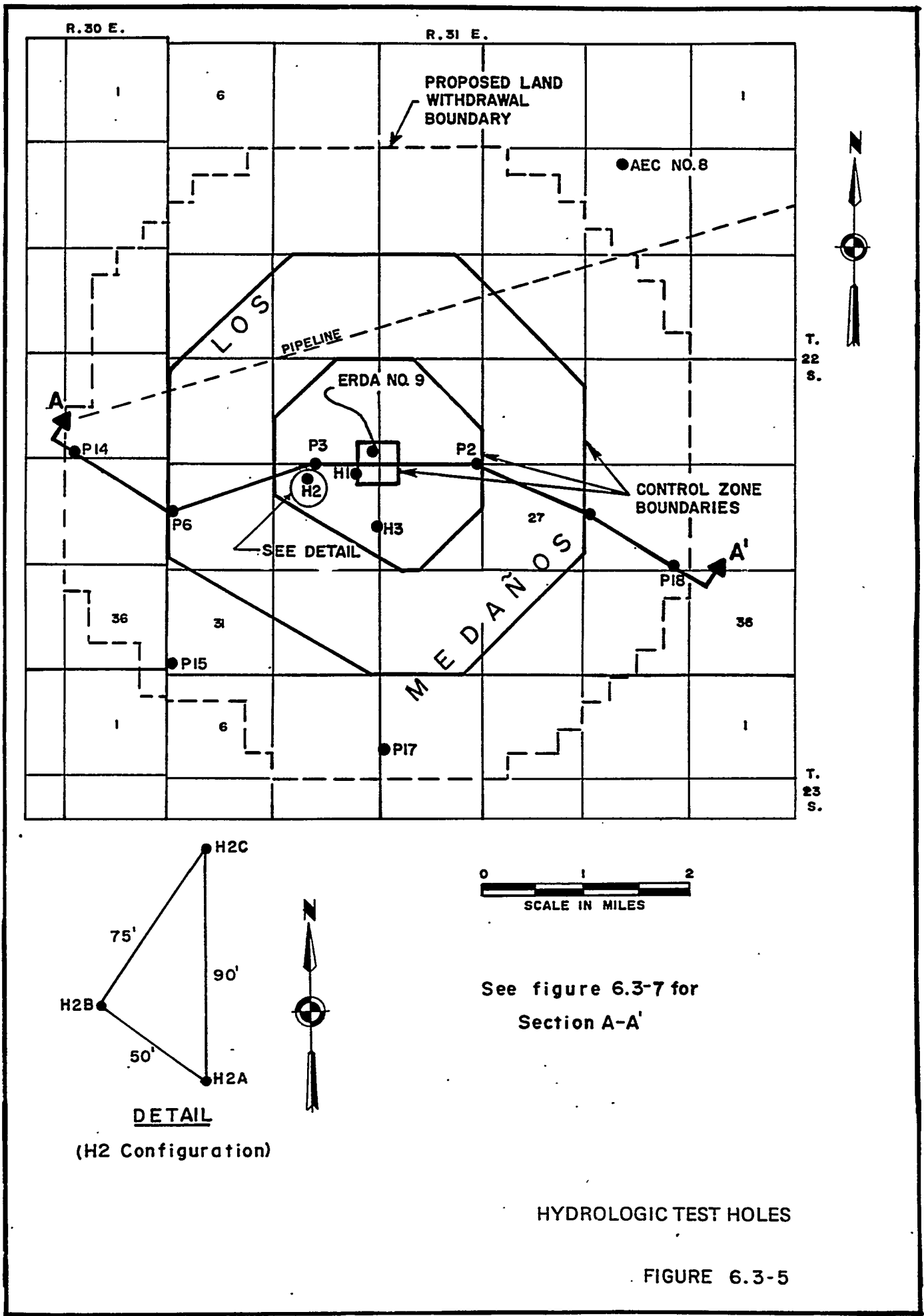
R.30 E.

R.31 E.

PROPOSED LAND
WITHDRAWAL
BOUNDARY

●AEC NO.8

N

T. 22 S.

LOS

PIPELINE

ERDA NO. 9

A

PI4

P3

P2

HI

H2

P6

CONTROL ZONE
BOUNDARIES

SEE DETAIL

H3

27

A'

PI8

MEDAÑOS

36

31

36

PI5

1

6

1

PI7

T. 23 S.

H2C

75'

90'

H2B

N

50'

H2A
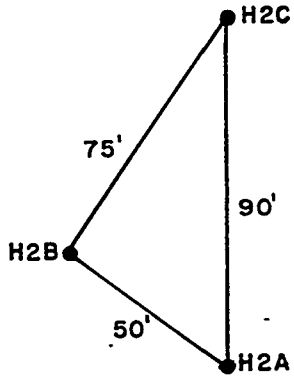
DETAIL

(H2 Configuration)

0   1   2
SCALE IN MILES

See figure 6.3-7 for
Section A-A'

HYDROLOGIC TEST HOLES

FIGURE 6.3-5

DEPTHS IN
FEET
0 ——————— Elevation of Ground Surface 3388.7 ft.

22 ——————
    Dune sand &
    Gatuna Formation

DEWEY LAKE

REDBEDS

502 ———————

RUSTLER

Magenta Dolomite
(560-584)
Culebra Dolomite
(670-694)
Top of Salt @ 718

FORMATION

820 ———————

SALADO

FORMATION

$10^{3/4}$ inch ∅ casing to 38 ft.

$6^{5/8}$ inch ∅ casing to 894 ft.

Cement grout.

2 inch ∅ tubing to
production packer (652 ft.)

Perforated interval, 564-592 ft.
(3-1/2 inch jet shots per foot)

Inflatable production packer at 652 ft.

Perforated interval, 675-703 ft.
(3-1/2 inch jet shots per foot)

Inflatable bridge plug at 795 ft.

Perforated interval, 813-837 ft.
(3-1/2 inch jet shots per foot)

Top cement plug 864 ft.

Status October 1977:

    Total depth drilled : 894 ft.
    Diameter of drilled hole : $9^{7/8}$ inch
    Monitoring Culebra through tubing
    Monitoring Magenta in annulus
    Contact zone not accessible (bridge plug)

CONSTRUCTION OF OBSERVATION WELL H-3

FIGURE 6.3-6

A'

P18

SURFICIAL
DEPOSITS

SANTA ROSA
SANDSTONE

DEWEY LAKE
RED BEDS

TOP OF RUSTLER
SALT

RUSTLER

FORMATION

SALADO

FORMATION

BED 124

—3500

—3000

—2500

—2000

—1500
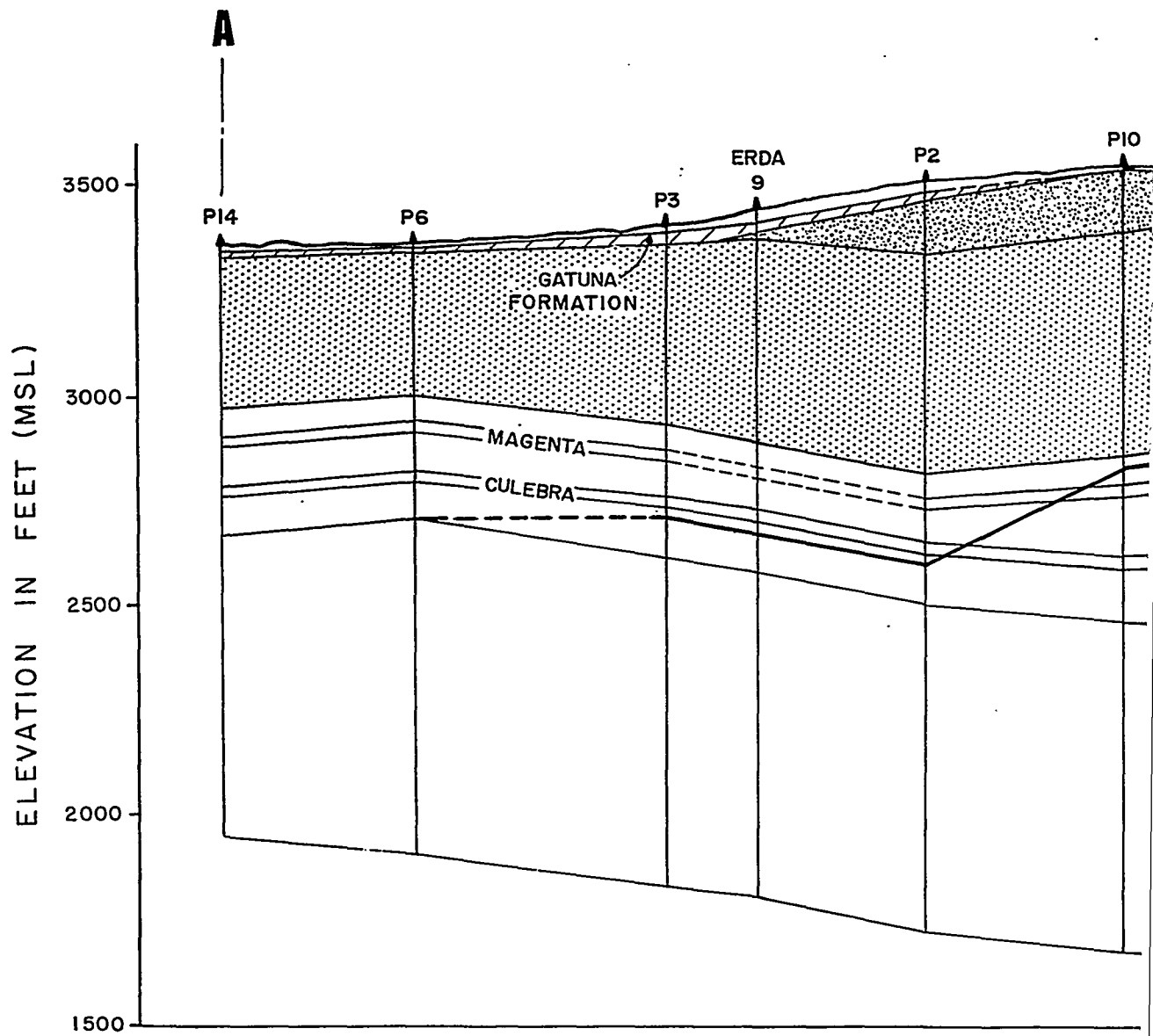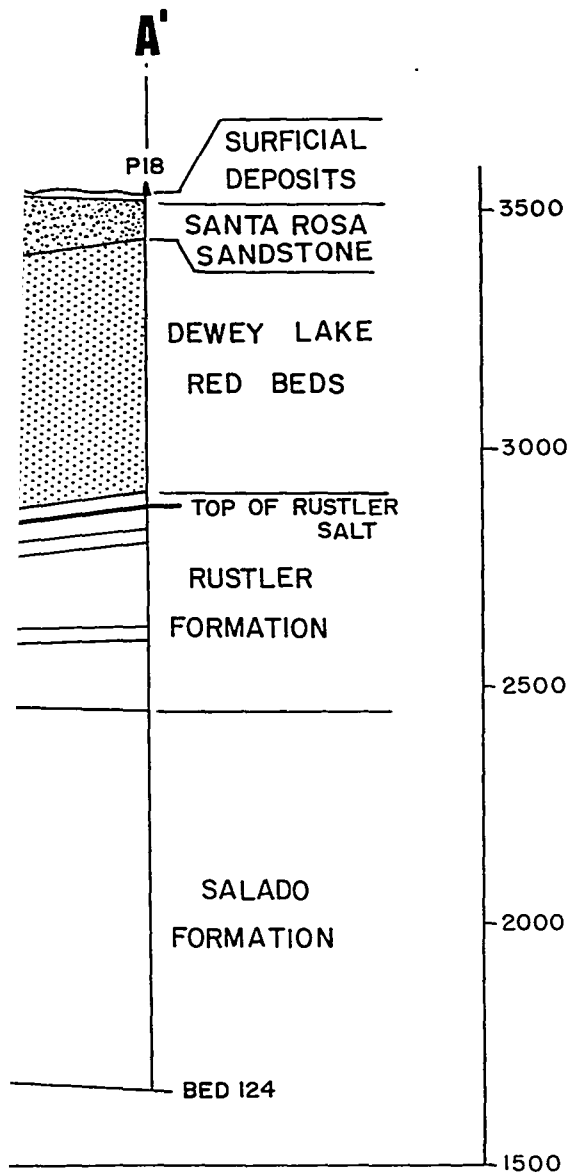
REFERENCES:

Lambert and Mercer, 1978 , fig.4, p.I–15

NOTE:

For location of Section see
Figure 6.3–5.

0   1   2   3 KM
0   1   2 MI
HORIZONTAL SCALE
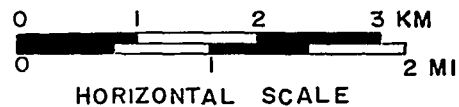
GEOLOGIC SECTION
THROUGH THE LOS MEDANOS AREA

FIGURE 6.3-7

EXPLANATION

DISSOLUTION WEDGE

EXTENT OF CENOZOIC FILL
DEEP CENOZOIC FILL

AREA SUBJECT TO EROSION
DURING JURASSIC TIME
(BACHMAN 1976)

Reference: Based on Figure I
from Anderson, 1978

DISSOLUTION FEATURES AND EXTENT
OF EROSION IN DELAWARE BASIN

FIGURE 6.3-8

B — Quahada Ridge

B' — Livingston Ridge

Mescalero caliche projected

Nash Draw

180'

120'

3300' 3300'

3100' 3000'

2900' 2900'

Top   of

220'

2700'

Salado

Formation   2700'

420'

Top   of

630'

marker   bed 124

750

2500'

2300'

2100'

ELEVATION IN FEET (MSL)

LINE OF SECTION

T.21 S.

B

B'

T.22 S.

SITE

N

R.30 E.   R.31 E.

0   1   2 miles

HORIZONTAL SCALE

Reference: Fig. II, USGS Open File
Report 74–194, 1974

RELATIONSHIP OF
NASH DRAW TO DISSOLUTION
IN SALADO FORMATION

FIGURE 6.3-9

Table 6.2-1. AREAL REQUIREMENTS OF THE WIPP SITE

Zone	Zone Use	Approximate Acreage
I	Surface Facilities	60-(100)
II	Underground Storage	1,860
III	1-mile wide zone surrounding Zone II No mining or drilling.	6,230
IV	1-mile wide zone surrounding Zone III. Mining and drilling in conformance with ERDA specifications are allowed.	10,810
	TOTAL	18,960

29.6 square miles

TABLE 6.2-2

SALIENT FEATURES OF MAJOR DAMS UPSTREAM AND

DOWNSTREAM FROM WIPP SITE

Name of Reservoir	River	Drainage Area (sq. mi.)	Type of Dam	Year Completed	Height (ft.)	Max. Storage Capacity (AF)	Purpose
Sumner	Pecos	4,390	earth	1937	143	258,500	Irrigation
McMillan	Pecos	16,990	earth	1908	40	66,600	Irrigation
Avalon	Pecos	18,070	earth	1907	40	36,600	Irrigation
Red Bluff	Pecos	20,720	earth	1937	98	405,000	Irrigation & Hydro-power
Two Rivers	Rio Hondo	963	earth	1963	93	262,221	Flood
	Rocky Arroyo	64	earth	1963	116		Control

TABLE 6.2-3

WATER USE DATA FOR THE PECOS BASIN

Use category	Surface-water and groundwater withdrawals (mgd) 1975[a]
Agriculture	1546
Steam-electricity	12
Manufacturing	0
Domestic	47
Commercial	8
Mining	151
Public lands	4
Fish hatcheries	3
Total	1771

SOURCE: U.S. Water Resources Council, Second National Assessment of Water and Related Land Resources, in press.

[a]The total groundwater withdrawal for 1975 was 1079 mgd.

TABLE NO. 6.2-4

PRECIPITATION AT CARLSBAD, N.M. (in inches)

Period of Record   1931-1960

MONTH	JAN.	FEB.	MARCH	APRIL	MAY	JUNE	JULY	AUG.	SEPT.	OCT.	NOV.	DEC.	ANNUAL
Max. Precip	2.31	1.93	4.27	3.99	12.28	6.24	5.48	4.41	7.36	6.13	1.55	2.12	33.94
Av. Precip.	0.44	0.37	0.46	0.54	1.76	1.33	1.56	1.60	1.94	1.61	0.35	0.47	12.43
Min. Precip.	0	0	0	0	0.18	0	0	0.01	0	0	0	0	4.40

SOURCE: U. S. Weather Bureau, 1961.

· TABLE NO. 6.2-5

TEMPERATURES AT CARLSBAD, N.M. (in °F)

Period of Record   1931-1960

MONTH	JAN.	FEB.	MARCH	APRIL	MAY	JUNE	JULY	AUG.	SEPT.	OCT.	NOV.	DEC.	ANNUAL
Max. Temp	50.4	54.8	61.2	69.1	74.6	83.6	84.2	84.6	80.6	70.8	57.4	52.6	66.3
Av. Temp.	43.8	48.4	54.8	63.3	71.4	79.8	81.4	80.8	74.2	64.1	51.5	44.7	63.2
Min. Temp.	35.2	43.6	47.8	60.1	68.4	73.4	77.4	76.7	70.2	58.2	45.8	37.5	60.3

SOURCE: U. S. Weather Bureau, 1961.

TABLE NO. 6.2-6

WATER QUALITY PARAMETERS (TIME-WEIGHTED AVERAGE)
FOR SAMPLING STATIONS ON THE PECOS RIVER,
OCTOBER, 1975, TO SEPTEMBER, 1976

Station No.	Discharge (cfs)	pH	Dissolved-solids concentration (mg/1)				
			Total	Chloride	Sulfate	Sodium	Calcium
08405000 (Carlsbad)	12	7.7	2,500	531	1100	322	334
08406500 (Near Malaga)	26	7.7	5,390	1690	1820	1030	524
08407000 (Pierce Canyon Crossing)	28	7.5	13,900	6500	2280	4020	551

SOURCE: U. W. Geological Survey, Water-Data Report NM-76-1.

TABLE NO. 6.3-1 AQUIFER CHARACTERISTICS OF THE GUADALUPIAN AGE ROCKS (ADAPTED FROM HISS, 1976, TABLES 6 AND 7)

Geologic Unit	Avg. Hydraulic Conductivity (ft/day)	Average Porosity (%)	No. of samples or tests	
			Conductivity	Porosity
Rock Core Analysis				
Tansill Fm.	0.006	4.23	399	381
Yates Fm.	0.026	9.74	11,287	11,387
Seven River Fm.	0.140	6.56	4,367	4,485
Queen Fm.	0.029	7.79	7,324	7,648
Grayburg Fm.	0.032	7.15	1,971	1,973
Grayburg-San Andres (Und.)	0.033	5.76	7,062	7,313
Glorieta Sandstone	0.027	9.16	3,128	3,115
Delaware Mt. Gp.	0.016	15.65	4,549	4,493
Pumping Tests (San Andres)				
T.20S, R.38E, Sec. 7	0.20		(Drawdown Test)	
Same well as above	0.20		(Recovery Test)	
T.22S, R.37E, Sec. 29	0.30		(Drawdown Test)	
Pumping Tests (Capitan)				
T.21S, R27E, Sec. 5	2.4		(Recovery Test)	
T.21S, R.28E, Sec. 30	16.0		(Recovery Test)	
T.21S, R.34E, Sec. 24	3.0		(Specific Capacity)	
T.21S, R34E, Sec. 14	1.7		(Specific Capacity)	
Same Well	1.9		(Drawdown Test)	
Same Well	1.4		(Recovery Test)	
T.24S, R36E, Sec 4	24.0		(Drawdown Test)	
T.24S, R36E, Sec. 16	7.4		(Specific Capacity)	

TABLE 6.3-2 -- Records of Wells in the Los Medanos Area, New Mexico
(Adapted from Cooley, 1972, Table 4)

Location Number	Altitude Above Mean Sea Level (feet)	Depth of Well (feet)	Diameter of Well Casing (inches)	Depth Below Land Surface (feet)	Date of Measure- ment	Geologic Source	Use and Remarks
19.32.34.434	3560	260	---	Dry	9-22-72	QTs, Trc, Trsr(?)	Unused; 3 wells at this locality; no access for entering casing in the other 2 wells.
19.33.26.244	3609	---	6	90.58	9-25-72	QTs, Trc(?)	Electric Submersible; stock.
26.244a	3609	101	---	90.93	9-25-72	QTs, Trc(?)	---
19.34.31.131	3620	53	6	Dry	9-25-72	QTs	Unused; 2 ft. of water in bottom of hole--probably does not represent true water level.
31.232	3632	120R	6	---	9-25-72	QTs, Trc(?)	Windmill; stock; "Hardin Well," no access to enter casing.
20.31.13.412	3440	30	6	1.12	9-18-72	QTs	Unused.
15.130	3460	105	6	62.10	9-18-72	QTs(?), Trsr	Unused.
15.130a	3460	79	6	63.39	9-18-72	QTs(?), Trsr	Unused; 5 wells at this location of which only 1 is an operating well.
15.130b	---	---	---	---	---	QTs(?), Trsr	Windmill; stock.
20.32. 1.312	3510	20	6	Dry	9-22-72	QTs	Unused; deepest of 4 wells at this location, all wells are dry.
24.333	3555	67	5	37.67	9-11-72	QTs	Unused
24.333a	3555	---	---	---	---	QTs(?)	Windmill; stock.
27.144	3545	30	---	23.67	9-18-72	QTs	Unused; no casing present.
36.214	3585	---	---	P43.88	9-18-72	QTs	Windmill; stock; 3 wells at this location at Bingham ranch, well pumping estimated at 2 gallons per minute.

TABLE 6.3-2 (continued)-- Records of Wells in the Los Medanos Area, New Mexico

Location Number	Altitude Above Mean Sea Level (feet)	Depth of Well (feet)	Diameter of Well Casing (inches)	Depth Below Land Surface (feet)	Date of Measure- ment	Geologic Source	Use and Remarks
20.33. 4.432	3555	4		Dry	9-22-72	QTs	Unused.
18.123	3521	249	6.5	245.58	9-25-72	Trc	Unused.
21.111	3536	49	6	36.90	9-25-72	QTs	Unused.
24.124	3630	680	12	405.15	9-22-72	Trc, Trsr(?)	Windmill; stock; "West Windmill," watersand at about 300 feet as reported by driller.
20.34. 4.444	3633	200	8	P174.08	10-2-72	Trc	Windmill; stock; "Robert's Well," old oil test drilled before 1930.
14.133	3648	230		190.25	10-2-72	Trc	Windmill; stock.
17.334	3640	220(?)	8	P129.68	10-2-72	Trc	Windmill; stock; "City Service Well," possibly oil test.
22.224	3655	220	12	196.49	10-2-72	Trc	Windmill; stock; "North Well," old oil test
34.432	3770	96	6	89.50	10-2-72	QTs	Windmill; stock.
21.30.18.333	3220	156	6	129.54	9-25-72	Pru	Unused.
22.423	3180	130	6	111.50	9-25-72	Pru	Unused.
21.31. 1.131	3580	30R	6	20.80	9-18-72	QTs	Windmill; domestic & in stock; at Campbell Ranch. "Grave Well."
1.241	3600	--	--	--	--	--	
2.221	3570	35	--	29.80	9-18-72	QTs	Windmill; stock.
7.331	3350	367	14	192.10	9-14-72	Pru, Prc (?)	Unused.
13.244	3600	68	6	Dry	9-13-72	QTs, Trc	Unused.
18.411	3310	--	6	158.32	9-14-72	Pru	Windmill; stock; "New Well."
30.421	3300	176	6	Dry	9-25-72	Pru	Unused.

TABLE 6.3-2 (continued)-- Records of Wells in the Los Medanos Area, New Mexico

Location Number	Altitude Above Mean Sea Level (feet)	Depth of Well (feet)	Diameter of Well Casing (inches)	Depth Below Land Surface (feet)	Date of Measurement	Geologic Source	Use and Remarks
21.32. 6.111	3598	54R	--	44.00R	9-18-72	QTs	Windmill; domestic & stock; at Allred Ranch; 2 wells at this location.
21.33. 2.231	3810	1150R	--	--	9-22-72	Trsr	Unused; could not pass tape below 550 feet in 1972.
2.420	3770	94	6	79.58	9-22-72	QTs	Windmill; stock.
4.434	3805	147	--	129.66	10-2-72	QTs(?), Trc	Unused.
4.434a	3805	127	--	Dry	10-2-72	QTs(?), Trc	Unused.
18.114	3890	150	--	140.75	9-12-72	QTs	Windmill; stock.
18.114a	3890	175	--	142.88	9-12-72	QTs	Unused.
18.123	3855	--	--	--	9-12-72	QTs(?)	Windmill; stock.
18.123a	3855	145	8	117.30	9-12-72	QTs	Unused.
18.131	3895	11	--	Dry	9-12-72	QTs	Unused.
25.421	3670	67	--	56.58	9-22-72	QTs	Windmill; stock; "West Well."
28.124	3688	210	8	179.00	9-22-72	Trc	Windmill; stock; "Standard Wells," 3 wells at this location.
22.30. 5.431	3120	225	14	53.25	9-19-72	Pru, Prc(?)	Unused.
6.444	3140	176	22	92.40	9-19-72	Pru	Unused.
7.244	3110	58	12	Dry	9-19-72	Pru	Unused.
10.311	3135	68	6	63.70	9-12-72	Pru	Unused; at Crawford Ranch.
20.120	3076	10	5	Dry	9-19-72	QTs, Pru	Unused.
32.111	3010	35	6	32.70	9-19-72	Pru	Unused.
22.31.15.130	3460	--	--	144.07	9-12-72	Trsr(?) Pdl	Windmill; stock.
15.130a	3460	--	--	145.50	9-12-72	Trsr(?) Pdl	Unused.

TABLE 6.3-2 (continued)-- Records of Wells in the Los Medanos Area, New Mexico

Location Number	Altitude Above Mean Sea Level (feet)	Depth of Well (feet)	Diameter of Well Casing (inches)	Depth Below Land Surface (feet)	Date of Measurement	Geologic Source	Use and Remarks
22.32.14.323	3717	380	--	367.80	9-13-72	Trsr	Jenson Jack; stock; "Comanche Wells."
14.324	3720	380(?)	--	370.40	9-13-72	Trsr	Windmill; stock; "Comanche Wells."
22.33. 5.321	3650	10	6	0.0	9-22-72		Windmill; stock; well on edge of Dagger Lake.
13.231	3515	490	6	388.05	9-21-72	Trc	Windmill; stock; "Roger's Well."
13.231a	3515	400	6	388.05	9-21-72	Trc	Windmill; stock.
20.244	3602	--	--	--	--		Unable to locate well in 1972.
23.30. 2.444a	3250	315	7	257.73	9-20-72	Prc	Windmill; stock; "Little Windmill," well 444 destroyed.
6.424	2980	--	6	0.0	9-20-72	--	Unused; "Nash Well," area flooded by lake.
19.123	3045	--	7	68.55	9-20-72	Prc	Windmill; stock.
21.122	3165	--	5	--	9-20-72	Pru, Prc(?)	Windmill; stock; "Indian Well," no access for
		204	5	179.25	4-6-59	Pru, Prc(?)	water level measurement.
22.234	3210	244	--	227.32	9-20-72	Pru, Prc(?)	Unused.
33.244	3438	696	--	--	--	Pru, Prc	Abandoned; at Gnome Site, plugged 6-25-69, USGS No. 5.
34.133	3413	518	--	433.91	9-25-72	Pru, Prc	Observation; at Gnome Site, USGS No. 4.
				433.67	12-12-61	Pru, Prc	
34.133a	3413	--	--	427.03	9-25-72	Pru, Prc	Unused; at Gnome Site, USGS No. 8.
34.234	3401	568	6	415.70	4-14-62	Pru, Prc	Observation; at Gnome Site, USGS No. 6, drld to 1499' & plugged back to 568'.
34.234a	3402	563	6	418.10	4-16-62	Pru, Prc	Observation; at Gnome Site, USGS No. 7, drld to 1507' & plugged back to 563'.
34.324	3426	567	--	441.67	9-25-72	Pru, Prc	Observation; at Gnome Site, USGS No. 1.
				442.40	9-22-60	Pru, Prc	

TABLE 6.3-2 (continued)-- Records of Wells in the Los Medanos Area, New Mexico

Location Number	Altitude Above Mean Sea Level (feet)	Depth of Well (feet)	Diameter of Well Casing (inches)	Depth Below Land Surface (feet)	Date of Measurement	Geologic Source	Use and Remarks
23.31. 6.320	3300	213	8	144.72	2-4-59	Pdl	Windmill; domestic.
6.320a	3300	400R	--	--	--	Pdl, Pru	Windmill; domestic; tape will not pass 222' in 1972.
6.444	3310	--	6	106.35	9-20-72	Pdl	Windmill; domestic.
7.240a	3315	--	6	62.27	9-20-72	Pdl	Windmill; stock.
17.310	3305	--	--	--	9-20-72	Pdl, Pru	Windmill; stock.
26.340	3451	--	6	250.47	9-20-72	Pdl	Windmill; stock.
29.113	3335	--	4	139.90	9-20-72	Pdl	Windmill; stock.
23:32. 3.311	3660	550R	8	--	9-13-72	Trsr	Windmill; stock.
3.311a	3660	--	10	204.18	9-13-72	Trsr	Unused.
21.241a	3680	515	--	480.75	9-21-72	Trsr	Windmill; stock.
		550	6	510.00R	4-13-59	Trsr	
23.33.12.312	3530	388	12	351.45	9-21-72	Trsr	Windmill; stock; "Allred Well."
17.423	3702	650(?)	8	504.40	9-21-72	Trc(?), Trsr	Submersible; stock "Graham Wells."
26.421	3645	173	6	165.15	9-21-72	Trc	Windmill; stock; "Tip Top Wells."
26.421a	3645	189	6	P184.00	9-21-72	Trc	Windmill; stock; "Tip Top Wells."
28.334	3675	544(?)	--	500.00R	11-27-53	Trc(?), Trsr	Windmill; stock & domestic; at Brinninstool Ranch, 2 wells at this location, tape will not pass 220' in either well.

Explanations

(1) Geologic source: QTs, surficial deposits; Trc, sandstone beds in the Chinle Formation; Trsr, Santa Rosa Sandstone; Pdl, Dewey Lake Redbeds; Pru, Rustler Formation above Culebra Dolomite Member, including Magenta Dolomite Members; Prc, Culebra Dolomite Member of Rustler Formation.

(2) Altitute: From topograhical maps.

(3) Depth of well: All depths of wells were obtained in 1972; all depths to water in the wells measured in 1972 or before are listed; R, reported depth; P, pumping level; < , less than.

TABLE 6.3-3: Water Quality Data (from Table 2, Mercer and Orr, 1978)
reported in parts per million

Monitor Well of Sample	Date of Sample	pH Units	Tempera- ture (Celsius)	Calcium (Ca)	Magnesium (Mg)	Sodium (Na)	Potassium (K)	Bicar- bonate (HCO₃)	Carbonate (CO₃)	Sulfate (SO₄)
Magenta·Dolomite										
H-1	5/10/77	7.2	22.0	1,000	460	6,200	840	93	0	3,600
H-2a	2/22/77	8.6	22.0	820	170	2,700	81	74	0	2,400
H-3	5/10/77	8.0	22.5	1,200	480	9,300	250	51	0	3,400
Culebra·Dolomite										
H-1	3/17/77	7.3	22.5	820	1,800	29,000	5,600	100	0	11,000
H-2b	2/22/77	8.4	21.5	690	160	2,100	91	59	5	3,000
H-2c	3/16/77	8.1	20.5	680	120	3,600	120	62	0	3,200
H-3	3/17/77	7.4	21.5	1,500	670	19,000	630	115	0	5,700
P-14	3/14/77	6.0	21.5	3,100	760	7,600	600	357	0	1,400
P-15	5/10/77	10.2	21.5	770	63	6,900	1,700	63	24	3,200
P-17	5/10/77	7.4	22.5	1,700	1,600	30,000	120	77	0	5,000
P-18	5/10/77	7.2	24.5	5,600	16,000	9,200	6,200	310	0	980
Rustler-Salado·Contact										
H-1	2/22/77	7.9	21.0	13,000	30,000	56,000	17,000	675	0	520
H-2c	2/23/77	5.9	20.5	9,200	25,000	66,000	9,100	199	0	1,300
H-3	2/24/77	7.6	21.5	18,000	25,000	59,000	14,000	467	0	370
P-14	2/24/77	7.2	24.5	570	1,200	120,000	1,300	222	0	10,000
Delaware·Sand										
AEC-8	9/22/77	6.0	30.0	10,000	2,500	55,000	860	420	0	240

Table 6.3-3 Continued

Monitor Well	Chloride (Cl)	Fluoride (F)	Silica (SiO_2)	Dissolved Solids (Sum of constitents)	Nitrate* +Nitrate (N)	Ortho* Phosphorus (P)	Boron* (B)	Iron* (Fe)	Manganese* (Mn)
Magenta·Dolomite									
H-1	10,000	2.0	1.7	22,200	0.04	0.03	3.3	0.22	0.95
H-2a	4,100	-	6.0	10,300	0.04	0.01	0.22	0.06	< 0.05
H-3	15,000	1.8	6.4	29,700	0.08	0.04	13.0	0.04	0.22
Culebra·Dolomite									
H-1	49,000	0.8	0.6	97,300	0.03	0.00	18.0	0.79	2.8
H-2b	2,800	2.0	1.7	8,890	0.01	0.03	9.5	0.02	0.2
H-2c	4,700	1.6	3.5	12,500	0.16	0.00	10.0	0.11	0.14
H-3	29,600	0.5	1.2	57,200	0.07	0.00	20.0	0.05	0.12
P-14	20,000	0.9	33	33,700	0.01	0.02	0.7	17	0.5
P-15	11,000	1.2	1.6	23,700	0.04	0.03	4.7	0.1	0.02
P-17	54,000	1.5	1.0	92,500	0.06	0.11	1.7	1.2	3.0
P-18	80,000	1.2	1.0	118,000	0.81	0.40	100.0	0.54	4.5
Rustler-Salado·Contact									
H-1	210,000	-	0.0	327,000	0.29	0.00	110	1.5	52
H-2c	200,000	-	2.0	311,000	1.1	0.00	150	2.5	78
H-3	210,000	-	1.0	327,000	0.77	0.00	1.9	1.5	3.8
P-14	180,000	-	2.0	313,000	0.34	0.08	1.7	2.1	3.4
Delaware Sand									
AEC-8	120,000	1.2	3.6	189,000	0.11	0.05	53	23	14.0

* Due to sampling conditions, analyses of NO_3^{-1}, PO_4^{-3}, BO_3^{-3}, Fe^{+2}, and Mn^{+2} are probably no more precise than $\pm 15\%$. The others have a precision of about $\pm 5\%$.

TABLE 6.3-4 Fluid Yield From Test Zones
(gallons per day)

Hole No.	Test Interval (depth in ft)	Magenta Dolomite	Culebra Dolomite	Salt Residue Zone in Rustler Fm.	Rustler-Salado Contact	Bell Canyon Sand
Open hole, drill stem tests (1)						
H-1	562 - 592	23.1				
	626 - 667			22.4		
	667 - 669		22.1			
	669 - 842				10.9	
H-3	558 - 608	14.1				
	672 - 703		2.3			
	703 - 780			1.8		
	800 - 868				2.6	
Open hole, bailing tests (2)						
H-2a	513 - 563	27				
H-2b	611 - 661		260			
H-2c	743 - 795				0.8[3]	
Cased hole with perforated interval, bailing tests (2)						
H-1	562 - 590	66				
	675 - 703		46[4]			
	803 - 827				1.0[5]	
H-2b	510 - 538	210				
H-2c	624 - 652		310			

TABLE 6.3-4 (continued) Fluid Yield From Test Zones
(gallons per day)

Hole No.	Test Interval (depth in ft)	Magenta Dolomite	Culebra Dolomite	Salt Residue Zone in Rustler Fm.	Rustler-Salado Contact	Bell Canyon Sand
Cased hole with perforated interval, bailing tests (2)						
H-3	562 - 590	(8640)[6]				
	675 - 703		200			
	813 - 837				11/32d[8]	
P-14	573 - 601		(5760)[7]			
	676 - 700				75	
P-15	410 - 438		50		2.0/42d[8]	
P-17	558 - 586		170			
	702 - 726				1.0/72d[8]	
P-18	912 - 940			0.5/33d[8]		
	1076 - 1100				0.5/73d[8]	
AEC-8	4844 - 4860					269[9]

NOTES:

(1)   Inflows measured over periods ranging from 11.5 to 37.5 hours.
(2)   Inflows monotired for periods ranging from 8 days to 217 days.   Rate based on inflow during first 24 hours.
(3)   Inflow of 14 gallons in 18 days (no other data).
(4)   Inflow of 416 gallons in 9 days (no other data).
(5)   Average trend after 33 days recovery.
(6)   Bailed 360 gallons in 1 hour with 6 feet of drawdown.
(7)   Bailed 720 gallons in 3 hours with no drawdown.
(8)   Early measurements inconclusive; inflow for period of days (d) indicated.
(9)   Recovery measured for only 2.8 hours.

TABLE NO. 6.3-5

OBSERVATION WELLS – MONITORING ZONES

WELL NO. (GROUND ELEV.)	ZONE TESTED	ACCESSIBLE DEPTH	INTERVALS ELEV.
H-1 (3403)	Magenta Culebra Rustler-Salado	562-590 675-703 803-827	2841-2813 2728-2700 2600-2576
H-2a	Magenta	No tests except levels	
H-2b	Culebra	510-538	2867-2839
H-2c (3377)	Culebra Rustler-Salado	624-652 743-795	2753-2725 2634-2582
H-3 (3389)	Magenta Culebra Rustler-Salado	562-590 675-703 813-837	2837-2799 2714-2686 2576-2552
P-14 (3358)	Culebra Rustler-Salado	573-601 676-700	2785-2757 2682-2658
P-15 (3310)	Culebra Rustler-Salado	410-438 532-556	2900-2872 2778-2754
P-17 (3340)	Culebra Rustler-Salado	558-586 702-726	2782-2754 2638-2614
P-18 (3479)	Culebra Rustler-Salado	912-940 1076-1100	2567-2539 2403-2379
AEC-8 (3532)	Bell Canyon (Upper) Bell Canyon (Lower)	4821-4827 4844-4860	[1289-1295]* [1312-1328]*

*Elevations in brackets are below mean sea level; all other
elevations are above msl. All depths and elevations are given in
feet.

TABLE NO. 6.3-6

POTENTIOMETRIC LEVELS
OCTOBER 1977
(Elevation in Feet)

Observation Well	Ground Surface Elevation	Magenta Dolomite	Culebra Dolomite	Rustler-Salado Contact	Delaware Sands "Upper"	"Lower"
H-1	3,403	3,154	3,013	Not Monitored[1]		
H-2a	3,377	3,128	Not Penetrated	Not Penetrated		
H-2b	3,377	3,081	3,026	Not Penetrated		
H-2c	3,377	Not Screened	3,021	34'/Month[2]		
H-3	3,389	3,141	2,984	Not Monitored[1]		
P-14	3,358	Not Screened	3,034	2,970		
P-15	3,310	Not Screened	3,002	2,975		
P-17	3,340	Not Screened	2,968	2,970		
P-18	3,479	Not Screened	8'/month[2]	40'/month[2]		
AEC-8	3,532	Not Screened	Not Screened	Not Screened	2,927	2,933

NOTES:

[1]The Rustler-Salado contact is accessible, but is temporarily off.

[2]Recovery Rate: Level in tubing had not reached static level in October, 1977

GCR CHAPTER 7

GEOCHEMISTRY

7.1 INTRODUCTION

In the context of this Geological Characterization Report, "geochemistry"
is taken here to include a description of chemical properties of geologic
media presently found in the surface and subsurface environments of
southeastern New Mexico in general, and of the proposed WIPP withdrawal
area in particular. "Chemical properties of geologic media" might be
extended to include a description of present understanding of chemical
processes which have taken or are taking place in southeastern New Mexico
rocks. This geochemistry chapter of the WIPP Geological Characterization
Report does not consider any aspect of artificially-introduced material,
temperature, pressure, or any other physico-chemical condition not native
to the rocks of southeastern New Mexico. These as-yet hypothetical
considerations belong in the realm of interactions between radioactive
waste and rock, a subject of the experimental programs initiated as part
of the WIPP studies that are not yet completed. Early experimental
results of radionuclide interactions with southeast New Mexico rocks and
fluids are reported in Chapter 9.

A substantial fraction of this chapter consists of original source
material, never before published in any format aside from reports of
investigations resulting from research contracts. Much of this material
is, however, in the process of being recast so as to be suitable for
presentation in various professional forums. Some material has already
been so presented.

Information contained herein was offered if the work involved was at a
suitable stage of completion so as to allow conclusions to be drawn.
Some subjects of investigation related to geochemistry require several
years more investigation, even for final site characterization, and are
discussed in Chapter 10, "Continuing Studies." Subjects of the present
chapter are those which provide background data of relevance to (1)

experimental programs involving radioactive waste and its interaction with geomedia, (2) borehole plugging, (3) the intrinsic physico-chemical stability of southeastern New Mexico rocks in the geologic past, and (4) safety assessment, which is described in other major documents relating to the proposed WIPP. These data include mineralogy, volatile constituents of rocks, the constitution, origin and history of liquids and gases found in rocks, and the lengths of time which have passed since the latest episodes of thermodynamic instability resulting in rock/fluid interactions.

In the absence of a satisfactory theoretically-formulated mathematical model which can accurately predict phase equilibria among complex evaporite minerals, an empirical approach, based on observed assemblages, is adopted here. Such modelling is beyond the scope of this document.

It will be noted that volatile contents of evaporites were determined by three different methods: static heating (Section 7.5.3), thermogravimetric analysis (Section 7.5.2) and counting of fluid inclusions (Section 7.6). Each set of data was collected for a different geochemical purpose, but results from all techniques show comparable amounts of volatile constituents in the evaporites. The most accurate results, however, are probably those derived from static heating.

7.2   THE MINERALOGY OF DELAWARE BASIN EVAPORITES AND RELATED ROCKS OF
        THE LOS MEDANOS AREA

7.2.1   Introduction

The foregoing sections on geology and stratigraphy have briefly mentioned generalized mineralogies of Delaware Basin rocks of the Los Medanos area. Here it becomes of interest to present a more thorough exposition of mineralogies. This is done for a variety of reasons: (1) mineralogies affect properties of rocks important to physical aspects of mining, (2) soluble minerals in rocks potentially give rise to solutions which can interact with waste and its containers, and (3) minerals in

rocks have various degrees of sorptive affinities for radionuclides and can serve to decrease their mobility. While this section is devoted mainly to an account of the minerals found in the main Ochoan evaporite section (Castile and Salado Formations), mineralogies of some Guadalupian rocks and some rocks above the main evaporite section are included. This information is particularly useful to the consideration of radionuclide mobility in rocks containing substantially more fluid than the evaporites, and is of fundamental importance to in situ experiments involving waste-rock interactions. Also, investigations of fluid inclusions, sources of volatiles, groundwater geochemistry and age-dating of rocks and waters are closely related to mineralogy.

7.2.2   Previous Work

Southeastern New Mexico evaporites have been economically important for many years because they contain the well-known McNutt Potash Zone in the middle part of the Salado Formation. Descriptions of mineralogies of the McNutt and adjacent portions of the Salado have been given in several previous reports covering much of the Permian Basin, and environs of southeastern New Mexico (Brokaw et al., 1972; Jones, 1973; Jones, 1974a; Jones, 1974b; Jones, 1975). A detailed review of the economic mineralogy of the McNutt Potash Zone underlying Los Medanos appears in Chapter 8 of this report. This section on mineralogy has been developed as background critical to mine design, waste-rock-fluid interactions, and other aspects of geochemistry, such as age-dating and radionuclide migration.

7.2.3   Overview of Evaporite Mineralogy

X-ray powder diffraction examination of 50 core samples from ERDA #9 in the center of the study area (Figure 4.1-2) has been completed. Only qualitative information was obtained from these preliminary cores in order to assess mineralogical variations among selected horizons.

As-received cores were crushed and ground to bulk powder to provide a representative sample of that zone, x-ray specimen mounts weres scanned

at $1°$/min on a diffractometer equipped with copper x-ray source, graphite monochrometer and scintillation detector.

Eight minerals were identified in the 50 samples:

1. anhydrite $CaSO_4$
2. clay $Al_2Si_4O_{10}(OH)_2 \quad xH_2O$
3. halite $NaCl$
4. loeweite $Na_{12}Mg_7(SO_4)_{13} \quad 15H_2O$
5. magnesite $MgCO_3$
6. polyhalite $K_2Ca_2Mg(SO_4)_4 \quad 2H_2O$
7. quartz SiO_2
8. sylvite KCl

Their occurrence is given qualitatively in Table 7.1 with a corresponding graphical distribution shown in Figure 7.1. Trace amounts of the potassium minerals sylvite and polyhalite were found in the proposed TRU horizon (2034-2110'), and the high-level horizon (2594-2692') was void of potash.

7.2.4 Mineralogy òf Fluid-Bearing Zones in the Rustler Formation and Delaware Mountain Group

Mineralogies of certain fluid-bearing rocks above and below the main evaporite sequence have been determined as background information for radionuclide sorption studies.

Magenta Member, Rustler Formation (AEC No. 8). The Magenta member of the Rustler Formation is largely ferroan dolomite, probably containing minor ankerite which gives rise to the reddish color in weathered outcrops. This rock also contains detrital quartz, and gypsum forms as crystals, filling the vugs in the dolomite, which can be up to several cm across.

Culebra Member, Rustler Formation (AEC No. 8). Like the Magenta, the Culebra member is largely dolomite, with traces of detrital quartz. In addition, small amounts of calcite are found.

Bell Canyon Sandstone (AEC No. 8). The Bell Canyon Formation is the uppermost unit in the Delaware Mountain Group immediately underneath the main evaporite sequence. It is mostly detrital quartz and major feldspar with a matrix of kaolinite and chlorite cemented with calcite and minor amounts of dolomite.

Cherry Canyon Sandstone (Pine Springs Outcrop). Although the Cherry Canyon Formation was not sampled in any WIPP exploratory borehole, its stratigraphic position directly underneath the Bell Canyon made it of interest in preliminary radionuclide sorption measurements. The detrital component is largely quartz, and the cement is mostly dolomite. Minor amounts of albite and microcline contribute to the detrital component, and minor amounts of gypsum and calcite are found in the cement.

7.3   DETAILED CHEMISTRY AND MINERALOGY OF SOLUBLE AND INSOLUBLE COMPONENTS OF THE SALADO FORMATION

7.3.1   Introduction

While this section deals primarily with results obtained from cores from AEC No. 7 and AEC No. 8, exploratory holes three miles northeast of the present study area (Figure 4.1-2), these holes provided material of sufficient lithologic similarity to ERDA No. 9 so as to be of value. The analytical strategy employs a normative-type calculation, in which mineralogical compositions are derived mathematically from bulk chemical compositions. The results of those calculations then can be compared to mineralogies determined petrographically or by x-ray diffraction. This section serves as fundamental background information for the chapters on silicate mineralogy and sources of volatile components within the evaporites.

7.3.2   Materials and Methods

Sample Preparation and Handling. The core samples as received were halved and one-half was retained while the remaining half was crushed and ground. The ground sample was size-distributed as shown in Table 7.2.

The samples were all double-wrapped for storage in plastic bags due to their hygroscopic nature. A portion of the crushed sample weighing approximately 20 grams was accurately weighed and dried in an oven at $70^{\circ}C$ for two hours to determine weight loss. The dried sample was then added to 200 ml of distilled water, stirred for 1 hour, and filtered. The filtered material was dried and weighed to determine the insoluble portion of the sample while the filtrate contained the soluble portion of the sample.

Analysis of Soluble Portion. The elements potassium, calcium, magnesium, silicon, iron, aluminum, and strontium were analyzed by standard atomic absorption methods using a Perkin-Elmer 403 Atomic Absorption Spectrophotometer. Sodium, typically difficult to analyze precisely, was analyzed using an Orion Specific Ion Sodium electrode and an Orion Research Model 801 pH meter. Sulfate was determined gravimetrically as barium sulfate; chloride was determined volumetrically by titrating with mercuric nitrate (Vogel, 1961)

Analysis of Insoluble Portion. The insoluble portion was separately analyzed only if the insoluble percentage was greater than 0.5% of the total sample weight. Samples containing less than 0.5% insolubles did not provide sufficient material for analysis, and it was deemed that even a major constituent in such a small percentage of the total would not contribute significantly to the sample behavior. A portion of the water-insoluble material weighing about 100 mg was dissolved in HF, using the following procedure in a teflon-lined high pressure bomb (Bernas, 1968; 1973) obtained from Parr Instruments. Nitric acid (1 ml) was added

to wet the sample and 3 ml of 50% HF were added. The bomb was assembled and placed in a 70°C oven for 2 hours. The contents of the bomb were quantitatively transferred to a polypropylene beaker containing 2.8 g of boric acid and about 30-40 ml deionized water. The boric acid was allowed to dissolve with stirring and the solution diluted to 100 ml in a volumetric flask and stored in a polyethylene bottle. A solution containing all of the matrix material was prepared for use in making standards for the atomic absorption spectrophotometer. All analyses were performed as described in the preceding section. Samples were tested for the presence of carbonates using concentrated HCl but only occasionally was a trace amount detected.

Thermal Analysis. Samples analyzed for weight loss upon heating were ground so that greater than 90% of the sample was smaller than 100 mesh. Each sample was dried for at least 3 days at 65°C in a thermostatically regulated oven. This temperature was chosen to avoid the long-term dehydration of gypsum described elsewhere in this report. Low temperature weight loss (70°C for 2 hours) was used to measure absorbed water. This weight loss is probably higher than for rock distant from the sample collection point owing to absorption of drilling water. Samples of 100 mg weight were heated for differential thermal analysis (DTA) using a Fisher 200A DTA apparatus at a rate of 10°C/min from 25°C to 500°C.

Thermogravimetric analysis was carried out with a Fisher 100A TGA apparatus and a Cahn Model R6 electrobalance at a rate of 5°C/min from 60°C to 500°C using 100 mg of sample material. A few samples were heated to 800°C and are described elsewhere in this subsection.

Results of Analyses. Whole-rock chemical analyses, soluble-insoluble fractions, and weight losses upon heating are presented in Appendix 7.A. These analyses are converted to relative numbers of moles of components by multiplying weight percents by appropriate values of 1000/molecular weight. The results are listed in Appendix 7.B. If the insoluble fraction of a sample exceeds 0.5 weight percent, separate calculations are provided for both the soluble and insoluble fractions of the sample.

7.3.3   Results and Discussion

Distribution of Mineral Phases. Chemical analyses may be used to
estimate, semiquantitatively, the amounts of constituent minerals present
in a rock. This is accomplished by distributing the quantitatively
determined chemical components among mineral phases known qualitatively
to be present in the rock. The method was as follows:

> The distribution of the total number of moles (Nt) of a given
> chemical component (c) among the various mineral phases (p) present
> in a rock is described by the equation

$$Nt,c = \Sigma \ (Np)\ (Nc,p)$$

where:

   Nt, c = the total number of moles of the component c in the rock

   Np = the total number of moles of each of the mineral phases p in the
   rock,

   Nc,p = the number of moles of the component c in one mole of phase p.

This equation is simply a statement of conservation of mass, indicating
that the total amount of a given chemical component must be distributed
among the minerals containing that component; this distribution is
controlled by the specific chemical compositions of the minerals.
An expression of the form of the above equation may be written for each
of the components present in a rock sample. For a given rock, one of
three conditions are possible for the set of simultaneous equations
describing the distribution of all components in that rock:

1) if the number of equations (1 for each component) is equal to
   the number of unknowns (the moles of each of the phases), an
   exact solution to the equations may be determined.

2) if the number of components exceeds the number of phases (more
   equations than unknowns) the system is overdetermined and a
   solution to the equations may be evaluated by a method such as
   least squares regression.

3) if the number of components is less than the number of phases
   (more unknowns than equations), the system is indeterminate.

If either of the first two criteria are met, the chemical composition of
the rock can be employed to calculate the quantitative amounts of
minerals known, qualitatively, to be present.

An important assumption for the treatment described above is that the
chemical composition of all mineral phases is known. This is necessary
in order to define $N_{c,p}$ for all phases in the mass balance equations. If
a mineral of variable composition is present in a rock sample (i.e., a
solid solution), an additional variable is introduced to the set of
equations; that is, the composition of the solid solution. This
additional variable may change a set of N equations and N unknowns
(condition 1 above) to an indeterminate set containing N + 1 unknowns.
If such is the case, it is necessary to employ some additional analytical
technique to determine the actual composition of the unknown. On the
other hand, if the solid solution is present in a rock meeting condition
2 above, it will suffice to simply introduce two values of N_p for the
phase; in other words, an unknown for the number of moles of each of the
pure end-members of the solid solution present. The composition of the
mineral is then defined by the relative number of moles of each of the
end-members present.

Qualitative mineralogy may be carried out by a variety of methods such as
x-ray diffraction and thin-section analysis in addition to
straight-forward examination. The chemical data obtained during this
study have been used to attempt to estimate relative amounts of minerals
present in the various samples. With only a few exceptions, the rocks
are made up essentially of halite, and other mineral phases are present
in comparatively minor or trace amounts.

Samples from the Carlsbad boreholes consist of two chemically distinct
fractions: (1) water-soluble chlorides and sulfates of sodium,
potassium, calcium, and magnesium, and (2) water-insoluble silicates of
potassium, magnesium, and aluminum with quartz and iron oxide. Minerals
of the first group generally contain stoichiometric compositions, whereas
those of the second group exhibit extensive compositional variation. In

the case of the soluble portion, sodium occurs mainly with chloride as halite, while the other cations combine in various proportions with sulfate (and only occasionally chloride) forming minerals such as polyhalite, anhydrite, and kainite. These sulfates are of importance because they contain hydrate water which may be released upon heating. Silicates also undergo dehydration at elevated temperatures, but generally much higher temperatures are required than for the soluble salts because the water must be derived through destruction of hydroxyl groups. Compositions of minerals from these two classes are listed in Table 7.3.

Recognizing that soluble potassium, calcium, and magnesium are combined with sulfate, a semiquantitative estimate of various sulfate phases may be made by plotting the relative numbers of moles of the cations on triangular composition diagrams. The compositions of various stoichiometric mineral phases in the sulfate group are shown on such a diagram in Figure 7.2. No sulfate of potassium alone is common in nature, so sylvite is placed at the potassium apex of the triangle. Also shown on this diagram are the chloride and chloride-sulfate of potassium and magnesium. Not shown on Figure 7.2 are the soluble sulfates containing sodium. After plotting a given sample composition in terms of relative numbers of moles of soluble K_2O, CaO, and MgO, the total number of moles of these cations is compared to the number of moles of sulfate determined analytically; if the two are equal, then the minerals in the rock are estimated using the location of the sample on the diagram. If the cation sum is greater than available sulfate, an appropriate amount of chloride is added to make up the charge balance. Relative amounts of chloride and sulfate are then used in conjunction with the cations to determine appropriate amounts of carnallite, kainite and/or sylvite. If on the other hand, cations are deficient relative to sulfate, then sodium is added to the sulfate group to form bloedite, glaserite and/or glauberite.

The addition of sodium or chloride must be compatible with the relative amounts of these two components in the analysis. Generally, these are

present in such large amounts that a small error in their contents provides sufficient amounts for addition to the potassium-calcium-magnesium-sulfate fraction. In many instances, it is found that when it is necessary to do such addition, the appropriate component (sodium or chloride) is present in excess of the other necessary to form halite. Where such addition is not compatible with the chemical analysis, examination must be made of the insoluble portion of the sample. Where anhydrite-gypsum is present in significant amounts in a sample, the relatively low solubility of $CaSO_4$ (and possibly polyhalite) causes this phase to appear in both the soluble and insoluble fractions.

Minerals of the insoluble fraction consist of quartz, iron oxide, and a variety of clay minerals which are difficult to identify due to fine-grain-size and compositional variability. Iron probably occurs chiefly as either hematite (much of the halite is tinted orange) or an equivalent hydrated form although it may substitute for aluminum to a minor extent in clay minerals.

According to our chemical analyses, the remainder of the insoluble fraction is made up of the components K_2O, Al_2O_3, MgO, and SiO_2. Because the first three of these generally occur combined with the fourth, potential mineralogy of the samples may be evaluated by comparing insoluble analyses to mineral compositions plotted on the compositonal triangle $K_2O-Al_2O_3-MgO$ shown in Figure 7.3. On this diagram, mixed-layer solid solution among potassium and magnesium montmorillonites and seawater-illite is indicated by the shaded area between these three endmember components. It should be noted that the chlorite composition plotted on Figure 7.3 is that which has been observed in present day seawater sediments and evaporites. Relative proportions and amounts of minerals occurring in a given sample are evaluated by distributing potassium, aluminum, and magnesium along appropriate limiting phase compositions. Silica is then distributed among these phases according to stoichiometry, and any excess occurring in the sample analysis is considered to be free quartz.

Halite is by far the most abundant mineral in the soluble fractions of the samples. In only a few cases is halite a minor or trace constituent. Polyhalite and anhydrite/gypsum are accessory minerals in most samples, and in two of these, $CaSO_4$, is a major component. In normative calculations for sulfate deficient samples, kainite and carnallite are included, whereas thenardite, glaserite, bloedite, and kieserite appear in sulfate-excess and balanced samples. These phases are rarely present in more than trace amounts and are calculated to occur in such small quantities as to be insignificant in terms of contributions to hydrate water. Sample 8-1652 (i.e., 1652 feet depth in AEC No. 8) is significantly different from other soluble material in that it is calculated to contain relatively large amounts of the soluble salts sylvite, polyhalite, leonite, and glaserite. The drilling log reports loss of mud at this point, so it is uncertain as to whether a rock is of exotic mineralogy, or one from which certain cations have been leached by moving drilling mud, or one which has exhibited the incongruent solubility of polyhalite, leaving a sample of abnormal chemistry.

Most of the insoluble analyses plot within the triangle bounded by the phases Mg chlorite-K feldspar-talc on Figure 7.3. These minerals are recognized to occur in evaporite sequences which have undergone mild diagenesis (P < 100 atm, T < 100°C), forming as a result of interaction of brine with amorphous aluminosilicate detrital material (Braitsch, 1971). The only other phases calculated to occur in the insoluble fraction are mixed-layer illite-montmorillonite, quartz, and iron oxide. It should be noted that the presence of the mixed layer silicate as well as chlorite and talc may be difficult to establish if they occur in very fine grain size. None of the observed silicate phases undergo dehydration below 500°C, according to the DTA.

Effects of Heating Samples. A number of different responses to heating were exhibited by the samples. Heating to 70°C was designed to measure absorbed water recognizing that gypsum dehydrates, according to thermochemical data, at about 70°C. In normal differential thermal analysis, gypsum undergoes stepwise dehydration to hemihydrite and

anhydrite at about 150° and 185^OC, respectively. Kopp, (University of Tennessee, pers. comm.) has observed that gypsum dehydrates upon fine grinding and prolonged heating at 70^OC, hence the observed DTA breakdown is probably a result of kinetic factors. Consequently, samples analyzed using thermogravimetric analysis were powdered and placed in an oven at 70^OC for several days prior to analysis of weight loss at elevated temperatures. Samples 7-1171 and 8-2563 both contain major $CaSO_4$, but only the latter showed gypsum-type dehydration. This appears to indicate that sample 7-1171 actually contained anhydrite whereas sample 8-2563 contained gypsum since only 8-2563 showed significant weight loss at 70^OC but both analyses summed to near 100%.

Essentially isothermal dehydration was observed over a continuum of temperatures from 100° to 500^OC for a large number of samples. In addition, weight loss over a 50° to 100^OC span in temperature was observed for most samples, but generally at temperatures above 300^OC. These two types of weight loss probably indicate single-mineral dehydration for isothermal loss, and dehydration as a result of mineral-mineral chemical interaction for the weight loss occurring over a large temperature span. Such solid interaction is demonstrated by sample 8-1953 which contains both anhydrite and polyhalite but minimal bloedite. Figure 7.4 shows the DTA curves for pure polyhalite and gypsum. Comparison of these two curves to that of sample 8-1953 shows the 325^OC exotherm of polyhalite to be lacking while the lower temperature endotherms of gypsum are present. We suggest the missing polyhalite endotherm is a result of chemical interaction between polyhalite and anhydrite somewhere between 200° and 325^OC. Such interaction among evaporite minerals should probably be investigated in some detail in terms of retention of hydrate H_2O.

A few samples were heated to 800^OC to get an indication of how much weight might be lost from samples at high temperatures ($>500^OC$). Of the nine samples examined under these "extreme" conditions, four began gaining weight at about 700^OC. One sample increased in weight by about 15% between 725° and 800^OC. This gain in weight is not a result of

oxidation of iron (eg. Fe^{+2} in chlorite) since sample 8-2050 did not contain any iron. That the gain in weight may be caused by formation of an extremely hygroscopic phase at high temperatures as a result of solid-solid chemical interaction upon heating. Whether or not such a phase forms would undoubtedly depend upon the initial mineralogy of the rock to provide the correct reactant phases since not all sample exhibited this weight gain. The water necessary for this rehydration is probably a result of the fact that the testing laboratory is cooled during the summer months (the analyses were run in early June) by evaporation which results in high relative humidity.

A composite histogram of weight loss of all samples at elevated temperatures is shown in Figure 7.5. The distribution appears to be log-normal with the maximum density near 0.25% weight loss upon heating $500^{\circ}C$. Over half of the samples (56%) show weight loss of 0.5% or less, and only 15 samples exceed 1%. Figures 7.6A and 7.6B are plots of sample weight loss vs depth for the two drill holes. Samples showing more than 1% weight loss upon heating are scattered throughout the depth range but are generally separated by more than one hundred feet of low-water-loss material. There is a broad correlation between higher weight loss and increasing insoluble content of sample, but no clearcut relationship is seen between weight loss and silica content. It is concluded that high temperature weight loss is contributed by both silicate and sulfate minerals. It can be stated in general, however, that samples showing less than 1% weight loss contain less than 10 wt % insoluble material.

7.3.4   Conclusion

Most of the samples showed very little water loss between 200° and $300^{\circ}C$ and there were only small water losses at temperatures $200^{\circ}C$ and $300^{\circ}C$. As can be seen by examining the data, there are several zones where there is essentially no change in sample behavior with heating to moderate temperatures. These areas show good potential as burial sites for nuclear waste.

7.4   DETAILED PETROLOGY AND SILICATE MINERALOGY OF SOME PERMIAN BASIN
       ROCKS

7.4.1 Introduction

The purpose of this section is to describe and evaluate the petrologic,
mineralogic and geochemical properties of designated core samples,
primarily from the ERDA - 9 drill hole and various grab samples exposed
in mines and at the surface, in connection with the WIPP (Waste Isolation
Pilot Plant) site evaluation.

ERDA - 9 penetrates the Mescalero Caliche, Gatuna Formation Santa Rosa
Sandstone, Dewey Lake Red Beds, Rustler Formation, Salado Formation and
the uppermost 50 feet of the Castile Formation (Figure 4.3-3). Primary
interest is focused on selected intervals within the Salado and uppermost
Castile Formations.

The general problems under study are: 1) the genesis of the dominantly
evaporite succession with associated silicates and 2) the extent of
post-depositional alteration of these sediments. The basic approach (and
analytical method) is broadly threefold. First, detailed study of the
occurrence and mineralogy of silicates, particularly clay minerals, in
the evaporite succession (disaggregation, size fractionation, x-ray
diffractometry). Second, bulk chemical analysis of whole rock, water
soluble, acid insoluble, and clay size fraction (x-ray fluorescence,
atomic absorbtion spectroscopy, other rapid procedures). Third,
macroscopic and microscopic petrography (handspecimen and microscope
mineral identification, description of form, texture and lithology of
mineral associations, and x-ray diffractometry of bulk samples).

7.4.2 Procedure

After core intervals were selected for study, cores were cut lengthwise,
mostly in the form of 1/2, less commonly 1/4, of the core. Criteria for
selection and additional procedures for analysis of these samples are

described in the following sections on the silicate mineralogy, geochemistry and petrography.

7.4.3 Silicate Mineralogy and Geochemistry

Systematic logging of ERDA - 9 core and accompanying gross mineralogy have been described in Chapter 4. This section is focused on selected segments of the core and examination of the paragenesis of minor constituents, namely the silicate minerals, their composition, and their interpretation in terms of depositional and postdepositional phenomena.

Silicate mineralogy and geochemistry have not been comprehensively studied within the Ochoan rocks and the Permian Basin. Adams (1969) has reported briefly on the occurrences of talc in argillaceous rocks as a part of this extensive study of bromine distribution throughout the section; specialized clay mineral determinations by Grim et al. (1961) and Fournier (1961) have been undertaken on a limited number of samples and with minimal regard to their detailed stratigraphic setting and geneses.

In an effort to provide substantially more complete understanding of the silicates associated with the Permian evaporites, some 70 samples of the ERDA - 9 core ranging from 300 feet below the Salado-Rustler contact (1163.3 foot depth) down to a few tens of feet below the Salado-Castile contact (2867.6 foot depth) were selected. The following criteria were used in the selection: (1) representation of major lithologies; (2) detailed representation of an apparent "cycle" of evaporite deposition which occurs repeatedly through the Salado Formation section; (3) representation of intervals under consideration for waste storage sites; (4) detailed representation of selected polyhalite-anhydrite occurrences toward interpreting the genesis of the unusually abundant polyhalite; and (5) representation of the sequences which may provide data for interpreting postdepositional solution and recrystallization phenomena. In Table 7.4, we list the samples by depth, gross lithology, and stratigraphic position, as well as by character of data obtained; Table 7.5 provides a cross-listing for relating sample number to depth.

<u>Sample Preparation and Analysis</u>. The core was split and one split
rebagged for future reference. One to 10 cm segments of the remaining
half were selected for analysis (petrographic, mineralogic, and/or
chemical) and sectioned off. A 1 cm slab of this was retained for
petrographic examination; the remainder was coarsely crushed and a split
retained for whole rock analysis. The larger fraction of the sample was
leached with excess demineralized water to dissolve the halite host.
This was repeatedly centrifuged, decanted, and rewashed to remove all
traces of dissolved halite from the residue. The residue was dried,
reweighed, and a split suspended in boiling EDTA solution in order to
separate the "acid-soluble" salts (sulfate and carbonate minerals)
following the procedure of Bodine and Fernalld (1973). Again, after
repeated centrifuging, decanting and washing to remove EDTA and to
dissolve solid components from the insoluble residue, the suspension was
dried and reweighed. Table 7.6 depicts the quantities of sample residues
insoluble in water and EDTA. A split of this fraction was resuspended in
water, thoroughly disaggregated with an ultrasonic probe, and separated
into the $>2\,\mu$m and $<2\,\mu$m (effective spherical diameter) fractions by
timed gravity settling. Oriented diffractometer mounts of the fine
fraction were prepared by pipetting several drops of each suspension onto
glass slides and air-drying. Smear (paste) mounts and mounts using the
conventional commercial powder mounts were used for the $<2\,\mu$m insoluble
fraction as well as for the other fractions. In addition, pellet or
uniformly compressed mounts or "briquettes" of these fractions prepared
for x-ray fluoresence were also used for diffraction.

Where sufficient sample was available, normal procedure for the silicate
fraction included: (1) diffraction data for the whole EDTA-insoluble
fraction using the briquettes or paste mounts; (2) oriented (sedimented)
clay-size mounts on glass which were air-dried, glycol saturated, heated
to 300°C, and heated to 500°C. Conventional x-ray diffractometer
traces were obtained at a scanning speed of $2^{\circ}2\theta$/min with Cu-radiation
and a curved crystal monochromator.

X-ray fluorescence work involved briquette mounts using the vacuum-path Norelco fluorescence goniometer with quartz and gypsum analyzing crystals. In this study, standard regression procedures are used along with matrix evaluation for calculating abundances from the raw data. However, at this time the data can only be reported in terms of a unit-slope regression from one standard. Because of the severe errors such a procedure may induce, only "semi-quantitative" chemical results are claimed for this report.

Silicate Mineralogy. The following silicate minerals have been identified in the course of this study; their distribution is given in Table 7.7.

Quartz - Quartz occurs throughout the entire interval of the stratigraphic section analyzed; however, it does not occur in every sample. Quartz is generally fine-grained ($<10\mu$m), subhedral to anhedral, and readily identified in diffraction traces by its very strong peak at 3.34Å and moderate peak at 4.26 Å; interference by the micas and mica-clays with the former and by potash feldspar for the latter only rarely preclude its ready identification.

Illite (mica-clay) - Illite also occurs throughout much of the stratigraphic interval. It is readily observable in diffraction traces with its strong 10Å and 3.34Å peaks and its moderate 5.0Å peak (001, 003, and 003 respectively). All illites observed in the core are dioctahedral as based upon (060) < 1.52 Å and (001, 002, and 003) <1.0, 5.1, and 3.44 Å respectively. Many of the illites contain recognizable but small quantities of interlayered smectite, presumably saponite or other trioctahedral varieties, based on the slight asymmetry of the (001) reflection.

Feldspar - Feldspar occurs frequently, but generally in small quantities, throughout the section and its identification is based principally on one or more diffraction maxima in the 3.17 - 3.30Å range. Unfortunately, its abundance is usually low and when coupled with the presence of other

minerals its diffraction maxima for resolving its composition and its thermal character are not interpretable; both plagioclase and K-feldspar have, on occasion, been recognized.

Chlorite - Chlorite is commonly a minor constituent and its presence is often difficult to establish. With a 14 Å periodicity its maxima can be masked by smectities, various interlayered species, and by the 7 Å minerals, kaolinite and serpentine. In glycol saturated specimens, the 14 Å peak from expandable clays can be removed and at $500^{\circ}C$ the 7 Å peak from kaolinite is lost. Even so with only a small amount present in such an assemblage it can remain undetected.

Talc - Talc is rare throughout the core. It is common in the ore zones (Adams, 1969) but appears to be nearly absent from the other lithologies. Talc is identified by very sharp, strong reflections at 9.5 and 3.15 Å (001 and 003); the former is quite distinct from the broad reflection at 9.0 - 9.7 from a regular interlayered chlorite-saponite (corrensite).

Serpentine - Serpentine, like talc, is relatively rare in the section and is confined to the lowermost interval (below 2820.3 and at or below the Salado-Castile contact) in rock salt and anhydrite. Serpentine is identified by strong peaks at ~7.3 Å and ~3.6 Å (001 and 002 respectively for a single-layered variety). These maxima are noticeably greater than the 7.0 - 7.2 Å and 3.5 - 3.65 Å reflections attributable to chlorite. In our samples, these larger spacings are characteristically sharp and are not accompanied by the odd (00) reflections of the 14 Å minerals.

Expandable Clays - Expandable clays, the smectities, vermiculites, and mixed-layer clays containing either of these constituents, are the dominant clays of the section and are ubiquitous (Table 7.8). We have recognized at least four such clays; however, their definitive identity has not yet been resolved.

a. Saponite (e.g. JS-CS-9 at 1466.9') expands to >16Å with glycol saturation and collapses to < 14Å upon heating, (further heating would yield an ~9.5Å peak).

b. (?) Illite-saponite (e.g. JL-CS-2 at 1440.5' JL-CS-10 at 1325.3') with an air-dried maximum at 10.2 - 10.3Å, glycol saturation at 10.0Å and with or without a less intense shoulder or separate peak at 11.3 - 12.1Å, and collapsing to 9.8Å at 300°C. We have not ruled out a mixed-layer talc saponite identification for this phase.

c. Chlorite-saponite (e.g. MB-CS-21 at 1404.6' and MB-CS-32 at 2541.5') exhibits a 14Å peak expanding to 15.5Å with glycol saturation and collapse to <14Å upon heating. The chlorite-vermiculite phase described by Fournier (1961) and Grim et al. (1961) is probably this chlorite-saponite; the expansion with glycol is too great for this to be a chlorite-vermiculite. In some cases the interlaying is random; in others it is regular and produces a distinct superlattice peak (~29Å); in most there is some regularity with a slight shoulder present in the 25-30° 2θ present (these shoulder "maxima" are exceedingly difficult to plot precisely and all contain ±0.3-0.5° 2θ definition).

Nearly all of the diffraction data in Table 7.8 can be assigned to one of these three clay phases, yet data from several samples are not yet resolved, e.g. MG-CS-13 at 2518.3. It should be noted that smectities are smectite-bearing mixed-layer clays which commonly appear to be "stripped" by the EDTA-dissolution of nonsilicates; they commonly show 12-13.8Å air-dried spacings. However, suspending these clays in $MgCl_2$ or NaCl solutions and then rewashing and redrying restores the appropriate 14-15Å spacing.

In Appendix 7.C, we present a number of the diffraction diagrams illustrating these silicate assemblages.

Distribution of Clay Materials. Some general but tentative observations
regarding these minerals throughout the section are:

(1) Serpentine appears to be restricted to the lower
    40 feet of the analyzed section; it most commonly occurs in
    anhydrite and associated rock salt.

(2) Talc is not restricted to assemblages from bitterns as suggested
    by Adams (1969).

(3) Interlayered illite-saponite (or talc-saponite) appears to be
    resricted to polyhalite lithologies or adjacent anhydrite. It
    appears to be absent from clay beds and associated rock salts and
    from the polyhalite-free remainder of the section.

(4) Expandable clays appear to show somewhat less relative abundance
    in clay beds (1244.8, 1247.2, 1328.6, 1441.7, and 1468.1 ft.) than
    in the silicate assemblages from the evaporite rocks.

(5) Furthermore, the mixed-layered clay species in each of these clay
    seams consists solely of the well developed regularly
    interstratified chlorite-saponite (corrensite).

7.4.4 Mineralogy of Duval Mine Samples

Several samples of wall-rock were taken from the 4th ore zone
(langbeinite level) of the Duval Nash Draw potash mine, about 5 miles
west-by-southwest from the study area. These samples include a dark
brown clay parting (the DV-4 series) taken from the upper boundary of the
4th ore zone.

Untreated oriented powders were scanned from 2 to 60 degrees two theta.
The untreated slide was glycolated by vapor-soaking on a rack in a
container filled partially with ethylene glycol. An additional oriented
powder was heated at $450^{\circ}C$. Both the glycolated and the heated
specimens were scanned from 2 to 3 degrees two theta.

Whole rock samples were analyzed by loading a small amount of randomly oriented rock powder in a Norelco powder holder. This powder was scanned from 5 to 80 degrees two theta and the resulting diffractogram compared to values compiled in the Joint Committee on Powder Diffraction Standards file to determine bulk mineralogic composition. Mineralogic abundances noted were estimates based on comparative peak intensities.

All samples x-rayed (both clays and whole rocks) were scanned with Ni-filtered CuKα radiation. A time constant of two seconds was used with a scintillation counter detector and pulse height analyzer. The goniometer slit system consisted of a divergent and anti-scatter slit of 1 degree and a 0.003 inch receiving slit.

The results for Duval Mine samples appear in Table 7.9. For comparison, "dirty salt" from about 2100 feet depth in ERDA No. 9 has about 8% by weight insolubles.

7.4.5 Chemical Composition

Since appropriate regressions for each component based on several standards have not yet been calculated and matrix effect corrections have not yet been made, the analyses in Table 7.10 must be considered as only semiquantitative. In most cases, most totals are between 85 and 98%; perfectly reasonable totals with the remainder being chiefly water. A few totals exceed 100% and a few others are less than 85%; these are unquestionably in error. These data, however, do illustrate a number of important relations and are compatible with the mineralogic data.

Thus for example, those analyses with high alkali content (JS-CS-2 at 1440.5', JC-CS-6 at 1441.5, MB-CS-27 at 2067.0, MB-CS-31 at 2512.5, MB-CS-13 at 2518.3, MB-CS-10 at 2705.8, and MB-CS-36 at 2758.4) show substantial feldspar with or without abundant mica-clay.

In general, the chemical data support the mineralogic determinations. The silicate fractions are extraordinarily high in MgO (~20-30 wt % MgO)

and correspondingly low in CaO ($\sim$1 wt % CaO); Al_2O_3 is low ($\sim$8-12 wt % Al_2O_3) for clay mineral assemblages. Thus, except for illite, our clays are trioctahedral with only chlorite containing appreciable Al_2O_3.

7.4.6 Petrography

Petrographic analysis, both macroscopic and microscopic, is used in three ways: first, determination of the mineralogy of samples; second, given the mineralogy of a sample, description of lithology; third, the primary utility of petrographic analysis in this study, description of the texture of the sample. Texture refers to grain or crystal size, shape (habit or form), orientation, relationships (such as nature of contacts between crystals or grains) among different minerals and lithologies.

Macroscopic Petrography.

Sample Preparation and Procedures - Slabs, approximately 1 cm thick, were cut lengthwise using a band saw, from the 1/2 or 1/4 core samples. One face of a remaining core sample was then polished using a sander with various grit sandpapers. The sample was not to be used for silicate mineralogy-geochemistry analysis in order to avoid contamination. The polishing enhanced textural detail. Faces were also polished on some slabs.

Samples were selected from the core in which mineralogy based on macroscopic identification was obscure or uncertain for x-ray diffractometry of the bulk sample. Conventional diffractometry methods, as described previously, were used.

Macroscopic Petrographic Description - The mineralogy, lithology and texture in the polished sections of all the core intervals selected were described. Appendix 7.D is a brief extract from 54 pages of sketches accompanied by textural descriptions of these core intervals. Table 7.11 is a summary of the gross lithology reported largely as macroscopic

mineral identification and core footage. Table 7.11 indicates that
macroscopic mineral identifications are generally reliable, especially
for coarse-grained minerals, but visual estimation of the relative
minerals abundances are less reliable. Estimates of relative abundances
based on x-ray diffraction analysis are regarded as "semi-quantitative"
and maybe in error, but it is still more reliable because of its greater
precision, if not accuracy, compared to visual estimation.

Plates 7.1 through 7.6 are photographs of polished faces of cores or
slabs illustrating typical textures. Plate 7.1 shows a variety of shapes
of halite in anhydrite. The occurrence as beds or laminae or irregular
lenses is inferred to be primary because halite and anhydrite can
precipitate jointly or alternately from evaporating seawater. The
apparent swallow-tail form of halite in laminated anhydrite is a problem
because no primary occurrence of this form of halite is known. The
swallow-tail form can occur as a twinned crystal of gypsum, but
coprecipitation of gypsum and anhydrite is thermodynamically impossible.
One interpretation is primary precipitation of calcium sulfate only as
gypsum in the form of rapidly growing swallow-tail twins and finely
crystalline aggregates. Then post-depositional alteration of the finely
crystalline aggregates to anhydrite takes place, and the twinned crystals
alter either directly to halite or first to anhydrite which then alters
to halite, with preservation of the primary swallow-tail forms. This
interpretation is favored by the almost exclusive dominance of gypsum
rather than anhydrite as the primary precipitate in modern environments
and lab experiments. Controversial thermodynamic analyses also favor
gypsum as the primary precipitate, even metastably.

Plate 7.2 also illustrates occurrence of halite in well laminated
anhydrite. This is interpreted as primary coprecipitation of halite and
gypsum with these textures followed by post-depositional alteration of
gypsum to anhydrite with preservation of primary texture.

Plate 7.3 illustrates an occurrence of halite and polyhalite. The
triclinic crystal system of polyhalite is unlikely to produce a
rectangular outline in cross section whereas the cubic habit of halite or

the orthogonal morphology of anhydrite would. Thus, the rectangular outline of the polyhalite body suggests post-depositional alteration of anhydrite, (to a lesser extent of halite) to polyhalite as does the occurrence of most polyhalite in irregular masses among halite masses. Thermodynamic and experimental considerations as well as observation of modern evaporites indicate that polyhalite does not precipitate·from evaporating seawater.

Plate 7.4 illustrates coarse, relatively pure halite with anhedral, granular texture. The halite contains small crystals of anhydrite, probably a post-depositional alteration product of a primary coprecipitate of halite and gypsum.

Plate 7.5 illustrates another texture of halite in anhydrite with traces of magnesite. As previously indicated, it is believed to result from primary co-precipitation of halite and gypsum with post-depositional alteration of gypsum to anhydrite with preservation of primary texture. Magnesite is not known to precipitate from evaporating seawater but calcite does, suggesting post-depositional alteration of a primary (probably calcium) carbonate to magnesium carbonate.

Plate 7.6 illustrates textures in a dominantly anhydrite rock. The occurrence of the swallow-tail form near the stratigraphic top of the specimen as well as previously related discussions suggest primary precipitation of gypsum followed by post-depositional alteration of anhydrite, which could occur shortly after deposition, with preservation of primary textures.

Microscopic Petrography.

Sample Preparation and Procedure - The 1 cm thick slabs were converted to standard and oversize thin sections following conventional procedures (with the following exceptions) to minimize chemical alteration of the sample. Fluid in contact with the sample was a pure vegetable cooking

oil. Temperatures during the thin sectioning process did not exceed 30°C. Samples were put in dessication jars during impregnation to minimize contact of fluid acetone with the sample.

Microscopic Petrographic Description - Plates 7.7 through 7.12B are photomicrographs of thin sections of rock samples from the Permian Basin of southeast New Mexico. The samples are not from ERDA-9 core but are representative of mineralogies, lithologies and textures commonly encountered in the core.

Plate 7.7 is a photomicrograph of relatively finely crystalline euhedral to subhedral halite. The crystal form, relative clarity (although containing very fine crystals of anhydrite) and occurrence of fluid inclusions as both negative crystals and subspherical forms all suggest little post-depositional alteration with the exception of alteration of primary gypsum to anhydrite.

In Plate 7.8 also dominantly of halite (typical of the rock in Plate 7.4), there is a startling contrast to the texture in Plate 7.7. Crystals in Plate 7.8 are anhedral to subhedral, cloudy, coarser and devoid of fluid inclusions (the apparent void in the lower left was produced by plucking of a cleavage fragment from the specimen during sectioning). Because the texture shown in Plate 7.7 is regarded as indicative of little post-depositional alteration, the texture in Plate 7.8 is considered as indicative of extensive alteration, greater than that required for the postulated gypsum to anhydrite alteration which is also postulated for very fine crystals of anhydrite within the halite in Plate 7.8. These contrasting textures are also apparent in thin sections of carbonate rocks. Bathurst, (1975, especially Chapter 12), deals with recognition of chemically precipitated calcite (analogous to Plate 7.7) versus calcite post-depositionally altered from argonite or some other form of pre-existing calcite (analogous to Plate 7.8). Bathurst uses and builds upon terminology and concepts of the causes and processes of these alterations developed by Folk (1965).

Plate 7.9 shows an occurrence of halite with sylvite. The irregular bodies and irregular contacts of the sylvite (as well as the anhedral nature of the halite and bodies of intimately mixed halite and sylvite) are interpreted to be the product of post-depositional alteration. This interpretation is also favored by the fact that sylvite does not occur as a primary precipitate in the marine evaporite succession.

Plates 7.10A and 7.10B show the irregular and gradational nature of the contact between polyhalite and halite and the concentration of opaques, probably hematite, along the contact. These observations and those discussed under Plate 7.3 are interpreted to be products of post-depositional alteration of either anhydrite or halite to polyhalite.

Plate 7.11 shows the microscopic texture typical of many laminated or banded anhydrites of the Castile and Salado Formations. Neither x-ray diffractometry nor staining techniques have been used to determine the mineralogy of the carbonate. This texture is interpreted as annual varves by Anderson et al. (1972).

Plate 7.12A and 7.12B show dominately massive anhydrite, typical of much of the unlaminated anhydrite in the Salado Formation but atypically cut by a veinlet of gypsum. The rock sample was taken from outcrop and the gypsum veinlet is interpreted to have been produced by alteration of anhydrite to gypsum during uplift and exposure.

The petrographic descriptions and interpretations generally agree with those in the classic and relevant report of Schaller and Henderson (1932).

7.4.7 Interpretations and Tentative Conclusions

1. All of the samples discussed under macroscopic and microscopic petrography exhibit mineralogy, lithology and textures which are indicative of post-depositional alteration of the sediments (dated at 204 million years in Section 7.8). It is believed that fluids

migrating through the sediments are responsible for most of these alterations. Interestingly, the alteration of primary gypsum to anhydrite would liberate abundant volumes of fluid.

2. The abundance of polyhalite and the atypical mineral assemblages (sylvite-langbeinite vs kainite/carnallite-kieserite) of the ore zones suggest either drastic recrystallization or a former primary evaporite depositional environment. The areal extent of the Ochoan rocks and their great thickness coupled with paleogeographic evidence and the marine character of the underlying Permian strata appear to preclude the second alternative. Further evidence of the post-depositional origin of the present assemblage includes the low and highly variable bromine values in the Salado Formation rock salts (Holser, 1966; Adams, 1969). Age dates on K-bearing salts, discussed later in this chapter, further suggest recrystallization shortly after deposition.

3. The general mineralogy and chemistry of the EDTA-insoluble (silicate) fractions of the evaporite beds throughout the Salado and uppermost Castile Formations preclude their detrital origin.

4. The silicate assemblages and their chemistry further supports the hypothesis of post-depositional alteration of these rocks -- at least throughout much of the Salado Formation.

   a. The predominance of smectites (saponite) and trioctahedral smectite-bearing clays suggest relatively immature assemblages. The silicate assemblages of the Zechstein (Permian) of Germany are almost entirely nonsmectitic except for the well-crystallized, well-ordered regular interstratified chlorite-(smectite/vermiculite) mineral corrensite (Fuchtbauer and Goldschmidt, 1969). The Haselgebrige (Permo-triassic) of the Austrian alps similarly contains no smectites nor even smectite-bearing mixed-layered clays (Bodine, 1971), and the same is true for the Silurian salts of New York (Bodine and Standaert, 1977). The development of the unusual illite-saponite/talc/ saponite phase with polyhalite suggests immaturity of the silicate

phase with respect to the evaporite phase. Any further phase changes that would take place in the silicate appear to be kinetically inhibited.

b. The variability of the clay assemblages and their lack of correlation with major evaporite lithologies bespeaks strongly of recrystallization accompanying migrating post-depositional pore fluids. Except for the unusual 10.3 Å phase with polyhalite, the only other lithic correlations are: (1) reasonably well crystallized corrensite as the only expandable clay in the discreet clay seams and (2) the occurrence of serpentine in the uppermost Castile Formation. The former is tentatively attributed to the "closed system" nature of the impermeable salzton beds; they were not subject to the attacks by a variety of migrating pore fluids of different composition. The latter relates to the vertical distance between K-Mg-bearing salt beds and the Castile Formation, which essentially comes in contact only with less mobile fluids in equilibrium with halite-anhydrite.

c. It is very tentatively suggested that many of the salzton seams formed through accumulation of silicate debris included in salts which have been dissolved; their association with the soluble K-Mg salt ore zones and with the extensive polyhalite replacement of anhydrite beds appears remarkable and may provide the geometry for the "plumbing system" in which migrating pore fluids circulated. It is also recognized that some of the salzton beds may well represent recrystallized detrital accumulations during periods of no evaporite deposition as suggested by Adams (1969). If migrating groundwaters do flow in some such controlled pattern, ore mineral distribution in each ore zone should reflect this, i.e. remnants of the primary carnallite-kieserite farthest from the source of the brines, enveloped by langbeinite and langbeinite-sylvite assemblages, in turn enveloped by langbeinite and langbeinite-sylvite assemblages, in turn enveloped by sylvite, and finally by barren halite. Similarly polyhalite

crystallization should be at a maximum under the
langbeinite-sylvite assemblage within a given "cell" and would
likely decrease both away from and toward the lateral pore fluid
source.

In summary, substantial evidence has been accumulated that there has been
extensive salt recrystallization, most noticeably within the McNutt ore
zone. This is considerably less noticeable in the lower Salado and
Castile Formations, but may simply reflect the far simpler evaporite
mineralogy and persistence of substantially more homogeneous compositions
within the pore fluids.

Preliminary computer modeling does, for example, substantiate that a
typical primary marine evaporite salt assemblage of
carnallite-kieserite-halite can, when under continued attack by migrating
halite-gypsum saturated pore fluids flowing down dip in a hypothetical
cell, generate a progression of salt facies with remnants of the primary
assemblages farthest from the source. Toward the source, the following
succession of assemblages would be found: langbeinite-carnallite-halite
(or langbeinite-kieserite-halite) then langbeinite-halite, then
langbeinite-sylvite-halite facies, then sylvite-halite, culminating
toward the source in a barren halite facies. At the same time, the K-Mg
rich pore fluids which were generated through ore mineral dissolution and
alteration would no longer be in equilibrium with anhydrite; anhydrite
would alter to polyhalite until the solution chemistry reached the
polyhalite-anhydrite equilibrium composition. The precise thermodynamic
conditions and mineralogic reactions which governed these alterations are
not known; however, the age of this recrystallization of evaporites has
been determined to be in excess of 204 million years. For more details
regarding this recrystallization which closely followed deposition, the
reader is referred to Section 7.8.

7.5   VOLATILES AND FLUID INCLUSIONS IN MINERALS OF THE SALADO FORMATION

7.5.1 Introduction

Sources of liquids and gases native to the evaporites must be considered. One source is the intergranular fluid to be found in the pore spaces between mineral crystals and lithic fragments. These fluids are discussed in detail in a subsequent section (7.7). Another fluid source is the water of crystallization chemically bound in hydrous minerals. Yet a third source is fluid inclusions inside the mineral crystals themselves, which can behave as separate micro-geochemical systems.

Data presented in the overview Section 7.5.2, and Section 7.5.3 result from heating bulk rock samples to recover all types of fluid. In the major portion of the Salado, the total recovered amounted to less than 0.5 weight percent of the rock. As discussed in the overview section, it was possible to separately identify: (1) loosely-bound volatiles, (2) chemically-bound volatiles, and (3) fluid inclusions.

The sections on mineral sources of water and on fluid inclusions endeavor to place the data in the context of the mineralogy of the rocks serving as hosts for the volatiles. It will be noted that geochemistry in the context of the mineralogy is a pervasive theme in all parts of the geochemistry section of this report. This is true for the sections which follow on groundwater geochemistry and radiometric age-dating also. It will also be noted that the characterization of geochemical properties of solutions in the Salado confirm the qualitative measurements of fluid inclusion solute contents.

This chapter contains considerable data which will assist in the anticipation of short and long term physico-chemical conditions likely to arise during the experiments involving heat-producing radioactive wastes.

7.5.2 Overview of Volatile Contents of Evaporites

Themogravimetric analyses of 35 selected core samples from ERDA No. 9
were made. These were many of the same samples which were qualitatively
examined for mineralogy by x-ray diffraction (refer to Section 7.2.3).

These analyses were made by suspending powdered samples from a.
microbalance while dry nitrogen flowed above the sample. The samples
were heated by 5°C/minute until the temperature reached 500°C and
were held there until gas evolution had ceased. A hygrometer was
inserted downstream to register qualitatively whenever moisture was
evolved.

The as-received salt core specimens were massive pieces approximately 4
inches in diameter and 1-2 inches thick. No attempt was made to obtain
homogenized samples by powdering the entire piece. Instead nuggets were
chiseled from the center of the specimen. The nuggets were crushed and
ground to a powder just prior to the weighing and transferring to the
microbalance system. A maximum of ten minutes elapsed between the start
of crushing and the start of analysis. Thus, the possible loss or gain
of moisture prior to testing was minimized. Powdered samples were
necessary to minimize decrepitation.

The complete test results are presented in Table 7.12. Figure 7.7
illustrates the typical kinds of weight-loss curves observed. About half
the specimens showed 0.5% weight-loss (curve A). Curve B is common with
the rapid weight-loss occurring sometimes at 300° and sometimes above
400°C. Some samples show two stages. Only two samples followed curve
C, where weight-loss was observed from the beginning of the run. The
weight-loss curves for all samples are filed and are available for
inspections.

Replicate runs were made in several cases, predominantly those which
showed the larger weight-losses, and good agreement, i.e. within 5%, was
observed.

All mass-loss is not due solely to water. Only the weight-loss below $300^{\circ}C$ can be attributed largely to water; the weight-loss at higher temperatures is in part due to decomposition of carbonates or other volatile-bearing minerals.

Results were correlated with the x-ray diffraction results previously reported in an effort to identify which minerals may be decomposing. No definite conclusions could be reached so selected samples were analyzed for the evolved gases by gas chromatography/mass spectrometry. In particular, this was done for the samples 2302.6, 2516.3, 2658.5, 2786.5 and 2821.0.

The highest weight-loss was experienced by sample 2302.6. Its total ion chromatogram (Appendix 7.E) shows data channel numbers calibrated approximately in terms of temperature. Conspicious peaks occur at $100^{\circ}C$, $250^{\circ}C$ and $300^{\circ}C$. Detailed mass spectra are given for $50^{\circ}C$, $100^{\circ}C$, $150^{\circ}C$, $200^{\circ}C$ and $250^{\circ}C$; the most prominent mass peak is 18, corresponding to water. At higher temperatures, mass 14 (monoatomic nitrogen) becomes abundant. Even at lower temperatures, mass 28 (diatomic nitrogen) is present.

Sets of peaks separated by 12 mass units, corresponding to carbon, (95, 83, 71; 81, 69, 57, 45) probably represent fragments of hydrocarbons present in the diesel oil which was the lubricant used to core the hole. The contribution of mass 44 (CO_2) to the spectrum is a minimum at $200^{\circ}C$ and rises again at higher temperatures. The low-temperature contribution is again probably due to the contaminant diesel oil.

At the highest temperatures, the mass peaks 15, 16, and 17 (CH_3, CH_4, O, OH) are accentuated along with 14, 18; and 28 (N, H_2O and N_2). All the individual ion chromatrograms for mass numbers 14, 18, 19, 20 and 44 have coincidental peaks at about $25^{\circ}C$ and $300^{\circ}C$. Water and carbon dioxide are almost continuously evolved over the entire temperature range, but the coincidence of all the peaks for N, H_2O, F(?) and CO_2 (mass peaks 14, 18, 19, and 44, respectively) implies that evolution of

these components at $250^{O}C$ and $300^{O}C$ is related to a common source. Since halite decrepitates, releasing its fluid inclusions at about $250^{O}C$, those inclusions appear to be the most probable source of volatiles evolved at $250^{O}C$. Similarly since polyhalite dehydrates at a temperature slightly above $300^{O}C$, fluid inclusions in that mineral might be also released at that temperature (see Section 7.3). A detailed treatment of fluid inclusions appears in a subsequent discussion.

Mass numbers 32, 48, 64 and 80 have sharp coincidental chromatogram peaks at channel 517. These mass numbers most probably represent O_2, SO^{+2}, (possibly O_3 made inside the mass spectrometer) SO_2 and SO_3 released from the sudden decomposition of a sulfate. Similarly mass 36 (HCl) is released in major quantity at this point. All these phenomena occur at a slightly lower temperature than the main $200^{O}C$ event, and their relationship with that event possibly indicates the presence of a very volatile sulfate phase rapidly decomposing when the halite fluid inclusions begin to rupture. Daughter crystals of gypsum in halite fluid inclusions would indicate a high concentration of sulfate in the inclusions (see subsequent discussion) and such a solution might give rise to the observed sulfur species in the mass spectrum.

The sample with the next greatest total mass loss (2786.5, 3.64%) is considered next. Many of the same features of the chromatograms in Appendix 7.E are observed here as in the previous sample. The main difference is the appearance of a large hump of many volatiles (H_2O, F, N_2, O_2) released at less than $100^{O}C$. This is consistent with the occurrence of clay minerals which can absorb various volatiles at surface and interlayer sites. Volatiles would be expected to be weakly bound at these sites. The same hump as before appears at $250^{O}C$, incorporating N, H_2O, HF(?), N_2, O_2, HCl, CO_2 and SO^{+2}, but only the postulated SO_2 species appears to be catastrophically released and is probably a product of ionization in the mass spectrometer.

A hump incorporating N, H_2O, HF, N_2, O_2, HCl, CO_2 and SO^{+2} occurs substantially below $300^\circ C$. This peak probably corresponds to release of water and other volatiles born of OH and fluid inclusions in the clay minerals, when the clays decompose upon dehydration.

Sample 2516.3 (2.15% mass loss) was unusual in that it contained magnesite. As is seen in the chromatograms in Appendix 7.E, the loss of H_2O and N_2 from various sources provides most of the pattern, which was not sampled at a temperature greater than about $240^\circ C$. There is almost a continuum of absorbed O_2 released. The most significant feature of this sample is the high-temperature loss of CO_2, presumably from the decomposition of magnesite.

Finally, the most abundant-type sample is considered: those which have mass losses less than 0.5%. These are characteristic of most of the main evaporite section and contain very little other than halite and anhydrite. Typical examples of these rocks are samples 2658.5 and 2821.0 (Appendix 7.E). The main difference between these two is the apparent larger number of types of volatile sites in the shallower sample. Absorbed N, H_2O, N_2, and O_2 form a large, broad hump at low temperature, with catastrophic release (of fluid inclusions?) of H_2O, N_2, HCl, and CO_2 at higher temperature in 2821.0. In 2658.5, the catastrophic release of H_2O, N_2, HCl, and CO_2 (with possibly some SO^{+2}) appears to occur in smaller episodes as various sets of fluid inclusions are ruptured at higher temperature.

7.5.3 Mineral Sources of Water in the Salado Evaporite Sequence

Introduction. The purpose of this section is to describe the mineralogy and petrologic characteristics of samples taken from two coreholes of the Salado salt from the boreholes AEC Nos. 7 and 8 in Lea and Eddy Counties, near Carlsbad, New Mexico, and the degree to which the evaporite rocks present would dehydrate if subjected to the heat generated by containers of radioactive wastes (radwaste). In a previous study, (Fallis, 1973) the general characteristics of evaporite deposits and their minerals were

described and a detailed mineralogic and petrologic study of two cores from the Hutchinson Salt near Lyons, Kansas, was made. The results at that time indicated that water losses ranging from 0.4 to 19.0 weight % might be anticipated if the surrounding rocks were heated to 100°C.

Sample splits corresponding to ones in this section were also discussed in Section 7.3. A comparison of those results and these is presented in the following section.

Sampling and Sample Preparation. Segments of the original 4 inch (10.2 cm) cores were split in half, lengthwise, for chemical analysis and weight loss determination by thermogravimetric analysis (previous section). Eighty-three samples (coded by core number and depth) arrived wrapped in plastic to reduce the possibility of absorption of moisture during shipping and handling. Core AEC-7 was drilled in Lea County, New Mexico, and core AEC-8 in Eddy County, New Mexico.

Throughout the sample preparation, care was taken to not expose any of the samples to water; however, since it was necessary to cut, grind and sieve various portions of the samples, it was not possible to completely protect them from exposure to moisture in the air. During those periods when samples were not actively being worked upon, they were kept in plastic bags, tightly-stoppered bottles, etc.

Since several different analyses were to be made, it was necessary to obtain representative sample splits which would correspond to each other as closely as possible. A more complete discussion of sample preparation is given in the thesis by Combs. However, for convenience, a brief summary of the methods used in sample preparation is given below:

1. A representative segment of each core sample was chosen and removed by sawing the original core (normal to the axis of the core) with a dry blade, masonry-type saw. This new segment was typically about three inches (8 cm) long.

2. Next, a slice was cut from each core segment (parallel to the axis of the core) with the approximate dimensions 3 x 2 x 1/2 inches (8 x 5 x 1 cm) for use in preparing the thin sections. The sections were prepared by Fred Roberts Petrographic Section Service, Monterey Park, California. They were cut using oil rather than water and mounted with an epoxy cement which was not heated.

3. About one-half of the remainder of each core segment was crushed and sieved, and representative portions selected to be analyzed by x-ray diffraction, x-ray spectroscopy and by static heating methods for water loss determination. (Later, some additional separations were made and portions of the samples selected for bromine analysis using x-ray spectrocopy. These procedures will be described briefly in the following sections.)

Analytical Methods Used in This Study. Several different kinds of analyses were performed on the samples received. The methods used include static weight loss determinations (water loss), mineralogical and petrological analysis, and some chemical analyses using x-ray spectrocopy.

The weight loss determinations were made in essentially the same manner as for samples studied from Lyons, Kansas, and which was reported previously (Fallis, 1973). Splits of the several samples (sample size generally ranged from 1.5 to 2.0 gms and in the 60 to 120 mesh size fraction) were heated to $102\pm5^{\circ}$C for periods ranging from 2 to 42 days. The results of repeated analyses indicated that the precision of weight loss determinations was generally $\pm$ .0.1 to 0.2%. When new sample splits were used, the "precision" dropped to approximately $\pm$ 0.2 to 0.3%. Some data concerning precision are presented in Appendix 7.F.

In addition to the weight loss determinations performed near 100°C, weight loss determinations were also made for several samples which had been heated to $170\pm5^{\circ}$ (for 2 days) and $300\pm10^{\circ}$C for (2 to 3 days). The results of the weight loss analyses are reported in Appendix 7.G and discussed in the following section.

Mineralogical and petrological analyses were made using x-ray diffraction and standard petrological techniques. A summary of important mineralogical and petrological data is given in Appendix 7.H and discussed following the next section. The chemical analyses were made using two variants of the x-ray spectrographic method, x-ray fluorescence analysis (wave length dispersive) and x-ray emission spectroscopy (non-dispersive). The chemical analyses were made primarily for bromine, which can be used to aid in the interpretation of the origin of evaporite deposits, and semi-quantitative analyses were made for chlorine, sulfur and iron.

Weight Losses for Cores, AEC NO. 7 and 8. Weight loss data for the samples studied are tabulated in Appendix 7.G and illustrated in Figure 7.8. In general, the weight losses are much less than those found for samples from the site at Lyons, Kansas. The range of weight loss values at $102\pm5^{\circ}$C for the Carlsbad samples (Salado salt), Cores Nos. 7 and 8 was from 0.0 to 3.5% with the majority of samples showing losses less than 0.5%, while the Hutchinson salt, Cores Nos. 1 and 2 was from 0.5 to 19.0%, and most of the samples showed weight losses from 1 to 5%. A plot of approximate range of water loss at $102\pm5^{\circ}$C to be expected at various depths is shown in Figure 7.9. This is based on data from both Lyons, Kansas and Carlsbad, New Mexico sites.

Based on the results of the various heat treatments, the following conclusions can be drawn concerning the behaviour of the samples from Carlsbad:

1.   Samples consisting almost entirely of halite and/or anhydrite show weight losses (up to 300°C) which are typically less than 0.5% and probably less than 0.3%. The final total loss will depend on the amounts of clay minerals and minor hydrated evaporite minerals, such as polyhalite, which are present.

2.   Larger water losses (>1% at $102\pm5^{\circ}$C) are generally associated with the presence of clay minerals (and/or gypsum) in more than trace amounts. The exact losses will depend on

the kinds and amounts of clays present, the temperatures to
which they are heated and the length of time for which they
. are heated.

3. At some temperatures between 170° and 300°C, polyhalite,
which is a common accessory mineral constituent in some parts
of the Salado salt, will start to break down. It can
contribute water to the extent of about 6% of its weight in
the rock being heated.

4. Although present in only minor amounts (or absent) in the
samples that were analyzed, there are other evaporite minerals
such as carnallite, kainite, leonite, etc., near the potash
ore zones (the McNutt potash zone at approximately 1600' to
1800').

The weight losses determined in Section 7.3 are compared with these in
Appendix 7.G. It should be noted that the earlier data were determined
by thermogravimetric analysis; hence, weight losses were not determined
at any fixed temperatures but at the actual temperatures at which the
decompositions were detected. In order to make the data more comparable,
the previous data were rearranged and weight losses taking place within
certain temperature ranges were combined. The reader is referred to
Section 7.3 for the specific temperatures at which weight losses
occurred. It should also be noted that the two sets of data are not
directly comparable, since the weight losses of this section were
accomplished by heating under static heating conditions for periods of 2
or more days, while the previous data were obtained under dynamic
conditions (much more rapid heating). As a general rule, the
decomposition temperature of any given mineral will be higher under
conditions of dynamic heating rather than static heating.

Even so, there is generally good agreement between the two sets of data
which were obtained by different investigators using different
techniques. Most minor discrepancies can be explained on the basis of

differences in the methods of analysis. Only a few real discrepancies seem to exist (such as for sample at 1697 in Core #7). This is to be expected since each group rceived different halves of the core and since Section 7.3 involved sample splits of the entire core segment while this work involved only a sample split corresponding to the portion of the core used in preparing the thin section. Since there are both vertical and lateral variations in mineral content within the cores, samples might occasionally have been analyzed which were mineralogically different.

The rocks being considered at the proposed WIPP site, New Mexico, appear to be much more favorable than those from Lyons, Kansas. Even so, some mineral water is still present and is apt to be released during the period when the rocks are heated by the waste containers. It will be important to determine the maximum temperatures to be reached, the volume of rock which will be heated, and the probable maximum volume of water which will be released.

Mineralogy and Petrology of Cores No. 7 and 8. In some respects the mineralogy and petrology of the core samples from Carlsbad are similar to those of the core samples from Lyons. Both cores were taken through evaporite sequences and hence encountered sedimentary sequences containing typical saline minerals such as halite, anhydrite and polyhalite. In addition, clay minerals, magnesite, gypsum, quartz, feldspar, carnallite, celestite (?), glauconite and kainite (?), were detected in smaller amounts. The presence of any of the other less common evaporite minerals in the samples studied is uncertain. In general, they only occur in such small amounts and/or such fine grain sizes that positive identification was not possible using the diffractometer and petrographic miscroscope. In Section 7.3 it was noted that several of these less common minerals are apparently present in many of the samples analyzed. Readers of this section should be aware that the analyses are based on the actual minerals observed (modal analysis) in thin section as supplemented by X-ray diffraction while the analyses presented in Section 7.3 were done by computer manipulation of the chemical analyses determined for each sample (normative analysis). Such

normative analyses can be quite useful, especialy when working with very fine grained or glassy materials. However, it should be noted that normative analyses may generate mineral assemblages which do not agree with the actual minerals present, as was pointed out in section 7.3.

Summaries of the mineralogic and petrologic features of the individual samples studies are presented in Appendix 7.H. For the reader's convenience, some general comments about the mineralogy and petrology of these samples are presented below. An excellent study of the mineralogy and petrology of the rocks in this region is given by Schaller and Henderson, 1932. Brief description of the major minerals noted in the Carlsbad samples follow.

Halite. Most of the halite is colorless and shows excellent cubic cleavage. These features, coupled with less low relief and isotropic optical character, make its identification easy. Sometimes the halite is colored red or orange by minute inclusions of hematite (or other iron oxides) or other minerals such as polyhalite. The grain size showed a wide range, from less than 1 mm (fine grained), to greater than 1 cm (coarse grained). Grains between 1 mm and 1 cm are considered to be medium grained.

Because halite fractures and cleaves so readily, it is difficult to determine whether the numerous breaks observed in thin sections were already present at depth or whether they developed during the coring operation, shipping, handling, thin section preparation, etc. More fractures are noted at the outer margins of each of the thin sections. However, some of them must have occurred prior to the taking of the core because they are filled (at least in part) with other minerals, petroliferous material, etc. In several cases fracture zones could be traced across the entire width of a thin section.

Inclusions (liquid, solid and gas) are common in the halite. During the preparation of some samples hydrogen sulfide (gas) was released. In many cases the inclusions are oriented with respect to the cubic crystal

planes. These oriented inclusions appear to represent hopper crystals which grew at the water surface in times of quiet water and are inferred to represent deposition from shallow water.

Intergrowths of relatively well-formed, cubic crystals of halite with clay and silt-size minerals are likewise inferred to represent very shallow conditions, perhaps even subaerial exposure for brief period.

"Patches" (regular to irregular, more or less equidimensional areas) and "stringers" (regular to irregular areas which are generally elongated in one direction) of anhydrite, polyhalite, clay and silt-sized minerals are common in halite. Sometimes these patches and stringers follow grain boundaries, but often they cut across grains. Where they follow grain boundaries, they may represent (nearly) simultaneous growth of the halite crystals and smaller amounts of the other mineral phase(s). Where they cut across grains, they presumably represent deposition of the minerals along zones of weakness or along which solutions passed. Enough of this latter material is present to demonstrate that there were opportunities for solutions to migrate through these relatively impermeable rocks, even though it is not possible to determine just how far the solutions actually traveled.

Anhydrite. Anhydrite was recognized on the basis of its relatively high birefringence, differences in relief upon rotation and cleavages at right angles. Normally, anhydrite shows parallel extinction, too, but because of twinning, replacement phenomena, etc., this characteristic was not always useful.

Anhydrite occurs in three major types. "Primary" anhydrite, which is commonly bedded, is very fine grained (much less than 1 mm) and somewhat fibrous in character. It also occurs in coarser-grained crystals and twinned crystals (sometimes over 1 cm long). At least some of these larger crystals appear to be pseudomorphs (replacement) after previously-existing gypsum crystals. Sometimes, very small amounts of questionable gypsum are noted nearby, perhaps as a result of partial

rehydration of the anhydrite. Finally, there are more or less isolated crystals and crystal clusters of anhydrite which occur in patches and stringers within the halite or are intergranular with halite. These may be associated with polyhalite and/or clay and silt-sized minerals. This type of anhydrite is thought to be authigenic (formed in place from fluids contained in the pores of the rock or passing through the rock).

Anhydrite can be replaced by polyhalite if fluids containing potassium, magnesium and additional sulfate ions are present. Many examples of this replacement were observed.

A few examples of bedded, nodular anhydrite were observed. The nodules may have originally been composed of gypsum which was later replaced by anhydrite. The origin of such bedded nodules is thought by some workers to represent depositions in very shallow water which was periodically exposed (Sabkha facies).

Polyhalite. Polyhalite was recognized on the basis of its relatively low birefringence, inclined extinction and complex twinning. (Unfortunately in some fine-grained material and/or mixtures, polyhalite and anhydrite can be confused because their optical properties of relief and birefringence are almost the same in certain orientations).

Much of the polyhalite observed is rather fine grained (much less than 1 mm in size for the individual cyrstallites) and often fibrous. However, some larger crystals are numerous, isolated crystals and crystal clusters were observed. Polyhalite is often reddish due to iron oxide inclusions, but this is not universally true.

Some of the polyhalite appeared to be a bedded form associated primarily with halite and lesser anhydrite. Polyhalite also is found replacing anhydrite and associated with nearby patches and stringers of clay and silt-sized minerals. Whether the clay, etc., provided some of the ions necessary for formation of polyhalite or just acted as a pathway for solutions passing through the rock cannot be determined.

Minor Minerals. Minor minerals were identified on the basis of their optical properties and X-ray diffraction analyses, which were occasionally aided by information contained in the well logs for the cores. Just a few brief comments for each mineral are given here.

Clay minerals. Overall, much less clay is present in the samples from Carlsbad than was present in the Lyons samples. X-ray diffraction peaks attributed to clay minerals were noted in nine samples from Core #7 and in fourteen samples from Core #8. Based on the X-ray patterns and peaks noted at approximately 7, 10, 11.5, 14 and 15 angstroms, major clay minerals present include illite, chlorite, mixed-layer clays and possibly some kaolinite.

Magnesite. Although well-crystallized magnesite was not detected in thin sections, some very fine-grained, relatively high birefringent phase was noted in some thin sections and magnesite peaks were detected in some thin sections and magnesite peaks were detected in a number of X-ray patterns. Schaller and Henderson (1932) stated that many of the clays in the samples they studied were magnesitic. The common association of polyhalite with clay and silt-sized minerals may be due in part to the magnesium ions in the magnesitic shales and clays.

Gypsum. Gypsum is monoclinic and in thin section has low birefringence and low, negative relief. Twins ("swallowtail") are fairly common. Well-crystallized gypsum was detected in only one thin section among the samples studied. In addition, several of the sections contained small amounts of questionable gypsum in association with anhydrite and/or polyhalite. However, the amounts present were much less than 1% and could not be confirmed by X-ray diffraction.

Quartz and feldspar. These minerals are present in two forms, as detrital (silt and very fine sand-sized) material deposited along with the clays, and also as authigenic minerals which formed in or near patches and stringers of clay and silt-sized minerals.

Sylvite. A few thin sections contain small amounts of sylvite which was recognized on the basis of its distinctive reddish purple color (due to iron oxide inclusions) and lower relief than halite. Most of the sylvite observed was associated with polyhalite as well as with halite. There were no samples from the sylvinite (mixed halite and sylvite) zones. Adams (1967) reported that not all sylvite is colored; however, in the thin sections studied, the distinctive color was useful in locating the small amounts present.

Carnallite. Only one section contains detectable carnallite. This mineral was suspected on the basis of nearby carnallite as noted in the well log. Its high negative relief and "metallic" luster due to inclusions were used to confirm its presence.

Celestite (?). In two or three thin sections some isolated spear-shaped crystals and clusters of crystals with relatively high relief were noted. Although no positive identification could be made, it is suspected that these are celestite, which is the most common strontium mineral present in evaporite deposits.

Glauconite. A few greenish, rounded grains of glauconite were noted, generally associated with the clay and silt-sized minerals. Not enough of this material was present to attempt to determine its origin or source.

Kainite(?). Kainite (?) was observed in only one thin section. It is a monoclinic mineral with moderate birefringence and negative relief.

Summary and conclusions. The results of this study indicate that the Salado Salt in the samples received is composed primarily of fine to coarse-grained halite with polyhalite, anhydrite, and clay minerals. Other minerals detected in small amounts include gypsum, magnesite, quartz, feldspar, sylvite, carnallite, celestite (?), glauconite, and kainite(?). It should be noted that the samples received for analysis were selected from halite-rich zones in most cases; hence, some of the rarer evaporite minerals such as kieserite, langbeinite, leonite,

bischofite, etc., noted by Schaller and Henderson (1932) were not detected either because they were absent from the specimens analyzed or present in amounts too small (or too fine grained) to identify.

There is much petrographic evidence that the Salado salt was deposited in rather shallow water and may have been exposed subaerially at times. This evidence includes the presence of numerous hopper crystals (which can develop at the air-water interface of quiet, shallow seas) and the intergrowth of euhedral grains of halite with clay and silt-sized minerals, anhydrite, and polyhalite. The latter texture can develop in an exposed, mud-flat type environment. Previous workers, such as Anderson, et al. (1972), have concluded that the underlying, Castile Formation was deposited in deep water, perhaps as much as 2100' (650 m) deep. Hence, there must have been a major change in environmental conditions between the deposition of Castile and that of the Salado.

Petrographic evidence also suggests that local fluids native to the Salado have been able to move through the Salado salt (during recrystallization) along beds and seams of clay and silt, and to a lesser degree along fractures (see Section 7.8). These paths are now marked by entrapped fluid inclusions, zones of altered minerals and zones along which new minerals have been deposited.

Water loss determinations for over eighty samples from cores #7 and #8, indicate a range of water loss (upon heating to $102\pm5^{\circ}$C) from 0.0 to 3.5%, which is considerably below the water losses for samples from Lyons, Kansas. It whould be noted that the samples from the Lyons site came from much shallower depths than those from the Carlsbad area. In the section on weight losses, the ranges of dehydration to be anticipated with respect to depth are shown graphically. It appears that the ranges determined for the relatively shallow Lyons site merge with the ranges determined for the deeper Carlsbad site.

Most of the dehydration water at relatively low temperatures (near 100°C) appears to come from clay minerals, although gypsum may make a

contribution for samples taken at shallow depths. At higher temperatures, polyhalite will start to contribute to the dehydration of water. This dehydration takes place somewhere between 170° and 300°C. Pure polyhalite rock can lose up to 6% water. In general, the purer halite beds have weight losses below 0.3 to 0.5%.

As far as can be determined from the samples available for study, the rock units present in the Salado salt seem to release much less water when dehydrated than do the rocks of the Hutchinson salt from Lyons. Hence, the site near Carlsbad would seem to be more favorable (in so far as dehydration water goes) than Lyons. However, these rocks are not totally without water, and most units will lose from 0.0 to 0.3% water when heated and some units may lose up to 3.5% water.

Finally, it was noted during the preparaton of some of the samples that H_2S (and possibly some natural gas) was released when the samples were crushed. No H_2S was detected mass spectrometrically (previous section), which probably attests to a sensitivity of the human nose for H_2S that is unapproachable even with the most sophisticated available instrumentation.

7.6 FLUID INCLUSIONS IN CORE SAMPLES FROM ERDA NO. 9

7.6.1 Introduction

Fluid inclusions in the host rock are of interest to several aspects of nuclear waste disposal. First, determination of their origin and nature may provide insight into the complex sequence of processes and events from original deposition of the salt through to the present; such insight may well be of value in site evaluation. Second, fluid inclusions provide one source of water (and other volatiles) that would certainly aid in the corrosion and eventual breach of the waste containers, and subsequent leaching of the waste itself. Third, fluid inclusions, and their reaction under the thermal pulse from hot wastes, could have an effect on important physical properties of the hot host rock, such as deformation rates and particularly melting.

7.6.2 Samples Studied

Most samples studied were taken from ERDA core No. 9, and came from the
following footage intervals:

From	To
1799.0	1799.5
1902.0	1902.3
2065.0	2065.4
2095.1	2095.5
2272.4	2272.7
2391.0	2391.3
2611.5	2611.8
2658.7	2659.0
2760.0	2760.2
2820.8	2821.2
2058.8	2059.0
2070.4	2070.6
2606.5	2606.9
2617.2	2617.7
2626.7	2627.0
2659.0	2659.2
2665.0	2665.1
2692.4	2692.6
2699.8	2700.0

In addition to the above "representative" samples, four nonrepresentative
samples from ERDA No.9 were selected because they contained plainly
visible large inclusions, suitable for special tests:

        2061.2 - 2061.6
        2064.5 - 2065.0
        2614.7 - 2615.0
        2518.5 - 2619.0

In order to test certain sample preparation and inclusion extraction procedures with no loss of important core, two pieces of core from AEC 8 were also picked:

$$2059.5 - 2059.8$$
$$2462.0 - 2462.9$$

In the Kerr-McGee potash mine, Lea County, New Mexico, northwest of the WIPP site a 4-m igneous dike has cut potash ore beds. As this represents a natural simulation of some of the heat effects of canister storage, it is instructive to examine the fluid inclusions in samples taken at measured distances from this dike:

MB-77-8	White halite 1-2 cm from dike
MB-76-3	Barren salt 0.2 m from dike
MB-76-4	"Ore" horizon 2.5 m from dike
MB-76-5	"Ore" -21 m from dike

Of these samples, the field evidence indicates that only MB-77-8 has been molten. The others show some mineralogical effects of the heating, but as sedimentary structures are preserved, they have presumably not melted (M. Bodine, personal communication).

7.6.3 Sample Preparation

Sections. A thick slice was cut from each sample using a diamond saw and ethyl alcohol lubricant. One side was fine ground with an alcohol slurry of abrasive (1200 grit), ultrasonically cleaned in alcohol, mounted on glass with cold-setting epoxy resin, and cured in 16 hrs. at room temperature. The section was then ground down on a lap, using an alcohol slurry, to 3-8 mm thickness (depending on opacity) and then polished by finer abrasives, ending with either 1200 grit or 0.3 µm Al_2O_3. Plates with fine-ground surfaces were examined using a matching silicone oil or saturated brine and coverglass. Coarse cleavages could be examined directly, without polishing.

A small section ($\sim$ 2 X 4 cm) was cut first, perpendicular to the core axis (when nature of sample permitted orienting), then one or more larger plates (5 X 8 cm) were cut parallel with the core axis.

<u>Coarse water-soluble residues</u>. 100- to 150- gram samples were dissolved in tap water at room temperature with frequent stirring. The solution was decanted frequently to remove dissolved salts and finely divided solids such as clays.

7.6.4   <u>Methods of study</u>

<u>Petrographic Examination</u>. All slides and preparations were examained with the petrographic microscope, but phases present other than halite were not determined due to the short time available and the redundancy with extensive mineralogical work by others. Most examination time was spent on finding and characterizing the nature, size, frequency and distribution of the fluid inclusions.

Considerable time was spent determining the volume of fluid inclusions in the plates, through counts of representative portions. This determination was based on measurements with a graduated ocular (calibrated with a stage micrometer) and several assumptions. <u>First</u>, the inclusions were considered to be cubes (based on observation); one edge was measured and then the volume calculated. Larger inclusions (~ 1mm edge length) that were obviously not cubes were estimated from the summation of a series of smaller cubes. <u>Second</u>, since bubbles were very rare (only about 0.1% of the inclusions), and small (~ 1% of inclusion volume), they were ignored. <u>Third</u>, most inclusions in these samples were of one or the other of two types (essentially the same as the types "A" and "B" discussed in a later section on Results), and any given small portion of salt contained only one type. As the bulk of the sample in any plate could be characterized easily into these two types the approximate volume percent of the samples for each type could be estimated. A ~ 500 mm^3 volume of the plate was then selected from each type, visually estimated to be representative of that type in that plate, and the volume percent of inclusions determined in it by measurement and counting, using a transparent grid template at 500X. The total volume percent of inclusions was then calculated from the weighted average. The weight percent of inclusion fluid was calculated, assuming the salt to have a density of 2.2 and the brine to be 1.3 g/cm^3. Large numbers of very tiny inclusions were estimated from counts and estimates of small

but visually representative volumes. Although the relative errors
involved in this step are large, the total contribution by these small
inclusions, even though they are extremely abundant, was very small.
Most of the fluid found was present as a small number of large inclusions
that could be measured more accurately. All inclusions over 200 μm
(edge length) in the count volume were measured. The overall measurement
error in volume percent of inclusions present is believed to be on the
order of $\pm 5\%$ of the value stated for a given plate. Other variables,
particularly rare, still larger, centimeter-sized inclusions that were
opened during coring or sample preparation (and hence not counted), and
the large difference between different plates from the same sample,
introduced much larger errors.

Heating Stage. The liquid in inclusions trapped as homogenous fluid at
above surface temperature shrinks on cooling, forming a bubble that
provides a measure of the amount of differential shrinkage of liquid and
host crystal. As the bubbles in the inclusions were small, relatively
little heating was needed to cause homogenization. Hence a new heating
stage was set up, consisting of a bath of silicone oil with an electric
immersion heater and thermometer. Temperature equilibration was achieved
through convection and frequent stirring. The individual runs were
approximately 2-3 hrs. in length. Many inclusions that had no bubble as
received developed one on cooling the silicone to $\sim -6^O C$ with solid
CO_2. On subsequent heating this bubble would decrease in volume but
persist as a very small bubble at room temperature. Heating was done on
the stage of a low power binocular microscope, since the inclusions were
large and scattered.

Freezing stage. The depression of the freezing point of the fluid in an
inclusion (i.e., the "freezing temperature") is a function of the
composition of the fluid. Using this techique under the microscope can
permit a quick measure of the salinity of 10^{-10} g of fluid, a far
smaller sample than can be measured by any other method. Metastable
supercooling is common, so most inclusions had to be cooled to very low
temperatures (three hours in CO_2-acetone at -78° or even LN_2 at
$-196^O C$) to cause freezing. Subsequent slow warming of the sample while

surrounded by rapidly circulating refrigerated acetone of known
temperature under the microscope permits recording the temperature of
disappearance of the various solid phases formed on freezing (salts,
hydrates, and ice), under equilibrium conditions.

If an inclusion is frozen completely to a mixture of solids, with no
liquid, it becomes rather opaque. On warming, the first melting wets the
crystal interfaces, suddenly making the mass more translucent, and
permitting recrystallization to coarser crystals with time. This is
called the "first melting temperature." It ranges from $-21^{\circ}C$ for pure
NaCl solutions to $-51^{\circ}C$ for $CaCl_2$ solutions.

Crushing stage. If a host crystal containing an inclusion with a bubble
is surrounded by a fluid and gradually crushed while under the microscope
so that the behavior of the bubble can be observed, the presence of
noncondensable gas in the bubble, and its pressure, can be determined.
The test is only crudely quantitative in terms of pressure (based on the
volume precent expansion), but it is extremely sensitive as a detector of
small amounts of gas. Less than one billion molecules of gas can be
detected readily. Numerous cleavage fragments of salt containing various
types of inclusions were crushed on several models of crushing stages to
determine the amount and pressure of any noncondensable gases present.

Coarse water-soluble residues. These were studied in oil immersion
mounts in hopes that some of these phases were sufficiently coarse to
contain fluid inclusions that would provide data on their conditions of
formation.

Decrepitation. A portion of the core weighing approximately 100 g was
split out with a rock splitter; where possible the outside core surface
was avoided, due to the probability of physical deformation and resultant
leakage of incluions. This piece was wrapped loosely in aluminum foil,
weighed, and heated to the run temperature ($150-250^{\circ}C$) over a period of
8 hours to avoid thermal shock, held at run temperature for 3-4 days,
cooled and reweighed to determine weight loss. Following this the
homogenization temperature range was redetermined for a series of

inclusions that appeared, on petrographic examination, to be representative. Crushing tests were also repeated on the heated samples to detect the presence of noncondensable gases under pressure.

7.6.5 Results of Petrographic Examination

Inclusions type A. This is the most abundant type by far. It consists of slightly rounded cubic cavities (Plates 7.13 and 7.14) filled with liquid and generally no other phase, except for rare tiny vacuum (shrinkage) bubbles that comprise ~1% by volume of those inclusions having bubbles. Only about 0.1% of the inclusions have bubbles, usually the larger inclusions only, but there are exceptions (see below). Type A inclusions occur as dense irregularly shaped clouds of randomly distributed but crystallographically oriented inclusions (e.g., Plate 7.16). In such dense arrays, individual inclusions are rarely over 20μ m on an edge (Plate 7.18), few are >5 μ m, and most are in the range 0.5-2.0 μ m, with the highest concentrations in the smallest sizes (Plate 7.19). Estimates of the maximum number of such inclusions, based on counts of representative volumes, show about one inclusion per 100 μ m^3, or 10^{10} per cm^3. If these are assumed to average one μ m^3 in volume, such cloudy halite would contain about one volume percent of fluid.

In addition to these irregular clouds, abundant type A inclusions occur in crystallographically arranged (cubic) planes and zones in the host halite, frequently with parallel inclusion-free zones (Plates 7.13 and 7.14).

In some zones type A inclusions grade into more sparsely distributed but larger inclusions ($\leq$ 100 μ m), as seen in Plates 7.14 and 23-24. These coarser inclusions may represent incipient recrystallization of the host. The distinction between these larger type A inclusions and type B (next section) may seem inexact, but actually there is little overlap.

Inclusion type B. Type B inclusions, although far less abundant than type A, carry most of the inclusion fluid in these samples, since they are much larger ($\geq$ 100 μ m to several millimeters). Although large, many have no bubble as found (Plate 7.20), but may develop one if cooled slightly ($\sim$ -7°C) and warmed back to room temperature. They are generally irregular if large ($\geq$ 500 μ m) and are more nearly euhedral negative cubes if smaller (Plates 7.15 and 7.17). They occur as single isolated inclusions in otherwise almost optically clear halite, and as dense groups of many inclusions, in part interconnected with tubular extensions (Plate 7.15).

The host halite for type B inclusions may occasionally have cloudy wisps of type A inclusions, but they are never immediately adjacent to a large inclusion (Plates 7.15 and 7.17). These features suggest that salt originally containing only clouds of "primary" type A inclusions has been partly or completely recrystallized to form coarser crystals of clear salt with type B inclusions. This interpretation is supported by the grain size of the host salt, which is almost always coarser in those parts of a sample containing type B inclusions (see Table 7.13 in next section on weight percent of fluid). The boundary between cloudy primary and clear recrystallized salt is sometimes curved (Plate 7.16). If it were straight, it might not be possible to distinguish it from a primary growth zone boundary between fast cloudy and slow clear growth. Most areas of type A occur as irregular masses within single crystals of mainly recrystallized halite (Plates 7.15 and 7.17).

Relatively few samples, particularly sample 1902.2, show birefringent crystals of an unidentified phase inside what appear otherwise to be type B inclusions. These are equant to bladed crystals of moderately high birefringence ($\sim$ 0.06) and moderate index of refraction (but well above that of the surrounding brine). Many are twinned (Plates 7.25 and 7.26), and when prismatic or bladed, the extinction positions are strongly inclined to the crystal elongation. As the distribution of these crystals is irregular, and as a similar birefringent phase occurs in some of the same samples (Plate 7.27) the occurrence in the inclusions might be interpreted as accidental trapping of solids present at the time of

trapping of the inclusions. All 10 inclusions in one group in sample
1902.2 (Plate 7.27) contain these crystals, in roughly the same amount
(estimated at ~ 5% by volume), thus suggesting that they are true
daughter crystals, formed by precipitation from the trapped fluid.
Another plane of inclusions in this same sample, only 400 μ m away,
contains only liquid (Plate 7.28) so it is concluded that the fluids
present during recrystallization changed in composition with time.

Inclusions Type C. This type is similar to type B in size, shape, and
occurrence, but rarer, and differs only in containing a relatively larger
gas bubble, of variable volume, but > 1% by vol. (Plate 7.29). A larger
gas bubble can originiate by several processes -- leakage, necking down,
higher temperature of trapping, or primary gas. The gas bubbles in these
inclusions are found to be under pressure (see "Results of crushing stage
studies"), so it is believed that such inclusions have trapped a mixture
of gas and liquid (i.e., primary gas). In some (e.g., Plate 7.30), such
inclusions have apparently formed by a refilling of an earlier type B
inclusion with a gas-liquid mixture along a crack.

Inclusion Type D. This type occurs in curving planes outlining some of
the individual crystal boundaries (Plates 7.31 and 7.32). It was
probably full of fluid under natural conditions, but as the grain
boundary permitted leakage and desiccation, these are now full of gas
(presumably air).

7.6.6 Weight Percent of Fluid

A summary of the results of measurements of the volume percent of fluid
in the inclusions is given in Table 7.13. In calculating these volumes
some simplifying assumptions had to be made, in addition to those
mentioned in Section 7.6.5. For simplicity the host salt volume counted
was categorized as type A or B on the basis of the maxiumum size of
inclusions it contained. If these were ≤ 1 mm, it was called type A.
This division is not the same as given in the descriptions of type A and
B inclusions, where ~ 100 μ m inclusions are considered as probably
indicative of recrystallization, but this has little effect on the
results, since on the average, over 90% of the fluid is present as type B

inclusions > 1mm in about 30% of the volume of the salt. Table 7.13 shows that these samples now contain a total of from 0.17 to 2.86% fluid by volume, and average 0.61. These values correspond to 0.1 to 1.7 weight percent fluid as extremes, and average 0.36 weight percent. These results are compatible with those reported in Sections 7.5.2 and 7.5.3.

These values have a measurement error of about ± 5% of the amount found. Much larger, however, is the variability introduced by the samples themselves. Thus three parallel plates were cut at ~ 3-cm intervals through samples 2272, and yielded 1.23, 0.36, and 0.20 volume percent fluid.

Even more important to consider is the bias inherent in these measurements due to substantial and unpreventable loss of inclusions. Examination of the cores showed some centimeter-sized cavities, the sites of former fluid inclusions. No inclusion this size could possibly be included in our count since the plates counted had to be <1 cm in thickness to be translucent. In addition, in situ all natural intergranular porosity in these salt beds was possibly full of fluids. The type D inclusions found represent probably only a trivial part of the total in situ water content present as such "imperfectly sealed fluid inclusion." Large scale in situ porosity tests would be needed to evaluate this variable.

7.6.7 Results of Heating Stage Studies

Only 35 inclusions were run, as listed in Table 7.14. These are mostly from type B inclusions. Some of these inclusions had to be cooled to below room temperature to nucleate a bubble before the run (Plates 7.20, 33 and 34). Why some very tiny inclusions have vapor bubbles (Plate 7.36), yet many large ones have persisted metastably as stretched liquid (i.e., one phase) is puzzling. The data are too sparsely distributed to determine whether the range of values (20.4 to 45.5°C) represents a real difference between samples. One group of inclusions in sample 2821 with birefringent daughter crystals showed no change in the crystals on heating to 24.5°C.

7.6.8 Results of Freezing Stage Studies

Inclusions in NaCl have a special type of behavior on freezing, as a result of reaction of the water of the inclusions with the walls to form the new incongruently-melting phase hydrohalite ($NaCl.2H_2O$), at temperatures below $+0.15^{\circ}C$. As a result, the inclusion enlarges and becomes full of birefingent crystals upon being held at low temperatures. Evidence of this expansion remains on warming to room temperature. Furthermore, the volume resulting from expansion to form ice is frequently larger than the original volume of the inclusion, and the inclusion's walls crack to relieve the pressure (Plate 7.35).

The freezing data are summarized in Table 7.15. If the solution present is simply NaCl and H_2O, the last crystal of hydrohalite will melt at $+0.15^{\circ}C$, assuming equilibrium has been obtained (which is an extremely slow process for this phase). Although only relatively few large type B inclusions were run, many smaller type A inclusions were also watched at the same time. None were found to have either first melting at -21° or freezing at $+0.15^{\circ}C$, so none consist of essentially pure NaCl solutions. Much hydrohalite formed in these inclusions, but as there were birefringent crystals (generally with birefringence less than that of hydrohalite) that persisted well above $+0.15^{\circ}C$, the last solid is a phase other than hydrohalite, and the solutions must contain significant quantities of materials other than NaCl (Plate 7.37). This is also very evident from the first melting temperatures.

7.6.9 Results of Crushing Stage Studies

Bubbles in types B and D inclusions from several samples were examined on the crushing stage. All disappeared immediately on opening, indicating that they consist of water vapor (at $\sim$ 20 mm pressure), and hence collapse at one atmosphere. The bubbles in several type C inclusions showed considerable expansion, however, indicating gas under pressure. Thus the bubble in the inclusions shown in Plate 7.38 expanded 270% by volume on opening (Plate 7.39), indicating that nearly three atmospheres of noncondensable gas is present. The composition of this gas is unknown at present.

A previously unrecorded inclusion deformation phenomenon was also observed in some inclusions that were in a sample that was under uniaxial stress on the crushing stage at room temperature but had not been broken to release the inclusions. These inclusions developed a scalloped pattern along the corners (Plate 7.40), presumably due to solution at points of stress concentration and redeposition elsewhere. This pattern developed over a relatively few minutes at effectively constant stress. At least some volume change occurred in this process, since the bubble in the inclusion disappeared at constant temperature.

7.6.10 Results of Study of Coarse Water-Insoluble Residues

The weight percent of such residues ranged from 0.005% (sample 2391 to 0.3% (sample 2821). Unfortunately, however, although there were a variety of phases present in the residues, none of the crystals contained visible fluid inclusions. Some samples emitted a petroliferous odor and showed oily films on the water surface during leaching; it is not known whether these represent contamination from the oil-based drilling mud used in part of the coring, or natural oil in the samples (as is present in other salt deposits, as integranular films and inclusions). No oil inclusions were seen in this work.

7.6.11 Decrepitation Tests

These tests were run only on the last nine samples of the first 19. A summary of the test data and results is given in Table 7.16. On examination of the material after the decrepitation tests, several general features were evident. The nature of the test is such that systematic inclusion counts before and after the test on the same sample are impossible. It was obvious that although most of the larger inclusions had decrepitated, and were empty, many small inclusions ($\leq \sim 100$ μ m) had not. These small inclusions appear perfectly normal in distribution, but almost all had developed appreciable vapor bubbles (Plate 7.41), with a vapor/liquid ratio that is obviously higher after heating than that present in two-phase inclusions before heating. Only the 150°C sample still had inclusions without bubbles; a few 10-20 μ m one-phase liquid inclusions were found there. All three samples showed some "steam" inclusions - cubic negative crystals with fillets of liquid

in the corners. No gas under pressure was found in any of the heated inclusions. In most cases, the weight losses increase with increasing run temperature; the several exceptions are probably a result of nonhomogeneous distribution of inclusion in the sample aliquots taken.

Homogenization temperatures were determined on two-phase inclusions remaining in the samples after the decrepitation tests. The results are given in Table 7.17, along with the volume percent of vapor phase, estimated from measurements of bubble diameters.

7.6.12   Study of Suite of Samples from Kerr-McGee

The three samples closest to the lamprophyre dike (See Chapter 3) yielded usable inclusions. (Sample MB-76-5 was too fine grained and opaque to be usable by the sample preparation techniques used here, and will not be considered futher in this report.) In all three samples about 15% of the small inclusions ($< \sim 20$ μm) were without bubbles as received. Most inclusions in all three samples were normal, two-phase inclusions with a small bubble. Homogenization temperatures were determined on a representative group of these two-phase inclusions in each, with results as shown in Table 7.18.

Freezing runs were made on inclusions in two of these samples. In both cases the first melting temperatures were well below that of a pure $NaCl-H_2O$ system ($< -28^{\circ}C$ for MB-77-8 and $< -31.0^{\circ}C$ for MB-76-4). On warming, the last solid phase to dissolve in both samples was an unidentified phase, presumably a hydrate other than $NaCl \cdot 2H_2O$. This dissolved at +11 to +18°C (MB-77-8) and at +4 to +7.2°C (MB-76-4).

One 75- μm inclusion was found in MB-77-8 that yielded an entirely different freezing behavior. This inclusion contains a single homogenous fluid at room temperature, presumed to be gas (Plate 7.43a). On cooling to the range -70 to -75°C this inclusion develops a number of grains of an unidentified solid (Plate 7.43f). On warming to about -68°C, a liquid/vapor meniscus becomes visible (Plate 7.43e), with solid grains

still present. The last of these grains disappears at $\sim -56^{\circ}C$ (Plate 7.43d); on further warming the liquid/gas meniscus becomes faint (Plate 7.43c) and the two homogenize, by expansion of the liquid, at $-20.9^{\circ}C$ (Plate 7.43b). This behavior is difficult to interpret in terms of composition. CO_2 has its triple point at $-56^{\circ}C$, in exact agreement with the disappearance of the solid phase at $-56^{\circ}C$ observed here, but obviously the inclusions cannot contain just CO_2, as there is liquid present at a lower temperature. The nature of the mixture of gases can only be guessed at this time.

The crushing tests in the Kerr-McGee mine samples were most revealing. The normal, small-bubble inclusions contain a vacuum bubble (i.e., water vapor at ~ 20 mm presure). Many inclusions that either had a very large bubble or appeared to contain gas only, from all three samples, were found to contain either vacuum (Plates 7.44 and 7.45), or a partial vacuum (Plates 7.46 and 7.47). These are probably from the trapping of bubbles of steam, with or without some noncondensable gas and brine. All three samples also contained a few inclusions with gas under greater than atmospheric pressure. These inclusions were one-phase as first observed, and except under special circumstances, it is not possible to distinguish between a vacuum, dense gas, or even liquid, in such single inclusions. It is only on crushing, when these inclusions formed bubbles of noncondensable gas in the surrounding fluid, that the internal pressure became evident. By measuring the size of the inclusions before crushing, and the diameter of the bubbles evolved, we obtain a crude measure of the internal pressure, assuming each unit volume expansion corresponds to one bar pressure. In a few inclusions, the contents changed to a two-phase, liquid + vapor system during the expansion (Plate 7.48), but usually the pressure release was too sudden to reveal if there was a transient two-phase condition. The volume expansion varies for different inclusions, from 30- to 40-fold (Plates 7.49 and 7.50) to a maxiumum of perhaps 100-fold (Plate 7.51). As the immersion medium used is an oil in which methane is probably readily soluble, this gas is more likely CO_2, since the bubbles dissolve in the oil very slowly.

Interpretation of the data from the Kerr-McGee mine samples is difficult at this time. The presence of an inclusion filled with a dense CO_2-rich (?) gas in sample MB-77-8, (in halite that was probably molten at the time of intrusion of the dike) is not unexpected, since there is a small amount (0.2-2%) of magnesite in the adjoining rock (M. Bodine, personal communication). The dike shows no evidence of carbonate alteration, however, and there is a problem in explaining the presence of inclusions of low-temperature, gas-free brine, apparently pure steam, and dense CO_2 in the same sample. Formation of these types at different times is obviously required, but there is no other indication of differences in conditions or time of origin.

The temperature at which the dense gas inclusion was trapped is of interest. Although the melting point of pure NaCl is $800^{\circ}C$, other materials present here in the potash ore zone (such as KCl) will lower this temperature. If we assume that the gas inclusion contains pure CO_2, the $-21^{\circ}C$ homogenization indicates a filling density of about 1.03 g/cm^3 (Roedder, 1965). Combining this with the estimate of confining pressure of ~ 38 MPa (380 bars) yields an obviously erroneous "trapping temperature" of $0^{\circ}C$. The several inconsistencies and difficulties in interpretation of the data from the Kerr-McGee samples cannot be resolved until additional studies are made.

7.6.13 Discussion

Geological Significance. Several aspects are evident from these various results. First, the fluids in all the inclusions, both type A in primary salt crystals and type B in recrystallized salt, are strongly saline brines, with significant amounts of other salts present in addition to NaCl. These brines differ from one inclusion to another, indicating that a range of fluids has been present at various times in these beds, but no inclusions with simple NaCl solutions were found, as are found in other salt beds and as might be expected if pure salt beds have been fractured in the presence of meteroically-derived (fresh) ground water. The original deposition of salt occurred from highly-concentrated brines, and

presumably all waters that have passed through these samples since have had dissolved in them amounts of other minerals in addition to NaCl. Such fluids have caused extensive recrystallization of the salt, and presumably other mineralogical changes, so that little of the original salt texture remains. <u>Second</u>, at some stage in this recrystallization, gas-liquid mixtures were present in the pores of these beds. <u>Third</u>, this recrystallization occurred at near-surface temperatures (20-45°C). <u>Fourth</u>, the movement of these fluids must have been slow, as the evidence of extensive inclusion metastability indicates very clean solutions, free from the solid nuclei present in most fast-moving near-surface waters.

The fluids from which the salt crystals making up these beds originally crystallized were exceedingly saline brines with much material other than NaCl in solution, as shown by the freezing data on primary inclusions in hopper salt. These hopper crystals appear to have grown on the surface and then to have sunk, as described by Dellwig (1955). All but about 1% of this original hopper salt texture has been eliminated by recrystallization at some unknown later time, yielding coarser, clearer crystals of salt, and presumably gross changes in the mineral assemblage other than halite. Some of the clear salt surrounding the chevron structures may represent crystallization of these hopper nuclei on the bottom of the basin, but most is believed to be from recrystallization. This recrystallization occurred in the presence of exceedingly saline brines and with much material other than NaCl in solution. The brine may have been composed essentially of fluids from the primary fluid inclusions, released during the recrystallization. It was trapped as large inclusions in the recrystallized salt and comprised the bulk of the liquid now present in the samples as studied in the laboratory. Although the salt beds now appear dry to the eye, the samples contain 0.1 to 1.7 weight % fluid as examined, and may contain more <u>in situ</u>. At some stage or stages early in the history of these beds, the fluids present in these rocks varied in composition. (See section 7.7) A very few were saturated with organic gases such as methane and actually contained bubbles of a separate gas phase. Others contained additional salts in solution, resulting in the precipitation of various crystalline solids

from the liquid within inclusions in halite. The relative time sequence of these various fluids is not known, and most inclusions have neither methane nor crystalline solids. The latest episode of any recrystallization has been dated at 204 million years, slightly younger than Permian.

Homogenization temperatures of inclusions in recrystallized salt range from 20.4 to 45.5°C. During burial, creep from recrystallization in a salt bed with intergranular films of solution should result in the hydrostatic pressure on fluids (during trapping in a crystal) being essentially equal to the lithostatic pressure. If an overburden of 5000 ft. (1524 m) is assumed to have been present during the recrystallization, the maxiumum pressure (lithostatic) would have been $\sim$ 38 MPa (380 bars). There are no PVT data on the specific fluids present in the inclusions, but if the data on a 25-percent NaCl solution are used, this pressure would suggest a maximum pressure correction of 36°C (Potter, 1977), and hence trapping (i.e., recrystallization) temperatures of 56-82°C. However, the true pressure correction may be lower, particularly since the fluids are more saline than 25-percent NaCl. Thus there is a drop of 12°C in the pressure correction on changing from 20-percent NaCl to 25-percent NaCl.

The presence of smooth planes of primary hopper salt inclusions of various sizes, separated by planes of inclusion-free salt, with the plane orientation horizontal, proves that these minute inclusions have not moved measurably since deposition, although they have been in a geothermal gradient presumably similar to that of the present for about 225 m.y.

The widespread occurrence of metastable phenomena in these inclusions, even in some large ones, suggests that fluid flow in the past through these beds has been very slow. Also, the fact that <u>all</u> inclusions that have been frozen prove to contain bitterns, and none was found with just NaCl-H$_2$O solution, proves that at no time during the history of these samples did ground water, saturated <u>only</u> with respect to NaCl, ever penetrate into these particular samples.

Nuclear Waste Disposal Significance. The most signficant aspects at this stage in the study are as follows: First, the amount of fluid water solution now present in the samples as fluid inclusions averages 0.36 weight percent. Second, although noncondensable gases are present under pressure in some inclusions, the total amount is very small. Third, the inclusions change dimensions signficantly within minutes at room temperatures when the host crystal is subjected to uniaxial stress; this might suggest more rapid movement of inclusions in a thermal gradient if simultaneously under stress, as in mine pillars. Fourth, and possibly most significantly, the distribution of primary inclusions indicates that they have not moved visibly (i.e., less than a few micrometers at most), in the 225 million years since they formed, yet they have been in the small but finite geothermal gradient all this time. All fluid inclusions can be expected to move when placed in a thermal gradient. Since there is usually a thermal coefficient of solubility, material will dissolve on one wall and precipitate on the other. The rate of movement is a complex function of numerous variables (including inclusion size), but the temperature coefficient of solubility is probably the most limiting parameter in the case of NaCl. In the pure system $NaCl-H_2O$, the solubility change per 100g H_2O is low, only $0.03gm/^{\circ}C$ in the range of $0-100^{\circ}C$. This increases by approximately a factor of two at the elevated temperatures expected near the wastes. This coefficient is comparable in the $NaCl-MgCl_2-H_2O$ system.

All these aspects will now be treated in expanded detail.

Amount of Water in the Beds. Although this is the most important single datum that might be obtained from inclusion studies, fluid inclusion counting can provide only approximate values. The nature of the samples and the necessary sample preparation are such that there is a bias toward low values built into these data. Superimposed on this uncertainty in accuracy is poor precision in the measurement, due to variability of the sample material. For example, adjacent slabs of the same sample showed a five-fold range. It is probable that precisely calibrated neutron logs, reflecting the amount of hydrogen in the beds, give a more accurate

evaluation of the total water present, since they would effectively integrate over a much larger sample and would include the effects of the liquid-filled intergranular cavities which these tests miss.

One important aspect of the inclusions on the properties of the salt is the effect of the constitutents present on the lowering of the temperature of melting, and on the amount of liquid present at any given temperature. In this connection it is important to note that the inclusions' fluid is not water, but a strong bittern with probably significant quantities of magnesium ions. This will certainly affect the temperature coefficient of solubility of NaCl in these liquids, and will have important effects on the vapor pressure of these liquids (see below).

Corrosive Gases in the Inclusions. Although gas analyses by mass spectrometry are still to be made on the inclusion fluids, it is evident from the crushing studies that the inclusions in these samples, at least, contain very little noncondensable gases. Although hydrogen sulfide was found as an important constituent of gases in a gas pocket in another drill hole, (ERDA-No. 6, Section 7.7), there can be very little, if any, in these inclusions. The human nose is a rather sensitive detector of H_2S, ordinarily responding to a minimum of $\sim 10^{-10}$ g. No odor of H_2S was detected during preparation of these samples, when relatively large volumes of inclusion liquid were exposed to the air. Gases such as HCl formed within the inclusions or by reactions of inclusion fluids with other minerals during heating, and under intense gamma radiation, may be a much more important cause for corrosion than those now present in the inclusions.

Effects of Water on Physical Properties of the Salt. The intergranular porosity in these salt beds, in situ, possibly contains some aqueous solution. Such fluids will tend to be squeezed out of the salt beds over geological time as recrystallization along grain boundaries and other processes permit compaction, just as the residual water in a sandstone is eliminated during the formation of a quartzite. Such flow will occur, however, only if there is an escape route for the fluid to take. As

pointed out very aptly by Baar (1977), there is much evidence from high pressure fluid pockets that salt rocks in situ are generally impermeable at depths exceeding about 300 m. It may well be that under such conditions, which preclude further "dewatering", the fluid in these intergranular films is still able to migrate short distances, enough to permit it to coalesce into "pockets", perhaps at points of slightly reduced pressure, just as a plastic shale will flow to the crest of folds in firmer rocks. These "pockets" might be represented in part as the short-lived seeps observed in potash mines.

Even if the intergranular liquid were to be removed completely, yielding a polycrystalline texture with salt crystals in true contact with each other, there is no driving force to remove the fluid inclusions from within the individual halite crystals. If such a salt bed is deformed to the point of rupture of salt crystals, any inclusions along the rupture will provide water to "lubricate" the fracture and hence lower the apparent strength of the rock. Although one might expect that a new fracture would preferentially follow planes of inclusions, as from the healing of former fractures, Gerlach and Heller (1966) have shown that the salt recrystallized in the vicinity of such a healed fracture is actually stronger than the adjacent unrecrystallized salt, and new fractures could not be made through the inclusions. Actually, most of the fluid in inclusions in the Carlsbad salt is in large, apparently randomly arrayed inclusions in recrystallized salt, and examination of fractures through such samples suggests that cracks induced in the laboratory experiments reported here have preferentially taken routes through such inclusions.

One example of the surprising effects of inclusion fluids on the properties of salt crystals is found in the behavior of fluid inclusions in single crystals of salt under uniaxial stress (Plate 7.40). Under these conditions, fluid inclusions visibly change shape, and volume, within a few minutes, at room temperature. This is a new inclusion phenomenon, never reported before.

Evidence of Previous Solution Movement in These Beds. The fluid inclusion evidence obtained so far on solution movements is encouraging in that it indicates at most only very slow movement, and suggests that part of the fluids now present in these beds may even be nearly Permian in age. The lack of any pure $NaCl-H_2O$ inclusions also argues against any previous sudden inrush of groundwater that could be trapped as inclusions in halite before it had time to acquire a full complement of other salts.

Movement of Inclusions in a Thermal Gradient. All fluid inclusions should move when the host crystal is placed in a thermal gradient. The nature and rate of such movement has been the subject of numerous studies, since it is of consequence in the chemical industry. Wilcox (1968) summarizes this extensive work (citing 111 references). Similar migration of inclusions is also an important cause for degradation of laser crystals grown at high temperatures by the Czochralski technique (Hopkins et al., 1976). Most liquid inclusions move up the thermal gradient, but if the vapor bubble is large relative to the liquid, and particularly if boiling occurs, the movement may be in the reverse direction (Wilcox, 1969; Anthony and Cline, 1972; Chen and Wilcox, 1972). The rate of movement is independent of inclusion size in many systems, but strongly (and directly) dependent on inclusion size in others (Wilcox, 1969); there may be a threshold size below which no movement occurs (~ 10 µ m in KCl; Anthony and Cline, 1971a). Large inclusions may break up during movement (Wilcox, 1968; Anthony and Cline, 1973). Many factors may affect the rate of migration, even in a given host, including gravity, composition, surface tension, inclusion shape, crystal anisotropy and imperfections, presence of a foreign gas, etc. In salt, since the thermal coefficient of solubility is small at surface temperatures, but increases greatly with increase in temperature, the rate of movement in a given gradient can be expected to increase with increase in ambient temperature. Higher ambient temperature also increases the travel rate by increasing the solubility, the diffusion coefficient, and the interface kinetics, and the increase in rate was found to be particularly striking in NaCl (Wilcox, 1968, p. 20). The

fact that the inclusions in Carlsbad salt have not moved measurably during geological time in the geothermal gradient is perhaps an indication of exceedingly slow rate, or perhaps a result of a very weak driving force.

Accurate prediction of behavior of in situ inclusions in the thermal gradient around a canister in salt cannot be obtained at this time, as there are too many uncontrolled variables. Since most inclusions at Carlsbad contain no bubble or only a very small bubble, they will move toward the canister, as was shown to occur at Project Salt Vault (Holdoway, 1974). The rate of this movement will depend most particularly on the inclusion size, the ambient temperature of the grain, the temperature gradient, and the temperature coefficient of solubility of NaCl in the particular inclusion fluid involved. The average distance that an inclusion must travel before it intersects a grain boundary will vary with the grain size of the salt, but seldom would be over 1 cm.

What can be expected when the inclusion reaches a grain boundary? Anthony and Cline (1971b) showed that grain boundaries in crystal aggregates tend to trap migrating droplets, but Anthony and Sigsbee (1971) showed that gas bubbles (10-50 μm) migrating in polycrystalline camphor could cross grain boundaries. However, migrating bubbles were observed to drag grain boundaries when the bubble concentration on the grain boundary was large. In Project Salt Vault, Holdoway (1974) says only that "little migration across grain boundaries appears to have occurred." Obviously, if a grain boundary is very tight, a large inclusion could cross it without effect. But if the grain boundary is composed of different material, the fluid could spread out along it as a film. Any such film should act as an inclusion, with material diffusing across it away from the heat source.

The behavior of an inclusion migrating to the wall of an open cavity (e.g., that holding the canister) will be different. On contacting the cavity, Anthony and Cline (1974) and Wilcox (1968, 1969) have shown that

some evaporation occurs, a vapor bubble forms, the inclusion seals itself, and now that it has a large bubble, it reverses direction and moves back the way it came, this time going down the gradient.

Decrepitation Release of Liquid Inclusions. In view of the expected slow migration rates of liquid inclusions in the thermal gradients established by the canisters, it seems probable that release of inclusion fluid by decrepitation will be an important process. An individual inclusion, if it is assumed to have rigid walls, to contain 25-percent NaCl solution, and to homogenize at $40^{\circ}C$, will develop 70.0 MPa (700 bars) internal pressure when heated to $100^{\circ}C$, and 200 MPa (2000 bars) at $200^{\circ}C$ (Potter, 1977). However, salt cannot stand such internal pressures without yielding. Even a strong, hard mineral such as quartz starts to decrepitate when the internal pressure in its fluid inclusion reaches 80 $\pm$ 3 MPs (800 $\pm$ 3 bars) (Khetchikov and Samoilovich, 1970), and halite can be expected to decrepitate when the internal (inclusion) pressure reaches four times the yield stress for monolithic halite, under no confining stress (Cline and Anthony, 1971).

When Carlsbad halites were heated, some of the inclusions decrepitated in part causing the samples to fragment, and yielding an average weight loss of 0.13% ($150^{\circ}C$), 0.22% ($200^{\circ}C$), and 0.73% ($250^{\circ}C$). This means that this much volatiles left the system. More inclusion fluid may well have been exposed, and merely lost water until its concentration of salts was such that the vapor pressure of H_2O at that temperature was less than one atmosphere. Salts in solutions in these brines (including materials other than NaCl as well) have effects on the vapor presure and hence on any vapor transport.

In addition to those inclusions that decrepitated, however, many inclusions remain sealed as liquid inclusions in the sample after heating, albeit in a changed form. These have permanently deformed their walls to form a larger chamber, and now have a much larger shrinkage bubble, proportional to the amount of expansion. (Why some decrepitate and others expand is at present unanswered; residual stresses in the host

crystal may be involved.) This expansion phenomenon is not new - it has been reported at various times in the past. It is the net result of several volume changes during heating of the inclusion. On heating, the host salt expands, enlarging the cavity as well. This effect is small, yielding a cavity volume increase of only 1.2% from 40 to 140°C. The fluid in the inclusion dissolves more salt from the walls on heating; the net volume effect of this (generally a decrease; i.e., an increase in cavity volume) will vary widely with the composition of the solution. Thermal expansion of the brine would develop high pressures if the walls were rigid, but instead, in the presence of liquid, the inclusion walls frequently just expand. The amount of expansion is roughly proportional to the temperature of heating, i.e., the inclusion fluid streches the walls until its internal pressure drops just below that needed to cause further stretching at that temperature. Nucleation of a vapor phase may even occur (Geguzin and Dzyba, 1973), in which case loss of water to the expanding vapor phase also helps to limit the expansion. Some of the thermodynamic variables of the process have been modeled by Cline and Anthony (1971) for the pure halite system.

7.7 THE GEOCHEMISTRY OF DELAWARE BASIN GROUNDWATERS IN RELATION TO THEIR HOST ROCKS

7.7.1 Introduction

Geochemical studies of waters found in Permian and younger rocks of the Delaware Basin (Southeast New Mexico, West Texas) have assumed a new importance in recent years. This began in 1975 when Sandia Laboratories, in cooperation with the United States Energy Research and Development Administration undertook studies of the suitability of Delaware Basin evaporite deposits for the long-term storage of radioactive wastes generated by the national nuclear defense program.

In particular, three aspects of fluid geochemistry have bearing on an understanding of the geology of the area:

1. Rock history - the relationships between dissolution features and nearby fluids which may have dissolved evaporites.

2. Fluid history - evidence of rock/fluid interactions preserved in fluid chemistry, indicating the complexities of fluid movement.

3. Fluid origins - the ultimate sources of fluids which have participated or have potential for participating in dissolution of evaporites.

Many of the waters considered here were bailed from preexisting wells with the assistance of the United States Geological Survey, between December, 1975, and June, 1976. In addition, boreholes for subsurface exploration of Los Medanos (the ERDA study area) tapped some fluid producing zones. These holes include ERDA No. 6,. which at a depth of 2711 feet produced saturated brine associated with H_2S-rich gas from the Castile Formation. In this hole, stratigraphic marker beds were found several hundred feet above their expected positions (Anderson and Powers, 1978). Nine holes penetrating the Rustler Formation have facilited hydrological testing and sampling of Rustler waters. Finally, samples of waters were collected from pools in Carlsbad Caverns. Table 7.19 is an inventory of water samples, together with their collection locations. New Mexico locations are given in Figure 7.10, showing their distribution with respect to the Capitan Limestone.

Three geochemical approaches will be followed in this subchapter. Each approach will consider a few examples of various "types" of water:

1. Solute chemistry - dissolved solids content.

2. Thermodynamics - equilibia and non-equilibria of a fluid-gas system.

3. Stable isotope ratios - variations in deuterium and oxygen - 18 content.

7.7.2 Data

Analytical results for the 29 waters are given in Table 7.20. Solute
analyses are expressed in mg/l, performed according to APHA (1971)
methods, with modifications by Collins (1975). Analyses by Martin Water
Laboratories have a precision of about $\pm$ 5 to 10%; others $\pm$ 3% (Table
7.19).

Stable isotope analyses were made according to Epstein and Mayeda (1953)
and Bigeleisen et al (1952), and are reported in " δ " notation as
deviation of the D/H or $^{18}O/^{16}O$ ratio from the corresponding ratio of
Standard Mean Ocean Water (SMOW) (Craig, 1961b, Epstein and Mayeda,
1953), in parts per thousand (‰, "per mille") for example:

$$\delta D = \frac{(D/H)\ sample - (D/H)SMOW}{(D/H)\ SMOW} \times 1000$$

The precision of $\delta\ ^{18}O$ values is better than $\pm$ 0.1‰ and that of δ D
is better than $\pm$ 1‰ .

Solutes. In this discussion "fresh water" is taken to contain less than
3000 mg/l total dissolved solids (TDS), and is potable at least to local
cattle. "Brackish water" refers to TDS contents between 3000 and 30000
mg/l. Brines are waters containing more than 30000 mg/l TDS. According
to these definitions, number 1, probably 18 and 26 through 29 (Table
7.19) are fresh waters, found in the Capitan and Santa Rosa Formations.
Numbers 2, 6, 11, 17, 22, 24 and probably 19 through 21 are brackish, and
include most Rustler waters, one Capitan and one Castile. The fresh and
brackish waters contain the solutes expected to be found in carbonate and
anhydritic or gypsiferous aquifers. All the other waters are brines, and
include the Salado, Morrow, Delaware (Bell Canyon) waters, two Castile,
one Capitan, and even two Rustler waters; these Rustler samples came from
the Culebra dolomite member, adjacent to halite-bearing parts of the
Rustler Formation.

Brines are treated in the most detail here, since their presence has implications regarding either their representation of original evaporite mother-liquors, or their solutes having been derived through rock-water interaction. Their geochemical complexity cannot be understood from solute chemistry alone, and a brine occurrence in a particular rock unit does not necessarily imply that the brine has interacted with its host rock.

The chloride/bromide ratios, where obtainable, of all the brines were between 430 and 900, compared to 292 for modern sea water (Collins, 1975). If the Permian Basin water had a Cl/Br ratio similar to that of sea water, as suggested by Holser (1963) for fluid inclusions in Kansas salt, then these Delaware Basin brines do not contain "original" Permian water as a major component. Since halite crystallizing from sea water selectively excludes bromide from the NaCl lattice, halite has a Cl/Br greater than 300 (Adams, 1969), as would brine resulting from the dissolution of halite. Hence, the sodium chloride in these brines has been dissolved from rocks, but not necessarily the rocks in which the brines were found.

Rather than discuss abundances of individual ions in brine solutions, it is more instructive to consider solute ions combined as solids which might be expected to precipitate from solution upon complete evaporation. Following the crystallization sequences compiled by Braitsch (1971), not only some similarities will be noted between the resulting normative mineral assemblages, but also some significant differences. Waters 16, 9, and 14 (Salado, Bell Canyon, Castile) will be presented as examples.

Water from the Duval Mine Vent Hole is similar to the other potash mine seeps (Numbers 3, 4 and 5) all of which are saturated solutions. Table 7.21 shows the relative proportions of minerals expected to precipitate from this solution. This assemblage is similar to that expected to precipitate from sea water, even though the relative proportions are different (note the overwhelming preponderance of carnallite). In view

of the incongruent dissolution of polyhalite resulting in a calcium-poor
solution, this brine is what one would expect for water which has
dissolved a potash deposit. Note the presence of normative borax, an
evaporite mineral not commonly reported in the Carlsbad potash district
(cf. Jones, 1975).

Waters from the more saline portions of the Capitan aquifer (numbers 11,
12 and 13) contain the normative assemblage dolomite-anhydrite-kainite(or
carnallite)-halite±sylvite, in various proportions, and are also
indicative of solutes obtained by dissolution of adjacent evaporites.

Water number 9, from the Bell Canyon Formation, is examined in Table
7.22. The solution is calcium-rich, as indicated by the less common
minerals tachyhydrite and antarcticite. These two minerals are not known
to precipitate from sea water, and together with a magnesium deficit
distinguish this water from a simple solution of primary evaporites.
Graf et al. (1966), have given attention to the origin of calcium
chloride waters, and emphasized shale ultrafiltration as an explanation.
Other possibilities include diagenetic reactions in which magnesium in
solution displaces calcium in carbonates to form dolomite, or in which
Mg-rich sheet silicates are formed, having given up more easily
replaceable cations such as Na and Ca (Grim, 1968), which were present in
the original minerals (kandites and smectities). Mg-rich sheet silicates
are present in the Ochoan evaporites overlying the Bell Canyon (see
subsection 7.4). Since brine number 9 is a saturated solution, and since
calcite, not dolomite is the prevalent carbonate mineral of the Bell
Canyon, neither dolomitization nor shale ultrafiltration (which tends
also to produce a low-Ca water, which has not yet been found) appears to
be a satisfactory model for the in situ evolution of Bell Canyon brine.
The sulfate deficiency could have arisen from biogenic degradation of
sulfate. The most likely explanation for the in situ Ca-enrichment is
ion exchange. This brine probably did not originate in the Bell Canyon,
but its solutes probably came from nearby evaporites.

Waters 8 and 10 have a much lower TDS content than does 9, but otherwise yield most of the same minerals. The high strontium content of all three could be taken to indicate that these waters have indeed participated in the recrystallization of carbonates, but probably not within the Delaware Mountain Group of sandstones, which includes the Bell Canyon Formation. According to the Sr/Ca studies of Oxburgh et al. (1959), this solution would have been in equilibrium with a calcite containing about 4000 ppm Sr, a value too high for most natural calcites and dolomites. The Sr in solution could easily have come from the diagenetic alteration of aragonite outside the Bell Canyon.

On July 30, 1975, borehole ERDA No. 6 produced saturated brine (number 14, Table 7.19) and H_2S-rich gas (0.16 cubic feet STP per gallon) from a fractured, gray, laminated Castile anhydrite unit 2711 feet below the surface. Similar phenomena in the Castile have been reported by oil companies, but with an order of magnitude more gas. The analysis of one other such brine (Shell Bootleg, number 15 in Table 7.19) is given in Table 7.20, and is quite similar to the ERDA No. 6 brine. The solutes are resolved in Table 7.23, and aside from thenardite and LiCl (resulting from an almost economic concentration of lithium) are similar to the case of the dissolved potash deposit. Na_2SO_4 has been previously reported in subsurface brines (Reeves, 1963), and thenardite is known to precipitate from local surface lakes. Lithium is a common component of evaporites formed near igneous rocks, but the nearest igneous rock is several kilometers away (Calzia and Hiss, 1978). The brine is sodium-rich and magnesium poor. Once again in terms of ion exchange, a loss of evaporite-derived magnesium into silicates, which give up sodium, appears to be the mechanism here, although this need not have taken place in the Castile. Such like processes may account both for magnesium depletion in the solution and the formation of magnesium silicates in the evaporite sequence.

Thermodynamics. The ERDA No. 6 gas and brine are the only fluids which lend themselves to multiphase thermodynamic considerations. The gas amounted to 1.22 liters (STP) per liter of liquid, and consisted of

55% CO_2, 28% H_2S, 15% CH_4, 1.5 N_2 and 0.5% C_2H_6, determined

mass spectrometrically. The H_2S is not saturated in the solution, even

in the light of the salting-out effect of high TDS content (Randall and

Failey, 1927), and amounts only to 0.02 molal. In order to examine the

role of sulfur in this system (the only multivalent element common to

both liquid and gas phases) a predominance area diagram (cf. Garrels and

Christ, 1965), was constructed for the system S-O-H with the variables pH

and oxygen partial pressure, and with total sulfur equal to 0.36 molal

(approximating the sulfate and H_2S in solution). The resulting diagram

is Figure 7.11, for the field-temperature of 25°C. The field-measured

pH is 6.3, and samples of the brine containing dissolved H_2S were

observed to precipitate elemental sulfur upon standing at atmospheric

conditions. The diagram shows that at pH 6.3, the sulfur field occurs

between the sulfate and H_2S fields. Thus, the diagram correctly

predicts the oxidation of H_2S to sulfur, and the sulfate and H_2S

cannot be in thermodynamic equilibrium with one another at pH < 7.

Unfortunately, the oxidation potential was not measured, and the precise

position of the ERDA No. 6 system on the diagram is not known. The most

probable origin of the H_2S is biogenic reduction of sulfate, an ion

abundant in the surrounding rocks as anhydrite as well as in solution.

Kuznetsov et al (1963), have indicated that bacteria such as

Desulfovibrio aestuarii can exist in saturated NaCl solutions, although

their activity is inhibited by bivalent cations, which are not prevalent

in the ERDA No. 6 brine.

Stable Isotopes. Analysis of water samples for their $^{18}O/^{16}O$ and D/H

ratios has been found to be a useful method of identifying the source of

water molecules, and to some degree identifying the types of interactions

the water has undergone in the presence of other phases.

Figure 7.12 is a δ D versus δ ^{18}O plot for Delaware Basin

groundwaters. Most of the earth's meteoric waters have isotopic

compositions which fall between the lines described by the equations:

$$\delta D = 8 \ \delta \ ^{18}O + 5 \ \text{(Epstein et al., 1965; 1970)}$$

and

$$\delta D = 8 \ \delta \ ^{18}O + 10 \ \text{(Craig, 1961a)}.$$

These lines are included in Figure 7.12, and the area between them is labelled "Meteoric Field."

Most of the points in Figure 7.12 lie in or near the meteoric field. Except for Carlsbad Caverns, a $\delta \ ^{18}O$ value of -7‰ and a δD value of -50 ‰ appears to be a good approximation to local meteoric water in the Delaware Basin. The Caverns are part of the hydrologic system independent of the rest of the Capitan. Their enrichment in D and ^{18}O reflects the water's origin from air mass conditions different from those which produce other Basin rains.

Bracketing the cluster of meteoric points are two dashed lines whose intervening field is labelled "evaporation." This field is the trajectory of isotopic compositions that the meteoric waters would follow during evaporation. The trajectory slope is 5, according to Craig et al. (1963). The few points that lie in or near the evaporation field (4 Rustler and 1 Castile) may indeed have suffered partial evaporation prior to infiltration, but definitely originated as metoric water.

The dashed line through the origin, also of slope 5, is the trajectory of isotopic compositions of evaporating sea water. This line is also valid for the evaporation of warm-climate coastal meteoric waters ($\delta \ ^{18}O \approx -2‰$, $\delta D \approx -10‰$, as indicated by the intersection of this line with the meteoric field. Such waters were postulated by Holser (1963; 1966) to have been potential contributors to the Delaware Basin. The figure shows that the waters of positive $\delta \ ^{18}O$ values are not the products of partial evaporation either of Delaware Basin water or of modern meteoric water. This conclusion is the same as that drawn from the Cl/Br ratios.

The environments in which the Salado, Morrow and Delaware (Bell Canyon)
waters were found involved a rock/water ratio that was very large, as
deduced from the low productivity of these reservoirs. Consequently, any
interaction involving isotopic exchange between these waters and host
rocks would tend to alter the isotopic composition of the water
toward δ D and δ^{18}O values consistent with equilibrium isotopic
fractionation between water and minerals in the rock. Calcite in the
Bell Canyon Sandstone had a δ^{18}O value of +25.1‰, a value only
slightly less than typical marine carbonate. This implies only minor
isotopic alteration of easily exchanged carbonate oxygen in the rock
through the action of water, and indicates lack of calcite-water isotopic
equilibrium in the Bell Canyon. The oxygen and hydrogen in clay minerals
are known to be readily exchangeable with water (O'Neil and Kharaka,
1976). The Delaware, Morrow and Salado waters have isotopic compositions
that are suggestive of at least partial isotopic exchange between local
meteoric waters and clay minerals in the sediments, in which the
mineral/water ratio was very large (cf. Savin and Epstein, 1970) for at
least several thousand years. Other mineral sources of exchangeable
oxygen and hydrogen are fluid inclusions, whose stable isotopes have yet
to be studied, and the water of crystallization of many evaporite
minerals. The potash seep waters may have interacted with hydrous
minerals. However, gypsum-water is the only such mineral-water system
for which the ^{18}O/^{16}O and D/H fractionation factors are known.

None of the waters have resulted directly from the dehydration of gypsum
to form anhydrite. If ERDA No. 6 were such a water, the point marked "G"
in Figure 7.12 would be the isotopic composition of the water from which
that gypsum precipitated (using the gypsum-water fractionation factors of
Fontes and Gonfiantini, 1967). "G" is not consistent with evaporating
Delaware Basin water, whose anticipated δ D - δ^{18}O trajectory was
discussed above. The isotopic composition of ERDA No. 6 brine is
consistent with an approach to isotopic equilibrium between water and
clay minerals, not necessarily in the Castile. Its isotopic exchange,
together with its history of cation exchange, has resulted in a brine
whose history appears to be similar to that of oil field brines of
Alberta and the Gulf Coast (cf. Clayton et al., 1966).

7.7.3 Summary

Many types of rock/fluid interactions are evident in the geochemistry of
groundwaters found in the Delaware Basin. It is not possible to
completely characterize these interactions from solutes or stable
isotopes alone, nor through a study of water alone without a similar
study of rock. In addition to fresh and brackish waters, which have
acquired solutes from their host rocks, the brines have here illustrated
three examples of various types of rock/fluid interactions:

1.   dissolution of evaporites (saline Capitan waters).

2.   dissolution of evaporites with isotopic exchange between fluid
      and rock (Salado potash seeps).

3.   dissolution of evaporites, isotopic exchange, and cationic
      exchange (Delaware, Morrow and ERDA No. 6 waters).

The latter two types indicate more profound interaction than the first,
since these involve changes in the water molecules themselves.

No original Permian waters could be identified. If much of the evaporite
section has been recrystallized, as Holser (1963) suggests, not even the
fluid inclusions are expected to preserve such waters.

7.8 RUBIDIUM-STRONTIUM SYSTEMATICS OF THE SALADO FORMATION, SOUTHEASTERN
     NEW MEXICO

7.8.1 Introduction

One of the important reasons for studying bedded salt deposits for a
radioactive waste repository is to determine their intrinsic geological
stability and to understand the behavior of alkali and alkaline earths in
such a system assuming leakage of isotopes such as ^{90}Sr and ^{137}Cs.

If it can be demonstrated that such isotopes are likely to be retained at or very near the possible leakage area, then the potential danger of such leakage is minimized. Alternately, if it is found that there has been widespread migration of alkali and alkaline earth elements in the prospective storage sites, then these sites may be unfavorable for retention of ^{90}Sr, ^{137}Cs, etc. assuming leakage occurs. Furthermore, if the latest episode of diagenetic evaporite recrystallization can be dated, arguments can be made for the geochemical requilibration of the evaporite assemblage into a thermodynamically stable configuration, reducing the liklihood of such events in the future.

To address this problem the WIPP study area and nearby sites were chosen for investigation, utilizing the well-established Rb-Sr geochronologic method of age determinations. This method is especially well suited for addressing alkali and alkaline earth retention and/or migration because of the species involved and its simplicity. Because of geochemical similarities (ionic radii, ionization potential, charge) Rb can be used as an analogue for Cs, and ^{90}Sr will behave as any other Sr isotope. Hence the Rb-Sr ages will allow, in theory, meaningful interpretation of the stability of the Salado Formation in terms of Rb and Sr retention and/or migration.

The basic age equation is:

$$T = \frac{(^{87}Sr/^{86}Sr)_m - (^{87}Sr/^{86}Sr)_o}{(^{87}Rb/^{86}Sr)_m \ (\lambda)}$$

where:

T = age in years

$(^{87}Sr/^{86}Sr)_m$ = measured isotopic ratio normalized to $(^{86}Sr/^{88}Sr) = 0.1194$ (the average abundance ratio in the earth)

$(^{87}Sr/^{86}Sr)_o$ = initial isotopic ratio before $^{87}Rb \ (\beta^-)^{87}Sr$ radiogenic decay (R_o) occurs.

$(^{87}Rb/^{86}Sr)_m$ = measured isotopic ratio

(calculated from Rb/Sr ratio).

(λ) = decay constant for ^{87}Rb

= 1.42 x 10^{-11}/y.

The $(^{87}Sr/^{86}Sr)_m$ term is the sum of

$(^{*87 + 87}N)Sr/^{86}Sr$

where *87 and ^{87}N refer to radiogenic and normal mass 87 respectively.

The initial ratio $(^{87}Sr/^{86}Sr)_o$ can either be assumed, determined by measurements on Rb-free phases formed at T =0, or determined by extrapolation from an isochron (i.e. line of slope $e^{T\lambda}$- 1 along which all samples of the same age and initial ratio but with different Rb/Sr ratios will fall; see Faure and Powell, 1972). The last of these choices is considered the most reliable due to natural variations of the initial ratios in nature, even from supposedly uniform, Rb-free, reservoirs.

7.8.2 Previous Work

K-Ar dating of evaporites has been shown by numerous investigators to be extremely risky (see discussion in Faure, 1977) due to loss of radiogenic ^{40}Ar by diffusion and other processes. Some K-Ar ages have beeen attempted for salts from the WIPP study area at Los Medanos (Shell Dev. Co.; 1973). For sylvites, minimum dates from 18 ± 8 to 74 ± 8 m.y. were obtained while two langbeinite-sylvite mixtures yielded nearly identical dates of 137 ± 8 and 147 ± 8 m.y. Only one very pure langbeinite (18%K) yielded a date of 245 ± 10 m.y.; this date is in excellent agreement with the 225-240 m.y. age range assigned to the Late Permian evaporites of the Castile and Salado formations.

The only other officially reported work is that by E. L. Tremba (1973; unpub. Ph.D. dissertation) in which he reports widely scattered data for evaporites from the Los Medanos area. Tremba's (1973) work was not directed toward problems of local alkali or alkaline earth migration, however, and composite samples were commonly taken which would, in

effect, mask any such local effects. He reports two model Rb-Sr dates of 241 ± 23 m.y. and 208 ± 8 m.y. respectively for (1) a K-ore zone from the Saunders Mine and (2) two separate aliquots of a water-soluble K-ore. An initial ratio of 0.7077 was used in both cases. For water soluble samples from mine faces within the Saunders Mine, Tremba reports a 129 ± 5 m.y. isochron but, without adequate justification, one point (#3SS) is omitted from the isochron calculation. As a model age for this one point yields an apparent model date of 330 m.y. (R_o = 0.708), then the significance of the 129 ± 8 m.y. date, based on only 4 of 5 samples, is difficult to interpret.

Similarly, five samples from Tremba's core 184, first ore zone, yield an apparent isochron date of 120 ± 28 m.y. but with an extremely high initial ratio of 0.7226 ± 0.0092. The argument is made that the two 120 to 129 m.y. isochrons can be explained by some type of Cretaceous "rehomogenization event". This interpretation can be criticized because 27 low-K samples from core 184 yield a mean $(^{87}Sr/^{86}Sr)_m$ = 0.7077 ± 0.0001; and any hypothesized rehomogenization event must explain how selective parts of the core can be affected whereas others are not. For example, Tremba argues that recrystallization involving polyhalite may have taken place at approximately 120 m.y. ago at which time the initial ratio was increased by rehomogenization to above 0.72; yet the data in Table 7.24 yield at least one sample (ERDA-9, 1759.1-1759.8) with $^{87}Sr/^{86}Sr_m$ = 0.7064. Furthermore, if one uses the individual points for Tremba's 129 m.y. isochron and assumes an initial ratio of 0.7077 (based on his data), a range in model dates results from about 185 m.y. to 100 m.y. (not counting sample EV-13 with a very low $^{87}Rb/^{86}Sr$ ratio). The reason for this apparent scatter is unanswered by Tremba's work.

7.8.3 Analytical Procedure

Sample Preparation. Samples studied thus far have been core segments from WIPP exploratory holes. The core segments were about four inches in diameter and ranged in length from 4 to 12 inches. These samples first

were trimmed by air saw to remove all outer surfaces that may have contacted drilling brines or been otherwise contaminated. Only the remaining prism of rock was retained for analysis; the outer portions were stored for possible use in the future.

Enough of the remaining inner portions were ground to -100 mesh.to produce approximately 200 g of rock powder. About 30 g of this.powder was quartered out and saved for whole rock analysis.

Separation of Water-Insoluble From Water-Soluble Material. The concentration of water-insoluble residue in a sample was determined during the separation of the soluble from the insoluble material. Approximately 60 g of powdered sample, weighed to the nearest 0.01 g, was placed in a 250 ml glass centrifuge tube together with about 175 ml of distilled and deionized H_2O. The bottle was then capped and the mixture shaken vigorously for about 3 minutes, centrifuged for 15 minutes and decanted into S and S 576 filter paper. This procedure was repeated with 175 ml of H_2O followed by a third leaching of 150 ml of H_2O.

The resulting solution was transferred into a Pyrex 600 ml beaker, which was placed on a $150^{O}C$ hotplate until no more liquid remained. The salt residue was then quantitatively removed from the beaker, weighed, and stored for analysis.

Separation of the < 2 Micron Fraction. The < 2 micron fraction was separated from the insoluble residue remaining from the above procedure. The insoluble residue was repeatedly washed and centrifuged until a disperson of the clay-sized material was obtained. The washed slurry was then put into 1000 ml cylinders for gravity settling. The length of time necessary for settling was calculated from the equation noted by Folk (1968). Fractions finer than 2 microns were siphoned off after the proper length of time had passed. A portion of the < 2 micron fraction was used for oriented slides (for x-ray diffraction analysis); the remainder was dried, ground to -100 mesh and used for Rb-Sr isotopic and other geochemical analyses.

X-ray Diffraction Analysis of Clay and Evaporite Minerals. Thus far,
identification of clay minerals has been based solely on x-ray
diffractograms, obtained from a Norelco wide range diffractometer.
Untreated oriented powders were scanned from 2 to 60 degrees two theta.
The untreated slide was glycolated by vapor-soaking on a rack in a
container filled partially with ethylene glycol. An additional oriented
powder was heated to 450°C. Both the glycolated and the heated
specimens were scanned from 2 to 30 degrees two theta.

Whole rock samples were analyzed by loading a small amount of randomly
oriented rock powder in a Norelco powder holder. This powder was scanned
from 5 to 80 degrees two theta and the resulting diffractogram compared
to values compiled in the Joint Committee on Powder Diffraction Standards
file to determine bulk mineralogic composition. Mineralogic abundances
noted were estimates based on comparative peak intensities.
All samples x-rayed (both clays and whole rocks) were scanned with
Ni-filtered CuK radiation. A time constant of two seconds was used
with a scintillation counter detector and pulse height analyzer. The
goniometer slit system consisted of a divergent and anti-scatter slit of
1 degree and a 0.003 inch receiving slit.

Rb-Sr Isotopic Analysis. Procedures for the dissolution of samples for
Rb-Sr isotopic analyses varied dependent on the samples mineralogic
composition. All samples were first weighed accurately and placed into a
100 ml teflon evaporating dish; the amount of sample to be dissolved was
determined to ensure at least 10 mg Sr and Rb would be in solution. The
sample was then spiked with ^{84}Sr and ^{87}Rb solutions. Samples which
contained silicate minerals were dissolved with 30 ml reagent grade HF
and 3 ml vycor distilled $HClO_4$ on a hot plate. Samples containing only
water soluble material were dissolved with 50 ml of distilled and
deionized H_2O and 10 ml of vycor distilled 6N HCl. Samples containing
large amounts of sulfate minerals were first dissolved in aqua regia and
then treated with HF and $HClO_4$.

After complete dissolution of the powder and evaporation of all HF and
$HClO_4$, the samples were digested with 25 ml of H_2O and 25 ml of HCl.

The mixture was then reduced to about 5 ml by slow evaporation and allowed to cool overnight. After cooling the solution was filtered through S and S #576 filter paper and loaded onto the top of a chromatography column charged with sulfonated polystyrene, a chromatographic grade cation exchange resin.

The column was washed with 2N HCl repeatedly while the effluent was flame tested for cationic composition. Rb and Sr fractions were collected at the appropriate intervals indicated by the flame test. The collected fractions were subsequently dried, redissolved and transferred to precleaned quartz microvials. The microvials, containing the samples, were fused, cooled and stored for mass spectrometric analysis.

All Rb and Sr concentrations were determined by standard isotope dilution techniques. All Rb and Sr isotopic ratios were measured using a 23 inch, 90 degree sector, solid source, single filament Nuclide mass spectrometer equipped with an electrometer and strip-chart recorder.

7.8.4 Results

Samples for the present study were provided from Sandia Laboratories drill cores AEC-8, ERDA--6, and ERDA 9 drill cores. Samples were studied for their Rb-Sr systematics by mass spectrometer and (Table 7.24, 7.25), mineralogy by x-ray diffraction (Table 7.26). Additional geochemical studies are planned (i.e., rare earth elements, by instrumental neutron activation analysis).

Samples have been divided into whole rocks, water soluble portions, and the minus-two micron fractions. This approach varies significantly from Tremba's (1973) approach in that he worked with water soluble and total water insoluble fractions; the latter were not treated for separation of authigenic from allogenic fraction. This will be discussed later.

Whole rocks may yield uncertain results due to the unknown nature of water insoluble fractions within them. Similarly, the water soluble fractions are meaningful only if the nature of the water insoluble

fraction is studied. This last point can best be addressed by detailed study of the clay-size (minus-two micron), authigenic minerals common to evaporites.

(1)   Whole rocks: the water insoluble content of whole rocks varies from less than 1 percent to 32 percent, with a mean of 6.5 percent if sample Dv-4D (clay rich) is omitted. The basic mineralogy of these samples is a halite rich assemblage with some samples rich in sylvite and/or polyhalite as well. Langbeinite-rich samples are rare. The Rb-Sr isochron for eleven samples is shown in Figure 7.13. The date of 132 m.y. must be considered very approximate as nine of the eleven samples plot essentially on the ordinate. Of these last eleven, nine are used to yield a reasonable estimate of initial ratio = 0.7081 ± 0.0005 (in agreement with Tremba's 1973 value of 0.7077).

(2)   Water soluble samples: in working with water soluble samples the assumption is made that ions released into solution will not be absorbed onto the surface of the insoluble material. This is probably true only if the insoluble material consists of allogenic quartz, feldspars, etc. but not clay minerals. An isochron for five water soluble samples yields an apparent date of 206 m.y. with R_o = 0.7084 (Figure 7.14). While this date is not unreasonable for the Permian-Triassic boundary, it is slightly low.

(3)   Minus-two micron fraction: the authigenic clay minerals which one might predict for an evaporite sequence are present in this fraction (Table 7.26). Of interest is that this material is (a) authigenic as demonstrated by the x-ray diffraction work and (b) is also the dominant part of the water insoluble fraction. Thus the apparent

isochron date (Figure 7.15) of 325 m.y. needs explanation. If one remembers that many of the clay partings in the potash mines are interpreted as being of aeolian origin, then it is very likely that such aeolian clay minerals will, in part, reflect their provenance. This has been noted before by Hurley et al. (1962) for minus-two micron clay minerals from the Bermuda Rise. Of interest here is that our 325 m.y. date (Figure 7.15) is virtually identical with Tremba's (1973) 331 m.y. date for total water-soluble material.

7.8.5 Discussion

There are several ways to treat the data gathered so far. First a composite of whole rocks, water soluble and minus-two micron size clay minerals yields an isochron date (Figure 7.16) of 165 $\pm$ 20 m.y. with R_o = 0.7115. This date must be interpreted as a minimum due to the fact that the best estimate of R_o is 0.7081 $\pm$ 0.0004 according to the data presented in Table 7.24.

It is also apparent that the whole rocks by themselves are, in general, too halite-rich and possess Rb/Sr ratios which are too low for isochron work. When to this is added the uncertainty introduced by the insoluble material mixed with possible pre-T_s (i.e. time of sedimentation) material smaller than two microns, plus some detrital feldspar, quartz, etc., then the whole rocks can be assumed to be unsuitable for the isochron work.

If the clay minerals in the minus-two micron fraction are aeolian, pre-T_s material may account for the pre-Permian date of 325 m.y. (Figure 7.15). Similarly, since the clay mineralogy (Table 7.26) is very typical of evaporite clay minerals, then an alternate explanation is that these clay minerals have acted as local sinks for some [*87]Sr presumably remobilized during and after lithification and diagenesis. A lower age limit for this event is set by the 206 m.y. date from the water soluble fraction.

When only the water soluble and minus-two micron clay mineral fractions are considered together, a 204 m.y isochron (Figure 7.17) results with R_o = 0.7137. This date is only somewhat lower than the Permian-Triassic boundary and can safely be interpreted as a minimum due to the high initial ratio (0.7137). This interpretation assumes, however, that the clay minerals equilibrated with the evaporite medium (i.e. salts plus brine plus remnant sea water) at the time of sedimentation and this point remains to be unequivocally demonstrated.

Many of the above mentioned uncertainties will almost certainly be resolved by additional samples now in various stages of analysis for Rb-Sr systematics plus additional samples not yet treated. Furthermore, scanning electron microscope studies are planned to help resolve the problems of aeolian versus non-aeolian authigenesis hypotheses regarding clay mineral occurrences. Finally, rare earth element (REE) data, when complete, will greatly enhance understanding of the evaporite-insoluble material systematics of the Los Medanos area.

7.8.6 Concluding Statements

These data are of importance to he WIPP in the Los Medanos area because: (1) Widespread recent rehomogenization of radiogenic ^{87}Sr would be obvious if consistently high ^{87}Sr/^{86}Sr ratios were determined either from Rb-poor phases or by extrapolation from all samples with high Rb/Sr to the ordinate (Figures 7.13-7.17). This is not the case, and in fact values for whole rocks yield a mean of 0.7081, and several isochrons yield extrapolated values from approximately 0.709 to 0.713. The entire set of data argues against large amounts of radiogenic ^{87}Sr-enriched brine, having been formed post-200 m.y. ago, subsequently leaving its imprint in the recrystallized minerals. (2) the Rb-Sr isochron based on water soluble fractions and clay minerals, Figure 7.17 yields a date of 204 m.y. This date, in view of R_o = 0.7137 (i.e. higher than 0.7084), must be interpreted as a minimum date pending further analyses. (3) The clay minerals (Table 7.26) are of special interest in that they are typical of evaporite clay minerals formed during evaporite diagenesis,

yet they have been interpreted as aeolian. If they are aeolian, then some mixture of kaolinite-montmorillonite-illite would be expected rather than the saponite-chlorite-montmorillonite-serpentine-talc-illite assemblage noted. Since the clay minerals yield (Figure 7.15) a pre-sedimentation apparent date of 325 m.y. with high R_o (0.7123), then it is possible that these clays acted as local sinks for radiogenic ^{87}Sr (and Rb?) released during early diagenesis from roughly 235 m.y to 204 m.y.; such an interpretation is consistent with the data obtained to date. Tremba (1973) has argued for some mid-Cretaceous "rehomogenization event" at about 120 m.y. ago but inspection of his data coupled with these data do not support such an hypothesis. (4) REE are especially sensitive as geochemical tracers and forthcoming data, coupled with continued Rb-Sr and other work, should permit resolution of some of the problems concerning alkali and alkaline earth retention/migration in the geologic past at the Los Medanos site.

7.9 URANIUM ISOTOPE DISEQUILIBRIUM IN GROUNDWATERS OF SOUTHEASTERN NEW MEXICO AND IMPLICATIONS REGARDING AGE-DATING OF WATERS

7.9.1 Introduction

History. Regional exploration of bedded salt deposits for a radioactive waste repository in the Delaware Basin (Permian, New Mexico) included boreholes into the evaporites and associated rocks. These rocks contained various amounts of fluids, already described (Lambert, 1978). Although the halite deposits of the Ochoan Epoch are the prime target of consideration for waste storage, the older rocks of the Guadalupian Epoch are included in the present study, because of the Capitan reef, a body of cavernous limestone which encircles the Basin. The Capitan not only is the dominant rock in the Carlsbad Caverns, but also supplies potable water to the city of Carlsbad. Therefore, it is appropriate to consider possible connections between the Capitan and accumulations of water found in pockets in the evaporites. Brine and gas pockets are known to occur in the Carlsbad district potash mines and in the Castile Formation (anhydrite and halite) underlying the Salado Formation.

One exploration hole, ERDA No. 6, drew national attention (Boffey, 1975), when it encountered an accumulation of saturated NaCl brine laced with Na_2SO_4, accompanied by H_2S-rich gas at 826 m below the surface. Discovery of this artesian fluid, together with bedding-plane dips in the host Castile Formation exceeding 70°, led to abandonment of that particular site. Geophysical investigations showed that this and other occurrences of brine and gas were associated with closed structure contours drawn for the Castile formation. These structures, restricted to a narrow strip of evaporites near the reef have been termed "salt anticlines" (Anderson and Powers, 1978). Core from the fluid-producing zone of ERDA No. 6 consisted of gray laminated anhydrite whose fractures were filled with massive crystalline white anhydrite (Plate 7.52). While isolated fluid accumulations are not rare in evaporites, the possible use of the region for radioactive waste disposal requires attention to the origin of this particular type of accumulation. In the extreme cases, the fluid originates directly from water from the Capitan Reef, or the water was entrapped in the Castile Formation at the time for evaporite deposition in the Permian. In the first case, the water would have an age little older than Capitan waters. In the second case, the water would be in excess of 230 million years old.

Implications. Indeed, the very presence of the ERDA No. 6 accumulation of fluid poses several questions:

1. How long has the water been confined in the pocket?

2. Does the time of the water's intrusion correspond to any significant known geologic events?

3. What is the source of the water?

4. How long has this pocket been disconnected from nearby aquifers such as the Capitan Reef, if it ever was connected?

·5. What are the limits to rates of influx (if any) or recharge and discharge (if any) of this fluid pocket?

6. To what degree does the ERDA No. 6 occurrence (or any other in the area) represent a flowing system?

6. Which radiometric clock should be used to age-date the water and what should be taken as initial conditions for age-dating?

7.9.2 Analytical Approach

General Geochemistry of Groundwaters. A number of groundwaters from the Delaware Basin have been characterized in terms of their general geochemistry with respect to their host rocks (Lambert, 1978). In terms of solutes, all waters from below the fresh-saline interface in the Capitan were similar to each other. In addition all shallow (≤ 300 m depth) waters were similar to one another and all deep (≥ 1000 m depth) waters were similar to one another. The ERDA No. 6 water was unique in its solute content, indicative of profound disequilibrium between solution and host rock and also between solution and associated gas phase.

In terms of D/H and $^{18}O/^{16}O$ ratios, Capitan and shallow waters all are similar and are of meteoric origin. (Carlsbad Caverns waters are also of meteoric origin, but are not related to other waters in the Capitan.) Deep water stable isotope ratios are similar to one another, and are not characteristically meteoric. ERDA No. 6 has uniquely non-meteoric isotopic ratios among those of Delaware Basin waters. No waters were found which represent original evaporite mother-liquor.

Experimental Procedures. In spite of the evidence that this fluid has experienced profound interactions with rock (Lambert, 1978), radioisotopes were examined to establish that the ERDA No.6 fluid was not of relatively recent origin. Plutonium concentration was determined by isotope dilution employing a spike of ^{244}Pu. The actual measurement was made on a three-stage thermal emission solid source mass spectrometer equipped with pulse counting for ion detection. The instrument has a very high abundance sensitivity (10^7) and low background, allowing for the determination of precise isotopic ratios on small samples amounting to 0.1 to 1 nanograms of plutonium. The plutonium concentration of the ERDA No. 6 brine was found to be less than 10^{-15} grams per gram, corresponding to the lower limit of analytical detectability. The absence of plutonium suggests the brine has been isolated at least since 1945, a date corresponding to the first atmospheric detonation of nuclear weapons.

Carbon 14 was measured in the CO_2, which amounted to 55% of the total gas collected from ERDA No. 6. Carbon 14 content was counted in a gas proportional detector whose efficiency was calibrated with the NBS oxalate standard. The result was the same as the background, which was about 2 counts per minute in a 1.5 liter detector at 2 atmospheres pressure. From this it was concluded either that the brine is older than about 30,000 years or possibly that carbonates in the host rock have diluted the carbon in the system with non-radioactive carbon.

The disequilibrium of the activity of ^{234}U relative to ^{238}U in natural waters has been attractive as an indicator of the age of groundwaters (Osmond and Cowart, 1976). ^{234}U and ^{238}U are related by the decay scheme:

$$^{238}_{92}U \xrightarrow[4.5 \times 10^9 a]{\alpha} \, ^{234}_{90}Th \xrightarrow[24d]{\beta^-} \, ^{234}_{91}Pa \xrightarrow[1 \text{ min}]{\beta} \, ^{234}_{92}U \quad (1)$$
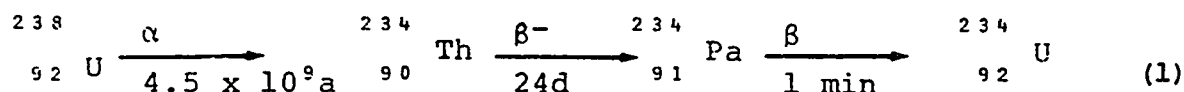
It has been proposed that excess ^{234}U builds up in confined waters as an aging effect as a result of the alpha-recoil of ^{234}Th, which ejects ^{234}Th out of the host rock crystal lattice into the water (Kigoshi, 1971; Kronfeld et al., 1975). From a knowledge of decay constants and initial activity ratio α_0 ($\alpha = \lambda_{234} N_{234} / \lambda_{238} N_{238}$), the time of confinement is calculated. It cannot be assumed, however, that the earth's natural abundance ratio, $\alpha = 1.00$, is a priori valid for a confined rock-water system. The water carried in with it an initial uranium concentration and original activity ratio, α_0. The water ultimately comes to thermodynamic equilibrium with its host rock and may leach or even deposit ^{234}U and ^{234}Th. Uranium concentrations and α -ratios of rocks and waters in this study were determined by isotope dilution mass spectrometry, described above. Figure 7.18 shows the locations of principal water samples of this study. Table 7.27 shows uranium conentrations and values of α for various waters.

7.9.3   Results and Discussion

The overleaf of Plate 7.52 shows the variations of U content and α in anhydrite of rock core taken from the zone which produced fluid in ERDA No. 6 (826 m, 2709 ft depth). Table 7.27 shows that in ERDA No. 6, both U concentration and α vary with time, until U concentration falls asymptotically to about 2 parts in 10^9, and α rises asymptotically to about 1.35. In the early part of a several-hour flow test, water samples were found to be contaminated with drill mud and spallations from metal pipe. By 1400 hours not only had the uranium reached steady state values, but the iron concentration had fallen from 260 parts in 10^6 (1130 hours) to a steady value of 5 parts in 10^6 (1400 hours), indicating the flushing out of drilling-introduced contaminants. Thus, the later samples are probably representative of the fluid accumulation.

The total variation in α among all water samples is relatively small (1.2 to 5.2). In contrast, absolute uranium content in the waters of Table 7.27 varies by more than two orders of magnitude. Similarly, rock material illustrated in Plate 7.52 shows a wide variation in U content: 1 to 2 parts in 10^6 for "original" laminated gray anhydrite down to 20 to 30 parts in 10^9 in the secondary white anhydrite fracture filling only a few centimeters away.

7.9.4   Applicaton of the Uranium Isotope Disequilibrium Model

If N_2 is the amount of ^{234}U present in a phase, and N_1 is the amount of ^{238}U, the change in ^{234}U content with time in the brine is

$$\left(\frac{dN_2}{dt}\right)_{brine} = \lambda_1 N_1 - \lambda_2 N_2 + Q_1 + Q_2, \qquad (2)$$

in which Q_1 is the rate of release of ^{234}Th (the parent of ^{234}U) from the rock, Q_2 is the rate of release of ^{234}U from the rock and λ_1 and λ_2 are decay constants for ^{238}U and ^{234}U, respectively.

Release rates Q_1 and Q_2 can be modeled in the fashion of Kigoshi (1971), who studied the release of ^{234}Th from zircon powder. He gave the accumulated activity of ^{234}Th in solution after time t as

$$(\lambda_{Th} \, N_{Th})_{brine} = 1/4 \; L \; S\rho \; (N_{238} \; \lambda_1)_{rock} \; (1 - e^{-\lambda_{Th}t}), \tag{3}$$

in which λ_{Th} is for ^{234}Th, L is the recoil distance of ^{234}Th in decay scheme (1) above, S is the surface area of parent rock, ρ is its density, and N_{238} is expressed as the number of ^{238}U atoms per gram of rock. Thus, the activity of ^{234}Th in the brine is related to the activity of ^{238}U in the rock by a proportionality constant, and, of course, the time-dependent term. When $t >> 24$ days, (3) can be approximated as

$$(\lambda_{Th} \, N_{Th})_{brine} \approx f_1 \cdot (\lambda_1 \, N_1)_{rock}, \tag{4}$$

in which f_1 is now the leach fraction of ^{234}Th, incorporating $1/4 \; L \; S \; \rho$ in (3). In general, ^{238}U activities in rock and coexisting brine will not be equal, but will be related by a distribution coefficient r, which is theoretically an equilibrium constant, neglecting the kinetics of dissolution and precipitation:

$$(\lambda_1 \, N_1)_{rock} = r \; (\lambda_1 \, N_1)_{brine} \tag{5}$$

In actual fact, the time required to achieve chemical equilibrium between rock and brine might be very long relative to the half-life of ^{234}Th. Q_1 now becomes

$$Q_1 = r \cdot f_1 \cdot (\lambda_1 \, N_1)_{brine} \tag{6}$$

Similarly, the amount of ^{234}U released is dependent on the decay of its precursor ^{238}U, and on the equilibrium ratio r, and on the leach fraction for ^{234}U, f_2:

$$Q_2 = r \cdot f_2 \cdot (\lambda_1 \, N_1)_{brine} \tag{7}$$

In addition, some fraction, f_3, of the ^{238}U will be leached from the rock,

$$\lambda_1 N_1 = r \cdot f_3 \cdot (\lambda_1 N_1)_{brine} + (\lambda_1 N_1)_{brine} \tag{8}$$

Now, equation (2) becomes:

$$\left(\frac{dN_2}{dt}\right)_{brine} = (\lambda_1 N_1)_{brine}\left[1 + r(f_1 + f_2 + f_3)\right] - \lambda_2 N_2 \tag{9}$$

If f is defined as a composite leach fraction $(f_1 + f_2 + f_3)$, the solution to (9) is:

$$N_2(t) = \frac{\lambda_1}{\lambda_2 - \lambda_1}(1+fr)N_1(t) + N_1(t=0)\frac{\lambda_2 N_2(t=0)}{\lambda_1 N_1(t=0)}\frac{\lambda_1}{\lambda_2}(1+fr)e^{-\lambda_2 t} \tag{10}$$

which allows us to express the solution in terms of $\alpha = \frac{\lambda_2 N_2}{\lambda_1 N_1}$:

$$\alpha_{brine} \doteq \frac{\lambda_2}{\lambda_2 - \lambda_1}(1+fr) + \left[\alpha_0 - \frac{\lambda_2}{\lambda_2 - \lambda_1}(1+fr)\right]e^{-(\lambda_2 - \lambda_1)t} \tag{11}$$

and since $\lambda_2 \gg \lambda_1$

$$\alpha_{brine} \approx 1 + fr + \left[\alpha_0 - 1 + fr\right]e^{-\lambda_2 t} \approx \alpha_b \tag{12}$$

The corresponding equation for the rock is:

$$\left(\frac{dN_2}{dt}\right)_{rock} = \lambda_1 (1 - f)(N_1)_{rock} - \lambda_2 (N_2)_{rock} \tag{13}$$

Since for a closed system, the $^{234}U/^{238}U$ equilibrium activity ratio is 1.000, the solution to (13) is:

$$N_2(t)_{rock} = \frac{\lambda_1}{\lambda_2 - \lambda_1}(1-f)N_1(t)_{rock} + \frac{\lambda_1}{\lambda_2}N_1(0)_{rock}e^{-\lambda_2 t} \tag{14}$$

$$- \frac{\lambda_1}{\lambda_2 - \lambda_1}N_1(0)_{rock}(1-f)e^{-\lambda_2 t}$$

which in terms of α is

$$\alpha_{rock} = \frac{\lambda_2}{\lambda_2 - \lambda_1} (1 - f) + e^{-(\lambda_2 - \lambda_1)t} - \frac{\lambda_2}{\lambda_2 - \lambda_1} (1 - f) e^{-(\lambda_2 - \lambda_1)t}$$

(15)

The approximation $\lambda_2 \gg \lambda_1$ reduces the equation (15) to

$$\alpha_{rock} \approx 1 - f + f e^{-\lambda_2 t} \approx \alpha_r$$

(16)

Let us now assume that the geochemical conditions (i.e. U content and α) observed in the ERDA No. 6 rock-fluid assemblage represent equilibrium conditions. This requires the mutual consistency of equations (12) and (16), and that

$$f = \frac{(\alpha_0 - 1)(\alpha_r - 1)}{\alpha_b - \alpha_0 + r(\alpha_r - 1)} .$$

(17)

Anhydrite found in the veins is the most recently formed phase in the core, and using the U values from 1709.4 white anhydrite (U = 33 parts in 10^9, $\alpha = 1.04$; Plate 7.52 overleaf), and the averages of the last two ERDA No. 6 brines in Table 7.27, (U = 2.01 parts in 10^9, $\alpha = 1.35$) equation (17) gives rise to the plot in Figure 7.19. Note the prominent singularity at $\alpha_0 = 2.01$, and that $\alpha_0 \leq 1.971$ at f = 1 (corresponding to 100% leaching, and $\alpha_0 \geq 2.052$ at f = -1 (corresponding to all the uranium in the rock having precipitated from the brine).

Solving equation (12) for t, we obtain an expression for the age of the brine:

$$t = \frac{\ln\left(\frac{\alpha_b - 1 - fr}{\alpha_0 - 1 - fr}\right)}{-\lambda_2} .$$

(18)

For values of $\alpha_0 \leq 1.971$, negative ages result. Only for values of $\alpha_0 \geq 2.052$ are realistic ages obtained. This result implies that there has been minimal leaching from the rock. Furthermore, it suggests rather that precipitation of uranium has occured from brine to rock which is consistent with reducing conditions implied by the presence of H_2S.

Clearly, the amount of precipitation which has occurred (negative leaching) is related to the original α_0 at the time of closure of the rock fluid system.

Values of α for nearby waters in the Capitan limestone (Table 7.27) which by proximity afford a possible source of water for the ERDA No. 6 brine pocket, are mostly in excess of 1.35. In addition, the ERDA No. 6 brine is not saturated in $CaSO_4$ (Lambert, 1978), and is not likely to have been responsible for the precipitation of substantial amounts of vein anhydrite. Furthermore, the limited volume of the brine pocket (Griswold, 1977) could not realistically be expected to dissolve and reprecipitate anhydrite in veins to the extent observed in the core. Therefore, the α_0 of the ERDA No. 6 brine must have been larger than 2.052, with very little interaction with the reservoir rock.

7.9.5 Model Ages Based on No Leaching

Values of α and α_0 will in this model allow an age determination of a water to be made. The highest α value thus far determined is 14.2, the result of isotope dilution mass spectrometry performed on a sample from Israel supplied by J. Kronfeld, which gave an α value of 10.1 ± 1.6 by alpha-spectroscopy (Kronfeld et al., 1975). In addition, the occurrence of waters elsewhere in the Delaware Basin (Table 7.27 suggests that a reasonable α_0 value might be 5.14 (in the Capitan limestone), the highest thus far found in the Basin. If the ERDA No. 6 brine represents water escaped from the Capitan, and its α_0 was on the order of 5, Figure 7.19 shows that its interaction with the ERDA No.6 reservoir rock (fractured Castile anhydrite) precipitated less than 6% of the rock's uranium from the brine.

Neither total concentration nor isotopic composition of uranium in the ERDA No. 6 brine was inherited through interaction with the Capitan limestone, for the ERDA No. 6 brine contains substantially more uranium that the Capitan waters (Table 7.27) presently do. Likewise, uniformity in the stable isotope composition of Capitan waters (Lambert, 1978) shows

that the peculiar stable isotope composition of ERDA No. 6 water cannot have arisen by interaction with the Capitan limestone. Composition of stable and unstable isotopes in ERDA No. 6 brine might have arisen from interaction between water and rocks encountered by the water if it moved from the Capitan to its ERDA No. 6 environment.

In its simplest form, equation (18), under conditions of no interaction between ERDA No. 6 brine and its reservoir rock, reduces to:

$$t = \frac{\ln\left(\dfrac{\alpha_b - 1}{\alpha_0 - 1}\right)}{-\ \lambda_2} \tag{19}$$

which very nearly corresponds to the combination of the solutions to the equations

$$\frac{dN_1}{dt} = -\ \lambda_1\ N_1$$

$$\frac{dN_2}{dt} = -\ \lambda_2\ N_2 + \lambda_1\ N_1$$

for which

$$t \approx \frac{\ln\left(\dfrac{\alpha_b - 1}{\alpha_0 - 1}\right)}{-\ \lambda_2 + \lambda_1} \tag{20}$$

The above conclusions allow limits to be assigned to the age of confinement of the ERDA No. 6 brine, and also to ages of waters in the Capitan. Equation (20) differs from equation (19) only by the approximation that

$$\frac{\lambda_2}{\lambda_2 - \lambda_1} \approx 1,$$

since $\lambda_2 = 2.806 \times 10^{-6}\ a^{-1}$ for ^{234}U
and $\lambda_1 = 1.537 \times 10^{-10}\ a^{-1}$ for ^{238}U.

Figure 7.20 shows the family of curves obtained from equation (20), using observed values of α from Table 7.29, and various values for α_0. The model ages indicated on Figure 7.19 for the ERDA No. 6 brine are less

than those in Figure 7.20 because 4 to 5 percent interaction between brine and rock (uranium precipitation) involves loss of uranium from solution by means other than radioactive decay. There is no evidence for any degree of chemical equilibrium between ERDA No. 6 rock and fluid. If we realistically limit f (Figure 7.19) to have a value between -0.02 and -0.50, the minimum age of the ERDA No. 6 occurrence is 570,000 years ($\alpha_0 = 6$). In actual fact, as the data of Kronfeld et al. (1975) suggest, maximum α_0 values are universally in the range 10 to 15, and the age is between 800,000 and 1,000,000 years. According to the no-interaction model, (Figure 7.20), if water escaped from the Capitan ($\alpha_0 = 5.14$) into the brine pocket, this must have occurred at least 880,000 years ago. The highest α_0 value (14.2) confirmed by isotope dilution mass spectrometry gives an age of 1,300,000 years.

If the Carlsbad area (near the Pecos River) is a major recharge area for much of the Capitan reef, and if Carlsbad water ($\alpha_0 = 5.14$) is the basis for age-dating other waters in the Capitan, ages between 300,000 and 1,100,000 years are obtained. The maximum α_0 (14.2) would imply that Capitan waters are at least 400,000 years old.

7.9.6 Implications and Conclusions

A mathematical model based upon analytical data has showed that the ERDA No. 6 occurrence of brine can be age-dated by the uranium-disequilibrium method. Combinations of leach fractions and ages were derived, and the interaction between rock and fluid was indicated to be minimal. If the brine pocket was once connected to the Capitan Reef, the most productive aquifer in the region, such connection was severed at least 500,000 years ago, and probably more than 900,000 years ago. The brine pocket has been stagnant ever since, and there is little evidence to indicate that chemical equilibrium has been established among the solid, liquid and gaseous phases involved in the brine pocket.

Even though the α value of the ERDA No. 6 brine was close to those of nearby metoric waters taken from the northern apex of the Capitan Reef, these α values are far removed from those of more remote meteorically-derived saline Capitan waters from the east and west arms of the reef (Carlsbad No. 7 and Shell No. 28). In fact, the remote waters appear to be younger than apex waters (Hackberry and Middleton), implying the groundwater flow in the reef is indeed toward the apex and recharge is in the east and west part of the reef.

Fresh and saline Capitan Reef waters have retained their meteoric D/H and $^{18}O/^{16}O$ ratios, even though the ages of some of them are comparable to that of ERDA No. 6. Although reef apex waters and ERDA No. 6 brine are radiometrically similar, the solutes and stable isotopes of ERDA No. 6 reflect a more profound rock/fluid interaction than Capitan waters have experienced. This interaction, however, is more likely to have taken place in rocks between the Capitan and the brine pocket than in the brine pocket itself.

The ERDA No. 6 reservoir rock has not replenished ^{234}U to the brine in spite of long contact. Furthermore, uranium mobility into the white recrystallized anhydrite from the gray laminated anhydrite from the gray laminated anhydrite was shown to be very low in this anoxic environment.

Dating by the uranium-disequilibrium method is not necessarily dependent on a closed system, and bounds on ages can be assigned. Requirements for $^{234}U/^{238}U$ dating include: α values of fluid and rock, leach rate, and knowledge of a value for original activity ratio, α_0. The α value for the rock is necessary to evaluate the degree of rock-fluid disequilibrium. The leach rate might be negligible even in a closed system. A unique solution to an age-dating problem, however, requires knowledge of initial conditions, just as in case of the well-established uranium-lead and carbon 14 age-dating techniques.

7.10 SUMMARY

Geochemical investigations of the WIPP site have been undertaken to
characterize and quantify the mineralogy and petrology of the Delaware
Basin evaporites and associated non-evaporites, volatile constituents and
fluid inclusions native to the evaporites, the geochemistry of
groundwaters native to the rocks, and the lengths of time that the
evaporites and groundwaters have existed in their present environments.
While these investigations have utilized a number of techniques of
analytical chemistry, the choice and analysis of samples, together with
interpretations of results, are carried out in the context of the WIPP
geology.

The most common mineral in the Permian (Ochoan) Salado Formation, which
is proposed for radioactive waste emplacement, is halite. Some of the
halite contains minor amounts of anhydrite, and traces of trioctahedral
clays and detrital minerals. Locally throughout the Salado Formation
marker beds of anhydrite and polyhalite occur at intervals of a few tens
of meters. Local accumulations of potassium and magnesium sulfates occur
in the McNutt potash zone in the upper part of the Salado.

The petrographic textures, geochronology, and the presence of minerals
which are not primary precipitates of sea water, such as sylvite and
polyhalite, indicate that much of the evaporite section last underwent
recrystallization more than 200 million years ago, shortly after Permian
deposition. The trace clay mineral fraction of the rock salt has
efficiently entrapped and held radiogenic strontium for at least the last
200 million years. The aqueous solutions involved in this
recrystallization were not in communication with fluids outside the
evaporite section.

Volatiles presently occur in the evaporite section as the
chemically-combined water of crystallization, hydroxyl-groups bound in
sheet silicates, short-lived seeps exposed in mines, and as
physically-entrapped inter- and intracrystalline fluid inclusions. The

total volatiles recovered from rock salt heated to 600°C typically amount to less than 0.5 weight percent (about 1.5% by volume). In addition to water, traces of nitrogen, CO_2 and contaminants from the coring operation are recovered from subsurface evaporite cores taken from boreholes. The fluid inclusions appear to have been entrapped at 20 to 45°C, and contain NaCl, $MgCl_2$ and minor amounts of other solutes. Fluid inclusions not affected by recrystallization have not moved in the ambient geothermal gradient since the Permian deposition.

Isolated pockets of aqueous solutions now found in the evaporites have no geochemical relationship to surface-derived meteoric waters or to groundwaters above and below the evaporites; neither do they represent original evaporite mother liquors. Such pockets probably are relics of the post-depositional recrystallization which took place more than 200 million years ago, at which time they might have inherited their geochemically distinct solute assemblages and stable isotope compositons.

Stable isotope and solute content studies of meteorically-derived groundwaters west of the WIPP site and peripheral to the Delaware Basin indicate that simple uptake of solutes from rocks with which they have come in contact did not alter their meteoric isotope ratios. Thus, waters participating in active dissolution of salt, which has not occurred in the Salado Formation at the WIPP site, could be readily identified by their geochemistry.

The origin and age of an artesian brine pocket in the Castile Formation, northeast of the WIPP site was evaluated by a uranium isotope disequilibrium model. It was concluded that this accumulation (encountered in borehole ERDA No. 6) has no connection with any other known groundwaters, and has been in its present environment for at least 880,000 years.

7.11 REFERENCES

Adams, S. S., 1967, Bromine in the Salado Formation, Carlsbad potash district, New Mexico: Unpublished Ph.D. Dissertation, Harvard University, 202 pp.

Adams, S. S., 1969, Bromine in the Salado Formation, Carlsbad potash district, New Mexico: New Mexico Bur. Mines Min. Res. Bull. 93, 112 p.

American Public Health Association, 1971, Standard methods for the examination of water and wastewater (13th ed.): APHA, Am. Water Works Assn., Water Pollution Control Fed: Washington, D. C.

Anderson, R. Y., Dean, W. E., Kirkland, D. W., and Snider, H. I., 1972, Permian Castile varved evaporite sequence, West Texas and New Mexico: Bull. Geol. Soc. Amer., v. 83, p. 59-86.

Anderson, R. Y., and Powers, D. W., 1978, Salt anticlines in the Castile-Salado evaporite sequence, northern Delaware Basin, New Mexico: N. Mex. Bur. Mines Min. Res. Circ. 159, in press.

Anthony, T. R. and Cline, H. E., 1971a, Thermal migration of liquid droplets through solids: Jour. Applied Physics, v. 42, no. 9, p. 3380-3387.

Anthony, T. R. and Cline, H. E., 1971b, The interaction of liquid droplets with a grain boundary in large accelerational fields: Philosop. Mag., v. 24, no. 189, p. 695-703.

Anthony, T. R. and Cline, H. E., 1972, The thermomigration of biphase vapor-liquid droplets in solids: Acta Metallur., v. 20, p. 247-255.

Anthony, T. R. and Cline, H. E., 1973, The stability of migrating droplets in solids: Acta Metallur., v. 21, p. 117-122.

Anthony, T. R., and Cline, H. E., 1974, Thermomigration of liquid droplets in salt, in Fourth Symp. on Salt, v. 1, A. H. Cougan, ed.: Cleveland, Ohio, Northern Ohio Geol. Soc., p. 313-321.

Anthony, T. R. and Sigsbee, R. A., 1971, The thermomigration of spherical bubbles through a transparent polycrystalline solid: Acta Metallur., v. 19, p. 1029-1035.

Baar, C. A., 1977, Applied salt-rock mechanics 1; the in-situ behavior of salt rocks: Elsevier Sci. Pub. Co., Amsterdam, 283 pp.

Bathurst, R. G. C. 1975, Carbonate Sediments and their Diagenesis, 2nd ed. Elsevier Scientific Publishing Company, New York, N.Y., 658 pp.

Bernas, B., 1968, New method for decomposition and comprehensive analysis of silicates by atomic absorption spectrophotometry: Anal. Chem. v. 40, p. 1682-1686.

Bernas, B., 1973, Acid pressure decomposition device for interference-free AA analysis: Amer. Lab., v. 5, no. 8, p. 41.

Bigeleisen, J., Perlman, M.L., and Prosser, H.C., 1952, Conversion of hydrogenic materials to hydrogen for isotopic analysis: Anal. Chem., v. 24, p. 1356-1357.

Bodine, M. W., Jr. 1971, Alteration of basic volcanic rocks by marine hypersaline brines, Hallstatt, Upper Austria: (Abstract), Geol. Soc. Am. Abstr., v. 3, p. 509.

Bodine, M. W., Jr. and Fernalld, T. H. 1973, EDTA dissolution of gypsum, anhydrite, and Ca-Mg carbonates: J. Sediment. Petrol. v. 43, p. 1152-1156.

Bodine, M. W., Jr. and Standaert, R. R., 1977, Chlorite and illite compositions from Upper Silurian rock salts, Retsof, New York: Clays and Clay Minerals, v. 25, p. 57-71.

Boffey, Philip M., 1975, Radioactive waste site search gets into deep water: Science, v. 190, p. 361.

Braitsch, O., 1971, Salt deposits -- their origin and composition, trans. P. J. Bureck and A. E. M. Nairn: Springer-Verlag, Heidelberg, p. 1-297.

Brokaw, A. L., Jones, C. L., Cooley, M. E., and Hays, W. H., 1972, Geology and Hydrology of the Carlsbad Potash Area, Eddy and Lea Counties, New Mexico: U.S. Geologic Survey open-file report 4339-1, 86 pages.

Calzia, J. P., and Hiss, W. L., 1978, Petrographic character and extent of an Oligocene basaltic dike system, northern Delaware Basin, New Mexico: N. Mex. Bur. Mines Min. Res. Circ. 159, in press.

Chen, K. H., and Wilcox, W. R., 1972, Boiling and convection during movement of solvent inclusions in crystals: Indust. Eng. Chem. Fundamentals, v. 11, no. 4, p. 563-565.

Clayton, R. N., Friedman, I., Graf, D. L., Mayeda, T. K., Meents, W. F., and Shimp, N. F., 1966, The origin of saline formation waters, I. Isotopic Composition: Jour. Geophys. Res., v. 71, p. 3869-3882.

Cline, H. E., and Anthony, T. R., 1971, Vaporization of liquid inclusion (sic) in solids: Philosoph. Mag., v. 24, p. 1483-1494.

Collins, A. G., 1975, Geochemistry of oilfield waters: Elsevier Scientific Publishing Company, Amsterdam, p. 1-496.

Craig, Gordon, L. I., and Horibe, Y., 1963, Isotopic exchange effects in the evaporation of water, I. Low-temperature experimental results: Jour. Geophys. Res., v. 68, p. 5079-5087.

Craig, H., 1961a, Isotopic variations in meteoric waters: Science, v. 133, p. 1702-1703.

Craig, H., 1961b, Standard for reporting concentrations of deuterium and oxygen - 18 in natural waters: Science, v. 133, p. 1833-1834.

Dellwig, L. F., 1955, Origin of the Salina salt of Michigan: Jour. Sed. Petrology, v. 25, p. 83-110.

Epstein, S., and Mayeda, T., 1953, Variaton of ^{18}O content of waters from natural sources: Geochim. Cosmochim. Acta, v. 4., p. 213-244.

Epstein, Sharp, R. P., and Gow, A. J., 1965, Six-year record of oxygen and hydrogen isotope variations in South Pole firn: Jour. Geophys. Res., v. 70, p. 1809-1814.

Epstein, 1970, Antarctic ice sheet: Stable isotope analyses of Byrd station cores and interhemispheric climatic implications: Science, v. 168, p. 1570-1572.

Fallis, S. M., 1973, Mineral sources of water and their influence on the safe disposal of radioactive wastes in bedded salt deposits: Unpublished Master's Thesis, University of Tennessee, Knoxville, 61 pp.

Faure, G., and Powell, J. L., 1972, Strontium isotope geology: Springer-Verlag, New York, 188 p.

Faure, G., 1977, Principles of Isotope Geology: J. Wiley & Sons, Inc., New York, 464 p.

Folk, R. L., 1965, Some Aspects of Recrystallization in Ancient Limestones, in L. C. Pray and R. C. Murray (eds.): Soc. Econ. Paleontologists and Mineralogists, Spec. Pub. 13, p 14-48.

Folk, R. L., 1968, Petrology of sedimentary rocks: Hemphill's, Austin, Texas, 170 p.

Fontes, J., and Gonfiantini, R., 1967, Fractionment isotopique de l'hydrogene dans l'eau de cristallisation du gypse: C. R. Acad. So. Paris, Ser. D., v. 265, p. 4-6.

Fournier, R. O., 1961, Regular interlayered chlorite-vermiculite in evaporite of the Salado Formation, New Mexico: U.S.G.S., Prof. Paper 424-D, p. 323-327.

Fuchtbauer, H. and Goldschmidt, H., 1969, Die Tonminerale der Zechsteinformation: Beitr. Mineral. Petrogr. v. 6, p. 320-345.

Garrels, R. M., and Christ, C. L., 1965, Solutions, minerals, and equilibria: Harper and Row, New York, p. 1-450.

Geguzin, Ya. E., and Dzyuba, A. S., 1973, Study of liquid inclusions in rock salt crystals in the entire range of their existence: Kristallografiya, v. 18, no. 7, p. 800-807 (in Russian; English abstract in Fluid Inclusion Research -- Proceedings of COFFI, v. 7, p. 62).

Gerlach, Hansludwig, and Heller, Siegfried, 1966, Uber Kunstliche Flussigkeitseinschusse in Steinsalzkristallen: Deutsche Gesell. Geol. Wiss., Reihe B., Mineralogie und Lagerstattenforschungen, Bd. 11, Heft 2, p. 195-214.

Graf, D. L., Meents, W. F., Friedman, I., and Shimp, N. F., 1966, The origin of saline formation waters, III. Calcium chloride waters: Illinois State Geol. Surv. Circ. 397, p. 1-60.

Grim, R. E., 1968, Clay Mineralogy (Second Edition), McGraw-Hill Book Company, New York, p. 1-596.

Grim, R. E., Droste, J. B., and Bradley, W. F., 1961, Diffraction data of a regular mixed layered clay mineral in an evaporite, in Eighth Natl. Conference on Clay and Clay Minerals: Pergamon Press, Inc., New York, p. 228-236.

Griswold, G. B., 1977, Site selection and evaluation studies of the Waste Isolation Pilot Plant (WIPP), Los Mendanos, Eddy County, New Mexico: Sandia Laboratories, SAND77-0946.

Hiss, W.L., 1975, Stratigraphy and ground-water hydrology of the Capitan aquifer, southeastern New Mexico and west Texas: unpublished ph.D. thesis, University of Colorado, Boulder, 396 p.

Holdoway, K. A., 1974, Behavior of fluid inclusions in salt during heating and irradiation, in Fourth Symp. on salt, v. 1, A. H. Coogan, ed.: Northern Ohio Geol. Soc., Cleveland, Ohio, p. 303-312.

Hopkins, R. H., Seidensticker, R. G., and Stewart, A. M., 1976, Degradation of Czochralski silicate oxyapatite crystals by the thermomigration of liquid drops: Jour. Crystal Growth, v. 33, p. 223-231.

Holser, W. T., 1963, Chemistry of brine inclusions in Permian salt from Hutchison, Kansas in J. L. Rau (ed.), Symposium on salt: Northern Ohio Geological Society, Cleveland, Ohio, p. 86-103.

Holser, 1966, Bromide geochemistry of salt rocks in J. L. Rau (ed.), Second Symposium on Salt: Northern Ohio Geological Society, Cleveland, Ohio, p. 248-275.

Hurley, P. M., Heezen, B. C., Pinson, w. H., and Fairbairn, H. W., 1963, K-Ar age values in pelagic sediments of North Atlantic: Geochim. Cosmochim. Acta, v. 27, p. 393-399.

Jones, C. L., 1973, Salt Deposits of Los Medanos Area, Eddy and Lea Counties, New Mexico, with sections on Ground-water Hydrology, by M. E. Cooley, and Surficial Geology, by G. O. Bachman: U.S. Geological Survey open-file report 4339-7, 67 pages.

Jones, C. L., 1974a, Salt Deposits of the Clovis-Portales Area, East-Central New Mexico: U.S. Geological Survey open-file report 74-60, . 22 pages.

Jones, C. L., 1974b, Salt Deposits of the Mescalero Plains Area, ·Chavez County, New Mexico: U.S. Geological Survey open-file report 74-190, 21 pages.

Jones, C. L., 1975, Potash Deposits in Part of Los Medanos Area of Eddy and Lea Counties, New Mexico: U.S. Geological Survey open-file report 75-407, 37 pages.

Khetchikov, L. N., and Samoilovich, L. A., 1970, The possibilities of the decrepitation method in mineral thermometry: Akad. Nauk S.S.S.R., Izvest., Ser. Geol., 1970, no. 7, p. 92-98 (in Russian; translated in Fluid Inclusion Research -- Proceedings of COFFI, v. 3, 1970, p. 94-100).

Kigoshi, Kunihiko, 1971, Alpha-recoil thorium-234: dissolution into water and the uranium-234/uranium-238 disequilibrium in nature: Science, v. 173, p. 47.

Kronfeld, J., Gradsztajn, E., Muller, H.W., Raddin, J., Yaniv, A., Zach, R., 1975, Excess ^{234}U: an aging effect in confined waters: Earth Planetary Sci. Letters, v. 27, p. 342.

Kuznetsov, S. I., Ivanov, M. V., and Lyalikova, N. N., 1963, Introduction to geological microbiology (transl. P. T. Broneer): McGraw-Hill Book Company, New York, p. 1-245.

Lambert, S. J., 1978, The geochemistry of Delaware Basin groundwaters: New Mexico Bur. Mines and Min. Res. Circ. 159, in press.

O'Neil, J. R., and Kharaka, Y. K., 1976, Hydrogen and oxygen isotope exchange reactions between clay minerals and water: Geochim. Cosmochim. Acta, v. 40, p. 241-246.

Osmond, J.K., and Cowart, J.B., 1976, The theory and uses of natural uranium isotopic variations in hydrology: Atomic Energy Review, v. 14, p. 621.

Oxburgh, V. M., Segnit, R. E., and Holland, H. D., 1959, Coprecipitation of strontium with calcium carbonate from aqueous solutions (abstr.): Bull. Geol. Soc. Amer., v. 70, p. 1653.

Potter, R. W., II, 1977, Pressure corrections for fluid-inclusion homogenization temperatures based on the volumetric properties of the system $NaCl-H_2O$: J. Research U.S. Geol. Survey, v. 5, no. 5, p. 603-607.

Randall, M., and Failey, C. F., 1927, The activity coefficient of gases in aqueous salt solutions: Chem. Rev., v. 4, p. 271-284.

Reeves, C. C., Jr., 1963, Subterranean natural brines produce sodium sulphate in West Texas: Ground Water, v. 1, p. 35-36.

Roedder, E., 1965, Liquid CO_2 inclusions in olivine bearing nodules and phenocrysts from basalts: Amer. Min., v. 50, p. 1746-1782.

Savin, S. M., and Epstein, S., 1970, The oxygen and hydrogen isotope geochemistry of clay minerals: Geochim. Cosmochim. Acta, v. 34, p. 25-42.

Schaller, W. T. and E. P. Henderson, 1932, Mineralogy of drill cores from the potash field of New Mexico and Texas: U. S. Geol. Surv. Bull. No. 833, 124 pp.

Shell Exploration and Production Research Center, 1973, Potassium-Argon dates on Permian potash minerals from southeastern New Mexico: Isochron/West, No. 6, p. 37.

Tremba, E. L., 1973, Isotope geochemistry of strontium in carbonate and evaporite rocks of marine origin: unpub. Ph.D. dissertaton, Ohio State Univ., 185 p.

Vogel, A. I., 1961, A Textbook of Quantitative Inorganic Analysis: 3rd Ed., John Wiley and Sons, Inc., N.Y., p. 462.

Wilcox, W. R., 1968, Removing inclusions from crystals by gradient techniques: Indust. Eng. Chem., v. 60, no. 3, p. 13-23.

Wilcox, W. R., 1969, Anomalous gas-liquid inclusion movement: Indust. Eng. Chem., v. 61, no. 3, p. 76-77.

Depth Below Surface (Feet)

	ANHYDRITE	HALITE	MAGNESITE	POLYHALITE

FIGURE 7.1

DISTRIBUTION OF MINERALS IN ERDA #9 CORE SAMPLES
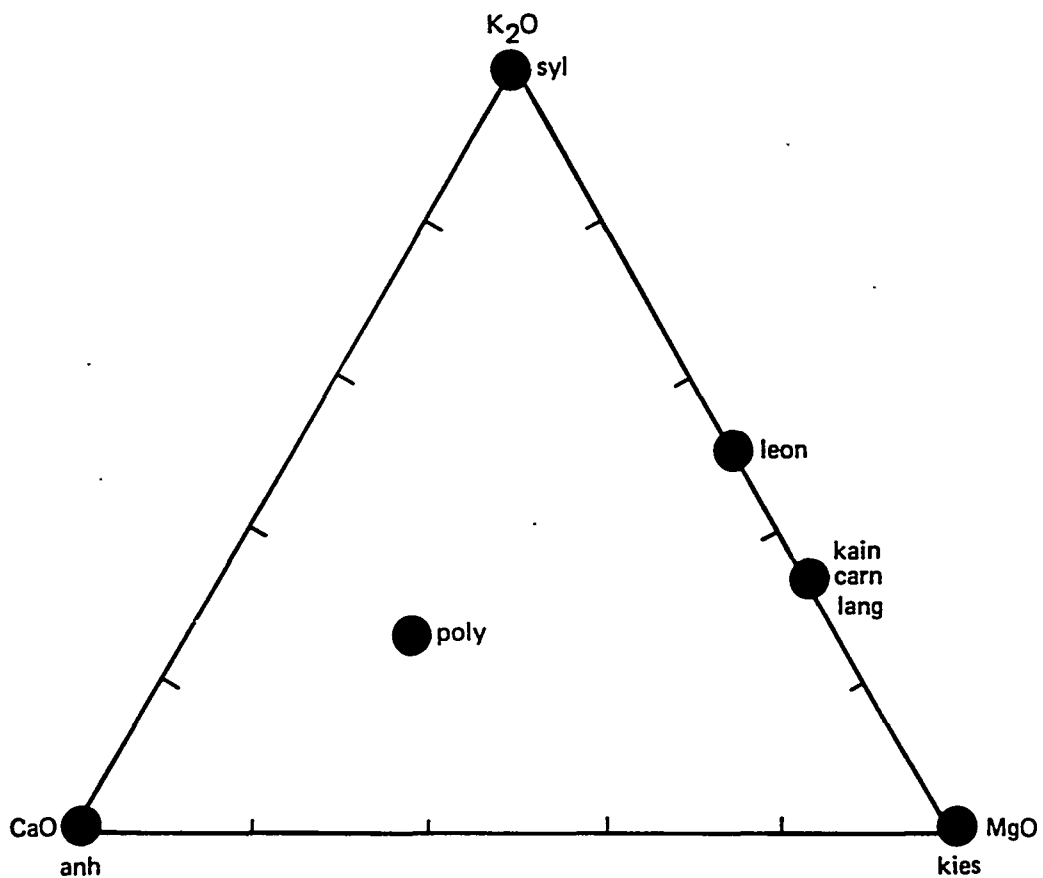
FIGURE 7.2

TRIANGULAR COMPOSITION DIAGRAM OF

SOLUBLE SULFATE-GROUP MINERALS
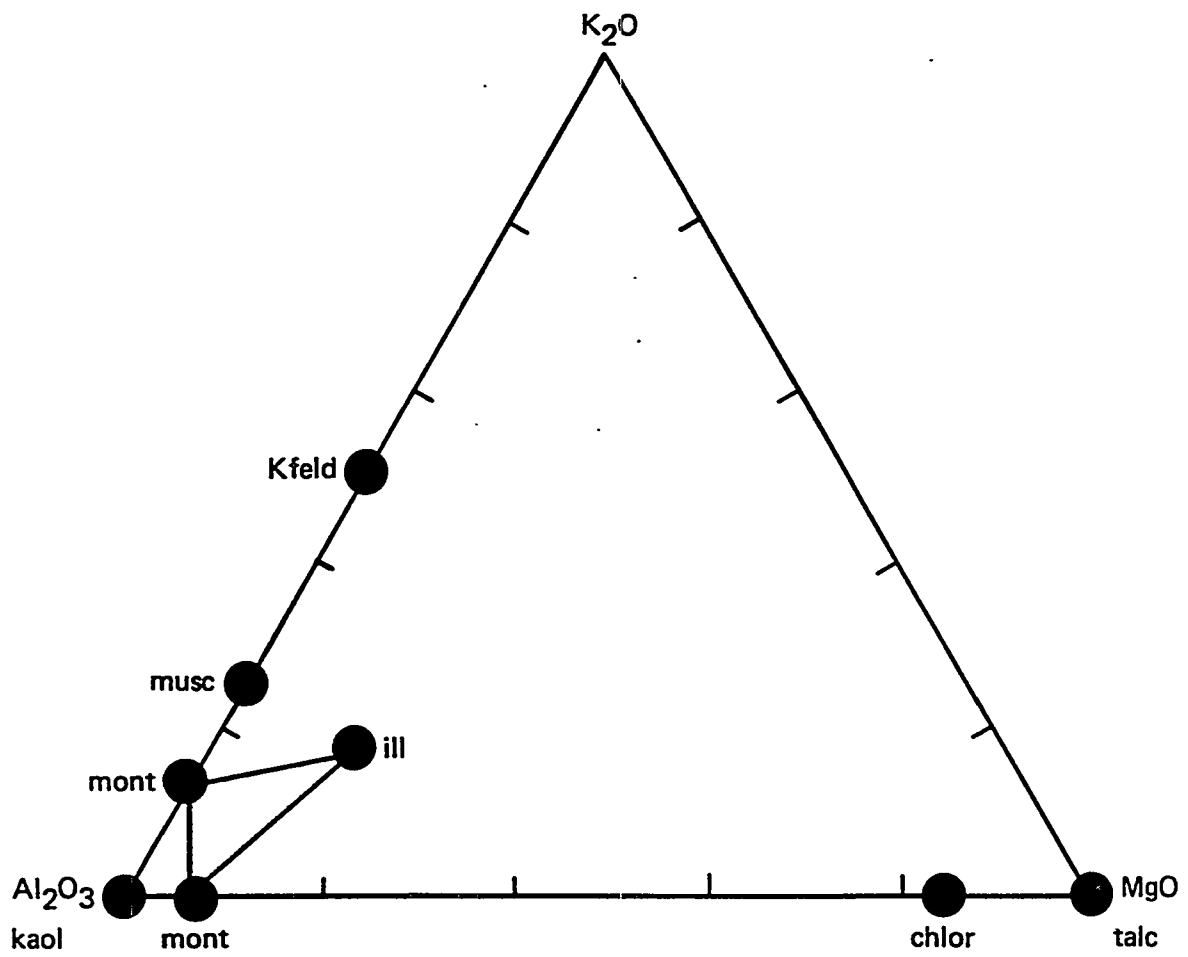
FIGURE 7.3

TRIANGULAR DIAGRAM OF

INSOLUBLE SILICATE-GROUP MINERALS

endotherm

exotherm

300

poly

gyp

8–1953
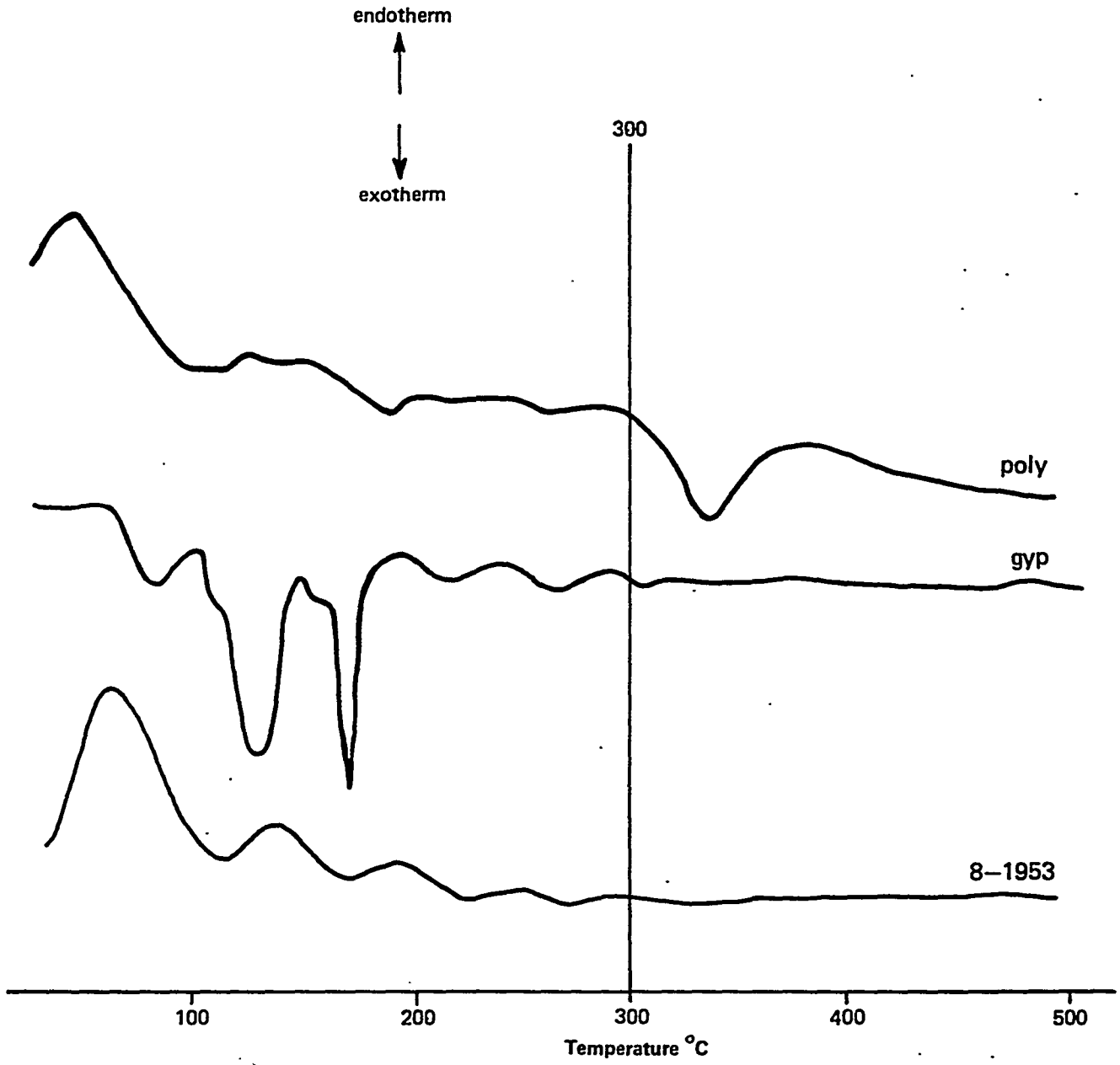
Temperature °C

FIGURE 7.4

DIFFERENTIAL THERMAL ANALYSIS CURVES

FOR GYPSUM AND POLYHALITE
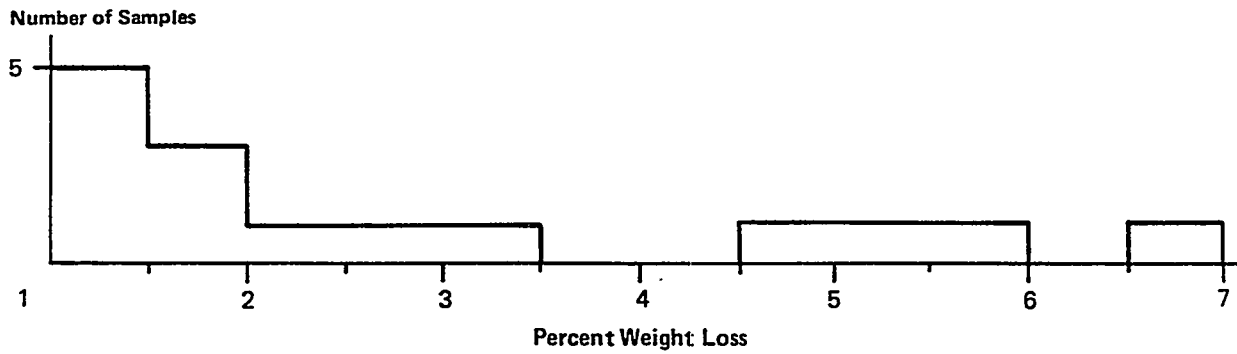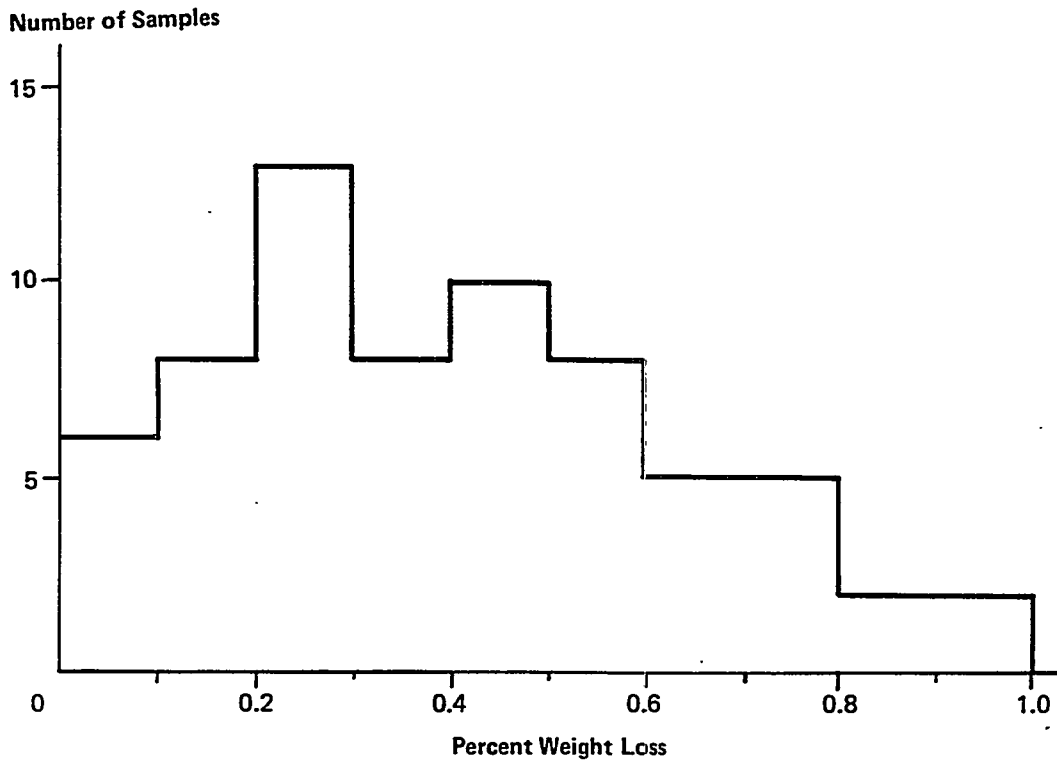
FIGURE 7.5

TOTAL WEIGHT LOSSES AT ELEVATED TEMPERATURES

(500°C) FOR CORES FROM AEC NOS. 7 AND 8

FIGURE 7.6A

AEC NO. 7 SAMPLE WEIGHT LOSSES VS. DEPTH

AT ELEVATED TEMPERATURES (500°C)

Sample Depth (Feet)

Off Scale
(6.84)

Percent Weight Loss
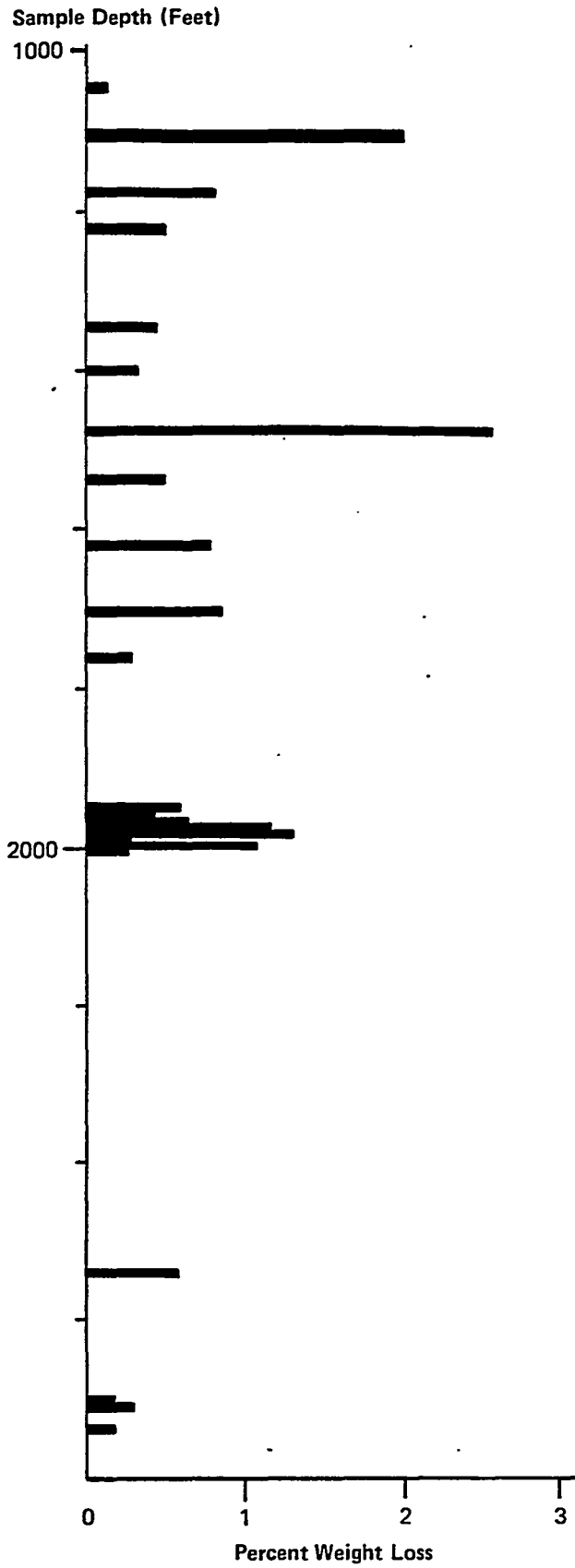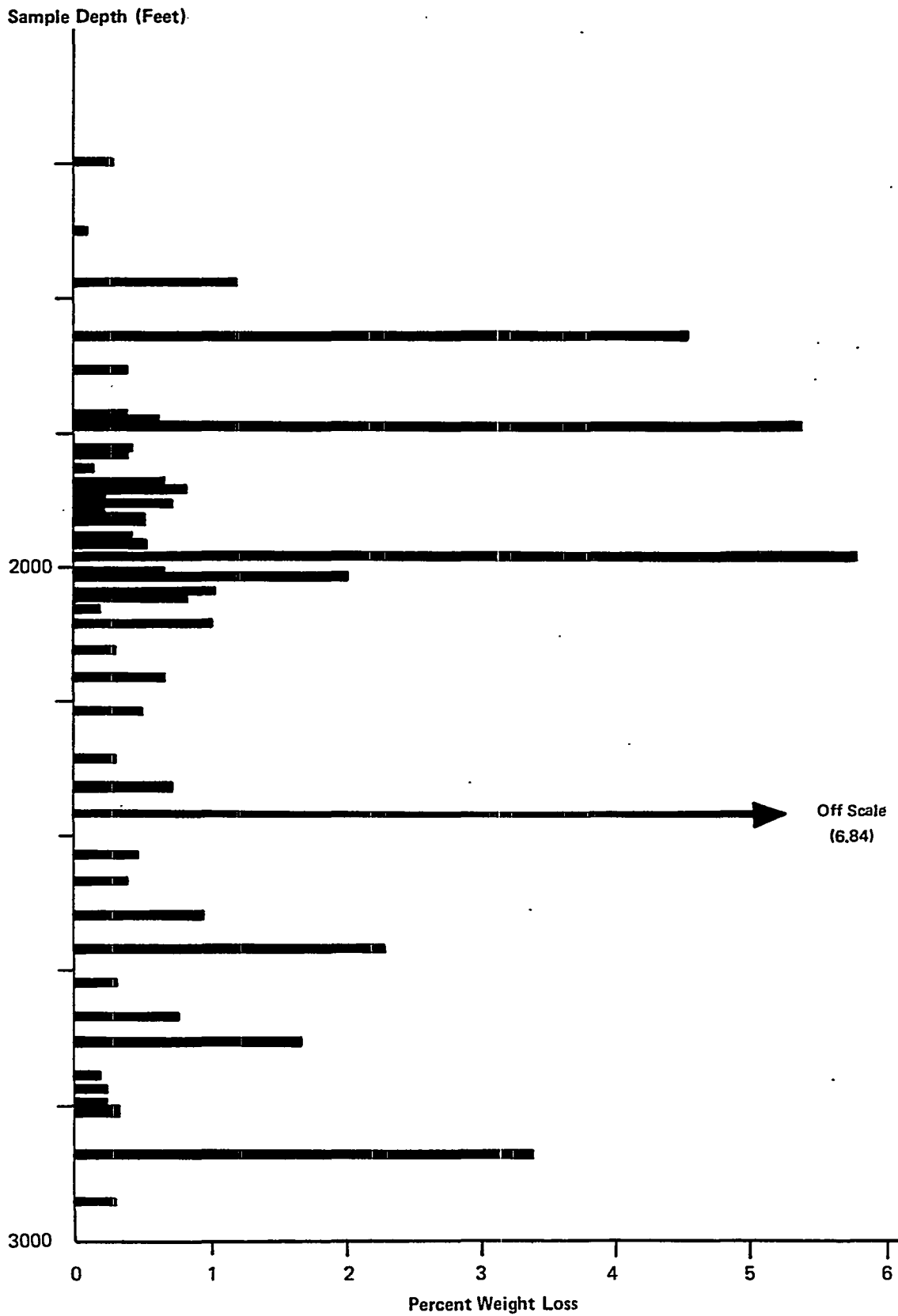
FIGURE 7.6B

AEC NO. 8 SAMPLE WEIGHT LOSSES VS. DEPTH

AT ELEVATED TEMPERATURES (500°C)

Percent Weight Loss

C

A
Typical Rock Salt

B

Polyhalite-Bearing
Rock Salt

Clay-Bearing
Rock Salt

Temperature °C
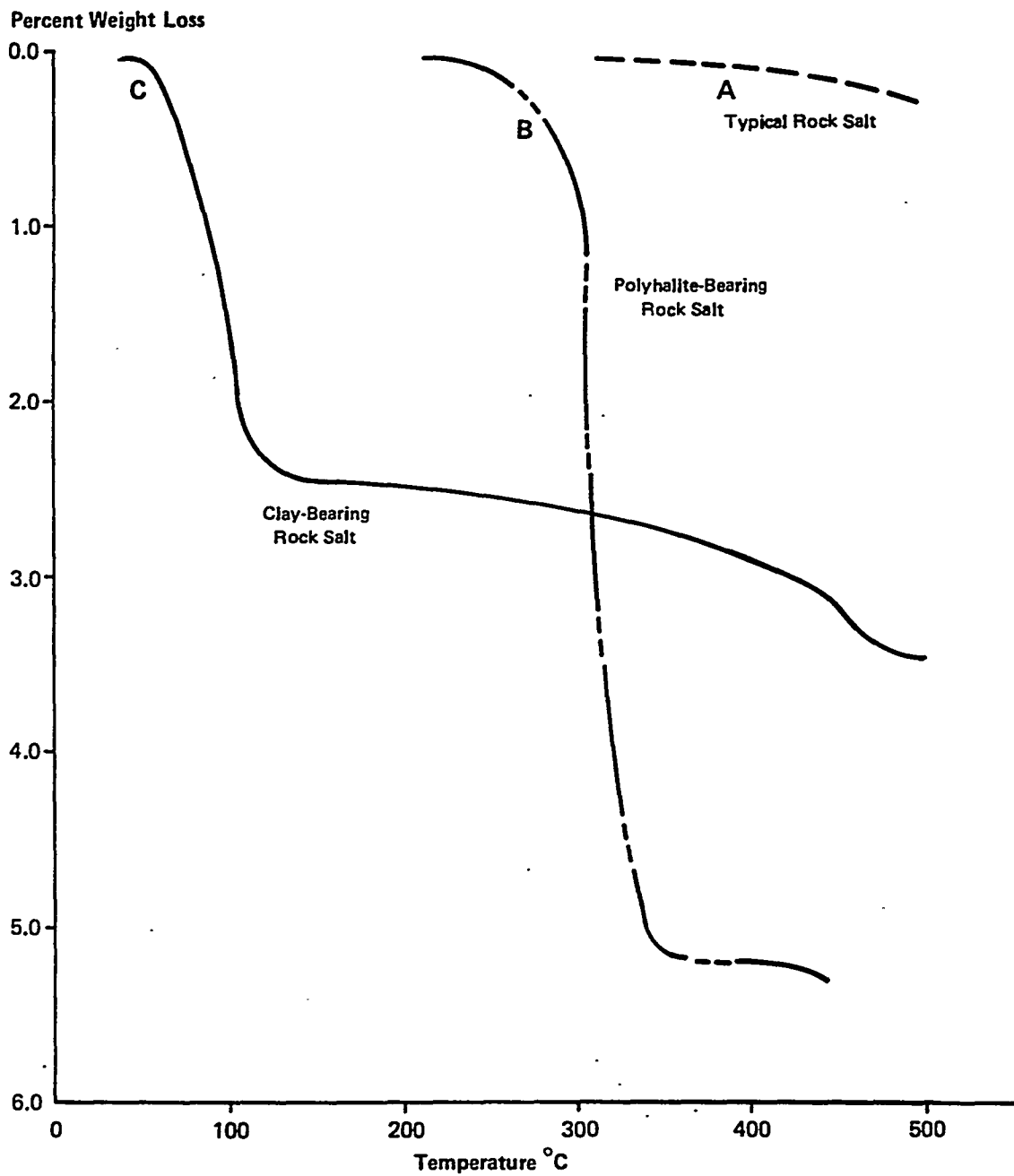
FIGURE 7.7

TYPICAL WEIGHT-LOSS CURVES FOR ERDA #9 EVAPORITE CORE
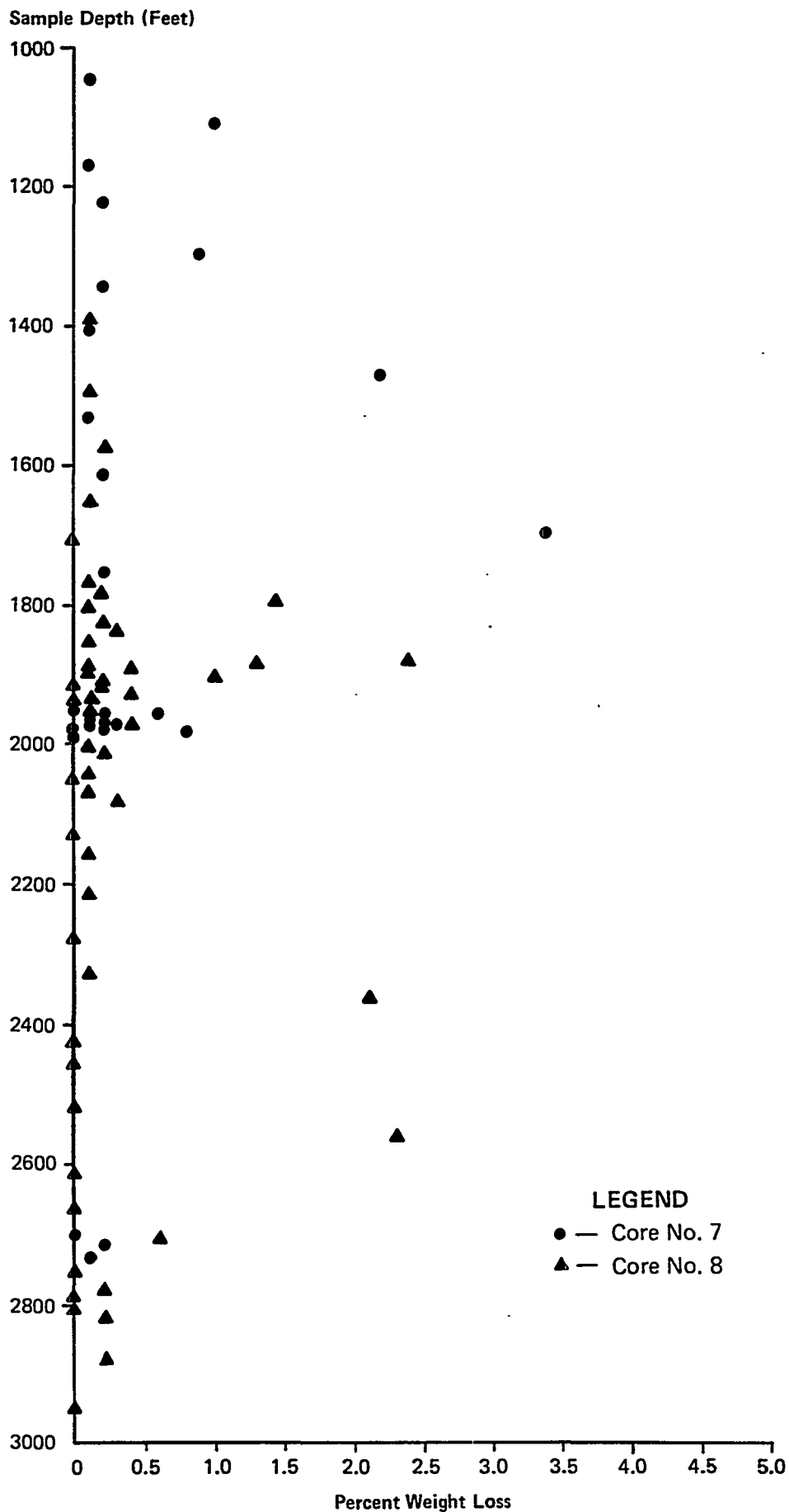
FIGURE 7.8 WEIGHT LOSS DATA FOR SAMPLES (102±5°C)

FROM CORES NO. 7 AND NO. 8 NEAR CARLSBAD, NEW MEXICO
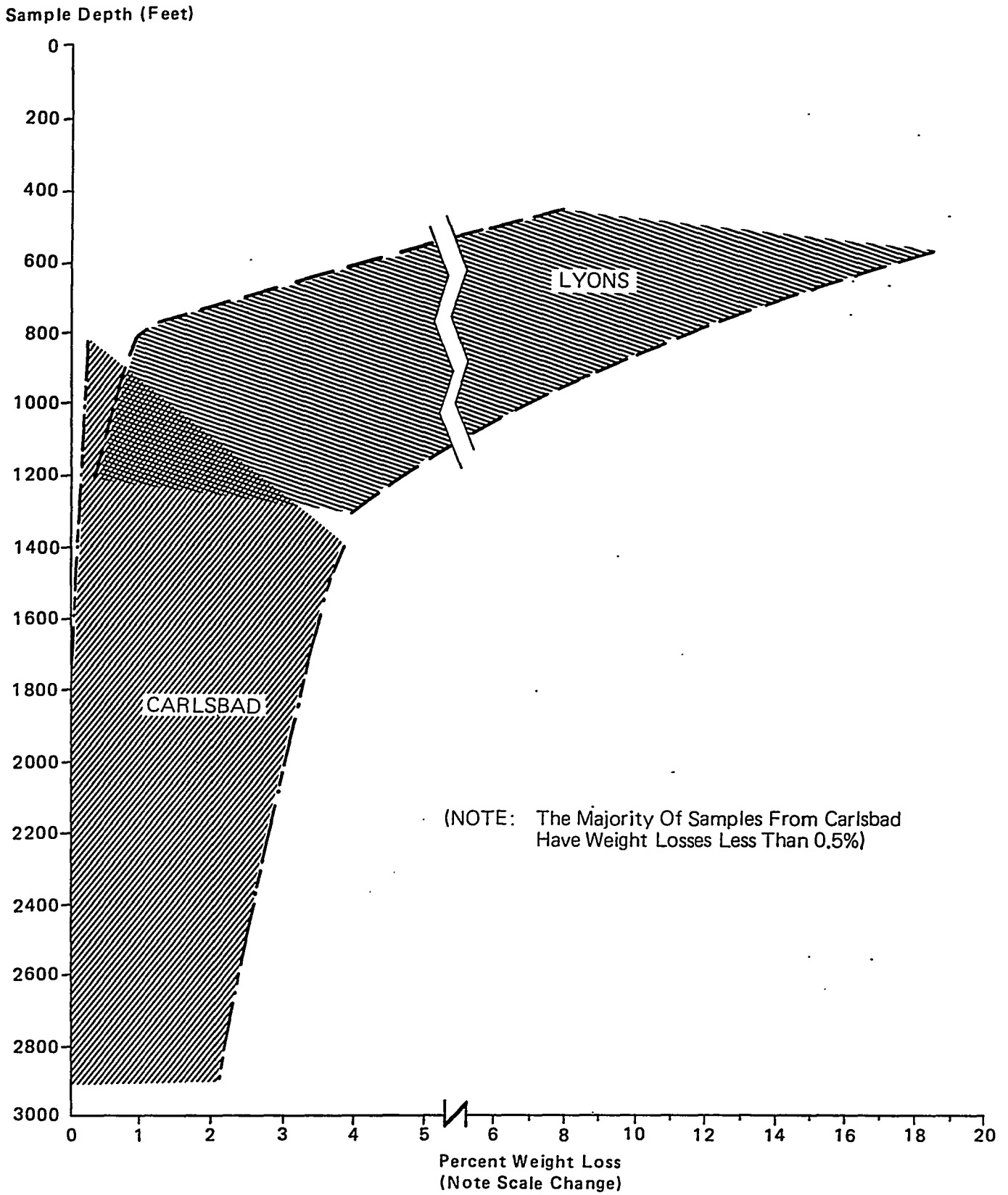
FIGURE 7.9 APPROXIMATE RANGE OF WEIGHT LOSS TO BE EXPECTED
At 102 + 5°C VS. DEPTH FOR SAMPLES FROM LYONS, KANSAS
AND CARLSBAD, NEW MEXICO
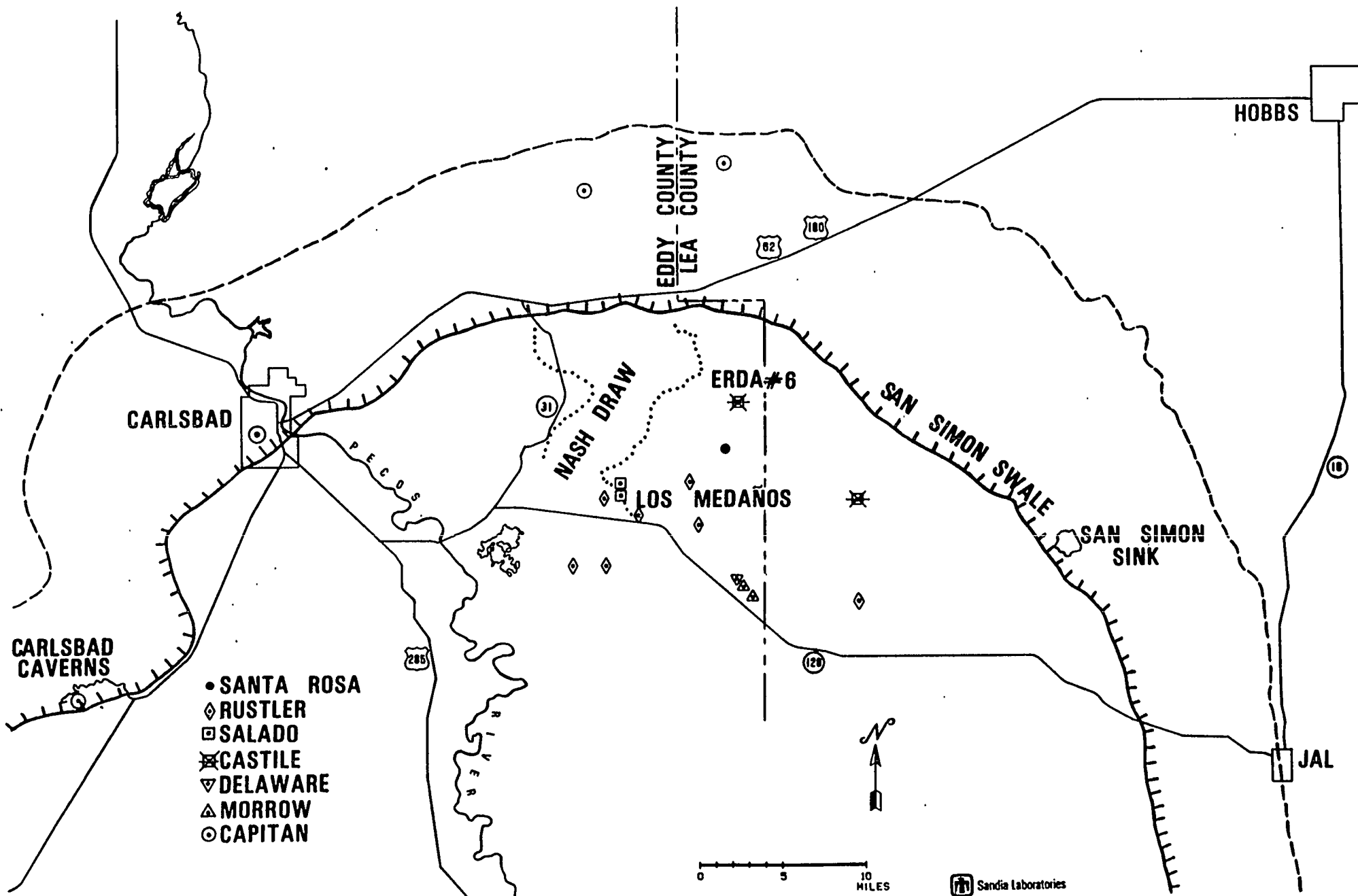
FIGURE 7.10 Map of the New Mexico portion of the Delaware Basin, showing locations of water sampling points in this study. The solid hachured line is the basinward margin of the Capitan Reef; the dashed line is the shelfward edge.

Legend:
- ● SANTA ROSA
- ◇ RUSTLER
- ▣ SALADO
- ✳ CASTILE
- ▽ DELAWARE
- △ MORROW
- ◉ CAPITAN

HOBBS

CARLSBAD

CARLSBAD CAVERNS

EDDY COUNTY / LEA COUNTY

ERDA #6

NASH DRAW

LOS MEDAÑOS

SAN SIMON SWALE

SAN SIMON SINK

JAL

PECOS RIVER

0 5 10 MILES

Sandia Laboratories
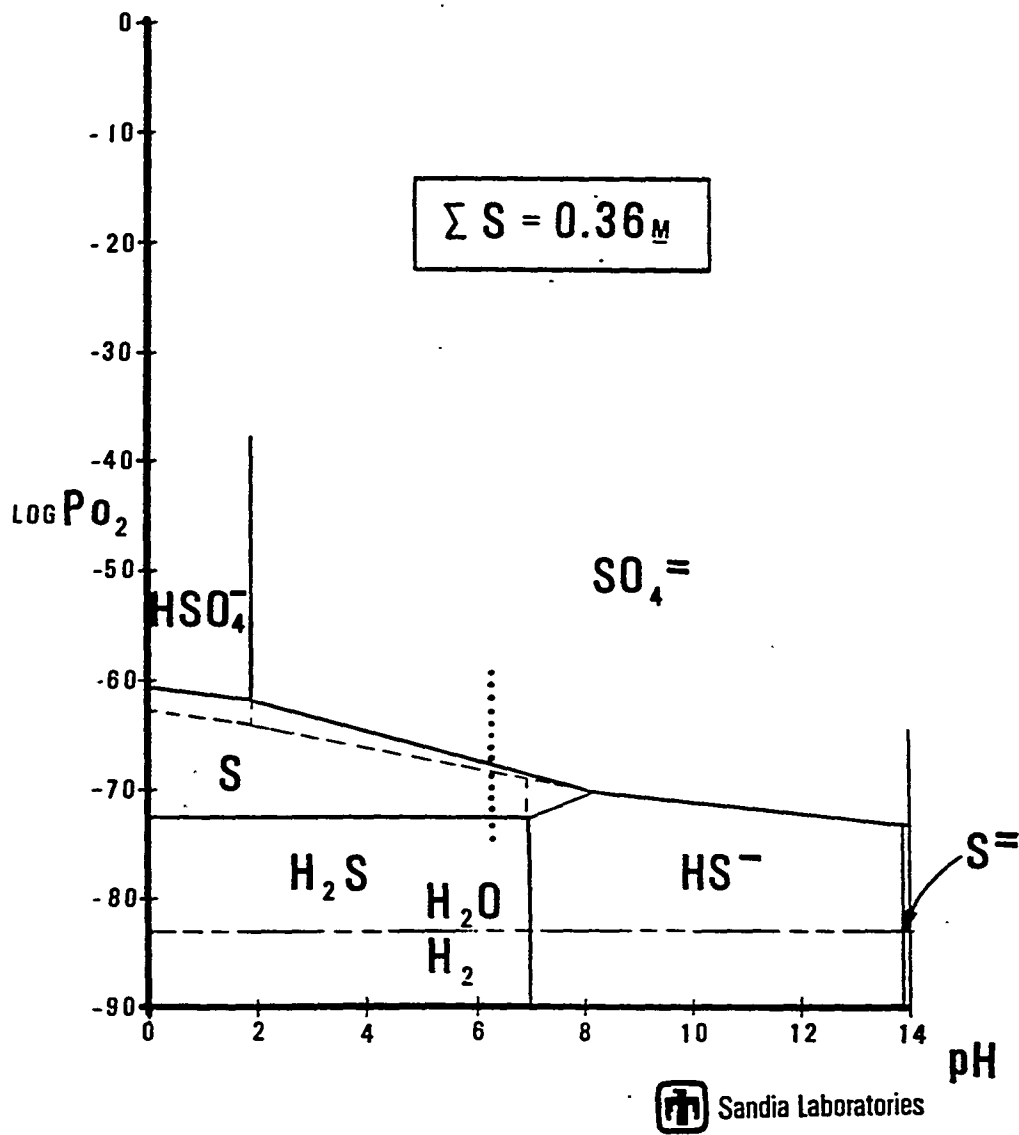
FIGURE 7.11 Predominance area diagram, oxygen partial pressure versus pH, for the System S-O-H at 25°C, 1 atmosphere and total sulfur concentration of 0.36m. Dashed lines are metastable extensions of boundaries. Dotted line represents the field-measured pH of ERDA No. 6, 6.3.
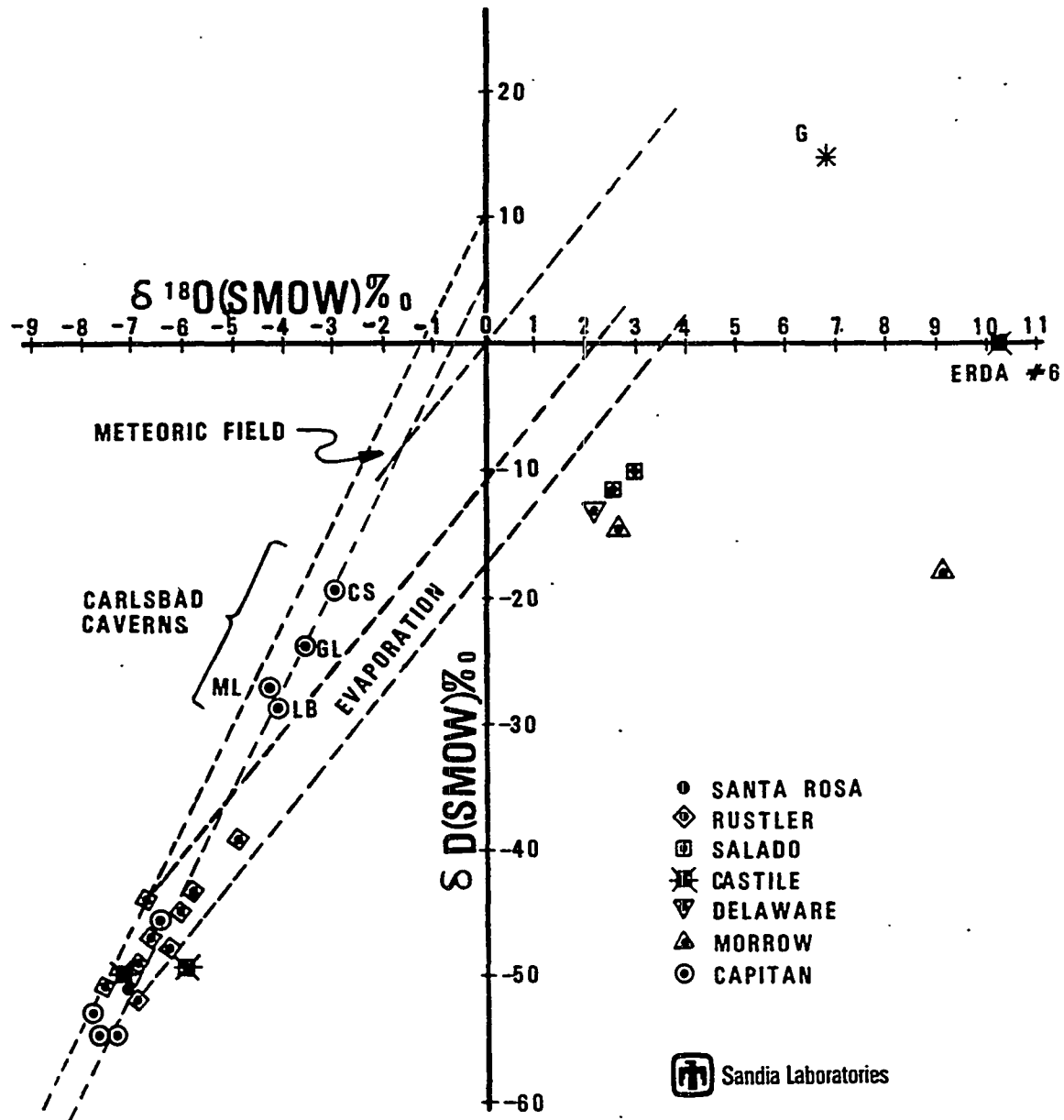
FIGURE 7.12 Stable isotope compositions, δD versus $\delta^{18}O$, for Delaware Basin groundwaters. Relationships are shown for meteoric waters, evaporating meteoric and sea waters. Hypothetical evaporite mother-liquor for gypsum (G) is shown for the case in which ERDA No. 6 is taken to be the water of crystallization for that gypsum.

FIGURE 7.13

Apparent Rb—Sr Isochron
Whole Rocks

$T = 132\,m.y.$
$R_0 = 0.7096$

$\frac{87}{Sr}/\frac{86}{Sr}$

$\frac{87}{Rb}/\frac{86}{Sr}$

7 data
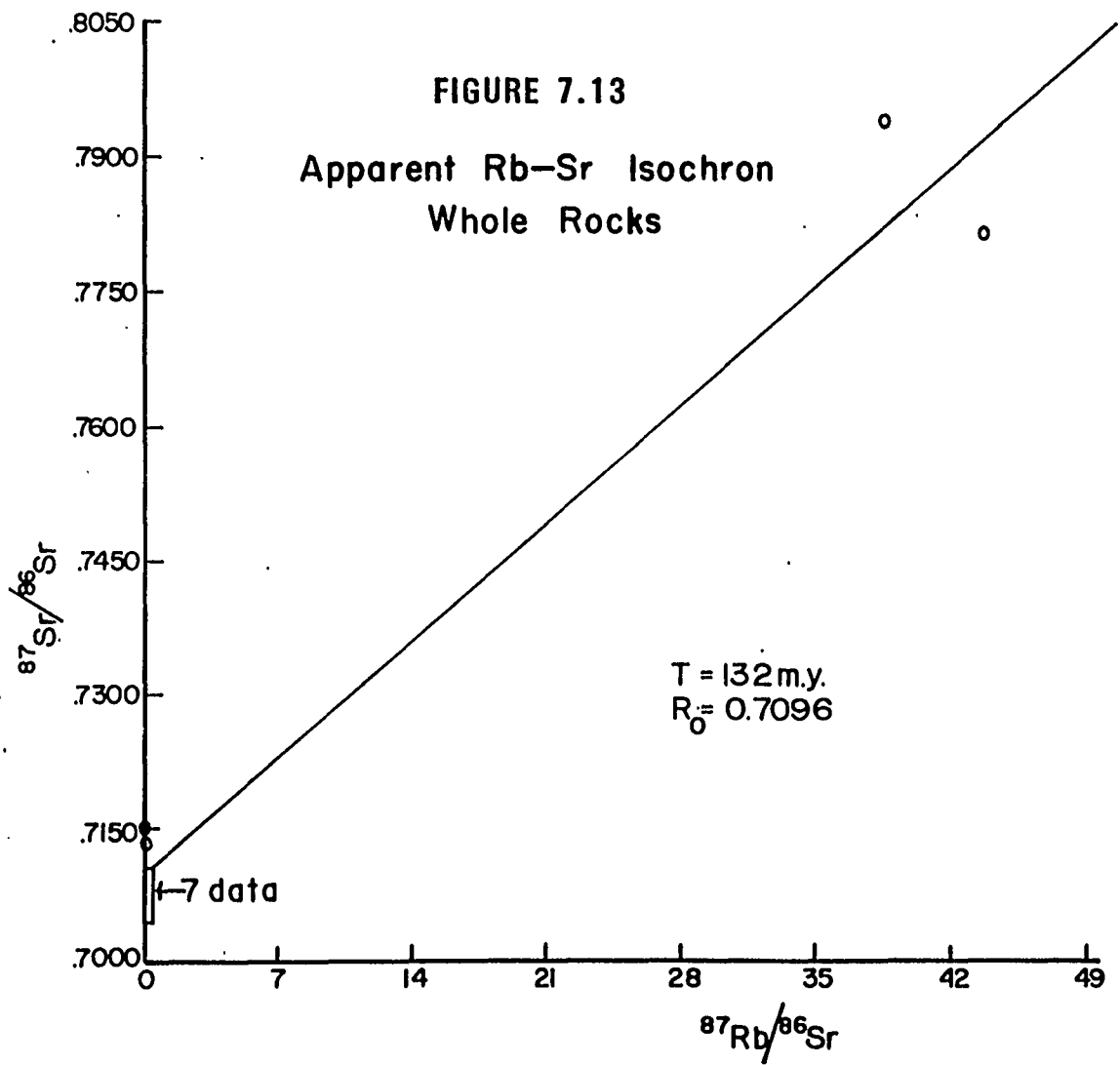
FIGURE 7.14

Apparent Rb–Sr Isochron
Water Soluble Fraction

$T = 206.1$ m.y.
$R_0 = 0.7084$

${}^{87}Sr/{}^{86}Sr$

${}^{87}Rb/{}^{86}Sr$

FIGURE 7.15

Apparent Rb — Sr Isochron
Clay Mineral (<2M) Fraction

$T = 325$ m.y.
$R_0 = 0.7123$
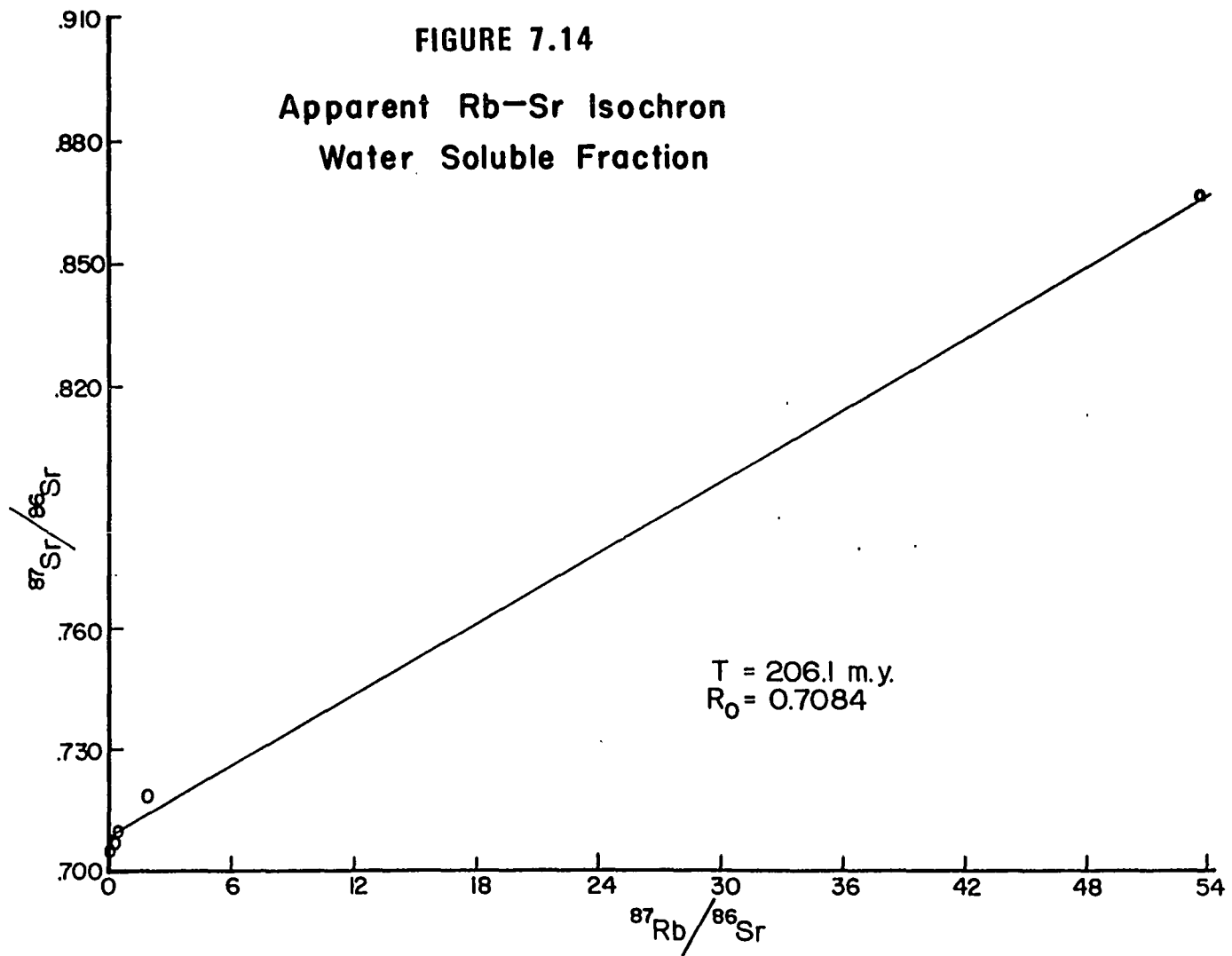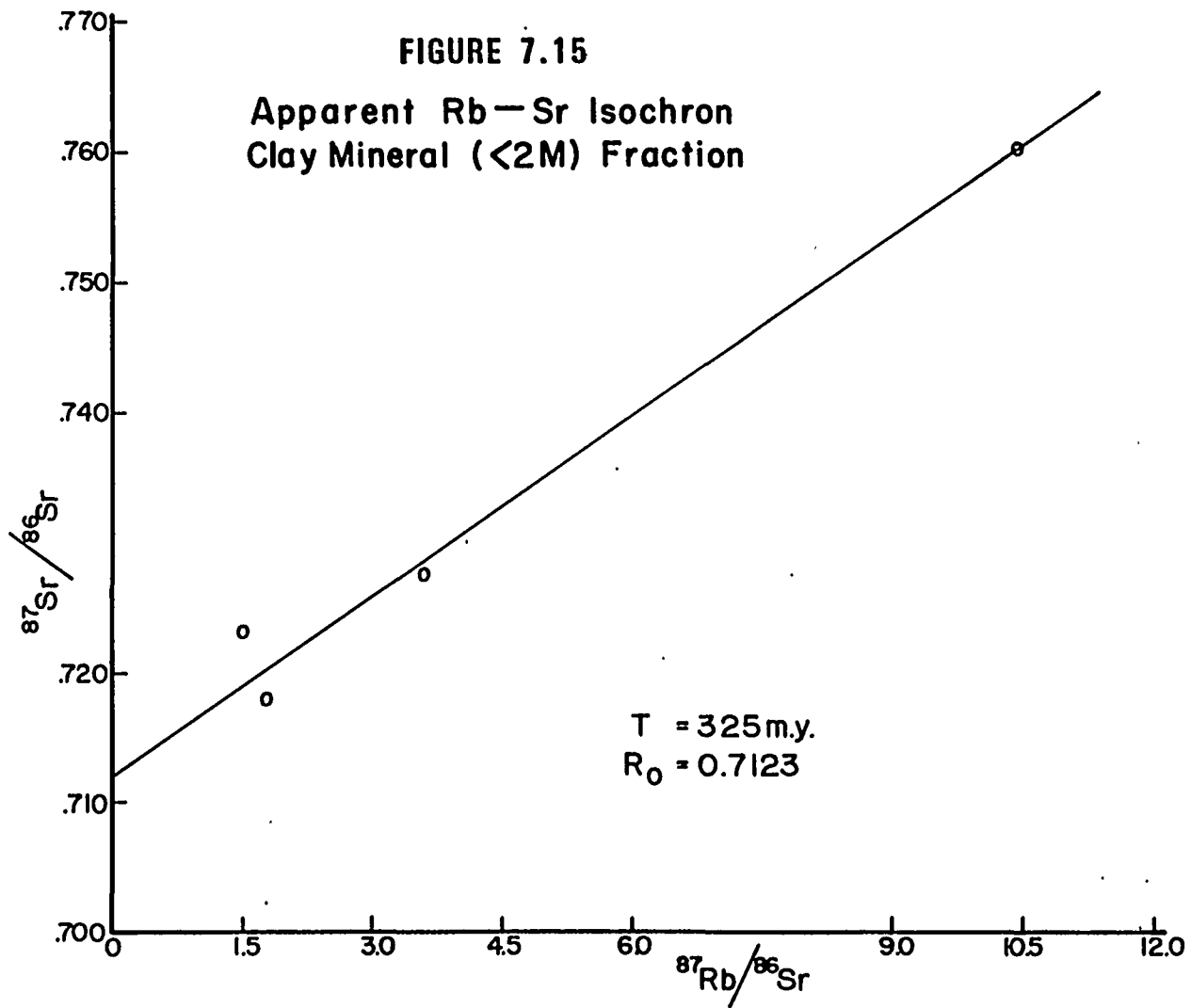
FIGURE 7.16

Apparent Rb–Sr Isochron
Composite of Whole Rock,
Water Soluble Fractions, and
Clay Minerals

T = 165 m.y.
R_O = 0.7115

FIGURE 7.17

Apparent Rb—Sr Isochron
Water Soluble and Clay Mineral Fractions
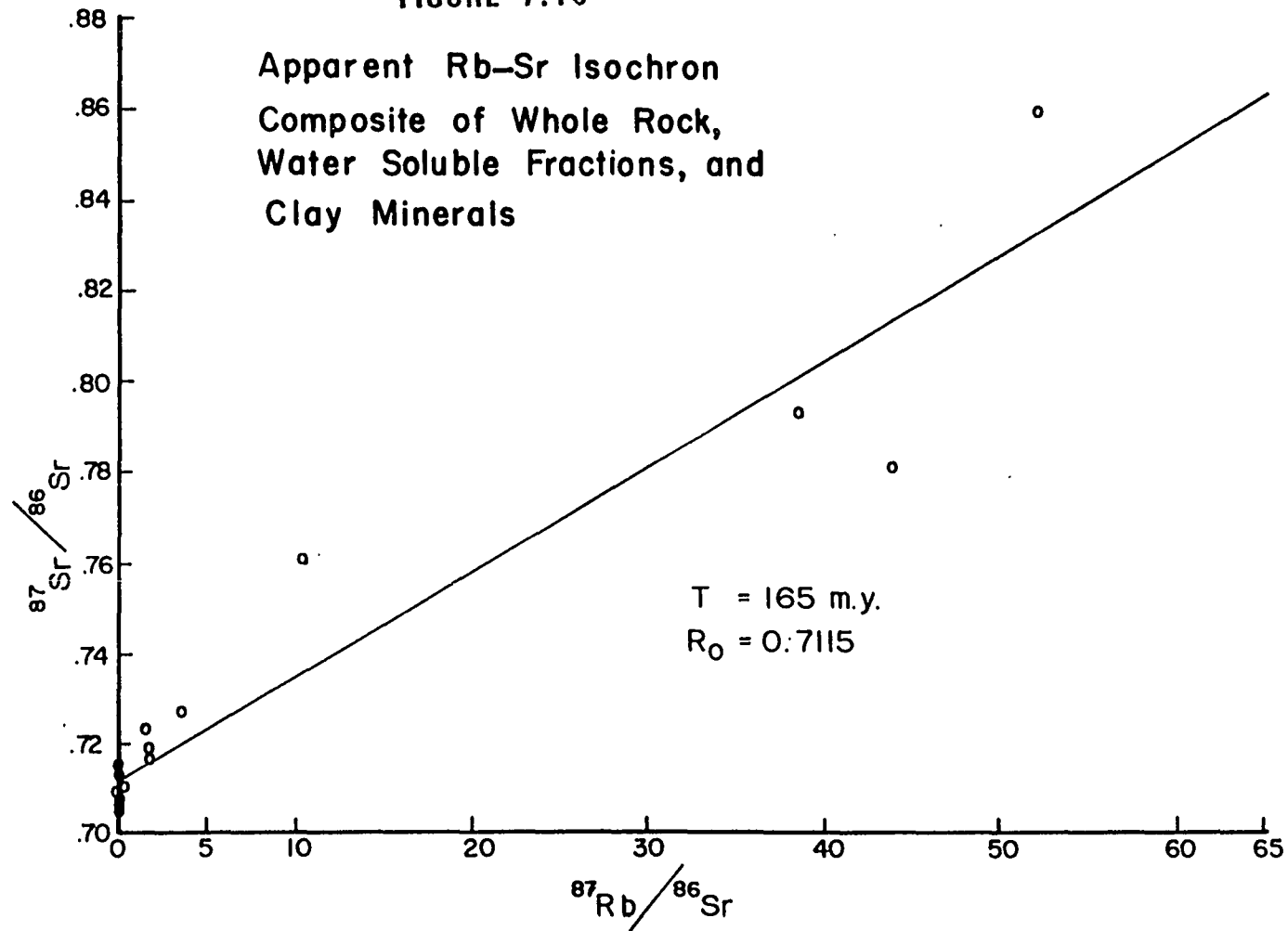
$T = 204$ m.y.
$R_0 = 0.7137$
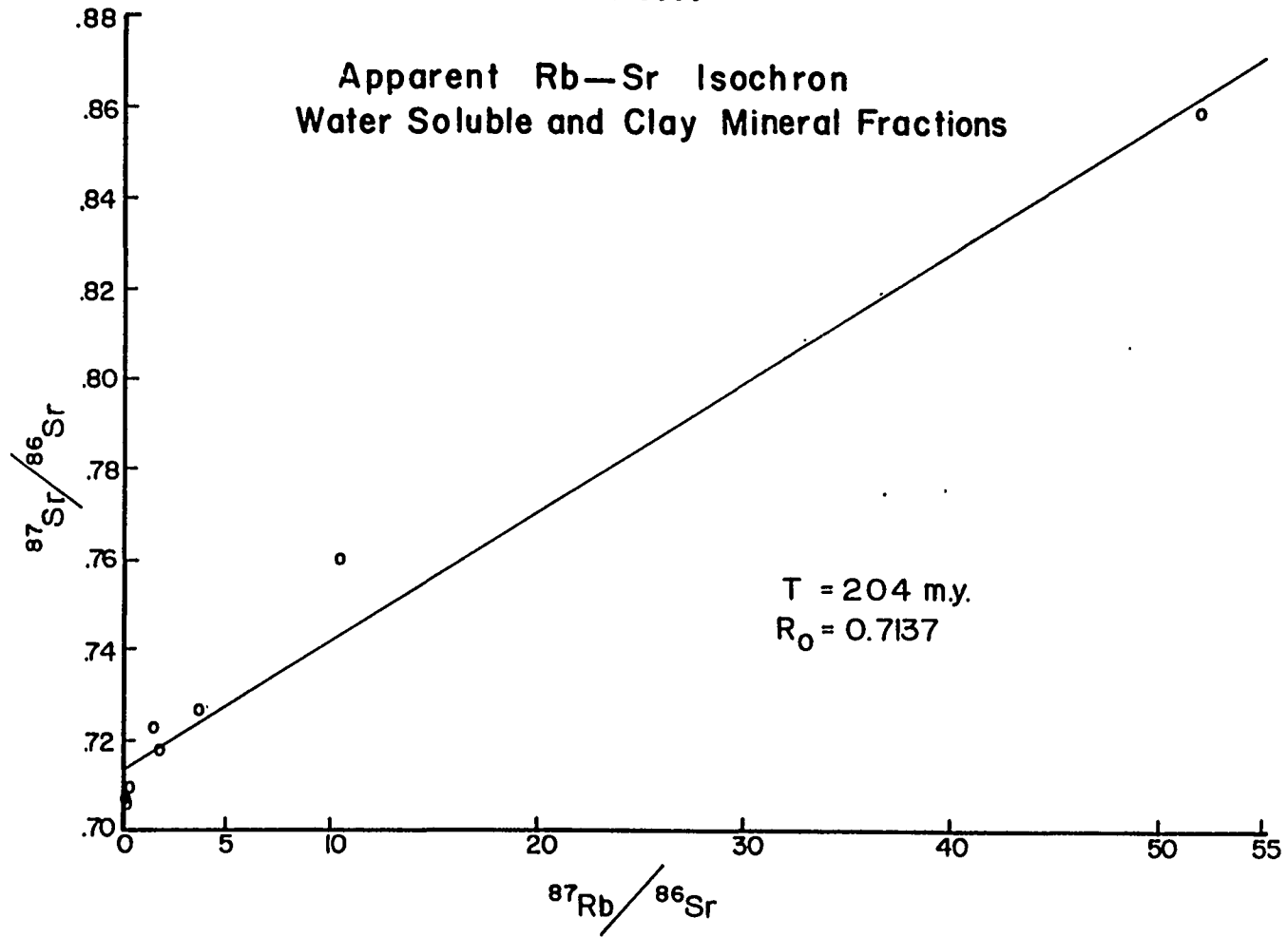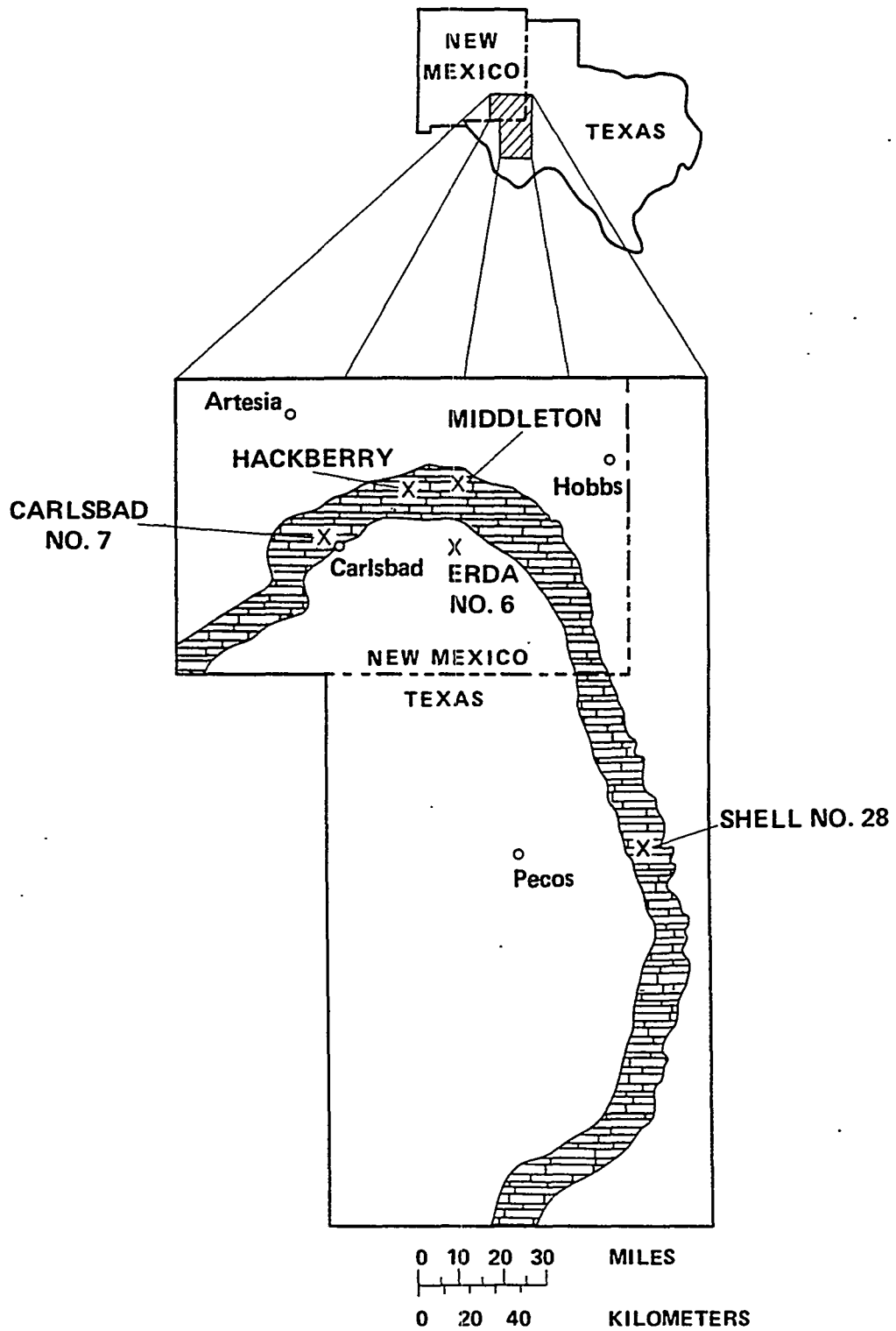
FIGURE 7.18 Map of a portion of the Delaware Basin (southeast
New Mexico, west Texas) showing locations of holes
whose fluids are sampled for [234] U/ [238] U-disequi-
librium age-dating. The brick-pattern shows the
surface projection and outcrop of the capitan reef
limestone. (from Hiss, 1975)

FIGURE 7.19   Graph of the equation $f = \dfrac{(\alpha_0 - 1)(\alpha_r - 1)}{\alpha_b - \alpha_0 + r(\alpha_r - 1)}$

for the ERDA No. 6 assemblage of rock and brine, in which $r = 16.42$, $\alpha_r = 1.04$, $\alpha_b = 1.35$.

Uranium disequilibrium ages for the brine are shown according to the equation

$$t = \dfrac{\ln\left(\dfrac{\alpha_b - 1 - fr}{\alpha_0 - 1 - fr}\right)}{-\lambda 2}$$

$a_0 = 1.971$
at $f = 1$

Uranium Leaching

5.7 X 10^5 yr.

7.8 X 10^5 yr.

9.4 X 10^5 yr.

Uranium Deposition

$a_0 = 2.052$
at $f = -1$
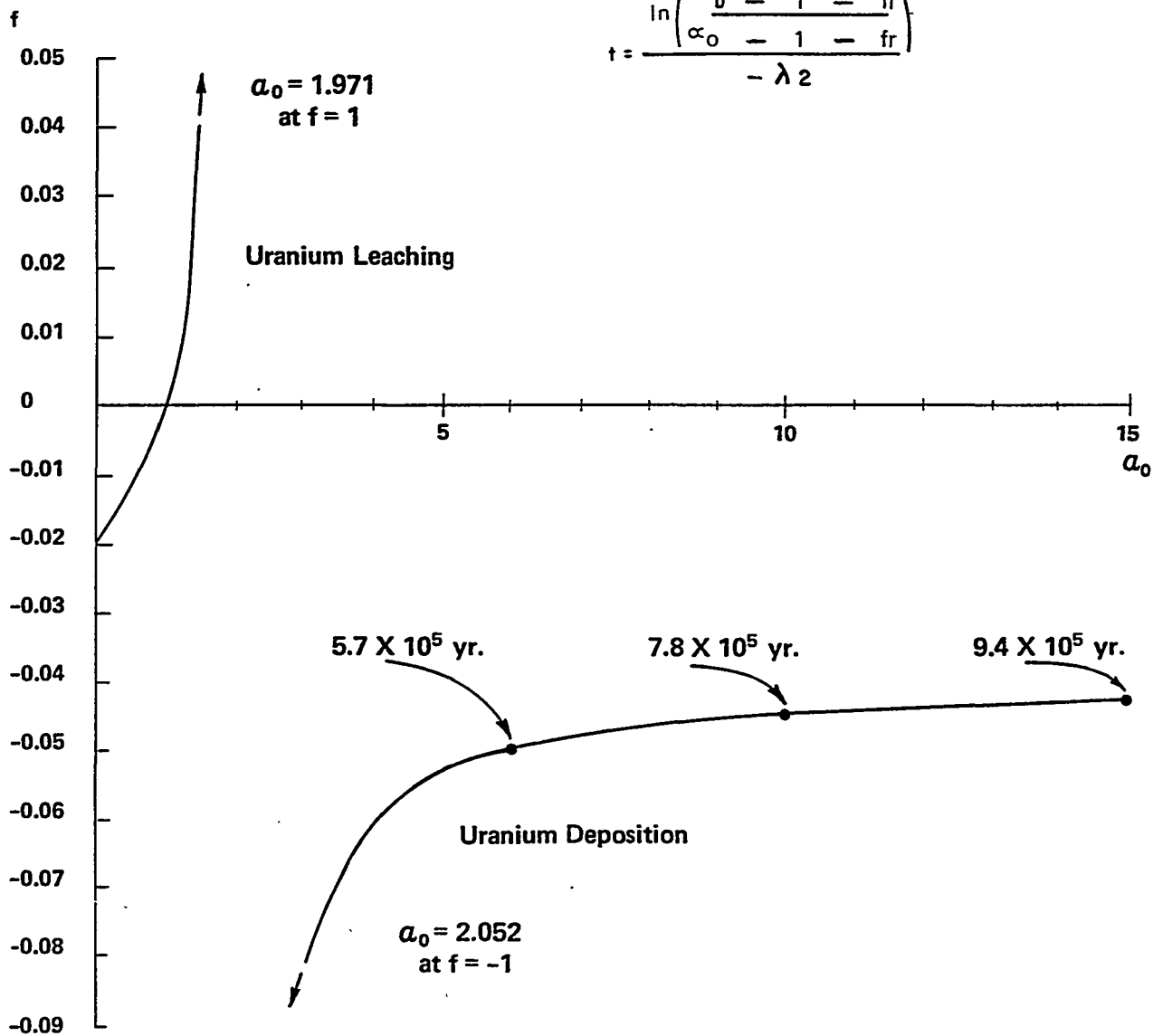
Note that the ERDA No. 6 assemblage is indicative of uranium deposition ($f < 0$) rather than uranium leaching.

t (age)
Million Years

$$a = {}^{234}U/{}^{238}U \text{ in solution}$$

$$t = \frac{\ln\left(\frac{a-1}{a_0-1}\right)}{-2.806}$$
(million years)

HACKBERRY

ERDA NO. 6

MIDDLETON

SHELL NO. 28

CARLSBAD NO. 7

a_0
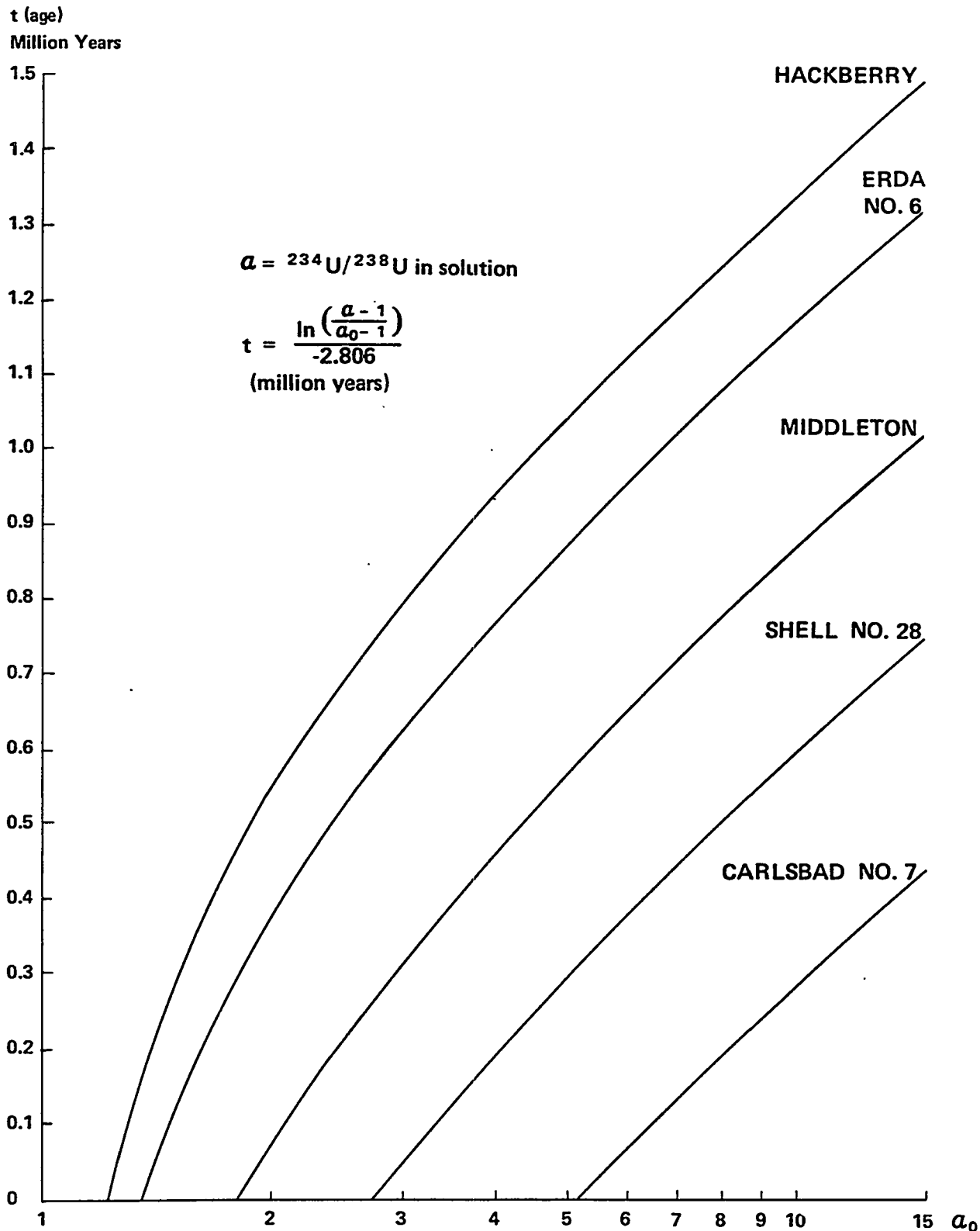
FIGURE 7.20   Uranium disequilibrium ages as a function of
original ^{234}U/ ^{238}U ratio, for Delaware Basin
groundwaters. These curves are derived from a
model involving no exchange or uranium between
rock and water.

TABLE 7.1. MINERAL CONTENT OF ERDA #9 CORE SAMPLES (M=MAJOR, T=TRACE).

ERDA 9
CORE #

(DEPTH IN FEET)	ANHYDRITE	CLAY	HALITE	LOEWEITE	MAGNESITE	POLYHALITE	QUARTZ	SYLVITE
1162.7	T		M					
1165.7	M		M					
1168.0	M		T					
1168.8			M					
1172.8			M			M		
1173.4	M				M		T	
1174.1			M			M		
1405.7			M		T			
1418.8						M		
1584.0			M					
1610.0			M					
1632.4	M				M			
1632.8						M		
1648.5			M	T				
2034.7	M		M				T	
2035.7	T		M					T
2036.3			M					
2065.0			M					
2067.5			M			T		
2302.6	M		T			M		
2413.7			M			M		
2414.2			M			M		
2415.6	M		M					
2512.0	M		M					
2516.3	M		M		T			
2518.8	M							
2528.7	M				T			
2529.0	M		T					
2538.5	M				T			

TABLE 7.1. MINERAL CONTENT OF ERDA #9 CORE SAMPLES (M=MAJOR, T=TRACE), continued

ERDA 9
CORE #

(DEPTH IN FEET)	ANHYDRITE	CLAY	HALITE	LOEWEITE	MAGNESITE	POLYHALITE	QUARTZ	SYLVITE
2541.0	•	•	M	•	•	•	•	•
2542.0	•	•	M	•	•	•	•	•
2593.2	M	•	•	•	•	•	•	•
2594.5	•	•	M	•	•	•	•	•
2597.0	T	•	M	•	•	•	•	•
2608.9	T	•	M	•	•	•	•	•
2614.7	•	•	M	•	•	•	•	•
2619.6	T	•	M	•	•	•	•	•
2658.5	M	•	M	•	•	•	•	•
2663.3	T	•	M	•	•	•	•	•
2696.4	M	•	M	•	T	•	•	•
2706.5	•	•	M	•	•	•	•	•
2711.9	T	•	M	•	T	•	•	•
2759.0	T	•	M	•	•	•	•	•
2768.5	M	T	M	•	•	•	•	•
2820.7	M	•	M	•	•	•	•	•
2820.6	T	•	M	•	•	•	•	•
2821.0	T	•	M	•	•	•	•	•
2826.5	T	•	M	•	•	•	•	•
2845.3	M	•	•	•	T	•	•	•
2848.8	M	•	•	•	•	•	•	•

TABLE 7.2

Size Distribution of Ground Samples

Mesh	% of Sample *
> 20	5.2
20-28	8.8
28035	19.9
35-65	57.0
65-100	6.1
100-200	2.9
< 200	0.2

*Total ≠ 100 due to rounding

TABLE 7.3

Listing of Minerals Named in Subsection 7.3

Mineral Name	Chemical Composition
Anhydrite	$CaSO_4$
Bloedite	$Na_2 Mg(SO_4)_2 \cdot 4H_2O$
Carnallite	$K Mg Cl_3 \cdot 6 H_2O$
Chlorite	$Mg_5Al_2Si_3O_{10}(OH)_8$
Glaserite	$K_3Na(SO_4)_2$
Glauberite	$Na_2Ca(SO_4)_2$
Gypsum	$CaSO_4 \cdot 2H_2O$
Halite	$NaCl$
Illite	$K_{0.6}Mg_{0.25}Al_{2.3}Si_{3.5}O_{10}(OH)_2$
Iron Oxides (FEOX)	$Fe_2O_3 \cdot XH_2O$
Kainite	$KMgCl SO_4 \cdot 11/4 H_2O$
K-Feldspar	$K Al Si_3O_8$
Kieserite	$MgSO_4 \cdot H_2O$
Langbeinite	$K_2Mg_2 (SO_4)_3$
Leonite	$K_2Mg(SO_4)_2 \cdot 4 H_2O$
Montmorillonite	$Mg_{0.16} Al_{2.33} Si_{3.67} O_{10}(OH)_2$
Polyhalite	$K_2Mg Ca(SO_4)_4 \cdot 2 H_2O$
Quartz	SiO_2
Sylvite	KCl
Talc	$Mg_3 Si_4 O_{10} (OH)_2$
Thenardite	$Na_2 SO_4$

TABLE 7.4

ERDA No. 9 Samples Chosen for Silicate Mineralogy

Depth (ft)	Sample	Gross Lithology	Stratigraphic Position
1163.3-1163.6	MB-CS-18	Rock salt	SALADO Fm.
1165.1	MB-CS-16	Anhydrite	
1166.17	MB-CS-17	o Anhydrite	
1167.5	MB-CS-1	Anhydrite	
1168.31	MB-CS-6	Anhydrite w/ halite	
1169.4-1169.5	MB-CS-19	Rock salt	
1172.9	MB-CS-5	Polyhalite	
1173.7-1173.8	MB-CS-20	Rock salt	
1242.5	JL-CS-24	Rock salt	
1242.9-1243.1	JL-CS-18	Polyhalite w/ halite	
1243.6-1243.7	JL-CS-27	Polyhalite w/ halite	
1244.2-1244.5	JL-CS-15	Rock salt w/ polyhalite	
1244.5-1244.8	JL-CS-16	Polyhalite w/ halite and clay	
1244.8	JL-CS-12	o Clay	
1245.0-1245.3	JL-CS-20	Rock Salt	
1246.7-1247.1	JL-CS-21	Rock Salt	
1247.1-1247.2	JL-CS-5	o Clay	
1325.2-1325.4	JL-CS-10	o Polyhalite w/ anhydrite veins	
1327.0-1327.2	JL-CS-23	Polyhalite	
1327.7-1327.8	JL-CS-26	Polyhalite w/ halite	
1328.2-1328.4	JL-CS-25	Polyhalite w/ halite and clay	
1328.6	JL-CS-3	o Clay	
1328.7-1329.8	JL-CS-17	Rock Salt	

Depth (ft)	Sample	Gross Lithology	Stratigraphic Position
1404.6-1404.7	MB-CS-21	Rock Salt	11th ore zone
1418.2	MB-CS-7	Anhydrite with clay seam	
1418.6	MB-CS-8	Polyhalite	marker bed 117
1440.4-1440.6	JL-CS-2	o Polyhalite w/ halite	
1441.0-1441.3	JL-CS-6	o Polyhalite	
1441.7	JL-CS-4	o Clay	
1466.4-1466.6	JL-CS-11	o Polyhalite w/ clay	
1466.8-1467.1	JL-CS-9	o Polyhalite w/ clay	
1467.7-1468.1	JL-CS-22	Rock salt w/ clay	
1468.1	JL-CS-14	o Clay	
1535.6-1535.8	JL-CS-8	Polyhalite w/ anhydrite	
1536.5	JL-CS-7	Anhydrite	
1536.5-1536.6	JL-CS-19	Polyhalite w/ clay	
1537.8-1537.9	JL-CS-18	o Polyhalite w/ anhydrite	
1584.4-1584.5	MB-CS-22	Rock salt	near 5th ore zone
1609.5-1609.8	MB-CS-23	Rock salt	
1649.4-1649.6	MB-CS-24	Rock salt	near 4th ore zone
2034.5	MB-CS-14	Anhydrite	
2035.6-2035.9	MB-CS-25	Rock salt	
2036.5-2036.7	MB-CS-26	Rock salt	
2037.3	MB-CS-4	o Anhydrite	

Depth (ft)	Sample	Gross Lithology	Stratigraphic Position
2065.3-2065.4	MB-CS-29	Rock salt	
2066.1	MB-CS-28	Rock salt	
2067.0	MB-CS-27	o Rock salt	
2414.8	MB-CS-30	Rock salt	⌒ 16 ft above marker bed 143
2512.5	MB-CS-31	o Rock salt	
2517.9	MB-CS-12	Anhydrite)	
2518.3	MB-CS-13	o Anhydrite)	
		)	Cowden Anhydrite
2528.0	MB-CS-11	Anhydrite)	
2541.2-2541.9	MB-CS-32	o Rock salt	
2608.9-2609.5	MB-CS-33	Rock salt	
2615.9-2616.4	MB-CS-41	Rock salt	
2616.4-2616.8	MB-CS-34	Rock salt	
2617.2-2617.7	MB-CS-35	Rock salt	
2705.2-1705.6	MB-CS-37	Rock salt	
2705.8	MB-CS-10	o Rock salt	

TABLE 7.4, continued

Depth (ft)	Sample	Gross Lithology	Stratigraphic Position
2758.2-2758.6	MB-CS-36	o Rock salt	
2819.1-2819.6	MB-CS-39	o Rock salt	
2820.2	MB-CS-15	o Anhydrite	
2820.3	MB-CS-2	Anhydrite	
2821.1-2821.7	MB-CS-38	Rock salt	
2827.3-2827.5	MB-CS-40	o Rock salt	
			2829
2846.0	MB-CS-9	o Anhydrite	
2848.4	MB-CS-3	o Anhydrite	CASTILE Fm.
2867.4-2867.6	MB-CS-42	Anhydrite	

o Samples subjected to semi quantitative analysis (see Table 7.10).

TABLE 7.5

Core depths of samples selected for mineralogic-geochemical analysis.

Sample	Depth (ft)		Sample	Depth (ft)
MB-CS-1	1167.5		MC-CS-36	2758.2-2758.6
-2	2820.3		-37	2705.2-2705.6
-3	2848.4		-38	2821.1-2821.7
-4	2037.3		-39	2819.1-2818.6
-5	1172.9		-40	2827.3-2827.5
MB-CS-6	1168.3		MC-CS-41	2615.9-2616.4
-7	1418.2		-42	2867.4-2867.6
-8	1418.6			
-9	2846.0			
-10	2705.8			
MB-CS-11	2528.0		JL-CS-1	1441.5
-12	2517.9		-2	1440.4-1440.6
-13	2518.3		-3	1328.6
-14	2034.5		-4	1441.7
-15	2820.2		-5	1247.1-1247.3
MB-CS-16	1165.1		JL-CS-6	1441.0-1441.3
-17	1166.2		-7	1536.5
-18	1163.3-1163.6		-8	1535.6-1535.8
-19	1169.4-1169.5		-9	1466.8-1467.1
-20	1173.7-1173.8		-10	1325.2-1325.4
MB-CS-21	1404.6-1404.7		JL-CS-11	1466.4-1466.6
-22	1484.4-1584.5		-12	1244.8
-23	1609.5-1609.8		-13	1467.5
-24	1649.4-1649.6		-14	1468.1
-25	2035.6-2035.9		-15	1244.2-1244.5
MB-CS-26	2036.5-2036.7		JL-CS-16	1244.5-1244.8
-27	2067.0		-17	1328.7-1329.8
-28	2066.1		-18	1537.8-1537.9
-29	2065.3		-19	1536.5-1536.6
-30	2414.8		-20	1245.0-1245.3

Core depths of samples selected for mineralogic-geochemical analysis.

Sample	Depth (ft)		Sample	Depth (ft)
MB-CS-31	2512.5		JL-CS-21	1246.7-1247.1
-32	2541.2-2541.9		-22	1467.7-1468.1
-33	2608.9-2609.5		-23	1327.0-1327.2
-34	2616.4-2616.8		-24	1242.5-1242.8
-35	2617.2-2617.7		-25	1328.2-1328.4
			JL-CS-26	1327.7-1327.8
			-27	1343.6-1343.7
			-28	1242.9-1243.1

TABLE 7.6

Quantities of water-leach and EDTA-leach residues in samples from
the ERDA-9 core. Sulfate lithologies (anhydrites and polyhalites)
and salztons were not subjected to water leach.

Hole Depth (ft)	Sample Number	Bulk wt. (g)	LEACH RESIDUES (Percent of bulk)		EDTA Residue wt. (g)	Lithology
			WATER	EDTA		
1163.5	MB-CS-18	1820	0.005	neg	neg+	rock salt
1165.1	MB-CS-16	40	>90	0.11	.043	anhydrite
1166.2	MB-CS-17	1229	>90	0.20	2.33	anhydrite
1167.5	MB-CS-1	38	>90	0.074	0.027	anhydrite
1168.3	MB-CS-6	358	>75	0.23	0.81	anhydrite
1169.4	MB-CS-19	209	0.36	0.005	0.011+√	rock salt
1172.9	MB-CS-5	40	>90	0.13	0.050	polyhalite
1173.7	MB-CS-20	259	0.012	neg	neg+	rock salt
1242.5	JL-CS-24	655	1.89	*	*	rock salt
1242.9	JL-CS-28	200	>75	0.76	1.52	polyhalite
1243.6	JL-CS-27	200	>75	0.60	1.21	polyhalite
1244.4	JL-CS-15	537	0.013	0.003	0.018	rock salt
1244.6	JL-CS-16	400	>75	1.13	4.51	polyhalite
1244.8	JL-CS-12	#	>90	>90	8.40	salzton
1245.1	JL-CS-20	400	6.18	1.15	4.60	rock salt
1246.8	JL-CS-21	747	0.21	*	*	rock salt
1247.2	JL-CS-5	#	>90	>90	2.70	salzton
1325.3	JL-CS-10	641	29.8	0.26	1.68	rock salt
1327.0	JL-CS-23	350	>75	0.25	0.89	polyhalite
1327.8	JL-CS-26	200	>75	0.30	0.61	polyhalite
1328.3	JL-CS-25	200	>75	1.13	2.26	polyhalite
1328.6	JL-CS-3	#	>90	>90	1.46	salzton
1328.7	JL-CS-17	1765	0.18	0.12	2.09	rock salt

Hole Depth (ft)	Sample Number	Bulk wt. (g)	LEACH RESIDUES (Percent of bulk)		EDTA Residue wt. (g)	Lithology
			WATER	EDTA		
1404.6	MB-CS-21	244	2.5	1.0	2.43	rock salt
1418.2	MB-CS-7	40	>90	20.80	8.32	anhydrite
1418.6	MB-CS-8	1120	>90	0.62	6.94	polyhalite
1440.5	JL-CS-2	200	>75	0.83	1.66	polyhalite
1441.2	JL-CS-6	600	>75	0.13	0.80	polyhalite
1441.7	JL-CS-4	#	>90	>90	2.92	salzton
1466.5	JL-CS-11	400	>75	0.42	1.67	polyhalite
1466.9	JL-CS-9	200	>75	3.99	7.97	polyhalite
1467.9	JL-CS-22	860	4.17	1.22	10.5	rock salt.
1468.1	JL-CS014	#	>90	>90	3.30	saltzon
1535.7	JL-CS-8	400	>75	0.44	1.76	polyhalite
1536.5	JL-CS-7	320	>75	2.63	8.41	anhydrite
1536.6	JL-CS-19	360	>75	0.37	1.33	polyhalite
1537.8	JL-CS-18	400	>75	0.55	2.19	polyhalite
1584.4	MB-CS-22	248	0.53	0.42	1.20+✓	rock salt
1609.6	MB-CS-23	473	0.037	0.017	0.081	rock salt
1649.5	MB-CS-24	176	1.6	1.1	1.90+✓	rock salt
2034.5	MB-CS-14	104	>90	3.9	4.07	anhydrite
2035.7	MB-CS-25	891	0.23	0.009	0.078+✓	rock salt
2036.6	MB-CS-26	810	0.23	0.025	0.20+✓	rock salt
2073.3	MB-CS-4	145	>90	5.0	7.28	anhydrite
2065.3	MB-CS-29	1085	0.18	0.11	1.17+✓	rock salt
2066.1	MB-CS-28	220	3.3	1.5	3.38	rock salt
2067.0	MB-CS-27	229	2.8	0.83	1.90	rock salt
24⁻ 8	MB-CS-30	421	36.3	0.049	0.21	rock salt

Hole Depth (ft)	Sample Number	Bulk wt. (g)	LEACH RESIDUES (Percent of bulk) WATER	EDTA	EDTA Residue wt. (g)	Lithology
2512.5	MB-CS-31	1073	1.79	0.074	0.074	rock salt
2517.9	MB-CS-12	40	>90	0.024	0.010+	anhydrite
2518.3	MB-CS-13	586	>90	0.55	3.20	anhydrite
2528.0	MB-CS-11	40	>90	0.23	0.094	anhydrite
2541.5	MB-CS-32	891	0.70	0.21	1.83	rock salt
2609.2	MB-CS-33	901	0.043	0.015	0.14+√	rock salt
2616.2	MB-CS-41	811	0.165	0.076	0.62+√	rock salt
2616.6	MB-CS-34	660	0.071	0.004	0.027+√	rock salt
2617.5	MB-CS-35	1015	1.17	0.18	1.83	rock salt
2705.4	MB-CS-37	638	13.3	0.65	4.14	rock salt
2705.8	MB-CS-10	450	>90	2.2	9.87	anhydrite
2758.4	MB-CS-36	421	6.6	0.77	3.25	rock salt
2819.3	MB-CS-39	982	2.2	0.27	2.65	rock salt
2820.2	MB-CS-15	520	>90	0.82	4.25	anhydrite
2820.3	MB-CS-2	640	>90	0.59	3.79	anhydrite
2821.4	MB-CS-38	916	1.25	0.039	0.36	rock salt
2828.7	MB-CS-40	920	1.22	0.13	1.17	rock salt
2846.0	MB-CS-9	200	>90	1.2	2.45	anhydrite
2848.4	MB-CS-3	656	>90	0.90	5.93	anhydrite
2867.5	MB-CS-42	240	>90	0.85	2.04	anhydrite

* Water-leach and EDTA-leach dissolutions of this sample not complete.
# Sample is hand-picked fragment of saltzton.
+ Reported as containing "negligible insoluble residue" Table 7.7.
√ A subsequent second dissolution of a substantially greater quantitiy of the sample yielded these data.

TABLE 7.7

Relative Abundances of minerals in EDTA-insoluble residues.

Sample	Depth (ft)	EDTA-insoluble residue				<2 μm fraction of residue				
		qtz	feld	hem	clay	il	ch	serp	talc	exp
MB-CS-18	1163.5	Negligible insoluble residue								
MB-CS-16	1165.1	XX	--	--	X	X	a	--	--	XX
MB-CS-17	1166.2	XX	x	--	XX	x	a	--	--	XX
MB-CS-1	1167.5	--	--	--	XX	X	--	--	--	XX
MB-CS-6	1168.3	XX	x	--	XX	x	a	--	--	XX
MB-CS-19	1169.4	Negligible insoluble residue								
MB-CS-5	1172.9	XX	--	--	x	x	--	--	--	XX
MB-CS-20	1173.7	Negligible insoluble residue								
JL-CS-12	1244.8	XX	x	--	XX	X	X	--	--	X
JL-CS-5	1247.2	XX	x	--	XX	XX	X	--	--	X
JL-CS-10	1325.3	a	--	--	XX	--	--	--	--	XX
JL-CS-3	1328.6	XX	X	--	XX	X	X	--	--	X

TABLE 7.7, continued

Relative Abundances of minerals in EDTA-insoluble residues (cont'd).

Sample	Depth (ft)	EDTA-insoluble residue				$<2\,\mu\mathrm{m}$ fraction of residue				
		qtz	feld	hem	clay	il	ch	serp	talc	exp
MB-CS-21	1404.6	XX	a	--	XX	x	x	--	X	XX
MB-CS-7	1418.2	--	x	--	XX	XX	X	--	--	X
MB-CS-8	1418.6	--	a	x	XX	x	x	--	--	XX
JL-CS-2	1440.5	X	XX	a	XX	a	a	--	--	XX
JL-CS-6	1441.2	X	XX	X	XX	XX	X	--	--	X
JL-CS-4	1441.7	--	X	--	XX	XX	X	--	--	X
JL-CS-11	1466.5	--	x	X	XX	XX	X	--	--	X
JL-CS-9	1466.9	XX	x	x	X	XX	X	--	--	XX
JL-CS-14	1468.1	X	X	--	XX	XX	X	--	--	XX

Relative Abundances of minerals in EDTA-insoluble residues (cont'd).

Sample	Depth (ft)	EDTA-insoluble residue				< 2 μm fraction of residue				
		qtz	feld	hem	clay	il	ch	serp	talc	exp
JL-CS-8	1535.7	--	X	x	XX	XX	x	--	--	XX
JL-CS-7	1536.5	a	--	--	XX	--	--	--	--	XX
JL-CS-18	1537.8	X	--	x	XX	XX	x	--	--	X
MB-CS-22	1584.4	Negligible insoluble residue								
MB-CS-23	1609.6	XX	X	x	XX	XX	X	--	--	XX
MB-CS-24	1649.5	Negligible insoluble residue								
MB-CS-14	2034.5	XX	--	--	x	x	x	--	--	XX
MB-CS-25	2035.7	Negligible insoluble residue								
MB-CS-26	2036.6	Negligible insoluble residue								
MB-CS-4	2037.3	XX	--	--	X	x	x	--	--	XX

TABLE 7.7, continued

Relative Abundances of minerals in EDTA-insoluble residues (cont'd).

Sample	Depth (ft)	EDTA-insoluble residue				$< 2 \mu$ m fraction of residue				
		qtz	feld	hem	clay	il	ch	serp	talc	exp
MB-CS-29	2065.3				Negligible insoluble residue					
MB-CS-28	2066.1	XX	a	--	XX	a	a	--	--	XX
MB-CS-27	2067.0	XX	X	x	XX	x	x	--	--	XX
MB-CS-30	2414.8	XX	X	--	X	a	x	--	--	XX
MB-CS-31	2512.5	X	--	a	XX	x	x	--	--	XX
MB-CS-13	2518.3	X	x	--	XX	a	a	--	--	XX
MB-CS-11	2528.0	--	--	--	XX	--	--	--	--	XX
MB-CS-32	2541.5	X	a	--	XX	X	X	--	--	XX

Relative Abundances of minerals in EDTA-insoluble residues (cont'd).

Sample	Depth (ft)	EDTA-insoluble residue				$< 2 \mu$ m fraction of residue				
		qtz	feld	hem	clay	il	ch	serp	talc	exp
MB-CS-33	2609.2			Negligible insoluble residue						
MB-CS-41	2616.2			Negligible insoluble residue						
MB-CS-34	2616.6			Negligible insoluble residue						
MB-CS-35	2617.5	XX	X	a	XX	XX	X	--	--	XX
MB-CS-37	2705.4	XX	X	a	X	XX	X	--	--	XX
MB-CS-10	2705.8	XX	X	a	X	X	x	--	--	XX
MB-CS-36	2758.4	XX	X	a	X	XX	X	--	--	XX

Relative Abundances of minerals in EDTA-insoluble residues (cont'd).

Sample	Depth (ft)	EDTA-insoluble residue				$< 2 \mu$ m fraction of residue				
		qtz	feld	hem	clay	il	ch	serp	talc	exp
MB-CS-39	2819.3	XX	X	--	X	XX	x	--	--	XX
MB-CS-15	2820.2	XX	--	--	XX	--	a	--	XX	X
MB-CS-2	2820.3	a	X	--	XX	XX	--	--	--	XX
MB-CS-38	2821.4	--	--	--	XX	--	--	XX	--	XX
MB-CS-40	2827.4	--	--	--	XX	--	--	XX	--	XX
MB-CS-9	2846.0	a	--	a	XX	--	--	XX	--	XX
MB-CS-3	2848.4	--	--	--	XX	--	--	X	--	XX

Relative Abundances of minerals in EDTA-insoluble residues (cont'd).

Sample	Depth (ft)	EDTA-insoluble residue				$< 2 \mu$ m fraction of residue				
		qtz	feld	hem	clay	il	ch	serp	talc	exp
MB-CS-42	2867.5	--	--	--	XX	--	x	X	--	X

Minerals: qtz = quartz; feld = feldspar; hem = hematite; il = illite; ch = chlorite; serp = serpentine; exp = expandable (smectite-bearing).

Relative abundances: XX = dominant constituent; X = major constituent; x = minor constituent; a = accessory constituent. All abundances based on relative intensities of major diffraction maxima.

TABLE 7.8

Low-angle diffraction maxima (Å) of expandable clays in the < 2 μ m fraction of the EDTA-insoluble residues.

Sample	Depth (ft)	Air-dried	Glycol-saturated	375°C (> 1hr)	500°C (> 1hr)
MB-CS-16	1165.1	14.5	n.d.	n.d.	n.d.
MB-CS-17	1166.2	13.8, 30.5	15.5, 32.7	13.8, (29.4)	13.6, (25.2)
MB-CS-1	1167.5	14.5	n.d.	n.d.	n.d.
MB-CS-6	1168.3	14.5, (25.2)	15.5, (35.3)	13.6, 31.6	13.2, 11.8, (27.6)
MB-CS-5	1172.9	14.3	n.d.	n.d.	n.d.
JL-CS-16	1244.6	13.8, 29.4	15.5, 11.2, 31.6	n.d.	n.d.
JL-CS-12	1244.8	13.6, 29.4	15.5, 31.5	13.6	13.2
JL-CS-20	1245.1	13.8, (30.5)	15.5, 34.0	n.d.	n.d.
JL-CS-5	1247.2	14.5, 30.5	15.5, 11.2, 31.6	14.3	13.6
JL-CS-10	1325.3	10.2	10.4, (12.1)	9.8	9.8, 11.0-11.9
JL-CS-3	1328.6	14.0, 30.5	15.5, 11.2, 31.6	14.5, (31.6)	12.6-14.7, (22.21)
MB-CS-21	1404.6	13.8, 31.6	15.8, 34.0	13.8, (32.7)	13.4, (29.4)
MB-CS-7	1418.2	13.8, (30.5)	n.d.	n.d.	n.d.
MB-CS-8	1418.6	13.4	15.5, (34.0)	13.6, (27.6)	11.6, (27.6)

TABLE 7.8, continued

Low-angle diffraction maxima (Å) of expandable clays in the < 2 μ m fraction of the EDTA-insoluble residues (cont'd).

Sample	Depth (ft)	Air-dried	Glycol-saturated	375°C (> 1hr)	500°C (> 1hr)
JL-CS-2	1440.5	10.3	10.2, 11.8	9.8	n.d.
JL-CS-6	1441.2	10.7, 13.6, (29.4)	11.3, 15.5, (31.6)	10.2, 13.0-14.3	10.0
JL-CS-4	1441.7	13.8, 31.6	15.5, 31.6	13.8, (29.4)	13.2
JL-CS-11	1466.5	13.8, 11.2, (30.5)	15.2, (32.7)	13.6, (26.0)	n.d.
JL-CS-9	1466.9	14.7	16.1	13.8	13.8
JL-CS-22	1467.9	14.1, 31.6	15.5, 34.0	n.d.	n.d.
JL-CS-14	1468.1	13.6, 30.5	15.5, 32.7	13.6	13.2
JL-CS-8	1535.7	10.3, 13.6	9.4, 11.5, 16.1	9.8, 13.6	9.7
JL-CS-7	1536.5	10.3	9.3, 11.3	9.9	9.8
JL-CS-18	1537.8	14.3, 32.7	15.8, 34.0	n.d.	n.d.
MB-CS-23	1609.6	12.3	n.d.	n.d.	n.d.
MB-CS-14	2034.5	13.8, 30.5	15.2, 31.6	14.0, 11.9, (31.6)	11.9, 13.2, 29.4
MB-CS-4	2037.3	13.5	15.5, 31.6	13.2, (28.5)	13.0

Low-angle diffraction maxima (Å) of expandable clays in the < 2 μ m fraction of the EDTA-insoluble residues (cont'd).

Sample	Depth (ft)	Air-dried	Glycol-saturated	$375^{\circ}C$ (> 1hr)	$500^{\circ}C$ (> 1hr)
MB-CS-28	2066.1	14.5, 30.5	15.5, 31.6	14.0, (29.4)	13.6, (30.5, 22.1)
MB-CS-27	2067.0	14.7, 29.4	16.7, 32.7	14.0, (29.4)	12.6, (26.0)
MB-CS-30	2414.8	13.8, 11.8, (29.4)	15.8, 12.8, (31.6)	13.8, 11.6, (24.5)	11.6, (26.0)
MB-CS-31	2512.5	12.6	n.d.	n.d.	n.d.
MB-CS-12	2517.9	12.8, 31.6	15.5, 31.6	n.d.	n.d.
MB-CS-13	2518.3	12.6, 26.0	17.0, 25.2	13.2, (26.8)	12.3, 10.3, 26.0
MB-CS-11	2528.0	13.2	n.d.	n.d.	n.d.
MB-CS-32	2541.5	13.8, 29.4	15.5, 31.5	13.4, (26.8)	14.2, (31.6)
MB-CS-35	2617.5	13.8, (29.4)	16.7, 32.7	13.8, (26.8)	12.6, 27.6
MB-CS-37	2705.4	14.5, 30.5	16.4, 34.0	13.8, (29.4)	12.5
MB-CS-10	2705.8	13.4	16.7, (35.3)	14.3, (30.5)	14.3, 11.8, (27.6)
MB-CS-36	2758.4	14.0, 29.4	16.4, 32 7	13.8, (29.4)	12.5, (29.4)

Low-angle diffraction maxima (Å) of expandable clays in the < 2 μm fraction of the EDTA-insoluble residues (cont'd).

Sample	Depth (ft)	Air-dried	Glycol-saturated	375°C (> 1hr)	500°C (> 1hr)
MB-CS-39	2819.3	14.5, 29.4	16.1, 31.6	14.5	13.6, (22.0)
MB-CS-15	2820.2	11.6, (26.8)	14.7, (27.6)	11.6, (24.5)	11.6, (26.8)
MB-CS-2	2820.3	14.5	----	10.4	9.8-17.7
MB-CS-38	2821.4	14.7	----	13.8	13.8
MB-CS-40	2827.4	14.7, 11.3	17.0	14.7	n.d.
MB-CS-9	2846.0	12.3, (24.5)	17.0, (28.5)	10.0 – 13.6, (29.4)	13.4
MB-CS-3	2848.4	12.3, (24.5)	17.3, (27.6)	12.63, (27.6)	11.6, (24.5)
MB-CS-42	2867.5	11.8	17.7	14.7	----

n.d. - data not yet determined

Values in parentheses, e.g. (30.5) represent diffraction maximum present only as shoulder.

TABLE 7.9

Mineralogy of Duval Mine Samples
4th Ore Zone

A. Evaporites

Mine Wall Samples	Halite	Sylvite	Polyhalite	Langbeinite
DV-1A	t	–	VA	–
DV-1B	VA	VA	–	–
DV-1C	VA	–	VA	t
DV-1D	VA	VA	t	–
DV-2A	A	VA	–	t
DV-2B	VA	–	A	–
DV-4A	A	–	VA	t
DV-4B	VA	–	–	–
DV-4C	VA	–	–	t
DV-4D	VA	–	–	t
DV-4E	t	t	–	VA
DV-5A	VA	–	–	–
DV-5B	VA	A	t	--

B. 2 Micron Fractions (Silicates)

Mine Wall Samples	Chlorite	Saponite	Chlorite-Saponite	Illite	Talc	Serpentine	Insoluble Residue (Wt. %)
DV-4B	t	–	VA	VA	t	A	15.7
DV-4C	–	–	VA	VA	t	A	12.3
DV-4D	t	t	VA	A	–	t	32.3
DV-5A	t	t	VA	A	t	A	10.3

VA : very abundant
A : abundant
t : tract
– : not detected

TABLE 7.10

Semiquantitive* chemical analysis of EDTA-insoluble fractions from ERDA-9 core.

	MB-CS-17	JL-CS-12	JL-CS-5	JL-CS-10	JL-CS-3	JL-CS-2	JL-CS-6	JL-CS-4
Depth (ft)	1166.2	1244.8	1247.1	1325.3	1328.6	1440.5	1441.2	1441.7
Lithology[+]	Anhydr.	Clay	Clay	Polyhal.	Clay	Polyhal.	Polyhal.	Clay

Weight Percent

SiO_2	59.	50.	50.	59.	52.	56.	45.	38.
TiO_2	.8	.9	1.2	.2	1.4	.4	.7	1.4
Al_2O_3	12.	13.	15.	12.	15.	6.2	2.5	18.
FeO[@]	1.2	2.4	3.8	1.3	3.2	5.3	14.	4.5
MgO	20.	25.	20.	32.	18.	20.	15.	19.
CaO	.01	.01	.04	.002	.008	.02	.03	.06
Na_2O	1.2	1.2	1.0	1.0	.5	2.4	1.4	1.6
K_2O	1.8	2.3	3.0	.3	3.3	2.9	2.0	4.6

Semiquantitive* chemical analysis of EDTA-insoluble fractions from ERDA-9 core.

	MB-CS-17	JL-CS-12	JL-CS-5	JL-CS-10	JL-CS-3	JL-CS-2	JL-CS-6	JL-CS-4
Depth (ft)	1166.2	1244.8	1247.1	1325.3	1328.6	1440.5	1441.2	1441.7
Lithology[+]	Anhydr.	Clay	Clay	Polyhal.	Clay	Polyhal.	Polyhal.	Clay

Atom Proportions (al = 1.0)

Si	4.2	3.2	2.9	4.3	3.0	7.6	15.	1.8
Ti	.04	.04	.05	.01	.06	.04	.2	.05
Al	1.0	1.0	1.0	1.0	1.0	1.0	1.0	1.0
Fe	.07	.13	.18	.08	.15	.61	4.0	.17
Mg	2.1	2.3	1.7	3.5	1.6	4.0	7.4	1.3
Na	.16	.15	.11	.14	.06	.64	92	.14
K	.16	.19	.22	.03	.24	.51	.87	.27

Semiquantitive* chemical analysis of EDTA-insoluble fractions from ERDA-9 core.

	JL-CS-11	JL-CS-9	JL-CS-14	JL-CS-18	MB-CS-4	MB-CS-27	MB-CS-31	MB-CS-13
Depth (ft)	1466.5	1467.0	1468.1	1537.8	2037.3	2067.0	2512.5	2518.3
Lithology[+]	Polyhal.	Polyhal.	Clay	Polyhal.	Anhydr.	Halite	Halite	Anhydr.

Weight Percent

SiO_2	34.	42.	41.	43.	54.	65.	41.	54.
TiO_2	.6	.6	1.2	.6	.8	1.0	.9	.4
Al_2O_3	10.	9.0	14.	8.8	12.	14.	14.	7.0
$FeO^@$	23.	3.7	3.3	8.2	3.7	4.7	N.D.	2.1
MgO	19.	29.	22.	21.	21.	9.3	18.	22.
CaO	.005	.005	.001	.03	.002	.02	.02	.04
Na_2O	1.3	.4	1.6	1.2	1.0	3.9	2.2	2.7
K_2O	2.9	2.6	4.1	2.0	1.5	4.1	2.6	2.5

Semiquantitive* chemical analysis of EDTA-insoluble fractions from ERDA-9 core.

	JL-CS-11	JL-CS-9	JL-CS-14	JL-CS-18	MB-CS-4	MB-CS-27	MB-CS-31	MB-CS-13
Depth (ft)	1466.5	1467.0	1468.1	1537.8	2037.3	2067.0	2512.5	2518.3
Lithology[+]	Polyhal.	Polyhal.	Clay	Polyhal.	Anhydr.	Halite	Halite	Anhydr.

Atom proportions (Al = 1.0)

Si	2.9	3.9	2.5	4.2	4.0	3.9	2.5	6.2
Ti	.04	.04	.05	.04	.04	.04	.04	.03
Al	1.0	1.0	1.0	1.0	1.0	1.0	1.0	1.0
Fe	1.7	.29	.17	.66	.23	.23	--	.20
Mg	2.4	4.0	2.0	3.1	2.3	.83	1.7	3.8
Na	.21	.07	.19	.22	.14	.45	.26	.60
K	.31	.31	.32	.25	.14	.31	.21	.37

Semiquantitive* chemical analysis of EDTA-insoluble fractions from ERDA-9 core.

	MB-CS-32	MB-CS-10	MB-CS-36	MB-CS-39	MB-CS-15	MB-CS-40	MB-CS-9	MB-CS-3
Depth (ft)	2541.5	2705.8	2758.4	2819.3	2820.2	2827.4	2846.0	2848.4
Lithology[+]	Halite	Halite	Halite	Halite	Anhydr.	Halite	Anhydr.	Anhydr.

Weight Percent

SiO_2	37.	61.	70.	67.	52.	33.	42.	44.
TiO_2	.8	.8	.8	.8	.1	.3	.2	.2
Al_2O_3	13.	12.	12.	12.	3.4	5.0	3.1	3.6
FeO[@]	3.4	4.4	3.4	3.3	.7	1.4	2.6	1.5
MgO	30.	17.	11.	13.	33.	29.	35.	37.
CaO	.002	.01	.1	.06	.007	1.0	.003	.003
Na_2O	1.0	2.9	2.3	2.1	1.6	.9	2.6	1.9
K_2O	1.7	1.8	1.4	1.8	.6	.9	3.3	.7

TABLE 7.10, continued

TABLE 7.10, continued

Semiquantitive* chemical analysis of EDTA-insoluble fractions from ERDA-9 core.

	MB-CS-32	MB-CS-10	MB-CS-36	MB-CS-39	MB-CS-15	MB-CS-40	MB-CS-9	MB-CS-3
Depth (ft)	2541.5	2705.8	2758.4	2819.3	2820.2	2827.4	2846.0	2848.4
Lithology[+]	Halite	Halite	Halite	Halite	Anhydr.	Halite	Anhydr.	Anhydr.

Atom proportions (Al = 1.0)

Si	2.5	4.5	5.1	4.7	13.	5.6	11.	10.
Ti	.04	.04	.04	.04	.02	.04	.04	.04
Al	1.0	1.0	1.0	1.0	1.0	1.0	1.0	1.0
Fe	.19	.27	.21	.19	.15	.20	.59	.30
Mg	2.8	1.8	1.2	1.3	12.	7.3	14.	13.
Na	.13	.41	.33	.29	.77	.30	1.4	.87
K	.15	.17	.13	.16	.19	.19	1.1	.21

* Calculated from 1:1 linear regression; matrix effects and other than unit regression slope not yet included.

+ Anhydr. = anhydrite; polyhal. = polyhalite.

@ Total iron as FeO.

TABLE 7.11

Mineralogy of Cores from ERDA No. 9

Core Footage	Gross Lithology (listed in decreasing order of (trace amount)	Bulk Mineralogy by X-ray Diffraction abundance, lower case indicates
1168.1	Anhydrite Halite Magnesite	Anhydrite Magnesite
1168.55	Anhydrite Halite Polyhalite	Anhydrite Halite Polyhalite
1173.5	Halite "Brown Material"	Halite Polyhalite trace 12Å (expandable) clay
1173.5	silty claystone or anhydrite	Anhydrite Polyhalite
1584.4	Halite "brown material" anhydrite	Halite polyhalite
1649.7	Halite polyhalite anhydrite	Halite polyhalite
2066.8	Halite '"brown material"	Halite Anhydrite quartz magnesite trace 10Å clay (illite) trace 14Å clay (chlorite)

Mineralogy of Cores from ERDA No. 9

Core Footage	Gross Lithology (listed in decreasing order of abundance, lower case indicates (trace amount)	Bulk Mineralogy by X-ray Diffraction
2067.4	see 2066.8	Halite polyhalite quartz? trace 12A^{o} (expandable) clay
2302	Polyhalite "White Material"	Anhydrite Polyhalite
2414.7	Polyhalite Halite Anhydrite	Halite Polyhalite
2415.0	see 2414.7	Polyhalite Anhydrite
2415.4	see 2414.7	Anhydrite
2529.5	Anhydrite magnesite?	Anhydrite Halite Magnesite
2538.5	Anhydrite Halite	Anhydrite Halite
2619.5	Halite anhydrite or magnesite	Halite Anhydrite
2820 B	Anhydrite Halite magnesite	Anhydrite Halite

TABLE 7.12

Weight Losses Observed Upon Heating of ERDA No. 9 Cores

Specimen No. (depth)	Total Weight-Loss (%)	Mass-Loss (%) At Mean Temperature Ranges		
		100°C	300°C	450°
2034.7	1.60	0.70	0.36	.057
2035.7	0.20	----	----	----
2065.0	0.35	----	----	----
2067.5	0.52	----	----	----
2302.6	5.40	----	5.10	0.17
2413.7	1.38	----	1.00	----
2414.2	3.13	----	2.90	----
2415.6	0.10	----	----	----
2512.0	0.14	----	----	----
2516.3	2.15	----	----	1.55
2518.8	0.32	----	----	----
2528.7	2.12	----	----	1.52
2529.0	3.12	----	----	2.94
2538.5	1.55	----	----	1.20
2542.0	6.39	----	6.19	0.20
2593.2	1.47	----	----	1.20
2594.5	0.36	----	----	----
2597.0	0.37	----	----	----
2608.9	0.17	----	----	----
2614.4	0.13	----	----	----
2619.6	0.22	----	----	----
2658.5	0.48	----	0.10	0.17
2663.3	0.50	----	----	0.29
2696.4	1.12	----	----	0.80
2706.5	0.37	----	----	----
2711.9	0.47	----	----	0.21
2759.0	0.28	----	----	----
2786.5	3.64	2.27	----	0.90
2820.7A	0.36	----	----	0.17
2820.6B	0.35	----	----	0.12
2821.0	0.40	----	0.19	----
2826.5	0.36	----	0.27	----
2845.3	1.42	----	----	1.21
2848.8	0.86	----	----	0.53

TABLE 7.13

Data on the volume percent of fluid now present in the salt cores from ERDA No. 9.

Depth interval (feet)	Type Sampled	Volume sampled (mm^3)	Approx. grain size (mm)	Fraction of total slide	Fluid % by vol.	Total % by vol., whole slide
1799.0-1799.5	B	500	5 to 10	1/4	1.66	
	A	500	1 to 5	3/4	0.17	0.54
1902.0-1902.3	B	500	2 to 8	1/5	0.866	
	A	500	0.5 to 3	4/5	0.11	0.26
2065.0-2065.4	B	500	20 to 50	5/6	3.4	
	A	500	20 to 50	1/6	0.20	2.86
2095.1-2095.5	B	500	3 to 15	1/10	2.58	
	A	500	3 to 15	9.10	0.039	0.29
2274.4-2272.7	(B	470	10 to 15	1/2	2.29	
	(A	470	5	1/2	0.17	1.23
" "	(B	510	5 to 7	2/5	0.86	
	(A	510	1 to 3	3/5	0.02	0.36
" "	(B	520	5 to 7	1/3	0.55	
	(A	520	1 to 3	2/3	0.02	0.20
2391.0-2391.3	B	460	10 to 15	1/10	1.17	
	A	460	3 to 10	9/10	0.12	0.22
2611.5-2611.8	B	530	5 to 25	1/5	0.79	
	A	530	2 to 5	4/5	0.015	0.17
2658.7-2659.0	B	360	5 to 10	1/4	1.18	
	A	360	2 to 8	3/4	0.039	0.32

TABLE 7.13, continued

Data on the volume percent of fluid now present in the salt cores from ERDA No. 9.

Depth interval (feet)	Type Sampled	Volume sampled (mm^3)	Approx. grain size (mm)	Fraction of total slide	Fluid % by vol.	Total % by vol., whole slide
2760.0-2760.2	B	460	5 to 8	1/5	0.96	
	A	460	3 to 5	4/5	0.27	0.40
2820.8-2821.2	B	490	3 to 8	1/4	0.87	
	A	490	2 to 5	3/4	0.31	0.45

TABLE 7.14

Homogenization temperatures (^{o}C) of two-phase
liquid + gas inclusions from ERDA No. 9 core
(numbers of inclusions run given in parentheses)

Depth interval	Homogenization temperatures
1799.0-1799.5	20.5(1), 21.0(1), 25(3)
1902.0-1902.3	25.1(1)
2065.0-2065.4	(none)
2095.1-2095.5	25.6(2), 34.5(1), 44.0(1), 45.5(2)
2272.4-2272.7	41.25(1), 42.5(1), 42.6(3)
2391.0-2391.3	23(4), 39(1)
2611.5-2611.8	(none)
2658.7-2659.0	43.0(1), 43.25(1), 43.5(1), 44(2), 45.0(1)
2760.0-2760.2	20.4(1), 21.6(1), 21.8(2)
2820.8-2821.2	22.5(1), 23.0(1), 25.5(1)

TABLE 7.15

Summary of freezing data (^{O}C), mainly on
type B inclusion in samples from ERDA No. 9 core

Depth	First melting temp.	Freezing temp.	Notes
1799	<-31.9	> +10	∿20% liquid at -31.9
1902	<-32	> +10	
2095	<-28.4	+15	∿20-25% xls at 0°C
"	-32.2	"	
2272	<-32.8	+11.8	∿50% xls at 0°C
2391	<-26.1	> +12.8	
2760	<-32	> +12.7	

TABLE 7.16

Test data and weight loss (in %) from decrepitation tests.
Roman numerals indicate amount of sample breakup after run:
I - unbroken; II - broken into 2 or 3 pieces;
III - broken into more than 3 pieces.

Core interval (ft)	Temperature, $^\circ$C		
	150	200	250
2058.8 - 2059.0	0.16 II	0.23 II	0.76 III
2070.4 - 2070.6	0.16 II	0.12 I	0.35 III
2606.5 - 2606.9	0.02 I	0.24 II	0.95 III
2617.2 - 2617.7	0.06 I	0.30 I	0.62 II
2626.7 - 2627.0	0.19 I	0.28 I	1.04 III
2659.0 - 2659.2	0.14 I	0.13 I	0.59 III
2665.0 - 2665.1	0.19 I	0.18 I	0.75 III
2692.4 - 2692.6	0.06 I	0.26 I	0.83 III
2699.8 - 2700.0	0.19 I	0.24 II	0.65 III
Average	0.13	0.22	0.73

Heating schedule (hours)

Room T to run T	7	9.5	8
Hold at run T	79	95	79
Run T to room T	~9	~9	~10

TABLE 7.17

Temperature of homogenization and volume % vapor
of two-phase inclusions in salt of samples after
decrepitation tests.

Decrepitation run temp. (^{O}C)	Homogenization temp. (^{O}C)		Number of inclusions runs	Volume % vapor phase; avg. for $\sim$ 25 inclusions
	Minimum	Maximum		
150	90	120	16	0.8
200	110	180	21	1.8
250	180	273	28	5.0

Note: Birefringent crystals, present in some of these inclusions, do not
disappear during homogenization runs.

TABLE 7.18

Temperature of homogenization of two-phase inclusions
in salt from near dike in Kerr-McGee mine,
Lea County, New Mexico.

Sample no.	Distance from dike (m)	Temp. of homogenization (^{O}C)		Number of inclusions run
		Minimum	Maximum	
MB-77-8	0.01 - 0.02	71	116	7
MB-76-3	0.2	60	110	6
MB-76-4	2.5	85	88*	9

* Two birefringent crystals remained unchanged, and a cubic crystal (KCl ?)
  dissolved at 82°C. (See Plate 7-42 for a similar inclusion.)

TABLE 7.19

INVENTORY OF FLUIDS SAMPLED FOR GEOCHEMICAL STUDIES
OF DELAWARE BASIN GROUNDWATERS

Sample No.	Sample Name	Formation Sampled	Location	Solutes	Stable Isotopes	Solute *Analyst
1	Carlsbad City #7	Capitan	T22S-R26E-S1	X	X	M
2	Duval Mine/Collector Ring	Rustler	T22S-R30E-S33	X	X	M
3	Duval Mine/Seep-BT26	Salado	T22S-R30E-S33	X	X	S
4	Duval Mine/Seep-BT48	Salado	T22S-R30E-S33	X	X	M
5	Duval Mine/Seep-BT58	Salado	T22S-R30E-S33	X		M
6	James Ranch	Rustler	T23S-R31E-S5	X	X	M
7	Fairview	Rustler	T23S-R32E-S36	X	X	M
8	Todd State 36-1	Morrow	T23S-R31E-S36	X	X	M
9	Todd Federal 26-4	Bell Canyon	T23S-R31E-S26	X	X	M
10	Todd Federal 26-1	Morrow	T23S-R31E-S26	X	X	M
11	Shell No. 28	Capitan	PSL Blk 74-S34(Texas)	X	X	M
12	Middleton	Capitan	T19S-R32E-S21	X	X	M
13	Hackberry	Capitan	T19S-R31E-S31	X	X	M
14	ERDA #6	Castile	T21S-R31E-S35	X	X	S
15	Shell Bootleg	Castile	T22S-R32E-S36	X		Sh
16	Duval Mine/Vent Hole	Salado	T22S-R30E-S33	X		M
17	UNM Pokorny	Castile	PSL Blk 61-S3(Texas)	X	X	M
18	Smith Livingston Ridge	Santa Rosa	T22S-R31E-S15		X	
19	Indian	Rustler	T23S-R30E-S21		X	
20	Mobley	Rustler	T23S-R30E-S19		X	
21	Mobley #3	Rustler	T23S-R30E-S2		X	
22	H1-Magenta	Rustler	R22S-R31E-S29	X	X	U
23	H1-Culebra	Rustler	T22S-R31E-S29	X	X	U
24	H3-Magenta	Rustler	T22S-R31E-S29	X	X	U
25	H3-Culebra	Rustler	T22S-R31E-S29	X	X	U
26	Green Lake	Capitan	Carlsbad Caverns		X	
27	Mirror Lake	Capitan	Carlsbad Caverns		X	
28	Longfellow's Bathtub	Capitan	Carbsbad Caverns		X	
29	Celery Stalk Pool	Capitan	Carlsbad Caverns		X	

* Analysts: M - Martin Water Laboratories
              S - Sandia
              Sh - Shell
              U - U.S. Geological Survey

TABLE 7.20

GEOCHEMICAL ANALYSES OF DELAWARE BASIN GROUNDWATERS
(Solutes in mg/l)

No.	pH	$\delta^{18}O$ ‰	δD ‰	Ca^{++}	Mg^{++}	Na^+	K^+	Cl^-	Br^-	SO_4^+	HCO_3^-	TDS	Other Information
T 1	7.2	− 7.9	−54	74	29	8	1	10	0	72	285	474	NO3:5
2	7.4	− 6.4	−48	1100	280	3600	405	6400	0	2500	122	14380	Sr:30
3	5.5	+ 3.0	−10	640	55400	27500	3000	236500	305	3650	1090	355085	BO3:660
4	5.4	+ 2.6	−12	500	62600	44400	30250	251500	530	3300	1170	395000	BO3:840
5	5.5			520	62000	46300	30250	250000	582	3100	1170	395000	BO3:990
6	7.6	− 5.0	−40	590	175	68	5	400	0	1570	190	3240	NO3:225
7	7.6	− 7.1	−53	590	200	120	3	142	0	2140	130	3350	
8	6.4	+ 2.7	−15	1600	240	11300	500	20600	23	300	380	35600	Sr:240
9	7.1	+ 2.2	−13	27600	6075	76700	1700	18500	410	210	215	295400	Sr:1750
10	6.6	+ 9.2	−18	4880	920	28700	200	55400	90	30	300	92400	Sr:1750
11	7.1	− 7.7	−56	940	280	2280	57	3900	0	2400	550	11300	
12	7.4	− 7.5	−55	1100	570	10600	330	17050		3720	300	33800	Sr:64
13	6.0	¬ 6.5	−46	2200	1680	68700	2950	110800		5150	132	192000	Sr:140,Fe:312
14	7.3	+10.3	0	130	350	112000	5100	186100	240	16000	1310	321000	BO3:650,Li:160
15	7.7			550	1860	124500		185000		16800	1480	330700	
16	5.8			1260	38500	49000	52500	241500	385	3600	700	388650	BO3:1160
17	1.6	− 6.0	−50	190	100	200	18	2700	0	570	0	3800	
18		− 7.2	−52										
19		− 6.3	−46										
20		− 6.9	−44										
21		− 5.9	−44										
22	7.4	− 6.8	−48	890	270	5700	70	8000		3900	92	18922	
23	7.6	− 7.0	−50	780	280	9400	190	12000		7400	105	30155	
24	7.4	− 7.3	−53	760	190	4200	100	5800		2600	1150	14800	
25	7.4	− 7.0	−53	1500	720	19000	450	33000		5200	88	60000	
26		− 3.6	−24										
27		− 4.3	−28										
28		− 4.2	−29										
29		− 3.0	−20										

TABLE 7.21

DUVAL MINE VENT HOLE WATER #16

. One liter of solution might be expressed as the
following amounts of common evaporite minerals:

0.006 moles	(1	gm)	$CaMg(CO_3)_2$	Dolomite
0.026 moles	(4	gm)	$CaSO_4$	Anhydrite
0.012 moles	(3	gm)	$KMgClSO_4 \cdot 11/4H_2O$	Kainite
1.343 moles	(370	gm)	$KMgCl_3 \cdot 6H_2O$	Carnallite
0.224 moles	(46	gm)	$MgCl_2 \cdot 6H_2O$	Bischofite
0.005 moles	(2	gm)	$Na_2B_4O_7 \cdot 10H_2O$	Borax
2.121 moles	(121	gm)	$NaCl$	Halite

TABLE 7.22

TODD FEDERAL 26-4 WATER #9

One liter of solution might be expressed as the following
amounts of common evaporite minerals:

0.10 moles	(52 gm)	$CaMg_2Cl_6 \cdot 12H_2O$	Tachyhydrite
0.04 moles	(4 gm)	$KMgCl_3 \cdot 6H_2O$	Carnallite
0.59 moles	(129 gm)	$CaCl_2 \cdot 6H_2O$	Antarcticite
3.34 moles	(195 gm)	$NaCl$	Halite

TABLE 7.23

ERDA 6 WATER #14

One liter of solution might be expressed as the following
amounts of common evaporite minerals:

0.003 moles	(1 gm)	$CaMg(CO_3)_2$	Dolomite
0.009 moles	(1 gm)	$MgCO_3$	Magnesite
0.011 moles	(3 gm)	$KMgClSO_4 \cdot 11/4H_2O$	Kainite
0.130 moles	(9 gm)	KCl	Sylvite
0.155 moles	(22 gm)	Na_2SO_4	Thenardite
0.048 moles	(14 gm)	$LiCl$	?
4.521 moles	(265 gm)	$NaCl$	Halite

TABLE 7.24

Rb-Sr Data for Evaporites from the Salado Formation

A. Whole Rocks

Core hole Interval	$(^{87}Sr/^{86}Sr)_N$	Rb (ppm)	Sr (ppm)	$^{87}Rb/^{86}Sr$
AEC-8				
1622.4-1622.9	0.7056	5.0	112.4	0.13
1636.6-1637.1 (sylvite rich portion)	0.7816	120.1	8.0	43.77
1645.0-1645.3	0.7150	0.40	48.2	0.02
1671.2-1671.8	0.7097	5.6	39.8	0.41
1715.4-1715.7	0.7089	0.07	90.9	0.02
1762.0-1762.3	0.7099	1.3	37.9	0.10
1782.2-1782.4	0.7137	0.30	5.7	0.15
ERDA-9				
1404.8-1405.8	0.7934	67.1	5.1	38.41
1648.5-1649.0	0.7079	0.47	44.7	0.03
1759.1-1759.8 (polyhalite rich portion)	0.7064	4.9	793.5	0.02
ERDA-6				
1421.0-1421.7	0.7095	0.60	156.2	0.01

B. Water Soluble Portions

ERDA-8				
1607.0-1608.0	0.7173	26.7	44.7	1.73
ERDA-9				
1408.8-1405.8	0.8601	70.8	4.0	51.87
1709.0-1709.5	0.7094	0.99	8.5	0.34
1713.6-1714.0	0.7072	2.0	34.1	0.17
1772.0-1772.4	0.7067	1.5	57.7	0.07

C. < 2 Micron Fractions (Clays)

AEC-8				
1607.0-1608.0	0.7229	42.9	82.2	1.51
1671.2-1671.8	0.7273	43.9	35.2	3.62
ERDA-9				
1404.8-1405.8	0.7608	84.5	23.6	10.40
1772.0-1772.4	0.7181	29.4	48.1	1.76

TABLE 7.25

% Insoluble Residue in Whole Rock

Core hole Interval	Insoluble Residue (percent)
AEC-8	
1607.0-1608.0	9.0
1610.8-1611.3	9.0
1622.4-1622.9	2.0
1636.6-1637.1	3.7
1645.0-1645.3	0.8
1671.2-1671.8	11.3
1715.4-1715.7	1.1
1782.2-1782.4	12.5
ERDA-9	
1404.8-1405.8	7.2
1621.9-1622.2	0.8
1633.6-1634.1	0.4
1648.5-1649.0	2.1
1652.8-1653.1	0.3
1709.0-1709.5	1.1
1713.6-1714.0	18.2
1759.1-1759.8	0.7
1772.0-1772.4	12.6

TABLE 7.26

Mineralogical Data

Core hole Interval	Halite	Sylvite	Polyhalite	Langbeinite
A. Whole Rocks (Evaporite Mineralogy by XRD)				
AEC-8				
1607.0-1608.0	VA	VA	–	–
1610-8-1611-3	VA	A	–	–
1622.4-1622.9	VA	A	–	–
1636.6-1637.1	VA	VA	t	–
1645.0-1645.3	VA	t	–	–
1671.2-1671.8	VA	t	t	–
1715.4-1715.7	VA	t	–	–
1762.0-1762.3	VA	t	–	–
1782.2-1782.4	A	A	A	t
ERDA-9				
1404.8-1405.8	A	t	VA	VA
1621.9-1622.2	VA	t	–	–
1633.6-1634.1	VA	t	–	–
1648.5-1649.0	VA	A	–	–
1652.8-1653.1	VA	t	–	–
1709.0-1709.5	VA	A	–	–
1713.6-1714.0	VA	A	–	–
1759.1-1759.8	VA	A	t	–
1772.0-1772.4	VA	A	t	–
ERDA-6				
1421.0-1421.7	VA	t	–	–

Mineralogical Data

Core hole Interval	Halite	Sylvite	Polyhalite	Langbeinite

B. 2 Micron Fractions (Clays, Minerals)

Core Hole Interval	Chlorite	Saponite	Chlorite/ Saponite	Illite	Talc	Serpentine
AEC-8						
1607.0-1608.0	–	–	VA	A	t	A
1610.8-1611.3	t	–	A	A	–	A
1622.4-1622.9	–	–	t	A	A	t
1636.6-1637.1	–	–	A	VA	t	t
1645.0-1645.3	t	–	A	A	t	A
1671.2-1671.8	–	–	VA	A	–	t
1715.4-1715.7	A	–	t	VA	–	VA
1762.0-1762.3	t	t	–	A	A	t
1782.2-1782.4	A	–	t	VA	VA	A
ERDA-9						
1404.8-1405.8	–	–	A	VA	t	A
1648.5-1649.0	A	–	A	VA	VA	VA
1713.6-1714.0	–	–	VA	A	A	VA
1772.0-1772.4	–	–	VA	A	t	A
ERDA-6						
1421.0-1421.7	–	–	t	t	VA	t

VA:	very abundant
A:	abundant
t:	trace
–:	not detected

TABLE 7.27

URANIUM CONCENTRATIONS AND ISOTOPIC RATIOS IN DELAWARE BASIN WATERS

Sample	U Concentration	$\alpha(^{234}U/^{238}U)$	$\delta^{18}O$ (SMOW)‰	δD (SMOW)‰
Shell	0.60 parts in 10^9	2.75	−7.7	−56
Middleton	0.54 parts in 10^9	1.81	−7.5	−55
Hackberry	0.02 parts in 10^9	1.22 ± 0.05	−6.5	−46
Carlsbad 7	0.05 parts in 10^9	5.14	−7.9	−54
ERDA 6 1140 hr.	89 parts in 10^9	1.11 ± 0.04		
ERDA 6 1212 hr.	4.8 parts in 10^9	1.26 ± 0.05		
ERDA 6 1445 hr.	2.14 parts in 10^9	1.37 ± 0.07	+10.3	0
ERDA 6 1520 hr.	1.88 parts in 10^9	1.33 ± 0.07		
ERDA 6 Drill Mud	67.2 parts in 10^9	1.19		
Brine Lake (Mud Ingredient)	56.3 parts in 10^9	2.04		

Arrows in these photographs point stratigraphically upward.
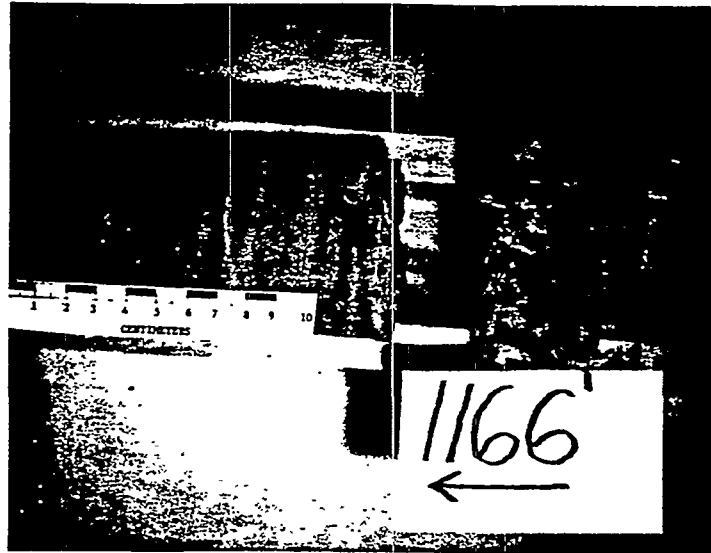
Plate 7.1. Core footage: 1165.4 to 1177.1 ft. (including 0.1 ft. gap) Brownish halite in gray anhydrite. Halite occurs as a thin bed at top of specimen, then as irregular lenses and thin laminae, finally as vertically elongate crystals, some with "swallow tail" form, near bottom of specimen. Locally horizontal laminae occur within the anhydrite due either to color change of the anhydrite or laminae of magnesite.
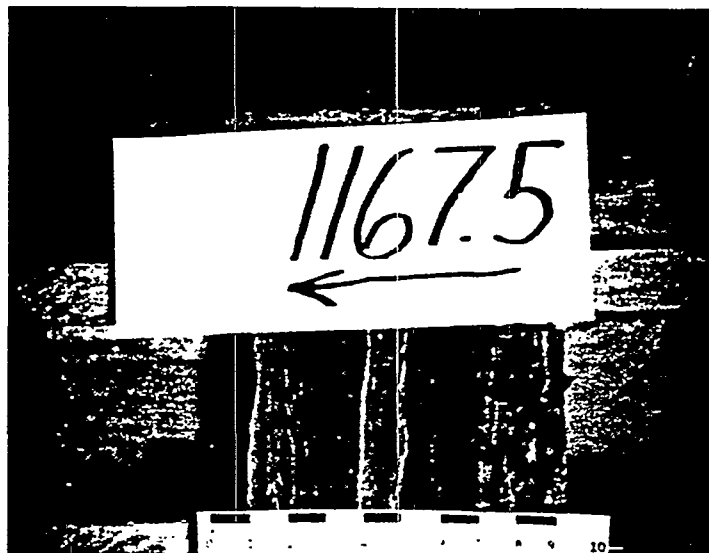
Plate 7.2. Core footage: 1167.5 ft. Dominantly light to dark gray, laminated anhydrite with thin, locally discontinuous, laminae of white magnesite and brownish, elongate halite oriented perpendicular to convex-upward, discontinuous laminae of light gray to white anhydrite.

Plate 7.3. Core footage: 2065.8 to 2066.6 ft.
Dominantly clear to milky white halite crystals, approx-
imately 10 mm in size, and reddish brown to pinkish brown
polyhalite. Note rectangular outline of polyhalite
body stratigraphically above the first 6 in 2066; but most
polyhalite occurs around halite crystal boundaries below
2066 label.
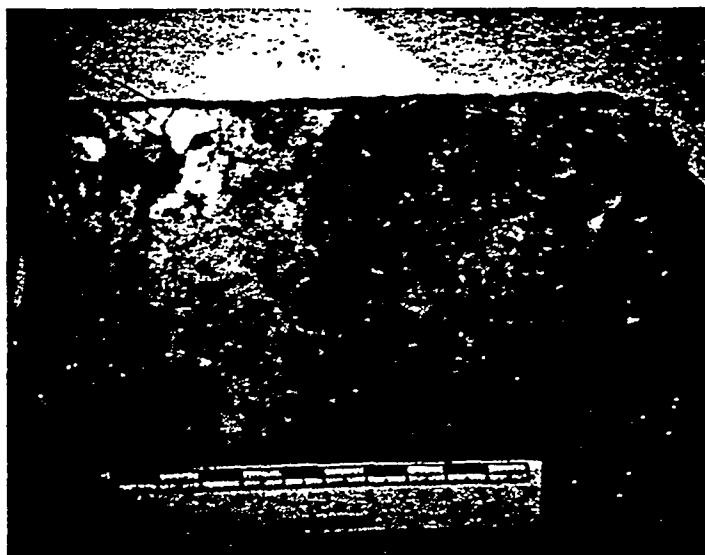
Plate 7.4. Core footage: 2615.0 to 2615.6 ft.
Dominantly coarse (ranging from 3 to 40, average 20 mm in
size) halite crystals, some with cubic form but most
anhedral, locally separated by microcrystalline white
anhydrite.

Plate 7.5. Core footage: 2705.8 ft. Coarse, ranging from 2 to 15 mm, light gray to black halite in white microcrystalline anhydrite and rare 1 to 2 mm bodies of pure white magnesite.
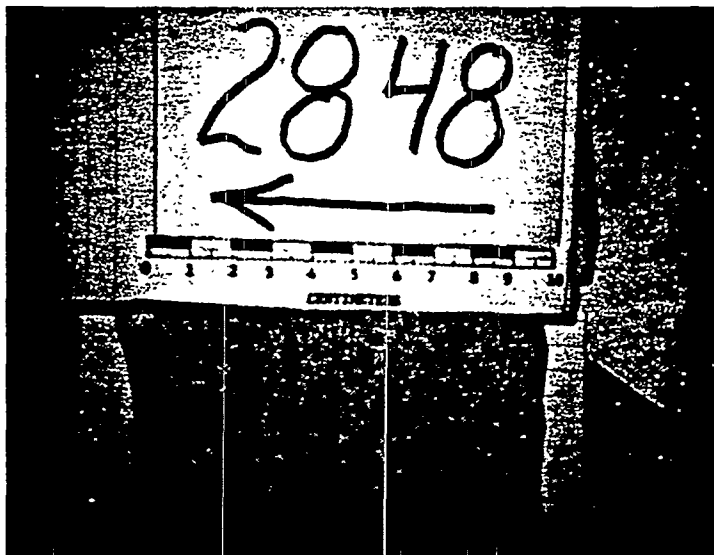
Plate 7.6. Core footage: 2848 ft. Varicolored (white and all shades of gray) anhydrite, some crystals near stratigraphic top of sample exhibit "swallow tail" form.
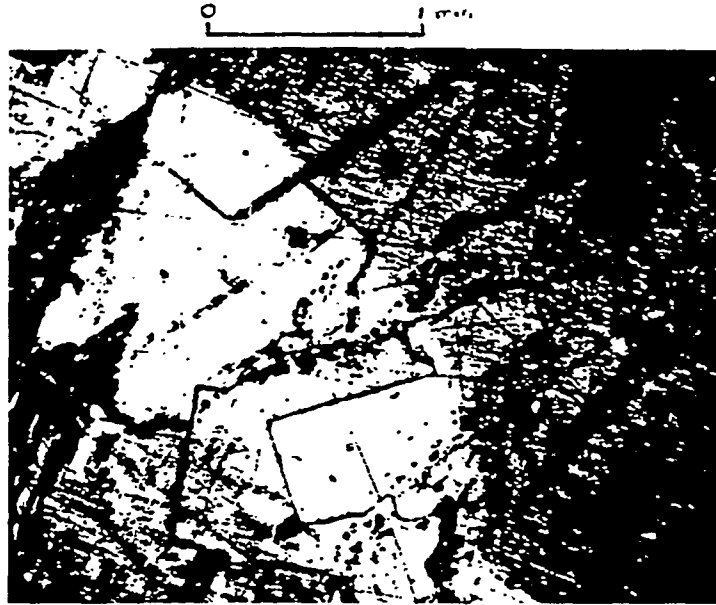
Plate 7.7. Photomicrograph (25X, plane light) of halite: many euhedral (cubic) to subhedral, relatively clear crystals locally containing fluid inclusions. Crystal size ranges from 0.5 to 1.5 mm. Compare with Plate 7.8.
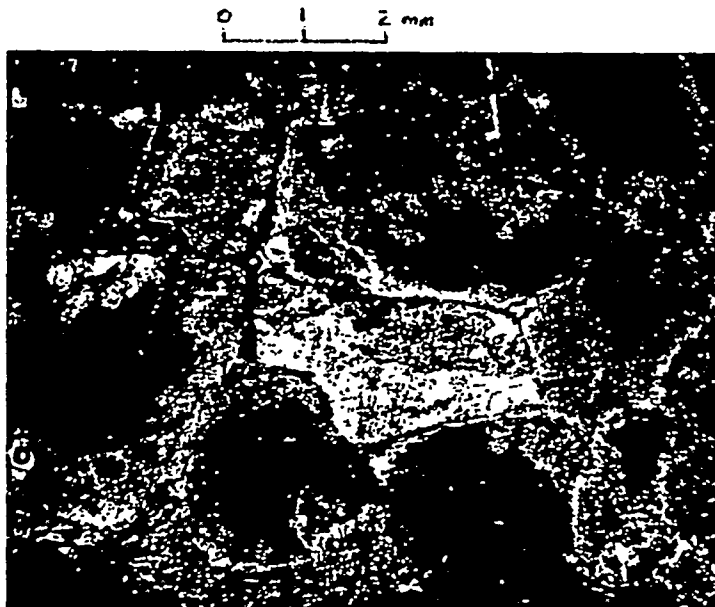
Plate 7.8. Photomicrograph (10X, plane light) of halite: subhedral to anhedral, cloudy crystals devoid of fluid inclusions. Crystal size ranges from 1.5 to 4.5 mm.
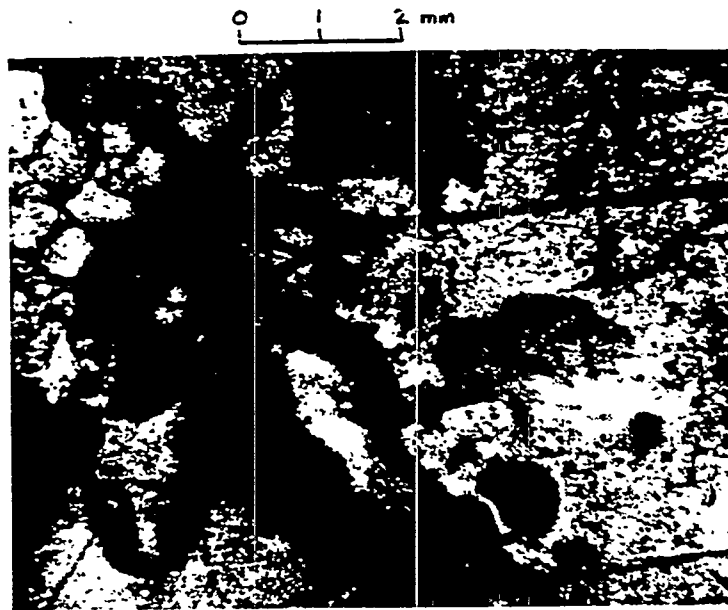
Plate 7.9. Photomicrograph (10X, plane light) of
sylvite (reddish, translucent to black, opaque in photo)
and halite: halite anhedra size ranges from 0.4 to 5 mm.
Two subhedra dominantly of sylvite occur within halite anhedra,
one subhedron/anhedron of mixed sylvite and halite occurs
within a coarse halite subhedron, but most sylvite occurs
as anastomosing bodies having gradational contacts with halite
between halite anhedra.
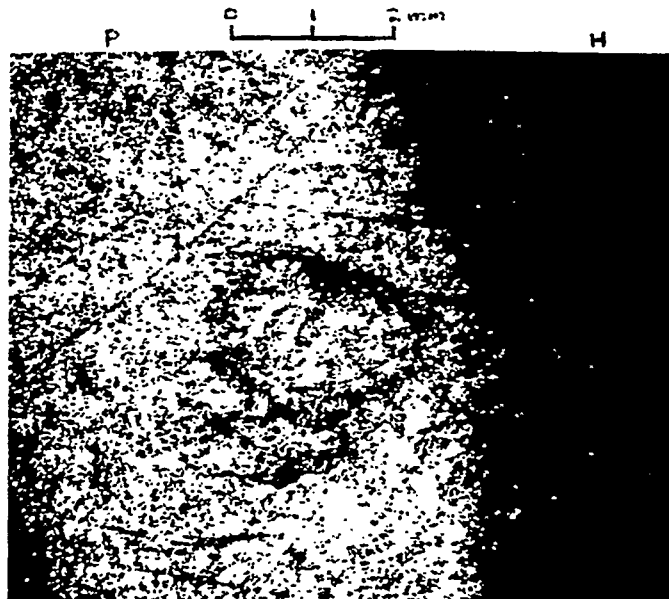
Plates 7.10A and 7.10B. Photomicrographs (10X, plane light in 7.10A, crossed nicols in 10B) of polyhalite (P) and halite (H): Polyhalite occurs as a cloudy anhedron (pinkish in hand specimen) locally containing smaller anhedra which are apparent due to concentrations of opaque (black in the photo, red under microscope reflected light) material, probably hematite. Concentrations of hematite also occur along the contact of polyhalite with halite which becomes extinct (black in 10B) under crossed nicols. The contact is irregular and gradational.
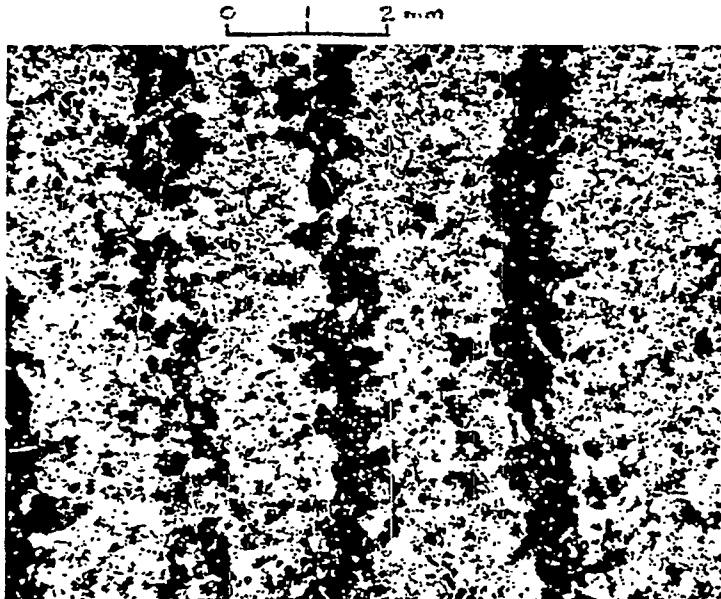
Plate 7.11. Photomicrograph (10X, plane light) of
laminated anhydrite and calcium or magnesium carbonate:
Dark thin laminae (approximately 1 mm thick) of dominantly
carbonate anhedra separate thin laminae (approximately
2 mm thick) of dominantly anhydrite anhedra.
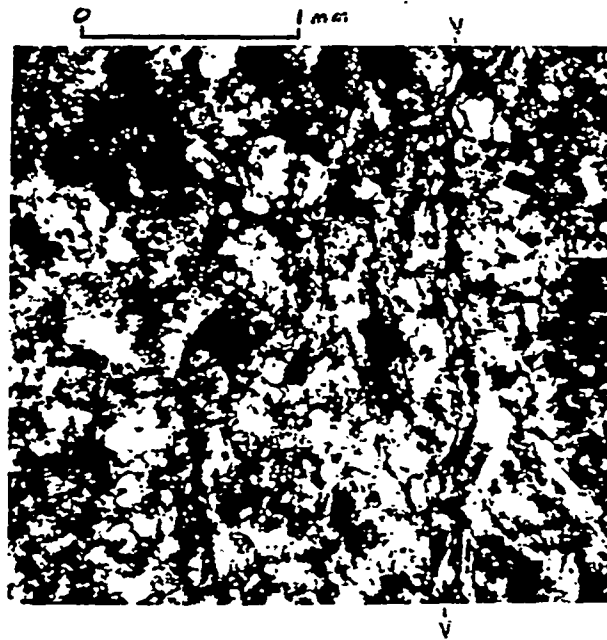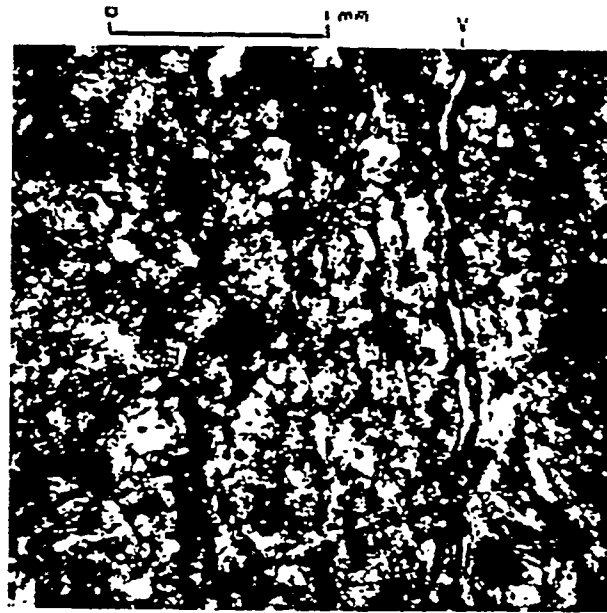
Plates 7.12A and 7.12B. Photomicrographs (25X, plane
light in Plate 7.12A, crossed nicols in Plate 7.12B)
of anhydrite with veinlet (V) of gypsum. Anhydrite occurs
as a mosaic of 0.04 to 0.4 mm anhedra and subhedra with
high order interference colors in 12B. Veinlet somewhat
discontinuous, is more apparent in 12A and consists of
very elongate irregular anhedra of relatively clear
gypsum with lower order interference colors than the
anhydrite in 12B. The veinlet is approximatedly strati-
graphically horizontal and is 0.06 mm thick, the width
of a single elongate gypsum anhedron.

1 mm
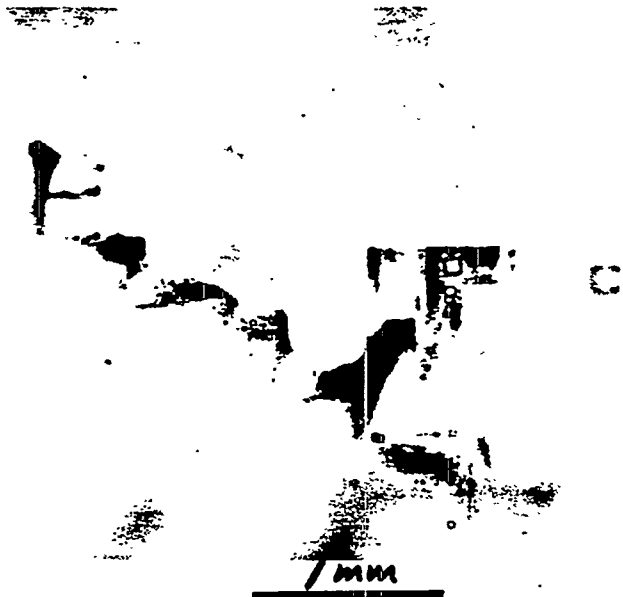
Plate 7.13 Group of dark unrecrystallized zones in
essentially inclusion-free single crystal of halite of
sample 2065. For detail on central area see Plate 7.14.

100 µm
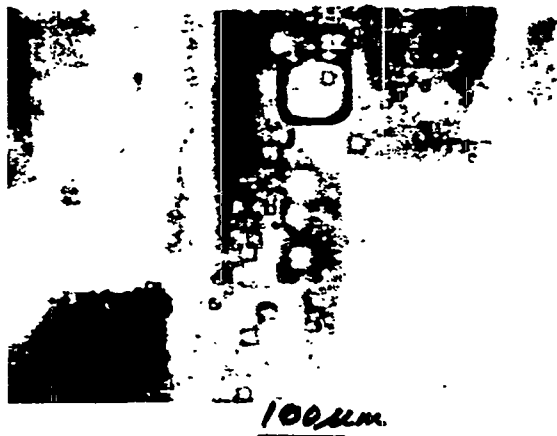
Plate 7.14 Detail of area in Plate 7.13 showing sharp
crystallographically controlled boundaries of inclusion-rich
zones (type A). Such boundaries may represent primary
crystallization features rather than recrystallization fronts.

Plate 7.15 Recrystallized part of sample 2065 with large numbers of type B inclusions with small bubbles (e.g., see arrow) and some dark, cloudy unrecrystallized portions (details in Plate 7.16).

Plate 7.16 One of the dark areas in Plate 7.15 showing dense cloud of primary type A inclusions with some primary banding (arrow), and sharp but curving (solution?) contact with crystallographically parallel but almost inclusion-free recrystallized salt (at top).

1 mm

Plate 7.17 Coarsely recrystallized part of sample 2760, with many large type B inclusions, each with bubbles (arrows). Dark clouds are masses of unrecrystallized salt with large numbers of tiny type A primary inclusions (see Plates 7.18 and 7.19).
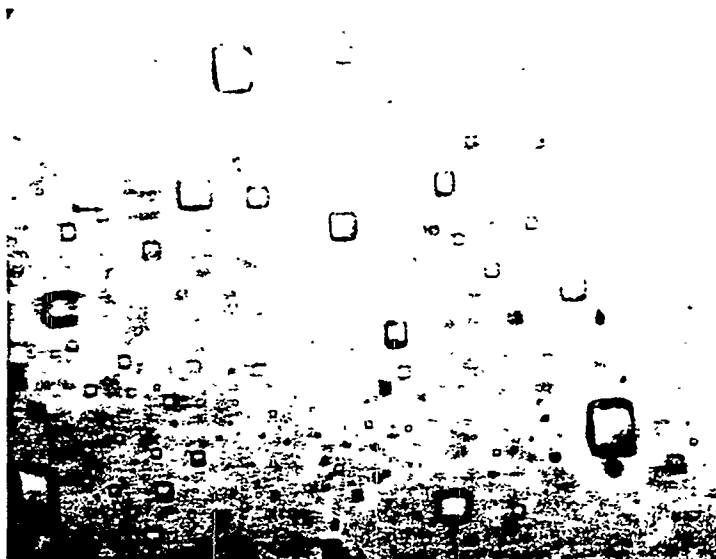
100 μm

Plate 7.18 Detail of one of the cloudy areas in Plate 7.17, showing high concentration of tiny type A inclusions. Most of these inclusions are < 1μm (see Plate 7.19).
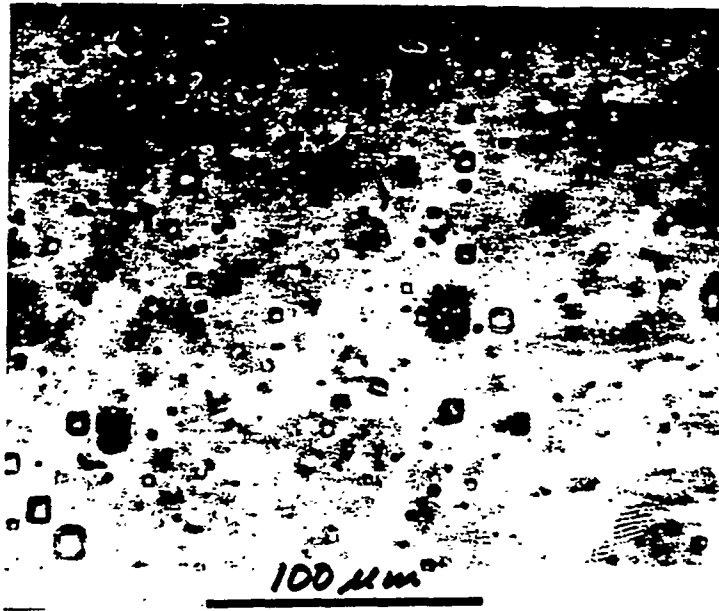
Plate 7.19 Detail of portion of Plate 7.18 that is relatively free of larger inclusions. The smallest inclusions are ≈ 0.5μm. All are type A. None of these inclusions contain a bubble.
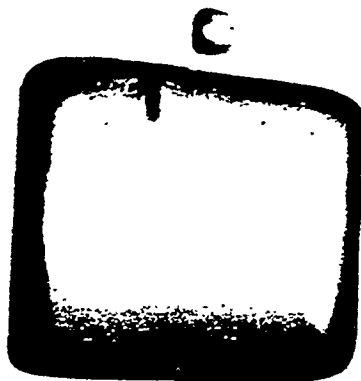
Plate 7.20 Inclusion in sample 2272.5 that contains only liquid, with no bubble, even though fairly large. Type B.
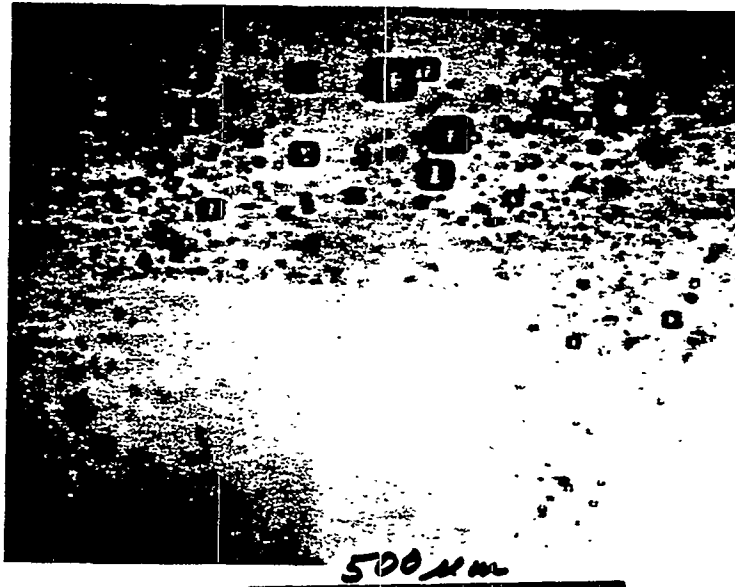
Plate 7.21 Unrecrystallized part of sample 1902 showing
primary cubic growth zone feature, delineated by a cloud
of tiny type A primary inclusions.
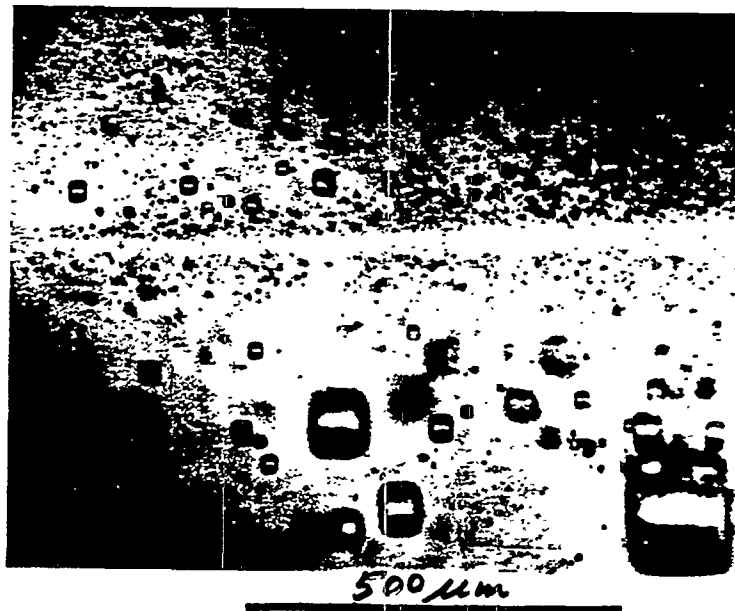
Plate 7.22 Unrecrystallized part of sample 1902 showing
thin inclusion-free zone through dense cloud of tiny type A
primary inclusions.

Plate 7.23 Oval grain of salt from sample 2760 containing
unrecrystallized core with tiny type A primary inclusions.
See Plate 7.24 for detail. Top of core is shown by arrow.
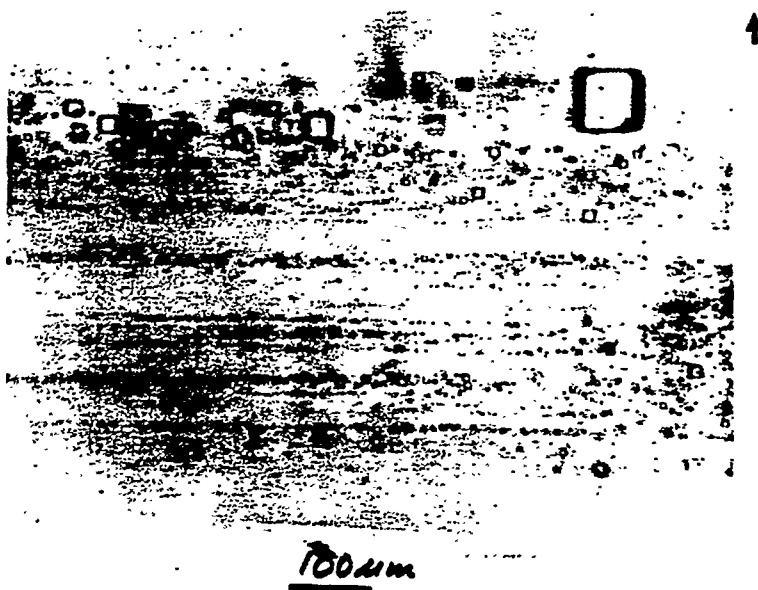
Plate 7.24 Enlgarged view of right central portion of
Plate 7.23, showing extremely fine banding of primary type A
inclusions, with inclusion-free zones between. Top of core
is shown by arrow.
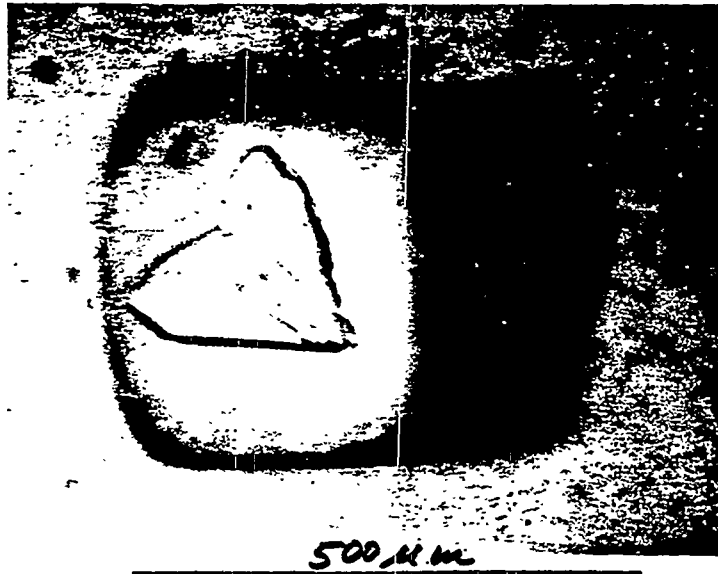
Plate 7.25 Inclusion (type B) in sample 1902 showing
twinned birefringent daughter crystal of unidentified
phase.

Plate 7.26 Daughter crystals of unidentified phase in
type B inclusion in sample 1902.2, with partly crossed
polarizers. Note twinning in largest crystal. Many inclusions
in this same sample have no daughter crystal or just a few tiny
crystals (see Plate 7.28).

Plate 7.27   Plane of type B liquid inclusions each with
a large number of unidentified bladed birefringent daughter
crystals, just 400 μm below another plane of inclusions
with no daughter crystals (Plate 7.28).   Inclusion in
Plate 7.26 with daughter crystals is similar in phase ratio
but not in same plane (out of focus in lower left here).
Sample 1902.2 partly crossed polarizers; birefringent mass
embedded in salt crystal at top may be the same phase.
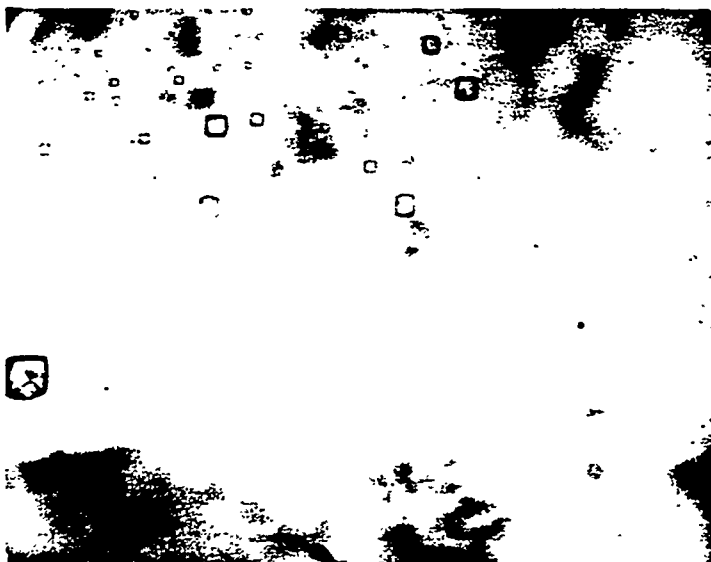
Plate 7.28   Plane of liquid type B inclusions, several with
bubble, but without daughter crystals, about 400 μm above a
plane of type B inclusions with a large number of unidentified
daughter crystals (Plate 7.27).   This lower plane is visible
but out of focus.   Sample 1902.2.   Inclusion of Plate 7.26 is
visible in lower left.

Plate 7.29   Large irregular type C inclusions in sample 2065 with "too large" bubbles.
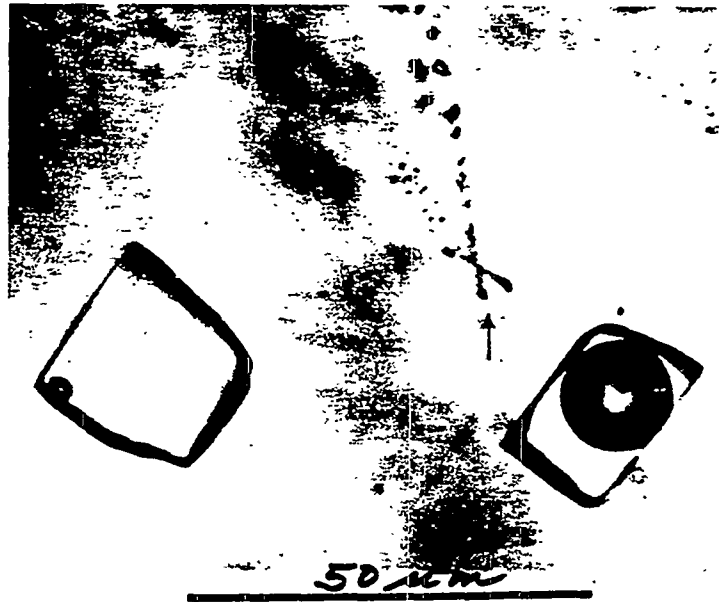
Plate 7.30   Pair of inclusions in sample 1902.   The one on left (Type B) with small bubble is typical of those in this sample; that on right (Type C) is on a healed fracture (see arrow) and has apparently been opened and the original fluid replaced with a gas-rich mixture under pressure.

1 mm →

Plate 7.31   Single crystal of salt in sample 2760 with
curving planes, outlined by type D inclusions, separating
it from adjacent grains.   Note also large type B inclusions
and mass of tiny type A primary inclusions in central core
of crystal.   Sample has probably undergone two stages of
recrystallization (see text).   Top of core is shown by arrow.

1 mm
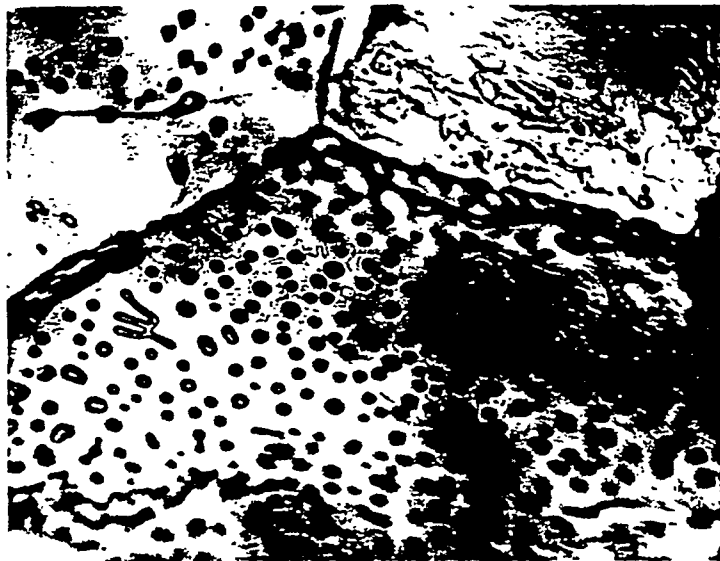
Plate 7.32   Fluid inclusions (gas; type D) on interface
between recrystallized salt crystals in sample 2760.   Note
120° junction.   Top of core is shown by arrow.
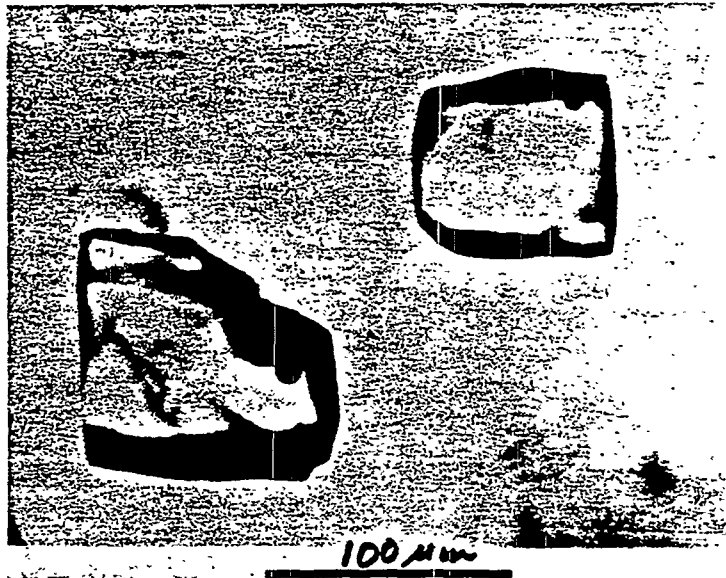
Plate 7.33 Large type B inclusions in sample 1799.1 homogenizing at 20.5°C (lower left) and 21°C (upper right). Photographed at ≈ 19°C.
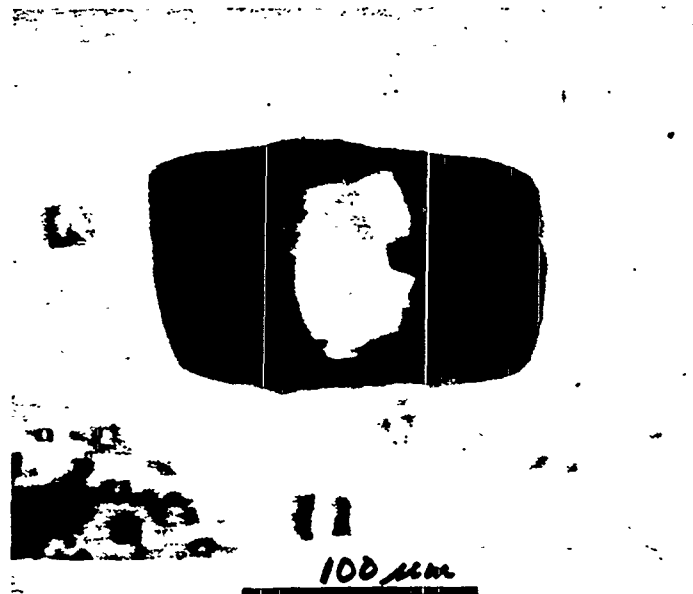
Plate 7.34 Large type B inclusion in sample 2760.1 homogenizing at 20.5°C. Photographed at ≈ 19°C.
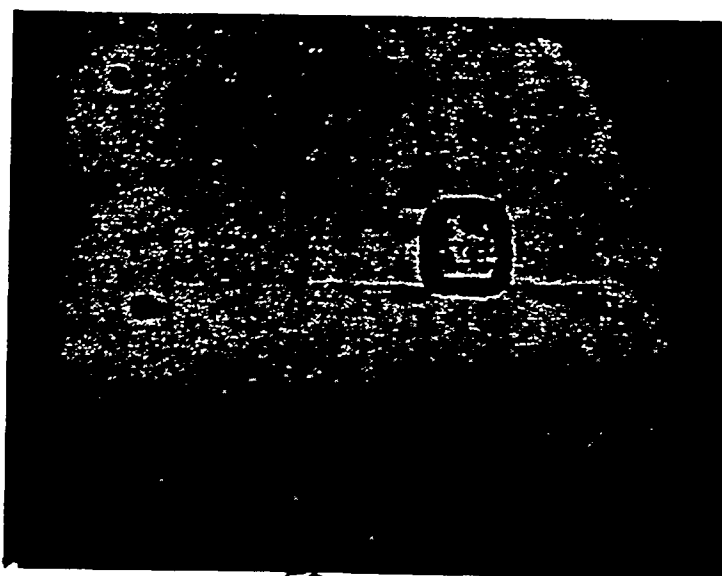
50 μm

Plate 7.35   Inclusion (type B) in sample 1902 after
freezing run, showing horizontal crack formed by expansion
on freezing, that is now a plane of tiny secondary fluid
inclusions; larger bubble than originally was present (due
to volume increase); and rounded halo of tiny inclusions
formed during freezing run (arrows), as a result of water
in inclusion reacting with halite of walls to form
$NaCl \cdot 2H_2O$, thus increasing inclusion volume.   See text.

10 μm

Plate 7.36   Minute primary inclusion in unrecrystallized salt
from sample 1902 at high magnification (1560 X).   The inclusion
in upper right is about 1.8 μm on an edge, and contains a
bubble of <0.5μm.   Resolution of bubble is poor as it is
generally in rapid motion even with an IR filter in optical
system and exposures must be long.   Many inclusions with no
bubble area are ≈ 0.5μm on an edge.

Plate 7.37 Sequence of photographs of type B inclusions in sample 2095.3 taken at the temperatures indicated during a freezing run. At -75.5^0C the inclusions contain a partly opaque mixture of solid grains of ice and salts. No change was visible on warming to -34.5^0C, but at -32.2^0C the mixture suddenly became more translucent and the grain size started to increase, indicating first melting. Extensive melting occurred around -4^0C, and the remaining crystals decreased to $\approx$ 20-25% at 0^0C. These were probably a hydrate but not all Nacl $2H_2O$, since a few were present at $+12^0$, and the last dissolved at $+15^0$C. The room temperature photo was taken after the run. The bubble size varies with phases present and temperature.

−4.

−12°

−32.2° 200μm

−34.5°
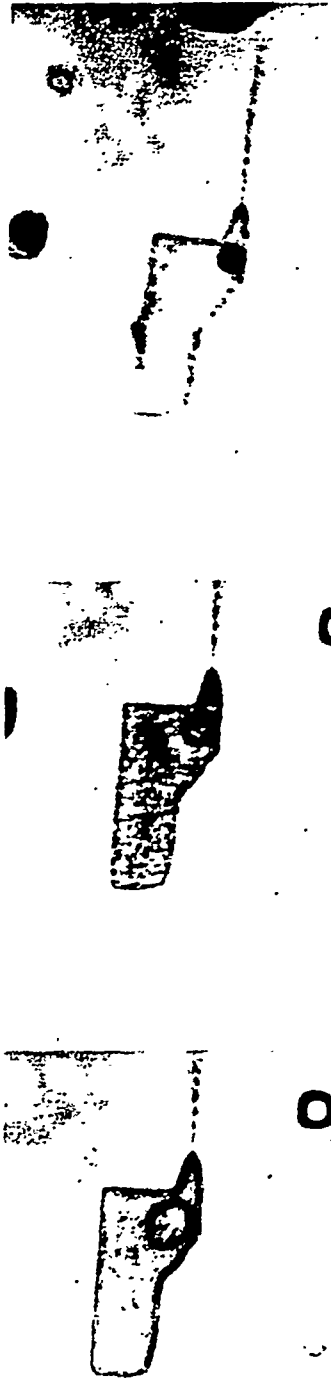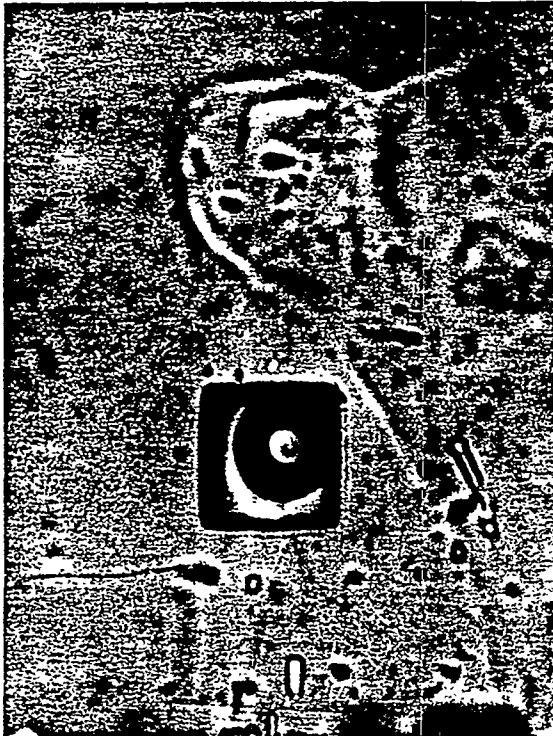
Plate 7.38 Inclusion from sample 2760, as found, with large bubble, viewed on crushing stage. The bubble contains gas under pressure (see Plate 7.39).

Plate 7.39 Same inclusion as seen in Plate 7.38, on crushing stage, after fracture has reached it. The bubble has expanded approximately 270% (vol) on pressure release.

Plate 7.40 Sequence of photographs of inclusion in sample
2760 on crushing stage. A shows the inclusion as found. The
sample was then stressed and immediately cracked (at right in
B), but the area of inclusion was still under stress, since
changes took place along edges of inclusion during next 10
minutes at constant stress (photo B). After 16 minutes at
constant stress (C) changes are more pronounced and bubble
is smaller; after 18 minutes bubble is gone (D).

In each of the following plates, the length of the scale bar is 100 μm.

Plate 7.41 (Photo 1) Group of small primary hopper-growth inclusions in ERDA-9 sample 2699.8-2700.0, after 250°C decrepitation run. These inclusions probably had no bubble originally, and now have one as a result of plastic deformation of the host salt. They now homogenize at temperatures as high as 273°C (Table 7.17).

Plate 7.42 (Photo 2) Solid phases (daughter crystals?) in inclusion in Kerr-McGee mine sample MB-76-4. The small rod-like crystal has parallel extinction, and the large cubic(?) crystal (KCl?) appears isotropic.

Plate 7.43 (Photo 3) Dense gas inclusion in Kerr-McGee mine sample MB-77-8, photographed at the approximate temperatures indicated (°C). See text, subchapter 7.5.

Plates 7.44 and 7.45 (Photos 4 and 5) Steam inclusions (arrows) in Kerr-McGee mine samples MB-76-3 (7.44) and MB-77-8 (7.45), now containing essentially vacuum, before (a) and after (b) being intersected by a fracture during crushing tests. The surrounding oil has filled the inclusions completely in (b).

Plates 7.46 and 7.47 (Photos 6 and 7) Gas inclusions in Kerr-McGee mine sample MB-77-8 containing gas at less than one atmosphere pressure, before (a) and after (b) being intersected by a fracture during crushing tests.

Plate 7.48 (Photo 8) High pressure gas inclusion in Kerr-McGee mine sample MB-76-4 before (a) and after (b) being intersected by a fracture during crushing.

Plates 7.49, 7.50 and 7.51 (Photos 9, 10, and 11) High pressure gas inclusions in Kerr-McGee mine samples MB-77-8 (7.49 and 7.51) and MB-76-3 (7.50), before (a) and after (b) being intersected by a fracture during crushing. The approximate volume expansion is 30-fold in 7.49, 40-fold in 7.50, and 100-fold in 7.51. Two bubbles formed in 7.49, and one in 7.50 (arrows).

1

2

a +22		**d** −56	
b −21		**e** −68	
c −30		**f** −75	

3

a

b

4
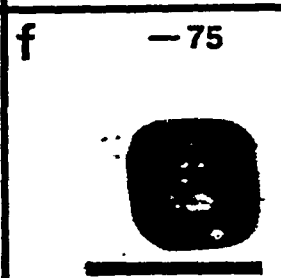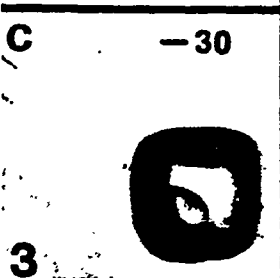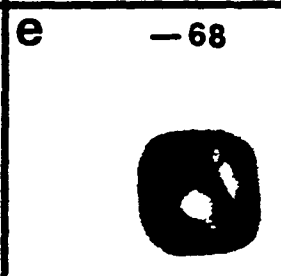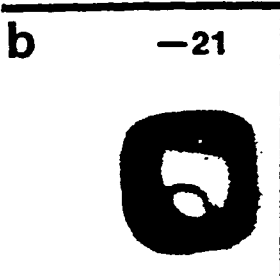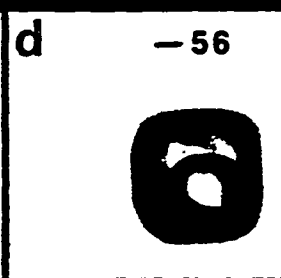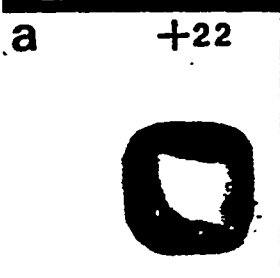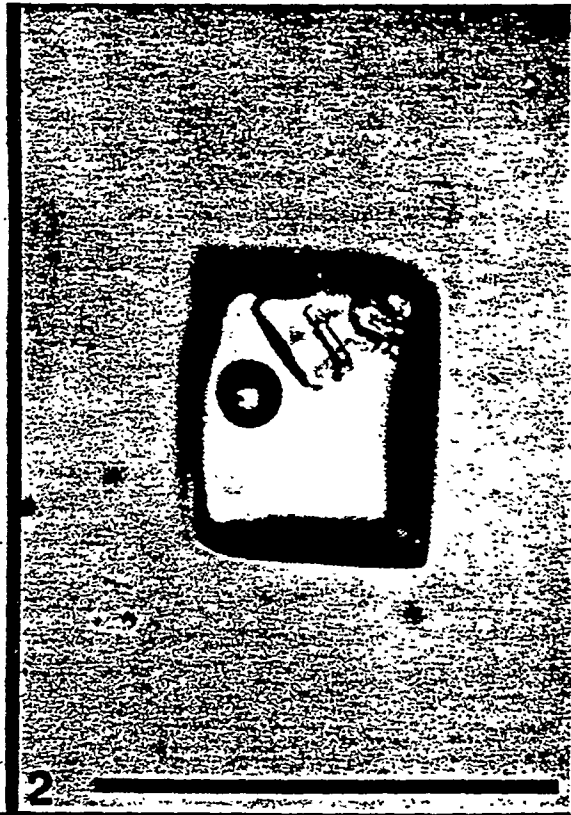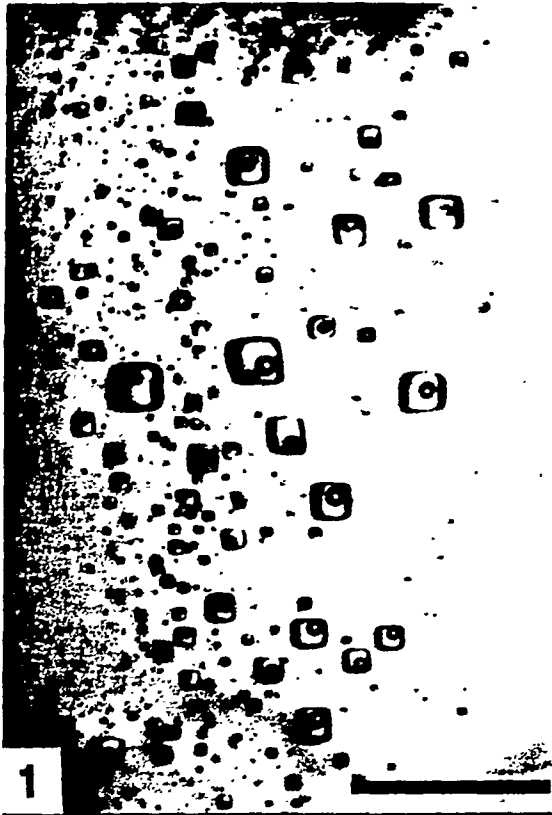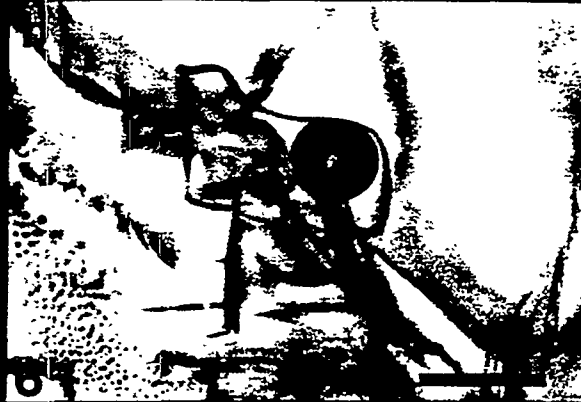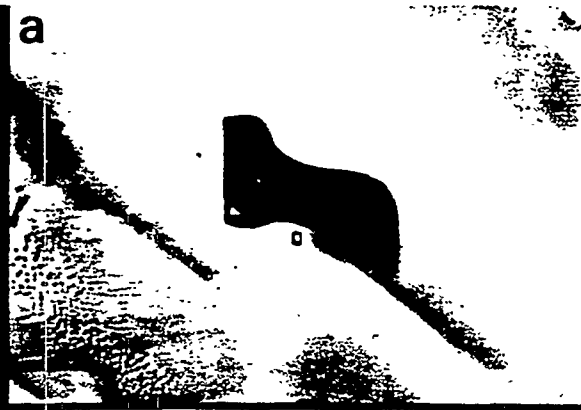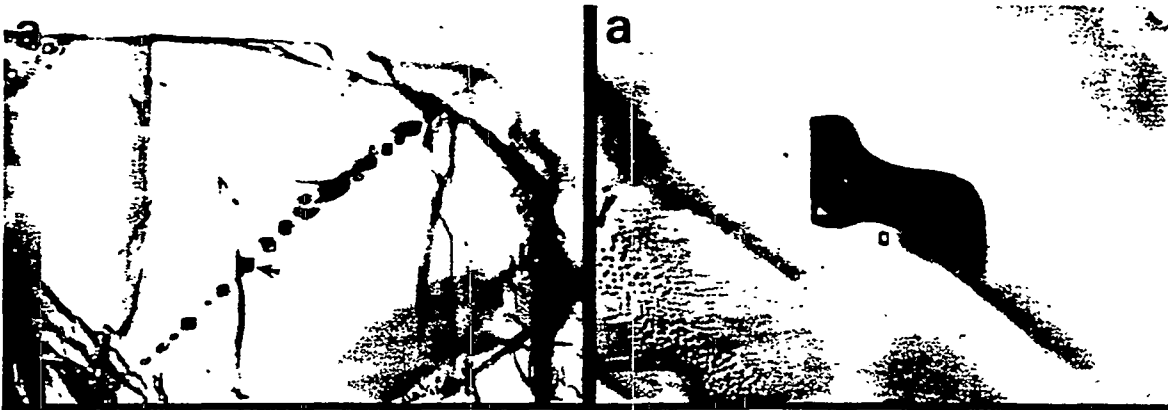
PLATE CAPTION

Plate 7.52 and Overleaf: Core fragments from Castile
anhydrite serving as host rock for the ERDA No. 6 brine
reservoir. Depths of origin, uranium contents and $^{234}U/^{238}U$
ratios are given in the overleaf for various parts of the core
fragments.

TOTAL U $\overset{a}{(^{234}U/^{238}U)}$ DEPTH (Ft.)

19.2 ppb   1.09   2708

1.61 ppm   1.02

33 ppb   1.04   2709.4

**coarsely
crystalline
anhydrite
(white)**

**laminated
calcite and
anhydrite
(gray)**

2.17 ppm   1.04   2709.9
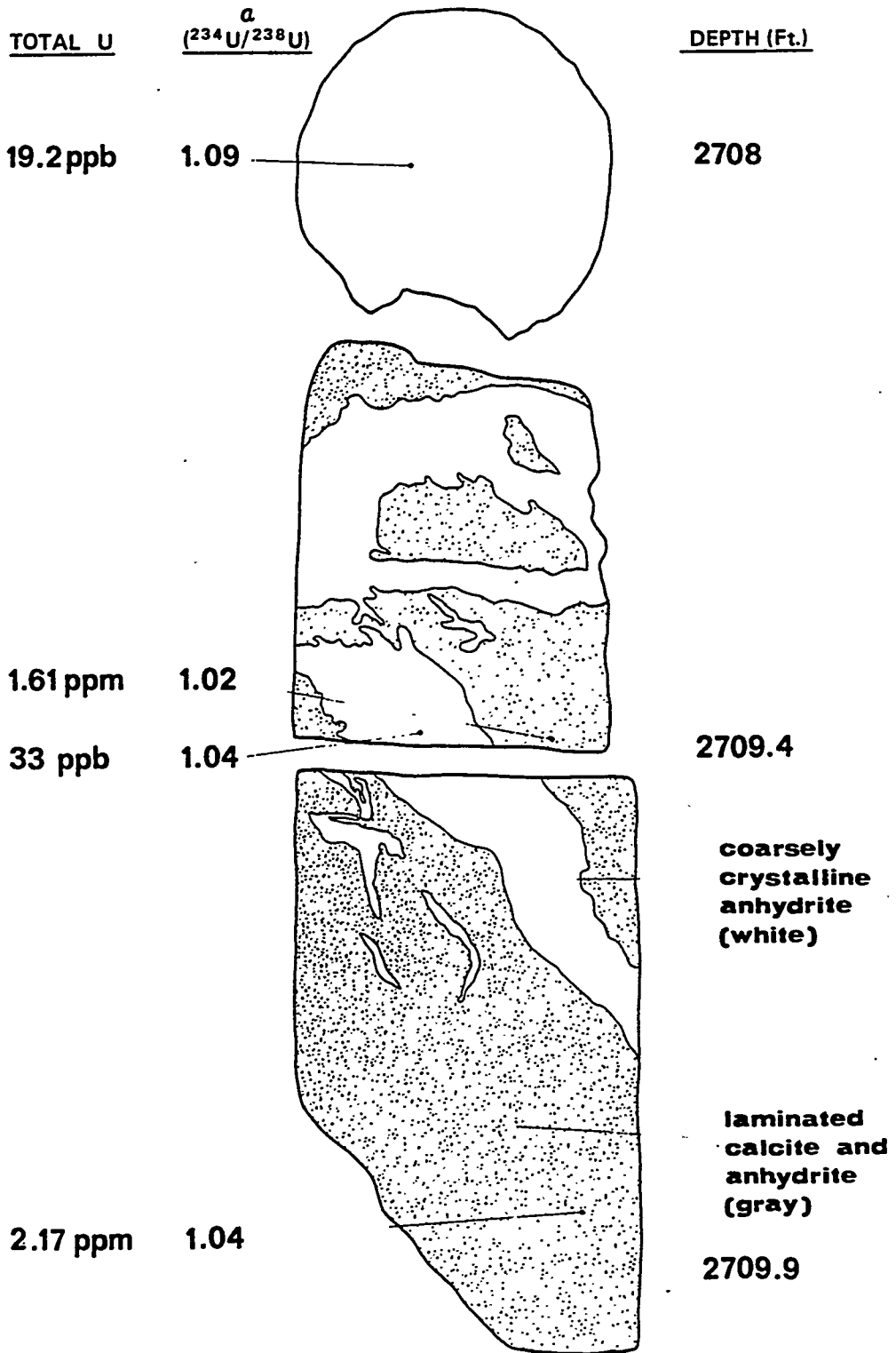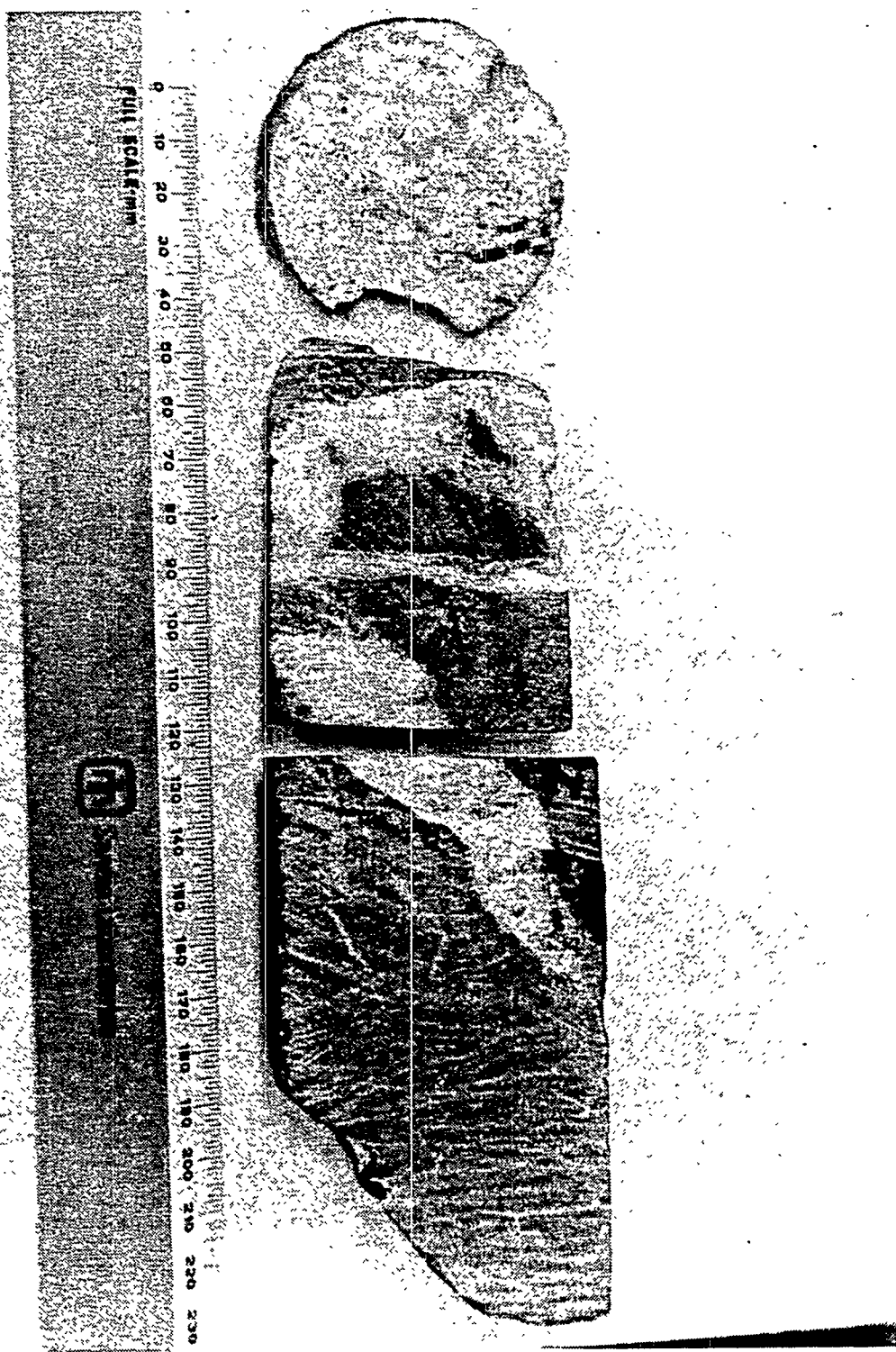
PLATE 7.52

8.1   INTRODUCTION

The northern portion of the Delaware Basin is known for production of
potassium salts and fluid hydrocarbons. An effort was made to select a
location for the WIPP that would minimize conflict with these resources.
It is likely, however, that some of these potash and hydrocarbon
resources underlie the site. The extent of potash mineralization has
been fairly well established because the potash mining industry has
released information concerning their exploratory drilling in the area.
Those findings were supplemented by information from 21 additional holes
drilled by the Department of Energy. Site selection criteria described
in Chapter 2 prescribe that the site be no closer than one mile from a
deep drill hole. This means that the potential hydrocarbon resource must
be evaluated by inference utilizing subsurface information from
surrounding areas. An investigation was also carried out to determine
the significance of other possible industrial minerals such as caliche,
gypsum, salt, uranium, sulfur, and lithium at or very near the WIPP
site. Table 8-1 summarizes the principal findings of resource studies.
Only potash and natural gas are considered to be significant exploitable
deposits as shown in Table 8-2. The economic resources denied in Zones
I-III are shown in Table 8-3.

8.2   ORGANIZATIONS INVOLVED IN RESOURCE EVALUATION, AND THEIR REPORTS

Numerous contractors representing both government and private companies
were engaged in the resource evaluation at the WIPP site. An outline of
work accomplished during this phase of the site characterization is given
in Table 8-4.

The listed studies quantify in-place resources and evaluate what portion
of those resources would be extractable. A legal determination is now
under way to establish values to the various mineral and oil and gas

lease holders within the site area. However, these studies deal with the present value of specific land tracts and as such are not pertinent to site chacterization.

8.3 POTENTIAL RESOURCES IN RELATIONSHIP TO STRATIGRAPHY AT THE WIPP SITE

Resource evaluation at the WIPP site took into consideration the existing stratigraphy of the site area. Each formation was evaluated for mineral deposits that were either known or that could exist based on the characteristics of the sediments present.

A stratigraphic column is given in Table 8-5 that indicates where in the geologic section specific types of deposits are considered to have a reasonable likelihood of occurrence. The table briefly describes the character, thickness, and median depth of each formation.

8.4 RESOURCE DESCRIPTION BY SPECIFIC COMMODITIES

The description of resources commences with the shallowest formation and proceeds down the stratigraphic column to the Precambrian.

8.4.1 Caliche

A thin layer of caliche (a whitish, calcium carbonate-rich material) underlies most of the site area. Exposures are normally obscured by dune sand, but it has been estimated that the caliche blanket covers approximately 80% of the site area. The average thickness is 4.3 feet, and the total resource has been estimated at 185 million tons (Siemers et al., 1978). The quality of caliche as determined by insoluble content (ranging from 21 to 69%) appears to be typical for caliche for this region.

Caliche is often used to surface dirt roads in southeast New Mexico. Small quarries dot the landscape, and several provided material for road construction to various drill locations within the WIPP site. This is the sole use for caliche in this region. Caliche is so extensive in this region that it can not be considered as either a limited resource or one that has significance to road construction of surrounding areas if land is withdrawn for the WIPP site.

8.4.2 Uranium

Uranium could occur in sediments such as those of the Gatuna, Santa Rosa or Dewey Lake Formations. However, no significant occurrence of uranium has been found within the Delaware Basin. Reducing environments favoring uranium deposition are absent as evidenced by the lack of organic debris, pyrite or humates in these formations. No signal indicative of economic or even marginal uranium concentrations was observed on gamma ray logs of the 36 holes drilled through these beds during site evaluation. The conclusion is that significant uranium deposits are most unlikely, even in beds which are considered to be the most favorable.

8.4.3 Gypsum

Dissolution of salt from the Rustler Formation has occurred over much of the site area. Waters accompanying this dissolution have caused partial conversion of anhydrite within the Rustler to gypsum. The conversion is not complete, however, and it is doubtful that high-quality gypsum would be persistent in any single bed. The maximum amount that could be present, assuming an aggregate thickness of 40 feet, amounts to 1.3 billion tons (Siemers et al., 1978). The quality and bed thickness are inferior to those in beds west of the WIPP site. Still farther west and south, extensive outcrops of high quality gypsum of the Castile Formation occur. The nearby availability of superior quality gypsum that can be mined by open pit methods leads to the conclusion that gypsum in the Rustler Formation can not be considered a likely economic resource.

8.4.4 Halite (Salt)

Halite is the dominant constituent of the Ochoan evaporites. The shallowest salt is in the Rustler, but dissolution of this formation has removed much of the Rustler salt except in the southeast quadrant of the WIPP site. On the other hand, salt beds persist under the site in the Salado and Castile Formations. The thickest and purest salt beds in the region are in the Castile. The State Bureau of Mines and Mineral Resources estimated 118 billion tons of salt in the Salado within the WIPP boundary (Siemers et al., 1978). The Castile Formation would add approximately 80 billion tons of additional salt resource.

As with gypsum and caliche, the immense halite deposits are not considered to have economic significance because of the prevalence of these deposits throughout the general area and the existence of adequate supplies closer to areas where salt is in demand.

8.4.5 Sulfur

A significant deposit of native sulfur is being exploited by the Frasch process approximately 50 miles south of the WIPP site in northeastern Culberson County, Texas. The occurrence is associated with brecciated and carbonatized anhydrite beds of the Castile Formation. Considerable exploration has been under way since discovery of the Culberson deposit, but that exploration has been aligned along the southern and western parts of the Delaware Basin where the Castile Formation either lacked halite during deposition or the halite has been removed by dissolution. The genesis of the deposits is believed to depend on a combination of bacterial action, induced fracture permeability and a source of hydrocarbons (presumably from upward escape of natural gas or crude oil along fractures from the Delaware Mountain Group). The closest analogy to such a setting in the northern part of the Delaware Basin and the vicinity of the WIPP site would be either "breccia pipes" or H_2S-laden brine reservoirs. Careful attention was given in selecting the WIPP site to avoid such structures; further investigation has not revealed any such structures, therefore, no sulfur deposits are expected.

8.4.6 Lithium

Lithium occurs in a concentration of 140 mg/L in a saturated brine
reservoir that was encountered during the drilling of ERDA 6. The hole
was located 2 miles northeast of the outer boundary of the WIPP site. A
similar reservoir was found in the Belco Hudson Federal No.1 gas well 1/4
mile outside Zone IV on the southwest side of the site. No analyses were
done for lithium in the latter well, but both reservoirs were at
equivalent stratigraphic positions (middle Castile), contained H_2S, and
were fully saturated brines. The concentration of 140 ppm lithium in
ERDA 6 verges on being economically extractable if the reservoir is of
sufficient size. Griswold (1977) estimated the reservoir volume at ERDA
6 to be on the order of 100,000 to 1 million bbl. If reservoirs are
limited to this size, they would not warrant development. At current
market price the in-place value of the lithium would not exceed $1
million.

There has been a deliberate attempt to locate the WIPP site in an area
free of brine reservoirs in the Castile. Extensive seismic surveys have
been run across the area to ensure that no anomalous structures occur in
the Castile Formation. The occurrences at ERDA 6 and at the Belco well
are associated with complex anticlinal structures and are easily
recognizable on seismic survey traces.

8.4.7 Potash

Method of Evaluation. Sylvite (KCl) and langbeinite
$(K_2Mg_2(SO_4)_3)$ exist under portions of the WIPP site (see Figures
8.2, 8.3, 8.4). Although an attempt was made to avoid such deposits
during the site selection process, it was not possible to do so
completely because other site selection factors such as avoiding deep oil
and gas test wells and the desire for uniform and thick salt beds at
reasonable depth took precedence.

The potash evaluation commenced in August, 1976, after the site was
chosen for detailed characterization. When chosen, the site was located
mostly outside the Known Potash Area defined by the Conservation Division
of the U.S. Geological Survey. Considerable potash exploratory drilling
had been done on the flanks of the site area by private industry, but it
is a requirement that the results of that drilling be held in confidence
by the USGS. However, Sandia Laboratories contacted each mining company
that had drilled in the vicinity and was granted access to the drill
records on a private basis. These records indicated that deposits of
commercial quality probably extended into the site area. The Department
of Energy (then ERDA) authorized an exploratory drilling program to
evaluate the potash deposits within the WIPP site. Technical direction
of this exploratory drilling program was given to the USGS. The drilling
program commenced in August and was completed by the end of November,
1976.

The Roswell, New Mexico, office of the Conservation Division of the USGS
was given the task of determining potash resources by combining the
results of DOE-sponsored drilling with records of drilling in the
vicinity of the site. Findings have been reported by John et al. (1978).

The DOE also engaged the services of the U.S Bureau of Mines (USBM) to
evaluate the extent to which the resources defined by the USGS could be
produced at a profit using existing mining and beneficiation practices.
The results of the study have been reported by the USBM (1977). The
essential conclusion was that langbeinite in the 4th ore zone could be
profitably mined in the northeast quadrant of the WIPP site. A band of
sylvite, contained mostly within the 10th ore zone on the north and west
sides of the sites, verged on being economically exploitable. Profitable
mining of the sylvite would require a higher price for muriate (KCl) than
current market value ($52/ton versus a current price of $43/ton).

Description of the Potash Exploration Drilling Phase. Figure 8-1 is a
map showing a land block, centered on the WIPP site, that measures 8
miles on a side. This land block constitutes the area investigated by

the USGS and USBM. All locations of drill holes are shown from which information was available as to the depth, thickness, grade, and mineral suite of ore beds. Note that a different symbol is used to denote holes drilled by DOE from those drilled by mining companies. Examination of the distribution of hole locations reveals that the drilling plan directed by the USGS included testing the entire WIPP area on a spacing of not less than one hole per square mile. The objective was to completely cover the site area following industry practice for reconnaisance exploration. The density of the holes is judged to be quite adequate for resource appraisal.

Drilling closely followed standard industry practices (Jones, 1978). Rotary techniques were used from the surface down to a point just above the uppermost ore zone. Drilling operations were then converted to coring using a brine saturated with potassium chloride as the drilling fluid. Core recovery was excellent in all 21 holes. The core recovered was examined, and zones of interest were "split" for chemical analysis. Routine check analyses were done by an independent laboratory. All cores, including the remaining half of sample splits and sample rejects (excess after assay), have been permanently stored.

The results of the analyses of the 21 exploratory holes are attached as Appendix 8A. Included in the list are hole AEC 8 (drilled at the old ORNL site) and 17 holes for which information is available for release either by permission of the mining company involved or because the lease or permit on which the hole was drilled has expired.

Calculation of Potash Resource Distribution, Volume and Grade. As previously stated, calculation of the in-place volume and grade was undertaken by the Roswell office of the Conservation Division of the USGS. Technical assistance was also provided by the Special Projects Branch of the USGS.

There are 61 exploratory holes in the 8 x 8 mile land block shown in Figure 8-1. Ore intercept information was available to the USGS on all

of these holes. Thus, while their calculations used all available data, some specific information pertaining to 22 industry drilled holes is not reported in Appendix 8A to protect proprietary information of individual companies as they so requested.

The reserve calculation commenced with assigning depth intercepts to significant mineralization within the various ore zones. There are 11 such ore zones within the McNutt member of the Salado Formation (see Figure 4.3-3b). The next step consisted of extrapolating continuity of individual ore zones between holes. The final step was to calculate the volume and grade for continuous blocks of mineralization. In addition, the Conservation Division utilized criteria they have established for classifying resources as either measured, indicated, unevaluated, or barren. The criteria are:

> Measured potash reserves - Tonnage is computed from dimensions revealed in workings and drill holes. The grade is computed from the results of detailed sampling and analyses. A minimum of three data points in any one ore zone meeting quality and thickness standards, no more than 1 1/2 miles (2.4 km) apart, have been used to delineate measured reserves.

> Indicated potash reserves - Tonnage and grade are computed partly from specific measurements, samples, or production data and partly from projection for a reasonable distance on geologic evidence. The sites available for inspection, measurement, and sampling are too widely or inappropriately spaced to permit the mineral bodies to be outlined completely or the grade established throughout.

> Unevaluated potash areas - Tonnage and grade have not been computed due to low density drilling and sampling, but are surrounded by measured and (or) indicated reserves.

> Barren and/or minor potash mineralization areas - Subeconomic resources that would require a substantially higher market value or a major cost-reducing technology for economical production.

Subeconomic resources also include other bittern minerals not
presently being recovered.

Potash resources were then quantified at three minimum grade and
thickness levels. Standard conditions for each class are shown in Table
8.6.

The intermediate conditions, termed "lease", conform with established
policy of the Department of Interior that any area known to contain
potash mineralization meeting or exceeding that standard and located on
Federal land can be acquired only through competitive bid. The standard
is based on judgment along with recognition that ores as low as these
grades have been successfully treated from time to time at one or more of
the potash refineries in the Carlsbad district. The conditions termed
"high" are roughly equivalent to the grade of langbeinite and sylvite
ores currently being mined in the district.

Results of the USGS Resource Estimate. The essential results of the USGS
resource calculations are best shown by three consecutive maps (Figures
8-2, 3 and 4) which commence with the lowest resource grade standards and
progress to the highest. For simplicity, measured and indicated
resources were combined. The majority of the resource meets the criteria
for "measured" because the entire WIPP site has been drilled on one mile
centers. The resource maps do not segregate the several mineralized ore
zones, and at times they are "stacked", e.g. the 4th and 10th may be
mineralized in the same area in plan even though they are
stratigraphically separated by about 180 feet.

Most of the WIPP site area is underlain by potash resources that meet the
low standards. No significant planimetric change occurs on raising the
standard to lease grades. However, at the high standard, which is
roughly equivalent to the current standard of producing mines, the WIPP
is nearly clear of potash deposits of interest (particularly Zones
I-III). Mining operations may be allowed in Zone IV, the outer boundary
of the WIPP site, under controlled conditions.

As grade standards are increased, the potash resources reduce, at more rapid rate on a mass weight basis than on a planimetric basis. Table 8-7 lists the tonnage of by ore zone, type, and location by Zone boundaries within the WIPP site.

For ease in interpretation, the data in Table 8-7 has been charted on Figures 8-5 and 8-6 for langbeinite and sylvite resources, respectively. The USGS recognized the 4th ore zone (langbeinite) and the 10th (mainly sylvite) as the two major mineralized ore zones in the WIPP site area (John et al., 1977). At lease grade, the 4th ore zone contains 115.4 million tons of langbeinite resource, of which only 24 million tons (21%) lies inside the outer boundary of Zone III. At the higher grade (8% K_2O as langbeinite) the tonnage under the WIPP reduces to 59 million tons, of which only 14.6 million tons (25%) lies inside the outer boundary of Zone III.

The 10th ore zone contains mostly sylvite, but a mixed assemblage containing both langbeinite and sylvite exists on the east side of the withdrawal area. At present only one operator in the Carlsbad district has a refinery capable of handling such ores. This operator is the leaseholder over part of this mixed ore zone. However, the langbeinite in the 10th ore zone would be difficult to beneficiate according to the USBM study (USBM, 1977, p.103). Therefore, the 10th ore zone is considered to be viable only for its sylvite content. With this restriction, the 10th ore zone contains 53.5 million tons of ore at lease standard under the entire WIPP site, of which 30.4 million tons (57%) are located within the outer boundary of Zone III. At the high standard, the total tonnage reduces to 38.8 million tons, of which only 9.8 million tons (25%) are inside Zone III.

Results of the USBM Valuation of Potash Resources. The USBM has performed an economic assessment of the potash resources that were defined by the USGS. The USBM study included beneficiation testing to determine the amenability of the various mineral assemblages to refining into marketable products. The USBM engineers visited most of the mines in the district to gather data concerning mining and refining techniques, power consumption, water use, etc. Then, knowing the location and grade

of potash deposits in the WIPP site area, they devised conceptual designs of various mining and processing facilities that would provide both the highest profit and efficient recovery of marketable products from the potash deposits. The approach followed what private industry would do in an evaluation of a potash prospect. No restriction was placed as to where physical mining could be done, or problems related to land acquisition or permitting. Resources adjacent to the WIPP site were considered in the mine development plans. In all, the USBM conceived 12 different conceptual plans for exploiting potash in this area. Each plan, called a mining unit, was evaluated leading to a conclusion that 8 were worthy of full cost analysis. The full findings have been reported by the USBM (1977).

The USBM concluded that only one mining unit (Unit B-1) could be considered economic under existing market conditions and technology (see Table 8.8).

Unit A-1 almost meets the economic requirement of 15% rate of return on invested capital set by the USBM. To make it viable one needs a price of $52.04 per ton of muriate without any increase in production costs. Muriate is currently selling at $43.40 for standard grade containing 62% K_2O (Source: July 1978 issue of Engineering and Mining Journal); however, the price for muriate has exceeded $60 per ton in the past.

Data within the USBM report indicate that the langbeinite resources associated with the Unit B-1 that lie within the boundary of WIPP amount to 48.46 million tons, of which only 13.33 million tons (27.5%) lie inside the outer boundary of Zone III. For Unit A-1 the corresponding numbers are 27.41 million and 0.9 million tons.

Summary of Conclusions Concerning Potash Resources in the WIPP Site. The site contains economically mineable reserves of langbeinite and possibly sylvite. If total rights withdrawal is a requirement to satisfy waste isolation, then the relevant quantities of potash resources are much greater than if mining is allowed in the Zone IV, the outer buffer zone. The relevant quantities are presented in Table 8-9.

The USGS has estimated that potash resources in southeast New Mexico (excluding the WIPP site) that meet lease standards are on the order of 5000 million tons of combined sylvite and langbeinite ores. Therefore, total withdrawal of potash lease rights at the WIPP site would account for about 7% of those resources; withdrawal of Zone I, II, and III rights would account for about 2%. No data are available for the Carlsbad potash district regarding what percentage of these resources would meet the standards deemed by the USBM to be mineable under today's conditions. In addition, the principal potash resource at the WIPP site consists of langbeinite. No estimates, either by USGS or USBM standards, are available for this ore alone. The Carlsbad district is the only area mining langbeinite in the free world. Langbeinite equivalent is produced in quantity, however, by combining sulfates of potassium and magnesium obtained from brine lakes. When the site was initially selected, most of the WIPP lay outside the Known Potash Area, however the 21 hole drilling program conducted as part of the WIPP potash evaluation resulted in discoveries sufficient to warrant expansion of that boundary (see Figure 8-1). The expansion conforms with USGS policy that potash resources meeting the lease standard must be placed within the enclave.

8.4.8   Hydrocarbons

Method of Evaluation. The WIPP site selection criteria dictated that deep drill holes (defined as those that penetrate through the Ochoan) be excluded from Zones I, II, and III. The objective was to maintain a one mile buffer between deep holes and Zone II, the zone in which waste is to be stored. This particular criterion is restrictive, because much of the Delaware Basin has been penetrated by wildcat test holes with an average density of about one hole per square mile. The present site is one of the few remaining portions of the Delaware Basin in New Mexico which will satisfy the criterion pertaining to deep holes. The absence of extensive drilling is due in part to the great depth (greater than 10,000 feet) to potentially favorable gas formations. In addition, potash deposits north and west of the site area precluded oil and gas exploration in those directions. Federal and State regulations have set aside potash

mineralized areas to protect underground mining operations from accidental entrance of methane gas. Therefore, most of the WIPP site is untested for deep reservoirs that might contain crude oil and natural gas. The evaluation must rely on projection of surrounding subsurface geologic information into the site area. There are four petroleum test holes in Zone IV of the WIPP site. Three holes tested the Delaware sands and were unproductive. The fourth was a deep gas test (15,000 feet) that was also unproductive.

The State Bureau of Mines and Mineral Resources performed a regional evaluation of the hydrocarbon resources in southeast New Mexico which was then used to further evaluate a four township area centered on the original ORNL site (Foster, 1974). This report is useful for the current WIPP site because, as indicated in Figure 8-7, the present site is still within the area studied.

Data contained in Foster's report provide a basis for estimating total hydrocarbon resources that might underlie the site area. By using a statistical approach, Foster arrived at a possible hydrocarbon content for each potential productive zone, commencing with the "Ramsey Sand," down to the top of the Precambrian basement. The Ramsey, the first potential pay zone, is located in the upper part of the Delaware Mountain Group. The lowest zones he considered to be potentially productive were dolomitic reservoirs in the Silurian/Devonian. His estimate was based on full development of any prospective area; therefore, total resources were estimated rather than the economics associated with their extraction. His resource estimate was based on the premise that geologic conditions beneath the site were as favorable as elsewhere in the study area and that each potential zone beneath an untested section would contain a proportionate share of the statistical average of hydrocarbons for that zone. The average was derived from success ratios and a conservative estimate of primary recovery of hydrocarbons as established by past exploration, development and production.

A consulting petroleum engineering firm, Sipes, Williamson and Aycock, Inc (SW&A), was engaged by Sandia Laboratories to conduct an economic evaluation of hydrocarbons in the site area. Based on known drilling costs and market conditions, they made a judgment as to what portion and which formations under the site were worthy of testing. The basic criterion was reasonable prospect for discovery with an economic reward to the operator of at least 10% return on his investment plus full recovery of costs. The essential conclusion of the SW&A study was that the Morrow unit has a high potential for successful discovery of natural gas. All other formations present were considered too high a risk to be the objective of a prudent wildcat test. Naturally, once a Morrow well was drilled it could encounter shallower productive pay zones, but the odds of such happening were deemed too speculative to be considered in the overall economics. The full findings of this study have been reported by Keesey (1976).

Structure maps of several horizons beneath the Ochoan evaporites have been compiled from seismic surveys that were either purchased from existing surveys or conducted as part of the WIPP site study. While the main purpose of these seismic surveys has been to understand the geologic aspects of the site area, they are also valuable for interpretation of potential hydrocarbon reservoirs. These structure maps were not available to Foster for his 1974 study, but they were to SW&A during their 1976 evaluation. The seismic studies have been reported by McMillan (1976) and G. J. Long & Associates (1976). Updated structural interpretations based on later seismic studies are now available. The recent changes have had little impact on the overall hydrocarbon evaluation.

Total Hydrocarbon Resources at the WIPP Site. The New Mexico Bureau of Mines study forms the basis of the evaluation of the total hydrocarbon resources in the site area (Foster, 1974). We assume there is a reasonable probability that Foster's estimated resources could exist under the site. However, this probably represents the upper bound of exploitable hydrocarbons.

The validity of the resource estimate rests on the subsurface geology and statistical probability. The geologic setting under the Ochoan evaporites is considered to be quite typical for this portion of the Delaware Basin; therefore the chance of finding oil or gas should approximate what has been found in similar areas near the site which have been more fully tested. However, since it is a regional statistical approach, it is possible that much more or much less than the average expected resource would be found if the site was actually drilled. The hydrocarbon evaluation is not as definitive as that for potash, which was actually confirmed by exploratory drilling. This would be self-defeating in the case of the deeper hydrocarbon resources since the area was selected to avoid such deep drill holes.

Foster's evaluation (Foster, 1974) took into account the occurrence of all known oil and gas accumulations in much of southeast New Mexico (Figure 8-7). The statistical base encompassed about 42 full townships equivalent to almost 1 million acres. The reserves for each oil pool or gas reservoir were estimated from the standpoint of actual or, where possible, projected production. Areas were then classed as developed or undeveloped based on the density and depth of drilling. From these data, Foster (1974) then determined the expected resource per section of land by assuming that the success of future drilling would have the same success ratio as in the past. A coincident assumption was that, while past wildcat drilling avoided the current WIPP site, the past economic incentive for drilling was low. Also, drilling restrictions pertaining to the Known Potash Enclave have prevented drilling, particularly on the west side of the WIPP area. There were more attractive areas available throughout the basin that satisfied the availability of private venture for exploration capital. These past constraints do not enter into the hydrocarbon potential estimates because the characterization of the site must take into consideration the long-term needs for mineral resources.

Figure 8-8 is taken from Foster (1974). Formations that he considered as potentially productive are shown opposite the stratigraphic column of sedimentary rocks underlying the Ochoan evaporites. Table 8-10 then

shows the potential resource he assigned to the various specific intervals but which were composited to more gross intervals. Further explanation is required pertaining to "wildcat" and "acreage" assignment of reserves.

The acreage method tests the success ratio of producing acreage versus the acreage considered to have been tested by wildcat drilling. The wildcat method considered a field, regardless of the number of wells in that field, as a single discovery. A success ratio was then determined by dividing the number of wildcat discoveries by the number of dry holes that were drilled to that formational depth. The acreage method normally results in a higher success ratio and, therefore, higher reserve estimates. In-place hydrocarbon resources for each zone within the WIPP site can be readily calculated from Foster's data by combining his estimate of in-place hydrocarbon resources per section (640 acres) with the known area for each zone of the WIPP site. The acreage method was used to prepare Table 8-11.

While the quantities given in Table 8-11 may appear large, they are brought into perspective by stating that all of the nearby region, i.e., the area studied by Foster, would contain 51 times the resource quantity under the WIPP site. The factor is simply the ratio of the total area evaluated by Foster (1512 square miles) divided by the area of the WIPP site (29.62 square miles). In addition, if hydrocarbon development is allowed in Zone IV, e.g., by deviated drilling, then the resource that would be withdrawn is reduced in proportion to the excluded area, i.e., from 29.62 square miles down to 12.73 square miles for a 43% reduction in restricted resources. The hydrocarbon resources remaining in Zones I, II, and III would account for only 0.84% of the total hydrocarbon resources Foster has estimated in the area immediately surrounding the WIPP site.

Estimate of the Economically Recoverable Hydrocarbon Resources. Sipes, Williamson, and Aycock, Inc. (SW&A) estimated the potentially economic hydrocarbon resources (Keesey, 1976). Their approach was to review the

existing geologic information pertaining to the area in and around the site and then to determine if the probability of oil and gas occurrences justified the risk of drilling and completing a well. The base area studied by SW&A consisted of a 20 x 20 mile block centered on the WIPP site (Figure 8-7). All available data were evaluated on each test that had been drilled within this 400 square mile area, with particular emphasis placed on deliverability and recoverable reserves.

SW&A found that 60 wells in this area were producing oil and/or gas from reservoirs in the Delaware Mountain, Bone Spring, Wolfcamp, Strawn, Atoka and Morrow. With the exception of the Atoka and Morrow, all other zones were considered as presenting too high a risk to justify the cost of wildcat drilling. Furthermore, even though an Atoka reservoir is being produced from a well located near the southwest corner of the WIPP site, SW&A concluded that that particular reservoir is being effectively drained by the single well. Offset drilling would enhance recovery rate but not total recovery.

The Morrow was considered to be worthy of testing, because of the high success ratio of wells drilled to that formation in the area around the site. Of 26 wells drilled to sufficient depth to test the Morrow, 23 were successfully completed as gas wells. A study of these wells revealed that the projected ultimate recovery ranged from insignificant to as much as 5.20 billion cubic feet (bcf) of natural gas. From the distribution of recoveries they concluded that the average successful Morrow well would recover 2.074 bcf of gas. This is in fair agreement with Foster's estimate for Pennsylvanian gas wells; he estimated 3.2 bcf per Morrow gas well if spaced at 320 acres per well.

Drilling and completion costs were then estimated for wells drilled to the Morrow (approximately 14,000 ft.). The estimate was $1.4 million. Using discounted cash flow analysis and the expected delivery rate and current gas price ($1.42 per 1,000 cu. ft. with 4% yearly escalation) they concluded that if a well produced 0.7 bcf over its lifetime it would

recover costs. Since the average well was more than twice this
production, it was apparent that drilling in the site area could be
justified.

Use was then made of the structure map on a limestone reflector horizon
in the Morrow based on data from seismic surveys (Figure 8-9) (Long,
1976). Tentative drilling sites were picked with weight given to the
flanks of anticlines because local experience indicates that productive
sand lenses would more likely occur at such localities. A total of 20
drill sites was selected (Figure 8-9). In favorable structural areas
wells were placed on a spacing of 320 acres per well. This spacing is
standard practice for wells of this depth in New Mexico. Depending on
proximity to producing wells and structural favorability, the 20 wells
were ranked as proven, probable or possible. The proven category was
limited to locations that would offset producing wells in the Los Medanos
field. Two locations were designated as proven, nine as probable, and
nine as possible.

The ultimate recovery of wells was adjusted to take into account the risk
factor associated with wildcat drilling. Proven wells were assigned
production of 2.07 bcf, probable wells 1.64 bcf, and possible wells 1.33
bcf per well for the southwest quadrant of the WIPP site. The estimated
reserves for locations in other parts were placed at 2.09 bcf for
probable and 1.67 bcf for possible reserves. No locations could be
considered as proven. The higher reserves assigned to these locations
were considered justifiable because shallower pay zones may be discovered
on the way down to the Morrow. This calculation yielded a total reserve
of 36.85 bcf of natural gas under the WIPP site (Table 8-12). Some
distillate would accompany this gas production. Foster (1974) estimated
that Pennsylvanian gas is accompanied by 14,950 barrels of distillate per
bcf of natural gas produced. Therefore, the 36.85 bcf of reserve under
the site should be expected to be accompanied by 550,900 bbl distillate.

Of the 20 drilling sites selected, 7 lie in Zone IV, 2 of which are
ranked as proven, 4 as probable, and 1 as possible. The aggregate

reserve of these 7 wells is 13.38 bcf of natural gas and 200,000 bbl of distillate. If drilling is allowed into Zone IV these hypothetical reserves could be recovered. The net balance that would be non-recoverable because of restrictions on drilling in Zones I, II, and III is 23.47 bcf of natural gas and 350,000 bbl of distillate.

Summary of Conclusion Concerning Hydrocarbon Resources. Table 8-13 summarizes the findings of the New Mexico Bureau of Mines resource study and the SW&A economic evaluation of the part of those resources considered attractive enough to be developed by the petroleum industry at 1977 prices and drilling costs.

The hydrocarbon resources remaining under the WIPP, if Zone IV is developed, amount to about 0.84% of that projected by Foster for the vicinity of the WIPP site. The total economic reserve, including Zone IV, amounts to approximately 90 days production of dry gas from southeast New Mexico.

8.4.9   Metalliferous Deposits in the Precambrian

Even the deepest oil/gas test near the WIPP site has not penetrated deep enough to encounter the Precambrian basement. A regional survey of test holes has been done by Foster and Stipp (1961). The basement may consist of slightly metamorphosed rhyolites and tuffs known as the Panhandle Volcanic Complex (Flawn, 1954). Such rocks hold potential for sulfide deposits. Geophysical techniques (induced polarization or electromagnetics) have a detection capability scarcely exceeding 1000 feet, while the Precambrian is at median depth of 18,000 feet beneath ground level at the WIPP site. No evaluation, therefore, is feasible for sulfide deposits. The depth is greater by a factor of almost two over the deepest mines in the world. Therefore, resources in the basement rocks, should they exist, are not likely to be attractive targets for exploitation.

8.5 SUMMARY

Potassium salts and fluid hydrocarbons are the only two resources thought
to be economically significant in the WIPP site area. The depth, volume
and richness of the deposits are the principal factors which will
determine when and if they might be exploited by a free-enterprise
system. Such economic evaluation has been conducted and reported in the
WIPP Environmental Impact Statement. Because economic aspects change,
they are not so relevant to site characterization as they are to
assessing the impacts of constructing the WIPP facility. Hence, in this
chapter, amounts and types of resources will be discussed rather than
their present economic value. The principal findings of resource studies
are summarized in Table 8-1.

If reasonable technologic and economic restraints are considered for
extracting, processing and marketing the resources then both the amounts
and types of exploitable deposits are greatly reduced. Only potash and
natural gas are considered to be significant in this respect (see Table
8.2). Even these reduced quantities should be considered as upper
estimates because of these assumptions: 1) complete mineral lease
ownership by a single company and 2) no conflict between the simultaneous
development of the shallow potash deposits and the deep gas reservoirs.

Economic resources are further reduced by allowing the mining of potash
and recovery of oil and gas by deviated drilling in Zone IV, the outer
buffer zone. If this is the case, then economic resources lying in the
inner zones are limited to those given in Table 8-3.

Caliche, salt, and gypsum are also present, but the abundance of these
minerals throughout the region leads to the conclusion that land
withdrawal for the WIPP will have little effect on present or future
requirements for them. Consideration was also given to the possible
presence of uranium in redbed-type sediments that overlie the
evaporites. The conclusion is that no significant uranium deposit
exists. Lithium occurs in a brine reservoir within the Castile Formation

northeast of the present site and may be present in a similar reservoir to the southwest. However, care has been taken to avoid such brine reservoirs within the site area. Consideration was also given to the possible existence of metalliferous deposits in the Precambrian basement under the site. However, the depth (about 18,000 feet below the ground surface) to Precambrian rocks would preclude mining even if mineral concentrations were present. No geologic or geophysical evidence exists to suggest that deposits are any more likely in the basement rock of the WIPP area than elsewhere in the region.

8.6 REFERENCES

Flawn, P. T., 1954, Summary of Southeast New Mexico Basement Rocks: Guidebook of Fifth Field Conference, New Mexico Geological Society, p 114-116.

Foster, R. W., 1974, Oil and Gas Potential of a Proposed Site for the Disposal of High-Level Radioactive Waste: Open-file report, New Mexico Bureau of Mines and Mineral Resources (work done under Contract No. AF(40-1)-4423 to ORNL).

Foster, R. W. and Stipp, T. F., 1961, Preliminary Geologic and Relief Map of the Precambrian Rocks of New Mexico: New Mexico Bureau of Mines and Mineral Resources, Circular 57.

Griswold, G. B., 1977, Site Selection and Evaluation Studies of The Waste Isolation Pilot Plant (WIPP), Los Medanos, Eddy County, New Mexico: SAND77-0946, Sandia Laboratories.

John, C. B., Cheeseman, R. J., Lorenz, J. C. and Millgate, M. L., 1978, Potash Ore Reserves in the Proposed Waste Isolation Pilot Plant Area, Eddy County, New Mexico: U. S. Geol. Surv. Open-file report 78-828.

Jones, C.L., 1978, Test Drilling for Potash Resources: Waste Isolation Pilot Plant Site, Eddy County, New Mexico: U.S. Geol. Surv. Open-file report 78-592.

Keesey, J. J., 1976, Hydrocarbon Evaluation Proposed Southeastern New Mexico Radioactive Material Storage Site, Eddy County, New Mexico: Sipes, Williamson and Aycock, Inc., Vols. I and II.

G. J. Long and Associates, Inc., 1976, Interpretation of Geophysical Data, Los Medanos and Vicinity: Report to Sandia Laboratories.

McMillan, C., 1976, Los Medanos Area: Permian Exploration Co., Report to Sandia Laboratories.

Siemers, W. T., Hawley, J. W., Rautman, C., and Austin, G., 1978, Evaluation of the Mineral Potential (excluding hydrocarbons, potash and water) of the Waste Isolation Pilot Plant Site, Eddy County, New Mexico: New Mexico Bureau of Mines and Mineral Resources, Report to Sandia Laboratories.

U. S. Bureau of Mines, 1977, Valuation of Potash Occurrences Within the Waste Isolation Pilot Plant Site in Southeastern New Mexico: Prepared for the ERDA.

LEGEND

O	Potash drill holes
⊠	ERDA potash drill holes
▢	Federal surface and mineral rights
▨	State surface and mineral rights
▨	Private surface and mineral rights
▢	Potash Enclave Boundary Extension, July, 1977
▨	Private surface, all mineral rights owned by Federal Government
▨	Private surface and mineral rights, except oil and gas federally owned

SCALE IN MILES

0   1/2   1   2   3

— N —

— — — Proposed WIPP site outline

— — — Zone boundaries and areas provided by ERDA

FIGURE 8-1

LOCATION OF POTASH EXPLORATION DRILL HOLES
IN THE VICINITY OF WIPP SITE
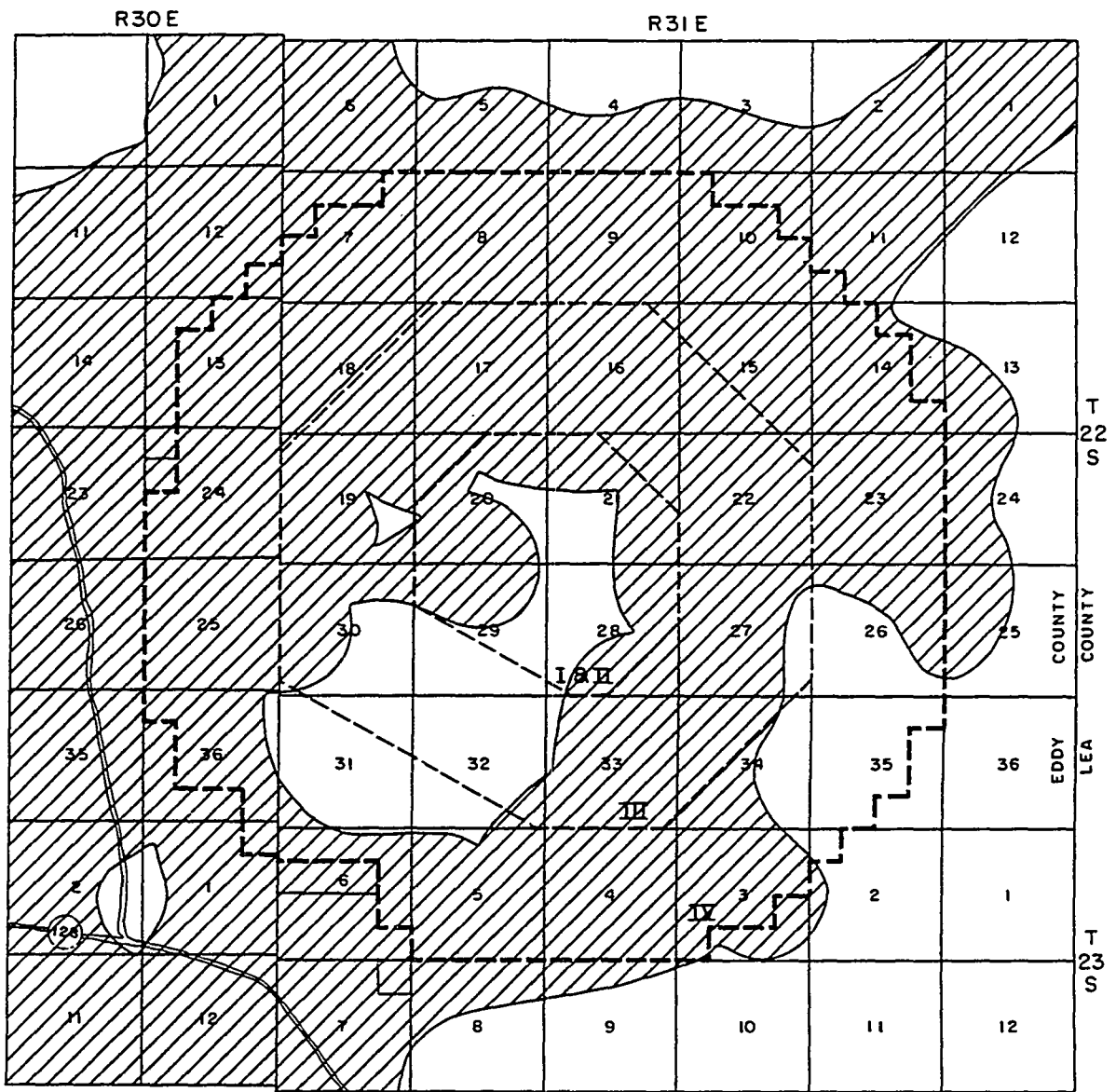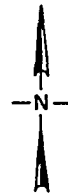
R30 E   R31 E

T 22 S
T 23 S

EDDY COUNTY / LEA COUNTY

Data provided by USGS Conservation
Division and ERDA

0   1/2   1   2   3

SCALE IN MILES

— N —

LEGEND

— — — Proposed WIPP site outline

— — — Zone boundaries and areas provided by ERDA

▨ Measured and indicated mineralization

Measured and indicated mineralization are at a cut off
of 3% K_2O as langbeinite or 8.0% K_2O as sylvite
or equivalent grade of mixed langbeinite-sylvite
occurring in a minimum 4-foot interval

FIGURE 8-2   LOW STANDARD POTASH RESOURCES
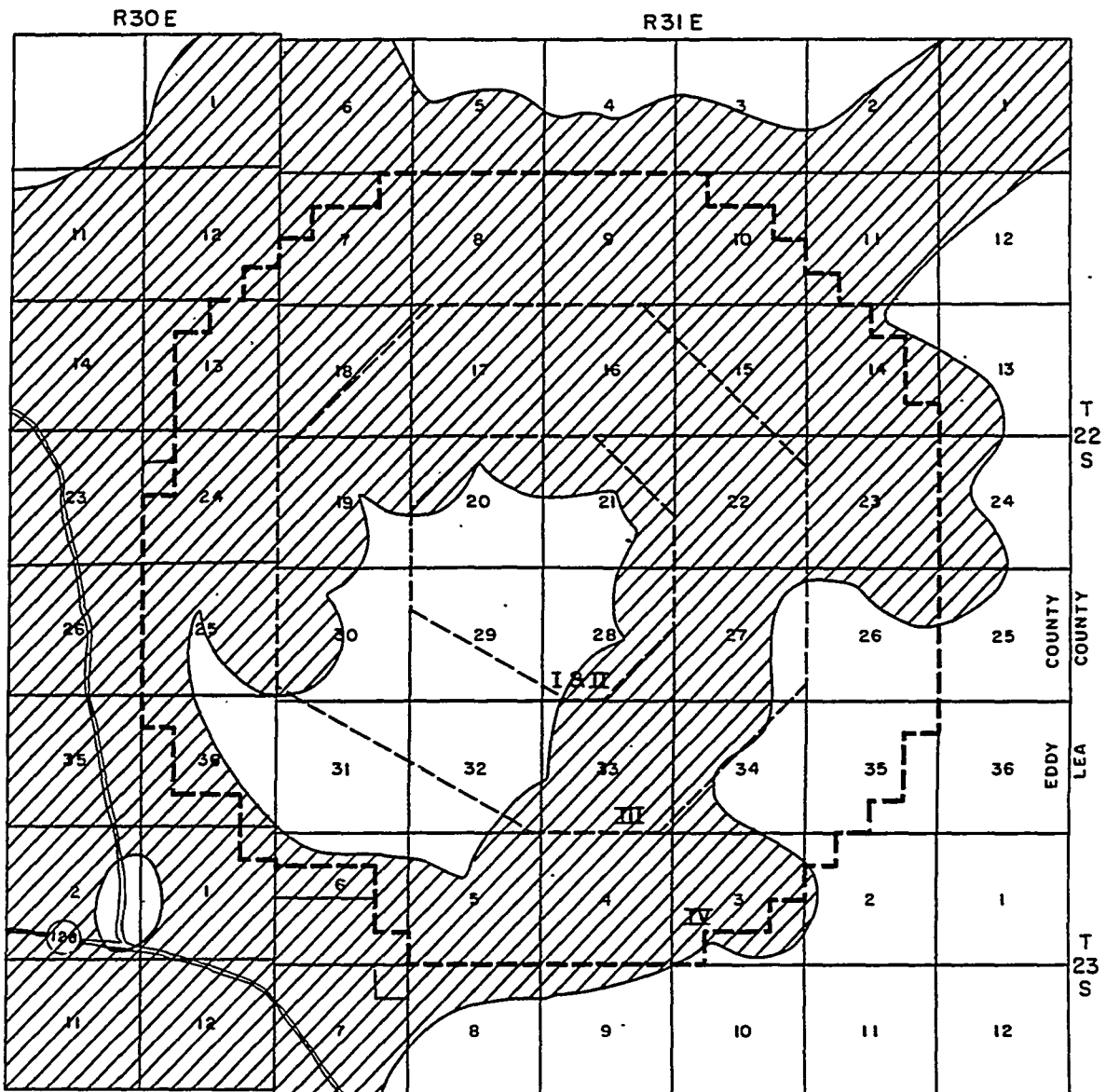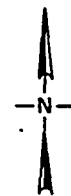
R30 E   R31 E

0   1/2   1   2   3

SCALE IN MILES

—N—

LEGEND

— — —   Proposed WIPP site outline

— — —   Zone boundaries and areas provided by ERDA

Measured and indicated mineralization

Measured and indicated mineralization are at a cut off
of 4% K₂0 as langbeinite or 10.0% K₂0 as sylvite
or equivalent grade of mixed langbeinite-sylvite
occurring in a minimum 4-foot interval

FIGURE   8-3   LEASE STANDARD POTASH RESOURCES
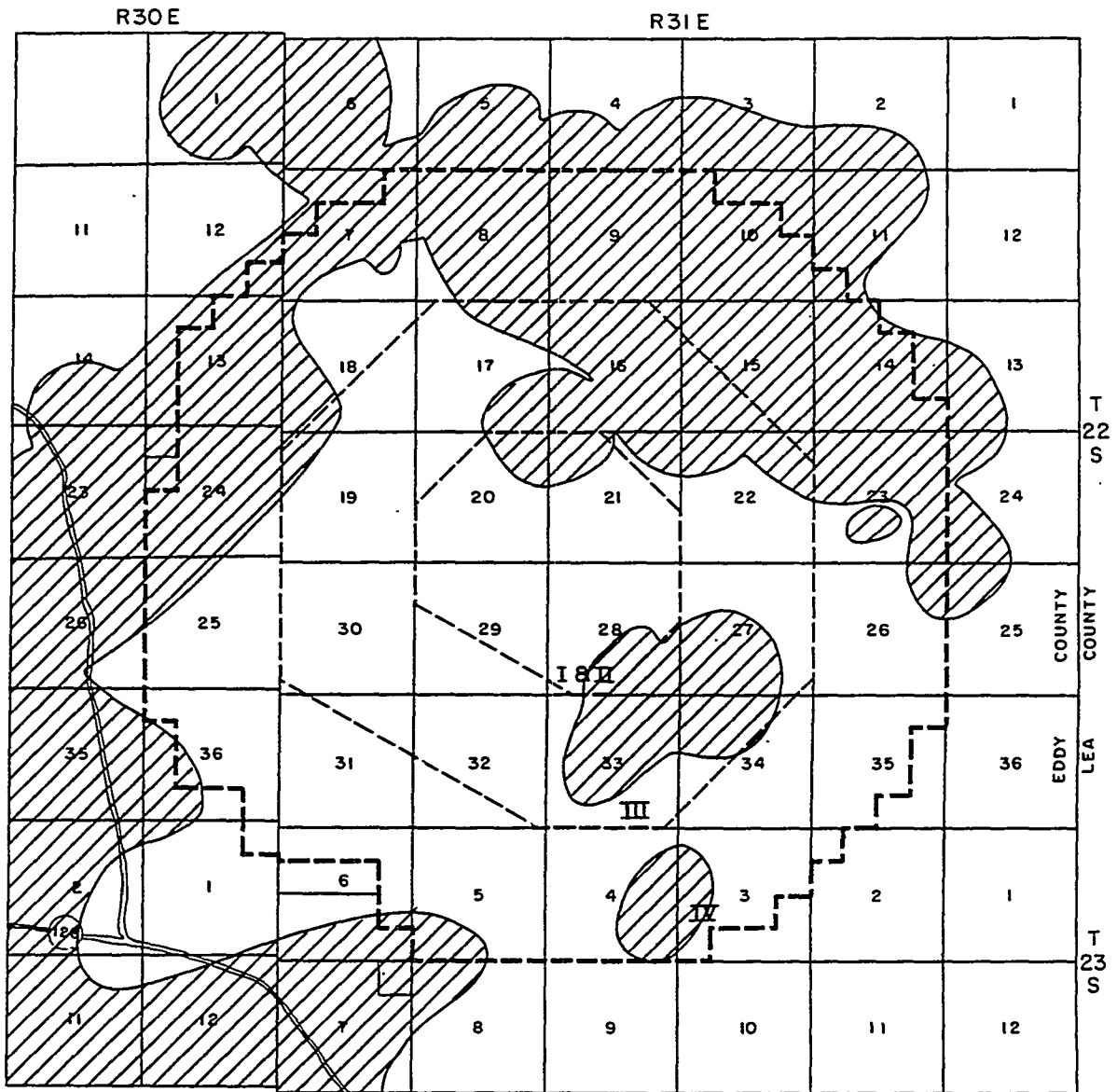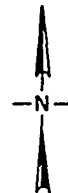
R30 E   R31 E

Data provided by USGS Conservation
Division and ERDA

0   1/2   1   2   3

SCALE IN MILES

— N —

LEGEND

— — —   Proposed WIPP site outline

— — —   Zone boundaries and areas provided by ERDA

Measured and indicated mineralization

Measured and indicated mineralization are at a cutoff
of 8% K$_2$O as langbeinite or 14.0% K$_2$O as sylvite
or equivalent grade of mixed langbeenite-sylvite
occurring in a minimum 4-foot interval

FIGURE 8-4   HIGH STANDARD POTASH RESOURCES
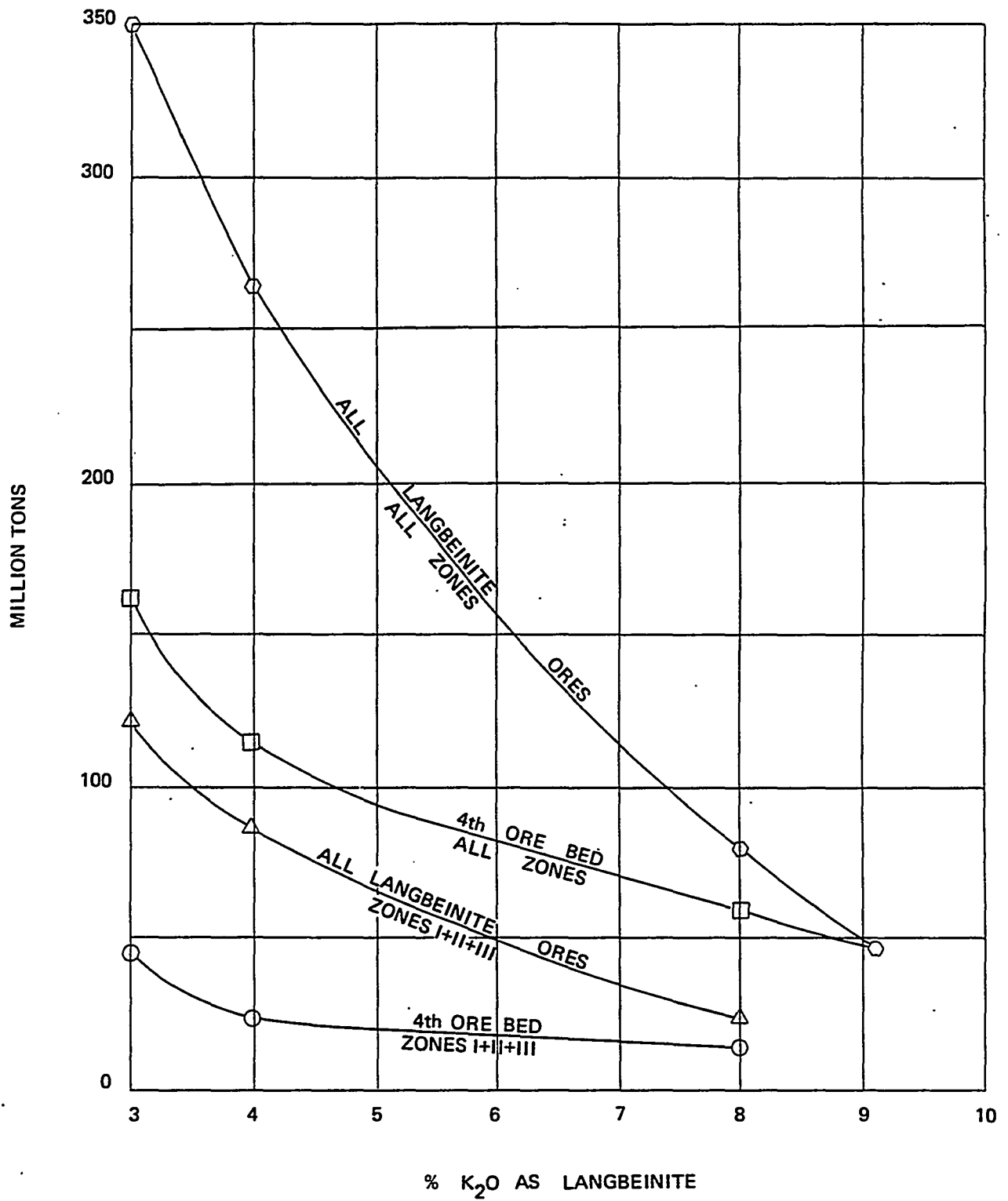
FIGURE 8-5.   LANGBEINITE RESOURCES
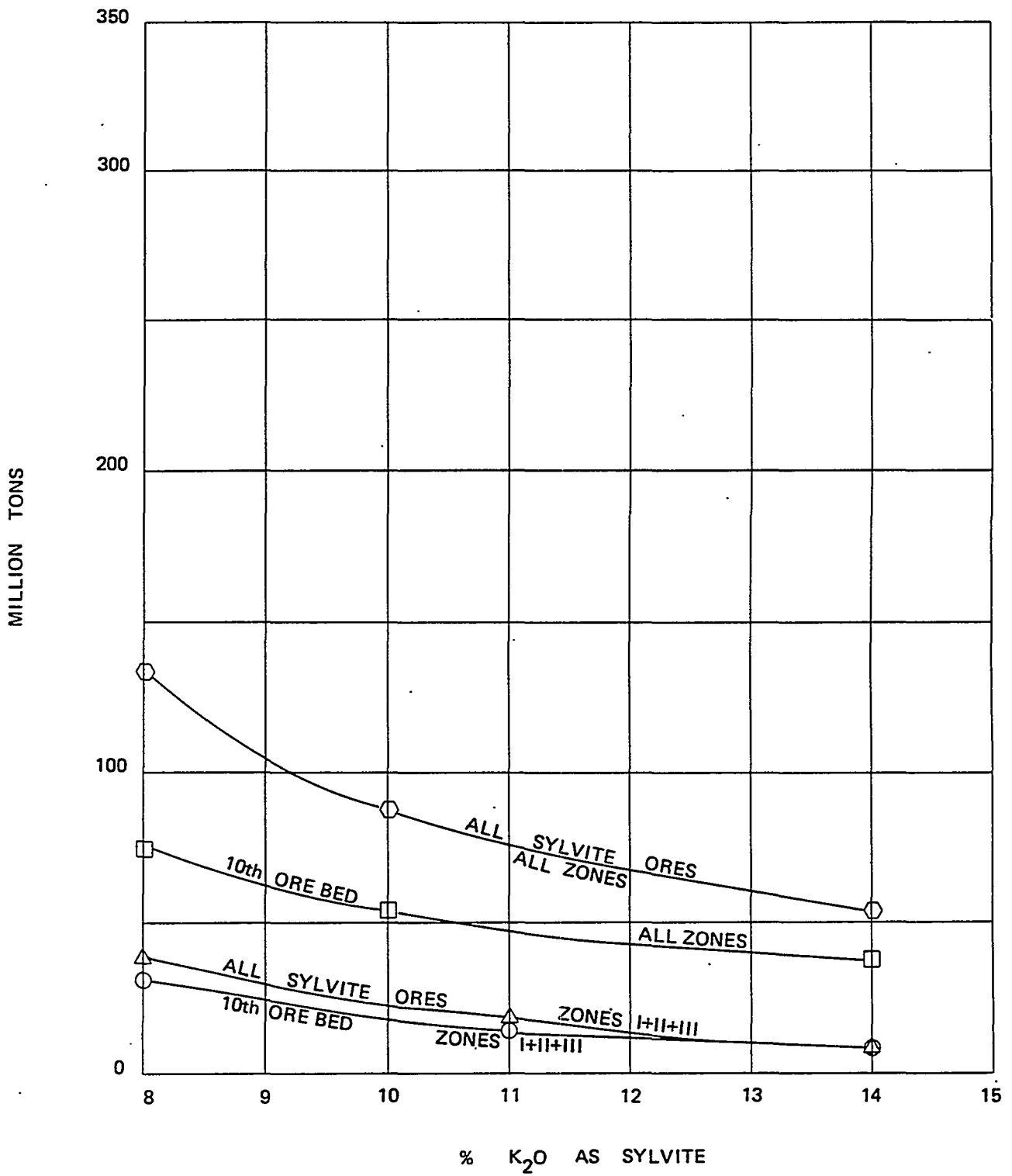
FIGURE 8-6. SYLVITE RESOURCES
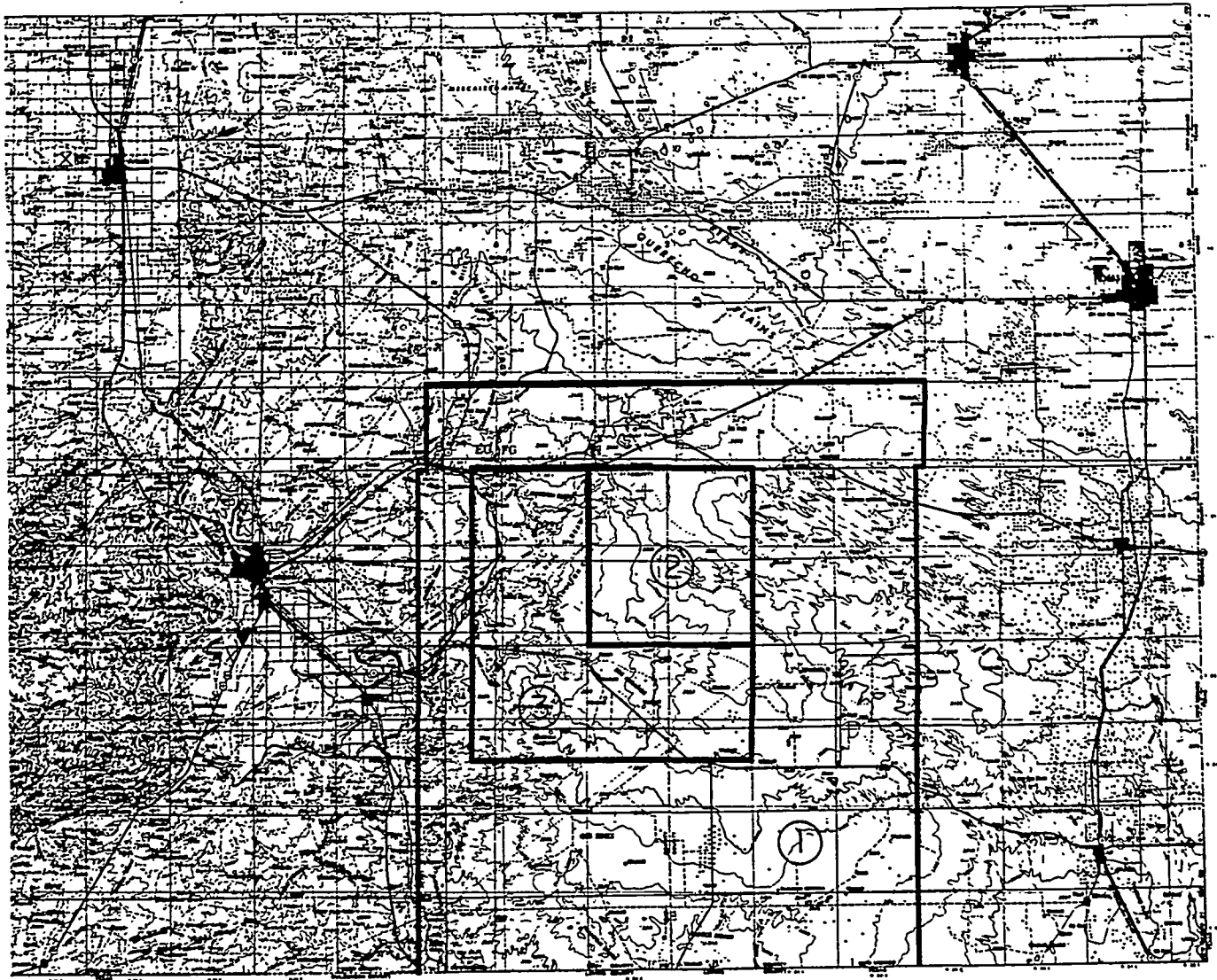
① NEW MEXICO BUREAU OF MINES STUDY AREA

② NEW MEXICO BUREAU OF MINES DETAILED STUDY CENTERED ON OLD ORNL SITE

③ SIPES, WILLIAMSON AND AYCOCK STUDY AREA CENTERED ON WIPP SITE

FIGURE 8-7

LOCATION OF HYDROCARBON RESOURCE STUDY AREAS

Elev.   Depth

3,000 — Ochoan
Triassic &
Younger

4,000 —

-750 — Ramsey Sand
Bell
5,000 — Canyon

-2,000 — Cherry
6,000 — Canyon

Delaware Mountain Group (2,900'-4,000')

-3,150 —
7,000 — Brushy
Canyon

8,000 —

-4,750 —

9,000 —

Bone
10,000 — Spring
(2,900'-3,500')

11,000 —

-7,650 —

Wolfcamp
12,000 — (1,000'-1,500')

-9,100 —
13,000 — Strawn
-9,700 — Atoka
-10,200 —
14,000 — Morrow
-10,950 — Barnett
-11,100 —
Mississippian
Limestone
15,000 —
-11,600 —
Woodford
-11,800 —
Silurian-
16,000 — Devonian
Carbonate

-13,050 —
Montoya
17,000 —
-13,500 — Simpson
-13,900 —
Ellenburger
-14,250 —
18,000 — Precambrian

Permian

Penn. (1,800'-2,100')

Miss. (550'-750')

Silurian-Devonian (1,250'-1,700')

Ordo-vician (1,000'-1,4000')

Potential pay zones.

5,000 ft.
4,000
3,000
2,000
1,000
500
0

FIGURE 8-8.   GEOLOGIC COLUMN AND POTENTIAL HYDROCARBON RESERVOIRS (ADAPTED FROM FOSTER, 1974)
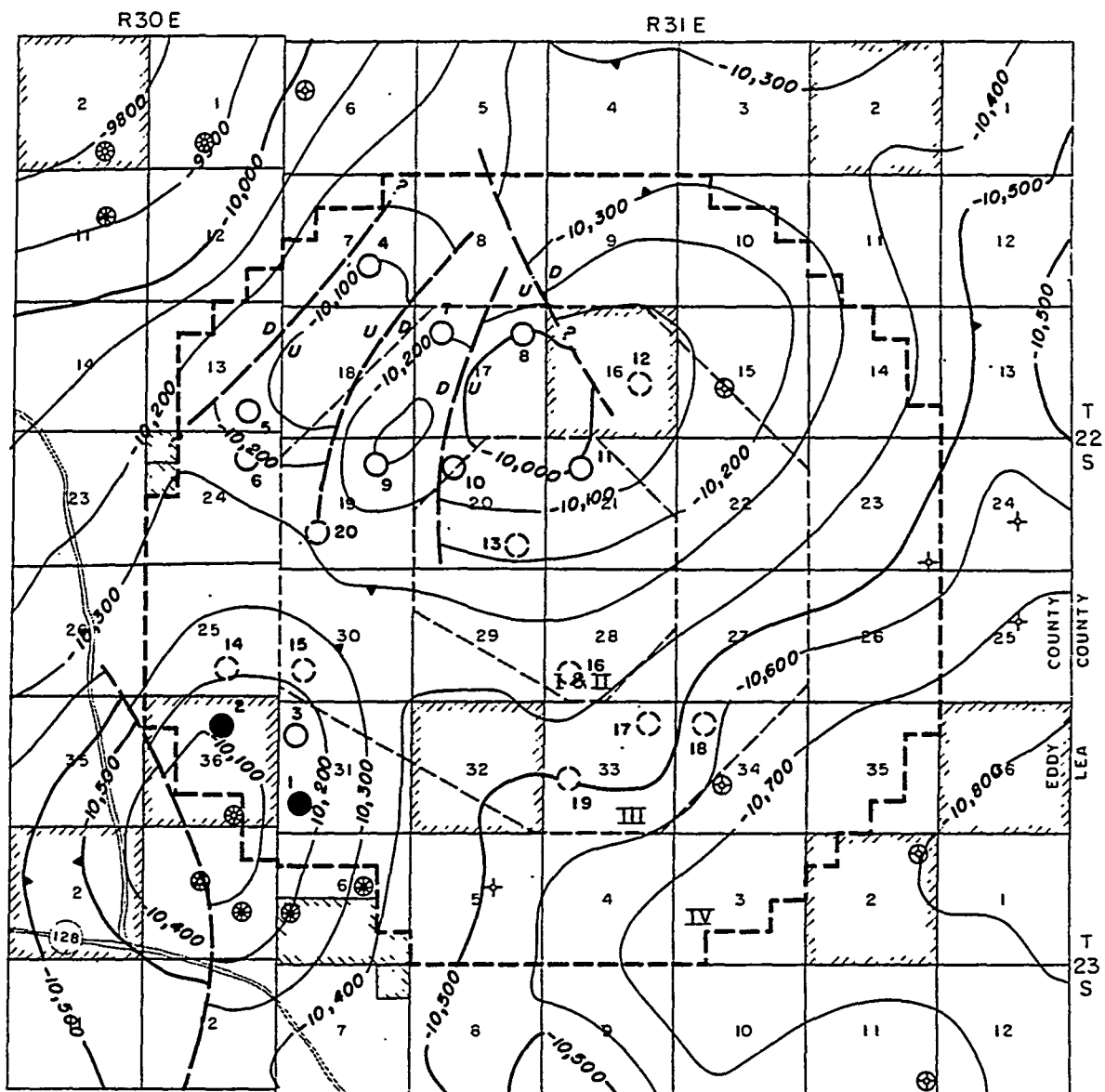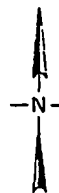
FIGURE 8-9

HYPOTHETICAL DRILLING SITES TO DEVELOP
POTENTIAL MORROW GAS RESERVOIRS

TABLE 8-1

TOTAL ESTIMATED RESOURCES AT WIPP SITE

Resource	Quantity	Depth	Richness
Caliche	185×10^6 tons	at surface	21-69% Insol.
Gypsum	1.3×10^9 tons	300-1,500 feet	Pure to mixed
Salt	198×10^9 tons	500-4,000 feet	Pure to mixed
Sylvite	88.5×10^6 tons	1600 feet	11.8 K_2O
Langbeinite	264.8×10^6 tons	1800 feet	6.10 K_2O
Crude Oil	37.7×10^6 bbls	4,000-20,000 feet	31-46° API
Natural Gas	490×10^9 cu. ft.	4,000-20,000 feet	1100 BTU/cu ft
Distillate	5.72×10^6 bbls	4,000-20,000 feet	53-56° API

TABLE 8-2

POTENTIAL ECONOMIC RESOURCES AT WIPP SITE

Resource	Quantity	Depth	Richness
Sylvite	27.43×10^6 tons	1,600 feet	13.33% K_2O
Langbeinite	48.46×10^6 tons	1,800 feet	9.11% K_2O
Natural Gas	36.85×10^9 cu ft	14,000 feet	1,100 BTU/cu ft
Distillate	0.55×10^6 bbls	14,000 feet	53° API

TABLE 8-3

ECONOMIC RESOURCES WITHIN ZONE I, II AND III AT WIPP SITE

Resource	Quality	Depth	Richness
Langbeinite	10×10^6 tons	1,800 feet	10% K_2O
Natural Gas	20×10^9 cu ft	14,000 feet	1,100 BTU/cu ft
Distillate	132×10^3 bbls	14,000 feet	53° API

TABLE 8-4

ORGANIZATIONS RESPONSIBLE FOR RESOURCE EVALUATION AND
KEY REPORTS CONCERNING RESOURCES

Organization	Responsibility	Reports
U.S. Geol Surv.	Potash Resources as related to ore grade and volume	John et al. (1978) Jones (1978)
U.S. Bur. of Mines	Determination as to what extent the potash resources reported by U.S.G.S could be economically mined and refined under today's technology and market	USBM (1977)
N.M. Bur. of Mines	Definition of resources and economics for caliche, salt, gypsum, brine, sulfur and uranium.	Siemers et al. (1978)
N.M. Bur. of Mines	Oil and gas resources. of a four township area which includes the WIPP site	Foster (1974)
Sipes, Williams and Aycock, Inc.	Determination of the economic viability of hydrocarbons under the WIPP site	Keesey (1976)
G.J. Long & Assoc. Inc., Permain Exploration Co.	Intrepretation of structure of Paleozoic sediments beneath Ochoan evaporites. These studies were useful in evaluation of hydrocarbons	Long (1976), McMillan (1976)

Table 8-5

POTENTIAL RESOURCES CORRELATED WITH STRATIGRAPHY

Formation	Thickness(ft)	General Character	Potential Resources	Evaluation
Mescalero Sand	0-15	Dune sand, fine grained	None	No resource
Caliche	0-5	Limestone, chalky	Caliche (in road construction)	Caliche is abundant throughout the area
Gatuna	0-375	Sandstone and siltstone	Uranium	Conditions apparently were oxidizing during deposition, and no uranium is apt to occur in the vicinity
Santa Rosa Sandstone		Sandstone	Uranium	Conditions apparently were oxidizing during deposition, and no uranium is apt to occur in this vicinity
Dewey Lake	487	Siltstone and sandstone some claystone	Uranium	Minor occurrences have been reported outside the WIPP site area. Gamma ray logs of 36 holes drilled within the site area showed no anomalies.
Rustler	310	Anhydrite and rock salt with subordinate dolomite, sandstone, claystone and polyhalite	Gypsum and salt	Abundant throughout the area, no advantage for site resources.
Salado	1976	Rock salt with subordinate anhydrite, polyhalite, potassium ores sandstone, and magnesite	Potassium salts, salt and gypsum	Langbeinite and sylvite occur in commercial quantities

Table 8-5 (Continued)

Formation	Thickness(ft)	General Character	Potential Resources	Evaluation
Castile	1400	Anhydrite and rock salt with subordinate limestone	Sulfur, salt, lithium in brine reservoirs	Salt is abundant throughout the area. Lithium concentration in brine is subeconomic today. Care has been taken to exclude brine reservoirs from site. Conditions and structures for sulfur deposits not known to exist at site.
Delaware Mtn. Group	3800	Fine grained sandstone (possibly a siltstone), shale, limestone, and dolomite	Oil and associated gas. Most favorable zone is the Ramsey sand	Reservoirs may exist, but small in comparison with the Morrow Formation
Bone Spring	3400	Limestone, fine-grained sandstone, and black shale	Oil and associated gas	Reservoirs may exist, but are small in comparison to the Morrow Formation
Wolfcamp (Hueco)	1480	Limestone, black shale, red or green shale, sandstone, and conglomerate	Oil and gas	Reservoirs may exist, but are small in comparison to the Morrow Formation
Strawn	300	Limestone, oolitic limestone and gray to black shale	Oil and associated gas	Reservoirs may exist, but are small in comparison to the Morrow Formation
Atoka	640	Limestone, oolitic limestone and gray to black shale	Natural gas	Commercial gas is being produced from near site. Atoka reservoirs are restricted in size, therefore, small likelihood of existence under the site
Morrow	1300	Limestone, oolitic limestone, gray to black shale, and sandstone	Natural	Commercial quantities of gas probably exist

Table 8-5 (Continued)

Formation	Thickness(ft)	General Character	Potential Resources	Evaluation
Mississippian	740	Black, angillaceous shale, black calcareous shale or shaly lime-stone, some sandstone	None	None likely
Siluro Ordovician	2100	Limestone, dolomite, chert, shale, black shale with rounded quartz grain inclusions, and small amounts of sandstone	Oil and gas. Most favorable zone is beneath the Woodford Shale	Oil and gas may be present in anticlinal situations
Precambrian		Not tested with in the WIPP site locality. Regional inference is that it consists of acidic volcanics or metasediments	Sulfide deposits	Considered too deep to exploit.

References: Siemers et al., 1978; Foster, 1974.

TABLE 8-6
STANDARD CONDITIONS FOR POTASH RESOURCES

Class	Type Ore	% K_2O	Thickness, ft
Low	Langbeinite	3	4
	Sylvite	8	4
Lease	Langbeinite	4	4
	Sylvite	10	4
High	Langbeinite	8	4
	Sylvite	14	4

Reference: John et al, 1978.

Table 8-7

POTASH RESOURCES, TONS x 10^6

I. Sylvite Ores

Ore Zone	Low Grade			Lease Grade			High Grade		
	I+II+III	IV	Total	I+II+III	IV	Total	I+II+III	IV	Total
10	30.4	44.4	74.8	16.5	37.2	53.7	9.8	28.9	38.7
9	3.7	6.6	10.3	1.2	4.8	6.0	--	0.7	0.7
8	5.0	43.1	48.1	1.0	27.8	28.8	--	13.7	13.7
Total	39.1	94.1	133.2	18.7	69.8	88.5	9.8	43.3	53.1

II. Langbeinite Ores

Ore Zone	Low Grade			Lease Grade			High Grade		
	I+II+III	IV	Total	I+II+III	IV	Total	I+II+III	IV	Total
10	25.0	30.6	55.6	24.6	24.8	49.4	9.7	0.9	8.8
5	11.6	14.6	26.2	10.9	13.3	24.2	--	1.6	1.6
4	46.5	114.5	161.0	24.0	91.4	115.4	14.6	44.4	59.0
3	14.6	19.9	34.5	9.6	16.0	25.6	--	--	--
2	24.2	49.5	73.7	18.7	31.5	50.2	1.9	7.9	9.8
Total	121.9	229.1	351.0	87.8	177.0	264.8	24.4	54.8	79.2

III. All Ores

Ore Zone	Low Grade			Lease Grade			High Grade		
	I+II+III	IV	Total	I+II+III	IV	Total	I+II+III	IV	Total
10	55.4	75.0	130.4	41.1	62.0	103.1	17.7	29.8	47.5
9	3.7	6.6	10.3	1.2	4.8	6.0	--	0.7	0.7
8	5.0	43.1	48.1	1.0	27.8	28.8	--	13.7	13.7
5	11.6	14.6	26.2	10.9	13.3	24.2	--	1.6	1.6
4	46.5	114.5	161.0	24.0	91.4	115.4	14.6	44.4	59.0
3	14.6	19.9	34.5	9.6	16.0	25.6	--	--	--
2	24.2	49.5	73.7	18.7	31.5	50.2	1.9	7.9	9.8
Total	161.0	323.2	484.2	106.5	246.8	353.3	34.2	98.1	132.3

Reference: John et al., 1978.

Table 8-8

ECONOMIC POTASH RESOURCES, TONS x 10^6

Mining Unit	Products	Recoverable Ore in Mining Unit	Recoverable Ore in WIPP Site	Percent in Zones I,II,III	Price[1] that Provides a 15 Percent ROR[2], $
B-1	Langbeinite	79.78	48.46	27.5	35.00
	Sulphate			27.5	88.50
A-1	Muriate	57.60	27.41	3.2	52.04
D-2	Langbeinite	87.93	23.57	0.7	36.51
	Sulphate			0.7	92.31
A-2	Muriate	98.32	51.80	7.6	61.73
C-2	Muriate	57.19	36.49	54.2	61.74
D-3	Langbeinite	140.27	42.45	23.5	42.26
	Sulphate			23.5	106.86
C-3	Muriate	70.64	52.87	57.5	67.52
A-3	Muriate	135.02	73.77	14.9	70.28

[1]Market price assuming no increase in production costs. Estimated weighted average annual price per ton of product, f.o.b., Carlsbad, New Mexico, used for evaluation.

[2]Rate of return

Reference: U.S. Bureau of Mines, 1977.

Table 8-9

SUMMARY OF POTASH RESOURCES, 10^6 TONS

| | In Place Resources (USGS Study) | | | | Mineable Today (USBM Study) | |
| | Lease Standard | | High Standard | | | |
	Langbeinite	Sylvite	Langbeinite	Sylvite	Langbeinite	Sylvite
Total Withdrawal	264.8	88.5	79.2	53.1	48.46	27.41*
Mining Permitted in Zone IV	87.8	18.7	24.4	9.8	13.35	0.9

*The USBM does not consider the sylvite contained in Unit A-1 to be mineable under today's market. To do so would require the price for muriate to be $52.04 per ton, or the investor must be willing to accept a rate of return less than 15%.

Table 8-10

POTENTIAL HYDROCARBON RESOURCES
EXPECTED IN VARIOUS FORMATIONS WITHIN THE DELAWARE BASIN

	Rating Geological		Rating Statistical		P.O.F.	Production Estimate — Acreage Oil (bbls)	Assoc. Gas (MCF)	Dist. (bbls)	Gas (MFC)	Oil (bbls)	Wildcat Assoc. Gas (MFC)	Dist. (bbls)	Gas (MCF)	Adjusted Rating Oil	Gas
Stratigraphic Unit	Oil	Gas	Oil	Gas											
Ramsey	IV		V		62	472,350	756,324			75,052	120,141			IV	
Delaware Mtn. Gp.	II		II		21	51,686	19,546			34,462	13,029			II	
Bone Spring	III		IV		39	193,952	379,738			88,170	172,610		.	III	
Wolfcamp	III	III	II	II	23	20,800	228,462	32,544	633,984	20,475	224,953	19,530	383,969	III	III
Pennsylvania	III	V	III	V	88	265,455				299,788	1,784,799	94,596	6,441,672	IV	IV
Mississippian	I	I	I	I	14										
Silurian/ Devonian	III	III	IV	IV	72	1,368,330	656,676	36,720	4,244,310	343,422	164,804	36,562	4,225,491	I	IV
Ordovician	I	II	I	III	63										

Table 8-10 (Continued)

Adjusted Production Estimate Section (640 Acres)

	Oil (bbls)	Assoc. Gas (MCF)	Dist. (bbls)	Gas (MFC)	Oil (bbls)	Assoc. Gas (MFC)	Dist. (bbls)	Gas (MCF)
Ramsey	472,350	756,324			75,052	120,141		
Delaware Mtn. Gp.	25,843	9,773			17,231	6,515		
Bone Spring	145,464	284,804			66,128	129,458		
Wolfcamp	15,600	171,347	24,408	475,488	15,356	168,715	14,648	287,979
Pennsylvanian	265,455	1,580,826	132,440	8,857,200	299,788	1,784,799	118,245	8,052,090
Mississippian								
Silurian Devonian	342,083	164,169	36,720	4,244,310	85,856	41,201	36,562	4,225,495
Ordovician								
	1,266,795	2,967,243	193,568	13,576,998	559,411	2,250,829	169,455	12,565,558

	Ratings	Calculated %
I:	Very low	25
II:	Low	50
III:	Moderate	75
IV:	High	100
V:	Very High	125

Taken from: R. W. Foster, 1974

Table 8-11

IN PLACE HYDROCARBON RESOURCES AT WIPP SITE*

Formation	Zone I+II+III			Zone IV			Total		
	Oil (bbls)	Nat. Gas (C.F.) $(x\ 10^9)$	Dist. (bbls)	Oil (bbls)	Nat. Gas (C.F.) $(x\ 10^9)$	Dist. (bbls)	Oil (bbls)	Nat. Gas (C.F.) $(x\ 10^9)$	Dist. (bbls)
Ramsey	6.0×10^6	9.6		8.0×10^6	12.8		14.0×10^6	22.4	
Delaware Group	3.3×10^5	0.1		4.4×10^5	0.2		7.7×10^5	0.3	
Bone Spring	1.9×10^6	3.6		2.5×10^6	4.8		4.4×10^6	8.4	
Wolfcamp	2.0×10^5	8.2	3.1×10^5	2.6×10^5	10.9	4.0×10^5	4.6×10^5	19.1	7.1×10^5
Pennsylvanian	3.4×10^6	132.9	1.7×10^6	4.5×10^6	176.3	2.2×10^6	7.9×10^6	309.2	3.9×10^6
Mississippian									
Silurian/ Devonian	4.4×10^6	56.1	4.7×10^5	5.8×10^6	74.5	6.3×10^5	10.2×10^6	130.6	1.1×10^6
Ordovician									
Total	16.2×10^6	210.5	2.5×10^6	21.5×10^6	279.5	3.2×10^6	37.7×10^6	490.0	5.7×10^6

* Based on Adjusted Production Estimate per Section (640 acres), Acreage method, Table 8-10. WIPP site contains 29.6 square miles or sections.

TABLE 8-12
ESTIMATE OF ECONOMIC HYDROCARBON RESOURCES AT WIPP SITE

Well Number	Natural Gas (BCF) Zone I, II, III			Natural Gas (BCF) Zone IV			Natural GAS (BCF) Total		
	Proven	Probable	Possible	Proven	Probable	Possible	Proven	Probable	Possible
1	---	---	---	2.07	---	---	2.07	---	---
2	---	---	---	2.07	---	---	2.07	---	---
3	---	---	---	---	1.64	---	---	1.64	---
4	---	---	---	---	2.09	---	---	2.09	---
5	---	---	---	---	2.09	---	---	2.09	---
6	---	---	---	---	2.09	---	---	2.09	---
7	---	2.09	---	---	---	---	---	2.09	---
8	---	2.09	---	---	---	---	---	2.09	---
9	---	2.09	---	---	---	---	---	2.09	---
10	---	2.09	---	---	---	---	---	2.09	---
11	---	2.09	---	---	---	---	---	2.09	---
12	---	---	1.67	---	---	---	---	---	1.67
13	---	---	1.67	---	---	---	---	---	1.67
14	---	---	---	---	---	1.33	---	---	1.33
15	---	---	1.33	---	---	---	---	---	1.33
16	---	---	1.67	---	---	---	---	---	1.67
17	---	---	1.67	---	---	---	---	---	1.67
18	---	---	1.67	---	---	---	---	---	1.67
19	---	---	1.67	---	---	---	---	---	1.67
20	---	---	1.67	---	---	---	---	---	1.67
	---	10.45	13.02	4.14	7.91	1.33	4.14	18.36	14.35
		Total	23.47		Total	13.38		Total	36.85

Plus Distillate 350,900 BBLS   Plus Distillate 200,000 BBLS   Plus Distillate 550,960 BBLS

Reference: Keesey, 1976.

TABLE 8-13
SUMMARY OF IN-PLACE AND ECONOMIC HYDROCARBON RESOURCES AT THE WIPP

	IN PLACE RESOURCES (NMBM STUDY)			ECONOMIC RESOURCES (SW&A STUDY)		
	Zone I,II,III	Zone IV	Total	Zone I,II,III	Zone IV	Total
Crude Oil 10^6BBLS	16.2	21.5	37.7	---	---	---
Natural Gas 10^9CUFT	210.5	279.5	490	23.47	13.38	36.85
Distillate 10^6BBLS	2.5	3.2	5.7	0.35	0.20	0.55

SPECIAL STUDIES

9.1 INTRODUCTION

The special studies presented in Chapter 9 cover issues of particular interest because the site is being characterized for radioactive waste isolation (the WIPP). The first special study presented is that of determining the thermophysical behavior of Southeastern New Mexico (SENM) rocks for mine design and the effects of heat-producing wastes, if placed in the WIPP. The second special study is to determine the site-specific sorptive capacities of SENM rocks for radionuclides flowing with SENM groundwaters. Characterization of the sorptive capacities of SENM rocks is required for safety assessment analysis of hypothetical failure events, not for site selection. Both of these studies are by no means complete and are continuing. The information presented here is an indication of the status of these studies in midyear 1978. Tabulations of test data are left to the references and future reports on specific subjects.

9.2 THERMOPHYSICAL PROPERTIES

9.2.1 Introduction

The thermophysical properties of New Mexico rock salt are being investigated to support the structural mine design and to evaluate the overall stability of bedded salt for the WIPP. A goal of this program is to develop constitutive relations which can be used in design and long-term stability calculations, commonly by finite element analyses (Dawson and Tillerson, 1977). Specific concerns are the stability of the facility during its life, the influence of ground motions on waste retrieval capabilities, and the effect of waste emplacement on the long term containment potential. The program was initiated in 1975.

Rock salts are weak, anelastic geological materials. They exhibit nonlinear response under practically all loading conditions at temperatures and pressures normally encountered in mining. Since salt

can experience large strains prior to failure, openings even at very shallow depths have been known to completely close and heal (Baar, 1977).

In long-established active mining districts, careful in situ observations and measurements have provided a basis for making reasonably reliable predictions of room deformation and failure (Baar, 1977). Some of this knowledge is applicable to the WIPP, although it cannot be directly applied to the WIPP because the behavior of rock salt is dependent upon the site, facility design, temperature and time involved. The rock mechanics program considers the particular problems posed by the longevity of the WIPP and by the unusual combination of mechanical and thermal loading anticipated in the repository.

Laboratory experiments have been severely criticized by some for not realistically representing in situ conditions, (Baar, 1977). However, laboratory experiments on rock salt are a useful step in material characterization, to establish limits of behavior. Ultimately, laboratory and in-situ test data coupled with modeling should lead to representative descriptions of material and structural behavior. As the WIPP is developed, in situ monitoring should enhance the validity of laboratory and modeling results.

The thermophysical behavior of rock salt has been modeled through various approaches, (e.g., Bradshaw and McClain, 1975; Fossum, 1977; Langer, 1967; Mraz, 1978; St. John, 1978; Serata, 1966, 1968, 1970; Serata and Cundey, 1978; Thompson and Ripperger, 1964; Thoms et al., 1973; Wahi et al., 1978). A widely accepted model which can translate laboratory data into a prediction of in situ salt behavior has not been developed.

Three broad areas were studied to identify the relative and site specific importance of various southeast New Mexico rock salt thermophysical properties. These three areas of study consist of: 1) petrography relevant to physical and mechanical properties, 2) general physical properties (density, moisture content, resistivity, etc.), and 3) thermal-mechanical properties (quasi-static and creep parameters).

Petrographic studies were conducted on mineralogically characterized core from AEC 7, AEC 8 and ERDA 9 to investigate structural petrographic changes between natural and experimentally-deformed samples (Callender & Ingwell, 1977). Identification of failure mechanisms by petrographic analyses will assist in selecting models to describe rock behavior.

Physical properties being measured for selected core include density, moisture content, porosity, permeability, electrical resisitivity, ultrasonic velocity, and thermal conductivity. Additional gas and brine permeability measurements are in progress at Sandia both on experimentally undeformed and deformed samples.

The following mechanical properties are being measured: uniaxial compressive strength, indirect (Brazilian) tensile strength, stress-strain behavior and ultimate stress in quasi-static triaxial compression, elastic moduli, principal strain ratios, elastic limit ("yield" stress), and creep rates. Additional tests address the effects of specimen machining, specimen aging due to stress relief during and after core retrieval, and specimen size, all of which could limit the field applicability of laboratory-determined results. The influence of sample size may be partially inferred from published data (e.g., Uhlenbecker, 1968; Dreyer, 1972; Szeki, 1978).

The data base for physical and thermal properties determined from core from the WIPP study area is still being compiled, and tests are continuing. Moreover, most of the results obtained to date pertain to rock salt alone, as opposed to other members of the stratigraphic column above and below the proposed repository horizons.

9.2.2 Petrography

Approximately 35 samples of experimentally undeformed and deformed salt were macroscopically and microscopically examined for mineralogy, fabric, and induced structure by J.F. Callender and T. Ingwell of the University of New Mexico (1977). Mineralogy of rock salt from southeast New Mexico has been described in detail in Chapter 7.

Between the depths of 1,000 and 2,000 feet, the samples are predominantly halite (NaCl) (range 47-98 percent) with lesser amounts of anhydrite ($CaSO_4$) (range 0-15 percent), polyhalite ($K_2MgCa_2(SO_4)_4 \cdot 2H_2O$) (range 0-18 percent), and clay and silt (range 0-44 percent). Halite is usually present in the core, except in samples from anhydrite layers and polyhalite seams. Anhydrite, clay and silt are generally present, while polyhalite occurs less commonly. Detailed stratigraphy of the WIPP study area is presented in the ERDA 9 corehole lithologic log, Figure 4.3.3.b.

Fabric In general, the undeformed rock salt specimens do not show well-developed linear or planar fabrics, aside from uncommonly-observed bedding. Locally, however, halite crystals show a faint to strong elongation, probably due to readjustment to local stresses. Certain fabric features within the cores may presumably have important local effects on salt deformation. These features include bubble trains, hopper crystals, cleavage, glide planes, grain boundaries, and clay zones (Callender and Ingwell, 1977).

Bubble trains are commonly aligned along cleaveage traces or grain boundaries in halite. The bubbles generally contain fluid, although some may also be gas or partially solid-filled (see section 7.6). Fracturing in experimentally deformed cores locally follows the bubble trains, and they are likely the site of small-scale structural weaknesses within halite. Once such fractures heal, the zones they followed become stronger than before (section 7.6) Hopper crystals, generally filled with clay, also tend to grow and be aligned along halite cleavage planes. In a number of samples, small-scale fracturing, induced by sample preparation or by disturbance during the coring operation in the field, is associated with zones of hopper crystals.

Cleavage, and fracture related to cleavage, is observed in halite. In euhedral, generally recrystallized, halite, the cleavage direction and grain boundary are coincident. In these cases, deformation along trends parallel to grain boundaries should certainly be facilitated. Similar relations, though less common, exist in subhedral halite. Translation

glide in halite is an important dislocation mechanism and has been described in the literature (c.f., Buerge, 1930; Clabaugh, 1962). Two glide planes, (110) and (001), have been recognized in both undeformed and deformed salt.

In summary, a local concentration of discrete fabric elements (e.g., hopper crystals, bubble trains) may be as statistically significant as planar or linear elements (such as bedding, cleavage alignment, or elongation) for the structural evaluation of the core, and local zones in deformed salt may play an important role in establishing fracture patterns.

Fracture. Analyses of fracture patterns in salt to date have been complicated by induced fracture during sample preparation and the field coring procedures used to obtain samples. The recognition of these induced fractures is generally fairly straightforward; however, the persistent question of local induced fracture arises during detailed study, and is a problem which cannot be easily resolved. Fortunately for the petrographer, many fractures are filled with clay, anhydrite, and polyhalite; these filled fractures give some insight into patterns in material before laboratory testing since they are clearly not a result of sample handling.

In general, fracture in undeformed salt core is relatively minor and is commonly associated with cleavage or grain boundary adjustments. It appears that fractures may have remained open at some stages of diagenesis for a sufficiently long period of time to be filled by sulfate or other solutions. A few unusual fracture geometries have been noted: en echelon fractures, generally with their major trend parallel to cleavage; circular fractures commonly around hopper crystals; fracture refraction across grain boundaries; jog and kink fractures; and fracture and local extension along glide planes. The number of fractures observed in the laboratory resulting from relief of the in situ confining stresses is unknown. Clay, anhydrite, and polyhalite have apparently flowed in some undeformed samples. Perhaps the best evidence for this statement is

local well-defined linear fabric in polyhalite and anhydrite, and the inclusion of halite in clay along grain boundaries.

In samples severely deformed by laboratory testing, fracture patterns are easily observed. In one sample a well-defined zone of cleavage and glide-plane fracture developed at about 40° to the compressional axis. Apparently, a network of interconnected fractures has been established in this zone which respects neither grain boundaries nor grain size. In contrast, another sample suggests that local fabric elements, particularly clay-rich zones, may affect fracture geometry and that planar fracture fabrics may not be as well-developed in clay-rich samples.

Fracturing of halite can be generated in the laboratory at relatively low confining pressures ($\leq$ 1500 psi) and moderately high strains (5 to 12 percent); this fracturing induces a fracture porosity in the material. At higher confining pressures, rock salt displays ductile behavior and it is difficult to induce fracturing. The position of the fracture pattern observed in the laboratory is related to both the stress direction and the local fabric elements. In addition, the crystal lattice of halite permits, through defects and crystallographic constraints (c.f., Hirth and Lothe, 1968), a complex dislocation system to develop.

9.2.3 Physical Properties

Measurements of physical properties of rock salt pertinent to the design of the WIPP have been conducted by several investigators. Some representative data are summarized in Table 9.2.3-1.

Density and Resistivity. Measurements were made on full dimension (4-1/2 inch diameter) core. The density determinations were performed following conventional laboratory procedures for determing bulk rock densities utilizing the buoyancy method. Commercial grade kerosene was used for buoyancy measurements. Direct current resistivity determinations were made using current densities of less than 0.20 microamperes per square centimeter (Elliot, 1976), and by downhole geophysical measurements (Griswold, 1977).

Volatile Mass Loss. Total volatiles, including water, were obtained by heating samples of Salado salt from the proposed repository levels to 300°C in several stages. Static weight loss determinations were made at each stage of heating (Kopp & Combs, 1975) and were reported in section 7.5.3.. In addition, thermogravimetric analyses were made by suspending powdered samples from a microbalance while dry nitrogen flowed over the sample. The samples were heated at 5°C/minute until the temperature reached 500°C and held there until gas evolution had ceased (see section 7.5.2 for details and data).

Permeability. Gas permeability of SENM rock salt has been measured for pressures up to 5000 psi and at room temperature to determine the tightness of the host rock to any gases evolved in the WIPP. The data developed by Sutherland (1978), are for argon gas at confining pressures to 2000 psi. A plot of permeability test results is shown on Figure 9.2.3-1. Sutherland's data demonstrate the influence of confining pressure (crack closure and healing) on permeability. Preloading of samples to near lithostatic confining pressures is required to obtain reproducible data in laboratory experiments. Other gases (air, nitrogen, argon) were measured by Core Labs (1977), Terra Tek (1978), and Shelby (1978). The Core Labs' tests followed API standards, however, they did not allow for crack healing. Shelby tested single crystal NaCl. The results of these measurements illustrate the following:

(1)   There is no correlation between measured permeabilities for as-received (stress-relieved) core samples;

(2)   Samples behave as if they are "healing" when subjected to a confining pressure on the order of their original in situ pressure (illustrated on Figure 9.2.3-1).

(3)   After an initial "healing" or "consolidation" period, the polycrystalline samples tested by Sutherland (1978) and Terra Tek (1978) have measured permeabilities of less than 0.05 microdarcys (the limit of resolution of their permeability measurement systems);

(4) There is little or no gas flow through the salt single crystals (less than 1 picodarcy) in the single crystal test apparatus of Shelby (1978). Therefore, the preferred flow channels through a core sample are believed to be along crystalline boundaries.

Thermal Conductivity. The thermal conductivity of several rock salt samples from core of AEC 8 were determined by a longitudinal heat flow apparatus. This apparatus was designed specifically for use with geologic core sections. Constant power is supplied to a heater at one end of the specimen until thermal equilibrium is established. The heat flux transducer and thermocouple outputs are then recorded allowing the thermal conductivity to be calculated from the readings (Acton, 1977). A plot of test results is shown on Figure 9.2.3-2.

Sonic Pulse Velocity. Measurements of compressional wave velocity were made both on laboratory samples (Kent and Wawersik, 1976) and by down hole geophysical methods (Griswold, 1977). Laboratory measurements were made both parallel and perpendicular to the core axis. No signficant variations (less than 0.02 Km/sec) were observed between the axial and transverse values of twenty measurements. The laboratory data were within 15% of the downhole geophysical values.

Summary of Data. Some physical properties are summarized in Table 9.2.3-1. In addition, permeability data are plotted on Figure 9.2.3-1 and thermal properties are shown in Figure 9.2.3-2. The experimental data are presented in the referenced documents.

9.2.4 Thermomechanical Properties

Introduction. It is the goal of laboratory stress-strain tests to develop constitutive relations which can be used in structural calculations. As the program progresses, a combination of finite element calculations using data obtained in the laboratory, empirical mine design methods and in-situ validation studies will serve to evaluate, in detail, certain aspects of the final WIPP design.

To achieve a valid and practical description of the behavior of rock salt from experiments in the laboratory, several programs are being conducted. These are: (1) Measurement of the mechanical response of SENM rock salts and other nearby rocks (e.g., anhydrite) over the domain of stresses and temperatures which may be expected in the WIPP; (2) Development of general models based on test results that are applicable to differing stress deformation and/or temperature histories; (3) Determination of mechanisms governing salt response in sufficient detail to allow the extrapolation of laboratory measurement in time; and finally (4) Establishment of relationships between laboratory samples of rock salt and salt masses in-situ.

This report summarizes the first series of laboratory tests, consisting primarily of short term "quasi-static" tests. These tests served to compare the response of WIPP salt with rock salts from other horizons and locations and to effectively scope the rock behavior for planning the long term creep tests. It is recognized that short term test behavior may be only partially indicative of long term behavior. Not all of the data developed is presented, particularly where detailed information has been published elsewhere. Instead, test values have been selected which are felt to best represent the behavior of the WIPP rock salt. Too few repetitive tests have been performed thus far to determine statistical significance of the data. This is due to the long times required to perform tests and the limited amount of rock salt core available to this test program from specific horizons of interest to WIPP.

A deliberate attempt was made to encompass a broad range of parameter variations including confining pressure and principal stress difference, i.e., mean stress and deviator stress, as well as temperature, time, loading rate, loading path, handling history, and specimen size. These variations covered a wider spectrum than might ordinarily be required to support the design of conventional mines or solution cavities. The approach is predicated on the unusual combination of anticipated mechanical and thermal loadings associated with WIPP. The experimental program plan also tried to address specific questions, for example,

concerning the effect of loading path, which were raised by critics of conventional quasi-static experiments in the past (Baar, 1977).

Testing was primarily conducted on rock salt samples from three horizons in the Salado Formation. The two horizons at 2,100+ feet and 2,600 to 2,700 feet represent the relatively pure halite from the proposed contact-handling (CH) and remote-handling (RH) levels, while the third horizon at 1,900 feet was chosen for study because it is clay rich salt.

The testing program through the summer of 1978 was generally divided into two segments, quasi-static tests and creep tests. Quasi-static properties were generated over a range of loading rates from d/dt $(\sigma_1 - \sigma_3)$ of 150 to 215 psi/min (RE/SPEC Inc. data, Gnirk et al., 1973, Hansen and Mellegard, 1977) to loading rates of 30 to 60 psi/min (Sandia data, Wawersik, 1977, 1978c). The 30 psi/min loading rate was chosen to match that of published data (Dreyer, 1972, Menzel and Schreiner, 1977). Creep tests were carried over a range of confining pressure $0 \leq \sigma_3 \leq 3,000$ psi, deviator stresses $1,500 \leq (\sigma_1 - \sigma_3) \leq 6,000$ psi, and temperatures of $24^\circ \leq T \leq 100^\circ C$ with a duration of up to 70 days. These loading rates were arbitrarily chosen as a means of scoping the behavior of SENM rock salt under conditions that may be encountered in the WIPP.

Apparatus, Experiments, Capabilities, and Data Handling. To support the determination of material properties of WIPP site rocks, a new triaxial facility was developed (Wawersik et al., 1976). Based on earlier experience (Wawersik and Brown, 1973; Gnirk et al., 1973; Wawersik, 1975), the present apparatus has the following capabilities.

> The apparatus accepts cylindrical specimens up to 4-1/4 inches diameter by 8.5 inches in length to accomodate the coarse grain size or rock salt.

> The system has a pressure rating of 10,000 psi; this is adequate to perform variable load path tests, for example, in triaxial compression, in triaxial extension, at constant maximum compression, etc.

The equipment is suitable to conduct both quasi-static tests and creep experiments.

Specimens can be heated uniformly to approximately 250°C in short-term tests and to 200°C to 220°C in long-term experiments.

Controlled, known temperature gradients can be applied for studies of fluid migration.

The equipment provides access to both specimen ends for possible venting or for measurements of pore pressure and permeability and for application of pore pressure, etc.

It provides both axial and radial deformation measurements. For uniform lateral deformation, this combination of strain measurements yields shear and volumetric strains.

The apparatus is equipped with multiple feed-throughs for use of instrumentation inside the pressure vessel.

Normally, hydrostatic and deviatoric loading are decoupled so that the hydrostatic response of all specimens can be defined and, more importantly, so that linear and bulk thermal expansion measurements can be determined as a function of temperature and pressure.

The apparatus and procedures allow for large, relatively unrestrained sample deformation.

Details of the test equipment (ranges, calibration procedures and precisions) are discussed elsewhere (Wawersik, 1975; Wawersik et. al., 1977; Wawersik, 1978a).Material and Test Specimens – The rock salt studied was machined from 4-1/4 inch diameter core obtained from zones at depths of 1,900 feet, 2,100 feet and 2,600 to 2,700 feet. Sample machining consisted of cylindrical and flat-end grinding following documented procedures which were designed to minimize the thickness of any shatter zones at the specimen surfaces. Alternatively, specimens were obtained by means of standard coring tools. Final specimen dimensions were nominally 2 inches or 4 inches in diameter, with a

length-to-diameter ratio of at least two. After machining, the
cylindrical surfaces of all samples were coated with a protective layer
of RTV silastic.

Quasi-static Rock Salt Properties. Quasi-static testing was conducted on
WIPP salt under hydrostatic pressures to 5,000 psi. Deviatoric loading
tests were performed to 3000 psi confining pressure and to temperatures
of 200°C. Variables of interest were: pressure (confining pressure,
mean stress), principal stress difference (deviator stress), time
(loading rate), temperature and load path. A separate study of the role
of the intermediate principal stress will also be initiated. The
importance of the foregoing variables was suggested by prior mine
measurements and by existing laboratory data (for example Schmidt, 1937;
U.S. Corps of Engineers, 1963; Le Comte, 1965; Hofer and Thoms, 1968;
Schlichta, 1969; Carter and Heard, 1970; Bradshaw and McClain, 1971;
Dreyer, 1972; Heard, 1972, Serata et al., 1972; Kern, 1973; Menzel and
Schreiner, 1977; Baar, 1977).

The term quasi-static is used in the conventional sense to denote a fixed
slow rate of loading. To avoid misunderstandings and undue
generalizations of these data, it is emphasized that most quasi-static
experiments were carried out at particular loading rates, e.g., 30
psi/min. It is important to realize that any data concerning the
mechanical behavior of WIPP rock salt under different loading conditions
must be inferred with proper regard to the time-dependent nature of the
material (Wawersik and Hannum, 1978).

Quasi-static data available to date include approximately 75 uniaxial
compression and indirect Brazilian tension tests at ambient temperature
on core from drill holes AEC 7 and 8 (Hansen and Gnirk, 1975). These
experiments were performed under the direction of Oak Ridge National
Laboratory prior to June, 1975. They include approximately 20
experiments on anhydrite and 5 tests on polyhalite. More recent
quasi-static data include approximately 50 tests on selected specimens
from the potential WIPP repository horizons (Wawersik et al., 1976;

Hansen, 1977; Hansen and Mellegard, 1977, Wawersik and Hannum, 1978).
Samples were machined from core of drill holes AEC 7 and ERDA 9.
Emphasis was placed on the response of rock salt from the storage horizon
at 2600 feet because of the added complexities of elevated temperatures
if heat producing wastes are placed in WIPP.

Selected representative mechanical properties in uniaxial compression and
indirect tension are listed in Table 9.2.4-1.

Quasi-static Triaxial Properties - Representative triaxial data are
listed on Table 9.2.4-2 for a range of confining pressures and
temperatures. Note that both tables 9.2.4.1 and 9.2.4-2 list secant
moduli (stress/total strain) and principal strain ratios ($\varepsilon_3/\varepsilon_1$) rather
than the elastic constants, that is, Young's modulus, E, and Poisson's
ratio. To calculate the intrinsic elastic constants it is necessary to
separate the nonelastic portion from the total deformation or to move
through stress states where elastic response dominates. This was
accomplished for New Mexico rock salt recently during unload/reload
cycles.

The constants obtained were $4.55 \times 10^6 \leq \varepsilon \leq 5.2 \times 10^6$ psi and
$0.17 \leq \nu \leq 0.24$ (Wawersik and Hannum, 1978). These values agree to
within 15% with those which were determined from borehole geophysical
data.

During initial deviatoric loading in the laboratory, nearly all
deformation of WIPP salt was nonelastic (Wawersik and Hannum, 1978). The
actual magnitude of this nonelastic deformation is likely to be sensitive
to the magnitude of the deviatoric stress which the core experienced
during drilling (Wawersik and Hannum, 1978), associated core damage and
subsequent core "relaxation" during core storage and handling.
Combinations of these factors probably account for the variations in
secant moduli and principal strain ratios in tables 9.2.4-1 and 9.2.4-2.

It is common practice in engineering to plot triaxial test data in the
form of Mohr's circles at the ultimate stress. The plots are made in the

stress space (σ,T) where σ and T denote normal and shear stresses, and an envelope is drawn tangent to the circles representing the ultimate shear stress of any value of confining pressure.

When the data from Tables 9.2.4-1 and 9.2.4-2 are plotted, three Mohr's circles which are normal for SENM rock salt are obtained in Figure 9.2.4-2A in stress space (σ,T) . The ultimate stresses can be approximated by a straight line (Coulomb) envelope of the form T = C + σ tan ϕ. In conventional engineering terminology, C is called the cohesion and ϕ , the angle of internal friction. In this case, at ambient temperatures, rock salt from the 2,700 foot level has an apparent cohesion of approximately 1,000 psi and an angle of internal friction of 33°. Similar data for other rocks are being used for mine pillar design. However, it should be recognized that the validity of these ultimate stress analyses rests on two assumptions: (1) failure is independent of the intermediate principal stress, and (2) failure is defined solely in terms of stresses and independent of strain, strain rate and time. Both of these assumptions are currently being evaluated for rock salt.

In contrast to other rocks, it is important to remember that rock salt undergoes large deformations long before the ultimate stress is reached. Since these deformations can exceed 15% even at ambient temperature, it is conceivable that a practial failure condition might incorporate a maximum deformation criterion. To illustrate this case, a Coulomb envelope was constructed (Figure 9.2.4-2B) which defines the stress magnitudes at an arbitrarily chosen constant value of strain (ϵ_1 = 2.5%). This value is the average strain at the ultimate stress of samples tested in uniaxial compression at ambient temperature and a loading rate of 30 psi/min. It can be seen that Figure 9.2.4-2B is different from the ultimate stress envelope in Figure 9.2.4-2A. Clearly, the shapes of the Mohr envelopes are highly dependent on failure criteria. The values obtained also depend on the manner in which the Mohr's envelope is drawn. In Figure 9.2.4-2A, a "best fit" straight line tangent to the circles was drawn; while in B, a parabola was drawn tangent to the circles.

Detailed Quasi-static Stress-Strain Relationships. Elastic constants, ultimate stresses, and stress or strain envelopes are useful for conventional failure stability analyses where rock is treated either as an elastic or as an elastic-plastic material. While such analyses have proven valuable in combination with careful engineering judgement, they are not always accurate. In view of the time-dependent nature of rock salt it is especially important that design calculations be based on a more comprehensive constitutive model. To initiate the development of such a model, detailed short-term quasi-static stress strain observations were made to identify the effects of pressure, deviatoric stress, (shear stress), temperature, and loading history. The influence of time as a discrete parameter is mainly considered in creep experiments.

Deviatoric Loading at Constant Confining Pressure. Deviatoric loading at constant confining pressure is the process of increasing the principal stress difference (deviator stress) from an initial state of hydrostatic compression. It is a necessary condition to induce substantial salt flow.

Typical quasi-static deviatoric loading data are shown in Figures 9.2.4-3 through 9.2.4-15. The key to these curves indicates sample depth in feet and (confining pressure in ksi and temperature in degree C). These stress strain curves depict complete continuous experimental records which indicate the manner in which all specimens were loaded. Deviator stress was applied incrementally rather than continuously. Actual force was raised quickly by some predetermined amount and then held constant for between 4 and 15 minutes while axial and lateral strains ε_1 and ε_2 (= ε_3) were monitored in time. The stepwise loading procedure made it relatively easy to control the mean applied loading rate while monitoring time dependent strains during load hold periods with a minimum of experimental error (Wawersik and Hannum, 1978). In most figures, these details of loading are omitted. As illustrated by the curve for sample 9-2601 in Figure 9.2.4-3, where smooth fits are made to the endpoints of each step in the actual stress strain record. Note that large changes in specimen cross sectional area at constant force during

all load hold intervals lead to considerable decreases in principal stress difference with time (Wawersik et al., 1977, 1978c). Conventional plots $(\sigma_1 - \sigma_3)$ versus ε_1 such as Figure 9.2.4-3 relate the present data to virtually all similar results for rock salt in the literature (for example, Schmidt, 1937; Heard, 1972; Dreyer, 1972, Menzel and Schreiner, 1977).

Considering Figures 9.2.4-3 through 9.2.4-6, three observations are particularly noteworthy.

1. Laboratory specimens of New Mexico rock salt have an initial elastic limit close to zero. Furthermore, this initial elastic limit appears to be the same following all hydrostatic pressure histories up to 5000 psi (Wawersik and Hannum, 1978).

2. Pressure appears to have a considerable effect on all properties of New Mexico rock salt except the elastic constants (Wawersik and Hannum, 1978). Specifically pressure controls the strain magnitudes, the ultimate stress and the relationships between the principal strain (Figures 9.2.4-5 and 9.2.4-6). Pressure effects are particularly evident at $(\sigma_1-\sigma_3)$ greater or equal 1200 psi.

3. New Mexico rock salt subjected to quasi-static laboratory compression can undergo substantial dilatancy which is associated with cataclasis, i.e., microfracturing. The magnitudes of the observed volume changes were significant particularly at low confining pressure and amounted to sizeable fractions of the observed shear strains near the ultimate stress (Wawersik and Hannum, 1978). Isovolumetric conditions of deformation are approached only at 3000 psi confining pressure. However, data at elevated temperature demonstrate that even comparatively minor amounts of dilatancy can have a considerable effect on the rate at which New Mexico rock salt deforms (Wawersik and Hannum, 1978).

Elevated Temperature Data. Elevated temperature experiments were carried out in two groups. First, the influence of temperature was considered at fixed confining pressures, for example, 500 psi (Figs. 9.2.4-7, 8 and 9). Then, the effect of pressure was evaluted at $200^{\circ}C$ (Figs. 9.2.4-10, 11 and 12). As expected (Bradshaw and McClain, 1971; Heard, 1972: Dreyer, 1972), temperature reduced the ultimate stress and increased the ductility (Fig. 9.2.4-7). Increasing the temperature is qualitatively equivalent to increasing confining pressure at ambient temperature. Cataclastic effects with considerable dilatancy are suppressed in favor of deformation modes which proceed at constant, or nearly constant, volume (Figs. 9.2.4-8 and 9.2.4-9). (Wawersik and Hannum, 1978)

Influence of Loading History. Effects of loading history are noted in several studies in the literature (for example, Schmidt, 1937; Sereta et al., 1972; Baar, 1977). To consider such effects, three sets of experiments were performed early in the experimental program. First, the influence of differing hydrostatic loading histories was tested. The results indicated no measurable effects on the behavior of rock salt from southeastern New Mexico during subsequent deviatoric loading (Wawersik and Hannum, 1978).

In the second group of experiments, quasi-static strains were measured as a function of load path in a conscious effort to separate the influences of load path and loading history as much as possible. The load paths employed are shown in Figure 9.2.4-15. They consist of:

1. Conventional triaxial tests at constant confining pressure (load path I).

2. Triaxial loading at constant mean stress $(\sigma m = \frac{1}{3} (\sigma_1 + \sigma_2 + \sigma_3)$ load path II).

3, Deviatoric loading at approximately constant maximum compression (load path III).

Figure 9.2.4-13 also identifies one test which combined load path III and I passing through points A, D, E, G, and H (Wawersik and Hannum, 1978). Table 9.2.4-3 provides a comparison of strains at several common stress states of Figure 9.2.4-13 with the strains ε_1 and ε_3 are numerically greatest along the path of constant confining pressure (load path I). The smallest ε_1 and ε_3 were obtained along the path of maximum pressure, either confining pressure or mean stress (load path III) (Wawersik and Hannum, 1978).

To evaluate load history even further, a third set of tests was performed. In these experiments, one sample was deformed in three successive stages at 3000, 500, and again at 3000 psi confining pressure. The response of this specimen was then compared with the strain behavior of individual samples which had been loaded deviatorically at 3000 psi and 500 psi confining pressure (Wawersik and Hannum, 1978). The results of the latter tests are shown in Figures 9.2.4-14 and 9.2.4-15. Notice particularly, that the stress strain record for the third load cycle of sample 7-2740.5 does not immediately converge to the stress strain records of specimens 7-2745 and 9-2601.5. Differences in results are obviously due to the influence of loading history (Wawersik and Hannum, 1978).

Interpretation of Quasi-static Data - In view of the quasi-static testing to date, as illustrated in the figures, the following observations were made repeatedly and establish broad guidelines which should be observed in modeling the thermomechanical behavior of New Mexico rock salt up to fracture and/or massive flow (ε_1 greater or equal 20%).

Rock salt from SENM in the laboratory is nonlinear under all loading conditions with an initial elastic limit ($\sigma_1 - \sigma_3$) approximately zero. Its intrinsic elastic properties can be evaluated accurately only in load/unload/reload cycles provided restrictions are imposed either on the loading (strain) rate or on the range of deviator stresses. However, given comparatively nonelastic strains, the intrinsic elastic behavior does not appear to be very important.

In the low confining pressure domain $\sigma_3 \leq 3000$ psi, rock salt behavior depends strongly on pressure and temperature. Both dependencies are reflected in ductility, ultimate stresses and in the variation between maximum and minimum principal strains or in the variations between volumetric strains and shear strains (Figures 9.2.4-4, 5, 8, 11, and 15).

A brittle mode of deformation (microfracturing) dominates rock salt deformation at ambient temperature, low confining pressure, and deviator stress in excess of approximately 1000 to 1500 psi. Accordingly, the overriding pressure effect under these conditions is pressure dependent dilatancy (Figures 9.2.4-4, 6 and 9). Brittle fracture, including creep fracture, i.e., macroscopic collapse and loss in load bearing ability are possible. At low (less than 1,000 to 1,500 psi) deviator stress, high temperature, and/or high pressure, salt deformation proceeds in a predominantly ductile manner at nearly constant volume. Particularly at high temperatures, pressure does not appear to further influence the nature of the governing deformation mechanisms. This is indicated by a pressure invariance (Figure 9.2.4-11) of the relationship between maximum and minimum compressive strains (shear and volumetric strains). However, observed differences in induced strain rate at a fixed loading rate but different confining pressures indicate that pressure influences the rate at which the governing deformation mechanisms, cataclastic or ductile flow, proceed.

It is recognized that available quasi-static stress strain data do not necessarily describe the properties of New Mexico rock salt over long periods of time. However, for lack of other information, quasi-static tests have been used to define the matrices of future creep experiments and to anticipate phenomena which might occur during creep. For example, emphasis is being placed on triaxial creep experiments as opposed to uniaxial tests. Simultaneous measurements are being made of both volumetric strains and shear strains in creep. Similar tests are not conducted routinely elsewhere and the apparatus to perform these tests is at the state-of-the-art in experimental rock mechanics.

Creep of Rock Salt   Creep tests on rock salt are continuing to evaluate
the long-term time-dependent behavior of New Mexico rock salt. Since
August, 1977, two sets of triaxial creep tests have been performed on
core from drill holes AEC 7 and ERDA 9, emphasizing the interval of 2600
to 2800 feet depth. Experiments were carried out over the range

$$0 \leq \sigma_3 \leq 3000 \text{ psi}, \; 1500 \leq (\sigma_1 - \sigma_3)$$
$$\leq 6000 \text{ psi}, \text{ and } 24^\circ \leq T \leq 130^\circ C.$$

Results indicate that in principle WIPP salt can undergo both transient
and steady state creep. Furthermore, limited data suggest that steady
state creep rates lie in the range from 10^{-10} sec^{-1} to 10^{-7}
sec^{-1}, depending strongly on stress state and temperature. Steady
state creep may have to be considered in WIPP design calculations; it was
not included in earlier wastes repository analyses which were conducted
in conjunction with in situ experiments during Project Salt Vault, Kansas
(Bradshaw and McClain, 1971).

To evaluate the nature of transient creep of the WIPP salt, 34 tests were
carried out on NX sized (two inch nominal diameter) core. Tests
durations vary between 0.5 and 500 hours (Hanson, 1977, and Hanson and
Mellegard, 1977). Initial efforts served to evaluate the significance of
transient creep on the possible repository conditions, to establish upper
(conservative) bounds for steady state creep rates at relatively low
deviator stress and temperature, and to test the applicability of a
pillar creep formula which has been widely used (Bradshaw and McClain,
1971):

$$E(t) = A(\sigma_1 - \sigma_3)^a T^b t^c \qquad (9.1)$$

The results of present transient creep data demonstrate significant
pressure effects which are consistant with all quasi-static observations
but are not predicted by equation 9.1.

Beyond that, however, at least one block of data appears to support equation 9.1 which in its generalized form is:

$$\epsilon = F_1(p)F_2(\sigma_1 - \sigma_3)F_3(T)F(\text{strain or time}) \quad (9.2)$$

Work is now in progress to estimate the error magnitudes which are associated with the use of equation 9.2 even under restricted conditions, e.g., $(\sigma_1 - \sigma_3) \leq 2{,}500$ psi and $\sigma_3 \leq 1{,}000$ psi. To accomplish this, numerical simulations are compared with the results of independent laboratory experiments which combine multiple creep runs with intermittent short-term stress variations at two different temperatures.

Time Dependent Fracture. To determine the long term strength of New Mexico rock salt, two approaches are being take. First, long-term laboratory creep tests are conducted to establish a relationship between strength and time. Obviously such tests are time consuming. Second, failure times may be calculated from creep flow and from estimates of the amount of nonelastic strain at the point of fracture. The nonelastic failure strain can be estimated by means of an empirical procedure which establishes a relationship between creep, time dependent fracture and quasi-static post failure characteristics (Wawersik, 1972). If this technique is applied to New Mexico rock salt, it appears that the range of stable creep prior to fracture at ambient temperature is:

$$\epsilon_1 \leq 2.5 \text{ to } 6\% \text{ at } \sigma_3 = 0 \text{ psi}$$

$$\epsilon_1 \leq 17 \text{ to } 20\% \text{ at } \sigma_3 = 500 \text{ psi}$$

Substantially greater stable creep occurs at $\sigma_3 = 3000$ psi confining pressure (Wawersik 1977). On Figure 9.2.4-18, photographs of core samples from ERDA #9 are shown that were deformed during triaxial testing (Hansen and Mellegard, 1977). Notice the large amount of strain test Numbers 6 and 7 have undergone without apparent major physical damage.

Applicability of Laboratory Measurements. Several investigations are underway to define the qualitative and quantitative applicability of laboratory experiments on WIPP salt to in-situ design predictions. Apart from numerical validation studies, measurements are in progress to determine the relaxation of core after drilling and to assess whether rock salt is damaged during field coring, recovery and storage. The latter efforts are supported by repeated tests on specimens with known laboratory stress histories to further define the effects of stress history, aging and specimen machine. In addition, numerical simulation are being conducted to balance the magnitude of deviatoric loading of salt core during drilling.

9.2.5 Summary and Conclusions

Data from the petrographic and physical properties studies show the WIPP horizon rock salt has low moisture content ($< 0.5\%$), is essentially impermeable ($< 5 \times 10^{-8}$ darcy) and has a high thermal conductivity ($\simeq 5.75$ watts/m$^{\circ}$k). These properties along with the studies of fabric and fracture indicate this rock salt is ideally suited from a physical standpoint for the storage of high temperature nuclear waste.

The initial elastic limit is close to zero for rock salt for any confining pressure. Although strengths for rock salt are substantial (unconfined compressive strength to 3700 psi and modulus to 2×10^{6} psi) the load bearing ability is dependent on time, temperature and confining pressure.

It has been shown that rock salt can experience large creep strains (25%) prior to loss of load bearing capacity. Gradual creep is an acceptable feature in the design of underground openings in rock salt as it allows the structure to close without a sizeable reduction in bearing strength and without the physical damage which is associated with fracture.

Laboratory testing is continuing to develop a constitutive model to describe the behavior of SENM rocks. The model will be used in computer codes to study the structural response of the geologic media to WIPP.

9.3 RADIONUCLIDE SORPTION ON WIPP ROCKS

9.3.1 Introduction

An important mechanism in retarding nuclide movement in groundwater is sorption. In the following discussion, this term will be used to encompass all mechanisms pertinent to interaction between nuclides and geomedia which include ion exchange, adsorption, and precipitation.

The ability of rocks to adsorb radionuclides and hinder their migration away from a geologic repository for radioactive waste is not a factor in site selection criteria (Chapter 2). Also, since sorptive affinity is not a fundamental invariant property of a rock sample, such as is mineralogy or total volatile content, radionuclide sorption properties were not discussed in Chapter 7 (Geochemistry). Nevertheless, quantification of rocks' affinities for radionuclide sorption, however, is NOT a generic problem which can be solved simply for all rocks. Since the only rational approach to the problem is to conduct experiments to determine radionuclide sorption properties for site-specific rocks and site-specific aqueous solutions, preliminary results of such experiments are reported as special studies. The results of special studies of radionuclide sorption are entirely dependent upon experimental conditions, just as in the measurement of quasistatic mechanical properties.

In some safety assessment modeling scenarios described for the escape of radionuclides from WIPP repository horizons, groundwters contact and leach the waste form, and eventually find their way out of the salt deposit into the surrounding rock and mineral strata. During this exit, the nuclide-bearing liquid would contact clay-containing halite in the repository horizon, polyhalite formations, anhydrite formations, and

finally the sandstone and dolomite formations which are the bounds of the evaporites. To a rough approximation, the concentration per unit mass of a given nuclide, sorbed on a solid mineral phase C_{solid} can be related to the concentration per unit volume, in the liquid phase C_{liquid}, by the relation:

$$C_{solid} = KC_{liquid}$$

where K is generally known as the distribution coefficient, Kd, with units of ml/g. The use of the term Kd implies an equilibrium condition for a given reaction which is both instantaneous and reversible. In the interaction of a nuclide with a complex mineral assemblage, neither condition may apply and the nuclide sorption observed can result from one or more sorption phenomena on one or more phases. To prevent confusion in nomenclature, the term Kd is used in this report, but with the understanding that what is being measured is a sorption coefficient which applies only to the system described and for the particular set of conditions used in making the measurement. Thus, the measurement of "Kd" does not reflect a fundamental thermodynamic property of rocks and/or solutions; it is rather a function of the experiment in which it is measured.

Ideally, sorptive affinities for radionuclides would be measured in situ in the geological formation of interest using long path lengths and available groundwater. This is not generally feasible and must be supplanted with data generated in a laboratory. Most of this section is an extract of SAND78-0297, "Interaction of Radionuclides with Geomedia Associated with the Waste Isolation Pilot Plant (WIPP) site in New Mexico" by R. G. Dosch and A. W. Lynch. It provides the results of a series of laboratory Kd measurements for various radionuclides and samples of different geological media from the vicinity of the WIPP site, and a discussion of the conditions used in making the measurements. The nuclides chosen for study have either a high potential for leaching and/or migration, a high radiotoxicity, or a chemistry similar to that of a nuclide with these properties. They included ^{137}Cs, ^{85}Sr, ^{131}I, ^{125}Sb, ^{144}Ce, ^{152}Eu, ^{153}Gd, ^{106}Ru, ^{243}Am, ^{244}Cm and ^{238}Pu.

A given set of conditions including pH, Eh, particle size, nuclide concentrations, and brine and/or groundwater simulant composition was defined prior to starting the work and maintained throughout. The Kd values reported are considered to be a set of preliminary baseline data for use in evaluating the effects of changes in those conditions which will undoubtedly be necessary as more information about the WIPP site itself and interactions of the waste forms with bedded salt become available.

The results of some parametric studies with lanthanide elements are also given. Significant differences in Kd's were observed as a result of varying pH and nuclide concentrations, and from the addition of trace quantities of organic contaminants to simulant solutions.

9.3.2 Geological Media

Sample Selection. The geological samples used in this work were taken from four inch diameter core samples from AEC #8 and ERDA #9 boreholes. (See Chapters 4 and 7 for descriptions of stratigraphy and mineralogy.) These include three samples from various rock formations (including the water-bearing rocks above and below the evaporites), four halite samples from the Salado Formation, and samples of polyhalite and Cowden anhydrite also from the Salado Formation.

The selection of the geological media for study was based on both the hydrology of the WIPP site and surrounding area and on a reasonable scenario for radionuclide transport from a bedded salt repository. The Magenta, Culebra, and Bell Canyon formations represent actual or potential aquifers.

Any path to the biosphere for water which may have contacted and leached a waste form would involve migration through halite formations, and also through anhydrite and polyhalite strata interspersed in the halite. Thus, these materials, along with the clay contained in the halite, are included in this study as they represent potential barriers to nuclide migration.

Sample Preparation. Culebra, Magenta, Bell Canyon, polyhalite, and anhydrite samples were reduced to a powder prior to use. Clays from the halite samples were obtained by dissolving core samples in deionized water, filtering and washing the insoluble residue, and drying at ambient temperature in air or vacuum.

9.3.3 Brine and Groundwater Simulants

The bulk of the Kd measurements reported herein were done using simulated brines and groundwater of the compositions given in Table 9.3-1. The Brine A composition is based on that expected in an aqueous solution in contact with potash deposits found in the vicinity of the WIPP site. The Brine B composition is typical of water in contact with halite deposits in the repository horizons. The groundwater Solution C composition is based on analyses of shallow groundwaters from the Los Medanos area (Lambert, 1978) above the evaporites and is intended to represent an "average" composition.

In determining Kd values for halite particles, saturated brines prepared from the particular core sample from which the halite had been taken were used as the liquid phase.

9.3.4 Solution Chemistry

Solutes. The use of simulated brines became necessary as both naturally occurring brines and core samples from repository horizons are currently available in very limited quantities. Simulants do offer the advantage of providing a reproducible matrix which allows for direct comparison of Kd data generated in different laboratories.

Potential problems in using simulants could arise from the absence of trace constituents which may be present in natural waters. If these are common inorganic species, the effect on Kd's would probably be negligible. However, trace quantities of organic compounds or dissolved gases such as hydrogen sulfide could produce significant changes in Kd

values should they tend to form stable complexes with some nuclides. The effect of trace quantities of organics which may be introduced into the repository as radwaste is being addressed and is discussed in Section 9.3.8.

Oxidation Potential. In aqueous migration from a deep geologic storage site, nuclides would most likely encounter both anoxic and aerobic conditions, in that order, as the biosphere is approached. The potential effect on Kd values could be many orders of magnitude; however, this should be limited to nuclides such as U, Np, and Pu which may undergo oxidation-reduction reactions in the potential range encountered.

Oxidizing conditions have been used to date·as they are believed to produce the "worst case" with respect to migration, i.e., the higher valence states of the previously mentioned actinides tend to have lower Kd's, and they will be encountered in any scenario leading to contamination of the biosphere.

Hydrogen Ion Activity. The effect of the pH is believed to be extremely important in both the solution chemistry and the adsorption mechanism involved in the Kd for a given geological media. Problems encountered in determining Kd values in systems where solution pH is varying are discussed in Section 9.3.8. Changes in the adsorption characteristics of clays, oxides, and some zeolite materials as a function of pH are well documented (Amphlett, 1964).

The initial pH values of 6.5, 6.5 and 7.5 for Brine A, Brine B and solution C simulants, respectively, were chosen as being representative of field pH measurements of natural brines and groundwaters in the Los Medanos area.

Radionuclide Concentation. Ideally, a distribution coefficient should be independent of concentration. This condition usually exists only over a narrow concentration range and, therefore, nuclide concentrations should be chosen which are somewhat representative of those expected in a

repository. The problem lies in the fact that little or no data exists to aid in estimating leaching rates under conditions expected after closure of a repository. These include glass or other waste forms at elevated temperature (70-200°C) and lithostatic pressure (2000 psi) in contact with "wet" salt or brine. Another presently unknown variable is the effect of radiolysis on leaching mechanisms and rates. Available leaching data primarily result from laboratory leaching experiments with simulated waste in distilled water at ambient temperature.

In order to simplify both sampling and counting operations in the initial work, an activity of approximately 1 μ Ci/ml was used for all determinations unless stated otherwise. The corresponding nuclide concentrations based on the suppliers' analyses of the isotopes used are listed in Table 9.3-2.

Unless otherwise stated, all distribution coefficient measurements were made using a single nuclide in the brines or groundwater to eliminate competing ion effects. The effect of the nuclide concentration on Kd's is of concern and some initial work in this regard is presented in Section 9.3.8.

9.3.5 Experimental Procedures

Apparatus, Sample Size and Sampling. Samples of rock, clay, anhydrite, polyhalite, or halite were weighed directly into polyethylene dropping bottles volumes of doped brine or groundwater were added. The ratio of liquid to solid was typically in the range of 30 to 35. Due to limited quantities of the clay samples, higher ratios (50-150) were used in experiments with clays.

The bottles were sealed by placing a piece of polyethylene film over the opening and replacing the bottle top. Agitation was provided by orbital, reciprocating, or wrist-action shakers. Samples for analysis were taken by replacing the polyethylene film with a 0.8 μ pore size Gelman filter, tightening the dropping bottle top down over the filter, and squeezing

the bottle to force 0.5 to 1.0 ml volumes into pre-weighed polyethylene vials. Quantitative volumes were determined from weight and density measurements. The filters were replaced with polyethylene film and the agitation continued.

Portions of all "feed" solutions were put in identical polyethylene dropping bottles, agitated, and sampled at the same time and in the same manner. The activity in the filtered "feed" samples were used as the initial solution activity in the Kd calculations.

Analyses. The activity in solutions containing ^{137}Cs, ^{85}Sr, ^{106}Ru, ^{131}I, ^{125}Sb, ^{152}Eu, ^{144}Ce, or ^{153}Gd was determined by x-ray spectroscopy. A Harshaw 3" x 3" NaI(Tl) scintillation crystal or an Ortec VIP Series Coaxial Ge(Li) solid state detector was used. Data was accumulated and processed by a PDP-11/20 computer system. ^{99}Tc beta activity was measured using a mica end-window Geiger tube or by liquid scintillation counting. Alpha activities were determined by liquid scintillation counting. Since only relative activities are needed to determine Kd's, units of cpm/ml were used in all calculations.

Equilibration Time. Samples of fission product nuclides were generally taken after 14-20 and 30-35 day equilibration periods. In some instances, more frequent sampling was done. Variation in Kd's between the two sampling times were generally within a factor of two and are believed to result from changes in concentration due to adsorption on container walls, filters, or pH changes in both the sample and feed solutions rather than from rock-nuclide sorption kinetics.

Equilibration times of 170 days were used in the actinide experiments. This extended period was dictated by delays in acquiring laboratory facilities rather than by experimental design.

9.3.6 Kd Data

The results of Kd measurements using the conditions described in previous sections are given in Tables 9.3-3 through 9.3-11. Each table represents a different geological sample and contains th Kd's determined for the various brine/groundwater-nuclide combinations listed and a pH range including the initial feed pH and final sample pH values. The Kd ranges given for the fission product nuclides include two or more measurements made during the course of the experiment. Error associated with these measurements is certainly the most significant at the high ($>10^4$) and low (<1) ends of the Kd range, where background to signal ratios are high or calculations are based on small differences in large numbers. Two-to-fivefold variations of Kd's between duplicate analyses in these regions were not uncommon. Another obvious source of uncertainty is sampling, both in picking a section of core to represent a geological formation and in taking small samples to represent the core. The magnitude of error due to heterogeneity in a given core sample is unknown, as multiple samples were not used in this survey.

9.3.7 Discussion of Kd Data

Cesium. Cesium adsorption from brines "A" and "B" on Culebra and Magenta samples, representing a potential aquifer region overlying the repository horizons, is minimal or non-existent with Kd's ranging from 0 to 2. Adsorption from groundwater C is slightly higher (Kd's from 4 to 10). In the potential aquifer underling the repository, the Bell Canyon Formation, Cs adsorption is significantly higher in the groundwater "C" simulant than in brine "B". This trend tends to support an ion exchange mechanism for Cs adsorption.

Similar results are observed on the samples associated with the repository horizons, with the exception of the polyhalite sample, which did not adsorb Cs from any of the solutions used.

Strontium. The adsorption of Sr on the rock samples from potential aquifer regions was very low with a Kd of 5 being the highest value observed in both brines and groundwater simulant.

Of the materials associated with the repository horizons, only the polyhalite sample showed any appreciable adsorption of Sr from the brine solutions that would be associated with the region.

The interstitial clay in the halite formation shows no tendency to adsorb Sr from the brine solutions (Tables 9.3-6 and (.3-9), and this may be attributed in part to the relatively high concentration of stable Sr used in the simulants. However, the same behavior was observed in an experiment where a brine prepared by dissolving a halite core and doped with < 0.3 ppm ^{85}Sr was cycled through a column of the halite particles from the same core (Tables 9.3-1 and 9.3-11). In this case, only a slight reduction in Sr activity was observed (which may have resulted from adsorption on the glass column or Tygon tubing used to circulate the brine); while ^{144}Ce was quantitatively removed by the halite.

Europium, Gadolinium and Cerium. These nuclides have been grouped together for discussion because their chemistries are very similar, particularly with respect to hydrolysis, and secondly, because they exhibited similar behavior in their interactions with the geomedia from the WIPP site.

With the exception of polyhalite samples, Kd's of greater than 10^3 for these nuclides were observed on all the geological samples with which they were contacted. Any interpretation of these data with respect to mechanism or comparison of the effects of different brines or geological media is difficult because of the contribution of hydrolysis and subsequent precipitation to the overall adsorption observed in the experiments.

For example, the polyhalite sample which was singled out as having Kd's of less than 10^3 for these nuclides (Table 9.3-7), also had final pH values which were lower than the rock or clay samples. Thus, the

apparent difference in Kd's may be a hydrolysis effect rather than be related to the polyhalite. The effect of hydrolysis is further discussed in Section 9.3.8.

Technetium and Iodine. Both of these nuclides are expected to exist as anionic species in natural groundwaters or brines and were used in the form of pertechnetate, TcO_4, and iodide, I, in this work.

Natural ion exchangers typically exhibit extremely low anion capacities, particularly in neutral or basic solution. In this work, the only material which showed significant adsorption of pertechnetate and iodide was a clay sample taken from a halite core (Table 9.3-9). The adsorption was observed in Brine A and groundwater C, but neither species appeared to be adsorbed from Brine B. The relatively high concentration of Tc used may have far exceeded the anion exchange capacity of some or all of the samples and this possibility is being investigated.

Ruthenium and Antimony. Difficulty was encountered in preparing the doped "A", "B", and "C" solutions due to the high concentrations of stable Ru and acid (4NHCl) in the [106]Ru solution used. Adjustment of pH after doping resulted in precipitation of > 95% of the Ru. The final feed solutions were estimated to contain approximately 0.10 μCi/ml of [106]Ru in "B" and "C" or 25 ppm total Ru.

General trends observed in the Kd measurements include: 1) higher Kd's for the clay minerals than for the rock samples, 2) higher Kd's in simulants "B" and "C" than observed in "A". The latter effect may be the result of brine composition, but more likely is a hydrolysis effect as the final equilibrium pH of "B" and "C" is higher than that in the "A" brine.

Antimony was added to the group of nuclides being studied late in this work, and there are not sufficient data available on which to base any general statements.

Actinides. The actinides used in this work were supplied as Am(III), Cm(III), and Pu(IV) solutions and used at face value. No attempts were made to determine the Pu species present in the simulant solutions after doping. The nominal activity of the actinides in the solutions used in this work was 1 µCi/ml, however, the final activities in the "feed" solutions were lower. The doping was done by adding the isotope solutions to containers and evaporating to dryness at room temperature. The brines or groundwater solutions were then added to the containers and the solutions were set aside for several days. The amount of isotope used was sufficient to provide an activity of 1.0 µCi per milliliter of solution if the entire amount was dissolved.

In general, the actinide concentrations in groundwater "C" at a pH of 7.3-7.4 are greater than those in the brine solutions in the 6.9-7 pH range. This is particularly true for ^{244}Cm, where the concentrations are 2 to 3 orders of magnitude lower in the brine solutions.

Kd values for the actinides of 300 or greater are observed for all the geological samples if the halite Kd's are based on weight of insoluble material rather than the weight of the total halite sample. In general, the Kd values in the groundwater "C" are higher than in Brine "B" which could result from hydrolysis due to higher pH in the "C" solutions; however, there are some cases where this Kd order is reversed.

The reasonably good agreement between the Kd values for the clay samples (Table 9.3-6) and the halite containing interstitial clay particles (Tables 9.3-5 and 9.3-11) suggests that the halite in the vicinity of the repository can serve as a barrier to actinide migration.

9.3.8 Parametric Effects

pH and Nuclide Concentration Effects on Kd. The first investigation into the contribution of the pH of the aqueous phase and effect of nuclide concentration on the sorption coefficient involved ^{152}Eu sorption from brines A and B and groundwater C on samples from the Magenta and Culebra Formations.

The experimental procedure used was the same as that described previously, except two blank samples of each feed solution were included instead of one. At the end of a two week equilibration period, the pH of the samples and feed solutions were measured. One of the feed B and C solutions was then adjusted so that its pH was equal to that observed in sample solutions containing that feed. A sodium carbonate solution was used for the pH adjustment, which was done over a period of three days. By the time analytical samples of the adjusted feeds were taken, the pH of some of them had increased and was higher than the corresponding sample. The pH of the Brine A feeds was not adjusted as the final values were the same as those in the samples.

The pH of the adjusted feeds decreased significantly during the first three months, probably due to adsorption of atmospheric carbon dioxide (Garrels and Christ, 1965). The pH of the solutions contacting the rock also varied with some increasing and others decreasing; however, the change was consistent within a given set of samples containing the same rock and solution.

Distribution coefficients calculated from both the feed activities and pH adjusted feed activities after two week and three month periods are listed in Table 9.3-12.

Europium is apparently more soluble in Brine A than in Brine B at the same pH or in the C composition at higher pH. The effect of adjusting the pH in B and C solutions definitely resulted in hydrolysis and formation of some species which did not pass through a 0.8μ filter. It is also of interest that significant decreases in activity in the pH-adjusted feeds were observed for all Eu concentrations used.

The Effect of Trace Organic Contaminants of Kd's of ^{152}Eu, ^{153}Gd and ^{144}Ce. One of the concerns in estimating migration rates of radionuclide in aqueous media is the ionic form of the nuclide of interest. Experiments have shown that the simple ionic forms of most polyvalent cations interact quite readily with geologic media from the

WIPP site via ion exchange or other sorption phenomena. These interactions serve to retard the movement of the ionic species relative to the aqueous matrix containing them.

The extent of the nuclide-geologic media interaction can be significantly altered by changes in the ionic form of the nuclide. Examples of such changes are redox reactions which may result in species of zero or negative charge types and reactions with available inorganic or organic ligands to form complex species with different chemical properties. One such change in properties might be enhanced mobility over that of the bare ion.

Investigations of the sorption changes due to complexation between organic ligands and radionuclides have been initiated by Robert T. Paine of the University of New Mexico. One source of organic ligands which may be present in large quantities in the repository is the plywood used in containers for shipping TRU waste. Samples of these containers are being refluxed in synthetic Brine B at 70°C, the maximum temperature expected in the transuranic (TRU) waste horizon in the repository. The initial samples of this brine, subsequently referred to as B*, were taken after 5 weeks of refluxing.

Although no significant physical degradation of the plywood was observed after this time period, chemical leaching did occur as evidenced by the coffee brown appearance of the brine. Gas chromatograph-mass spectrometer analysis of the brine indicated the presence of organic material, but identificaton was inconclusive. Infrared spectroscopy was used to examine carbon tetrachloride and benzene-acetone extracts from the brine. The extracted organic material fell into the general class of esterified rosin compounds, but no specific indentification was possible. Qualitative observation indicated that the brine contained extremely small amounts of organic material. Neither solvent system extracted the colored species from the brine.

The effect of plywood extract on lanthanide distribution coefficients (Kd's) was determind by measuring Kd's for ^{153}Gd, ^{144}Ce and ^{152}Eu between five geologic media from the WIPP site and the brine B* containing the plywood extract, and comparing these values with Kd's obtained in identical experiments using pure Brine B. The results are given in Table 9.3-13.

Although both the B and B* brines were doped initially with the same concentrations of tracers, there is a significant difference in the activity of the final samples taken. This could result from adsorption on the polyethylene containers or hydrolysis and subsequent filtration of hydrated oxides of the tracer elements through the 0.8 μ filters. In either case, the effect occurs to a significantly lesser extent in the brine B*, which is probably the result of interaction between the tracers and some ligand extracted from the plywood to form complexes which are less susceptible to hydrolysis.

The difference in Kd values could also result from complex formation. The complexing ligand may be a rosin derivative, many of which form very stable compounds with heavy metals. It may also be the species which causes the brown coloration of the brine. Observation of the analytical samples taken from the brine B* samples showed that the clay material had completely decolorized the brine. The other materials decolorized the B* samples to varying degrees, as given below in order of decreasing color intensity remaining in solution:

Feed > Magenta > Culebra ≈ Bell Canyon > Cowden > Clay solution

Similar work will be done using extracts which are being prepared from other organic materials expected to be associated with TRU waste such as rubber gloves, swipes, detergents, etc. Based on lanthanide·results, an experimental matrix will be designed to study the actinide elements.

The Effect of Oxidation State on Radionuclide Sorption. An additional approach to understanding the behavior of actinides under site specific conditions in WIPP is the study of the behavior of various oxidation

states of the actinides (particularly plutonium) in the presence of various components of the WIPP strata. This work is being performed at Argonne National Laboratory by Sherman Fried and Arnold Friedman.

Relatively concentrated solutions of actinides (0.01 M) whose oxidation states were determined by inspection of their optical absorption spectra were prepared and allowed to react with saturated WIPP brines, and with rocks from the WIPP site. Since it was assumed that in the final stages of a WIPP repository oxygen might be absent in the rock salt, the preparations were made in vacuo to identify species present under such conditions.

Solutions of plutonium were prepared in such a way that samples sealed in optical absorption cells at approximately 10^{-6} atmosphere of O_2 could be examined from time to time to observe changes in absorption peaks (if any) and thus determine the stability of the particular oxidation state as a function of time.

In the case of plutonium preparations, the isotope ^{242}Pu was employed. This was done to minimize radiolysis effects (specific activity Pu^{242} = 4.5×10^3 d/m/μg vs. $1/15 \times 10^5$ d/m/μg for ^{239}Pu). It is felt that while the behavior of plutonium in these concentrated solutions may be substantially different than tracer Pu migrating in an aquifer where the radiation field will be much less, it is nevertheless a good approximation to the conditions immediately in the vicinity of the canister when an amount of radioactivity has just leached out.

The various oxidation states of Pu were prepared by electrolytic means or oxidation by ozone as the case required, in order to avoid the introduction of extraneous ions which might affect the results.

The solutions of Pu compounds ($PuCl_3$, $PuCl_4$, and PuO_2Cl_2) were prepared directly in the absorption cell. The concentrations were generally of the order of 0.01 M. In a typical case, 4 ml of saturated WIPP brine "A" (Table 9.6-1) was introduced into the optical cell and

evaporated to dryness in a stream of nitrogen. After this operation, the proper amount of Pu compound was pipetted in the cell and evaporated to dryness with the salts from the WIPP brine.

The cell was attached to the vacuum line and evacuated until the pressure was $\sim 10^{-6}$ atm. De-aerated water was then distilled under vacuum until the amount of solution equals that which originally pipetted into the cell.

These samples of various Pu compounds were examined from time to time observing any changes in intensity or wavelength of absorption peaks corresponding to the oxidation state in question.

The resulting samples prepared for measurement of changes in intensity of the optical absorption spectra are Pu(III), Pu(IV) and Pu(VI) in water, and in saturated WIPP brine solution.

No definite changes in absorption peaks corresponding to changes in oxidation state were observed. The Pu(IV) solutions were so dilute, because of precipitation from the hydrolysis of Pu(IV), that little or no characteristic absorption peaks could be observed at all. The Pu(III) solutions, whose absorption peak is at about 6000 $\overset{\circ}{A}$, also showed little or no detectable change over the time interval of the experiment (2-4 months).

The Pu(VI) as PuO_2Cl_2, surprisingly, is insoluble in saturated WIPP brine. The level of solubility is so small that no absorption peaks could be seen at all. In order to be sure that this case is not one of very slow rate of solution, the sealed absorption cells are being rotated with periodic abosorption spectrum determinations.

Some absorption studies have already been carried out with Pu(IV) and Am(III) on anhydrite and dolomite from the WIPP site (see previous sections).

Work is presently underway with the Argonne National Laboratory Analytical Chemistry Group to develop procedures for the determination of the oxidation potential of WIPP salt, dolomite and anhydrite slurries, particularly those employing oxidation-reduction indicators.

Crude reaction rates and K_D values of Pu(III) and Am(III) with Magenta and Culebra dolomites in waters that have been equilibrated with the individual rock are in the table.

Rock Type	Radionuclide	Reaction Time (hr)	K_D
Magenta (gypsiferous dolomite)	Pu	50	41
	Am	400	47
Culebra (silty dolomite	Pu	1	19
	Am	1	84

It should be understood that these reaction rates are crude and that the K_D values are somewhat indeterminable because of varying quantities of radionuclides "plating out" on the walls of the containers. These experiments will be repeated as a function of temperature. Since these determinations were made on tablets of rock of known dimensions, the surface absorption coefficients can be calculated, these perhaps being more applicable to migration along fissures and cracks, where the surface absorption coefficient is

$$S_c = \frac{\text{activity/ml liquid}}{\text{activity/cm}^2 \text{ solid}}$$

The installation of a controlled atmosphere box has made it possible to study the absorption of the various oxidation states of Pu without the perturbing effects of atmospheric oxygen.

9.3.9 Summary

A survey of the potential of geological media from the vicinity of the Waste Isolation Pilot Plant site in Southeastern New Mexico for retardation of radionuclide migration via an aqueous carrier has been completed. Solution simulants representing water in equilibrium with potash minerals or halite zones and a typical groundwater were spiked with radionuclides and contacted with geological samples to obtain sorption coefficients, Kd's. The samples were taken from potential aquifers above and below the repository horizons and from bedded salt deposits in the repository horizons. The nuclides chosen for study represent those with a high potential for leaching and/or migration, high radiotoxicity, or those with a chemistry similar to nuclides with the aformentioned properties. They included ^{137}Cs, ^{85}Sr, ^{131}I, ^{99}Tc, ^{125}Sb, ^{144}Ce, ^{152}Eu, ^{153}Gd, ^{106}Ru, ^{243}Am, ^{244}Cm and ^{238}Pu.

A very general summation of the Kd results in brine simulants is as follows: Anionic species, TcO_4^- and I^-, showed little or no tendency to adsorb on any of the geological media (Kd's $\leq$ 1), with the possible exception of a clay material from a halite stratum (Kd < 5). Cs and Sr Kd's were also generally less than 1, but values in the range of 10-20 were observed on several minerals. Ru Kd's ranged from 25 to >10^3, depending on the brine and geological materials. The lanthanide and actinide Kd's were typically > 10^3, with only polyhalite showing significantly lower adsorption.

In the groundwater simulant, Tc and I showed the same behavior. The Kd's of the other nuclides were slightly higher, particularly those of Cs and Sr. This would be expected if the sorption were due to an ion exchange mechanism, but, in the case of the lanthanides and actinides, may also result from an increased contribution of hydrolysis to the Kd due to the higher pH of the groundwater simulant.

Important parameters in Kd measurements include solid sample form, simulant compositon, Eh and pH, and radionuclide concentration. In the Kd survey measurements, an initial set of these parameters was selected and, wherever possible, was used throughout the work. Parametric studies with Eu involving pH, trace organic constituents in the simulant solutions, and radionuclide concentrations have shown that significant differences in Kd's can be observed by varying any of those parameters.

A general observation which can be made from data obtained to date is that a Kd represents an empirical value for nuclide adsorption, which includes the effects of physical adsorption, ion exchange, and hydrolysis or other precipitation processes. The utility of a given Kd value is unambiguous only for that set of conditions used in making the measurement. Kd information which is used in modeling radionuclide migration should be in the form of a range of values generated in parametric studies under the variety of conditions postulated for a specific repository site.

For the WIPP site, rock salt, anhydrite, polyhalite and water-bearing dolomites and sandstones show an affinity for radionuclide sorption. Sorptive capacity as measured by batch Kd experiments generally expressed Kd > 0. Even small values of Kd (0 <Kd< 1) are effective in retarding the movement of radionuclides in groundwater.

9.4 REFERENCES

Acton, R.V., 1977, Thermal conductivity of SE New Mexico rocksalt and anhydrite: unpublished Sandia Laboratories preliminary report.

Amphlett, C.B., 1964, Inorganic Ion Exchangers, Elsevier, Amsterdam.

Baar, C.A., 1977, Applied Salt-Rock Mechanics 1: Elsevier Scientific, New York.

Bradshaw, R.L. and McClain, W.C., 1971, Project Salt Vault, a demonstration of the disposal of high-activity solidified waste in underground salt mines: Oak Ridge National Laboratories #4555.

Buerger, M.J., 1930, Translation-gliding in crystals of the NaCl structural type: Am. Mineralogist, v. 15, p. 174-187; p. 226-238.

Callender, J.F. and Ingwell, T., 1977, Structural Petrology of Undeformed and Experimentally Deformed Halite samples from USERDA Site #7 and #9, Report, SAND78-7076, Department of Geology, University of New Mexico.

Carter, N.L. and Heard, H.C., 1970, Temperature and rate dependent deformation of halite: Amer. Jour. Sci. 269, 193.

Clabaugh, P.S., 1962, Petrofabric study of deformed salt: Science, v. 136, p. 389-391.

Core Laboratories, 1977, Special core analysis study for Sipes, Williamson and Aycock, unpubl. consulting report to Sandia Laboratories by Sipes, Williamson and Aycock, Inc.

Dawson, P.R. and Tillerson, J.R., 1977, Comparative evaluations of the thermomechanical responses for three high level waste canister emplacement alternatives: Report, SAND77-0388, Sandia Laboratories.

Dreyer, W.E., 1974, Results of recent studies on the stability of crude oil and gas storage in salt caverns. 4th Symp. on Salt, A. H. Coogan, Ed.

Dreyer, W., 1972, The Science of Rock Mechanics: Trans. Tech. Publ. Cleveland, Ohio.

Elliot Geophysical Company, 1976, A laboratory investigation of the density and resistivity physical properties of drill core sample ERDA #9: consulting report to Sandia Laboratories.

Fossum, A.F., 1977, On the structural behavior of progressively mined solution cavities in salt, Journal of Applied Mechanics, v. 44, Series E, No. 4, p. 565-570.

Garrels, R.M. and Christ, C.L., 1965, "Solutions, Minerals and Equilibria," Freeman, Cooper & Co., San Francisco.

Mraz, D., 1978, Theoretical predictions confirmed by in-situ rock behavior in a deep potash mine: in 19th U.S. Rock Mechanics Symp., ed Y.S. Kim, Reno, Nevada.

Russel, J.E., 1978, A Creep Model for Rock Salt, Fifth Int. Salt Symps., Hamburg, Germany.

Schlichta, P.J., 1969, Growth, deformation, and defect structure of salt crystals: Geol. Soc. Am., Sp. Paper 88, 598.

Schmidt, W., 1937, Festigkeit and Verfestigung von Steinsalz: Zeitschr. Angew. Min., 1., 1.

Serata, S., 1966, Continuum theory and model of rock salt structure: in second symposium on salt, ed Jon L. Rau, Cleveland, Ohio.

Serata, S., 1968, Application of continuum mechanics to design of deep potash mines in Canada: Int. J. Rock Mech. Min. Sci., 5:293-314.

Serata, S., 1970, Prerequisites for application of finite-element method to solution cavities and conventional mines: in Third Symposium on Salt, ed., J.L. Rau and L.F. Dellwig, Cleveland Ohio.

Serata, S., 1972, The Serata stress control method of stabilizing undergound openings: Proc. 7 Can. Rock Mech. Symp. Edmonton, March 1971, pp. 99-118.

Serata, S., and Cundey, T.E., 1978, Rheological method of salt county design for underground storage of solid liquid, and gaseous matters: in 19th U.S. Symp. on Rock Mech. ed. Y.S. Kim, Reno, Nevada.

Serata, S., Sakuri, S., and Adachi, T., 1972, Theory of aggregate rock behavior based on absolute three-dimensional testing (ATT) of rock salt: in Basic and Applied Rock mechanics, Proc. 10th U.S. Symp. Rock Mech., K.E. Gray (ed.), AIME.

Shelby, J.E., 1978, Permeability of Sodium Cloride: Sandia Laboratories interoffice memo, Albuquerque, New Mexico.

St. John, C.M., 1978, Computer models and the design of underground radioactive waste repositories, M.I.T. Special Summer Session on Rock Engineering, June 1978.

Sutherland, H.J., 1978, Permeability of SENM rock salt: Sandia interoffice memo, Albuquerque, New Mexico.

Szeki, A, 1978, Influence of Volume on Creep Behavior of Rocksalt Pillars, Fifth. Int. Salt Sympos., Hamburg, Germany.

Terra Tek Inc., 1978, Gas permeabilities of SENM salt: consulting memo to Sandia Laboratories, Albuquerque, New Mexico.

Thompson, E., and Ripperger, E.A., 1964, An Experimental Technique for the Investigation of the Flow of Halite and Sylvinite, Proc. 6th Symp. Rock Mech., E.M. Spokes and C.R. Christiansen, eds., AIME.

Thoms, R.L., Char, C.V., and Bergeron, W.J., 1973, Finite Element Analysis of Creep in Rock-Salt Pillar Models, Proc. 14th, Symp. Rock Mech., H.R. Hardy and R. Stefanko eds., AIME.

Uhlenbecker, F.W., 1968, Verformungsmessungen in der Grube und erganzende Laboruntersuchungen auf dem Kaliwerk Hattorf (Werra-Revier) im Hinblick auf eine optimale Festlegung des Abbauverlustes bei grobtmoglicher Sicherheit der Grubenbaue, PhD Thesis, TH Clausthal.

U.S. Corps. of Engineers, 1963, Project Dribble, Petrographic examination and physical tests of cores, Tatum Salt Dome, Mississippi: Army Engineers Waterway Experiment Station, Techn. Rep. No. 6-614.

Wahi, K.K., Maxwell, D.F., Hofmann, 1978, Explicit finite-difference simulations of Project Salt Vault: in 19th U.S. Rock Mech. Symp., ed. Y.S. Kim, Reno, Nevada.

Wawersik, W.R. and Brown, W.S., 1973, Creep Fracture of Rock, Techn. Report UTEC 73-197, Univ. of Utah,

Wawersik, W.R., 1975, Technique and apparatus for strain measurements on rock in constant confining pressure experiments. Rock Mech. v. 7, 231.

Wawersik, W.R., 1977, Sandia Laboratories Albuquerque, New Mexico, Inter office memos, August and November.

Wawersik, W.R., 1978a, Large specimen triaxial apparatus for rock testing to 70 MPa confining pressure and 225°C: to be published.

Wawersik, W.R., 1978b, Effects of pressure, deviator stress and temperature on transient creep of rock salt at low confining pressure: AGU, Vol 59 No. 4, Apr. 78 p. 376.

Wawersik, W.R., 1978c, Sandia Laboratories, Albuquerque, New Mexico, Inter Office Memo, January.

Wawersik, W.R., Callender, J.F., Weaver, R., and Dropek, R.K., 1976, Preliminary determination of mechanical properties on rock salt from southeastern New Mexico. Pre-Proc., 17th U.S. Symp. Rock Mech., Univ. Utah Exp. St..

Wawersik, W.R. and Hannum, D.W., 1978, Mechanical behavior of New Mexico rock salt in triaxial compression up to 200°C: 5th Int'l Salt Symp. Hamburg, Germany, June 1978.
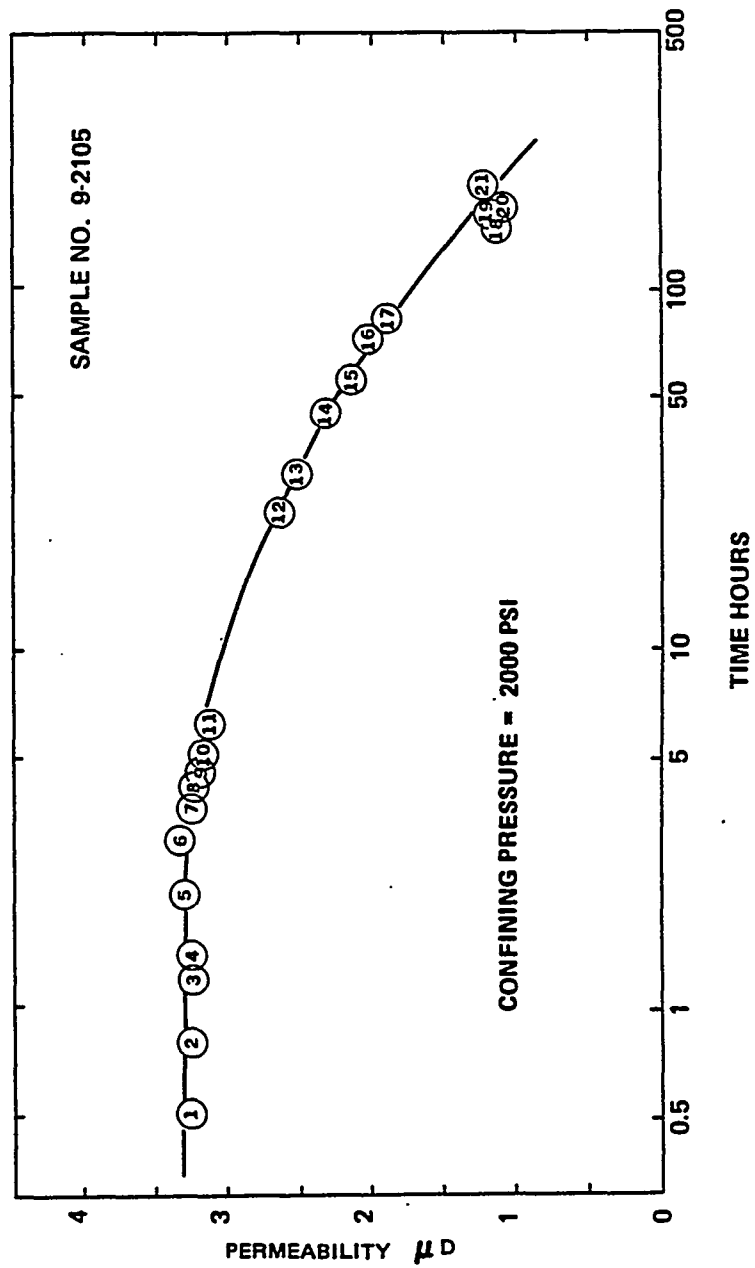
ARGON PERMEABILITY OF ROCK SALT SAMPLE AT 2000 PSI

CONFINING PRESSURE

FIGURE 9.2.3-1
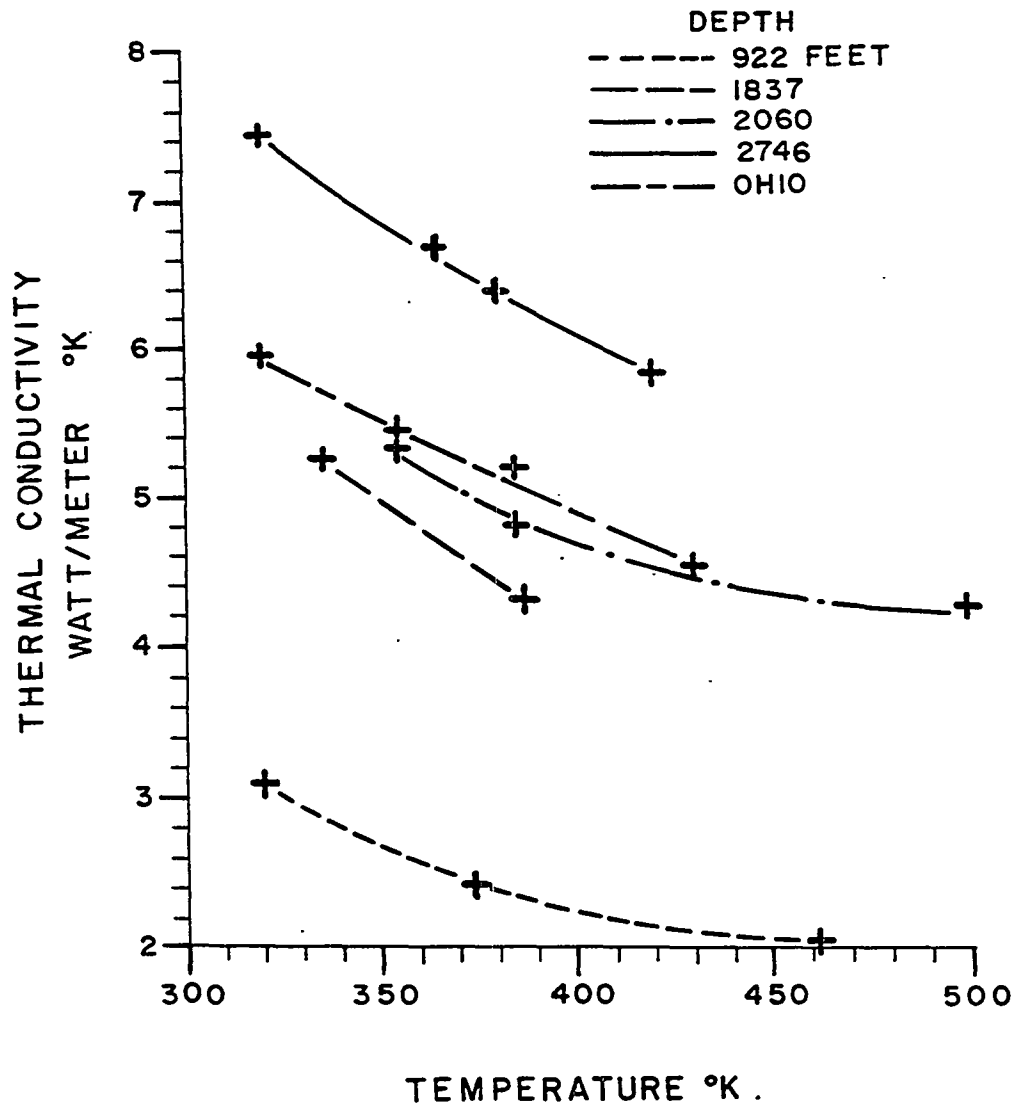
THERMAL CONDUCTIVITY OF ROCKSALT

CORE SECTIONS CONTAINING 50%

OR MORE HALITE, WELL AEC 8

From: Acton, 1977
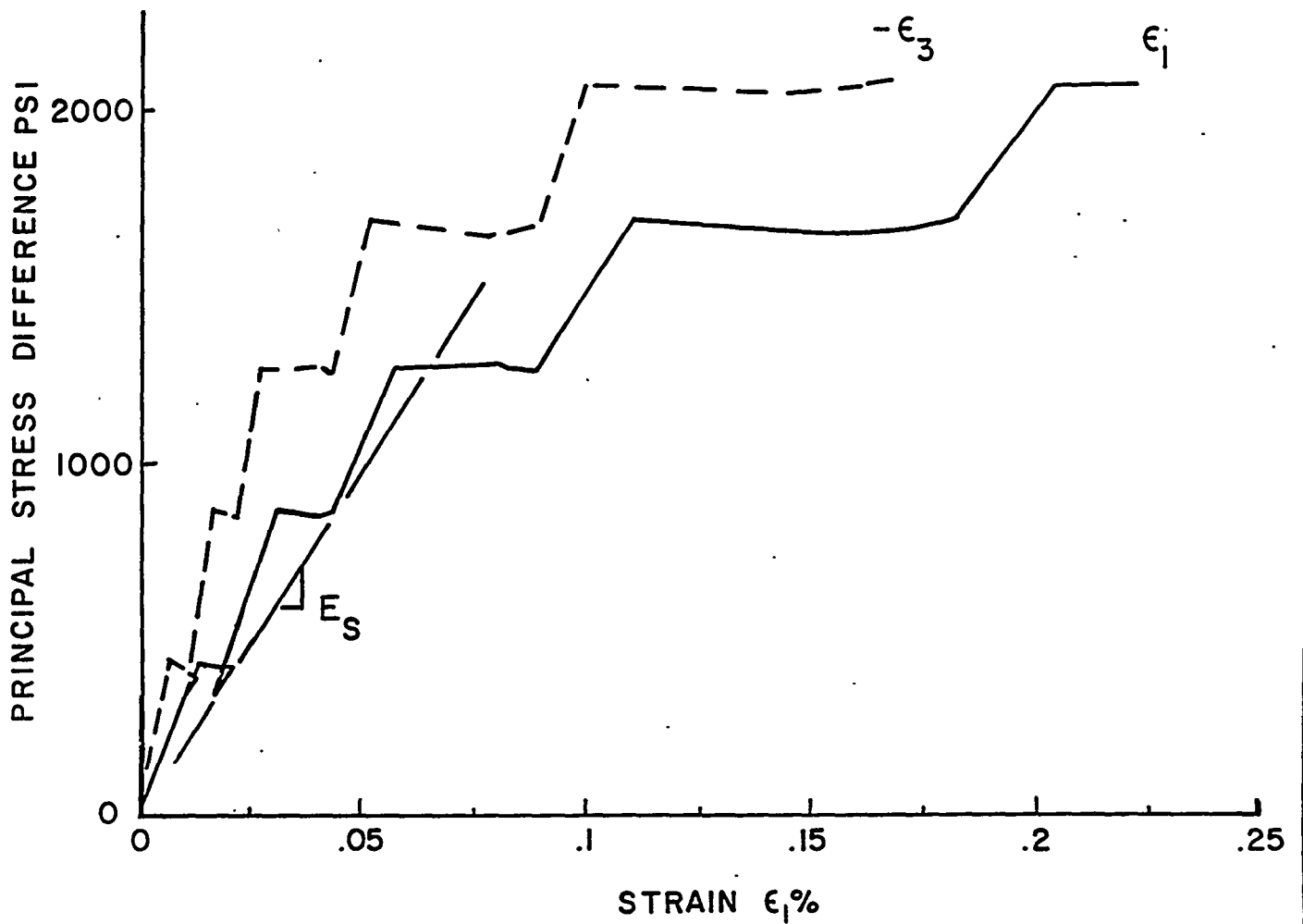
FIGURE 9.2.3-2

KEY

$- - - -$ 7-2745 (3.0, 23)
Hole No. — Sample depth in ft. (Conf. pressure in ksi, Temp. in °C)

TRIAXIAL STRESS-STRAIN CURVES IN

REGIME OF SMALL PRINCIPAL STRESS DIFFERENCES

AND STRAIN

From: Wawersik and Hannum, 1978

FIGURE   9.2.4-1

CONFINING PRESSURE	PRINCIPAL STRESS DIFFERENCE	AXIAL STRAIN AT FAILURE
σ_3	$(\sigma_1 - \sigma_3)$	ε_1
0 psi	3000 psi	2.5%
500	6000	15
3000	>10,000	>20

APPARENT COHESION C = 1000 psi

APPARENT ANGLE
OF FRICTION . $\emptyset$ = 33°
T = 23°

$\emptyset = 33°$
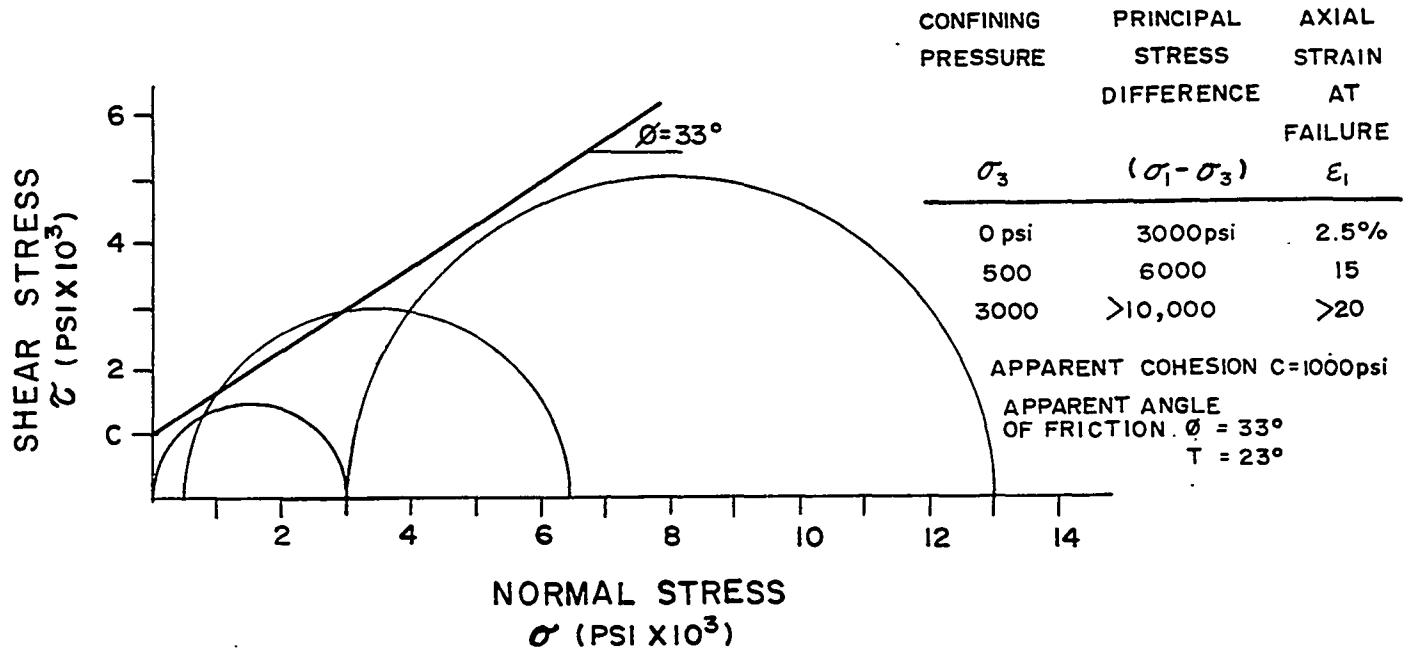
A. MOHR'S ENVELOPE AT ULTIMATE STRENGTH

CONFINING PRESSURE	PRINCIPAL STRESS DIFFERENCE	AXIAL STRAIN
σ_3	$(\sigma_3 - \sigma_1)$	ε_1
0 psi	3000 psi	2.5%
500	4500	2.5
3000	5250	2.5

T = 23°
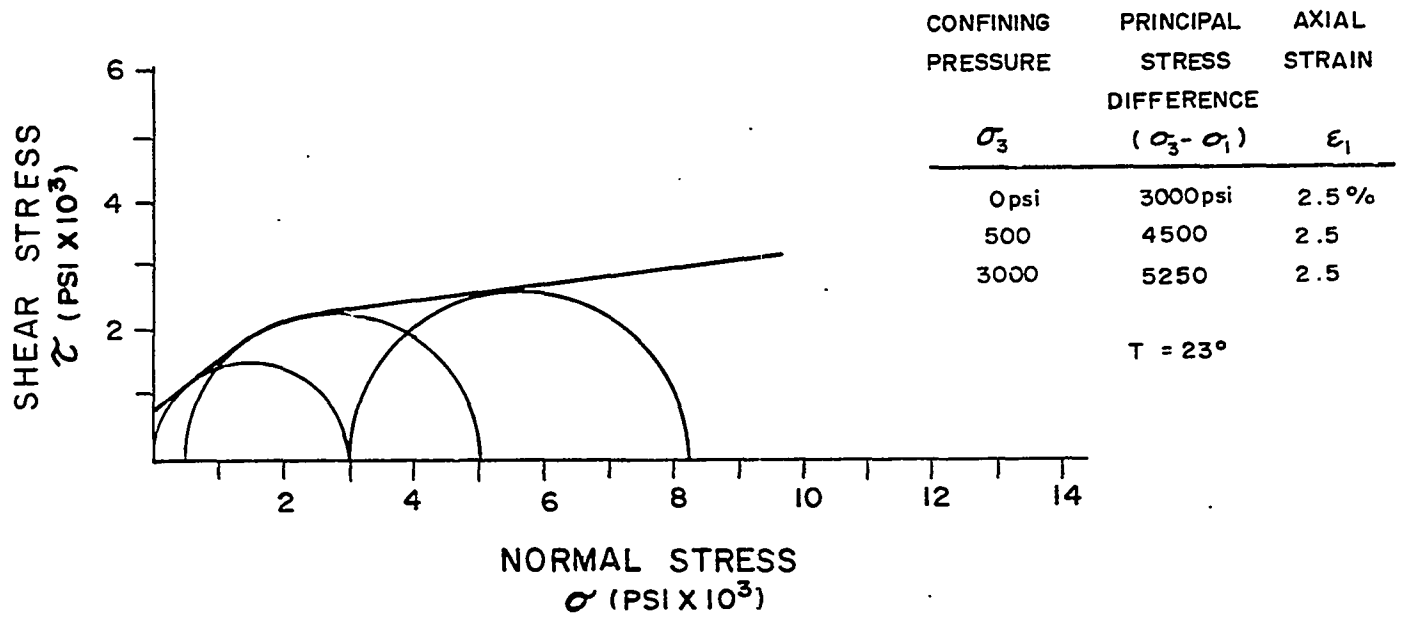
B. MOHR'S ENVELOPE AT CONSTANT STRAIN

NOTES:

1. THE SAME TEST DATA WERE USED TO
   GENERATE BOTH ENVELOPES.
   (TABLE 9 III, 9 IV ; WAWERSIK, 1977)

2. THESE QUASI-STATIC PROPERTIES
   DO NOT ACCOUNT FOR ANY STRENGTH
   DETERIORATION WITH TIME.

FIGURE   9.2.4-2
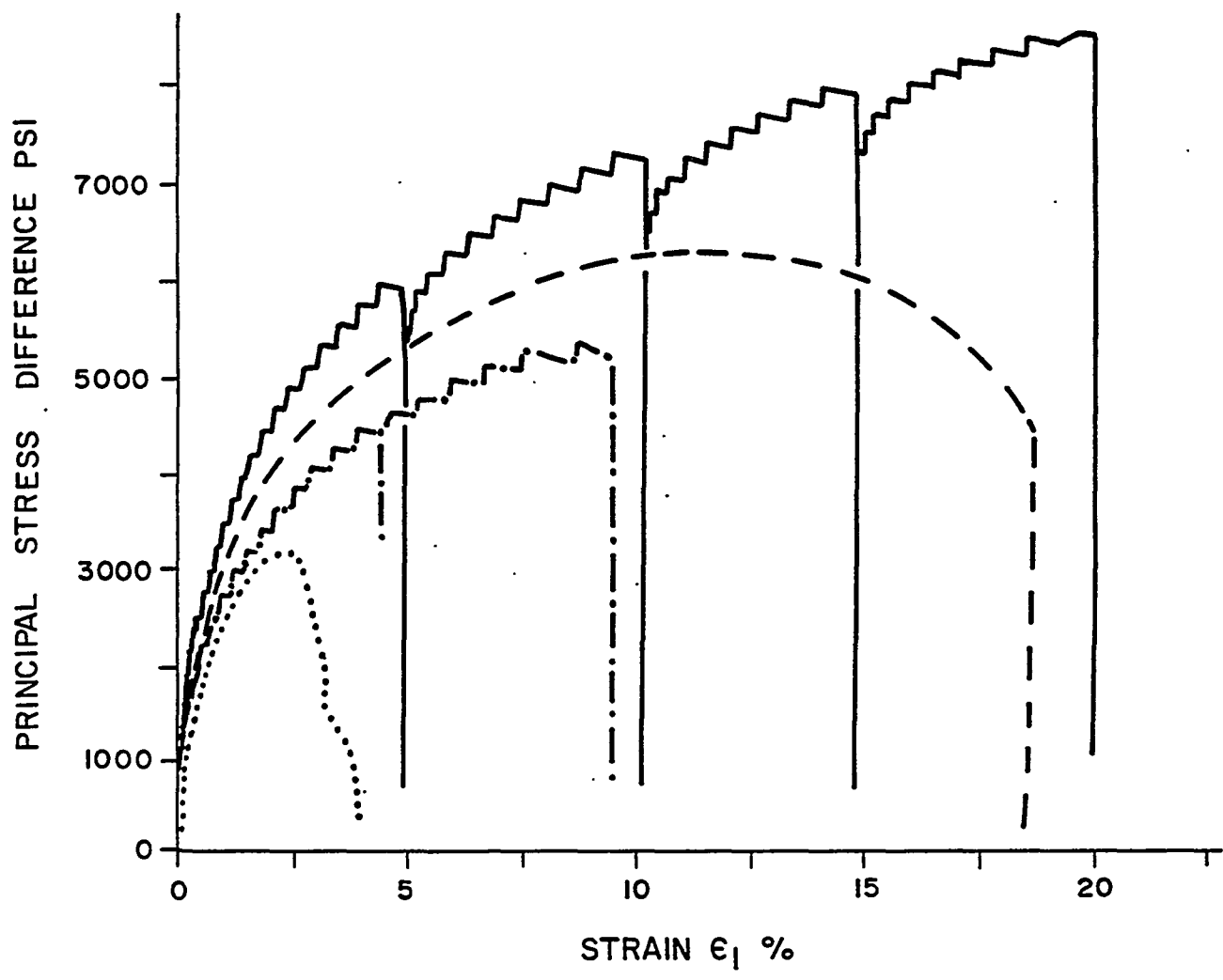
KEY

9-2676 (0, 23)
Hole No. — Sample depth in ft. (Conf. pressure in ksi, Temp. in °C)
7-2837 (.25, 23)
9-2601 (.50, 23)
9-2601.5 (3.0, 23)

CONVENTIONAL QUASI-STATIC TRIAXIAL

STRESS-STRAIN DATA AT AMBIENT TEMPERATURE

EFFECT OF PRESSURE

From: Wawersik and Hannum, 1978

FIGURE 9.2.4-3
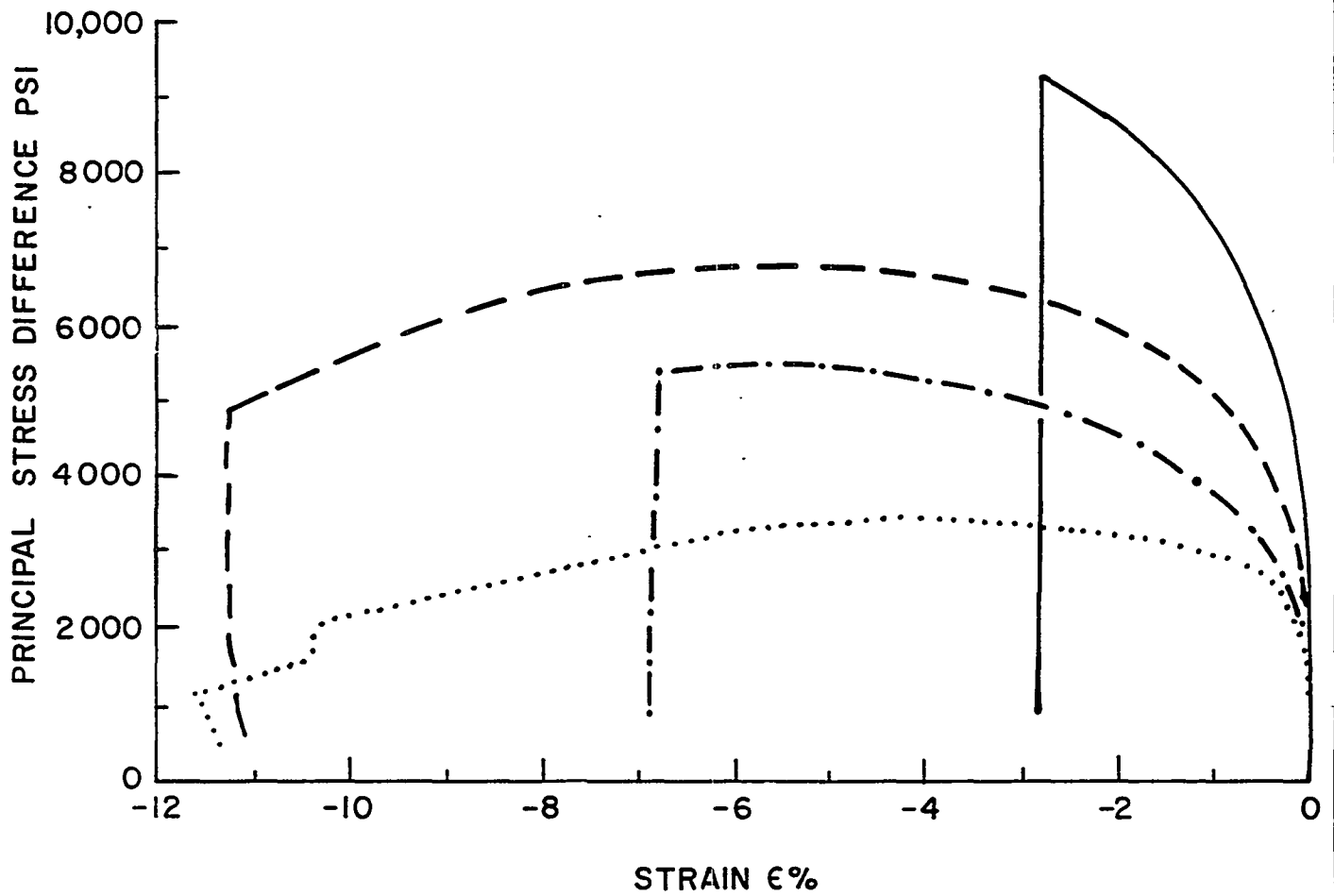
KEY

.... 9-2676 (0, 23)
Hole No. — Sample depth in ft. (Conf. pressure in ksi, Temp. in °C)
— · — 7-2837 (.25, 23)
— — 9-2601 (.50, 23)
——— 9-2601.5 (3.0, 23)

PRINCIPAL STRESS DIFFERENCE VS. VOLUMETRIC

STRAIN FOR TEST OF FIGURE 9.2.4-3
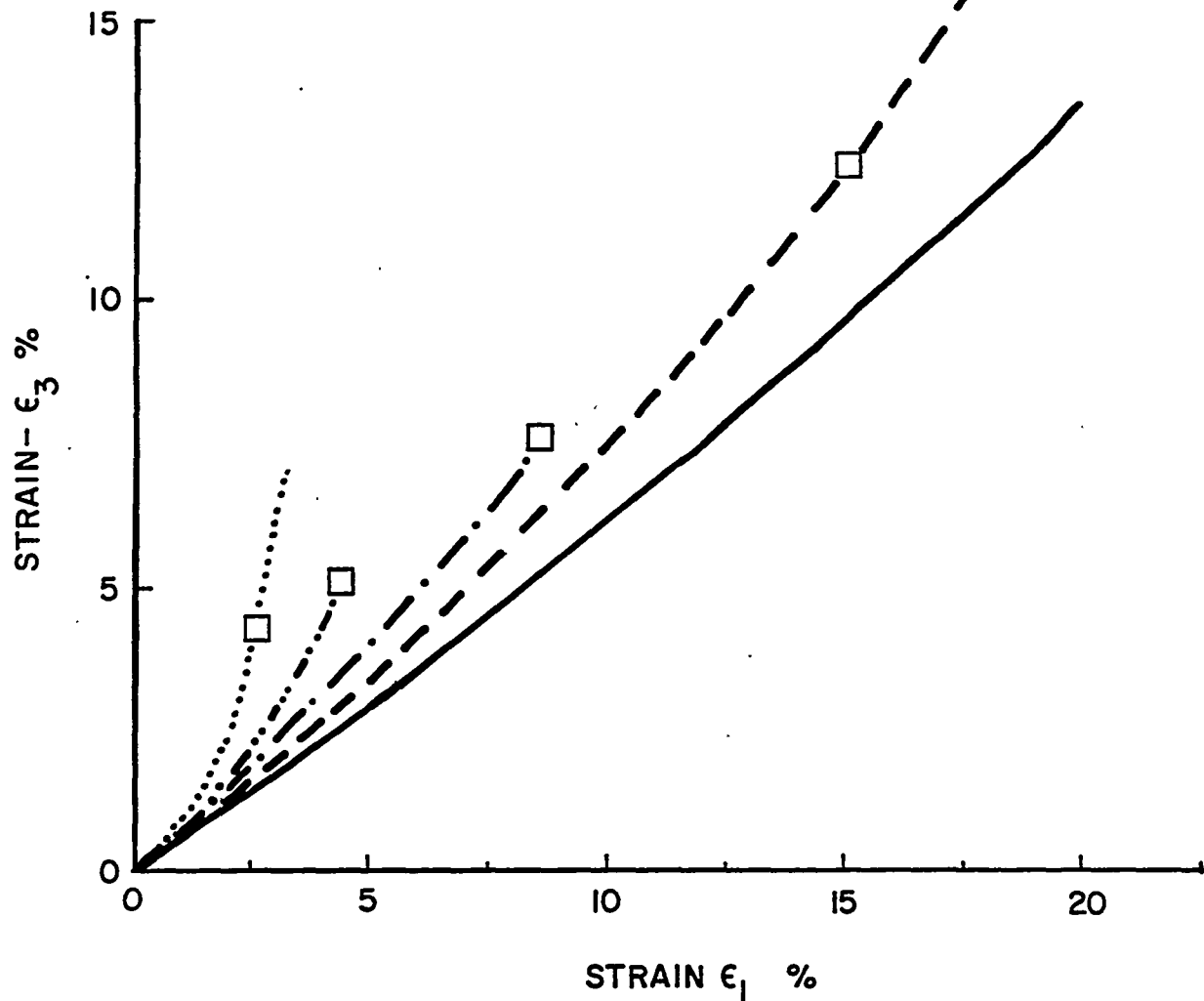
From: Wawersik and Hannum, 1978

FIGURE 9.2.4-4

KEY

··········	9-2676 (0, 23)
	Hole No. — Sample depth in ft. (Conf. pressure in ksi, Temp. in °C)
—··—	9-2689 (.10, 23)
—·—	7-2837 (.25, 23)
— —	9-2601 (.50, 23)
——	9-2601.5 (3.0, 23)

NOTE: Open squares identify approximate strains at ultimate stresses.

TRIAXIAL VARIATION OF LATERAL STRAIN VS. AXIAL STRAIN FOR TEST OF FIGURE 9.2.4-3
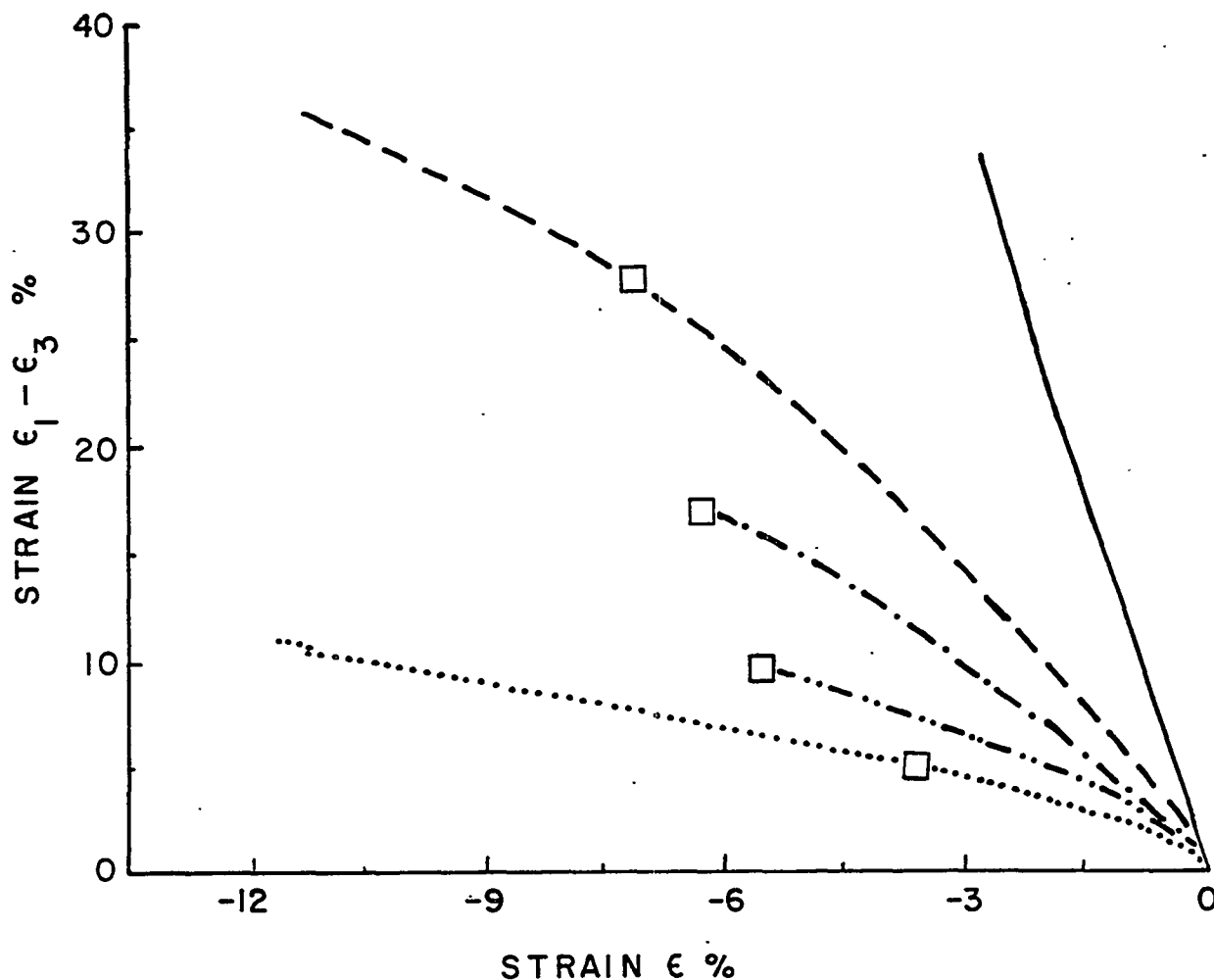
From : Wawersik and Hannum, 1978

FIGURE 9.2.4-5

KEY

.... 9-2676 (0, 23)
　　　　　Hole No. — Sample depth in ft. (Conf. pressure in ksi, Temp. in °C)
—..—　 9-2689 (.10, 23)
—.—　 7-2837 (.25, 23)
— —　 9-2601 (.50, 23)
———　 9-2601.5 (3.0, 23)

NOTE: Open squares identify approximate strains at ultimate stresses.

TRIAXIAL VARIATION OF SHEAR STRAIN VS
VOLUMETRIC STRAIN FOR TESTS OF FIGURE 9.2.4-3

From: Wawersik and Hannum, 1978

FIGURE 9.2.4-6

KEY
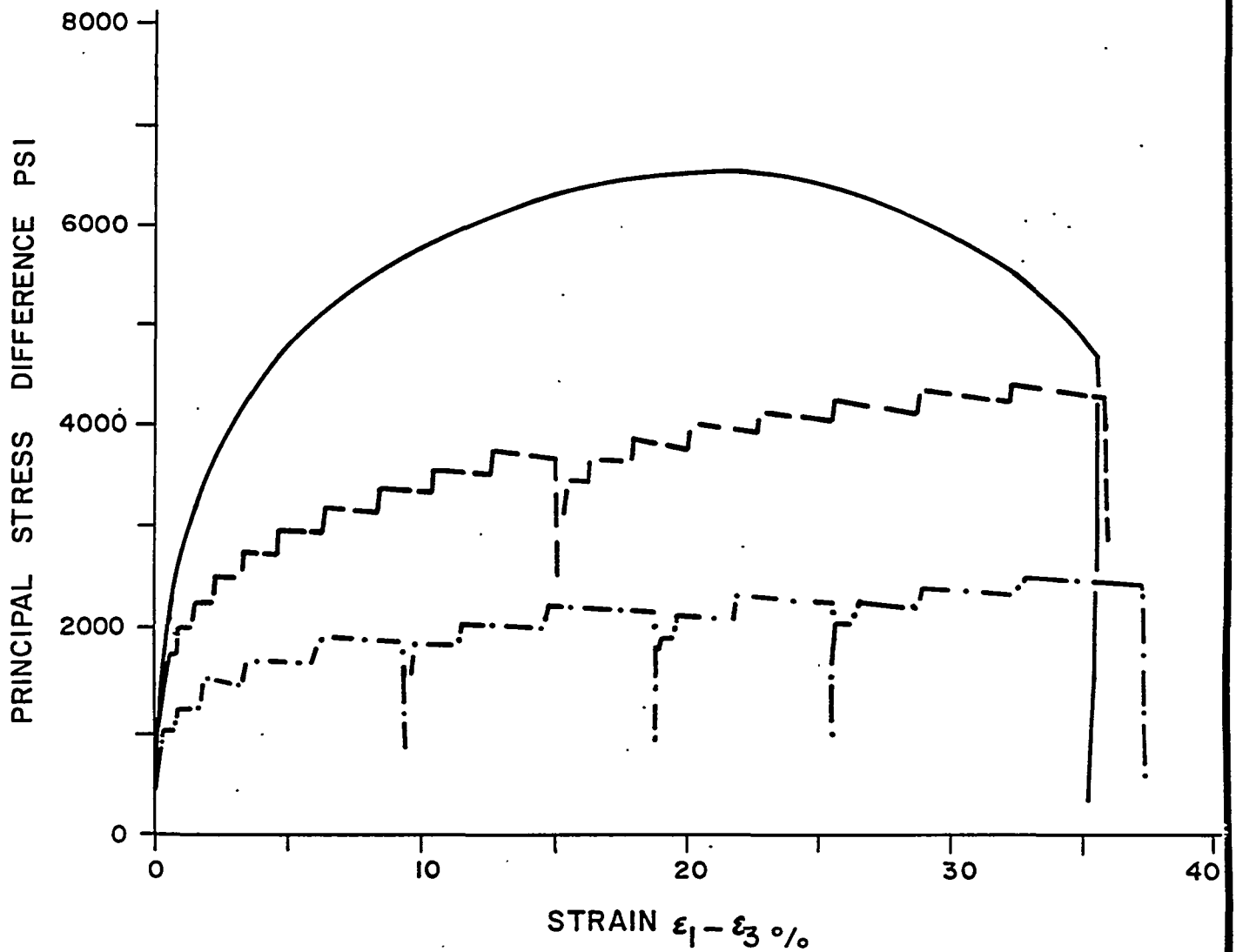
9-2601 (.50, 23)
Hole No. — Sample depth in ft. (Conf. pressure in ksi, Temp. in °C)
9-2673.4 (.50, 100)
9-2604 (.50, 200)

TRIAXIAL STRESS-STRAIN CURVES AS A FUNCTION

OF TEMPERATURE AT CONSTANT CONFINING PRESSURE

From: Wawersik and Hannum, 1978

FIGURE 9.2.4-7
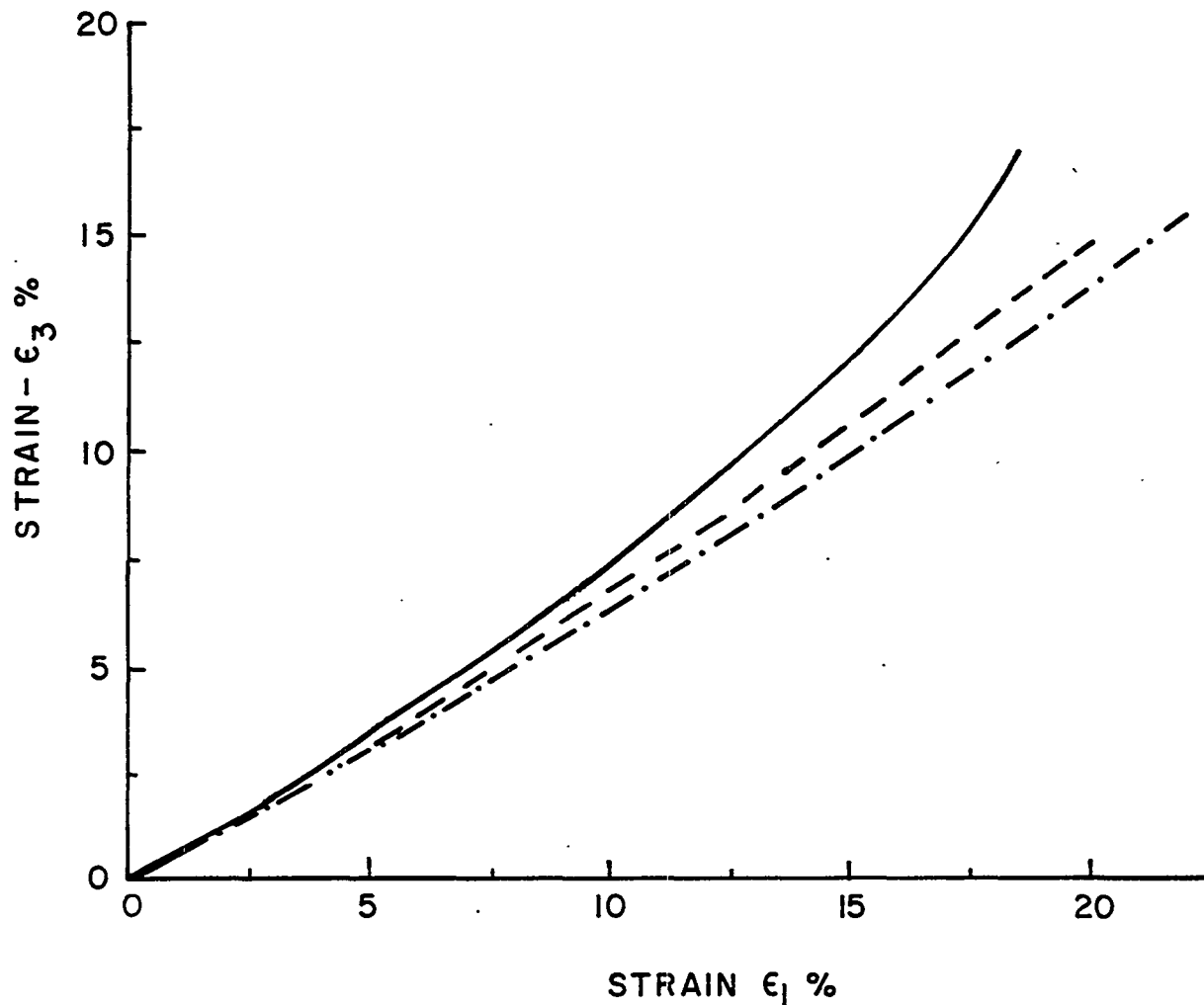
VARIATION OF LATERAL VS. AXIAL STRESS

FOR TESTS OF FIGURE 9.2.4-7
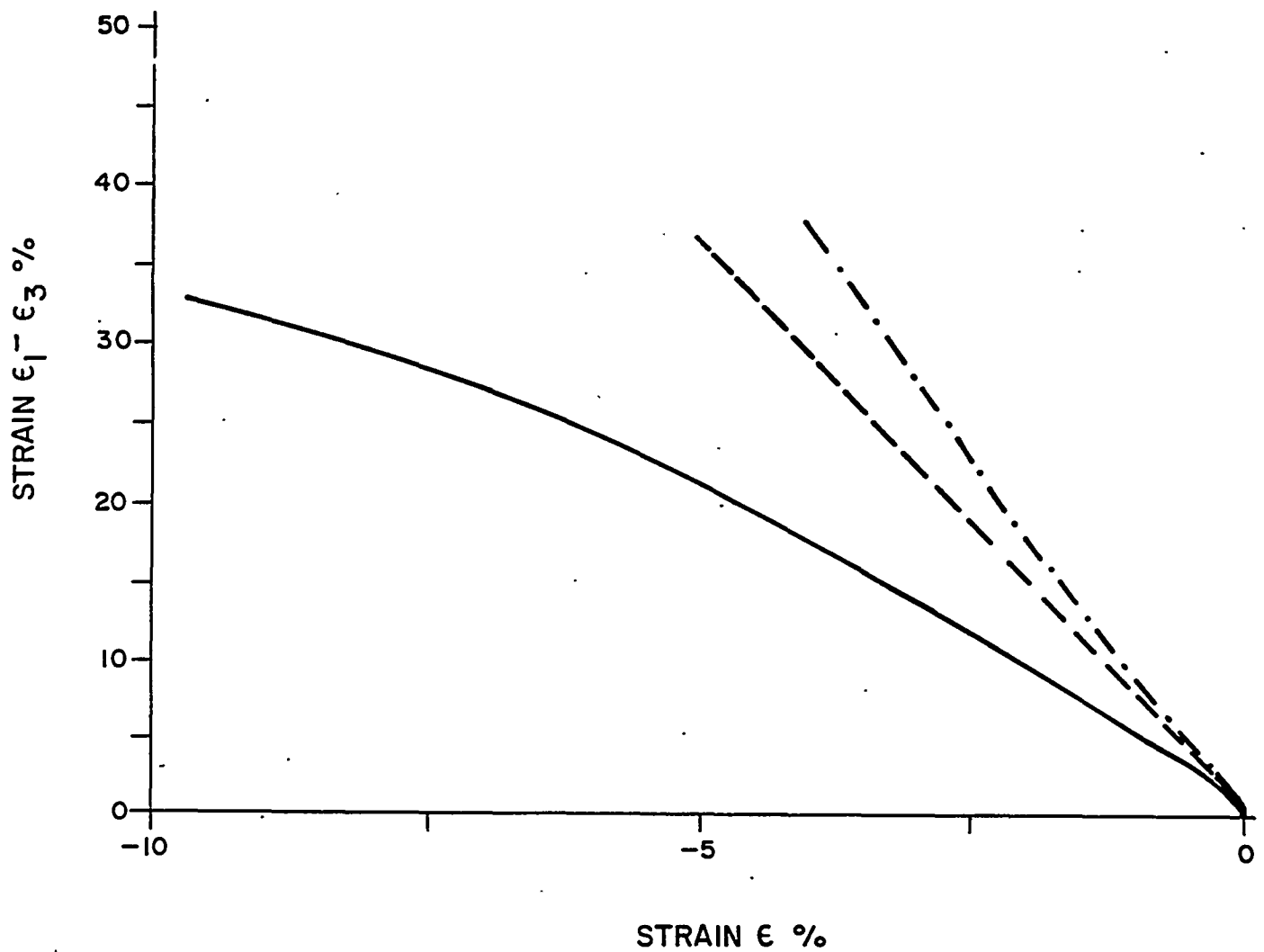
From: Wawersik and Hannum, 1978

FIGURE 9.2.4 - 8

KEY

———	9-2601 (.50, 23)
	Hole No. — Sample depth in ft. (Conf. pressure in ksi, Temp. in °C)
— —	9-2673.4 (.50, 100)
—·—	9-2604 (.50, 200)

VARIATION OF SHEAR-STRAIN VS. VOLUMETRIC

STRAIN FOR TESTS OF FIGURE 9.2.4-7

From: Wawersik and Hannum, 1978

FIGURE 9.2.4-9
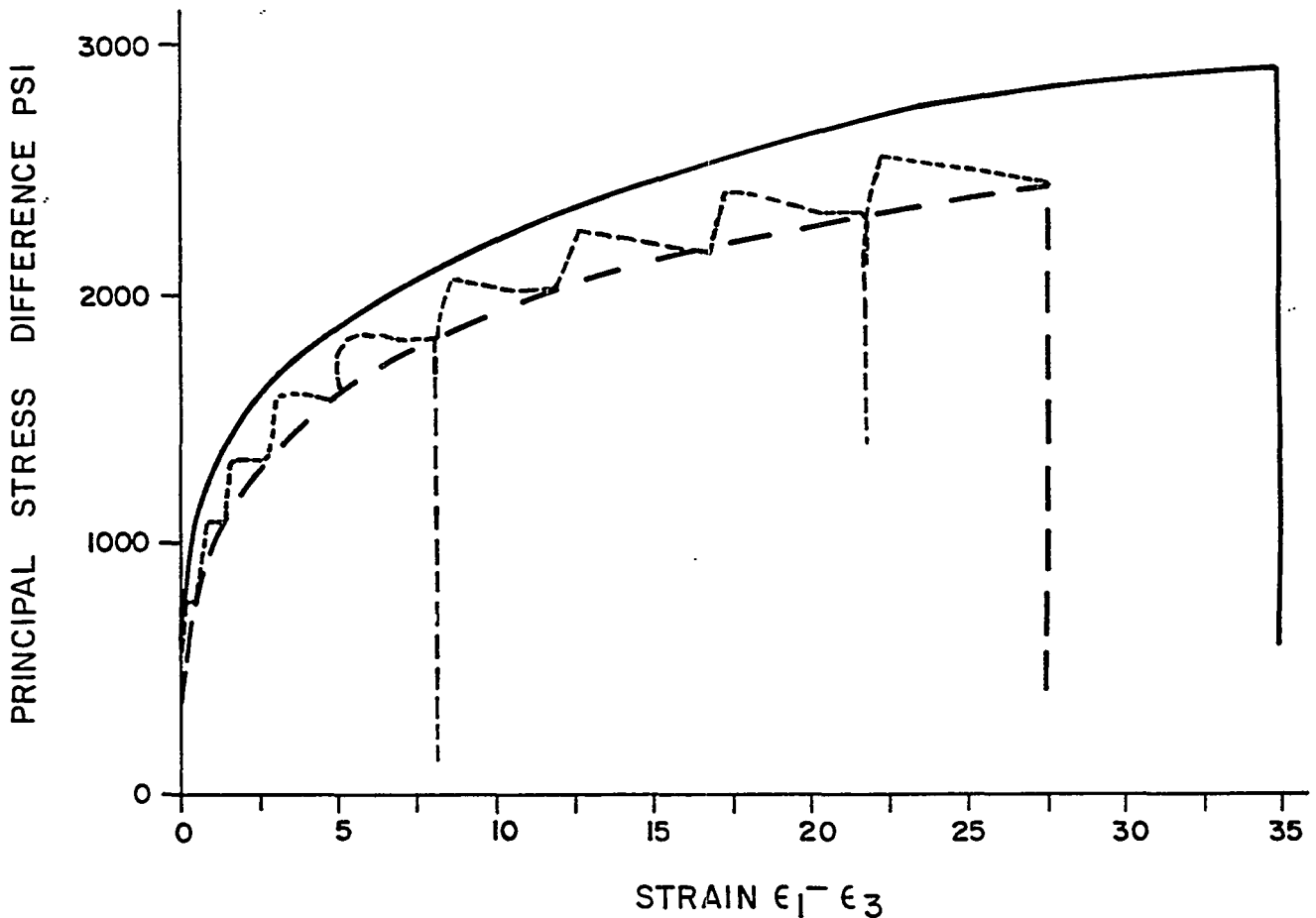
KEY

———————	7-2740 (.50, 200)
	Hole No. — Sample depth in ft. (Conf. pressure in ksi, Temp. in $^{\circ}$C)
— — —	7-2744 (3.0, 200)
- - - - -	Actual load path

TRIAXIAL STRESS STRAIN CURVES AS A

FUNCTION OF CONFINING PRESSURE AT

200°C
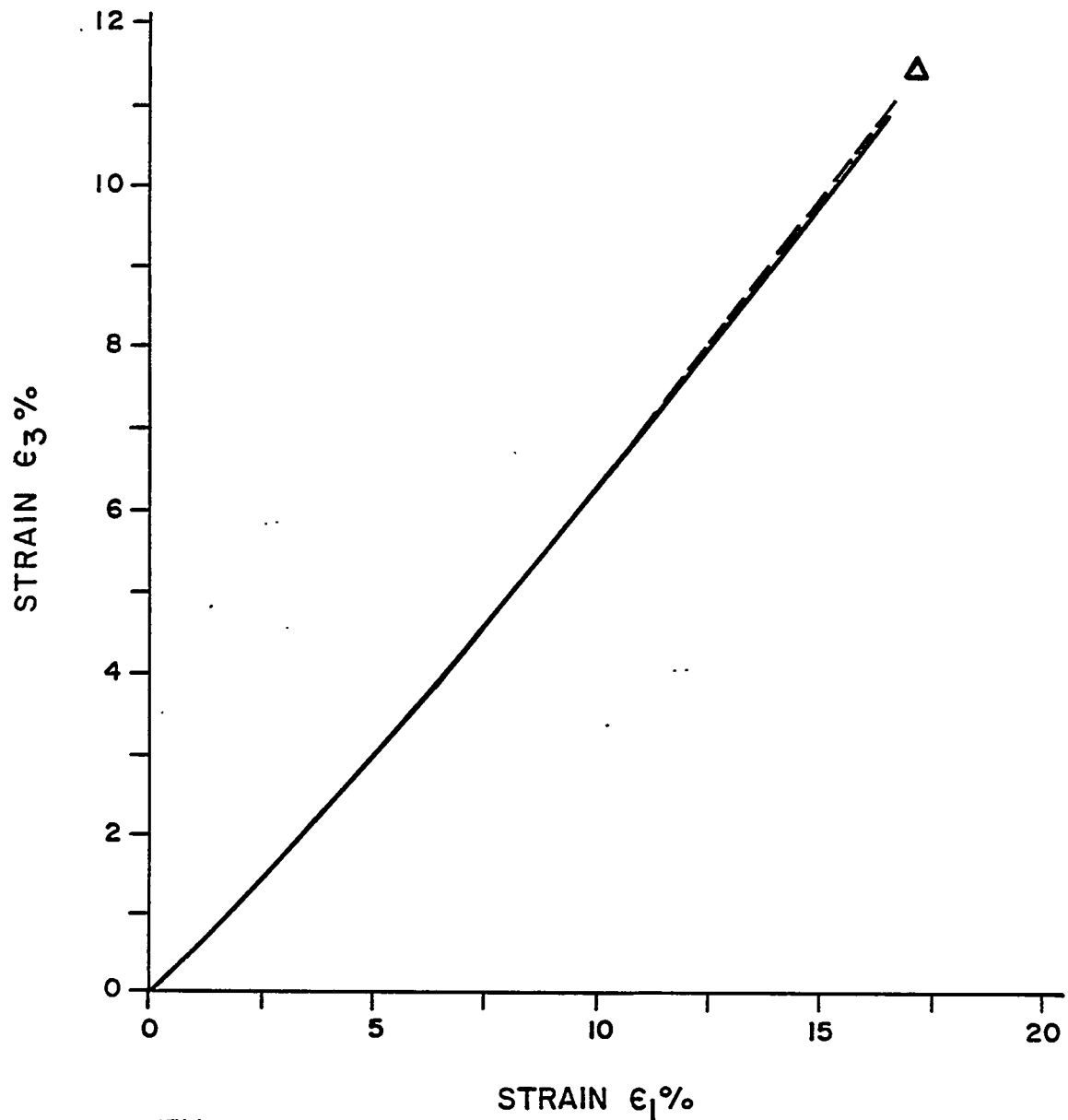
From: Wawersik and Hannum, 1978

FIGURE 9.2.4-10

KEY

△	7-2836 (0, 200)
	Hole No. — Sample depth in ft. (Conf. pressure in ksi, Temp. in °C)
——	7-2740 (.50, 200)
– – –	7-2744 (3.0, 200)

VARIATION OF LATERAL STRAIN VS. AXIAL STRAIN

FOR TESTS OF FIGURE 9.2.4-10

(PLUS ONE ADDITIONAL TEST
IN UNIAXIAL COMPRESSION)

From: Wawersik and Hannum, 1978
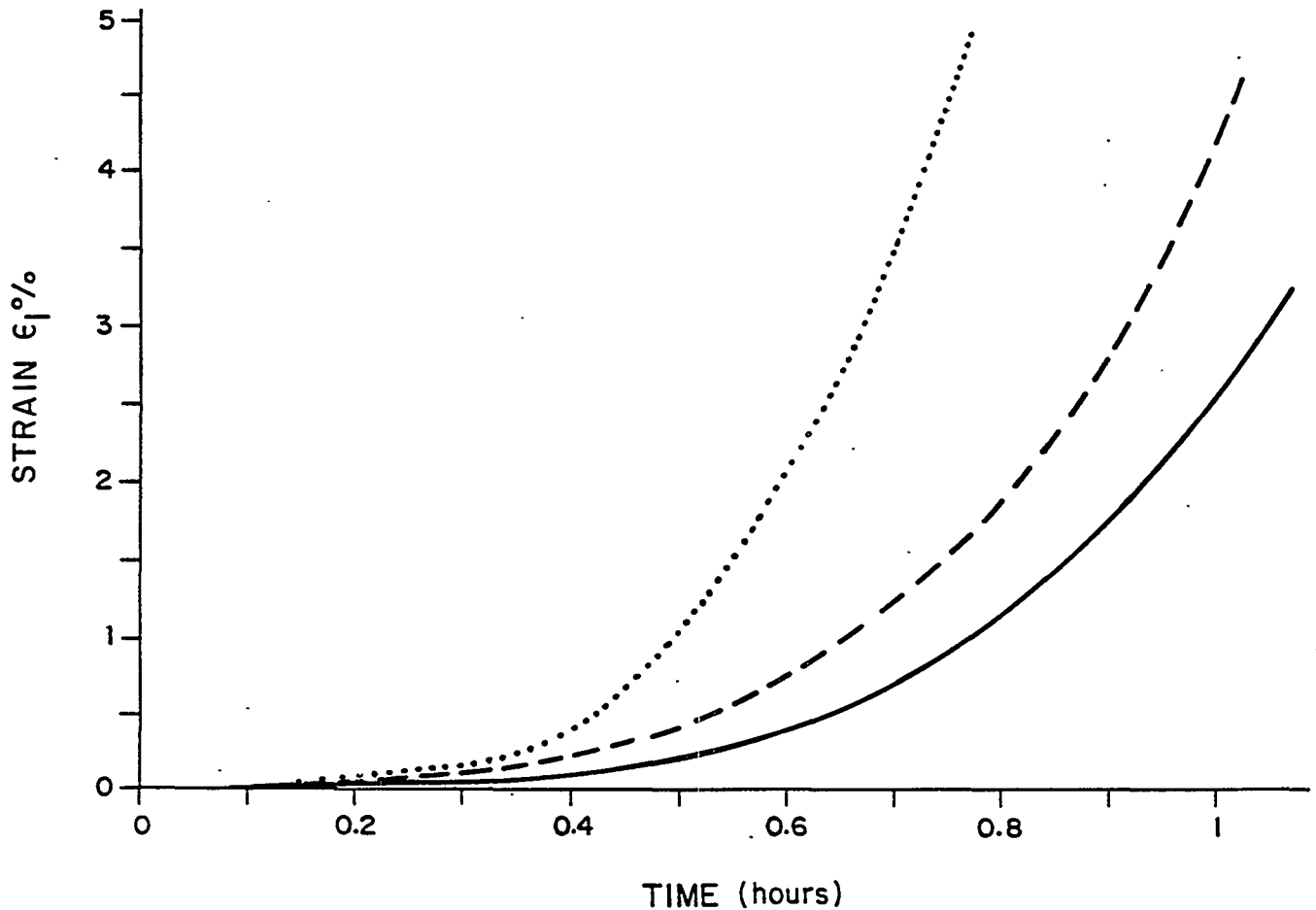
FIGURE 9.2.4-11

KEY

·········· 7-2836 (0, 200)
Hole No. — Sample depth in ft. (Conf. pressure in ksi, Temp. in °C)
— — 7-2740 (.50, 200)
——— 7-2744 (3.0, 200)

AXIAL STRAIN VS. TIME FOR TEST OF

FIGURES 9.2.4-IO AND 9.2.4-II
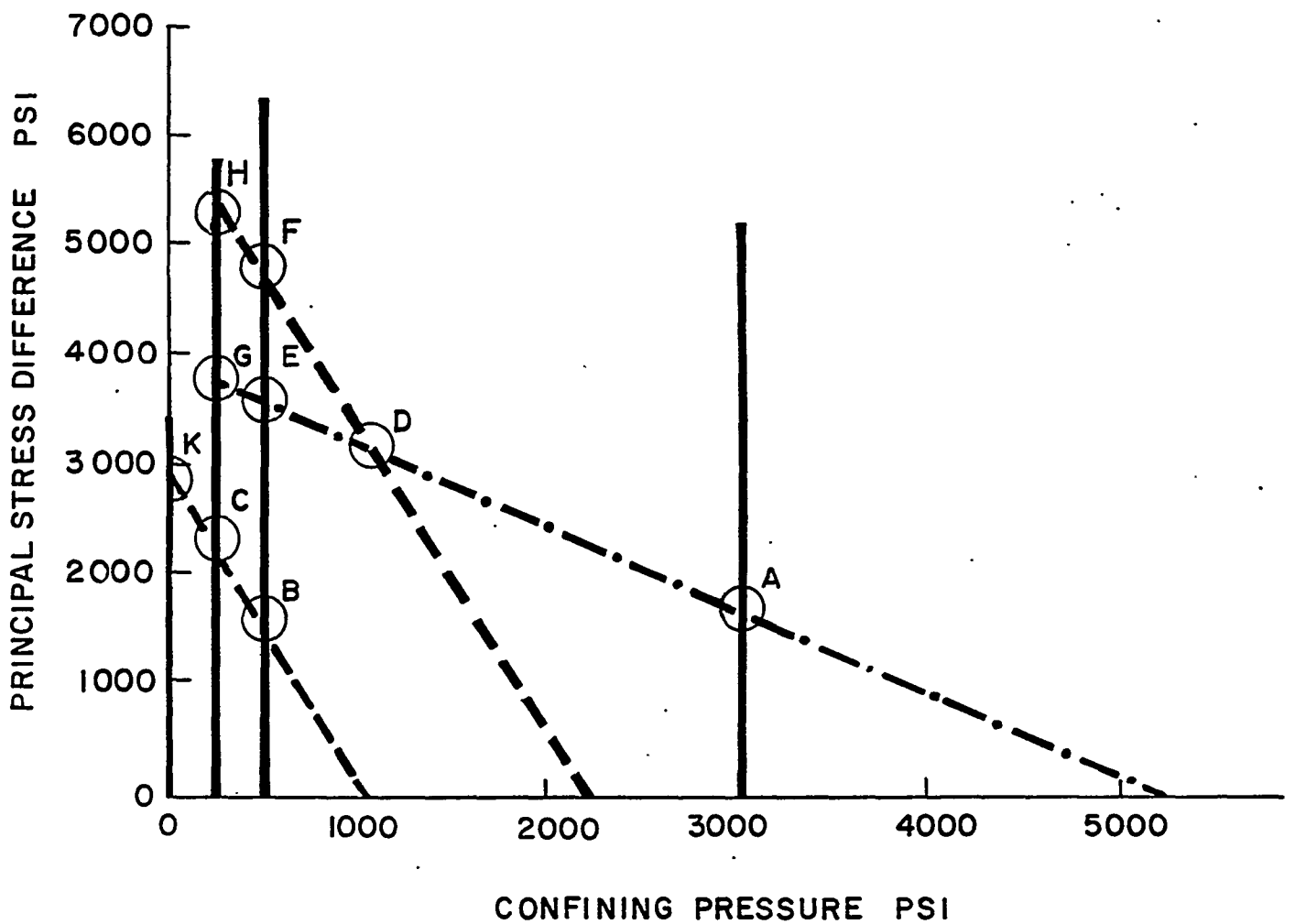
From: Wawersik and Hannum, 1978

FIGURE 9.2.4-12

MAP OF THREE NON-PROPORTIONAL LOAD PATHS

AND COMMON STRESS STATES

(POINTS A THROUGH K)

From : Wawersik and Hannum, 1978

FIGURE 9.2.4-13

KEY
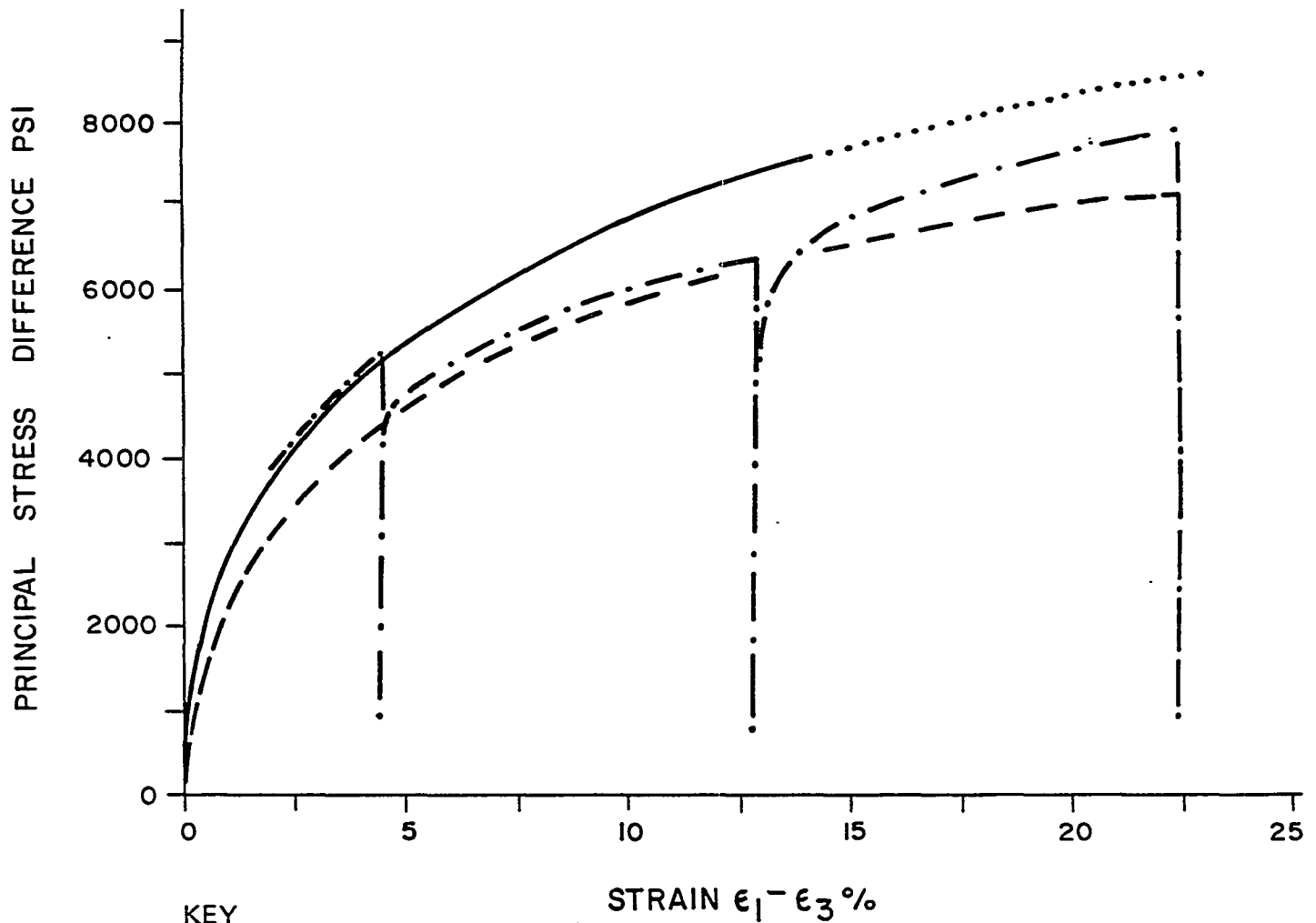
— — — 7-2725 (.50, 23)
Hole No. — Sample depth in ft. (Conf. pressure in ksi, Temp. in °C)
———— 7-2745 (3.0, 23)
—·—·— 7-2740.5 (3.0/.50/3.0, 23)
··········· 9-2601.5 (3.0, 23)

NOTE: The partial code 3.0/.50/3.0 identifies prevailing confining pressures between $(\sigma_1 - \sigma_3) = 0$ and first unload/reload cycle, first and second unload/reload cycle, and between second unload/reload cycle and final unloading trace.

STRESS-STRAIN CURVES

FOR SAMPLE SUBJECTED TO

ONE OR MORE CONFINING PRESSURES
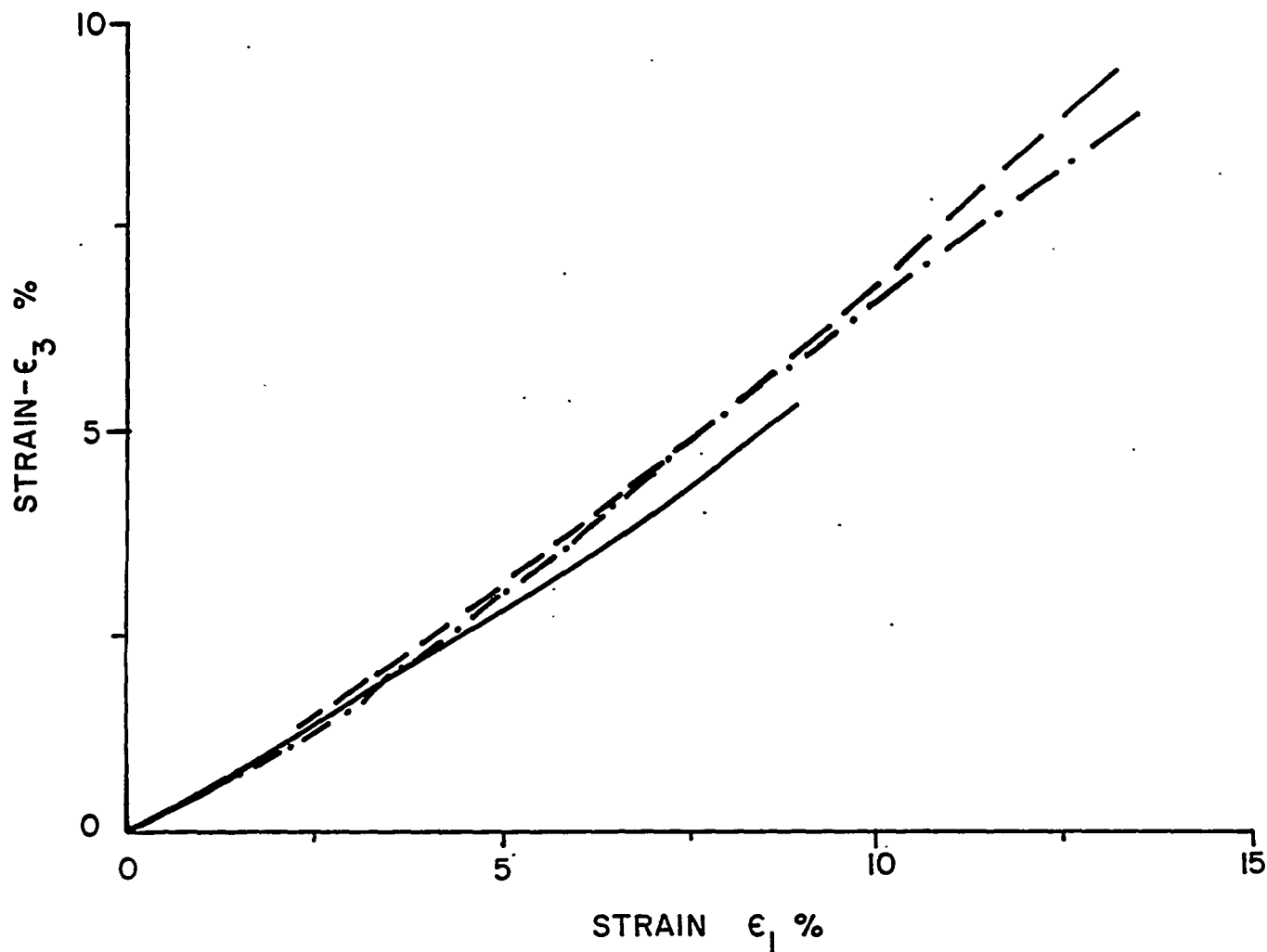
From: Wawersik and Hannum, 1978

FIGURE 9.2.4-14

KEY

--- --- 7-2725 (.50, 23)
                Hole No. — Sample depth in ft. (Conf. pressure in ksi, Temp. in °C)
———— 7-2745 (3.0, 23)
—·—·— 7-2740.5 (3.0/.50/3.0, 23)

VARIATION OF LATERAL STRAIN VS.

AXIAL STRAIN FOR TESTS OF FIGURE 9.2.4-14

From : Wawersik and Hannum, 1978
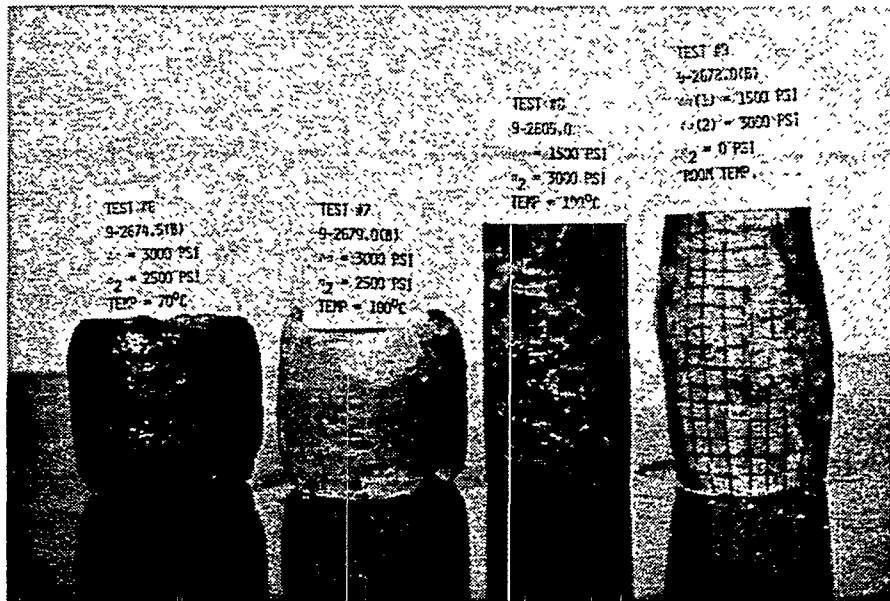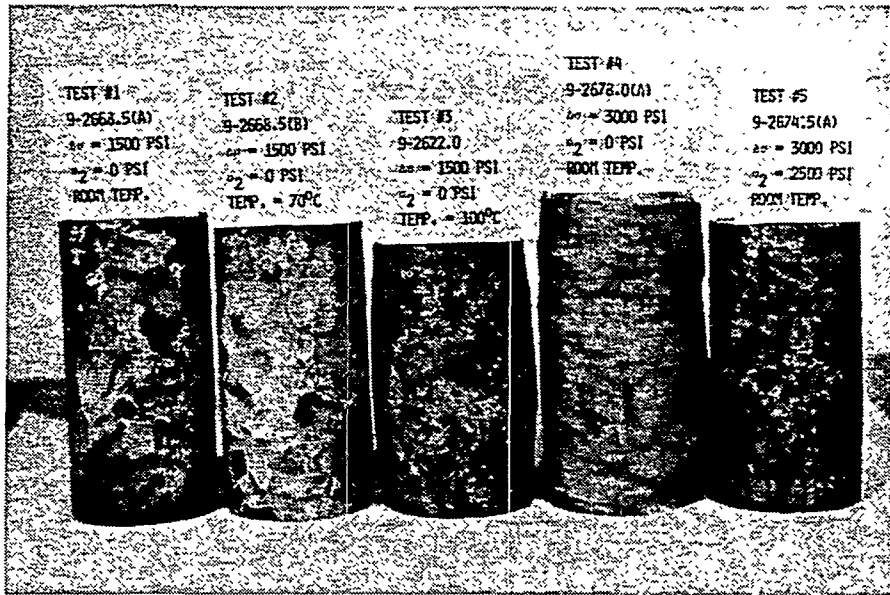
FIGURE 9.2.4-15

DEFORMED CORE SAMPLES OF ROCK SALT
FROM DRILL HOLE ERDA #9

FROM: HANSEN and MELLEGARD, 1977   FIGURE 9.2.4—16

Table 9.2.3-1: Physical properties of rock from WIPP study area

Material	Depth (ft)	Density (gm/cc)	Avg. Porosity (Range) (%)	Mass (Moisture) Loss (% to ≤ 300°C)	Resistivity in Ohm Meters	Avg. Air Permeability (Range) in (md)[2]	(P) Wave[3] Velocity (Km/sec)
Rock Salt	2000-2100	2.18	0.4 (0.1-0.8)	N[1] - 1.0	58,100	0.01 (0.0003-0.17)	(4.42-4.62)
Rock Salt	2600-2700	2.18	0.5 (0.3-0.7)	N - 0.4	(4,900-230,000)	-	-
Anhydrite		2.80	-	-	-	-	-
Polyhalite	-	2.70	-	-	-	-	-
Siltstone	-	2.26	-	-	-	-	-

[1]N - None Measured

[2]Core Labs Data; see also Figure 9.2.3-1

[3]Note: P Wave velocities determined in the lab agree to 15% with those measured downhole on borehole ERDA 9 (Griswold, 1977).

Table 9.2.4.-1 - Representative unconfined mechanical properties of rock salt from the WIPP study area

Material	Drillhole/ Approx. Depth (ft)	Uniax. Compr. Strength (psi)	Strain at failure percent	Brazilian Tensile Strength (psi)	Initial Elastic Limit $(\sigma_1 - \sigma_3)$ (psi)	Secant Modulus $\times 10^6$ (psi)	Principal Strain Ratio	Principal Strain Ratio, $\varepsilon_3/\varepsilon_1$ at Failure
Rock Salt	AEC 7,8/1900	2450	≥ 1.7	200	≤ 750	1.94	0.33	-
Rock Salt	AEC 7,8/2700	3700	3.6	240	≤ 750	1.94	0.34	-
Rock Salt	ERDA 9/2100	2400	1.6	-	< 200	-	-	1.6
Rock Salt	ERDA 9/2700	3300	2.9	-	< 200	-	-	2.1

Note: Loading rates - $30 \leq \frac{d}{dt} (\sigma_1 - \sigma_3) \leq 215$ psi/min

1 Megapascal (MPa) equals about 145 psi
Symbols < and > denote experimental uncertainty.

Table 9.2.4-2 – Representative triaxial compression data for rock salt from the WIPP study area

Drillhole/ Depth (ft)	Confining Pressure (psi)	Temp. (^oC)	Ultimate (max) Princ. Stress Diff. (psi)	Ultimate (max) Strain, ϵ_1 Percent	Initial Elastic Limit ($\sigma_1 - \sigma_3$) (psi)	Secant Modulus $x10^6$ (psi)	Principal Strain "Poissons'" Ratio	Max. Obs. Princ. Strain Ratio
ERDA 9/2100	500	23	6000	12	$\leq$100	2.7	0.20	– 0.72
ERDA 9/2100	3000	23	>9000	>20	$\leq$100	2.7	0.20	– 0.65
ERDA 9/2600- 2700	500	23	6300	15	$\leq$100	2.7	0.20	– 0.80
ERDA 9/2600- 2700	3000	23	> 8900	>20	$\leq$100	2.7	0.20	– 0.67
AEC 7/2700- 2800	500	23	> 6200	>13	$\leq$100	2.7	0.21	– 0.71
AEC 7/2700- 2800	500	100	$\approx$ 4200	$\geq$18	$\leq$100	–	–	– 0.69
AEC 7/2700- 2800	500	200	$\approx$ 2400	>17	$\leq$100	2.4	–	– 0.68
AEC 7/2700- 2800	300	200	> 2750	>17	$\leq$100	–	–	–
ERDA 9/2600	500	200	> 2500	>22	$\leq$100	–	–	– 0.68

Note: Loading rate d/dt $(\sigma_1 - \sigma_3)$ = 30 to 60 psi/min.

Table 9.2.4-3 Deviatoric Load Path Data For Figure 9.2.4-13

Reference Point In Figure 15	Load Path	$(\sigma_1 - \sigma_3)$ PSI	$\sigma_2=\sigma_3$ PSI	σm PSI	ϵ_1 %	$-\epsilon_3$ %
A	I	1600	2970	3550	0.17	0.07
	III	1640	3020	3570	0.075	0.05
B	I	1520	520	1015	0.357	0.175
	II	1500	520	1015	0.3	0.168
C	I	2200	260	1040	o.782	0.441
	II	2250	250	1015	0.769	0.476
D	II	3190	1120	2180	1.35	0.786
	III	3150	1120	2160	0.73	0.454
E	I	3540	520	1670	1.38	0.828
	II	3580	510	1700	1.12	0.705
F	I	4700	490	2090	4.04	2.434
	II	4740	510	2120	3.92	2.430
G	I	3840	250	1490	2.486	1.85
	III	3780	250	1500	1.49	1.01
H	I	5240	250	1990	8.58	7.81
	III & I	5140	260	2000	6.41	5.46
	II	5320	276	2070	5.71	3.79
K	I	2950	0	990	1.49	1.47
	II	2950	15	1000	1.58	1.19

Table 9.3-1

REPRESENTATIVE BRINES/SOLUTIONS
FOR
WIPP EXPERIMENTATION

Ion	Brine "A" (mg/liter) ($\pm$ 3%)	Brine "B" (mg/liter) ($\pm$ 3%)	Solution "C" (mg/liter) ($\pm$ 3%)
Na^+	42,000	115,000	100
K^+	30,000	15	5
Mg^{++}	35,000	10	200
Ca^{++}	600	900	600
Fe^{+++}	2	2	1
Sr^{++}	5	15	15
Li^+	20	-	-
Rb^+	20	1	1
Cs^+	1	1	1
Cl^-	190,000	175,000	200
SO_4^{--}	3,500	3,500	1,750
$B\ (BO_3^{---})$	1,200	10	-
HCO_3^-	700	10	100
NO_3^-	-	-	20
Br^-	400	400	-
I^-	10	10	-
pH (adjusted)	6.5	6.5	7.5
specific gravity	1.2	1.2	1.0

Table 9.3-2

Nominal Concentration of Nuclides Used in Kd Measurements

Nuclide	Concentration, ppm
^{137}Cs	0.012
Stable Cs	1.0
^{85}Sr	0.03 - 0.3
Stable Sr	5 - 15
^{106}Ru	2500
^{99}Tc	59
^{152}Eu	0.1 - 1.0
^{144}Ce	3×10^{-4}
^{131}I	5×10^{-5}
^{153}Gd	0.2 - 2.0
^{125}Sb	≤ 0.01
^{243}Am	5.4
^{244}Cm	0.012
^{238}Pu	0.058

Table 9.3-3

Distribution Coefficients on Samples From the Magenta Dolomite

Fission Product
Distribution Coefficients

	pH range	Cs	Sr	I,Tc	Eu,Gd	Ru
Brine A	6.5 - 6.9	< 1	1	0 - 1.5	$> 5 \times 10^3$	40-50
Brine B	6.5 - 7.5	< 1	1	< 1	$> 5 \times 10^3$	500-600
Sol'n C	7.5 - 8.2	4	5	0 - 1.5	$> 10^4$	400-550

Actinide
Distribution Coefficients

	pH range	Pu	Am	Cm
Brine B	6.5 - 7.8	5.4×10^3	3.1×10^2	1.3×10^3
Sol'n C	7.5 - 8.2	2.4×10^3	2.4×10^3	4.2×10^4

Table 9.3-4

Distribution Coefficients on Samples From the Culebra Dolomite

Fission Product
Distribution Coefficients

	pH range	Cs	Sr	I,Tc	Eu,Gd	Ru
Brine A	6.5 - 6.9	< 1	< 1	< 1	$> 10^4$	25 - 35
Brine B	6.5 - 7.6	1-2	1-2	< 1	$> 10^4$	640 - 660
Sol'n	7.5 - 8.2	7-10	4-5	< 1	$> 10^4$	240 - 400

Actinide
Distribution Coefficients

	pH range	Pu	Am	Cm
Brine B	6.5 - 7.8	2.1×10^3	2.6×10^3	1.2×10^4
Sol'n C	7.5 - 8.3	7.3×10^3	2.2×10^4	1.1×10^5

Table 9.3-5

Distribution Coefficients on Halite From The
2056' Horizon of ERDA #9 Borehole

Actinide Distribution
Coefficients [1]

pH range	Pu	Am	Cm
7.0 - 7.1	17	306	354
	(1.0×10^4)	(1.8×10^5)	(2.1×10^5)

1) The Kd values in parentheses were calculated
   from the weight of water insoluble material
   in the halite. The lower values are based on
   the total weight of halite taken.

Table 9.3-6

Distribution Coefficients on Samples of Clay From The 2186.6' Horizon of AEC #8 Borehole

Fission Product Distribution Coefficients

	pH range	Cs	Sr	I,Tc	Gd,Eu	Ru
Brine A	6.5 - 7.0	< 1	< 1	< 2	$> 2.5 \times 10^3$	150-180
Brine B	6.5 - 7.7	4-6	< 1	< 1	$> 10^4$	$> 2 \times 10^3$
Sol'n C	7.5 - 7.8	80-120	3-6	< 1	$> 10^4$	$> 1 \times 10^3$

Actinide Distribution Coefficients

	pH range	Am	Pu	Cm
Brine B	6.5 - 8.0	1.1×10^3	4×10^4	1.9×10^4
Sol'n C	7.5 - 8.4	3.5×10^3	1.8×10^5	4.2×10^5

Table 9.3-7

Distribution Coefficients on Samples of Polyhalite From the 2304' Horizon of ERDA #9 Borehole

Fission Product Distribution Coefficients

	pH range	Cs	Sr	Eu,Ce [1]	Sb	Tc
Brine A	6.5 - 7.0	< 1	5-10	10-20	< 1	< 1
Brine B	6.5 - 7.2	< 1	19-22	430-700, 50-55	0.9-1.5	< 1
Sol'n C	7.5 - 7.6	< 1	35-40	100-200, 40-60	3-4	< 1

1) Where two ranges of values are given, the first refers to Eu and the second to Ce.

Table 9.3-8

Distribution Coefficients on Sample of Cowden Anhydrite
From the 2562' Horizon of AEC #8 Borehole

Fission Product
Distribution Coefficients

	pH range	Gd,Eu,Ce
Brine B	6.5 - 7.9	$> 10^3$

Actinide Distribution
Coefficients

	pH range	Am	Pu	Cm
Brine B	6.5 - 7.9	2.9×10^2	6.7×10^3	4.2×10^3
Sol'n C	7.5 - 8.2	2.2×10^3	7.7×10^4	1.8×10^5

Table 9.3-9

Distribution Coefficients on Samples of Clay from
the 2725' Horizon of AEC #8 Borehole

Fission Product Distribution Coefficients

	pH range	Cs	Sr	Eu,Gd [1]	Tc,I [1]	Ru
Brine A	6.6 - 7.0	4-9	< 1	$> 10^3$, $2.8-4 \times 10^2$	3.5-4.5, 0-3.5	90-120
Brine B	6.7 - 7.4	3-6	< 1	$> 10^4$	< 1	$> 10^3$
Sol'n C	7.5 - 8.0	34-40	30-45	$> 10^4$, $>3 \times 10^3$	0.7-1.5, 0.5-4	$> 10^3$

Actinide Distribution Coefficients

	pH range	Am	Pu	Cm
Brine B	6.5 - 7.8	310	7.2×10^4	2.7×10^3
Sol'n C	7.4 - 8.4	2.3×10^3	4.0×10^4	1.6×10^5

1) Where two ranges of values are given, the first refers to
the first element listed and the second range is for the
second element listed.

Table 9.3-10

Distribution Coefficients on Samples of Bell Canyon Formation

Fission Product Distribution Coefficients

	pH range	Cs	Sr	Eu	Sb	Tc
Brine B	6.5 - 7.4	14-16	< 1	$> 10^4$	5-8	< 1
Sol'n C	7.5 - 7.9	130-140	1-5	$> 10^4$	20-25	< 1

Table 9.3-11

Distribution Coefficients on Halite Samples From the
2611' Horizon of ERDA #9 Borehole

Column Experiment

Column Bed: 7.5 g of Halite in 1 cm diameter column

Solution: Saturated Halite Solution, 200 ml

Flow: 1 Bed volume/min.

	% of Initial Activity in Solution	
Time (days)	^{85}Sr	^{144}Ce
0	100	100
1	98.0	26.7
4	96.8	0.9
8	98.4	0

Actinide
Distribution Coefficients[1]

pH range	Am	Pu	Cm
7.0 - 7.3	11	59	56
	(3.8×10^3)	(2.11×10^4)	(2×10^4)

(1) The Kd values in parentheses were calculated using the weight of
water insoluble material in the clay. The lower values are based
on the weight of halite taken.

Table 9.3-12

^{152}Eu Distribution Coefficients (Kd's)

Rock	Simulant	Nominal ^{152}Eu(μCi/ml)	Kd$^{(1)}$ 2 week	Kd$^{(1)}$ 3 month	Kd$^{(2)}$ 2 week	Kd$^{(2)}$ 3 month
Culebra	A	0.01	1.7×10^4	1.5×10^4	--	--
"	A	0.1	3.6×10^4	2.1×10^4	--	--
"	A	1.0	1.8×10^4	4.3×10^4	--	--
"	B	0.01	3.4×10^3	1.6×10^3	--	7.6×10^3
"	B	0.1	1.1×10^4	3.6×10^3	--	1.3×10^3
"	B	1.0	3.7×10^3	3.9×10^3	8.8×10^2	1.4×10^3
"	C	0.01	2.8×10^4	1.3×10^4	--	1.1×10^4
"	C	0.1	2.7×10^4	2.6×10^4	--	1.9×10^4
"	C	1.0	2.0×10^4	1.4×10^4	1.2×10^3	9.6×10^3
Magenta	A	0.01	1.4×10^4	6×10^3	--	--
"	A	0.1	1.9×10^4	2.0×10^4	--	--
"	A	1.0	1.2×10^4	1.4×10^4	--	--
"	B	0.01	2.8×10^3	8.6×10^2	--	4×10^2
"	B	0.1	8.3×10^3	3.7×10^3	--	1.3×10^3
"	B	1.0	1.1×10^3	1.2×10^3	3.5×10^2	4.0×10^2
"	C	0.01	2.0×10^4	1.7×10^4	--	1.3×10^4
"	C	0.1	3.6×10^4	2.2×10^4	--	1.6×10^4
"	C	1.0	1.4×10^4	1.5×10^4	7.7×10^2	1.3×10^4

(1) Kd based on activity in feed solutions.

(2) Kd based on activity in pH adjusted feed solutions.

Table 9.3-13

Comparison of ^{153}Gd, ^{144}Ce, and ^{152}Eu Kd's in Brine B and Brine B* Containing Plywood Extract

14 Day Equilibration

Sample	Brine	^{153}Gd cpm/ml	^{153}Gd Kd	^{152}Eu cpm/ml	^{152}Eu Kd	^{144}Ce cpm/ml	^{144}Ce Kd
Feed	B	24,200	-	20,230	-	5,120	-
Feed	B*	38,090	-	38,090	-	7,080	-
Culebra	B		4.2×10^3		9.9×10^3		1.5×10^3
"	B*		6.3×10^2		6.6×10^2		6.0×10^2
Magenta	B		2.5×10^3		3.4×10^3		1.4×10^3
"	B*		6.5×10^1		7.0×10^1		1.1×10^2
Bell Canyon	B		3.4×10^3		3.4×10^3		3.2×10^3
"	B*		1.3×10^2		1.5×10^2		2.3×10^2
Cowden	B		2.6×10^3		2.2×10^4		2.2×10^3
"	B*		3.7×10^2		4.0×10^2		5.1×10^2
High Clay	B		6.8×10^3		8.5×10^4		1.2×10^3
"	B*		8.7×10^3		2.8×10^4		2.5×10^3

28 Day Equilibration

Sample	Brine	^{153}Gd cpm/ml	^{153}Gd Kd	^{152}Eu cpm/ml	^{152}Eu Kd	^{144}Ce cpm/ml	^{144}Ce Kd
Feed	B	23,260	-	20,170	-	4,800	-
Feed	B*	33,350	-	35,210	-	5,910	-
Culebra	B		4.3×10^3		8.3×10^3		3.3×10^3
"	B*		2.1×10^3		1.8×10^3		1.3×10^3
Magenta	B		3.5×10^3		2.5×10^3		$\geq 10^4$
"	B*		1.4×10^2		1.6×10^2		2.5×10^2
Bell Canyon	B		4.2×10^3		2.7×10^3		3.2×10^3
"	B*		1.5×10^2		1.7×10^3		3.2×10^2
Cowden	B		$\geq 10^5$		5.4×10^3		1.8×10^3
"	B*		4.7×10^2		4.8×10^2		5.3×10^2
Hi Clay	B		6.5×10^3		8.7×10^3		6.1×10^3
"	B*		1.9×10^4		3.2×10^4		5.9×10^3

10.1   INTRODUCTION

Continuing studies for the WIPP primarily encompass those geological processes that need to be understood in order to more quantitatively assess the safety of converting the WIPP to a repository. The processes of importance are tectonic, geochemical, hydrologic, and climatic. The studies indicated within this chapter generally relate to these major processes. In addition, a few studies indicated in this chapter relate to minor continuing efforts of site characterization. This chapter will serve to enumerate issues which remain to be addressed relevant to the safety of converting WIPP to a repository. It is not intended here that specific plans and schedules be presented.

The organization of Chapter 10 follows that of previous chapters.

10.2   SITE SELECTION

In line with the differentiation made in Chapter 2 between site selection, site characterization, and site confirmation, the activities of site selection and site characterization are nearly complete. The confirmation of the WIPP site for a repository will necessitate the continuing studies indicated in Sections 10.3 through 10.9.

10.3   REGIONAL GEOLOGY

Continuing studies of the regional geology focus mainly on the processes of tectonics and climate through studies of paleoclimates and various manifestations of past tectonic activity.

10.3.1 Paleoclimatology

The purpose of paleoclimatic studies in southeastern New Mexico is to develop the local timing and magnitude of past climatic changes and their relation to observed geology to help assess the possible effects of future changes on a repository.

The primary method of paleoclimatic study is to examine cores of Pleistocene or Recent sediments for fauna and flora which are indicative of past climatic conditions. In addition, organic matter or ash falls may, if suitable, be dated radiometrically to provide time control.

Studies of paleoclimate are underway with preliminary analysis of core taken in San Simon Sink from borehole WIPP 15. Fauna and flora are being separated from the sediment for paleontological analyses, and suitable organic material is being separated for radiocarbon analysis. These studies of the San Simon material will be completed in 1979 to yield an initial profile of climatic changes. Further coring in other locations may be undertaken at that time, if necessary, to supplement the record. The final stage of this study will be to integrate the local climatic changes into the information about regional climates and to determine the relationship between climatic changes and related processes such as subsurface salt dissolution and resultant subsidence (see Section 10.6).

10.3.2 Regional Tectonic Studies

The purpose of various studies of regional tectonics is to assess the long-term effects of tectonic forces on a repository.

Several studies together contribute to information about regional tectonics and include the seismological studies discussed in Section 10.5.

LANDSAT. A preliminary examination of LANDSAT photos has been completed and is reported in Chapter 3. In addition, the WIPP site and surrounding regions will be re-examined in 1979 with more sophisticated image

enhancement to determine the presence and location of more subtle
lineaments. Field evaluation of the interpretations will be undertaken
as required.

Leveling Surveys. Releveling of some existing first-order vertical
control lines was carried out in 1977, and about 300 km of new lines were
established. These new lines, some of which traverse Nash Draw and the
WIPP site, will be periodically releveled to establish a data base for
separating regional tectonic effects from local effects perhaps due to
dissolution (see Section 10.6).

West Texas Salt Flats Graben. Releveling and seismology studies indicate
active tectonic displacement on the west Texas salt flats graben.
Seismic reflection records will be examined and test coring conducted in
1979 to determine if the sediments will yield a record of tectonic
disturbance that will contribute to information about the tectonic forces
likely to affect a repository located in the Delaware Basin.

10.4 SITE GEOLOGY

The purpose of continuing studies of site geology are to refine the data
base for assessment of the safety of a repository there, and to
contribute some additional details of site characterization. The methods
and studies as such are quite varied.

10.4.1 Geologic Mapping

Geologic mapping continues on the WIPP site and in the area, particularly
under a study of the stability of the WIPP site. This study, being
conducted by the USGS, is concerned with mapping caliche and related
sediments to provide more conclusive data on the length of time the area
has been stable, and the rates at which areas around the site have been
disturbed.

10.4.2 <u>Aeromagnetic Survey</u>

A very high resolution aeromagnetic survey will be initiated during FY79 to examine the WIPP site and several special features. The survey of the site will primarily be to determine if any dikes have intruded the evaporites at the site since dikes might form a pathway for fluid flow. Several of the domal features mentioned in Chapters 3, 4, and 6, two of which are considered to be breccia pipes, will be examined to determine if a magnetic signature is associated with disturbance of the magnetic red beds. The tool, if proven applicable, might then be used for prospecting to support continuing studies of breccia pipes as indicated in 10.6.

10.5 SEISMOLOGY

The purpose of continuing seismological studies is to provide data for facility design and to expand the data base contributing to an understanding of tectonic processes affecting a repository in the Delaware Basin. Seismological studies are supported by arrays of stations near points of interest.

10.5.1 <u>Near-Site Activity</u>

The careful characterization of near-site background activity, as indicated in Chapter 5, is the dominant seismic issue affecting the WIPP site. Station CLN has been operating near the site since 1974, and continues to operate. It is planned to augment this station so that at least three stations will be operating at the site to better define near-site seismicity.

10.5.2 <u>Central Basin Platform</u>

An array of stations has been operating near Kermit, Texas, since 1976 to evaluate the seismic activity on the Central Basin Platform and to explore the relationship, if any, between this activity and the massive

fluid injection for secondary oil recovery operations occurring in that area. This array will continue to operate both for this purpose and because the assessment of seismic activity at the WIPP site may partly depend on an understanding of the relationship between fluid injection and seismic activity should injection occur in oil fields near the site.

10.6 CONTINUING STUDIES IN HYDROLOGY

10.6.1 Introduction

Hydrology is a major consideration when examining the feasibility for locating a nuclear waste disposal site. Two factors are directly related to hydrology: (1) the geologic stability of the formation in which the waste products will be stored, and (2) the occurrence of water as a transport medium for radionuclides. Unsaturated waters migrating along the surfaces of the salt beds will dissolve salt; therefore, an examination of magnitude and direction of fluid flow and fluid chemistry in formations above and below the salt is necessary. Additionally, the direction and rate of fluid movement both above and below the storage horizon should be evaluated to predict the movement of radionuclides should they be accidentally discharged into the aquifers.

10.6.2 Purpose of Hydrologic Testing

Two hydrology-related questions are to be answered in evaluating the suitability of the proposed WIPP site.

1. What is the geologic stability of the Salado Formation?

2. Should the primary containment barrier (the salt) fail or an accident occur, where and how rapidly will radionuclides be transported by groundwater?

Three factors need to be investigated to examine the integrity of the Salado within the site: (1) the Rustler-Salado contact is to be examined

geophysically and petrologically within the WIPP area to determine if dissolution is presently occurring, (2) the dissolution front (as defined by the edge of the shallow dissolution zone in the Nash Draw) needs to be located more precisely, (3) the estimated rate of dissolution is to be refined.

The hydraulic gradients and rates of fluid movement in the series of fluid bearing zones that overlie the Salado require further definition. Estimates of concentrations of aqueous species (and when and where they might appear) may then be refined for specific safety-assessment modeling scenarios describing radionuclide escape into these groundwater systems and migration out of the area. In addition, formations which do not presently contain water but exhibit some degree of permeability are to be tested to see what rates of movement would be, should they contain water or other fluids at some later time.

10.6.3 Direction and Rate of Fluid Migration

If radionuclides were to reach fluid bearing zones in the Rustler, they would be transported away from the site by the groundwater system. To evaluate the impact of such an accident on the surrounding area, hydraulic gradients and hydraulic conductivities of fluid bearing zones overlying the salt beds will be determined or modified. Data for these determinations will be acquired by pumping tests on hydrologic test holes or measurements of the recovery time of fluid levels in bailed holes. Tracer tests will be conducted where they may contribute useful information.

A series of hydrologic tests is planned in holes placed near the periphery of the proposed land withdrawal area. After additional testing of some existing holes, control points for the potentiometric surfaces and for hydraulic conductivities will have been established for the periphery with a spacing of 2 to 3 miles. These data will allow construction of more detailed potentiometric surface maps for the site area. The potentiometric contours will be meshed with the results from

the Nash Draw program to the west. Consequently, the potentiometric surface and hydraulic conductivity data required for modeling efforts of long-term safety assessment will be obtained for an area extending from the northeast part of the study area to Malaga Bend on the Pecos River (an area of about 200 square miles).

The borehole plugging program requires data from both laboratory and in situ permeability measurements. These permeability measurements, both in the evaporites and in aquifers, will provide additional data for the safety assessment work.

10.6.4 Dewey Lake Redbeds

The Rustler Formation and the shallow dissolution zone in Nash Draw have demanded the attention of this program because they are fluid-bearing. The Dewey Lake Redbeds are also of some significance since fluids are present in sandstone lenses. Although the redbeds are only locally saturated, two possibilities exist for additional water to enter the formation: a climatic change to a high rainfall period, or migration of fluids from below into the redbeds.

Tests in two types of holes are being considered: existing holes, and at least one new hole specifically designed for Dewey Lake testing. The casing in existing holes will be perforated opposite permeable zones as identified from analyses of logging and drilling records.

The standard hydrologic testing procedures will allow calculation of the transmissivity of fluid bearing strata in the Dewey Lake Redbeds or other permeable zones that might be expected to contain fluids at some future time.

10.6.5 Long-Term Monitoring

The peripheral hydrologic test holes, which now include four potash holes, will be configured for long-term monitoring. This long-term

monitoring may show what changes are taking place in the hydraulic gradients which in turn may indicate increased or decreased flow, and variations in rates of recharge or discharge. Moreover, depending on the extent of the monitoring system, a warning network for information on fluid threats to the integrity of the repository is obtained.

The Dewey Lake Redbed hole(s) can be monitored to detect fluid movement that may not be present except during high precipitation cycles of long or short duration.

The test holes drilled in Nash Draw would be monitored to detect changes in the hydrologic regime along the Rustler-Salado contact. Because the Culebra is the main producer of water west and south of the WIPP area, it is desirable to monitor this fluid-bearing strata to determine its relationship with the shallow dissolution zone and to provide additional data for modeling the safety assessment modeling scenarios.

10.6.6 Surface Hydrology

Surface hydrology must be examined climatologically with the aid of surface mapping. Records of annual rainfall and intensity and duration of storms (particularly high intensity, 24 hour, 50 and 100 year recurring storms) are available. This information, in conjunction with surface mapping (from aerial photographs, topographic maps, or both) of contributory drainage will provide the basis to estimate amounts of runoff and amounts of infiltration in the study area. Because of the high evapotranspiration and the caliche layer below surficial sands, infiltration estimates are expected to be only a small portion of the calculated recharge.

Photogrammetric and field mapping is planned to locate and describe springs which may issue from the Dewey Lake Redbeds or the shallow dissolution zone. Several springs are suspected to be located west of the site, and discharge measurements could aid in the identification of the formations from which they issue. Geochemical monitoring of many

such springs, including the Malaga Bend seeps and the Pecos River salt
load, will add to this overall understanding of hydrologic system
dynamics.

10.6.7 Overview of Deep Hydrologic Testing

Three objectives for deep aquifer testing to complement the site-specific
shallow aquifer investigations in the WIPP study area are:

(1) To obtain static bottom-hole pressure measurements in the deep
     aquifer zones, for the refinement of previous estimates of local
     potentiometric surfaces, hydraulic gradients, and hydraulic
     conductivities.

(2) To determine the bounds of the formational reservoirs.

(3) To obtain fluid samples for geochemical analyses.

Three wells suitable for hydrologic testing (Badger, Cabin-Baby,
Cotton-Baby) are located within the site area. Each well will have to be
re-entered and plugged, in accordance with methods now under study, or
maintained as monitoring wells. Deep hydrologic data will be developed
from these well to obtain site-specific information on the Delaware
zones. Testing outside the study area involves two additional wells (AEC
No. 8 and ERDA No. 6).

10.6.8 Long-Term Monitoring of Deep Wells

A number of wells could be equipped for long-term monitoring of the
Delaware zone to show what changes, if any, are taking place in the
hydraulic gradient, which in turn indicate fluid movement in the
reservoir. Periodic fluid samples can be obtained to identify increased
flow or chemical changes in the ground water system.

10.6.9 Continuing Studies in Salt Dissolution and Overburden Subsidence

Program Objectives. The program of investigation of dissolution and subsidence has four fundamental purposes, and one special-case consideration:

1. To correlate surficial collapse features and deposits with subsurface dissolution, in order to develop criteria for an evolutionary pattern of collapse.

2. To characterize subsurface dissolution products adjacent to the WIPP site.

3. To determine the behaviour of fluids in dissolution products adjacent to the WIPP site.

4. To analyze potential impacts of evolution of dissolution products at and near the WIPP site with respect to repository breachment and radionuclide transport.

The special case is to determine the nature of subsidence over mines in salt, and its effects on the overlying groundwater system.

An elaboration of these purposes follows.

Nash Draw Investigations. Nash Draw is believed to have originated by some combination of surface erosion and subsidence following subsurface dissolution. If the process of formation is overwhelmingly erosion, then the potential for removal of overburden at the WIPP site is probably about the same as it has been in Nash Draw. If, however, the process is overwhelmingly dissolution of salt and subsequent collapse of the overburden, the potential extension of Nash Draw toward the WIPP by dissolution will be more quantitatively described. At present, there is no conclusive way of defining an instantaneous rate of growth of Nash Draw toward the WIPP site; therefore, the only alternative is to

understand the processes which have resulted in Nash Draw, and
incorporate their implications into the mathematical modeling efforts
directed toward safety assessment involving the WIPP site in general, and
radionuclide escape and migration in particular.

First, the Nash Draw program is a series of core holes, which will be
geophysically logged. This operation will obtain data to serve three
·purposes: 1) reveal the subsurface of Nash Draw stratigraphy at
carefully chosen points, 2) reveal the relationships between the
subsurface structure and surface features and deposits, 3) reveal how
much halite and anhydrite (or gypsum) has been removed by dissolution.

Second, the Nash Draw program is a source of geologic material for
petrographic and geochemical examination. Examination of thin sections
of recovered rock will allow the mineralogy of dissolution products to be
determined, i.e. identification of what was dissolved and what remains.
Mineralogy and textures of dissolution residues and cemented collapse
fill can then be compared with those of dissolution features sampled in
other programs, such as the one to investigate the cemented rubble
chimneys (often called "karstic domal features" or "breccia pipes").
Geochemical analyses of core materials for trace constituents will reveal
their degree of interaction with groundwaters, and possibly an age of
formation. Also, permeabilities to fluids can be obtained from cores.

Third, the Nash Draw core holes will become a series of hydrology test
holes. The brine flow underlying Nash Draw has been attributed
responsibility for much of the dissolution and collapse observed today.
The safety assessment scenarios for radionuclide escape and migration
involve movement from WIPP into Rustler Formation waters into the shallow
dissolution zone and out at Malaga bend on the Pecos River. It behooves
us to understand the hydrologic relationships between the shallow
dissolution zone and the Rustler water-bearing rocks in Nash Draw in
order to verify that models of radionuclide transport are representative
of the physical system.

<u>Cemented Rubble Chimney Investigations</u>. One of the "karstic domal
features" described by J. D. Vine (called Hill "C") was encountered at
the level of the McNutt potash zone by Mississippi Chemical Corporation.
It was found to be a chimney in the Salado Formation filled with
clay-cemented brecciated rock belonging to strata above the McNutt.
Similarly a breccia-filled chimney was encountered in drilling near a
circular hill near the Wills-Weaver Mine. There are numerous other
erosion-breached domes such as Vine's Hill "C" in the vicinity of Nash
Draw; the subsurface expression of them, if any, is virtually unknown.
It is desirable that a hole be drilled to a depth at which no more
brecciated rock is found. Hydrologic observation (including water
sampling and static water-level measurements) in fluid-bearing zones of
the structure itself and in "bedrock" and in nearby rocks will help to
determine the degree of hydraulic connection of the structure with
aquifers of regional extent.

Petrographic analyses of recovered core will allow comparisons to be made
with dissolution products recovered from Nash Draw investigations,
described previously. Such material also lends itself to geochemical
analyses for the determination of rock-water interaction history and
age. Similarly, fluid analyses will provide an indication of how the
fluids have interacted with their host rocks, helping to determine the
processes at work in such structures.

Since modeling of radionuclide escape and migration must take into
account fluid movement, cemented rubble chimneys should be evaluated for
their potential as paths for such movement. They should also be
evaluated as members of the evolutionary pattern of dissolution and
collapse features, and might be generically related to the development of
Nash Draw. Consequently, it is desirable to measure <u>in situ</u> the
permeability of the structure. In addition, the hydrologic relationships
between the chimney and surrounding rocks should be understood in order
to formulate a complete hydrologic model for risk assessment.

Mine Subsidence Investigations. The potash producers in southeastern New Mexico mine in two stages -- the primary recovery which leaves rooms separated by large pillars, and the secondary recovery in which they may "rob the pillars" and ultimately remove almost 95% of the ore. Second-mining requires abandonment almost immediately thereafter, because there is no longer a large enough local pillar system to hold up the roof. And so, the roof slowly sags, and subsidence is propagated to the surface.

While investigations of subsidence over mines do not bear directly on the four program objectives, mining is certainly a particular cause of subsidence and perhaps an indirect agent for initiating dissolution. If subsidence over a mine causes fracturing of water bearing rocks above, locally increased permeability might allow circulation of groundwater to underlying evaporites through the fractures to start dissolution.

The amount of subsidence and its potential for enhancement of salt dissolution of the Salado Formation over the WIPP if the McNutt potash zone were to be mined is unknown. If this subsidence program were to lead to a satisfactory means to predict subsidence and its effects, in particular dissolutioning, the control zone restrictions currently prescribed around the WIPP could possibly be relaxed. It is possible that minor subsidence will occur over the closed WIPP mine because it will not be possible to backfill the repository to the same packing density as original rock. Therefore, it is desirable to evaluate the effect of mining and subsequent subsidence on the local groundwater system in the subsiding overburden.

10.6.10 Modeling of Regional Hydrology

Hydrologic modeling has one basic objective, to support risk assessment work by describing the movement of fluids in this region in as much detail as possible. The movement of fluids affects the expected period of integrity of the repository and the movement of radionuclides from the repository. To fulfill this objective, the modeling emphasizes several

aspects. The first aspect is interpretation and explication of the data collected in field programs designed to delineate the regional flows. The second is to suggest where data are insufficient and more field or laboratory work is required. The third aspect is the simulation of experiments which cannot be performed in the field. Two examples for . simulations are: consequences of perturbations to regional flow patterns caused by the existence of a repository, and consequences of changes in regional flow patterns due to alterations in rainfall patterns or due to man's activities.

The fourth aspect is prediction of the movement and concentrations of radionuclides consistent with fluid movement determined in part by the release scenarios developed for WIPP.

Implementation is based on the modification and use of certain 2-D and 3-D computer codes available for hydrologic modeling. Code verification based on field data already collected is in process. Supporting laboratory programs designed to provide parameters as absorption coefficients, permeabilities, etc., are already underway.

10.7   CONTINUING STUDIES IN GEOCHEMISTRY

10.7.1   Introduction

Detailed accounts of geochemical data reported in Chapter 7 have provided the pressing need of fundamental information for (1) conceptual design of WIPP operational facilities, and (2) formulation of site-specific process scenarios to be used in the consequence safety assessment effort. An evaluation of the available data has shown that the completed studies are not entirely sufficient to support WIPP experimental programs. These programs include borehole plugging, laboratory rock mechanics, in-mine rock mechanics, in-mine heater experiments, in-mine high-level waste emplacement experiments, laboratory waste-rock interaction experiments, radionuclide transport through rocks, and waste encapsulation studies.

In addition, the long-term safety assessment effort has lacked
information about geological processes associated with so-called
"geological anomalies" such as igneous dikes and cemented rubble chimneys.

10.7.2   Mineralogy and Petrology

The data concerning assemblages of evaporite minerals in the Salado
Formation which were presented in Chapter 7 have addressed the types of
minerals found and their relative (qualitative) abundances. While this
has been useful in selection of candidate horizons for waste emplacement,
it has been of limited use to the quantitative measurements of thermal
and physical properties of evaporite rocks (see Chapter 9).

It has been found that a small change in the quantitative mineralogical
proportions in a rock sample has a large non-linear effect on thermal
properties, for example. Chapter 7, together with its executive summary
in Chapter 1, has pointed out the variability in the mineralogical
composition of rocks in the Permian evaporite section.

In addition, quantitative mineralogy and petrology is required for
development of materials to be used in the plugging of shafts and
boreholes. The long-term thermodynamic stability of a grout plug, for
example, cannot be evaluated without an intimate knowledge of mineral
phases in both grout and rock, so that free energy calculations can be
made for degradation reactions which might occur between the two.
Compatibility of grout with rock and groundwater will be an essential
factor requiring thorough evaluation to provide confidence in the
long-term sealing of boreholes and shafts which penetrate from surface to
repository horizons.

10.7.3   Volatiles Characterization

Chapters 7 and 9 have alluded to the variability in volatile content of
evaporites and how the variation affects fundamental rock properties.
Chapter 7 has addressed the volatile component in detail mostly in view

of mass loss experienced by heated rock. The entire mass loss cannot be ascribed to water alone. Indeed, Chapter 7 briefly addressed the chemical species which were found in a few selected rock samples, and even so, considerable variation was observed. Experiments are planned to simulate high-level-waste-canister heat in a potash mine, in order to quantize the devolatilization products. Unambiguous interpretations of the experimental results derived therefrom require an understanding of the volatile components native to the rock before heating begins. Furthermore, the interpretations also require an understanding of the fundamental differences between potash ore zones and actual repository zones, since the results of devolatilization in one will certainly not be directly applicable to the other without taking into consideration the native differences.

10.7.4   Origins of Evaporite Assemblages

It was pointed out in Chapter 7 that many of the evaporite mineral assemblages observed in the Permian section cannot have precipitated from a seawater-like solution. Furthermore, the thermodynamic properties of some minerals, such as the almost ubiquitous polyhalite, are virtually unknown. Similarly its mode of origin is entirely unknown, and has been long regarded wholly as a product of recrystallization, commonly replacing anhydrite.

The present assemblages not only contain non-primary evaporite minerals, but also have a magnesium deficiency relative to other evaporites in the world. The sink for this magnesium presumably lost during recrystallization has not been identified. The observations of Chapter 7 urge that a thermodynamic understanding of the environments and processes of evaporite recrystallization be sought. In this way the water loss that the evaporites have experienced (during recrystallization) can be estimated, and confidence can be gained regarding what mineralogical changes (if any) are likely to take place in response to waste emplacement.

The techniques used in deducing the origins of evaporite assemblages include chemical quantitative analyses of minerals, petrographic paragenetic examination, and stable isotope, radioisotope and trace element analyses.

10.7.5   Igneous Dike

In Chapter 4, there was mention of a northeast-trending igneous dike intruding the evaporites on the west side of Nash Draw west of the WIPP study area. The characterization of the dike was based on the Yeso Hills and Kerr-McGee mine occurrences, together with an aeromagnetic survey. In order to come to an understanding of the marginal effects (i.e., dike-salt-fluid interactions), the following pursuits are recommended:

1. Collection and study of additional samples from farther away from the Kerr-McGee dike occurrence.
2. Determination of:
    a. K-Ar ages of the alteration micas in the dikes
    b. Drilling angle holes with coring at appropriate intervals, to sample the dike and the effects of the dike upon the host rock system.

The dike appears to be a natural laboratory experiment involving high-temperature interactions among salts, groundwaters, and "alien" mineralogies such as emplaced waste would also represent.

10.7.6   Trace Elements and Age-Dating

A continued effort is desirable in age-dating and trace element studies, in order to support investigative efforts contemplated for the so-called "geologic anomalies." The activities are, specifically:

1. Chemical and isotopic study of exposed collapse structure in underground workings of Mississippi Chemical Mine.

a. If waters have percolated through this structure in very recent times then this may be reflected in oxygen isotopic study of grain coatings, etc. Rb-Sr studies of clay minerals should give an indication of Rb, Sr and ($^{87}Sr/^{86}Sr$) redistribution relative to clay minerals removed from the collapse structure.

b. Scanning electron microscope/microprobe study of grain boundaries: supplemented by instrumental neutron activation analysis (INAA) for adsorbed elements (alkalies, alkaline earths, rare earth elements).

c. Rare Earth Elements (REE) distribution in all primary and secondary phases most likely to have been affected by solutions.

2. REE (and other key trace element) abundance in major facies of drill core from WIPP site. At present trace element data are very sporadic and obtained by different techniques so that real differences due to analytical precision and accuracy are suspect. Detailed INAA study of various phases from the same stratigraphic horizons over a wide lateral extent are desirable to establish realistic background data for the REE (i.e. because the REE are commonly used as analogues for the transuranics) so that REE data from dike-salt contact zones and elsewhere can be proprly assessed. If the REE distribution is extremely variable then local variations due to solution, recrystallization, contact effects will be difficult to interpret; if the REE show a more or less uniform distribution pattern and abundance then such effects can be closely scrutinized.

3. Dike-evaporite contact effects. Samples from the lamprophyre dike (T = ~ 35 MYBP) which is observed in the underground workings of the Kerr-McGee Mine offers a unique chance to examine the effects of a local, high temperature source in contact with several evaporite phases.

10.7.7   Reef and Back-Reef Waters

There is at present some degree of confusion surrounding the source and discharge of water in the Capitan Reef surrounding the Delaware Basin. Chapter 7 has shown that the greater portion of the water in the Reef cannot have come from direct infiltration into outcrops in the Guadalupe and Glass Mountains, nor from rocks in the Basin. Therefore, the relationships between the Reef and its lagoonal facies (back-reef) stratigraphic equivalents are likely source and sink candidates. These relationships are best deduced by combinations of stable isotope, uranium isotope, and solute analyses of reef and back-reef waters. An extensive water-sampling of these areas is required for this. The results of this geochemical mapping of regional groundwater flow would be used in the long-term safety assessment modelling effort and the final publication of the regional groundwater mathematical model.

10.7.8   Future Work on Fluid Inclusions

In addition to the obvious necessity of making studies on samples from the actual strata to be used for high level waste storage, a variety of approaches need to be explored. Fluid inclusions near the waste canisters might decrepitate in the thermal pulse; the conditions under which this will occur can and should be explored experimentally. (studies are continuing of inclusions in a suite of salt samples collected at various distances from a dike penetrating the salt horizons; this provides a natural analog.) The identification of the daughter minerals in some inclusions, and their thermal behavior, as well as bubble movement in a thermal gradient, will provide additional compositional information. The gases released on crushing or heating should be explored, as well as the leakage of gases (or water) out of inclusions. This would be pertinent both for interpretation of K/Ar ages and in corrosion problems. The actual chemical composition of the larger inclusions and their isotopic composition (particularly H/D and O^{16}/O^{18}) can be determined by existing methods. This would help in

understanding the complex sequence of interactions of pore (and inclusion) fluid with the original salt beds to yield the present mineralogy.

10.8 RESOURCES

Sandia Laboratories has no continuing studies of resources at the WIPP site.

10.9 SPECIAL STUDIES

10.9.1 <u>Purpose</u>. The objective of thermophysical and radionuclide sorption studies on SENM rocks is to determine their characteristics as required by the structural mine design, <u>in situ</u> experimental, and long-term safety analyses programs. As with other continuing studies, these special studies are a means to an end, not an end in themselves.

10.9.2 <u>Thermophysical Properties</u>

<u>Scope</u>. A continuing assessment of the thermophysical properties of SENM rocks is envisioned because of the broad range of questions posed about radioactive waste isolation. These problems range from the plasticity of salt to the migration of brine in salt; many are not answered by a cursory investigation. Establishing a data base, for instance, for the analyses of long-term creep, is time consuming. It is not anticipated that evaluation of physical rock properties will be pivotal in mine, experiment or repository design; however, that is intrinsically impossible to guarantee. Such evaluations may very well be pivotal in considerations of retrievability of high-level waste experiments, in which high temperatures tend to accelerate creep. Thus, physical rock property determinations, such as the micromechanics of rock deformation, are a prudent pursuit to provide additional confidence in geologic isolation.

Continuing Studies. The primary object of the continuing experimental rock mechanics program is to understand and model the thermomechanical behavior of the WIPP salt. This will be accomplished through studies of transient creep data at pressures exceeding 1500 psi and at a principal stress difference less than 2000 psi where there is a paucity of data. In addition, petrographic investigations will continue to identify the governing deformation mechanisms.

Other studies relevant to the long-term stability of the WIPP include measurements of gas and brine permeabilities on previously deformed core and measurements of gas permeabilities at elevated temperatures. Studies are also planned in the area of thermal expansion coefficients and brine migration in salt under thermal gradients. Migration of fluid inclusions is being given attention, because of the brine's corrosive potential and because the capacity of fluid inclusions to carry radionuclides through rock salt is not known.

Rock mechanic programs will also be initiated to determine the mechanical properties of the WIPP site rock other than rock salt. These studies will be directed toward the engineering performance and construction characteristics of the non-salt rock which will influence the design and construction of shafts to the repository levels.

Mineralogic and petrographic studies will be conducted on core to support the physical rock properties determinations as required. This information is required to determine the phase systems in the rocks being investigated. A similar set of studies support the geochemical analyses, Chapter 7. The variations in mineral assemblage, grain size, fluid inclusion content, and petrofabric which have been observed in evaporite rocks have also given rise to variations in physical properties, which could only qualitatively be taken into account in the investigations reported here.

The arbitrary separation of mineralogical and physical rock properties from geology and hydrology that has often occurred in other studies is

being avoided in the comprehensive studies being performed for the WIPP. The relations of rocks found at the proposed repository horizons to those found in an in situ test bed located elsewhere (e.g., nearby potash mine) are being evaluated. Quite possibly, mineralogic and fabric changes may cause discrepancies in results from one site to another.

10.9.3 Radionuclide Sorption Properties

Scope. A continuing assessment of WIPP rocks ability to inhibit the migration of radionuclides away from the repository is envisioned to augment the batch Kd determinations, which were used in preliminary calculations of radionuclide travel time in site-specific escape scenarios. A realistic approach to safety assessment requires data to be generated (mostly in the laboratory) under simulated physiochemical conditions anticipated in subsurface evaporites and related rocks of southeast New Mexico. The laboratory experiments in radionuclide migration would ultimately be evaluated by SENM field experiments involving the emplacement and observation of movement of non-radioactive tracers which are chemically analogous to radionuclides.

Continuing Studies. Whereas previous "Kd" measurements reflect the degree to which radionuclide soprtion on rocks takes place in static, closed systems, scenarios involving the entrainment of radionuclides in moving groundwater imply that a variety of physiochemical conditions will be encountered in the subsurface.

Now that the radionuclides of interest have been identified, different oxidation states of those radionuclides which might give rise to different mobilities in WIPP environments will next be identified. Investigations of effects on sorption of parameters such as pH, radionuclide concentration in solution, and oxidation potential will then proceed with the oxidation states of species of interest. These parameterization experiments will culminate in the simulation of radionuclide migration in flow-through experiments involving actual WIPP rocks and solutions, at the anticipated physiochemical conditions.

Appendix 7.A (Ref. sec. 7.3)

Whole Rock Chemical Analyses, Soluble-Insoluble
Fractions, Mineralogy, and Weight Losses
upon Heating.

TOTAL ANALYSIS

HOLE #   7
DEPTH = 1044.2 FEET

SOLUBLE =   99.72 %
INSOLUBLE =   0.28 %

COMPONENT	WT %
SO3	0.55
NA	38.56
NA2O	0.0
K	0.03
K2O	0.0
MGO	0.04
CAO	0.43
SIO2	0.0
FE2O3	0.0
AL2O3	0.0
CL	60.40
WEIGHT LOSS ON HEATING	
70	0.10
HI TEMP	0.0
TOTAL	100.39

MAJOR: HAL
MINOR: ANH
TRACE: CARN

TOTAL ANALYSIS

HOLE # 7
DEPTH = 1107.5 FEET

SOLUBLE = 69.47 %
INSOLUBLE = 30.53 %

COMPONENT	WT %
SO3	20.88
NA	20.28
NA2O	6.63
K	0.0
K2O	4.48
MGO	4.57
CAO	1.84
SIO2	8.30
FE2O3	0.27
AL2O3	1.24
CL	30.78
WEIGHT LOSS ON HEATING	
70	0.12
125	0.10
200	0.40
350-400	1.37

TOTAL	101.26

MAJOR: HAL
MINOR: POLY, LANG, KFELD, TALC, QTZ
TRACE: CHLOR, FEOX

TOTAL ANALYSIS

HOLE # = 7
DEPTH = 1171.5 FEET

SOLUBLE = 37.10 %
INSOLUBLE = 62.90 %

COMPONENT	WT %
SO3	39.73
NA	12.56
NA2O	0.88
K	1.91
K2O	0.0
MGO	0.70
CAO	25.13
SIO2	0.63
FE2O3	0.06
AL2O3	0.0
CL	18.87
WEIGHT LOSS ON HEATING	
70	0.14
300-400	0.58
425	0.08
TOTAL	101.27

MAJOR: HAL, ANH
MINOR: POLY
TRACE: SYL, BLOED, QTZ, FEOX

TOTAL ANALYSIS

HOLE # = 7
DEPTH = 1221.0 FEET

SOLUBLE = 99.51 %
INSOLUBLE = 0.49 %

COMPONENT	WT %
SO3	2.02
NA	38.79
NA2O	0.0
K	0.06
K2O	0.0
MGO	0.10
CAO	0.88
SIO2	0.01
FE2O3	0.0
AL2O3	0.0
CL	58.31
WEIGHT LOSS ON HEATING	
70	0.30
100-200	0.14
375-425	0.07
TOTAL	101.17

MAJOR: HAL
MINOR: ANH
TRACE: POLY, LANG, QTZ

TOTAL ANALYSIS

HOLE #   7
DEPTH =   1343.0 FEET

SOLUBLE =   99.74 %
INSOLUBLE =   0.36 %

COMPONENT	WT %
SO3	0.99
NA	38.60
NA2O	0.0
K	0.35
K2O	0.0
MGO	0.15
CAO	0.66
SIO2	0.01
FE2O3	0.0
AL2O3	0.0
CL	59.40
WEIGHT LOSS ON HEATING	
70	0.27
300-350	0.16
TOTAL	100.95

MAJOR: HAL
MINOR: ANH, POLY
TRACE: QTZ

TOTAL ANALYSIS

HOLE #   7
DEPTH = 1402.5 FEET

SOLUBLE =   99.97 %
INSOLUBLE =   0.03 %

COMPONENT	WT %
SO3	0.11
NA	39.67
NA2O	0.0
K	0.06
K2O	0.0
MGO	0.06
CAO	0.02
SIO2	0.0
FE2O3	0.0
AL2O3	0.0
CL	59.78
WEIGHT LOSS ON HEATING	
70	0.19
400-500	0.12
TOTAL	100.04

MAJOR: HAL
MINOR:
TRACE: POLY

TOTAL ANALYSIS

HOLE # 7
DEPTH = 1468.5 FEET

SOLUBLE = 93.66 %
INSOLUBLE = 6.34 %

COMPONENT	WT %
SO3	2.88
NA	34.44
NA2O	0.0
K	0.37
K2O	0.07
MGO	1.85
CAO	0.19
SIO2	2.15
FE2O3	0.24
AL2O3	0.07
CL	53.61
WEIGHT LOSS ON HEATING	
70	1.27
100-150	0.36
175	0.10
250	0.07
375	0.34
400-500	0.45
TOTAL	98.46

MAJOR: HAL
MINOR: KAIN, KIES
TRACE: POLY, KFELD, TALC, QTZ

TOTAL ANALYSIS

HOLE # 7
DEPTH = 1534.0 FEET

SOLUBLE = 99.86 %
INSOLUBLE = 0.14 %

COMPONENT	WT %
SO3	1.67
NA	36.10
NA2O	0.0
K	0.52
K2O	0.0
MGO	0.22
CAO	0.64
SIO2	0.01
FE2O3	0.0
AL2O3	0.0
CL	57.76
WEIGHT LOSS ON HEATING	
70	0.22
200	0.01
400-500	0.24
TOTAL	97.53

MAJOR: HAL
MINOR: POLY
TRACE: KAIN, QTZ

TOTAL ANALYSIS

HOLE #   7
DEPTH = 1615.0 FEET

SOLUBLE =   98.69 %
INSOLUBLE =   1.31 %

COMPONENT	WT %
SO3	4.56
NA	35.06
NA2O	0.0
K	1.05
K2O	0.0
MGO	0.71
CAO	1.47
SIO2	0.23
FE2O3	0.04
AL2O3	0.07
CL	55.95
WEIGHT LOSS ON HEATING	
70	0.34
100	0.09
350-400	0.37
TOTAL	99.94

MAJOR: HAL
MINOR: POLY, KAIN
TRACE: CHLOR, MONT

TOTAL ANALYSIS

HOLE # 7
DEPTH = 1698.0 FEET

SOLUBLE = 95.35 %
INSOLUBLE = 4.65 %

COMPONENT	WT %
SO3	0.58
NA	36.47
NA2O	0.0
K	0.06
K2O	0.07
MGO	1.20
CAO	0.34
SIO2	2.07
FE2O3	0.25
AL2O3	0.61
CL	58.35
WEIGHT LOSS ON HEATING	
70	0.82
350	0.03
TOTAL	100.85

MAJOR: HAL
MINOR: ANH, CARN, KIES
TRACE: POLY, ILL, QTZ, FEOX

TOTAL ANALYSIS

```
HOLE #    7
DEPTH =  1755.0  FEET

SOLUBLE  =   99.60  %
INSOLUBLE =   0.40  %
```

COMPONENT	WT %
SO3	0.65
NA	38.12
NA2O	0.0
K	0.23
K2O	0.0
MGO	0.13
CAO	0.08
SIO2	0.02
FE2O3	0.0
AL2O3	0.0
CL	59.54
WEIGHT LOSS ON HEATING	
70	0.19
200	0.04
300-400	0.05
TOTAL	99.45

```
MAJOR:   HAL
MINOR:
TRACE:   LEON, QTZ
```

TOTAL ANALYSIS

HOLE # 7
DEPTH = 1952.5 FEET

SOLUBLE = 99.30 %
INSOLUBLE = 0.70 %

COMPONENT	WT %
SO3	3.18
NA	37.14
NA2O	0.0
K	0.75
K2O	0.03
MGO	0.54
CAO	0.79
SIO2	0.34
FE2O3	0.03
AL2O3	0.05
CL	57.00
WEIGHT LOSS ON HEATING	
70	0.14
350-450	0.44

TOTAL	100.43

MAJOR: HAL
MINOR: POLY
TRACE: LEON, CHLOR, KFELD, FEOX

TOTAL ANALYSIS

HOLE # 7
DEPTH = 1954.0 FEET

SOLUBLE = 97.46 %
INSOLUBLE = 2.54 %

COMPONENT	WT %
SO3	0.73
NA	37.94
NA2O	0.0
K	0.18
K2O	0.06
MGO	0.56
CAO	0.52
SIO2	1.34
FE2O3	0.09
AL2O3	0.23
CL	58.38
WEIGHT LOSS ON HEATING	
70	0.32
350-400	0.09
TOTAL	100.44

MAJOR: HAL
MINOR: POLY
TRACE: ANH, CHLOR, KFELD, TALC, FEOX

TOTAL ANALYSIS

HOLE # 7
DEPTH = 1957.5 FEET

SOLUBLE = 99.16 %
INSOLUBLE = 0.84 %

COMPONENT	WT %
SO_3	1.72
NA	38.38
NA_2O	0.0
K	0.36
K_2O	0.01
MGO	0.41
CAO	2.18
SIO_2	0.37
FE_2O_3	0.04
AL_2O_3	0.11
CL	59.00
WEIGHT LOSS ON HEATING	
70	0.20
300-400	0.12
TOTAL	102.90

MAJOR: HAL
MINOR: ANH
TRACE: POLY, CHLOR, KFELD, FEOX

TOTAL ANALYSIS

HOLE # 7
DEPTH = 1961.0 FEET

SOLUBLE = 99.10 %
INSOLUBLE = 0.90 %

COMPONENT	WT %
SO3	0.49
NA	39.14
NA2O	0.0
K	0.21
K2O	0.01
MGO	0.25
CAO	0.19
SIO2	0.42
FE2O3	0.04
AL2O3	0.08
CL	58.83
WEIGHT LOSS ON HEATING	
70	0.07
100	0.16
150-200	0.16
TOTAL	100.05

MAJOR: HAL
MINOR: POLY
TRACE: CHLOR, KFELD, TALC, QTZ, FEOX

TOTAL ANALYSIS

HOLE #   7
DEPTH = 1967.0 FEET

SOLUBLE =   99.94 %
INSOLUBLE =   0.06 %

COMPONENT	WT %
SO3	3.03
NA	39.58
NA2O	0.0
K	0.90
K2O	0.0
MGO	0.23
CAO	0.94
SIO2	0.0
FE2O3	0.01
AL2O3	0.0
CL	58.74
WEIGHT LOSS ON HEATING	
70	0.20
300-350	0.28
450-500	0.65
TOTAL	104.62

MAJOR: HAL
MINOR: POLY
TRACE: FEOX

TOTAL ANALYSIS

HOLE # 7
DEPTH = 1969.0 FEET

SOLUBLE = 98.05 %
INSOLUBLE = 1.95 %

COMPONENT	WT %
SO3	0.32
NA	38.76
NA2O	0.0
K	0.08
K2O	0.0
MGO	0.22
CAO	0.08
SIO2	0.15
FE2O3	0.02
AL2O3	0.04
CL	60.60
WEIGHT LOSS ON HEATING	
70	0.43
100	0.08
400-500	0.20
TOTAL	100.98

MAJOR: HAL
MINOR:
TRACE: ANH, KAIN, CHLOR, TALC, QTZ, FEOX

TOTAL ANALYSIS

HOLE # 7
DEPTH = 1973.0 FEET

SOLUBLE = 98.63 %
INSOLUBLE = 1.37 %

COMPONENT	WT %
SO3	0.26
NA	38.46
NA2O	0.0
K	0.06
K2O	0.03
MGO	0.53
CAO	0.07
SIO2	0.66
FE2O3	0.01
AL2O3	0.13
CL	59.58
WEIGHT LOSS ON HEATING	
70	0.19
170	0.07
380	0.02
450+	0.12
TOTAL	100.19

MAJOR: HAL
MINOR: POLY, KIES
TRACE: KAIN, CHLOR, FKELD, TALC, QTZ, FEOX

TOTAL ANALYSIS

HOLE # 7
DEPTH = 1975.0 FEET

SOLUBLE = 99.93 %
INSOLUBLE = 0.07 %

COMPONENT	WT %
SO3	0.19
NA	38.93
NA2O	0.0
K	0.06
K2O	0.0
MGO	0.07
CAO	0.09
SIO2	0.0
FE2O3	0.0
AL2O3	0.0
CL	60.38
WEIGHT LOSS ON HEATING	
70	0.17
400-500	0.07

TOTAL	100.03

MAJOR: HAL
MINOR:
TRACE: ANH, KAIN

TOTAL ANALYSIS

HOLE # 7
DEPTH = 1978.5 FEET

SOLUBLE = 91.07 %
INSOLUBLE = 8.93 %

COMPONENT	WT %
SO3	2.82
NA	32.52
NA2O	1.96
K	0.44
K2O	0.13
MGO	2.62
CAO	0.98
SIO2	2.89
FE2O3	0.37
AL2O3	1.06
CL	51.89
WEIGHT LOSS ON HEATING	
70	0.36
200	0.04
300-400	0.17
450-550	1.10
TOTAL	99.35

MAJOR: HAL
MINOR: POLY, CHLOR
TRACE: ANH, LANG, BLOED, FEOX

TOTAL ANALYSIS

HOLE #   7
DEPTH =   1983.0   FEET

SOLUBLE = 100.00   %
INSOLUBLE =   0.0   %

COMPONENT	WT %
SO3	1.11
NA	36.00
NA2O	0.0
K	0.61
K2O	0.0
MGO	0.40
CAO	0.46
SIO2	0.01
FE2O3	0.0
AL2O3	0.0
CL	59.20
WEIGHT LOSS ON HEATING	
70	0.29
125	0.03
275	0.05
350-400	0.14
TOTAL	98.30

MAJOR: HAL
MINOR: DOLY, KAIN
TRACE: QTZ

TOTAL ANALYSIS

HOLE # 7
DEPTH = 1986.5 FEET

SOLUBLE = 99.71 %
INSOLUBLE = 0.29 %

COMPONENT	WT %
SO3	0.17
NA	38.20
NA2O	0.0
K	0.04
K2O	0.0
MGO	0.03
CAO	0.21
SIO2	0.01
FE2O3	0.0
AL2O3	0.0
CL	60.66
WEIGHT LOSS ON HEATING	
70	0.10
TO 500	0.0
TOTAL	99.71

MAJOR: HAL
MINOR: ANH, POLY
TRACE: KAIN, QTZ

TOTAL ANALYSIS

HOLE #   7
DEPTH = 1993.5 FEET

SOLUBLE =   99.55 %
INSOLUBLE =   0.45 %

COMPONENT	WT %
SO3	2.96
NA	38.25
NA2O	0.0
K	1.68
K2O	0.0
MGO	0.79
CAO	2.30
SIO2	0.0
FE2O3	0.0
AL2O3	0.0
CL	53.81
WEIGHT LOSS ON HEATING	
70	0.19
100	0.05
350-400	0.80
TOTAL	101.28

MAJOR: HAL
MINOR: POLY
TRACE:

TOTAL ANALYSIS

HOLE #   7
DEPTH = 2537.0 FEET

SOLUBLE =   91.43 %
INSOLUBLE =   8.57 %

COMPONENT	WT %
SO3	46.62
NA	0.93
NA2O	4.93
K	0.90
K2O	0.0
MGO	13.02
CAO	4.37
SIO2	13.98
FE2O3	1.13
AL2O3	3.26
CL	2.63
WEIGHT LOSS ON HEATING	
70	0.47
100	0.09
TO 500	0.0
HI TEMP	8.68
TOTAL	109.58

MAJOR: ANH
MINOR: HAL, KIES
TRACE: BLOED, FEOX

TOTAL ANALYSIS

HOLE # 7
DEPTH = 2703.0 FEET

SOLUBLE = 98.97 %
INSOLUBLE = 1.03 %

COMPONENT	WT %
SO_3	1.46
NA	38.36
NA_2O	0.0
K	0.02
K_2O	0.01
MGO	0.26
CAO	0.79
SIO_2	0.25
FE_2O_3	0.06
AL_2O_3	0.05
CL	58.89
WEIGHT LOSS ON HEATING	
70	0.24
150	0.03
550	0.12

TOTAL	100.54

MAJOR: HAL
MINOR: ANH
TRACE: POLY, CHLOR, KFELD, TALC, FEOX

TOTAL ANALYSIS

HOLE # 7
DEPTH = 2716.3 FEET

SOLUBLE = 99.63 %
INSOLUBLE = 0.37 %

COMPONENT	WT %
SO3	0.44
NA	39.44
NA2O	0.0
K	0.01
K2O	0.0
MGO	0.01
CAO	0.18
SIO2	0.01
FE2O3	0.0
AL2O3	0.0
CL	61.00
WEIGHT LOSS ON HEATING	
70	0.22
350	0.04
TOTAL	101.72

MAJOR: HAL
MINOR: ANH
TRACE: POLY, TALC

TOTAL ANALYSIS

HOLE # 7
DEPTH = 2736.0 FEET

SOLUBLE = 99.67 %
INSOLUBLE = 0.33 %

COMPONENT	WT %
SO3	0.42
NA	39.75
NA2O	0.0
K	0.01
K2O	0.0
MGO	0.06
CAO	0.51
SIO2	0.01
FE2O3	0.0
AL2O3	0.0
CL	59.88
WEIGHT LOSS ON HEATING	
70	0.08
TO 450	0.03
TOTAL	101.08

MAJOR: HAL
MINOR: ANH
TRACE:

TOTAL ANALYSIS

HOLE # 8
DEPTH = 1391.5 FEET

SOLUBLE = 98.99 %
INSOLUBLE = 1.01 %

COMPONENT	WT %
SO3	1.14
NA	39.34
NA2O	0.0
K	0.31
K2O	0.02
MGO	0.27
CAO	0.53
SIO2	0.40
FE2O3	0.27
AL2O3	0.10
CL	58.07
WEIGHT LOSS ON HEATING	
70	0.04
110	0.03
350-400	0.19
TOTAL	100.71

MAJOR: HAL
MINOR: POLY
TRACE: CHLOR, ILL, QTZ, FLUX

TOTAL ANALYSIS

HOLE # 8
DEPTH = 1495.3 FEET

SOLUBLE = 99.83 %
INSOLUBLE = 0.17 %

COMPONENT	WT %
SO3	1.12
NA	38.00
NA2O	0.0
K	0.12
K2O	0.0
MGO	0.13
CAO	1.62
SIO2	0.01
FE2O3	0.0
AL2O3	0.0
CL	59.97
WEIGHT LOSS ON HEATING	
70	0.05
200	0.03
TOTAL	101.22

MAJOR: HAL
MINOR:
TRACE: CARN

TOTAL ANALYSIS

HOLE #   8
DEPTH = 1573.0 FEET

SOLUBLE =   97.72 %
INSOLUBLE =   2.28 %

COMPONENT	WT %
SO3	5.11
NA	34.63
NA2O	0.0
K	0.18
K2O	0.02
MGO	1.71
CAO	0.45
SIO2	0.02
FE2O3	0.0
AL2O3	0.01
CL	54.11
WEIGHT LOSS ON HEATING	
70	0.04
100	0.20
160	0.09
350-450	0.85
TOTAL	97.42

MAJOR: HAL
MINOR: (?) POLY, KIES
TRACE: (?) ILL

TOTAL ANALYSIS

HOLE #   8
DEPTH =   1652.0   FEET

SOLUBLE =   48.61 %
INSOLUBLE =   51.39 %

COMPONENT	WT %
SO3	51.04
NA	4.07
NA2O	4.24
K	18.59
K2O	0.99
MGO	4.58
CAO	3.93
SIO2	0.35
FE2O3	0.07
AL2O3	0.04
CL	7.35
WEIGHT LOSS ON HEATING	
70	0.09
300+	4.43
TOTAL	99.77

MAJOR: HAL
MINOR: POLY-(?) SYL, LEON, GLAS
TRACE: ILL, QTZ, FEOX

TOTAL ANALYSIS

HOLE #   8
DEPTH = 1705.0 FEET

SOLUBLE   =   99.71 %
INSOLUBLE =   0.29 %

COMPONENT	WT %
SO3	1.18
NA	38.79
NA2O	0.0
K	0.35
K2O	0.0
MGO	0.17
CAO	0.44
SIO2	0.01
FE2O3	0.0
AL2O3	0.0
CL	58.64
WEIGHT LOSS ON HEATING	
70	0.15
170	0.02
400-500	0.15
TOTAL	100.19

MAJOR: HAL
MINOR:
TRACE: POLY

TOTAL ANALYSIS

HOLE #   8
DEPTH =   1770.0   FEET

SOLUBLE =   98.79 %
INSOLUBLE =   1.21 %

COMPONENT	WT %
SO3	1.95
NA	35.75
NA2O	0.33
K	0.56
K2O	0.02
MGO	0.55
CAO	1.75
SIO2	0.48
FE2O3	0.0
AL2O3	0.12
CL	57.29
WEIGHT LOSS ON HEATING	
70	0.09
170	0.06
400	0.20
TOTAL	99.15

MAJOR: HAL
MINOR: ANH, KAIN
TRACE: ILL, QTZ

TOTAL ANALYSIS

HOLE # 8
DEPTH = 1787.0 FEET

SOLUBLE = 99.43 %
INSOLUBLE = 0.57 %

COMPONENT	WT %
SO3	3.01
NA	37.24
NA2O	0.0
K	0.69
K2O	0.01
MGO	0.54
CAO	0.70
SIO2	0.21
FE2O3	0.03
AL2O3	0.04
CL	58.00
WEIGHT LOSS ON HEATING	
70	0.32
100	0.04
300-400	0.23
TOTAL	101.06

MAJOR: HAL
MINOR: POLY, KAIN
TRACE: CHLOR, QTZ, FEOX

TOTAL ANALYSIS

HOLE #   8
DEPTH =   1794.5   FEET

SOLUBLE   =   75.34   %
INSOLUBLE =   24.66   %

COMPONENT	WT %
SO3	0.70
NA	29.75
NA2O	1.16
K	0.42
K2O	0.63
MGO	6.65
CAO	0.04
SIO2	7.80
FE2O3	0.46
AL2O3	1.91
CL	45.14

WEIGHT LOSS
ON HEATING

70	0.44
150	0.27
425+	4.70
TOTAL	100.07

MAJOR: HAL
MINOR: CARN, CHLOR, KFELD, TALC, QTZ
TRACE: POLY, FEOX

TOTAL ANALYSIS

HOLE # 8
DEPTH = 1804.0 FEET

SOLUBLE = 99.74 %
INSOLUBLE = 0.26 %

COMPONENT	WT %
SO3	0.28
NA	39.43
NA2O	0.0
K	0.06
K2O	0.0
MGO	0.04
CAO	0.70
SIO2	0.01
FE2O3	0.0
AL2O3	0.0
CL	59.94
WEIGHT LOSS ON HEATING	
70	0.02
200	0.05
TOTAL	100.79

MAJOR: HAL
MINOR: ANH
TRACE: CARN

TOTAL ANALYSIS

HOLE #   8
DEPTH = 1829.0 FEET

SOLUBLE =   99.03 %
INSOLUBLE =   0.97 %

COMPONENT	WT %
SO3	0.02
NA	39.87
NA2O	0.0
K	0.05
K2O	0.02
MGO	0.29
CAO	0.01
SIO2	0.29
FE2O3	0.04
AL2O3	0.08
CL	58.81
WEIGHT LOSS ON HEATING	
70	0.16
200	0.23
TOTAL	99.87

MAJOR: HAL
MINOR:
TRACE: ANH, CARN, CHLOR, KFELD, TALC, FEOX

TOTAL ANALYSIS

```
HOLE #    8
DEPTH =  1838.0  FEET

SOLUBLE  =   97.53  %
INSOLUBLE =   2.47  %
```

COMPONENT	WT %
SO3	0.80
NA	37.58
NA2O	0.0
K	0.26
K2O	0.10
MGO	0.48
CAO	0.05
SIO2	0.13
FE2O3	0.16
AL2O3	0.27
CL	58.38
WEIGHT LOSS ON HEATING	
70	0.39
TO 500	0.0
TOTAL	98.60

MAJOR: HAL
MINOR:
TRACE: POLY, SLY, LEON, CHLOR, KFELD, FEOX

TOTAL ANALYSIS

HOLE #   B
DEPTH = 1856.7 FEET

SOLUBLE =   99.96 %
INSOLUBLE =   0.04 %

COMPONENT	WT %
SO3	2.70
NA	36.08
NA2O	0.0
K	1.62
K2O	0.0
MGO	0.03
CAO	1.56
SIO2	0.0
FE2O3	0.0
AL2O3	0.0
CL	56.66
WEIGHT LOSS ON HEATING	
70	0.07
350	0.03
TOTAL	98.79

MAJOR: HAL
MINOR: ANH, SYL, POLY
TRACE:

TOTAL ANALYSIS

HOLE # 8
DEPTH = 1875.0 FEET

SOLUBLE = 70.94 %
INSOLUBLE = 29.06 %

COMPONENT	WT %
SO3	0.42
NA	25.64
NA2O	0.0
K	0.31
K2O	2.28
MGO	9.55
CAO	0.63
SIO2	15.30
FE2O3	1.23
AL2O3	3.00
CL	40.92
WEIGHT LOSS ON HEATING	
70	0.22
125-200	0.42
TOTAL	99.92

MAJOR: HAL
MINOR: CARN, KFELD, TALC
TRACE: POLY, CHLOR

TOTAL ANALYSIS

HOLE #   8
DEPTH = 1884.0 FEET

SOLUBLE =   80.58 %
INSOLUBLE =   19.42 %

COMPONENT	WT %
SO3	3.76
NA	27.10
NA2O	0.0
K	6.98
K2O	1.80
MGO	5.09
CAO	1.66
SIO2	9.02
FE2O3	0.60
AL2O3	1.99
CL	44.06
WEIGHT LOSS ON HEATING	
70	0.36
350-400	0.44
TOTAL	102.86

MAJOR: HAL
MINOR: ANH, CARN, KFELD, TALC, FEOX
TRACE: CHLOR

TOTAL ANALYSIS

HOLE # 8
DEPTH = 1890.0 FEET

SOLUBLE = 99.98 %
INSOLUBLE = 0.02 %

COMPONENT	WT %
SO3	0.77
NA	38.78
NA2O	0.0
K	0.10
K2O	0.0
MGO	0.10
CAO	0.95
SIO2	0.0
FE2O3	0.0
AL2O3	0.0
CL	59.33
WEIGHT LOSS ON HEATING	
70	0.05
300-400	0.08
TOTAL	100.18

MAJOR: HAL
MINOR:
TRACE: ANH, CARN

TOTAL ANALYSIS

HOLE #   8
DEPTH =   1894.3 FEET

SOLUBLE   =   95.43 %
INSOLUBLE =   4.57 %

COMPONENT	WT %
SO3	0.12
NA	37.90
NA2O	0.0
K	0.06
K2O	0.13
MGO	0.74
CAO	0.03
SIO2	2.43
FE2O3	0.20
AL2O3	0.43
CL	57.78
WEIGHT LOSS ON HEATING	
70	0.30
TO 500	0.0
TOTAL	100.12

MAJOR: HAL
MINOR: QTZ
TRACE: ANH, CARN, CHLOR, KFELD, TALC, FEOX

TOTAL ANALYSIS

HOLE #   8
DEPTH = 1898.5 FEET

SOLUBLE =   98.53 %
INSOLUBLE =   1.47 %

COMPONENT	WT %
SO3	0.55
NA	38.81
NA2O	0.71
K	0.07
K2O	0.01
MGO	0.26
CAO	0.12
SIO2	0.45
FE2O3	0.02
AL2O3	0.07
CL	57.97
WEIGHT LOSS ON HEATING	
70	0.16
TO 500	0.0
TOTAL	99.20

MAJOR: HAL
MINOR:
TRACE: POLY, BLOED, CHLOR, TALC, FEOX

TOTAL ANALYSIS

HOLE #   8
DEPTH =   1900.0 FEET

SOLUBLE   =   99.96 %
INSOLUBLE =   0.04 %

COMPONENT	WT %
SO3	3.20
NA	38.14
NA2O	0.0
K	0.98
K2O	0.0
MGO	0.47
CAO	0.39
SIO2	0.0
FE2O3	0.0
AL2O3	0.0
CL	57.60
WEIGHT LOSS ON HEATING	
70	0.17
300-400	0.64

TOTAL	101.63

MAJOR: HAL
MINOR: LEON
TRACE: POLY

TOTAL ANALYSIS

HOLE #   8
DEPTH = 1905.0 FEET

SOLUBLE =   96.98 %
INSOLUBLE =   3.02 %

COMPONENT	WT %
SO3	0.20
NA	38.67
NA2O	0.0
K	0.13
K2O	0.03
MGO	0.93
CAO	0.45
SIO2	0.91
FE2O3	0.14
AL2O3	0.25
CL	57.91
WEIGHT LOSS ON HEATING	
70	0.36
375	0.26
TOTAL	100.24

MAJOR: HAL
MINOR:
TRACE: POLY, CHLOR, KFELD, TALC

TOTAL ANALYSIS

HOLE #   8
DEPTH = 1910.0 FEET

SOLUBLE =   99.02 %
INSOLUBLE =   0.98 %

COMPONENT	WT %
SO3	0.53
NA	39.64
NA2O	0.0
K	0.0
K2O	0.30
MGO	0.31
CAO	0.44
SIO2	0.34
FE2O3	0.04
AL2O3	0.08
CL	59.04
WEIGHT LOSS ON HEATING	
70	0.06
375	0.04
TOTAL	100.82

MAJOR: HAL
MINOR: POLY
TRACE: ANH, CHLOR, KFELD, TALC, QTZ, FEOX

TOTAL ANALYSIS

HOLE # 8
DEPTH = 1913.1 FEET

SOLUBLE = 97.71 %
INSOLUBLE = 2.29 %

COMPONENT	WT %
SO3	0.06
NA	38.48
NA2O	0.0
K	0.06
K2O	0.05
MGO	0.55
CAO	0.01
SIO2	0.91
FE2O3	0.13
AL2O3	0.21
CL	59.27

WEIGHT LOSS
ON HEATING

70	0.11
120	0.03
260	0.03
400+	0.04
TOTAL	99.94

MAJOR: HAL
MINOR:
TRACE: KAIN, CHLOR, KFELD, TALC, QTZ, FEOX

TOTAL ANALYSIS

HOLE #   8
DEPTH =   1916.2 FEET

SOLUBLE =   99.85 %
INSOLUBLE =   0.15 %

COMPONENT	WT %
SO_3	0.92
NA	36.48
NA_2O	0.0
K	0.21
K_2O	0.0
MGO	0.13
CAO	0.44
SIO_2	0.0
FE_2O_3	0.0
AL_2O_3	0.0
CL	57.71
WEIGHT LOSS ON HEATING	
70	0.13
250	0.02
350-400	0.10
TOTAL	98.29

MAJOR: HAL
MINOR: POLY
TRACE: ANH

TOTAL ANALYSIS

HOLE # 8
DEPTH = 1923.0 FEET

SOLUBLE = 98.30 %
INSOLUBLE = 1.70 %

COMPONENT	WT %
SO3	1.06
NA	38.03
NA2O	0.0
K	0.05
K2O	0.08
MGO	0.09
CAO	0.20
SIO2	0.60
FE2O3	0.10
AL2O3	0.16
CL	58.43
WEIGHT LOSS ON HEATING	
70	0.19
300	0.06
450+	0.24
TOTAL	99.29

MAJOR: HAL
MINOR: POLY
TRACE: KAIN, CHLOR, ILL, KFELD, QTZ, FEOX

TOTAL ANALYSIS

HOLE #   8
DEPTH = 1930.0 FEET

SOLUBLE =   98.99 %
INSOLUBLE =   1.01 %

COMPONENT	WT %
SO3	2.81
NA	35.71
NA2O	0.08
K	1.03
K2O	0.01
MGO	0.46
CAO	0.20
SIO2	0.18
FE2O3	0.07
AL2O3	0.04
CL	56.74
WEIGHT LOSS ON HEATING	
70	0.05
350-400	0.42
TOTAL	97.80

MAJOR: HAL
MINOR: POLY
TRACE: LEON, CHLOR, KFELD, TALC, FEOX

TOTAL ANALYSIS

```
HOLE #     8
DEPTH =  1933.0  FEET

SOLUBLE   =   99.62 %
INSOLUBLE =    0.38 %
```

COMPONENT	WT %
SO_3	0.78
NA	38.03
NA_2O	0.0
K	0.15
K_2O	0.0
MGO	0.09
CAO	0.65
SIO_2	0.01
FE_2O_3	0.01
AL_2O_3	0.0
CL	59.81
WEIGHT LOSS ON HEATING	
70	0.19
200	0.09
TOTAL	100.19

```
MAJOR:  HAL
MINOR:  ANH, POLY, KAIN
TRACE:  QTZ, FEOX
```

TOTAL ANALYSIS

HOLE #   8
DEPTH = 1938.0 FEET

SOLUBLE =   99.86 %
INSOLUBLE =   0.14 %

COMPONENT	WT %
SO3	2.91
NA	35.63
NA2O	0.0
K	0.68
K2O	0.0
MGO	0.84
CAO	1.02
SIO2	0.0
FE2O3	0.0
AL2O3	0.0
CL	59.45
WEIGHT LOSS ON HEATING	
70	0.13
125	0.14
275	0.05
350-400	0.17
TOTAL	101.16

MAJOR: HAL
MINOR: POLY, KAIN
TRACE:

TOTAL ANALYSIS

HOLE # 8
DEPTH = 1953.2 FEET

SOLUBLE = 99.91 %
INSOLUBLE = 0.09 %

COMPONENT	WT %
SO3	2.30
NA	39.50
NA2O	0.0
K	0.30
K2O	0.0
MGO	0.42
CAO	1.23
SIO2	0.01
FE2O3	0.0
AL2O3	0.0
CL	57.63
WEIGHT LOSS ON HEATING	
70	0.05
250	0.05
375	0.03
425	0.29
TOTAL	101.90

MAJOR: HAL
MINOR: ANH, POLY
TRACE: BLOED, TALC

TOTAL ANALYSIS

HOLE # 8
DEPTH = 1967.0 FEET

SOLUBLE = 95.13 %
INSOLUBLE = 4.87 %

COMPONENT	WT %
SO3	1.25
NA	35.99
NA2O	2.73
K	0.57
K2O	0.09
MGO	1.21
CAO	0.41
SIO2	0.76
FE2O3	0.10
AL2O3	0.20
CL	57.52
WEIGHT LOSS ON HEATING	
70	0.28
190	0.04
+00-500	0.20
TOTAL	101.35

MAJOR: HAL
MINOR: POLY, KAIN, TALC
TRACE: CHLOR, FEOX

TOTAL ANALYSIS

HOLE #   8
DEPTH = 1986.0 FEET

SOLUBLE   =   36.72 %
INSOLUBLE =   63.28 %

COMPONENT	WT %
SO_3	60.87
NA	0.36
NA_2O	5.83
K	0.0
K_2O	26.07
MGO	1.83
CAO	5.12
SIO_2	0.54
FE_2O_3	0.17
AL_2O_3	0.85
CL	0.15
WEIGHT LOSS ON HEATING	
70	0.07
300-400	5.81
TOTAL	107.67

MAJOR: (?) GLAS, ANH, LEON
MINOR:
TRACE: HAL, FEOX

TOTAL ANALYSIS

HOLE #   8
DEPTH =   2006.0 FEET

SOLUBLE   =   99.50 %
INSOLUBLE =   0.50 %

COMPONENT	WT %
SO3	2.37
NA	37.59
NA2O	0.0
K	1.03
K2O	0.0
MGO	0.31
CAO	0.06
SIO2	0.01
FE2O3	0.0
AL2O3	0.0
CL	57.17
WEIGHT LOSS ON HEATING	
70	0.20
350-400	0.29
450	0.13
475	0.04
TOTAL	99.70

MAJOR: HAL
MINOR: KAIN, BLOED
TRACE: POLY, QTZ

TOTAL ANALYSIS

HOLE # 8
DEPTH = 2017.0 FEET

SOLUBLE = 95.20 %
INSOLUBLE = 4.80 %

COMPONENT	WT %
SO3	0.62
NA	35.66
NA2O	0.0
K	0.06
K2O	0.04
MGO	0.53
CAO	1.02
SIO2	2.02
FE2O3	0.28
AL2O3	0.70
CL	57.09
WEIGHT LOSS ON HEATING	
70	0.22
100	0.02
300-400	0.17
ORGANIC	1.59
TOTAL	100.02

MAJOR: HAL
MINOR: ANH
TRACE: SYL, CAIN, CHLOR, FEOX, ILL

```
                TOTAL ANALYSIS
                ----------------


             HOLE #   8
             DEPTH =  2039.0  FEET

             SOLUBLE =   98.94  %
             INSOLUBLE =  1.06  %

                ----------------


             COMPONENT              WT %
             ----------            ------

               SO3                  5.50

               NA                  35.02

               NA2O                 0.0

               K                    1.56

               K2O                  0.03

               MGO                  0.70

               CAO                  1.58

               SIO2                 0.27

               FE2O3                0.07

               AL2O3                0.05

               CL                  54.01

             WEIGHT LOSS
             ON HEATING

                     70             0.21

                    100             0.05

                300-400             0.49

                    425             0.27

                                  ------

               TOTAL               99.81


         MAJOR:  HAL
         MINOR:  POLY, KAIN
         TRACE:  KFELD, TALC, FEOX
```

TOTAL ANALYSIS

```
    HOLE # =   8
    DEPTH  =  2050.0  FEET

    SOLUBLE   =  28.61  %
    INSOLUBLE =  71.39  %
```

COMPONENT	WT %
SO3	54.99
NA	8.00
NA2O	4.90
K	0.05
K2O	0.04
MGO	0.31
CAO	7.10
SIO2	0.33
FE2O3	0.0
AL2O3	0.0
CL	12.44
WEIGHT LOSS ON HEATING	
70	0.11
475	0.68
TOTAL	88.95

```
MAJOR:  ANH
MINOR:  HAL
TRACE:  QTZ
```

TOTAL ANALYSIS

HOLE # 8
DEPTH = 2068.0 FEET

SOLUBLE = 98.84 %
INSOLUBLE = 1.16 %

COMPONENT	WT %
SO3	2.49
NA	37.41
NA2O	0.0
K	0.08
K2O	0.01
MGO	0.31
CAO	0.89
SIO2	0.38
FE2O3	0.05
AL2O3	0.07
CL	55.99
WEIGHT LOSS ON HEATING	
70	0.04
250	0.10
TOTAL	97.82

MAJOR: HAL
MINOR: ANH, TALC, BLOED
TRACE: POLY, CHLOR, FEOX

TOTAL ANALYSIS

```
HOLE #    8
DEPTH =  2084.0  FEET

SOLUBLE   =   92.00  %
INSOLUBLE =    8.00  %
```

COMPONENT	WT %
SO3	2.64
NA	34.46
NA2O	1.87
K	1.02
K2O	0.19
MGO	1.48
CAO	0.73
SIO2	2.07
FE2O3	0.25
AL2O3	0.37
CL	52.19
WEIGHT LOSS ON HEATING	
70	0.17
140	0.05
350-400	0.27
450-550	0.22
TOTAL	97.98

```
MAJOR:  HAL
MINOR:  CHLOR, TALC, QTZ
TRACE:  KFELD, FEOX
```

TOTAL ANALYSIS

HOLE #   8
DEPTH = 2130.0 FEET

SOLUBLE =   99.61 %
INSOLUBLE =   0.39 %

COMPONENT	WT %
SO3	2.31
NA	37.79
NA2O	0.0
K	0.42
K2O	0.0
MGO	0.25
CAO	0.75
SIO2	0.03
FE2O3	0.0
AL2O3	0.0
CL	57.16
WEIGHT LOSS ON HEATING	
70	0.11
125	0.07
350-400	0.10
TOTAL	99.38

MAJOR: HAL
MINOR: POLY
TRACE: ANH, QTZ

TOTAL ANALYSIS

HOLE # 8
DEPTH = 2162.0 FEET

SOLUBLE = 98.90 %
INSOLUBLE = 1.10 %

COMPONENT	WT %
SO3	1.56
NA	36.77
NA2O	0.55
K	1.23
K2O	0.03
MGO	0.65
CAO	0.93
SIO2	0.23
FE2O3	0.06
AL2O3	0.05
CL	59.99
WEIGHT LOSS ON HEATING	
70	0.14
300-400	0.48
TOTAL	102.67

MAJOR: HAL
MINOR: ANH, POLY, SYL
TRACE: KFELD, TALC, FEOX

TOTAL ANALYSIS

HOLE #   8
DEPTH =   2217.0   FEET

SOLUBLE =   99.78 %
INSOLUBLE =   0.22 %

COMPONENT	WT %
SO3	0.0
NA	39.14
NA2O	0.0
K	0.07
K2O	0.0
MGO	0.02
CAO	0.12
SIO2	0.01
FE2O3	0.0
AL2O3	0.0
CL	59.75
WEIGHT LOSS ON HEATING	
70	0.04
300-400	0.40
TOTAL	99.77

MAJOR: HAL
MINOR:
TRACE: ANH, POLY, SLY, QTZ

TOTAL ANALYSIS

HOLE #   8
DEPTH = 2280.0 FEET

SOLUBLE = 100.00   %
INSOLUBLE =   0.0   %

COMPONENT	WT %
SO3	0.39
NA	37.91
NA2O	0.0
K	0.12
K2O	0.0
MGO	0.09
CAO	0.25
SIO2	0.02
FE2O3	0.0
AL2O3	0.0
CL	60.23
WEIGHT LOSS ON HEATING	
70	0.19
350	0.08
TOTAL	99.28

MAJOR: HAL
MINOR: ANH, CARN
TRACE: POLY, QTZ

TOTAL ANALYSIS

```
HOLE #    8
DEPTH =  2326.0  FEET

SOLUBLE  =    95.44 %
INSOLUBLE =    4.56 %
```

COMPONENT	WT %
SO3	0.18
NA	37.83
NA2O	0.0
K	0.06
K2O	0.03
MGO	1.39
CAO	0.17
SIO2	1.15
FE2O3	0.12
AL2O3	0.25
CL	57.93
WEIGHT LOSS ON HEATING	
70	0.11
100-150	0.03
450+ MIN	0.56
TOTAL	99.81

```
MAJOR:  HAL
MINOR:  TALC
TRACE:  HAL, CARN, CHLOR, FLUX
```

TOTAL ANALYSIS

HOLE #   8
DEPTH = 2366.3 FEET

SOLUBLE =   31.37 %
INSOLUBLE =   68.63 %

COMPONENT	WT %
SO3	47.32
NA	0.62
NA2O	3.76
K	0.0
K2O	10.67
MGO	6.40
CAO	3.37
SIO2	10.68
FE2O3	0.01
AL2O3	1.57
CL	1.17
WEIGHT LOSS ON HEATING	
70	0.43
200-375	4.81
375-500	1.60

TOTAL	92.41

MAJOR:
MINOR: KAIN, KFELD, TALC, QTZ
TRACE: HAL, SYL

TOTAL ANALYSIS

HOLE #   8
DEPTH =   2427.5 FEET

SOLUBLE =   99.36 %
INSOLUBLE =   0.64 %

COMPONENT	WT %
SO3	2.58
NA	39.42
NA2O	0.0
K	0.01
K2O	0.01
MGO	0.05
CAO	0.35
SIO2	0.10
FE2O3	0.01
AL2O3	0.01
CL	59.88
WEIGHT LOSS ON HEATING	
70	0.03
300-400	0.40
TOTAL	102.85

MAJOR: HAL
MINOR: ANH
TRACE: POLY, BLOED, KFELD, TALC, QTZ, FEOX

TOTAL ANALYSIS

HOLE #   8
DEPTH =   2460.0 FEET

SOLUBLE =   99.21 %
INSOLUBLE =   0.79 %

COMPONENT	WT %
SO3	1.14
NA	38.75
NA2O	0.0
K	0.03
K2O	0.01
MGO	0.20
CAO	0.62
SIO2	0.19
FE2O3	0.03
AL2O3	0.06
CL	57.00

WEIGHT LOSS
ON HEATING

70	0.17
125	0.05
350	0.08
450	0.07

TOTAL	98.40

MAJOR: HAL
MINOR: ANH
TRACE: KAIN, CHLOR, KFELD, TALC, FEOX

TOTAL ANALYSIS

HOLE # 8
DEPTH = 2519.6 FEET

SOLUBLE = 99.36 %
INSOLUBLE = 0.64 %

COMPONENT	WT %
SO3	0.17
NA	40.42
NA2O	0.0
K	0.02
K2O	0.0
MGO	0.01
CAO	0.03
SIO2	0.0
FE2O3	0.0
AL2O3	0.0
CL	60.31
WEIGHT LOSS ON HEATING	
70	0.08
480	0.06
TOTAL	101.74

MAJOR: HAL
MINOR:
TRACE: POLY

TOTAL ANALYSIS

HOLE # 8
DEPTH = 2563.0 FEET

SOLUBLE = 7.11 %
INSOLUBLE = 92.89 %

COMPONENT	WT %
SO3	40.59
NA	1.47
NA2O	6.06
K	0.05
K2O	0.54
MGO	14.73
CAO	24.37
SIO2	6.25
FE2O3	0.96
AL2O3	1.86
CL	1.05
WEIGHT LOSS ON HEATING	
70	1.87
100-150	0.19
175	0.07
450+ MIN	0.11
TOTAL	100.17

MAJOR: ANH
MINOR: CHLOR, KFELD, TALC, FEOX
TRACE: HAL, LANG

TOTAL ANALYSIS

HOLE #   8
DEPTH = 2615.5 FEET

SOLUBLE   =   99.74 %
INSOLUBLE =   0.26 %

COMPONENT	WT %
SO3	0.86
NA	38.58
NA2O	0.0
K	0.05
K2O	0.0
MGO	0.02
CAO	0.58
SIO2	0.0
FE2O3	0.01
AL2O3	0.0
CL	59.37
WEIGHT LOSS ON HEATING	
70	0.21
300-350	0.06
TOTAL	100.00

MAJOR: HAL
MINOR: ANH
TRACE: POLY, FEOX

TOTAL ANALYSIS

HOLE # 8
DEPTH = 2665.5 FEET

SOLUBLE = 99.08 %
INSOLUBLE = 0.92 %

COMPONENT	WT %
SO_3	0.98
NA	38.68
NA_2O	0.0
K	0.02
K_2O	0.01
MGO	0.22
CAO	0.35
SIO_2	0.23
FE_2O_3	0.04
AL_2O_3	0.06
CL	59.14
WEIGHT LOSS ON HEATING	
70	0.25
400-500	0.48
TOTAL	100.46

MAJOR: HAL
MINOR: ANH, CHLOR
TRACE: POLY, KFELD, TALC, FEOX

TOTAL ANALYSIS

HOLE # 8
DEPTH = 2706.0 FEET

SOLUBLE = 98.75 %
INSOLUBLE = 1.25 %

COMPONENT	WT %
SO3	1.13
NA	37.09
NA2O	0.64
K	0.03
K2O	0.03
MGO	0.19
CAO	0.68
SIO2	0.27
FE2O3	0.27
AL2O3	0.07
CL	58.60
WEIGHT LOSS ON HEATING	
70	0.16
300	0.05
380	0.75
400+	0.70
TOTAL	100.66

MAJOR: HAL
MINOR: ANH
TRACE: POLY, CHLOR, KFELD, TALC, FEOX

TOTAL ANALYSIS

HOLE #   8
DEPTH = 2758.0 FEET

SOLUBLE =   99.22 %
INSOLUBLE =   0.78 %

COMPONENT	WT %
SO3	1.70
NA	37.20
NA2O	0.83
K	0.08
K2O	0.01
MGO	0.18
CAO	1.14
SIO2	0.06
FE2O3	0.01
AL2O3	0.02
CL	58.07
WEIGHT LOSS ON HEATING	
70	0.11
250	0.05
TOTAL	99.46

MAJOR: HAL
MINOR: ANH
TRACE: POLY, CHLOR, KFELD, TALC, FEOX

TOTAL ANALYSIS

HOLE # 8
DEPTH = 2779.0 FEET

SOLUBLE = 99.62 %
INSOLUBLE = 0.38 %

COMPONENT	WT %
SO_3	1.09
NA	37.41
NA_2O	0.0
K	0.01
K_2O	0.0
MGO	0.03
CAO	1.80
SIO_2	0.0
FE_2O_3	0.0
AL_2O_3	0.0
CL	58.53
WEIGHT LOSS ON HEATING	
70	0.21
HI TEMP	0.0
TOTAL	99.46

MAJOR: HAL
MINOR: CARN, ANH
TRACE:

TOTAL ANALYSIS

HOLE # 8
DEPTH = 2794.0 FEET

SOLUBLE = 99.79 %
INSOLUBLE = 0.21 %

COMPONENT	WT %
SO3	0.99
NA	37.86
NA2O	0.0
K	0.02
K2O	0.0
MGO	0.01
CAO	0.68
SIO2	0.0
FE2O3	0.0
AL2O3	0.0
CL	60.58
WEIGHT LOSS ON HEATING	
70	0.18
HI TEMP	0.0
TOTAL	100.53

MAJOR: HAL
MINOR: ANH
TRACE: POLY

TOTAL ANALYSIS

HOLE #   8
DEPTH = 2802.5 FEET

SOLUBLE =   99.55 %
INSOLUBLE =   0.45 %

COMPONENT	WT %
SO3	1.76
NA	38.39
NA20	0.0
K	0.02
K20	0.0
MGO	0.01
CAO	0.22
SIO2	0.0
FE203	0.0
AL203	0.0
CL	58.19
WEIGHT LOSS ON HEATING	
70	0.10
170	0.02
375	0.02

TOTAL	99.16

MAJOR: HAL
MINOR: ANH
TRACE: BLOED, POLY

TOTAL ANALYSIS

HOLE #   8
DEPTH = 2809.0 FEET

SOLUBLE   =   99.09 %
INSOLUBLE =   0.91 %

COMPONENT	WT %
SO3	2.02
NA	38.56
NA2O	0.0
K	0.01
K2O	0.01
MGO	0.04
CAO	1.09
SIO2	0.04
FE2O3	0.0
AL2O3	0.01
CL	59.70
WEIGHT LOSS ON HEATING	
70	0.15
150-200	0.09
400	0.24
TOTAL	101.56

MAJOR: HAL
MINOR: ANH
TRACE: POLY, BLOED, POLY, KFELD, QTZ

TOTAL ANALYSIS

HOLE #   8
DEPTH = 2820.5 FEET

SOLUBLE   =   99.46 %
INSOLUBLE =   0.54 %

COMPONENT	WT %
SO3	1.67
NA	38.42
NA2O	0.0
K	0.01
K2O	0.0
MGO	0.03
CAO	0.29
SIO2	0.06
FE2O3	0.0
AL2O3	0.0
CL	58.50
WEIGHT LOSS ON HEATING	
70	0.18
400+	0.18
TOTAL	99.34

MAJOR: HAL
MINOR: THEN, ANH
TRACE: POLY, TALC

TOTAL ANALYSIS

HOLE #   8
DEPTH = 2879.0 FEET

SOLUBLE =   96.41 %
INSOLUBLE =   3.59 %

COMPONENT	WT %
SO3	4.15
NA	32.65
NA2O	0.93
K	0.02
K2O	0.01
MGO	0.13
CAO	1.54
SIO2	0.13
FE2O3	0.01
AL2O3	0.01
CL	55.79

WEIGHT LOSS
ON HEATING

70	0.06
TO 500	0.0
500+	3.31
TOTAL	98.74

MAJOR: HAL
MINOR: GLAUB, ANH
TRACE: POLY, KFELD, TALC, FEOX

TOTAL ANALYSIS

HOLE #   8
DEPTH = 2948.0 FEET

SOLUBLE =   97.32 %
INSOLUBLE =   2.68 %

COMPONENT	WT %
SO3	5.34
NA	37.30
NA2O	0.0
K	0.01
K2O	0.01
MGO	0.03
CAO	0.79
SIO2	0.06
FE2O3	0.01
AL2O3	0.0
CL	55.51
WEIGHT LOSS ON HEATING	
70	0.20
150	0.02
450	0.02
500	0.02
TOTAL	99.32

MAJOR: HAL
MINOR: GLAUB, ANH
TRACE: LANG, TALC, QTZ, FEOX

Appendix 7.B (Ref. sec. 7.3)

Whole Rock Chemical Analyses in Soluble and

Insoluble Fractions & Moles times 1000

HOLE # 7
DEPTH = 1044.2 FEET
TOTAL

COMPONENT	WT %	MOLES
SO3	0.55	6.87
NA	38.56	1677.25
NA2O	0.0	0.0
K	0.03	0.77
K2O	0.0	0.0
MGO	0.04	0.99
CAO	0.43	7.67
SIO2	0.0	0.0
FE2O3	0.0	0.0
AL2O3	0.0	0.0
CL	60.40	1703.61

HOLE # 7
DEPTH = 1107.5 FEET

SOLUBLE
69.47 WT % OF TOTAL

HOLE # 7
DEPTH = 1107.5 FEET

INSOLUBLE
30.53 WT % OF TOTAL

COMPONENT	WT %	MOLES	WT %	MOLES
SO3	9.24	115.41	11.63	145.27
NA	20.28	882.12	0.0	0.0
NA2O	0.0	0.0	6.63	106.97
K	0.0	0.0	0.0	0.0
K2O	3.70	39.28	0.77	8.17
MGO	2.24	55.57	2.33	57.80
CAO	1.61	28.71	0.23	4.10
SIO2	0.0	0.0	8.30	138.13
FE2O3	0.0	0.0	0.27	1.69
AL2O3	0.01	0.10	1.24	12.16
CL	30.78	868.26	0.0	0.0
SUBTOTAL	67.86 %		31.40 %	
MEASURED =	69.47		30.53	

```
HOLE #   7                          HOLE #   7
DEPTH =    1171.5  FEET             DEPTH =    1171.5  FEET

SOLUBLE                             INSOLUBLE
   37.10 WT % OF TOTAL                 62.90 WT % OF TOTAL
```

COMPONENT	WT %	MOLES	WT %	MOLES
SO3	1.92	23.98	37.81	472.27
NA	12.56	546.32	0.0	0.0
NA2O	0.0	0.0	0.88	14.20
K	1.91	48.85	0.0	0.0
K2O	0.0	0.0	0.0	0.0
MGO	0.47	11.66	0.23	5.71
CAO	1.65	29.42	23.48	418.69
SIO2	0.01	0.17	0.62	10.32
FE2O3	0.0	0.0	0.06	0.38
AL2O3	0.0	0.0	0.0	0.0
CL	18.87	532.30	0.0	0.0

```
SUBTOTAL    37.39  %              63.08  %
MEASURED =  37.10                62.90
```

HOLE #   7
DEPTH =   1221.0   FEET

TOTAL

COMPONENT	WT %	MOLES
SO3	2.02	25.23
NA	38.79	1687.26
NA2O	0.0	0.0
K	0.06	1.53
K2O	0.0	0.0
MGO	0.10	2.48
CAO	0.88	15.69
SIO2	0.01	0.17
FE2O3	0.0	0.0
AL2O3	0.0	0.0
CL	58.31	1644.85

```
HOLE #    7
DEPTH =    1343.0  FEET
TOTAL
```

COMPONENT	WT %	MOLES
SO3	0.99	12.37
NA	38.60	1678.99
NA2O	0.0	0.0
K	0.35	8.95
K2O	0.0	0.0
MGO	0.15	3.72
CAO	0.66	11.77
SIO2	0.01	0.17
FE2O3	0.0	0.0
AL2O3	0.0	0.0
CL	59.40	1675.60

```
HOLE #      7
DEPTH =     1402.5   FEET
TOTAL


COMPONENT          WT %          MOLES
---------          ----          -----

   SO3             0.11           1.37

   NA             39.67        1725.53

   NA2O            0.0            0.0

   K               0.06           1.53

   K2O             0.0            0.0

   MGO             0.06           1.49

   CAO             0.02           0.36

   SIO2            0.0            0.0

   FE2O3           0.0            0.0

   AL2O3           0.0            0.0

   CL             59.78        1686.32
```

	HOLE # 7 DEPTH = 1468.5 FEET SOLUBLE 93.66 WT % OF TOTAL		HOLE # 7 DEPTH = 1468.5 FEET INSOLUBLE 6.34 WT % OF TOTAL	
COMPONENT	WT %	MOLES	WT %	MOLES
SO3	0.98	12.24	1.89	23.61
NA	34.44	1498.04	0.0	0.0
NA2O	0.0	0.0	0.0	0.0
K	0.37	9.46	0.0	0.0
K2O	0.0	0.0	0.07	0.74
MGO	0.52	12.90	1.32	32.75
CAO	0.18	3.21	0.01	0.18
SIO2	0.03	0.50	2.12	35.28
FE2O3	0.0	0.0	0.24	1.50
AL2O3	0.0	0.0	0.07	0.69
CL	53.61	1512.27	0.0	0.0
SUBTOTAL	90.13 %		5.72 %	
MEASURED =	93.66		6.34	

```
HOLE #   7
DEPTH =   1534.0   FEET

TOTAL
```

COMPONENT	WT %	MOLES
SO3	1.67	20.86
NA	36.10	1570.25
NA2O	0.0	0.0
K	0.52	13.30
K2O	0.0	0.0
MGO	0.22	5.46
CAO	0.64	11.41
SIO2	0.01	0.17
FE2O3	0.0	0.0
AL2O3	0.0	0.0
CL	57.76	1629.34

HOLE #   7
DEPTH =   1615.0   FEET

SOLUBLE
    96.69 WT % OF TOTAL

HOLE #   7
DEPTH =   1615.0   FEET

INSOLUBLE
    1.31 WT % OF TOTAL

COMPONENT	WT %	MOLES	WT %	MOLES
SO3	3.58	44.72	0.98	12.24
NA	35.06	1525.01	0.0	0.0
NA2O	0.0	0.0	0.0	0.0
K	1.05	26.85	0.0	0.0
K2O	0.0	0.0	0.0	0.0
MGO	0.69	17.12	0.02	0.50
CAO	1.39	24.79	0.08	1.43
SIO2	0.03	0.50	0.21	3.49
FE2O3	0.0	0.0	0.03	0.19
AL2O3	0.0	0.0	0.07	0.69
CL	55.95	1578.28	0.0	0.0

| SUBTOTAL | 97.75 % | | 1.39 % | |
| MEASURED = | 98.69 | | 1.31 | |

HOLE # = 7 DEPTH = 1698.0 FEET

HOLE # = 7 DEPTH = 1698.0 FEET

SOLUBLE 95.35 WT % OF TOTAL

INSOLUBLE 4.65 WT % OF TOTAL

COMPONENT	WT %	MOLES	WT %	MOLES
SO3	0.58	7.24	0.0	0.0
NA	36.47	1586.34	0.0	0.0
NA2O	0.0	0.0	0.0	0.0
K	0.06	1.53	0.0	0.0
K2O	0.0	0.0	0.07	0.74
MGO	0.28	6.95	0.92	22.82
CAO	0.33	5.88	0.01	0.18
SIO2	0.04	0.67	2.03	33.78
FE2O3	0.0	0.0	0.25	1.57
AL2O3	0.0	0.0	0.61	5.98
CL	58.35	1645.98	0.0	0.0
SUBTOTAL	96.11 %		3.89 %	
MEASURED =	95.35		4.65	

HOLE # 7
DEPTH = 1755.0 FEET

TOTAL

COMPONENT	WT %	MOLES
SO3	0.65	8.12
NA	38.12	1658.11
NA2O	0.0	0.0
K	0.23	5.88
K2O	0.0	0.0
MGO	0.13	3.23
CAO	0.08	1.43
SIO2	0.02	0.33
FE2O3	0.0	0.0
AL2O3	0.0	0.0
CL	59.54	1679.55

```
HOLE #   7                              HOLE #   7
DEPTH =    1952.5  FEET                 DEPTH =    1952.5  FEET

SOLUBLE                                 INSOLUBLE
  99.30 WT % OF TOTAL                     0.70 WT % OF TOTAL
```

COMPONENT	WT %	MOLES	WT %	MOLES
SO3	3.03	37.85	0.15	1.87
NA	37.14	1615.49	0.0	0.0
NA2O	0.0	0.0	0.0	0.0
K	0.75	19.18	0.0	0.0
K2O	0.0	0.0	0.03	0.32
MGO	0.42	10.42	0.12	2.98
CAO	0.78	13.91	0.01	0.18
SIO2	0.01	0.17	0.33	5.49
FE2O3	0.01	0.06	0.02	0.13
AL2O3	0.0	0.0	0.05	0.49
CL	57.00	1607.90	0.0	0.0

```
SUBTOTAL    99.14  %                    0.71  %
MEASURED =  99.30                       0.70
```

	HOLE # 7 DEPTH = 1954.0 FEET		HOLE # 7 DEPTH = 1954.0 FEET	
	SOLUBLE 97.46 WT % OF TOTAL		INSOLUBLE 2.54 WT % OF TOTAL	
COMPONENT	WT %	MOLES	WT %	MOLES
SO3	0.73	9.12	0.0	0.0
NA	37.94	1650.28	0.0	0.0
NA2O	0.0	0.0	0.0	0.0
K	0.18	4.60	0.0	0.0
K2O	0.0	0.0	0.06	0.64
MGO	0.17	4.22	0.39	9.68
CAO	0.51	9.09	0.01	0.18
SIO2	0.02	0.33	1.33	22.13
FE2O3	0.0	0.0	0.09	0.56
AL2O3	0.0	0.0	0.23	2.26
CL	58.38	1646.83	0.0	0.0
SUBTOTAL	97.93 %		2.11 %	
MEASURED =	97.46		2.54	

	HOLE # 7 DEPTH = 1957.5 FEET SOLUBLE 99.16 WT % OF TOTAL		HOLE # 7 DEPTH = 1957.5 FEET INSOLUBLE 0.84 WT % OF TOTAL	
COMPONENT	WT %	MOLES	WT %	MOLES
SO3	1.32	16.49	0.41	5.12
NA	38.38	1669.42	0.0	0.0
NA2O	0.0	0.0	0.0	0.0
K	0.36	9.21	0.0	0.0
K2O	0.0	0.0	0.01	0.11
MGO	0.24	5.95	0.17	4.22
CAO	2.18	38.87	0.0	0.0
SIO2	0.03	0.50	0.35	5.82
FE2O3	0.0	0.0	0.04	0.25
AL2O3	0.0	0.0	0.10	0.98
CL	59.00	1664.32	0.0	0.0
SUBTOTAL	101.51 %		1.08 %	
MEASURED =	99.16		0.84	

	HOLE # 7 DEPTH = 1961.0 FEET SOLUBLE 99.10 WT % OF TOTAL		HOLE # 7 DEPTH = 1961.0 FEET INSOLUBLE 0.90 WT % OF TOTAL	
COMPONENT	WT %	MOLES	WT %	MOLES
SO3	0.49	6.12	0.0	0.0
NA	39.14	1702.48	0.0	0.0
NA2O	0.0	0.0	0.0	0.0
K	0.21	5.37	0.0	0.0
K2O	0.01	0.11	0.01	0.11
MGO	0.07	1.74	0.18	4.47
CAO	0.19	3.39	0.0	0.0
SIO2	0.01	0.17	0.42	6.99
FE2O3	0.0	0.0	0.04	0.25
AL2O3	0.0	0.0	0.08	0.78
CL	58.83	1659.52	0.0	0.0
SUBTOTAL	98.95 %		0.73 %	
MEASURED =	99.10		0.90	

```
HOLE #    7
DEPTH =   1967.0  FEET

TOTAL


COMPONENT        WT %          MOLES
---------        ----          -----

   SO3           3.03          37.85

   NA           39.58        1721.62

   NA2O          0.0           0.0

   K             0.90          23.02

   K2O           0.0           0.0

   MGO           0.23          5.71

   CAO           0.94          16.76

   SIO2          0.0           0.0

   FE2O3         0.01          0.06

   AL2O3         0.0           0.0

   CL           58.74        1656.98
```

	HOLE # 7 DEPTH = 1969.0 FEET		HOLE # 7 DEPTH = 1969.0 FEET	
	SOLUBLE 98.05 WT % OF TOTAL		INSOLUBLE 1.95 WT % OF TOTAL	
COMPONENT	WT %	MOLES	WT %	MOLES
SO3	0.32	4.00	0.0	0.0
NA	38.76	1685.95	0.0	0.0
NA2O	0.0	0.0	0.0	0.0
K	0.08	2.05	0.0	0.0
K2O	0.0	0.0	0.0	0.0
MGO	0.11	2.73	0.11	2.73
CAO	0.08	1.43	0.0	0.0
SIO2	0.01	0.17	0.14	2.33
FE2O3	0.0	0.0	0.02	0.13
AL2O3	0.0	0.0	0.04	0.39
CL	60.60	1709.45	0.0	0.0
SUBTOTAL	99.96 %		0.31 %	
MEASURED =	98.05		1.95	

HOLE # 7
DEPTH = 1973.0 FEET

SOLUBLE
98.63 WT % OF TOTAL

HOLE # 7
DEPTH = 1973.0 FEET

INSOLUBLE
1.37 WT % OF TOTAL

COMPONENT	WT %	MOLES	WT %	MOLES
SO3	0.26	3.25	0.0	0.0
NA	38.46	1672.90	0.0	0.0
NA2O	0.0	0.0	0.0	0.0
K	0.06	1.53	0.0	0.0
K2O	0.0	0.0	0.03	0.32
MGO	0.13	3.23	0.40	9.92
CAO	0.06	1.07	0.01	0.18
SIO2	0.03	0.50	0.62	10.32
FE2O3	0.0	0.0	0.01	0.06
AL2O3	0.0	0.0	0.13	1.28
CL	59.58	1680.68	0.0	0.0

SUBTOTAL   98.58   %   1.20   %

MEASURED =   98.63   1.37

HOLE # 7
DEPTH = 1975.0 FEET

TOTAL

COMPONENT	WT %	MOLES
SO3	0.19	2.37
NA	38.93	1693.35
NA2O	0.0	0.0
K	0.06	1.53
K2O	0.0	0.0
MGO	0.07	1.74
CAO	0.09	1.60
SIO2	0.0	0.0
FE2O3	0.0	0.0
AL2O3	0.0	0.0
CL	60.38	1703.24

HOLE # 7 DEPTH = 1978.5 FEET

SOLUBLE 91.07 WT % OF TOTAL

HOLE # 7 DEPTH = 1978.5 FEET

INSOLUBLE 8.93 WT % OF TOTAL

COMPONENT	WT %	MOLES	WT %	MOLES
SO3	2.74	34.22	0.08	1.00
NA	32.52	1414.53	0.0	0.0
NA2O	0.0	0.0	1.96	31.62
K	0.44	11.25	0.0	0.0
K2O	0.0	0.0	0.13	1.38
MGO	0.37	9.18	2.25	55.82
CAO	0.96	17.12	0.02	0.36
SIO2	0.0	0.0	2.89	48.09
FE2O3	0.0	0.0	0.37	2.32
AL2O3	0.0	0.0	1.06	10.40
CL	51.89	1463.75	0.0	0.0
SUBTOTAL	88.92 %		8.76 %	
MEASURED =	91.07		8.93	

HOLE # 7
DEPTH = 1983.0 FEET
TOTAL

COMPONENT	WT %	MOLES
SO3	1.11	13.86
NA	36.00	1565.90
NA2O	0.0	0.0
K	0.61	15.60
K2O	0.0	0.0
MGO	0.40	9.92
CAO	0.46	8.20
SIO2	0.01	0.17
FE2O3	0.0	0.0
AL2O3	0.0	0.0
CL	59.20	1669.96

HOLE # 7
DEPTH = 1986.5 FEET
TOTAL

COMPONENT	WT %	MOLES
SO3	0.17	2.12
NA	38.20	1661.59
NA2O	0.0	0.0
K	0.04	1.02
K2O	0.0	0.0
MGO	0.03	0.74
CAO	0.21	3.74
SIO2	0.01	0.17
FE2O3	0.0	0.0
AL2O3	0.0	0.0
CL	60.66	1711.14

HOLE # 7
DEPTH = 1993.5 FEET

TOTAL

COMPONENT	WT %	MOLES
SO3	2.96	36.97
NA	38.25	1663.77
NA2O	0.0	0.0
K	1.68	42.97
K2O	0.0	0.0
MGO	0.79	19.60
CAO	2.30	41.01
SIO2	0.0	0.0
FE2O3	0.0	0.0
AL2O3	0.0	0.0
CL	53.81	1517.91

HOLE # 7
DEPTH = 2537.0 FEET

TOTAL

COMPONENT	WT %	MOLES
SO3	46.62	582.31
NA	0.93	40.45
NA2O	4.93	79.54
K	0.90	23.02
K2O	0.0	0.0
MGO	13.02	323.00
CAO	4.37	77.92
SIO2	13.98	232.65
FE2O3	1.13	7.08
AL2O3	3.26	31.97
CL	2.63	74.19

	HOLE # 7 DEPTH = 2703.0 FEET SOLUBLE 98.97 WT % OF TOTAL		HOLE # 7 DEPTH = 2703.0 FEET INSOLUBLE 1.03 WT % OF TOTAL	
COMPONENT	WT %	MOLES	WT %	MOLES
SO3	0.73	9.12	0.74	9.24
NA	38.36	1668.55	0.0	0.0
NA2O	0.0	0.0	0.0	0.0
K	0.02	0.51	0.0	0.0
K2O	0.0	0.0	0.01	0.11
MGO	0.06	1.49	0.20	4.96
CAO	0.78	13.91	0.01	0.18
SIO2	0.04	0.67	0.21	3.49
FE2O3	0.01	0.06	0.05	0.31
AL2O3	0.0	0.0	0.05	0.49
CL	58.89	1661.21	0.0	0.0
SUBTOTAL	98.89 %		1.27 %	
MEASURED =	98.97		1.03	

```
HOLE #    7
DEPTH =    2716.3  FEET
TOTAL
```

COMPONENT	WT %	MOLES
SO3	0.44	5.50
NA	39.44	1715.53
NA20	0.0	0.0
K	0.01	0.26
K20	0.0	0.0
MGO	0.01	0.25
CAO	0.18	3.21
SI02	0.01	0.17
FE203	0.0	0.0
AL203	0.0	0.0
CL	61.00	1720.73

```
HOLE #    7
DEPTH =    2736.0  FEET

TOTAL


COMPONENT        WT %         MOLES
-----------      ------       -------

    SO3          0.42          5.25

    NA          39.75       1729.01

    NA2O         0.0           0.0

    K            0.01          0.26

    K2O          0.0           0.0

    MGO          0.06          1.49

    CAO          0.51          9.09

    SIO2         0.01          0.17

    FE2O3        0.0           0.0

    AL2O3        0.0           0.0

    CL          59.88       1689.14
```

	HOLE # 8 DEPTH = 1391.5 FEET SOLUBLE 98.99 WT % OF TOTAL		HOLE # 8 DEPTH = 1391.5 FEET INSOLUBLE 1.01 WT % OF TOTAL	
COMPONENT	WT %	MOLES	WT %	MOLES
SO3	1.07	13.36	0.07	0.87
NA	39.34	1711.18	0.0	0.0
NA2O	0.0	0.0	0.0	0.0
K	0.31	.7.93	0.0	0.0
K2O	0.0	0.0	0.02	0.21
MGO	0.21	5.21	0.06	1.49
CAO	0.52	9.27	0.01	0.18
SIO2	0.0	0.0	0.39	6.49
FE2O3	0.0	0.0	0.27	1.69
AL2O3	0.0	0.0	0.10	0.98
CL	58.07	1638.08	0.0	0.0
SUBTOTAL	99.52 %		0.92 %	
MEASURED =	98.99		1.01	

HOLE # 8
DEPTH = 1495.3 FEET

TOTAL

COMPONENT	WT %	MOLES
SO3	1.12	13.99
NA	38.00	1652.89
NA2O	0.0	0.0
K	0.12	3.07
K2O	0.0	0.0
MGO	0.13	3.23
CAO	1.62	28.89
SIO2	0.01	0.17
FE2O3	0.0	0.0
AL2O3	0.0	0.0
CL	59.97	1691.68

HOLE # 8
DEPTH = 1573.0 FEET

SOLUBLE
97.72 WT % OF TOTAL

COMPONENT	WT %	MOLES
SO3	3.40	42.47
NA	34.63	1506.31
NA2O	0.0	0.0
K	0.18	.4.60
K2O	0.0	0.0
MGO	1.65	40.93
CAO	0.29	5.17
SIO2	0.0	0.0
FE2O3	0.0	0.0
AL2O3	0.0	0.0
CL	54.11	1526.38
SUBTOTAL	94.26 %	
MEASURED =	97.72	

HOLE # 8
DEPTH = 1573.0 FEET

INSOLUBLE
2.28 WT % OF TOTAL

WT %	MOLES
1.71	21.36
0.0	0.0
0.0	0.0
0.0	0.0
0.02	0.21
0.06	1.49
0.16	2.85
0.02	0.33
0.0	0.0
0.01	0.10
0.0	0.0
1.98 %	
2.28	

HOLE # 8
DEPTH = 1652.0 FEET

SOLUBLE
48.61 WT % OF TOTAL

COMPONENT	WT %	MOLES
SO3	19.80	247.31
NA	4.07	177.03
NA2O	0.0	0.0
K	18.59	475.45
K2O	0.0	0.0
MGO	4.12	102.21
CAO	0.19	3.39
SIO2	0.0	0.0
FE2O3	0.0	0.0
AL2O3	0.0	0.0
CL	7.35	207.33

SUBTOTAL   54.12 %

MEASURED = 48.61

HOLE # 8
DEPTH = 1652.0 FEET

INSOLUBLE
51.39 WT % OF TOTAL

	WT %	MOLES
SO3	31.24	390.21
NA	0.0	0.0
NA2O	4.24	68.41
K	0.0	0.0
K2O	0.99	10.51
MGO	0.46	11.41
CAO	3.74	66.69
SIO2	0.34	5.66
FE2O3	0.07	0.44
AL2O3	0.04	0.39
CL	0.0	0.0

41.12 %

51.39

```
HOLE #    8
DEPTH =    1705.0   FEET

TOTAL
```

COMPONENT	WT %	MOLES
SO3	1.18	14.74
NA	38.79	1687.26
NA2O	0.0	0.0
K	0.35	8.95
K2O	0.0	0.0
MGO	0.17	4.22
CAO	0.44	7.85
SIO2	0.01	0.17
FE2O3	0.0	0.0
AL2O3	0.0	0.0
CL	58.64	1654.16

HOLE # 8
DEPTH = 1770.0 FEET

SOLUBLE
98.79 WT % OF TOTAL

COMPONENT	WT %	MOLES
SO3	1.78	22.23
NA	35.75	1555.02
NA2O	0.0	0.0
K	0.56	14.32
K2O	0.0	0.0
MGO	0.52	12.90
CAO	1.75	31.21
SIO2	0.01	0.17
FE2O3	0.0	0.0
AL2O3	0.0	0.0
CL	57.29	1616.08

SUBTOTAL   97.66 %
MEASURED = 98.79

HOLE # 8
DEPTH = 1770.0 FEET

INSOLUBLE
1.21 WT % OF TOTAL

WT %	MOLES
0.17	2.12
0.0	0.0
0.33	5.32
0.0	0.0
0.02	0.21
0.03	0.74
0.0	0.0
0.47	7.82
0.0	0.0
0.12	1.18
0.0	0.0

1.14 %
1.21

HOLE # 8
DEPTH = 1787.0 FEET

SOLUBLE
99.43 WT % OF TOTAL

COMPONENT	WT %	MOLES
SO3	3.01	37.60
NA	37.24	1619.84
NA2O	0.0	0.0
K	0.69	17.65
K2O	0.0	0.0
MGO	0.40	9.92
CAO	0.70	12.48
SIO2	0.01	0.17
FE2O3	0.0	0.0
AL2O3	0.0	0.0
CL	58.00	1636.11
SUBTOTAL	100.05 %	
MEASURED =	99.43	

HOLE # 8
DEPTH = 1787.0 FEET

INSOLUBLE
0.57 WT % OF TOTAL

WT %	MOLES
0.0	0.0
0.0	0.0
0.0	0.0
0.0	0.0
0.01	0.11
0.14	3.47
0.0	0.0
0.21	3.49
0.03	0.19
0.04	0.39
0.0	0.0
0.43 %	
0.57	

```
                    HOLE #    8                        HOLE #    8
                    DEPTH =    1794.5  FEET            DEPTH =    1794.5  FEET

                    SOLUBLE                            INSOLUBLE
                    75.34 WT % OF TOTAL                24.66 WT % OF TOTAL

COMPONENT       WT %            MOLES              WT %            MOLES
---------       ----            -----              ----            -----

   SO3          0.70            8.74               0.0             0.0

   NA           29.75           1294.04            0.0             0.0

   NA2O         0.0             0.0                1.16            18.72

   K            0.42            10.74              0.0             0.0

   K2O          0.0             0.0                0.63            6.69

   MGO          0.44            10.92              6.20            153.81

   CAO          0.03            0.53               0.01            0.18

   SIO2         0.02            0.33               7.78            129.47

   FE2O3        0.0             0.0                0.46            2.88

   AL2O3        0.0             0.0                1.91            18.73

   CL           45.14           1273.34            0.0             0.0
                -----                              -----

SUBTOTAL        76.50   %                          18.15   %

MEASURED =      75.34                              24.66
```

```
HOLE #      8
DEPTH =     1804.0  FEET
TOTAL
```

COMPONENT	WT %	MOLES
SO3	0.28	3.50
NA	39.43	1715.09
NA2O	0.0	0.0
K	0.06	1.53
K2O	0.0	0.0
MGO	0.04	0.99
CAO	0.70	12.48
SIO2	0.01	0.17
FE2O3	0.0	0.0
AL2O3	0.0	0.0
CL	59.94	1690.83

	HOLE # 8 DEPTH = 1829.0 FEET SOLUBLE 99.03 WT % OF TOTAL		HOLE # 8 DEPTH = 1829.0 FEET INSOLUBLE 0.97 WT % OF TOTAL	
COMPONENT	WT %	MOLES	WT %	MOLES
SO3	0.02	0.25	0.0	0.0
NA	39.87	1734.23	0.0	0.0
NA2O	0.0	0.0	0.0	0.0
K	0.05	1.28	0.0	0.0
K2O	0.0	0.0	0.02	0.21
MGO	0.06	1.49	0.23	5.71
CAO	0.01	0.18	0.01	0.18
SIO2	0.01	0.17	0.29	4.83
FE2O3	0.0	0.0	0.04	0.25
AL2O3	0.0	0.0	0.08	0.78
CL	58.81	1658.96	0.0	0.0
SUBTOTAL	98.83 %		0.67 %	
MEASURED =	99.03		0.97	

	HOLE # 8 DEPTH = 1838.0 FEET SOLUBLE 97.53 WT % OF TOTAL		HOLE # 8 DEPTH = 1838.0 FEET INSOLUBLE 2.47 WT % OF TOTAL	
COMPONENT	WT %	MOLES	WT %	MOLES
SO3	0.80	9.99	0.0	0.0
NA	37.58	1634.62	0.0	0.0
NA2O	0.0	0.0	0.0	0.0
K	0.26	6.65	0.0	0.0
K2O	0.0	0.0	0.10	1.06
MGO	0.11	2.73	0.37	9.18
CAO	0.05	0.89	0.0	0.0
SIO2	0.01	0.17	0.12	2.00
.FE2O3	0.0	0.0	0.16	1.00
AL2O3	0.0	0.0	0.27	2.65
CL	58.38	1646.83	0.0	0.0
SUBTOTAL	97.19 %		1.02 %	
MEASURED =	97.53		2.47	

HOLE #   8
DEPTH =   1856.7 FEET
TOTAL

COMPONENT	WT %	MOLES
SO3	2.70	33.72
NA	36.08	1569.38
NA2O	0.0	0.0
K	1.62	41.43
K2O	0.0	0.0
MGO	0.03	0.74
CAO	1.56	27.82
SIO2	0.0	0.0
FE2O3	0.0	0.0
AL2O3	0.0	0.0
CL	56.66	1598.31

HOLE # 8 DEPTH = 1875.0 FEET SOLUBLE 70.94 WT % OF TOTAL			HOLE # 8 DEPTH = 1875.0 FEET INSOLUBLE 29.06 WT % OF TOTAL	
COMPONENT	WT %	MOLES	WT %	MOLES
SO3	0.42	5.25	0.0	0.0
NA	25.64	1115.27	0.0	0.0
NA2O	0.0	0.0	0.0	0.0
K	0.31	7.93	0.0	0.0
K2O	0.0	0.0	2.28	24.20
MGO	0.33	8.19	9.22	228.73
CAO	0.43	7.67	0.20	3.57
SIO2	0.01	0.17	15.29	254.45
FE2O3	0.0	0.0	1.23	7.70
AL2O3	0.0	0.0	3.00	29.42
CL	40.92	1154.30	0.0	0.0
SUBTOTAL	68.06 %		31.22 %	
MEASURED =	70.94		29.06	

	HOLE # 8 DEPTH = 1884.0 FEET SOLUBLE 80.58 WT % OF TOTAL		HOLE # 8 DEPTH = 1884.0 FEET INSOLUBLE 19.42 WT % OF TOTAL	
COMPONENT	WT %	MOLES	WT %	MOLES
SO3	3.76	46.96	0.0	0.0
NA	27.10	1178.77	0.0	0.0
NA2O	0.0	0.0	0.0	0.0
K	6.98	178.52	0.0	0.0
K2O	0.0	0.0	1.80	19.11
MGO	1.44	35.72	3.65	90.55
CAO	1.65	29.42	0.01	0.18
SIO2	0.01	0.17	9.01	149.94
FE2O3	0.0	0.0	0.60	3.76
AL2O3	0.0	0.0	1.99	19.52
CL	44.06	1242.88	0.0	0.0
SUBTOTAL	85.00 %		17.06 %	
MEASURED =	80.58		19.42	

```
HOLE #    8
DEPTH =    1890.0  FEET

TOTAL
```

COMPONENT	WT %	MOLES
SO3	0.77	9.62
NA	38.78	1686.82
NA2O	0.0	0.0
K	0.10	2.56
K2O	0.0	0.0
MGO	0.10	2.48
CAO	0.95	16.94
SIO2	0.0	0.0
FE2O3	0.0	0.0
AL2O3	0.0	0.0
CL	59.33	1673.62

```
HOLE #    8
DEPTH =    1894.3  FEET          HOLE #    8
                                 DEPTH =    1894.3  FEET

SOLUBLE                          INSOLUBLE
95.43 WT % OF TOTAL              4.57 WT % OF TOTAL
```

COMPONENT	WT %	MOLES	WT %	MOLES
SO3	0.12	1.50	0.0	0.0
NA	37.90	1648.54	0.0	0.0
NA2O	0.0	0.0	0.0	0.0
K	0.06	1.53	0.0	0.0
K2O	0.0	0.0	0.13	1.38
MGO	0.08	1.98	0.66	16.37
CAO	0.03	0.53	0.0	0.0
SIO2	0.0	0.0	2.43	40.44
FE2O3	0.0	0.0	0.20	1.25
AL2O3	0.0	0.0	0.43	4.22
CL	57.78	1629.90	0.0	0.0
SUBTOTAL	95.97 %		3.85 %	
MEASURED =	95.43		4.57	

```
                    HOLE #    8                          HOLE #   8
                    DEPTH =    1898.5  FEET              DEPTH =   1898.5  FEET

                    SOLUBLE                              INSOLUBLE
                    98.53 WT % OF TOTAL                  1.47 WT % OF TOTAL

    COMPONENT       WT %           MOLES                 WT %           MOLES
    ---------       ----           -----                 ----           -----

       SO3          0.55            6.87                 0.0            0.0

       NA          38.81         1688.13                 0.0            0.0

       NA20         0.0             0.0                  0.71          11.46

       K            0.07            1.79                 0.0            0.0

       K20          0.0             0.0                  0.01           0.11

       MGO          0.08            1.98                 0.18           4.47

       CAO          0.11            1.96                 0.01           0.18

       SIO2         0.01            0.17                 0.44           7.32

       FE203        0.0             0.0                  0.02           0.13

       AL203        0.0             0.0                  0.07           0.69

       CL   •      57.97         1635.26                 0.0            0.0
                  ------                                ----

    SUBTOTAL       97.60  %                              1.44  %

    MEASURED =     98.53                                 1.47
```

```
HOLE #      8
DEPTH =     1900.0  FEET
TOTAL


COMPONENT        WT %         MOLES
---------        ----         -----

    SO3          3.20         39.97
    NA          38.14       1658.98
    NA2O         0.0           0.0
    K            0.98         25.06
    K2O          0.0           0.0
    MGO          0.47         11.66
    CAO          0.39          6.95
    SIO2         0.0           0.0
    FE2O3        0.0           0.0
    AL2O3        0.0           0.0
    CL          57.60       1624.82
```

	HOLE # 8 DEPTH = 1905.0 FEET SOLUBLE 96.98 WT % OF TOTAL		HOLE # 8 DEPTH = 1905.0 FEET INSOLUBLE 3.02 WT % OF TOTAL	
COMPONENT	WT %	MOLES	WT %	MOLES
SO3	0.20	2.50	0.0	0.0
NA	38.67	1682.04	0.0	0.0
NA2O	0.0	0.0	0.0	0.0
K	0.13	3.32	0.0	0.0
K2O	0.0	0.0	0.03	0.32
MGO	0.10	2.48	0.83	20.59
CAO	0.44	7.85	0.01	0.18
SIO2	0.0	0.0	0.91	15.14
FE2O3	0.0	0.0	0.14	0.88
AL2O3	0.0	0.0	0.25	2.45
CL	57.91	1633.57	0.0	0.0
SUBTOTAL	97.45 %		2.17 %	
MEASURED =	96.98		3.02	

	HOLE # 8 DEPTH = 1910.0 FEET			HOLE # 8 DEPTH = 1910.0 FEET	
	SOLUBLE 99.02 WT % OF TOTAL			INSOLUBLE 0.98 WT % OF TOTAL	
COMPONENT	WT %	MOLES		WT %	MOLES
SO3	0.53	6.62		0.0	0.0
NA	39.64	1724.23		0.0	0.0
NA2O	0.0	0.0		0.0	0.0
K	0.0	0.0		0.0	0.0
K2O	0.29	3.08		0.01	0.11
MGO	0.10	2.48		0.20	4.96
CAO	0.44	7.85		0.0	0.0
SIO2	0.01	0.17		0.33	5.49
FE2O3	0.0	0.0		0.04	0.25
AL2O3	0.0	0.0		0.08	0.78
CL	59.04	1665.44		0.0	0.0
SUBTOTAL	100.05 %			0.66 %	
MEASURED =	99.02			0.98	

HOLE # 8
DEPTH = 1913.1 FEET

SOLUBLE
97.71 WT % OF TOTAL

COMPONENT	WT %	MOLES
SO3	0.06	0.75
NA	38.48	1673.77
NA2O	0.0	0.0
K	0.06	1.53
K2O	0.0	0.0
MGO	0.06	1.49
CAO	0.0	0.0
SIO2	0.01	0.17
FE2O3	0.0	0.0
AL2O3	0.0	0.0
CL	59.27	1671.93

SUBTOTAL   97.94 %
MEASURED =   97.71

HOLE # 8
DEPTH = 1913.1 FEET

INSOLUBLE
2.29 WT % OF TOTAL

WT %	MOLES
0.0	0.0
0.0	0.0
0.0	0.0
0.0	0.0
0.05	0.53
0.48	11.91
0.0	0.0
0.90	14.98
0.13	0.81
0.21	2.06
0.0	0.0

1.77 %

2.29

HOLE # = 8
DEPTH = 1916.2 FEET

TOTAL

COMPONENT	WT %	MOLES
SO3	0.92	11.49
NA	38.48	1673.77
NA2O	0.0	0.0
K	0.21	5.37
K2O	0.0	0.0
MGO	0.13	3.23
CAO	0.44	7.85
SIO2	0.0	0.0
FE2O3	0.0	0.0
AL2O3	0.0	0.0
CL	57.71	1627.93

HOLE # 8
DEPTH = 1923.0 FEET

SOLUBLE
98.30 WT % OF TOTAL

COMPONENT	WT %	MOLES
SO3	0.10	1.25
NA	38.03	1654.20
NA2O	0.0	0.0
K	0.05	1.28
K2O	0.0	0.0
MGO	0.05	1.24
CAO	0.08	1.43
SIO2	0.01	0.17
FE2O3	0.0	0.0
AL2O3	0.0	0.0
CL	58.43	1648.24
SUBTOTAL	96.75 %	
MEASURED =	98.30	

HOLE # 8
DEPTH = 1923.0 FEET

INSOLUBLE
1.70 WT % OF TOTAL

	WT %	MOLES
SO3	0.95	11.87
NA	0.0	0.0
NA2O	0.0	0.0
K	0.0	0.0
K2O	0.08	0.85
MGO	0.03	0.74
CAO	0.12	2.14
SIO2	0.59	9.82
FE2O3	0.10	0.63
AL2O3	0.16	1.57
CL	0.0	0.0
SUBTOTAL	2.03 %	
MEASURED =	1.70	

```
            HOLE #    8
            DEPTH =    1930.0  FEET            HOLE #    8
                                               DEPTH =    1930.0  FEET
            SOLUBLE
            98.99 WT % OF TOTAL               INSOLUBLE
                                               1.01 WT % OF TOTAL

COMPONENT       WT %         MOLES            WT %          MOLES
--------        ----         -----            ----          -----

   SO3         2.81         35.10            0.0           0.0

   NA          35.71        1553.28          0.0           0.0

   NA2O        0.0          0.0              0.08          1.29

   K           1.03         26.34            0.0           0.0

   K2O         0.0          0.0              0.01          0.11

   MGO         0.33         8.19             0.13          3.23

   CAO         0.19         3.39             0.01          0.18

   SIO2        0.0          0.0              0.18          3.00

   FE2O3       0.0          0.0              0.07          0.44

   AL2O3       0.0          0.0              0.04          0.39

   CL          56.74        1600.56          0.0           0.0
               -----                         -----

SUBTOTAL       96.81    %                    0.52    %

MEASURED =     98.99                         1.01
```

```
HOLE #      8
DEPTH =      1933.0   FEET

TOTAL


COMPONENT          WT %          MOLES
---------          ----          --------

   SO3             0.78           9.74

   NA             38.03        1654.20

   NA2O            0.0            0.0

   K               0.15           3.84

   K2O             0.0            0.0

   MGO             0.09           2.23

   CAO             0.65          11.59

   SIO2            0.01           0.17

   FE2O3           0.01           0.06

   AL2O3           0.0            0.0

   CL             59.81        1687.17
```

```
HOLE #      8
DEPTH =      1938.0   FEET

TOTAL


COMPONENT          WT %            MOLES
---------          ----            -------

   SO3             2.91            36.35

   NA             35.63          1549.80

   NA2O            0.0             0.0

   K               0.68           17.39

   K2O             0.0             0.0

   MGO             0.84           20.84

   CAO             1.02           18.19

   SIO2            0.0             0.0

   FE2O3           0.0             0.0

   AL2O3           0.0             0.0

   CL             59.45          1677.01
```

```
HOLE #      8
DEPTH =    1953.2  FEET

TOTAL


COMPONENT        WT %          MOLES
---------        -----         -------

  SO3            2.30          28.73

  NA             39.50         1718.14

  NA2O           0.0           0.0

  K              0.30          7.67

  K2O            0.0           0.0

  MGO            0.42          10.42

  CAO            1.23          21.93

  SIO2           0.01          0.17

  FE2O3          0.0           0.0

  AL2O3          0.0           0.0

  CL             57.63         1625.67
```

HOLE # 8
DEPTH = 1967.0 FEET

SOLUBLE
95.13 WT % OF TOTAL

COMPONENT	WT %	MOLES
SO3	1.25	15.61
NA	35.99	1565.46
NA2O	0.0	0.0
K	0.57	14.58
K2O	0.0	0.0
MGO	0.23	5.71
CAO	0.40	7.13
SIO2	0.0	0.0
FE2O3	0.0	0.0
AL2O3	0.0	0.0
CL	57.52	1622.57
SUBTOTAL	95.96 %	
MEASURED =	95.13	

HOLE # 8
DEPTH = 1967.0 FEET

INSOLUBLE
4.87 WT % OF TOTAL

WT %	MOLES
0.0	0.0
0.0	0.0
2.73	44.05
0.0	0.0
0.09	0.96
0.98	24.31
0.0	0.0
0.76	12.65
0.10	0.63
0.20	1.96
0.0	0.0
4.86 %	
4.87	

	HOLE # 8 DEPTH = 1986.0 FEET		HOLE # 8 DEPTH = 1986.0 FEET	
	SOLUBLE 36.72 WT % OF TOTAL		INSOLUBLE 63.28 WT % OF TOTAL	
COMPONENT	WT %	MOLES	WT %	MOLES
SO3	22.99	287.16	37.88	473.15
NA	0.36	15.66	0.0	0.0
NA2O	0.0	0.0	5.83	94.06
K	0.0	0.0	0.0	0.0
K2O	14.68	155.84	11.39	120.91
MGO	0.62	15.38	1.20	29.77
CAO	0.87	15.51	4.25	75.78
SIO2	0.0	0.0	0.54	8.99
FE2O3	0.0	0.0	0.17	1.06
AL2O3	0.0	0.0	0.85	8.34
CL	0.15	4.23	0.0	0.0
SUBTOTAL	39.67 %		62.11 %	
MEASURED =	36.72		63.28	

```
HOLE #    8
DEPTH =    2006.0  FEET

TOTAL


COMPONENT          WT %          MOLES
---------          ----          -----

   SO3             2.37          29.60

   NA             37.59        1635.06

   NA2O            0.0            0.0

   K               1.03          26.34

   K2O             0.0            0.0

   MGO             0.31           7.69

   CAO             0.06           1.07

   SIO2            0.01           0.17

   FE2O3           0.0            0.0

   AL2O3           0.0            0.0

   CL             57.17        1612.69
```

HOLE # 8 2017.0 FEET
DEPTH =

SOLUBLE
95.20 WT % OF TOTAL

COMPONENT	WT %	MOLES
SO3	0.55	6.87
NA	35.66	1551.11
NA2O	0.0	0.0
K	0.06	1.53
K2O	0.0	0.0
MGO	0.08	1.98
CAO	0.96	17.12
SIO2	0.02	0.33
FE2O3	0.0	0.0
AL2O3	0.0	0.0
CL	57.09	1610.44

SUBTOTAL   94.42   %

MEASURED =   95.20

HOLE # 8 2017.0 FEET
DEPTH =

INSOLUBLE
4.80 WT % OF TOTAL

WT %	MOLES
0.07	0.87
0.0	0.0
0.0	0.0
0.0	0.0
0.04	0.42
0.44	10.92
0.06	1.07
2.01	33.45
0.28	1.75
0.70	6.87
0.0	0.0

3.60   %

4.80

| | HOLE # 8 DEPTH = 2039.0 FEET | | HOLE # 8 DEPTH = 2039.0 FEET | |
| | SOLUBLE 98.94 WT % OF TOTAL | | INSOLUBLE 1.06 WT % OF TOTAL | |
COMPONENT	WT %	MOLES	WT %	MOLES
SO3	4.88	60.95	0.62	7.74
NA	35.02	1523.27	0.0	0.0
NA2O	0.0	0.0	0.0	0.0
K	1.56	39.90	0.0	0.0
K2O	0.0	0.0	0.03	0.32
MGO	0.50	12.40	0.21	5.21
CAO	1.57	28.00	0.01	0.18
SIO2	0.0	0.0	0.26	4.33
FE2O3	0.0	0.0	0.07	0.44
AL2O3	0.0	0.0	0.05	0.49
CL	54.01	1523.55	0.0	0.0
SUBTOTAL	97.54 %		1.25 %	
MEASURED =	98.94		1.06	

	HOLE # 8 DEPTH = 2050.0 FEET		HOLE # 8 DEPTH = 2050.0 FEET	
	SOLUBLE 28.61 WT % OF TOTAL		INSOLUBLE 71.39 WT % OF TOTAL	
COMPONENT	WT %	MOLES	WT %	MOLES
SO3	3.92	48.96	51.08	638.02
NA	8.00	347.98	0.0	0.0
NA2O	0.0	0.0	4.90	79.06
K	0.05	1.28	0.0	0.0
K2O	0.0	0.0	0.04	0.42
MGO	0.02	0.50	0.29	7.19
CAO	0.55	9.81	6.55	116.80
SIO2	0.0	0.0	0.33	5.49
FE2O3	0.0	0.0	0.0	0.0
AL2O3	0.0	0.0	0.0	0.0
CL	12.44	350.92	0.0	0.0
SUBTOTAL	24.98 %		63.19 %	
MEASURED =	28.61		71.39	

HOLE # 8
DEPTH = 2068.0 FEET

SOLUBLE
98.84 WT % OF TOTAL

COMPONENT	WT %	MOLES
SO3	2.49	31.10
NA	37.41	1627.23
NA2O	0.0	0.0
K	0.08	2.05
K2O	0.0	0.0
MGO	0.03	0.74
CAO	0.87	15.51
SIO2	0.02	0.33
FE2O3	0.0	0.0
AL2O3	0.0	0.0
CL	55.99	1579.41
SUBTOTAL	96.89 %	
MEASURED =	98.84	

HOLE # 8
DEPTH = 2068.0 FEET

INSOLUBLE
1.16 WT % OF TOTAL

WT %	MOLES
0.0	0.0
0.0	0.0
0.0	0.0
0.0	0.0
0.01	0.11
0.28	6.95
0.02	0.36
0.37	6.16
0.05	0.31
0.07	0.69
0.0	0.0
0.80 %	
1.16	

	HOLE # 8 DEPTH = 2084.0 FEET		HOLE # 8 DEPTH = 2084.0 FEET	
	SOLUBLE 92.00 WT % OF TOTAL		INSOLUBLE 8.00 WT % OF TOTAL	
COMPONENT	WT %	MOLES	WT %	MOLES
SO3	2.05	25.61	0.59	7.37
NA	34.46	1498.91	0.0	0.0
NA2O	0.0	0.0	1.87	30.17
K	1.02	26.09	0.0	0.0
K2O	0.0	0.0	0.19	2.02
MGO	0.35	8.68	1.13	28.03
CAO	0.72	12.84	0.01	0.18
SIO2	0.01	0.17	2.07	34.45
FE2O3	0.01	0.06	0.24	1.50
AL2O3	0.0	0.0	0.37	3.63
CL	52.19	1472.21	0.0	0.0
SUBTOTAL	90.81 %		6.47 %	
MEASURED =	92.00		8.00	

HOLE # 8
DEPTH = 2130.0 FEET

TOTAL

COMPONENT	WT %	MOLES
SO3	2.31	28.85
NA	37.79	1643.76
NA2O	0.0	0.0
K	0.42	10.74
K2O	0.0	0.0
MGO	0.25	6.20
CAO	0.75	13.37
SIO2	0.03	0.50
FE2O3	0.0	0.0
AL2O3	0.0	0.0
CL	57.16	1612.41

	HOLE # 8			HOLE # 8	
	DEPTH = 2162.0 FEET			DEPTH = 2162.0 FEET	
	SOLUBLE			INSOLUBLE	
	98.90 WT % OF TOTAL			1.10 WT % OF TOTAL	
COMPONENT	WT %	MOLES		WT %	MOLES
SO3	1.31	16.36		0.25	3.12
NA	36.77	1599.39		0.0	0.0
NA2O	0.0	0.0		0.55	8.87
K	1.23	31.46		0.0	0.0
K2O	0.0	0.0		0.03	0.32
MGO	0.45	11.16		0.20	4.96
CAO	0.93	16.58		0.01	0.18
SIO2	0.0	0.0		0.23	3.83
FE2O3	0.0	0.0		0.06	0.38
AL2O3	0.0	0.0		0.05	0.49
CL	59.99	1692.24		0.0	0.0
SUBTOTAL	100.68 %			1.38 %	
MEASURED =	98.90			1.10	

HOLE #   8
DEPTH =   2217.0 FEET
TOTAL

COMPONENT	WT %	MOLES
SO3	0.0	0.0
NA	39.14	1702.48
NA2O	0.0	0.0
K	0.07	1.79
K2O	0.0	0.0
MGO	0.02	0.50
CAO	0.12	2.14
SIO2	0.01	0.17
FE2O3	0.0	0.0
AL2O3	0.0	0.0
CL	59.75	1685.47

HOLE # 8
DEPTH = 2280.0 FEET
TOTAL

COMPONENT	WT %	MOLES
SO3	0.39	4.87
NA	37.91	1648.98
NA2O	0.0	0.0
K	0.12	3.07
K2O	0.0	0.0
MGO	0.09	2.23
CAO	0.25	4.46
SIO2	0.02	0.33
FE2O3	0.0	0.0
AL2O3	0.0	0.0
CL	60.23	1699.01

```
HOLE #     8
DEPTH =    2326.0   FEET

INSOLUBLE
   4.56 WT % OF TOTAL


COMPONENT        WT %           MOLES
---------        ----           -------

   SO3           0.0            0.0

   NA            0.0            0.0

   NA2O          0.0            0.0

   K             0.0            0.0

   K2O           0.03           0.32

   MGO           1.31          32.50

   CAO           0.03           0.53

   SIO2          1.14          18.97

   FE2O3         0.12           0.75

   AL2O3         0.25           2.45

   CL            0.0            0.0
                 ----

SUBTOTAL         2.88  %

MEASURED =       4.56
```

| | HOLE # 8
DEPTH = 2366.3 FEET | | HOLE # 8
DEPTH = 2366.3 FEET | |
| COMPONENT | SOLUBLE
31.37 WT % OF TOTAL | | INSOLUBLE
68.63 WT % OF TOTAL | |
	WT %	MOLES	WT %	MOLES
SO3	16.19	202.22	31.13	388.83
NA	0.62	26.97	0.0	0.0
NA2O	0.0	0.0	3.76	60.66
K	0.0	0.0	0.0	0.0
K2O	7.47	79.30	3.19	33.86
MGO	2.77	68.72	3.63	90.05
CAO	0.16	2.85	3.21	57.24
SIO2	0.01	0.17	10.67	177.57
FE2O3	0.0	0.0	0.01	0.06
AL2O3	0.0	0.0	1.57	15.40
CL	1.17	33.00	0.0	0.0
SUBTOTAL	28.39 %		57.17 %	
MEASURED =	31.37		68.63	

```
                HOLE #    8                          HOLE #    8
                DEPTH =    2427.5  FEET              DEPTH =    2427.5  FEET

                SOLUBLE                              INSOLUBLE
                  99.36 WT % OF TOTAL                  0.64 WT % OF TOTAL

COMPONENT        WT %        MOLES              WT %              MOLES
---------       -----       -------            -----             -------

   SO3           2.22       27.73               0.36             4.50

   NA           39.42     1714.66               0.0              0.0

   NA2O          0.0         0.0                0.0              0.0

   K             0.01        0.26               0.0              0.0

   K2O           0.0         0.0                0.01             0.11

   MGO           0.01        0.25               0.04             0.99

   CAO           0.31        5.53               0.04             0.71

   SIO2          0.0         0.0                0.09             1.50

   FE2O3         0.0         0.0                0.01             0.06

   AL2O3         0.0         0.0                0.01             0.10

   CL           59.88     1689.14               0.0              0.0
                -----                           -----

SUBTOTAL        101.85  %                        0.56  %

MEASURED =       99.36                          0.64
```

HOLE # 8
DEPTH = 2460.0 FEET

SOLUBLE
99.21 WT % OF TOTAL

COMPONENT	WT %	MOLES
SO3	1.14	14.24
NA	38.75	1685.52
NA2O	0.0	0.0
K	0.03	0.77
K2O	0.0	0.0
MGO	0.03	0.74
CAO	0.62	11.06
SIO2	0.0	0.0
FE2O3	0.0	0.0
AL2O3	0.0	0.0
CL	57.00	1607.90
SUBTOTAL	97.57 %	
MEASURED =	99.21	

HOLE # 8
DEPTH = 2460.0 FEET

INSOLUBLE
0.79 WT % OF TOTAL

WT %	MOLES
0.0	0.0
0.0	0.0
0.0	0.0
0.0	0.0
0.01	0.11
0.17	4.22
0.0	0.0
0.19	3.16
0.03	0.19
0.06	0.59
0.0	0.0
0.46 %	
0.79	

```
HOLE #      8
DEPTH =      2519.6   FEET
TOTAL
```

COMPONENT	WT %	MOLES
SO3	0.17	2.12
NA	40.42	1758.16
NA2O	0.0	0.0
K	0.02	0.51
K2O	0.0	0.0
MGO	0.01	0.25
CAO	0.03	0.53
SIO2	0.0	0.0
FE2O3	0.0	0.0
AL2O3	0.0	0.0
CL	60.31	1701.27

HOLE # 8 DEPTH = 2563.0 FEET			HOLE # 8 DEPTH = 2563.0 FEET	
SOLUBLE 7.11 WT % OF TOTAL			INSOLUBLE 92.89 WT % OF TOTAL	
COMPONENT	WT %	MOLES	WT %	MOLES
SO3	1.49	18.61	39.10	488.38
NA	1.47	63.94	0.0	0.0
NA2O	0.0	0.0	6.06	97.77
K	0.05	1.28	0.0	0.0
K2O	0.0	0.0	0.54	5.73
MGO	0.07	1.74	14.66	363.68
CAO	0.60	10.70	23.77	423.86
SIO2	0.0	0.0	6.25	104.01
FE2O3	0.0	0.0	0.96	6.01
AL2O3	0.0	0.0	1.86	18.24
CL	1.05	29.62	0.0	0.0
SUBTOTAL	4.73 %		93.20 %	
MEASURED =	7.11		92.89	

```
HOLE #      8
DEPTH =      2615.5  FEET
TOTAL
```

COMPONENT	WT %	MOLES
SO3	0.86	10.74
NA	38.58	1678.12
NA2O	0.0	0.0
K	0.05	1.28
K2O	0.0	0.0
MGO	0.02	0.50
CAO	0.58	10.34
SIO2	0.0	0.0
FE2O3	0.01	0.06
AL2O3	0.0	0.0
CL	59.37	1674.75

HOLE # 8
DEPTH = 2665.5 FEET

SOLUBLE
99.08 WT % OF TOTAL

COMPONENT	WT %	MOLES
SO3	0.98	12.24
NA	38.68	1,682.47
NA2O	0.0	0.0
K	0.02	0.51
K2O	0.0	0.0
MGO	0.01	0.25
CAO	0.35	6.24
SIO2	0.01	0.17
FE2O3	0.0	0.0
AL2O3	0.0	0.0
CL	59.14	1668.27
SUBTOTAL	99.19 %	
MEASURED =	99.08	

HOLE # 8
DEPTH = 2665.5 FEET

INSOLUBLE
0.92 WT % OF TOTAL

WT %	MOLES
0.0	0.0
0.0	0.0
0.0	0.0
0.0	0.0
0.01	0.11
0.21	5.21
0.01	0.18
0.22	3.66
0.04	0.25
0.06	0.59
0.0	0.0
0.55 %	
0.92	

HOLE # 8
DEPTH = 2706.0 FEET

SOLUBLE
98.75 WT % OF TOTAL

COMPONENT	WT %	MOLES
SO3	1.12	13.99
NA	37.09	1613.31
NA2O	0.0	0.0
K	0.03	0.77
K2O	0.0	0.0
MGO	0.01	0.25
CAO	0.68	12.13
SIO2	0.01	0.17
FE2O3	0.0	0.0
AL2O3	0.0	0.0
CL	58.60	1653.03
SUBTOTAL	97.54 %	
MEASURED =	98.75	

HOLE # 8
DEPTH = 2706.0 FEET

INSOLUBLE
1.25 WT % OF TOTAL

	WT %	MOLES
SO3	0.01	0.12
NA	0.0	0.0
NA2O	0.64	10.33
K	0.0	0.0
K2O	0.03	0.32
MGO	0.18	4.47
CAO	0.0	0.0
SIO2	0.27	4.49
FE2O3	0.27	1.69
AL2O3	0.07	0.69
CL	0.0	0.0
SUBTOTAL	1.47 %	
MEASURED =	1.25	

HOLE # 8
DEPTH = 2758.0 FEET

SOLUBLE
99.22 WT % OF TOTAL

COMPONENT	WT %	MOLES
SO3	1.70	21.23
NA	37.20	1618.10
NA2O	0.0	0.0
K	0.08	2.05
K2O	0.0	0.0
MGO	0.01	0.25
CAO	1.14	20.33
SIO2	0.0	0.0
FE2O3	0.0	0.0
AL2O3	0.0	0.0
CL	58.07	1638.08
SUBTOTAL	98.20 %	
MEASURED =	99.22	

HOLE # 8
DEPTH = 2758.0 FEET

INSOLUBLE
0.78 WT % OF TOTAL

WT %	MOLES
0.0	0.0
0.0	0.0
0.83	13.39
0.0	0.0
0.01	0.11
0.17	4.22
0.0	0.0
0.06	1.00
0.01	0.06
0.02	0.20
0.0	0.0
1.10 %	
0.78	

```
HOLE #   8
DEPTH =   2779.0   FEET
TOTAL
```

COMPONENT	WT %	MOLES
SO3	1.09	13.61
NA	37.41	1627.23
NA2O	0.0	0.0
K	0.01	0.26
K2O	0.0	0.0
MGO	0.03	0.74
CAO	1.80	32.10
SIO2	0.0	0.0
FE2O3	0.0	0.0
AL2O3	0.0	0.0
CL	58.53	1651.06

HOLE # 8
DEPTH = 2794.0 FEET
TOTAL

COMPONENT	WT %	MOLES
SO3	0.99	12.37
NA	37.86	1646.80
NA2O	0.0	0.0
K	0.02	0.51
K2O	0.0	0.0
MGO	0.01	0.25
CAO	0.68	12.13
SIO2	0.0	0.0
FE2O3	0.0	0.0
AL2O3	0.0	0.0
CL	60.58	1708.89

```
HOLE #    8
DEPTH =    2802.5  FEET
TOTAL
```

COMPONENT	WT %	MOLES
SO3	1.76	21.98
NA	38.39	1669.86
NA2O	0.0	0.0
K	0.02	0.51
K2O	0.0	0.0
MGO	0.01	0.25
CAO	0.22	3.92
SIO2	0.0	0.0
FE2O3	0.0	0.0
AL2O3	0.0	0.0
CL	58.19	1641.47

	HOLE # 8 DEPTH = 2809.0 FEET SOLUBLE 99.09 WT % OF TOTAL		HOLE # 8 DEPTH = 2809.0 FEET INSOLUBLE 0.91 WT % OF TOTAL	
COMPONENT	WT %	MOLES	WT %	MOLES
SO3	2.02	25.23	0.0	0.0
NA	38.56	1677.25	0.0	0.0
NA2O	0.0	0.0	0.0	0.0
K	0.01	0.26	0.0	0.0
K2O	0.0	0.0	0.01	0.11
MGO	0.01	0.25	0.03	0.74
CAO	0.96	17.12	0.13	2.32
SIO2	0.0	0.0	0.04	0.67
FE2O3	0.0	0.0	0.0	0.0
AL2O3	0.0	0.0	0.01	0.10
CL	59.70	1684.06	0.0	0.0
SUBTOTAL	101.26 %		0.22 %	
MEASURED =	99.09		0.91	

	HOLE # 8 DEPTH = 2820.5 FEET SOLUBLE 99.46 WT % OF TOTAL		HOLE # 8 DEPTH = 2820.5 FEET INSOLUBLE 0.54 WT % OF TOTAL	
COMPONENT	WT %	MOLES	WT %	MOLES
SO3	1.30	16.24	0.37	4.62
NA	38.42	1671.16	0.0	0.0
NA2O	0.0	0.0	0.0	0.0
K	0.01	0.26	0.0	0.0
K2O	0.0	0.0	0.0	0.0
MGO	0.01	0.25	0.01	0.25
CAO	0.10	1.78	0.19	3.39
SIO2	0.03	0.50	0.03	0.50
FE2O3	0.0	0.0	0.0	0.0
AL2O3	0.0	0.0	0.0	0.0
CL	58.50	1650.21	0.0	0.0
SUBTOTAL	98.37 %		0.60 %	
MEASURED =	99.46		0.54	

	HOLE # 8 DEPTH = 2879.0 FEET			HOLE # 8 DEPTH = 2879.0 FEET	
	SOLUBLE 96.41 WT % OF TOTAL			INSOLUBLE 3.59 WT % OF TOTAL	
COMPONENT	WT %	MOLES		WT %	MOLES
SO3	2.17	27.10		1.97	24.61
NA	32.65	1420.18		0.0	0.0
NA2O	0.0	0.0		0.93	15.00
K	0.02	0.51		0.0	0.0
K2O	0.0	0.0		0.01	0.11
MGO	0.01	0.25		0.12	2.98
CAO	0.59	10.52		0.95	16.94
SIO2	0.02	0.33		0.12	2.00
FE2O3	0.0	0.0		0.01	0.06
AL2O3	0.0	0.0		0.01	0.10
CL	55.79	1573.77		0.0	0.0
SUBTOTAL	91.25 %			4.12 %	
MEASURED =	96.41			3.59	

HOLE # 8
DEPTH = 2948.0 FEET

	SOLUBLE 97.32 WT % OF TOTAL		INSOLUBLE 2.68 WT % OF TOTAL	
COMPONENT	WT %	MOLES	WT %	MOLES
SO3	3.41	42.59	1.92	23.98
NA	37.30	1622.45	0.0	0.0
NA2O	0.0	0.0	0.0	0.0
K	0.01	0.26	0.0	0.0
K2O	0.0	0.0	0.01	0.11
MGO	0.01	0.25	0.02	0.50
CAO	0.54	9.63	0.25	4.46
SIO2	0.01	0.17	0.05	0.83
FE2O3	0.0	0.0	0.01	0.06
AL2O3	0.0	0.0	0.0	0.0
CL	55.51	1565.87	0.0	0.0
SUBTOTAL	96.79 %		2.26 %	
MEASURED =	97.32		2.68	

Selected x-ray diffraction traces of EDTA-insoluble residues from the ERDA-9 core.

I-2. MB-CS-42: Serpentine and saponite; the sharp maxima at 12.2 and 24.5$^{\circ}2\theta$ are basal spacings of serpentine's 7Å periodicity. The broad peak at 7.25$^{\circ}2\theta$ (air-dried) becomes a broad weak shoulder at ∿5$^{\circ}2\theta$ upon glycol saturation and is saponite.

 A. <2μm EDTA-insoluble residue, air-dried.
 B. Bulk EDTA-insoluble residue, glycol-saturated.

I-3. MB-CS-15: Talc and smectite (saponite); sharp peaks at 9.5 and 28.5$^{\circ}2\theta$ are basal spacings of talc's 9.5Å periodicity; they do not shift with glycol-saturation. The broad low-angle peak again is saponite; accessory amounts of serpentine also present.

 A. <2μm EDTA-insoluble residue, air-dried.
 B. Bulk EDTA-insoluble residue, glycol-saturated.

I-4. MB-CS-17: Regularly interstratified mixed-layer chlorite-saponite (corrensite); distinct strong superlattice reflection at 2.9$^{\circ}2\theta$ (air-dried) which expands to 2.7$^{\circ}2\theta$ with glycol-saturation. The peak at 6.4$^{\circ}2\theta$ (air-dried) expands to 5.6$^{\circ}2\theta$.

 A. <2μm EDTA-insoluble residue, air-dried.
 B. <2μm EDTA-insoluble residue, glycol-saturated.

I-5. JL-CS-9: Randomly interstratified mixed-layer chlorite-saponite; air-dried peak at 6.1$^{\circ}2\theta$ expands to 5.5$^{\circ}2\theta$ with glycol saturation. Illite (8.7, 17.6, and 26.6$^{\circ}2\theta$), minor serpentine (12.3 and 13.1$^{\circ}2\theta$), and minor feldspar (27.4$^{\circ}2\theta$) also present.

 A. <2μm EDTA-insoluble residue, air-dried.
 B. <2μm EDTA-insoluble residue, glycol-saturated.

I-6. MB-CS-13: Saponite; reflections at 6.1 and 27.3$^{\circ}2\theta$ which expand to 5.2$^{\circ}2\theta$ upon glycol saturation. A small quantity of a regularly interstratified mixed-layer clay (small superlattice peak at 2.4$^{\circ}2\theta$) also present.

 A. <2μm EDTA-insoluble residue, air-dried.
 B. <2μm EDTA-insoluble residue, glycol saturated.

I-7. JL-CS-2: Randomly interstratified mixed-layer clay, either talc-saponite or illite-saponite; single strong maximum at 8.6$^{\circ}2\theta$ becomes pronounced doublet at 9.6 and 7.6$^{\circ}2\theta$ with glycol saturation.

 A. <2μm EDTA-insoluble residue, air-dried.
 B. <2μm EDTA-insoluble residue, glycol-saturated.

°2θ Cu Kα

°2θ Cu Kα

°2θ K_α
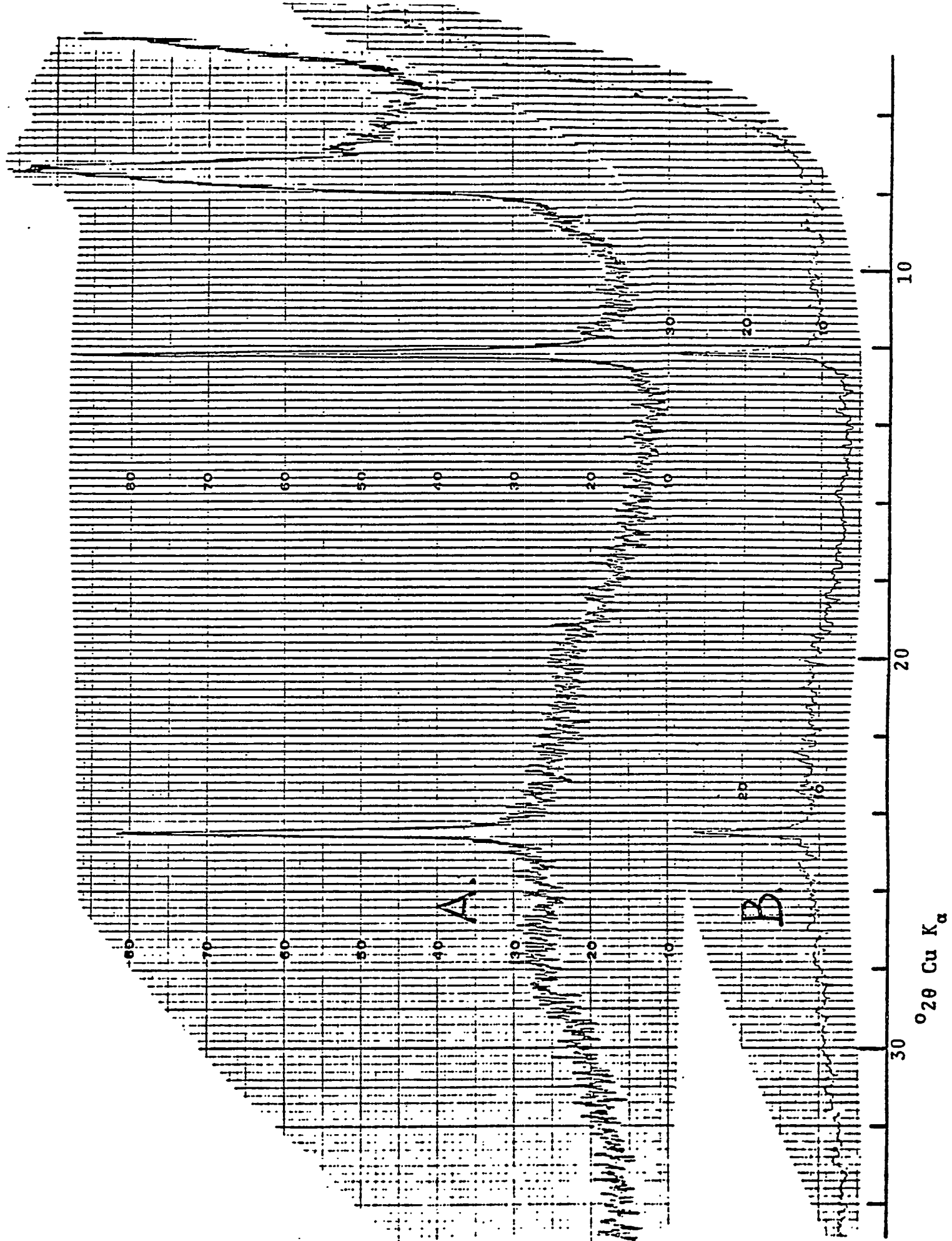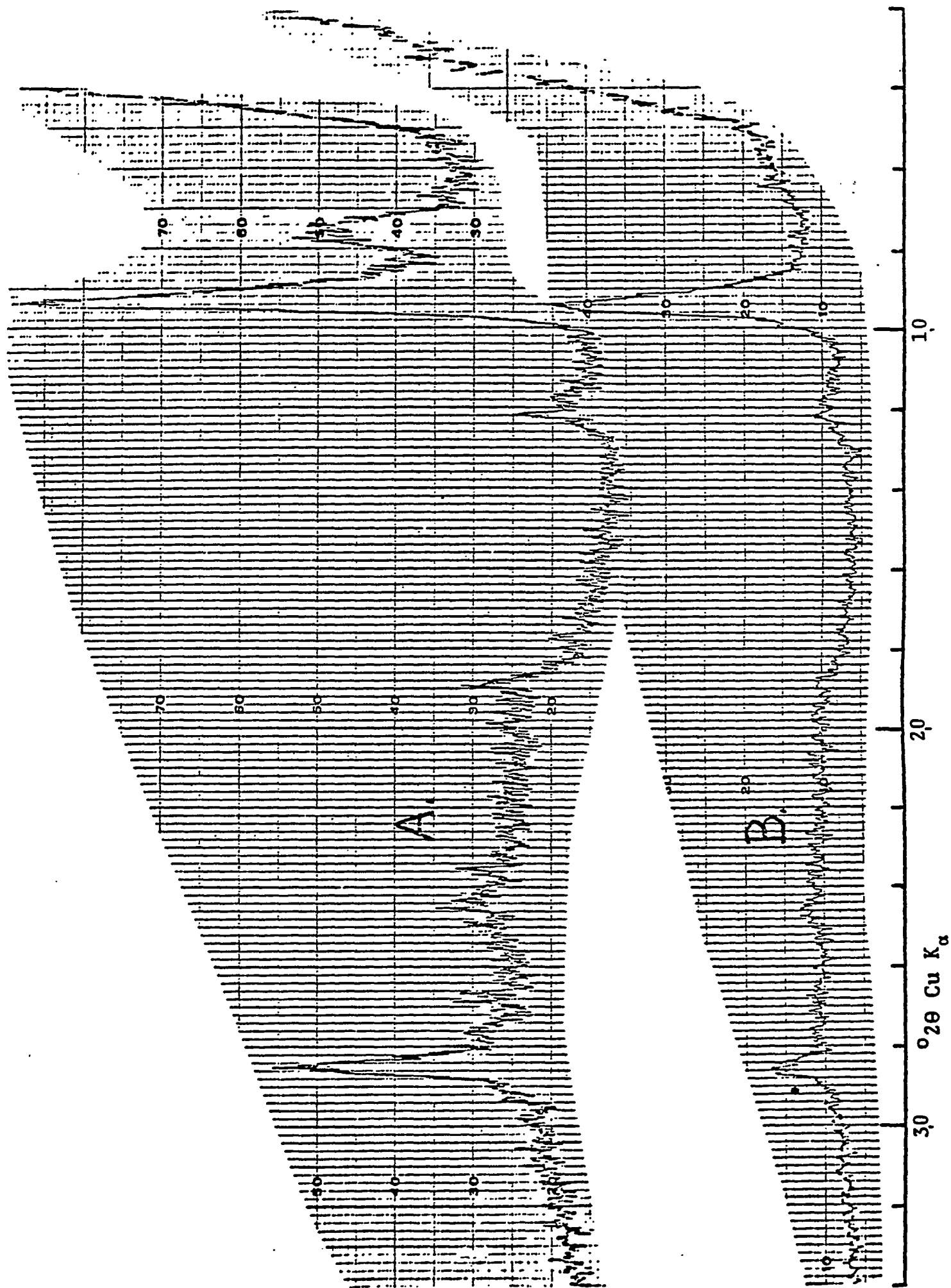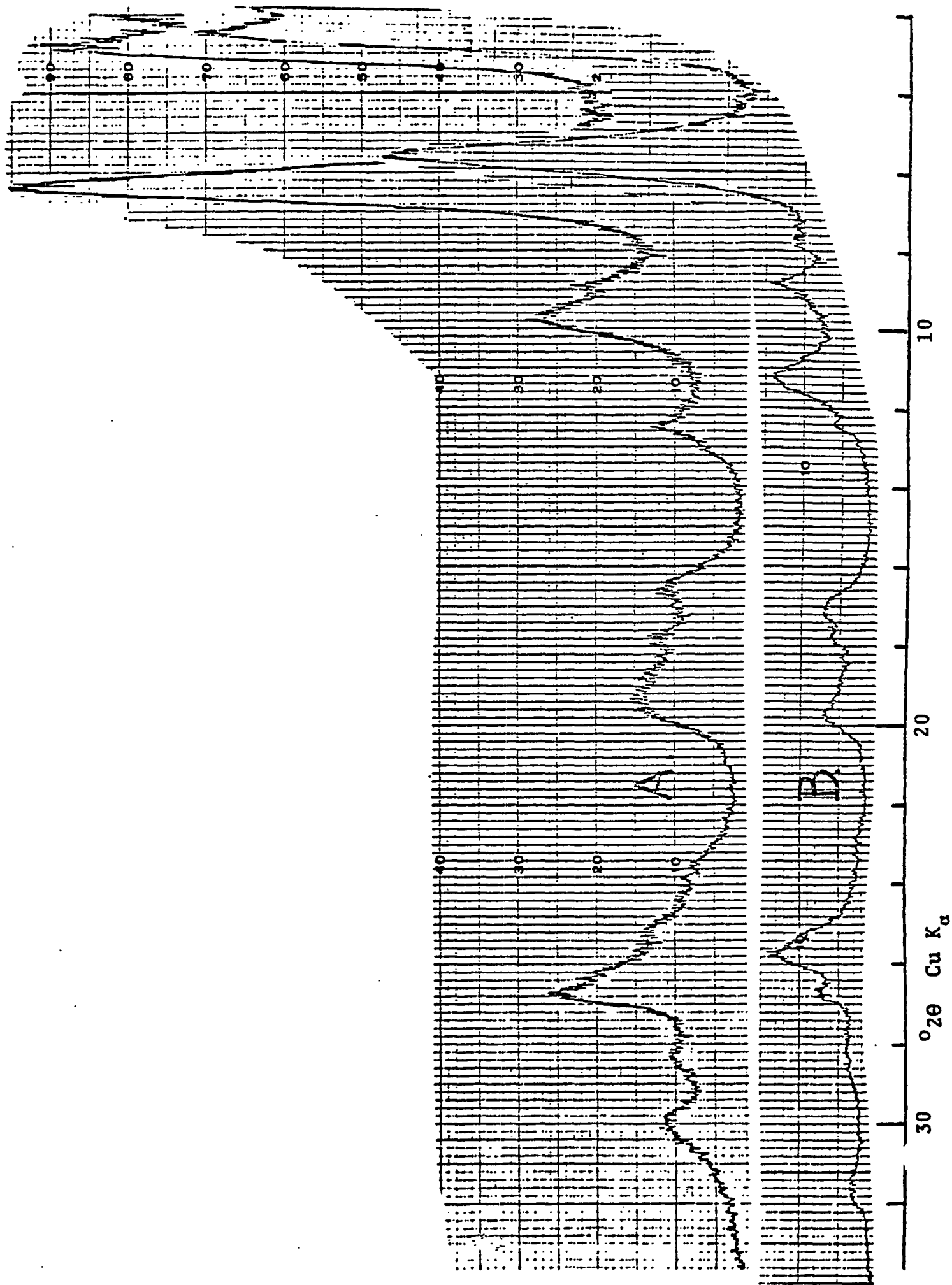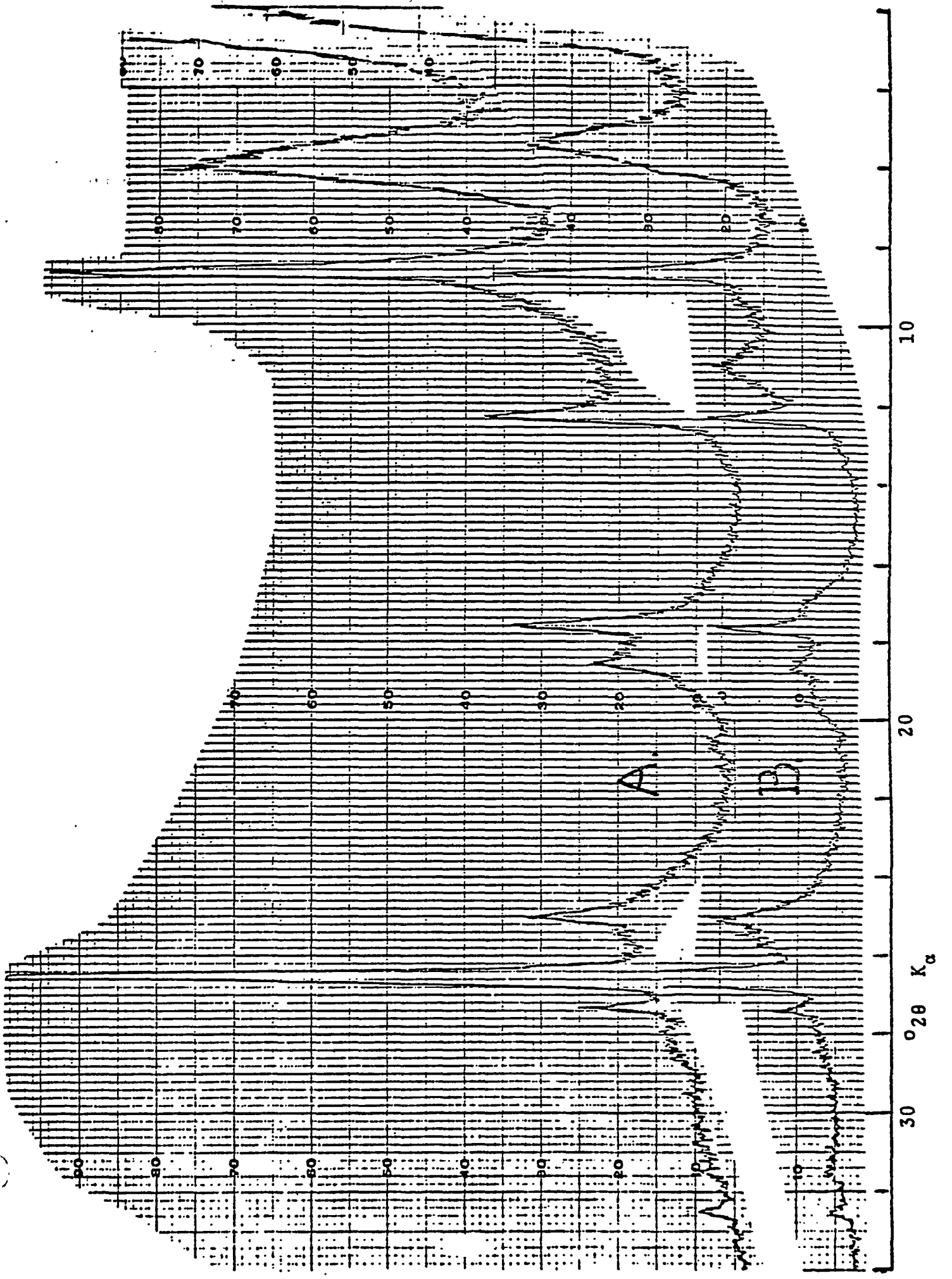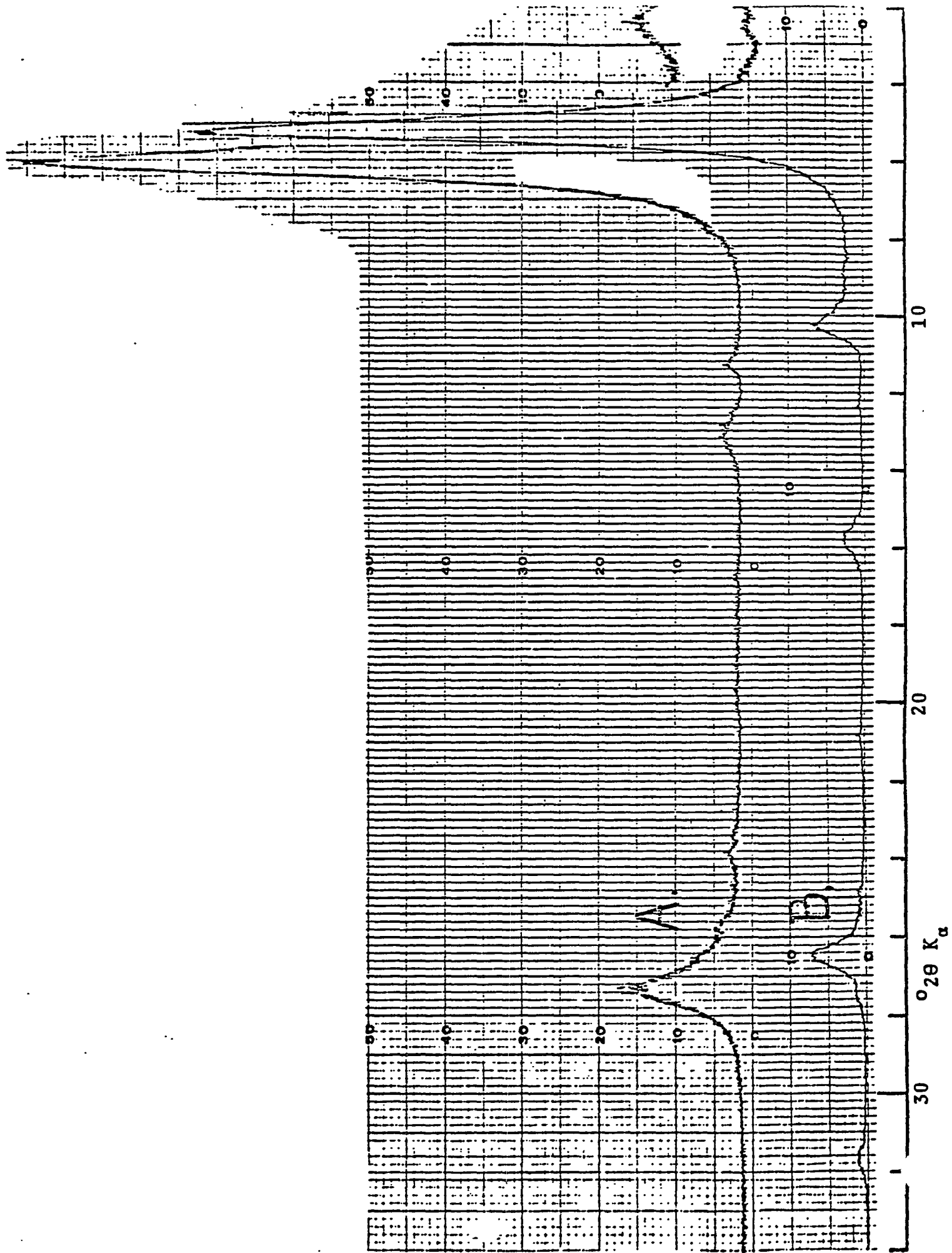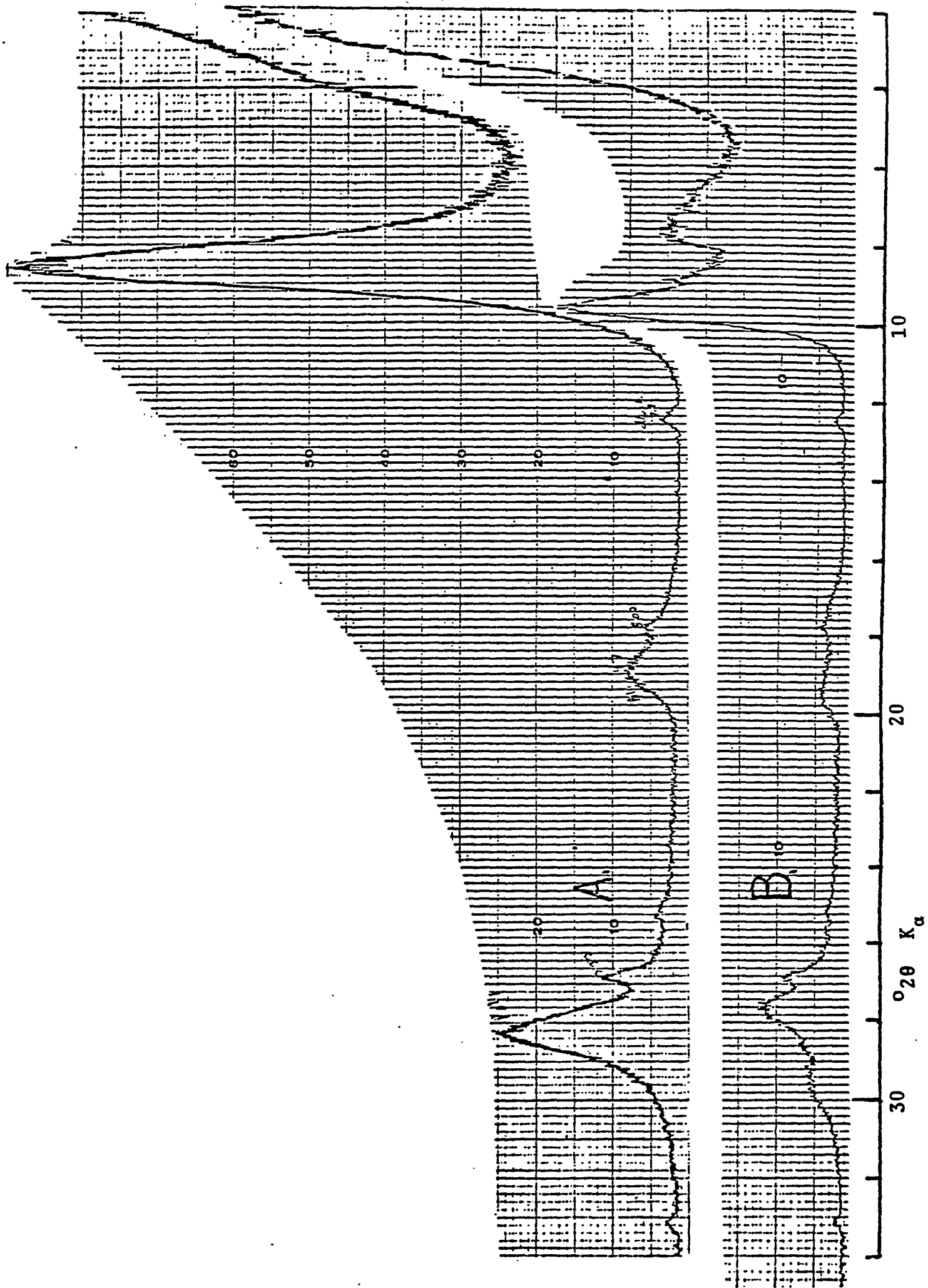
APPENDIX 7.b (Ref. sec. 7.4)

Core Footage (Sandia Core Photo #), Informal Lithology and Detailed
   Macroscopic Core Description

   FI in left column indicates abundant fluid inclusions.

   + just to left of right column indicates description incorpo-
      rates stratigraphic variation within that interval.

Abbreviations and Meanings used in Core Description (right column)

anhy or anhyd	anhydrite
ave	average
brwn	brown
dom	dominant
fg	fine grained or finely crystalline
inc	increasing
irreg	irregular
L	length
lams	laminae or laminations
lite or lt	light
loc	local or locally
max	maximum
repl	replacement
struc	structure
thk	thick or thickness
W	Width
w/	with
Xtals or Xtalline	crystals or crystalline
μX	microcrystalline

Core Footage (Sandia Photo #)	Informal Lithology	Macroscopic (aided by binocular microscope) Core Description
1162.7 (27) 1163.7	Halite	lite brwn, clear, anhedral Xtals (1cm), sharp Xtal boundaries of halite minor 1-4mm thk, lenses of lite gray, µX, anhydrite rimmed with polyhalite
1165.2 (28) 1166.6	Anhydrite w/ halite "crystal growth"	dominantly gray, µX anhydrite w/ slight color banding (gray-lite gray) with: lenses (1/2 to 1 cm thk.) of brown, clear to opaque, poorly defined anhedral Xtals, of halite layers (1 to 4 cm thk) of vertically elongate (L/W=2 to 3, L=2mm to 3 1/2 cm), locally swallow-tail, Xtals of halite
1167.3 (28) 1168	Banded Anhydrite	banding of dominantly gray, µX anhydrite laminae (5-10mm thk) with white, thin (<1mm) laminae of µX magnesite locally a few anhedral (some swallow tail) Xtals of halite, locally vertically elongate or radiating
1168 (29) 1168.25	Anhydrite	similar to 1165.2 - 1166.6 but including laminae (~1mm thick) of magnesite
1168.25 (29) 1169.9	brick-red Polyhalite and Halite	dominantly anhedral (rare euhedral) 1/2 cm Xtals of halite, clear to cloudy with red, µX polyhalite between and in halite crystals
1172.6 (30) 1173.5	Banded Polyhalite	prominant banding but mineralogy obscure - "brown mineral" typically opaque, microcrystalline or massive halite, orange to orange brown poorly bounded anhedra ~1/2 cm - silty claystone or anhydrite? locally contorted banding

Core Footage (Sandia Photo #)	Informal Lithology	Macroscopic (aided by binocular microscope) Core Description
1173.5 (31) 1174.7	Halite	halite – clear to red, anhedral Xtals (ave 1/2 cm, max 2 cm) red from polyhalite stain; minor anhydrite
1404.7 (103) 1405.7	11th ore zone (leonite, kainite?)	polyhalite (± halite?) white & cloudy to blood red, massive w/ irreg. patches of dark gray claystone and irreg patches of pale yellow mineral (kainite-leonite?) massive patches are both vertically and horizontally elongate
1418 (106-107) 1418.8	Marker Bed 117, polyhalite plus mud	dominantly massive red polyhalite (w/ microscopic granular texture) laminations 1/2 to 1 1/2 cm thk alternating w/ clay laminae (<2mm thk) which are black & wavy [near 1418 – claystone w/ poor horizontal fissility plus "brown mineral" which looks like halite but has bitter taste]
1584 (160) 1584.9	5th ore zone, very dirty	dominantly halite – clear anhedra ~1 cm (max 2 cm) locally stained by "brown mineral" μXtalline coatings & locally patches a few mm in size; minor patches of gray μX anhydrite
1609.1 (168) 1610.3	Clear Halite (~2 ft above polyhalite)	dominantly halite – brwn (due to polyhalite stain?) indistinct anhedral about 1 1/2 cm; minor evenly dispersed polyhalite stain, and patches (~2mm) of gray material (anhydrite or clay?)
1632 (175) 1632.8	Mudstone	near top: banded anhydrite – claystone; anhydrite dark gray, μX – laminae up to 2mm thk, locally vertically elongate masses or Xtals; claystone lite grey, laminae from 1/2mm to 1/2 cm (thk inc. upward) near base: polyhalite w/ gray clay

Core Footage (Sandia Photo #)	Informal Lithology	Macroscopic (aided by binocular microscope) Core Description
1648.5 (180-181) 1649.7	4th ore zone halite, bloedite, vanthoffite	dominantly halite - lite brown anhedra ~3/4 cm locally red, µXtal polyhalite as stain & repl. of halite - some lenses and Xtal coatings of gray µX anhydrite?
2034.3 2037.3	Halite	↑ dominantly halite: finely crystalline & clayey near top - coarsely crystalline & banded anhydrite &/or polyhalite near center - finely crystalline & banded ↑ w/ anhydrite near base
2065.2 2067.6	Halite	dominantly coarsely Xtalline (~2 cm) clear, anhedral halite w/ patches, lenses & stains of "brown material" (polyhalite, carnallite, glauberite?) loc w/ radiating acicular texture
2301.6 (384) 2302.7	lite colored Polyhalite	dominantly red, µX polyhalite - locally crinkly flakes & irreg. patches of white fg. material
2413.6 FI (418-419) 2415.7	pure & impure Polyhalite	↑ dominantly poorly thickly banded polyhalite w/ sub-equal lenses of anhydrite & halite polyhalite: pinkish brown to red, µX halite: med. to coarsely Xtal, usually anhedral but some euhedra, typically clear anhydrite: layers, lenses and interXtalline patches, ↑ gray, µX, locally brown
2512 (450) 2512.5	dirty Halite	dominantly halite-gray, clear to cloudy, anhedral, 1 cm Xtal; minor light gray anhydrite as interXtalline patches
2515.6 (452+) 2519.2	typical massive Cowden Anhy.	↑ (halite above 2516.9) faintly banded gray, µX, anhydrite w/ wispy lenses of magnesite ↑ very minor halite

Core Footage (Sandia Photo #)	Informal Lithology	Macroscopic (aided by binocular microscope) Core Description
2527.7 (456+) 2529.2	typical laminated Cowden Anhy.	laminations of gray, μX, anhydrite - lam up to 1 1/2 cm (some needle like & loc radiating into magnesite) white, opaque μX magnesite lams, wavy, <1mm to 3mm thk
2538.5 (459) 2539.4	base of Cowden Anhy.	top: faintly banded (color) μX anhydrite, minor patches of halite ↑ dominantly coarsely Xtalline (~1 cm) clear, anhedral halite w/ lenses & interXtalline anhydrite base: similar to middle but halite Xtal size decreases to ~1mm
2541 (460) 2542.5	dirty halite just below Cowden	dominantly halite - gray, clear to cloudy, anhedral Xtals (ave 1 cm, <1mm to 3 cm) minor anhydrite (or magnesite?) - interXtalline patches (1 or 2 cm by 2mm)
2606.5 2608.8	Halite	dominantly halite - typically clear but some cloudy, white to gray anhedra typically ~1 cm but three 3 cm thk zones of ave size ~2mm which tend to be gray; minor anhydrite - interXtalline gray, μX
2614.7 2615.6	Halite	dom. halite - clear white euhedra & subhedra, most anhedra, ave 2 cm (<1mm to 4 cm); minor anhydrite - lt gray to white, μX, interXtalline
2615.9 FI 2619.5	Halite	↑ 15.9 - 16.5 dom halite - clear, white to gray, anhedra, ave 2 cm (1/2 - 6 cm) w/ v minor gray-white, μX, interXtalline anhyd or magnesite 16.5 - 18.4 dom halite - clear to cloudy, white to gray anhedra, ave 1 cm (<1mm - 2 cm) locally "chevron struc" within (& across) Xtals w/ minor gray-white, μX, interXtalline anhyd or magnesite ↑ 18.4 - 19.5 similar to 15.9 - 16.5

Core Footage (Sandia Photo #)	Informal Lithology	Macroscopic (aided by binocular microscope) Core Description
(2705.7) 2704.8 (509) (2706.8) 2706.5	mottled Anhy & Halite	dominantly halite – coarsely Xtalline (1 to 1 1/2 cm) anhedral, clear to white cloudy cut at ~45° by zones more finely Xtalline halite and mixed w/ up to 30% interXtalline gray, µX, anhydrite (w/ minor magnesite)
2758 (526) 2759.3	dirty Halite	dom halite – light to dk gray, anhedra, ave ~1 cm (<1mm to 3 cm) w/ minor anhydrite – dk gray, µX (but some microlites) as interXtall material
2819.1 (545) 2819.8	clean Halite, slightly banded	dom halite – cloudy, white to lt. gray, anhedral; faint banding by ave Xtal size variation from 1/2 to 1 cm, finer Xtalline tends to be whiter; minor thin horizontal lenses (rare patches), white, µX (rare microlites)
2819.9 (545) 2820.9A	see above	dom anhydrite – lt gray to dk gray (locally banded), µX; subordinate halite – irreg lenses & patches (frequently thin & horiz elongate) unusually sharp contacts between anhydrite & halite
2820 B (545–546) 2820.6B	see above	same as 19.9 – 20.9A except anhydrite locally brown and may contain magnesite
2820.6B (546) 2821.9	see above	dom halite – cloudy, white, anhedral, ave 1 cm (<1mm to 2 cm); very rare lense of wh to lt gray, µX anhydrite possibly w/ magnesite
2826.5 2827.5	dirty Halite	dom halite – poorly developed banding from clear, to cloudy white, to opaque dk gray, anhedral crystals ave 1/2 – 1 cm some magnesite (or anhydrite) – thin irreg seams & wavy lams (both horiz), white, µX

Core Footage (Sandia Photo #)	Informal Lithology	Macroscopic (aided by binocular microscope) Core Description
2845.6	massive light Anhydrite	dom anhydrite – mottled from clear to white & cloudy to gray to dk gray
2846.4	(in Castile)	sub. magnesite – thin seams and irreg patches, μX
2847.8	banded light	dom anhydrite – banded from clear, to white & cloudy, to gray to dk gray, to black; clear tends to occur
2849.1	Anhydrite	in laminae & lenses, locally "enterolithic" contortions and w/ smooth lower contacts & irreg "swallowtail" upper contacts; subordinate magnesite

Appendix 7.E (Ref. sec. 7.5)

Gas Chromatograms and Mass Spectra
of Volatiles from Selected Samples
of Core from ERDA No. 9

Mass spectra are reported as intensity (normalized
to the highest mass peak) as a function of
mass/charge ratio (in atomic mass units).
Gas chromatograms are reported as intensity of
elution peaks (normalized to the highest elution peak)
as a function of relative elution time (in
arbitrary units).

SALT SAMPLE   2302.6
        TOTAL ION CHROMATOGRAM   X6
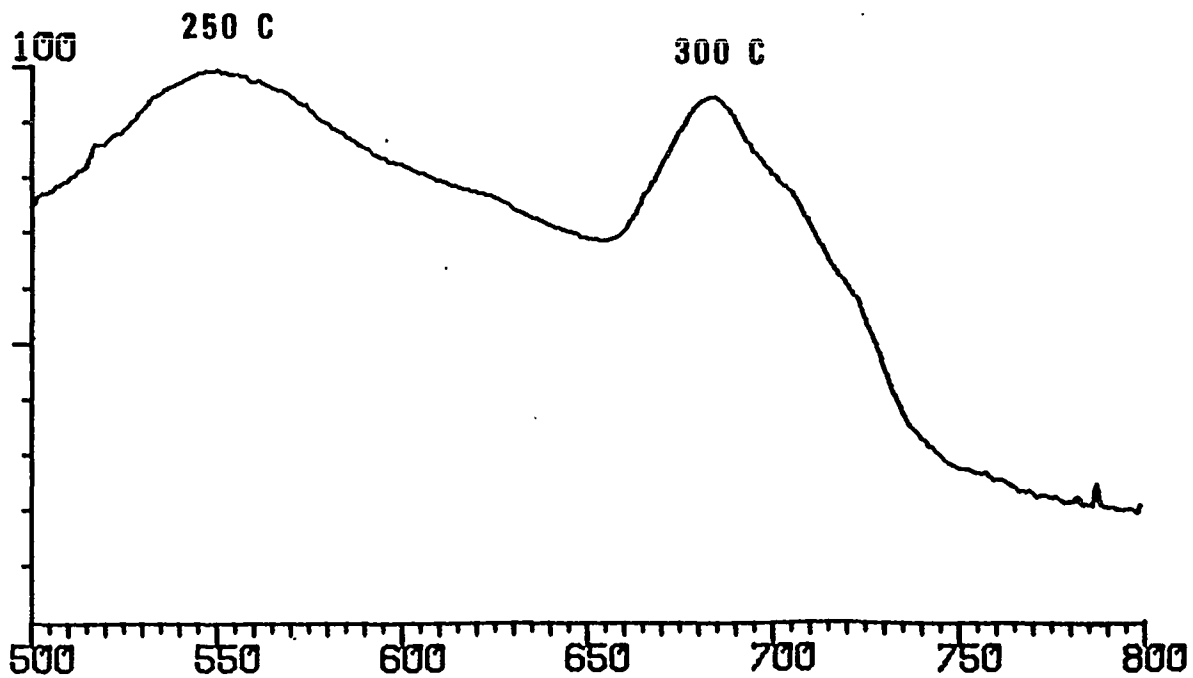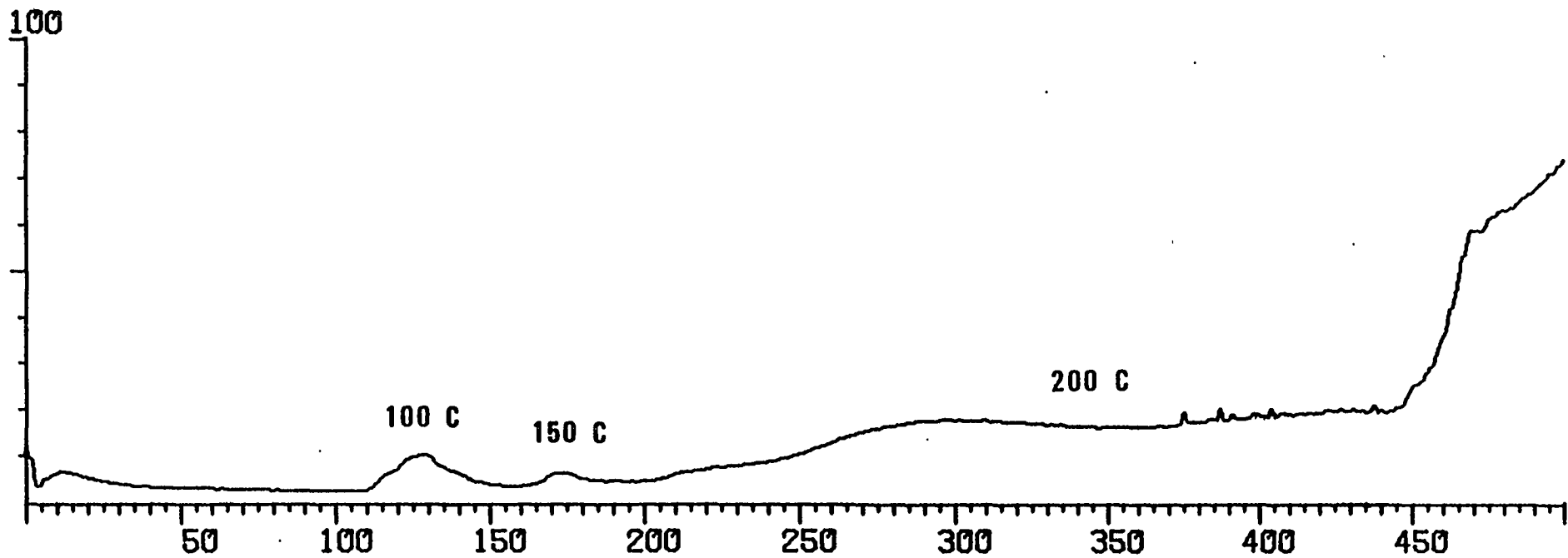
SALT SAMPLE

12   MASS SPECTRA   50C X3   2302.6

100

50

150   100   50
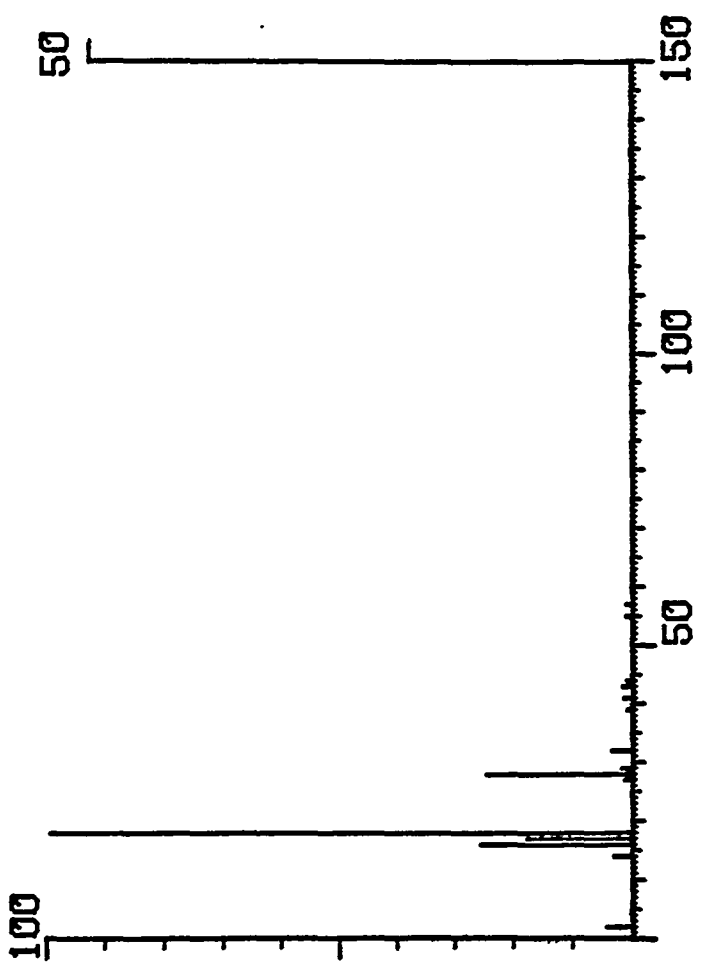
SALT SAMPLE 2302.6
128 MASS SPECTRA 100C X3
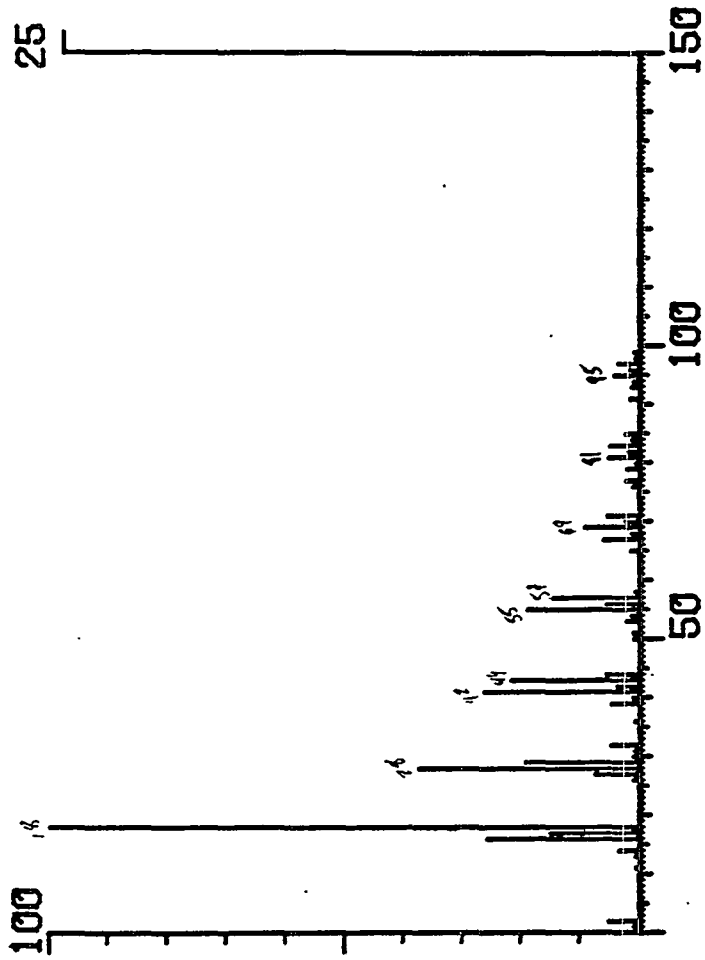
SALT SAMPLE

174   MASS SPECTRA   150C X3   2302.6
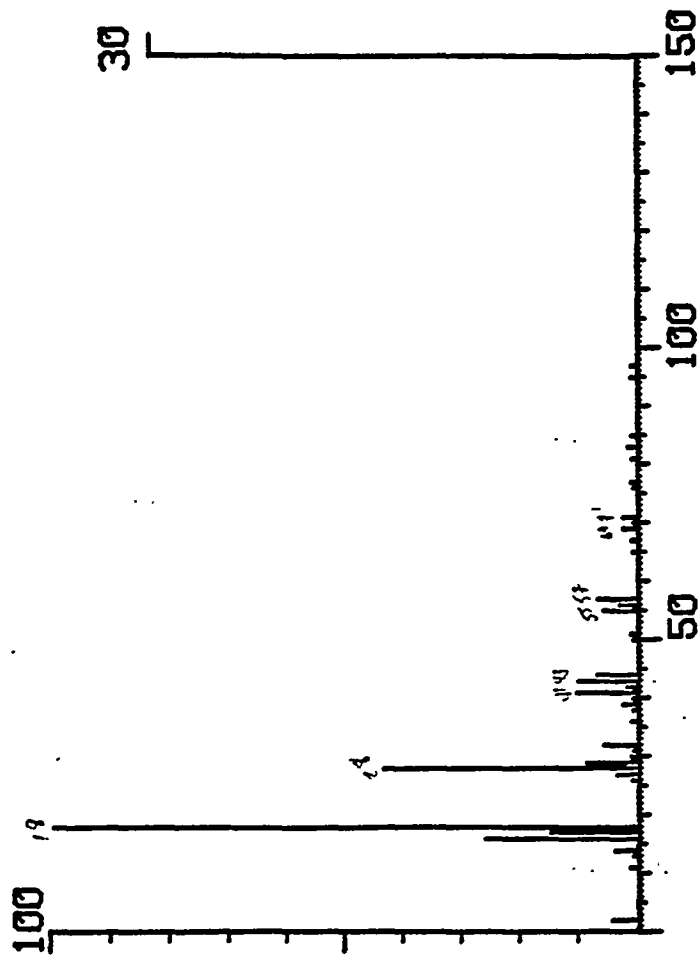
SALT SAMPLE   2302.6
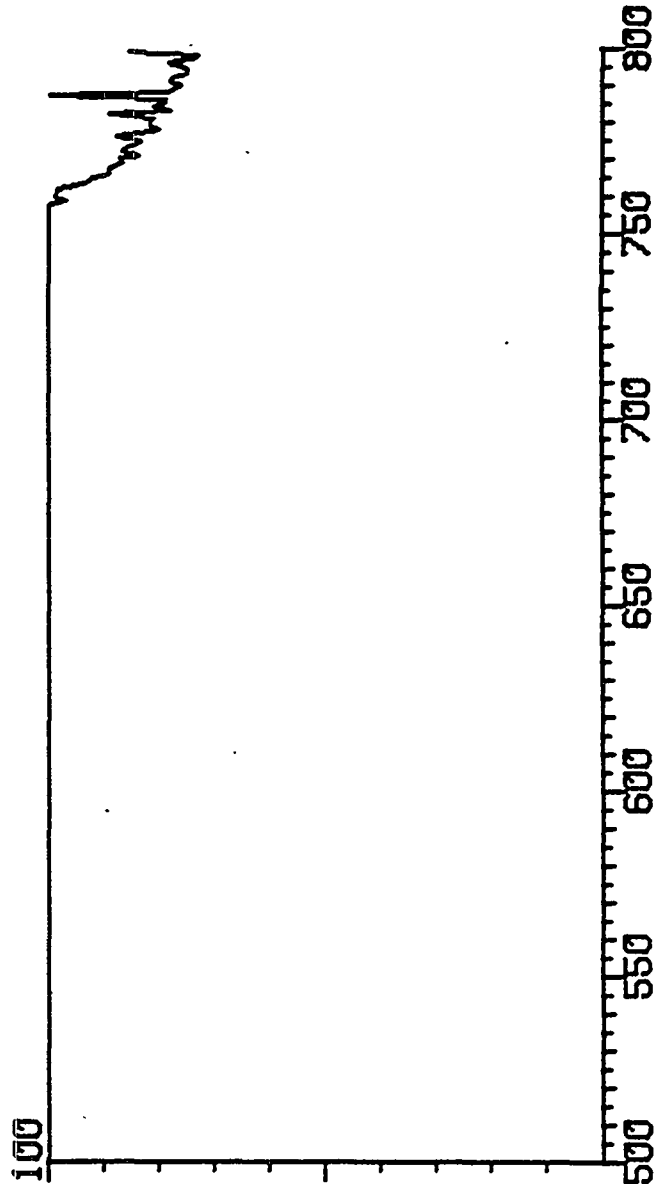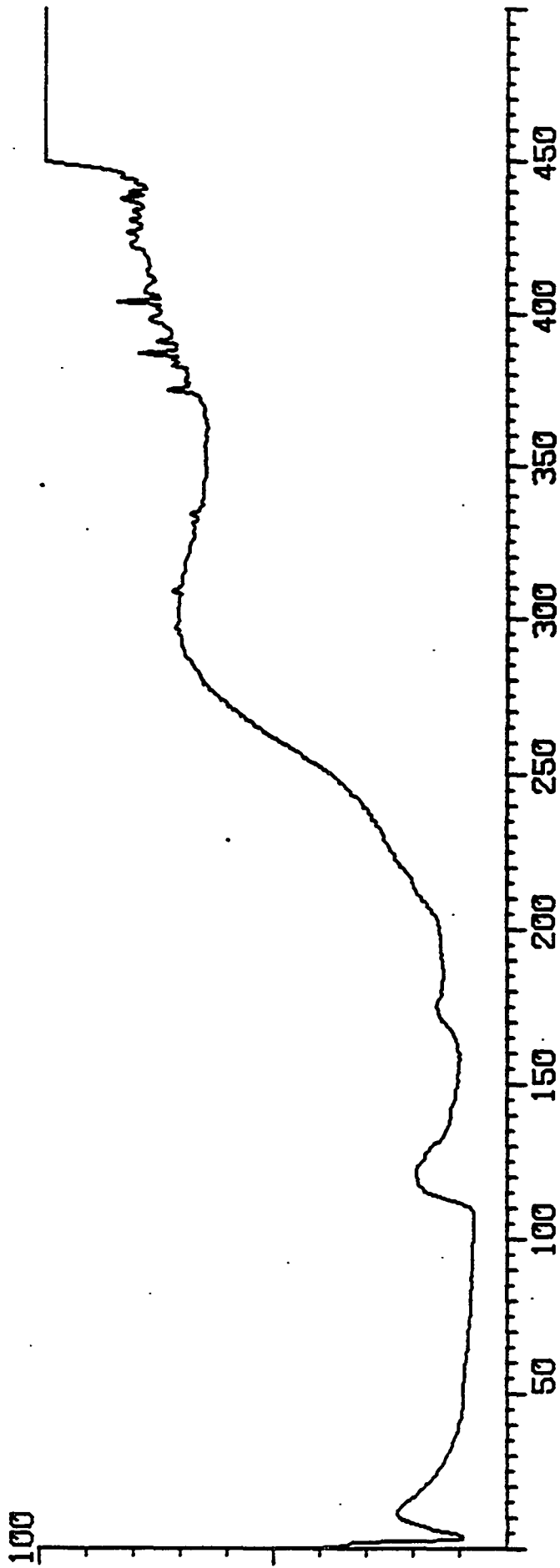# 297   MASS SPECTRA   200C X4
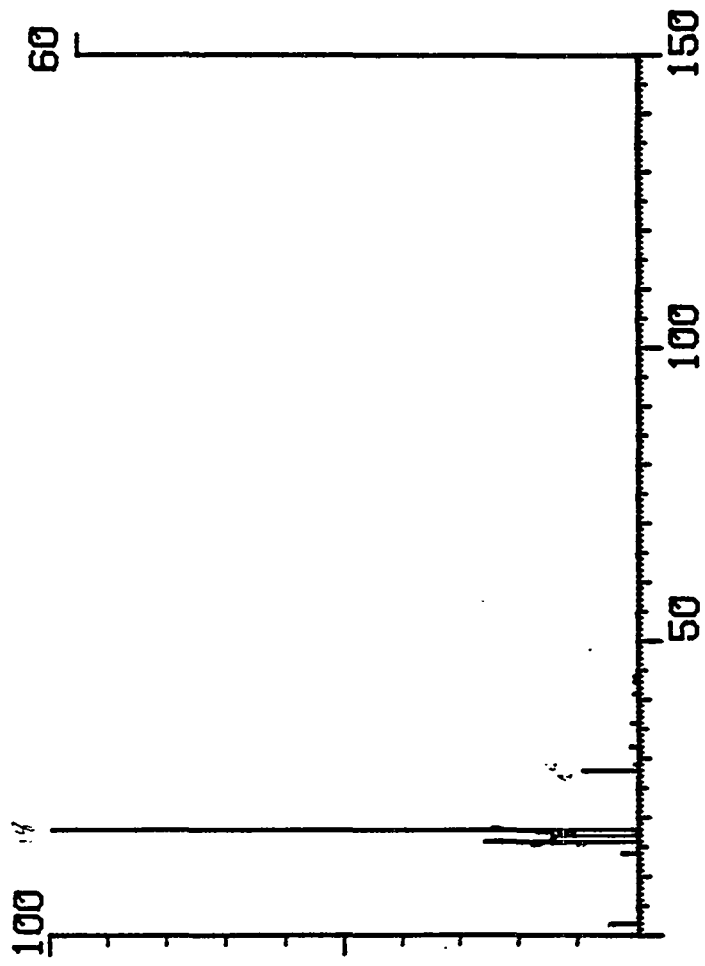
SALT SAMPLE   2302.6

550   MASS SPECTRA   250C X4
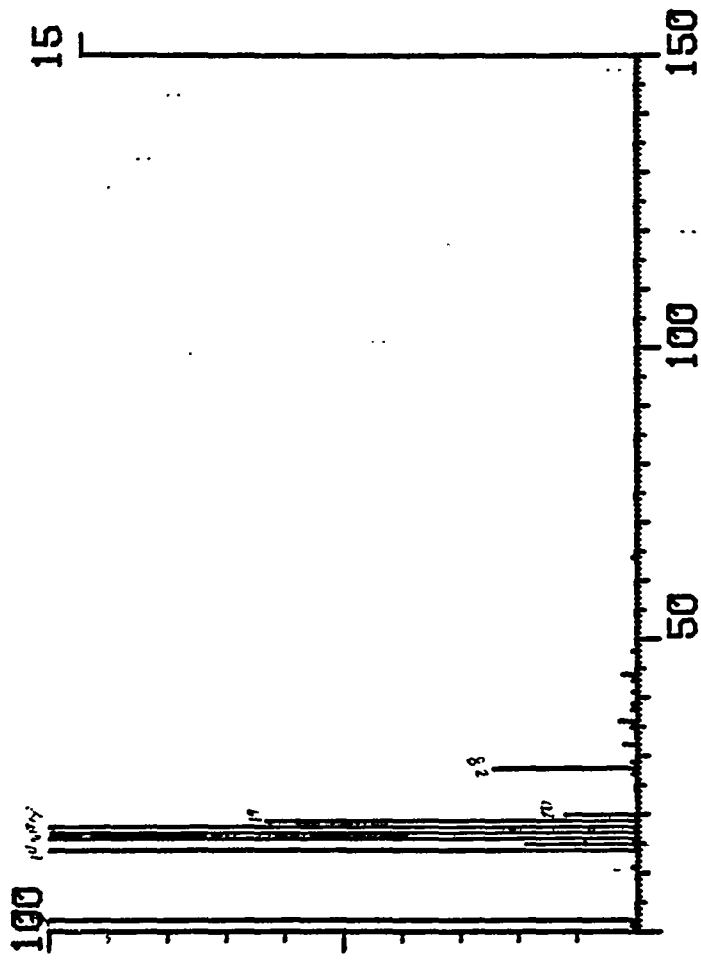
SALT SAMPLE   2302.6
686   MASS SPECTRA   300C X4

SALT SAMPLE

MASS 14 SEARCH X5
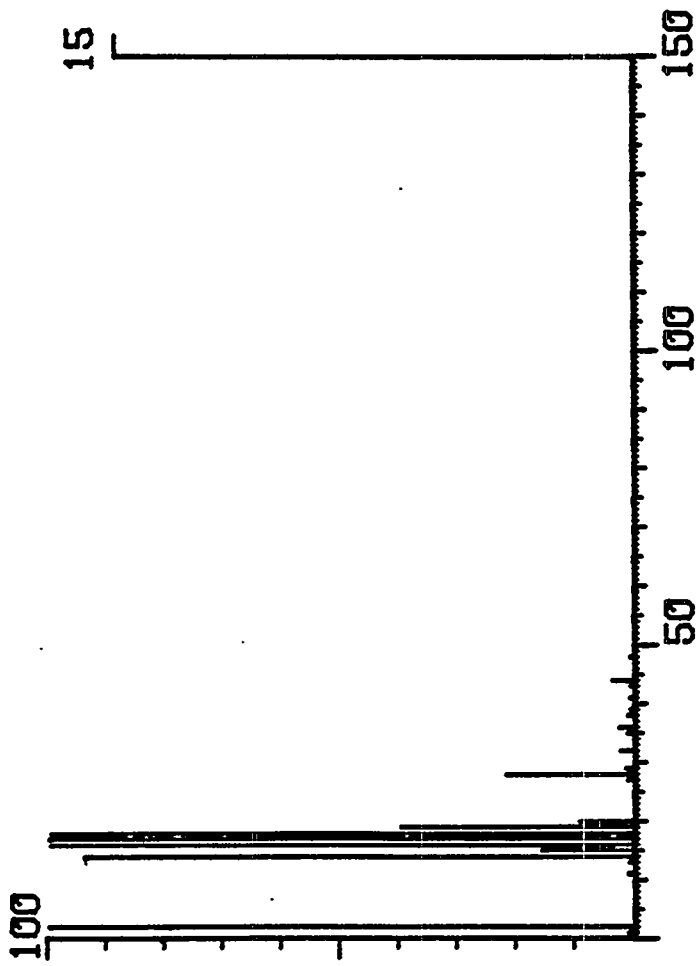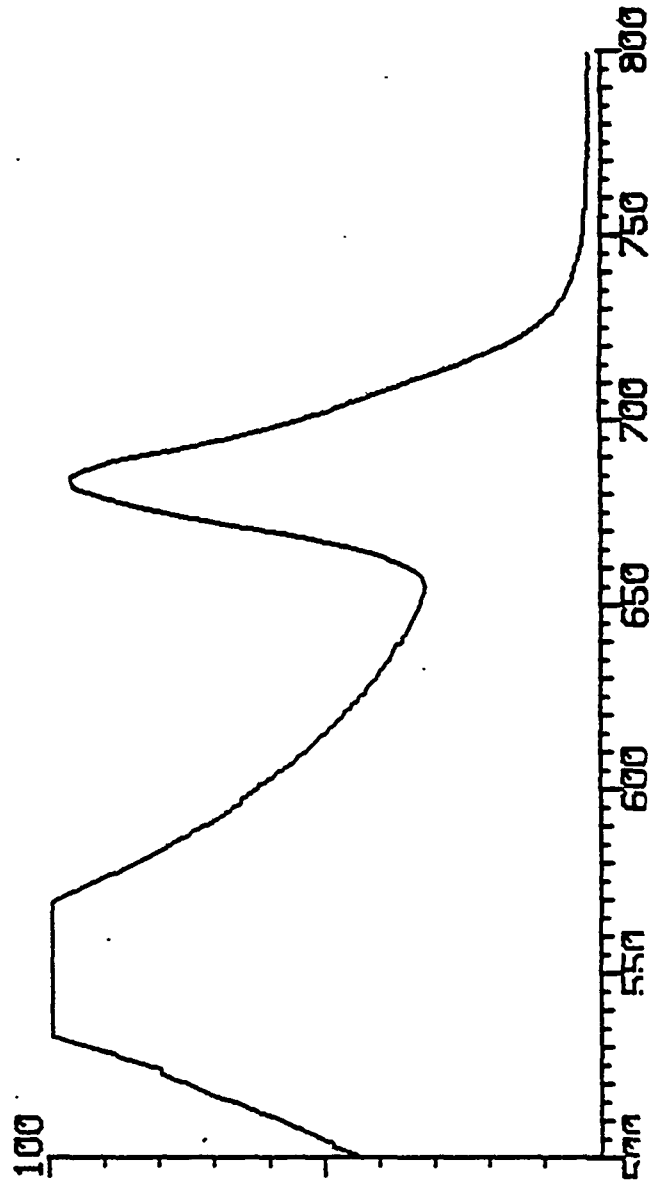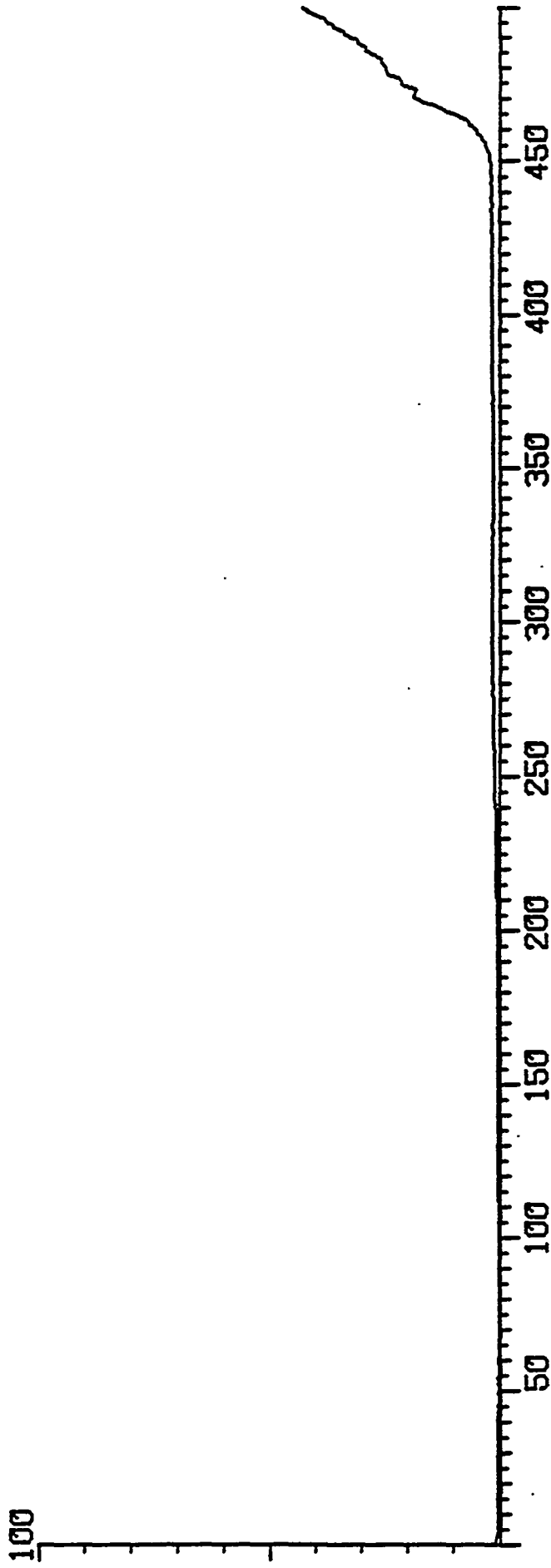
2302.6

SALT SAMPLE
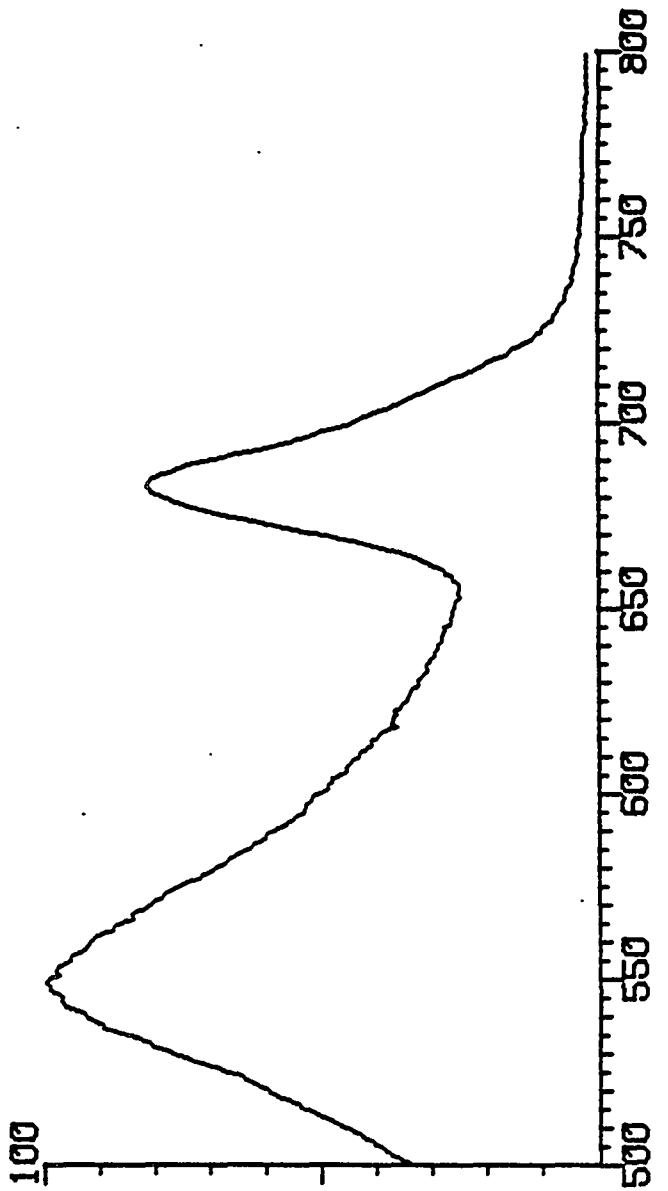
2302.6

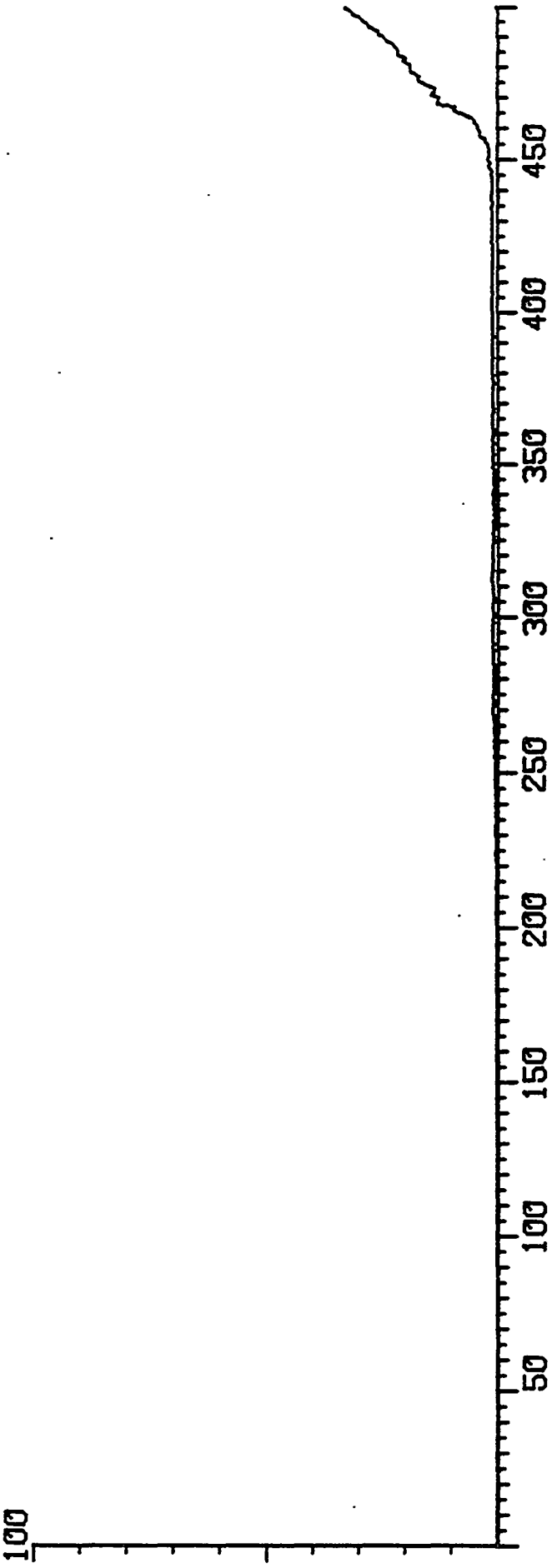MASS 18 SEARCH X4

SALT SAMPLE

MASS 19 SEARCH X4   2302.6
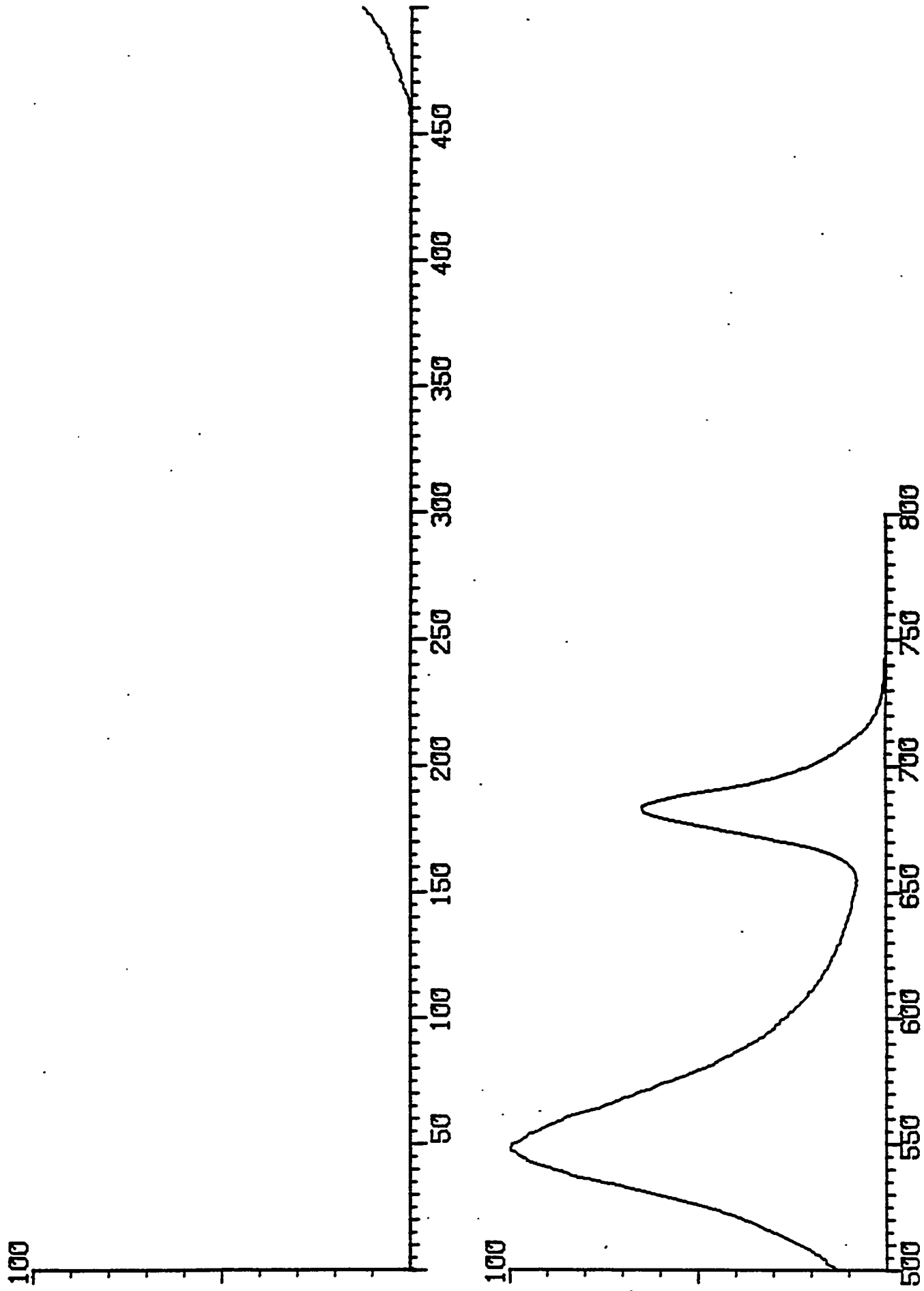
SALT SAMPLE   2302.6

MASS 20 SEARCH X3

SALT SAMPLE

MASS 32 SEARCH X2   2302.6

SALT SAMPLE   2302.6

MASS 36 SEARCH X2

SALT SAMPLE

MASS 44 SEARCH X2
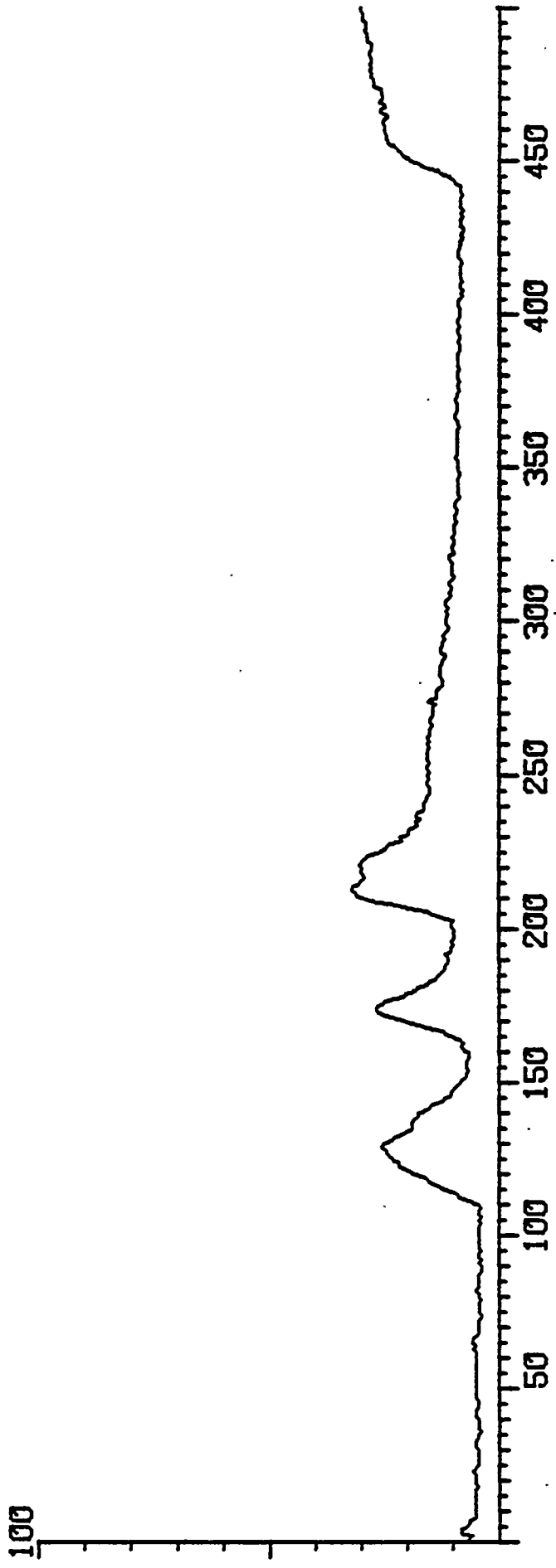
2302.6
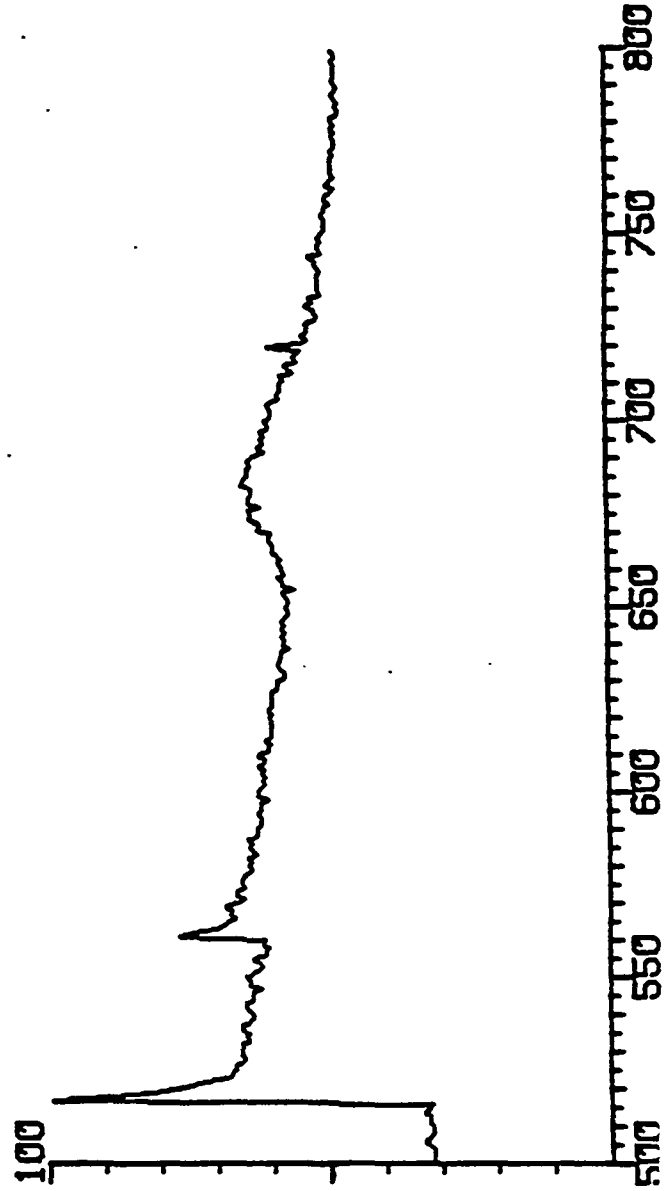
SALT SAMPLE   2302.6

MASS 48 SEARCH X1

SALT SAMPLE
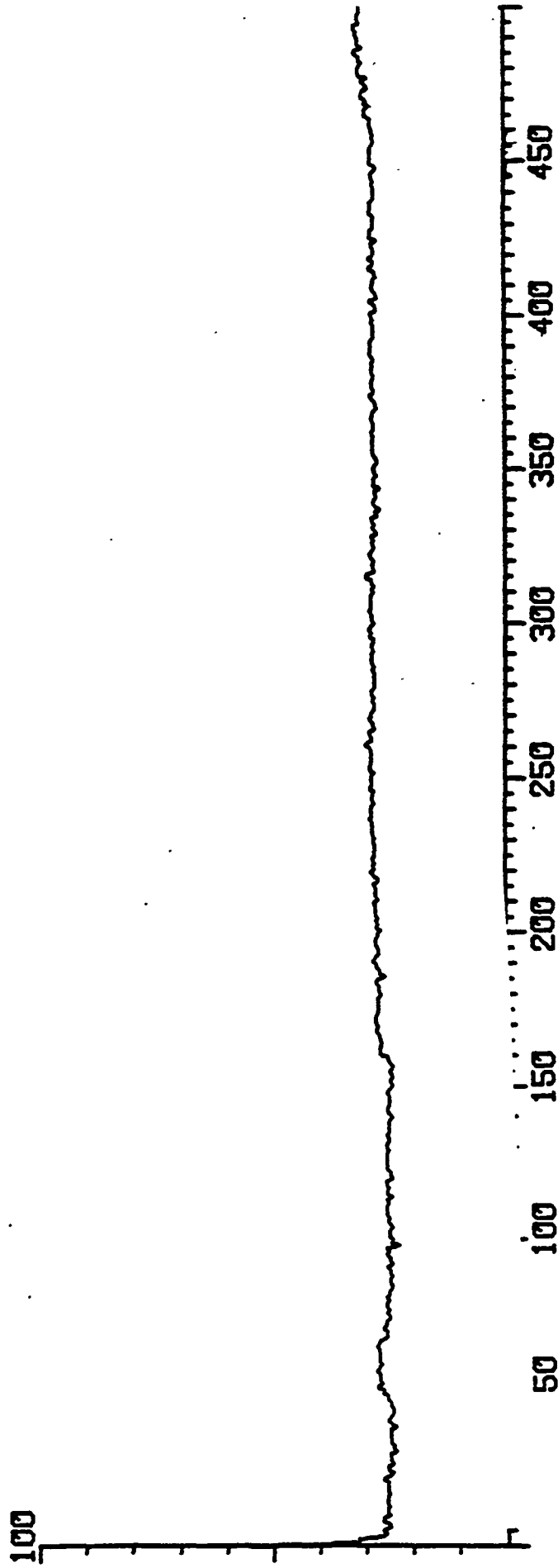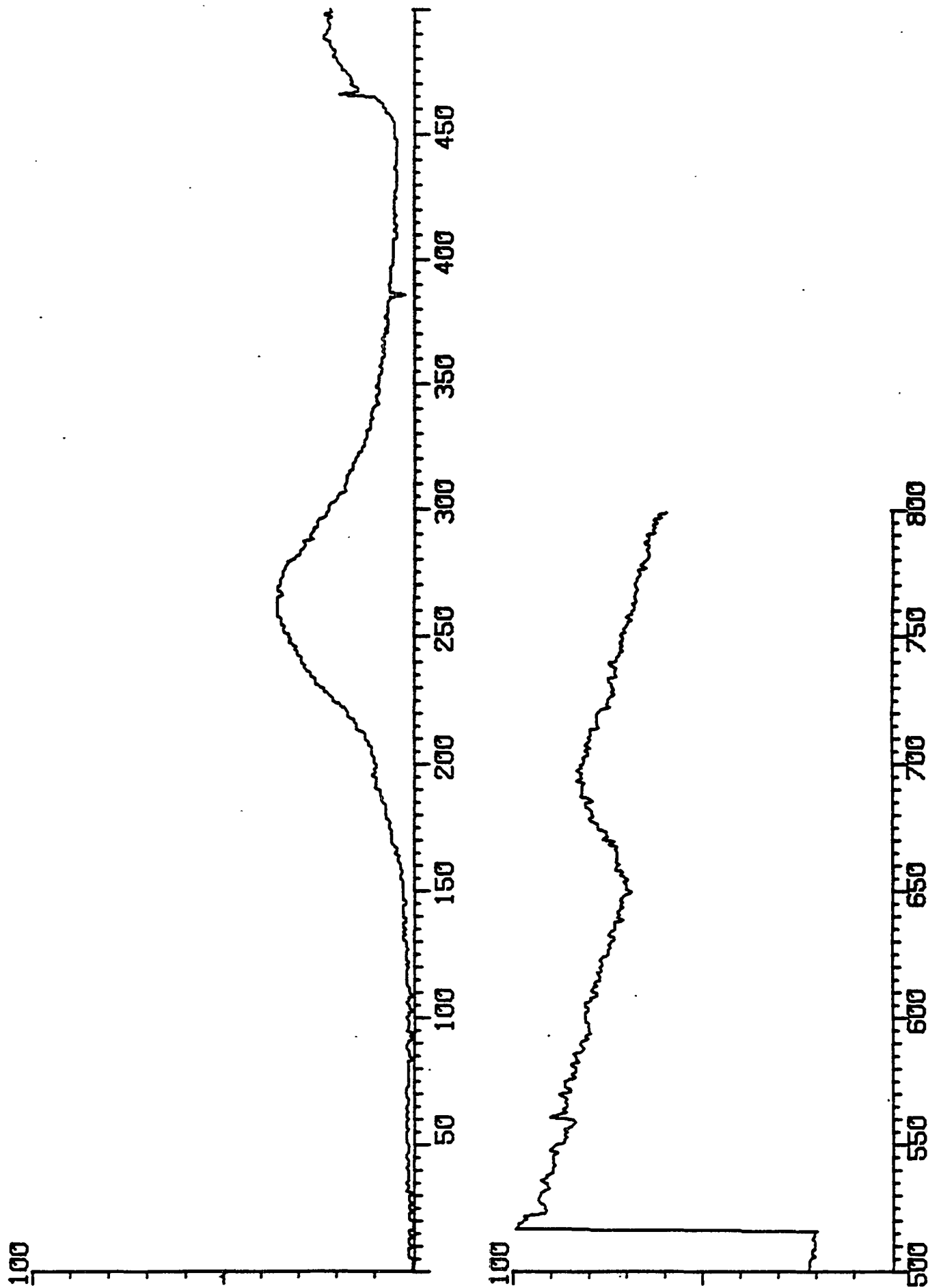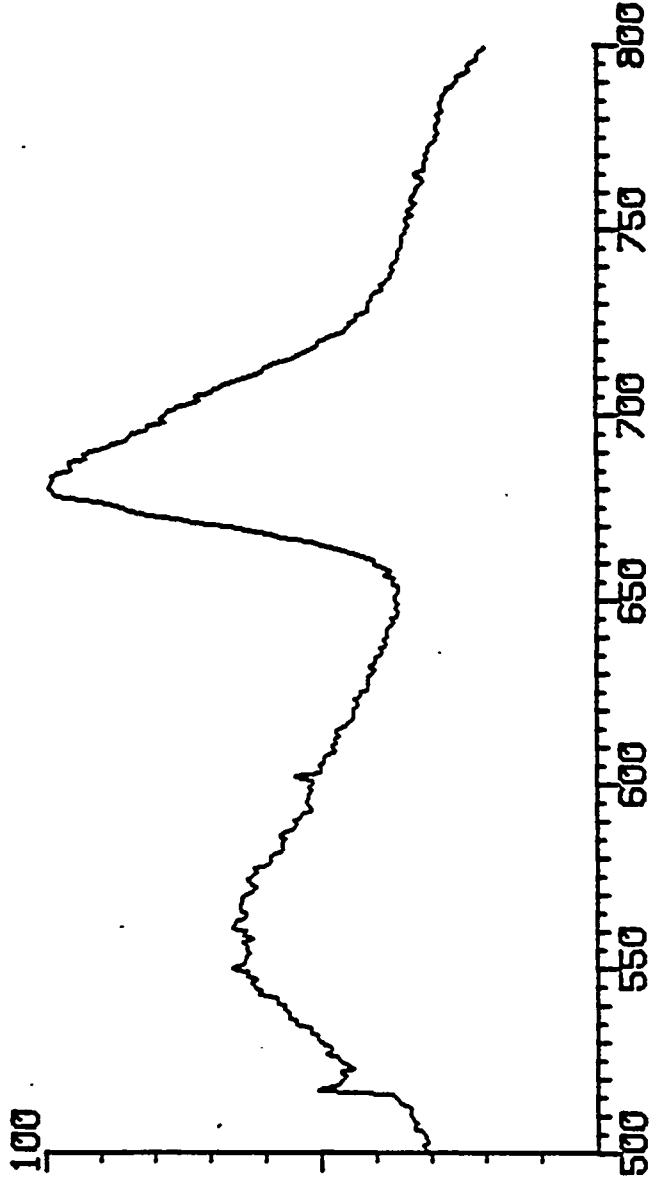
2302.6

MASS 64 SEARCH X1

SALT SAMPLE   2302.6

MASS 80 SEARCH X1

SALT SAMPLE   2302.6

517   CH 517 – CH 522 X1
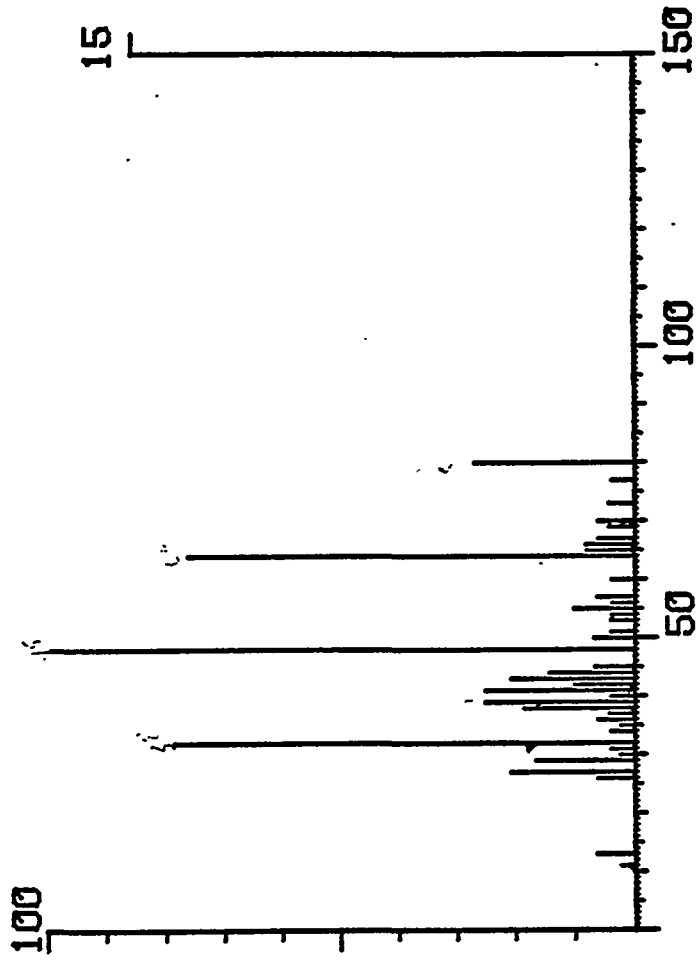
SALT SAMPLE   2516.3
            TOTAL ION CHROMATOGRAM

100

SALT SAMPLE   2516.3

MASS 18 SEARCH X3

100
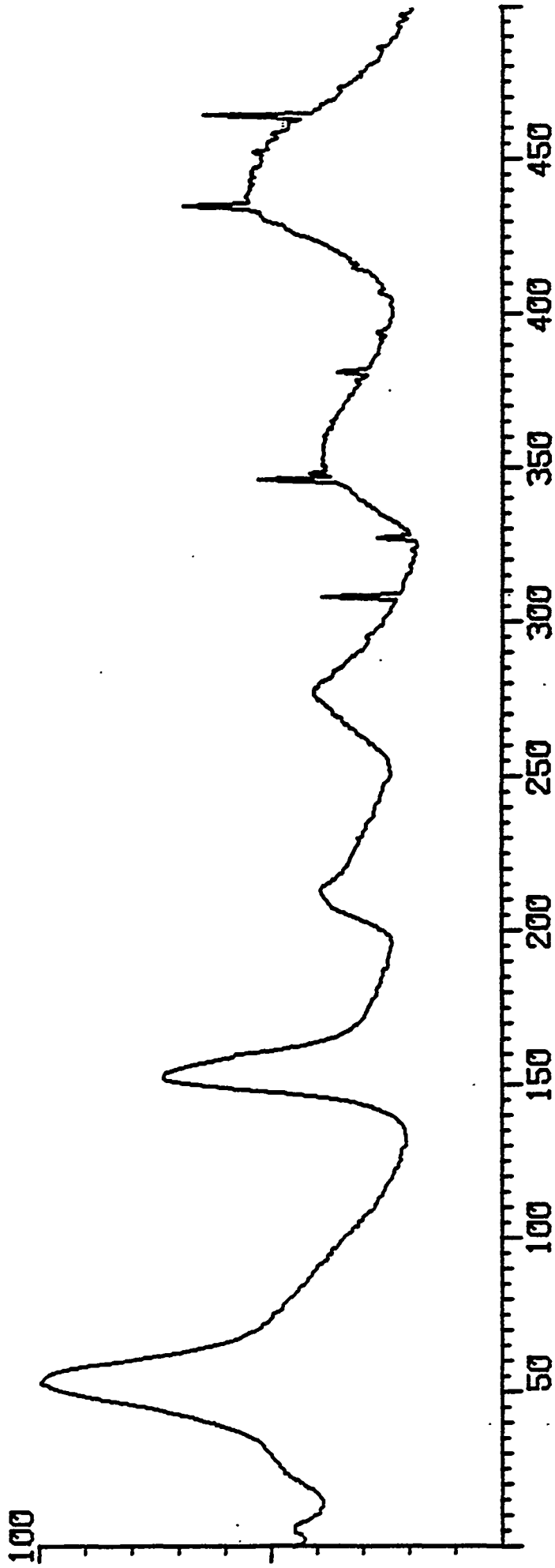
SALT SAMPLE   2516.3

MASS 28 SEARCH X3

100

50   100   150   200   250   300   350   400   450
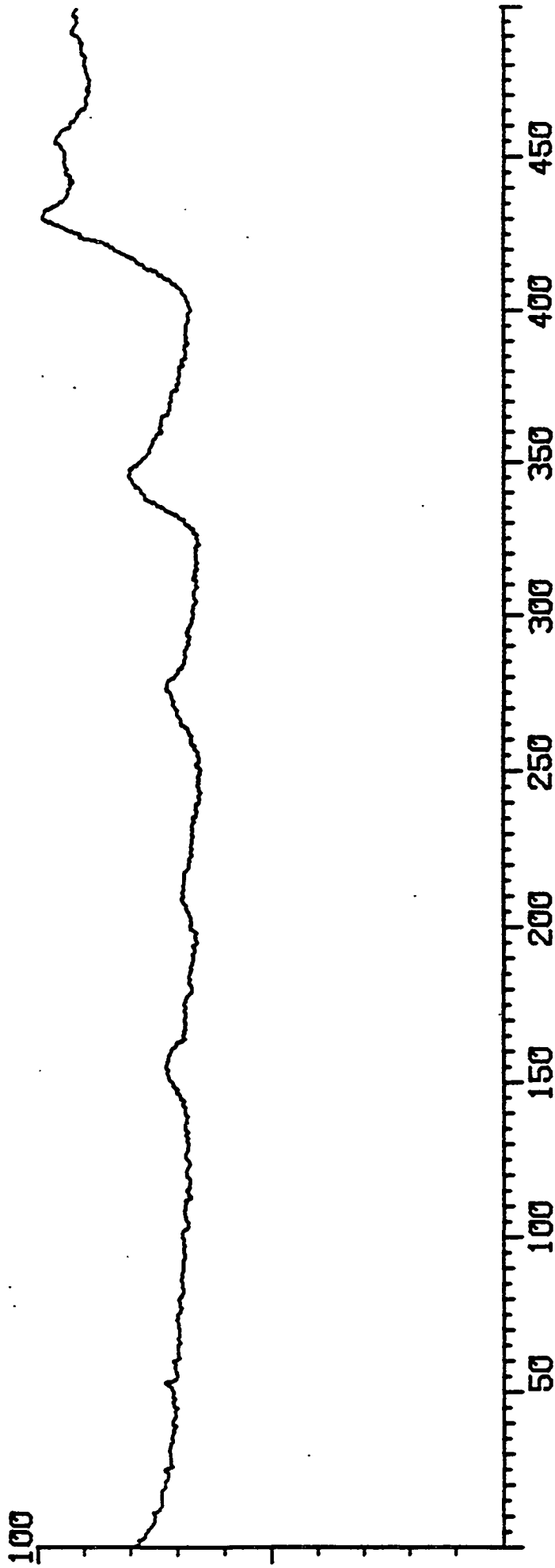
SALT SAMPLE   2516.3

MASS 32 SEARCH X2

100

50   100   150   200   250   300   350   400   450

SALT SAMPLE   2516.3

MASS 36 SEARCH X2

100

50   100   150   200   250   300   350   400   450
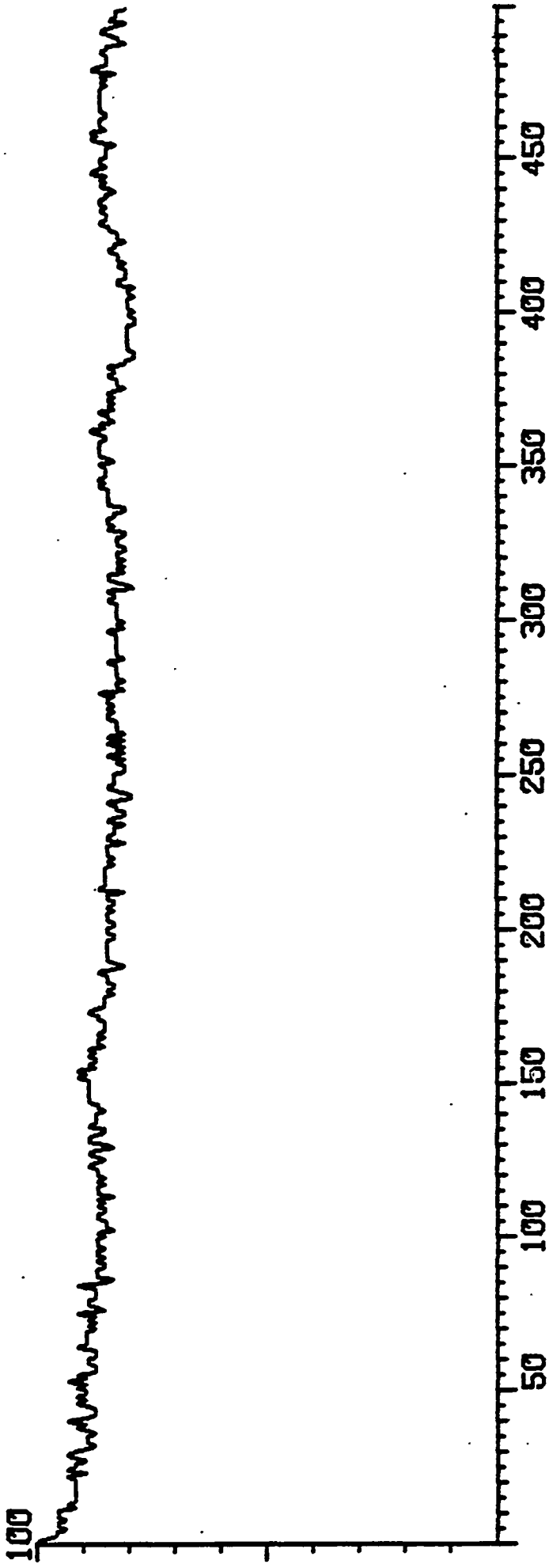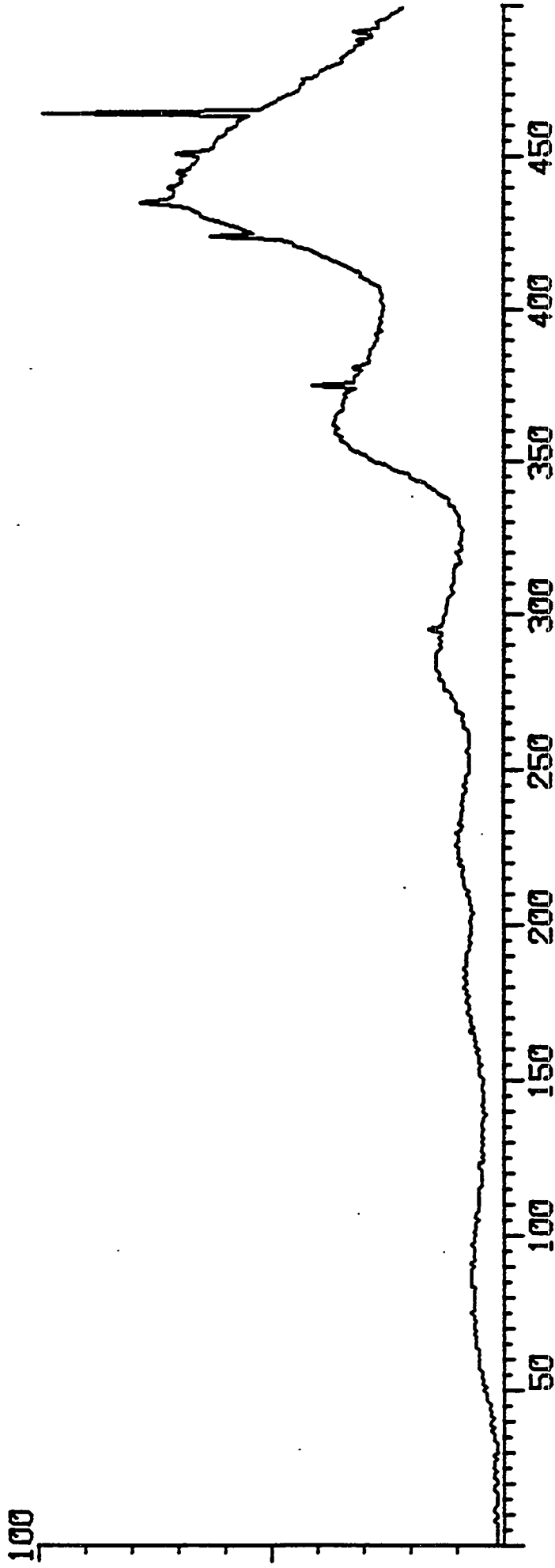
SALT SAMPLE   2516.3
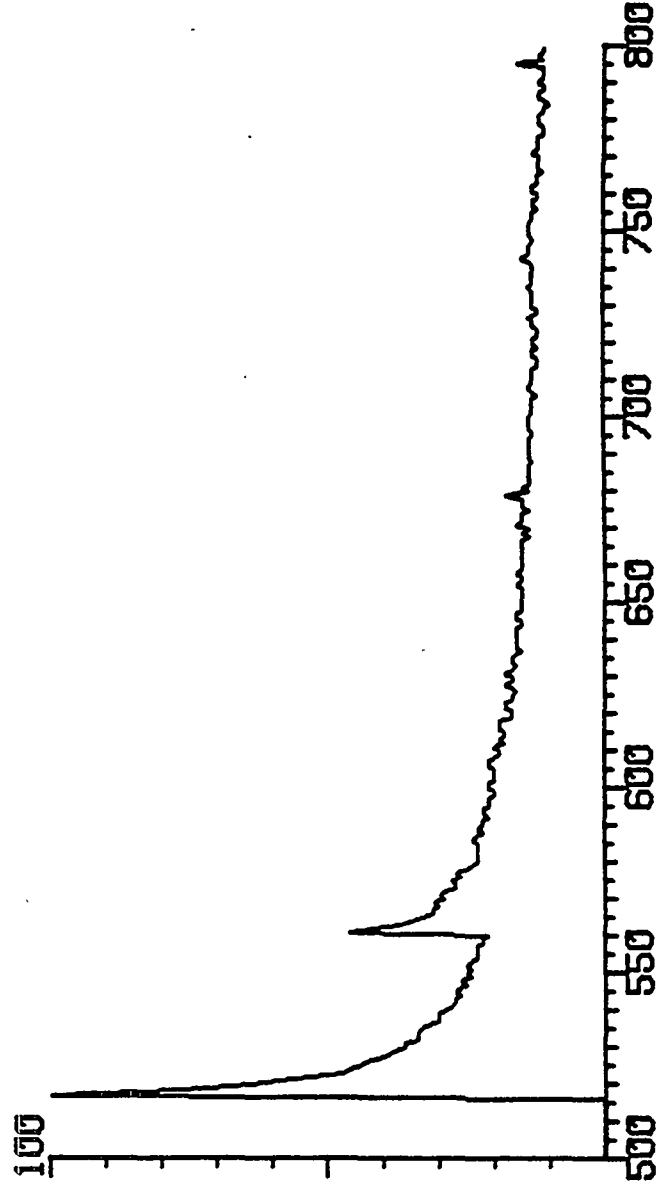
MASS 44 SEARCH X3
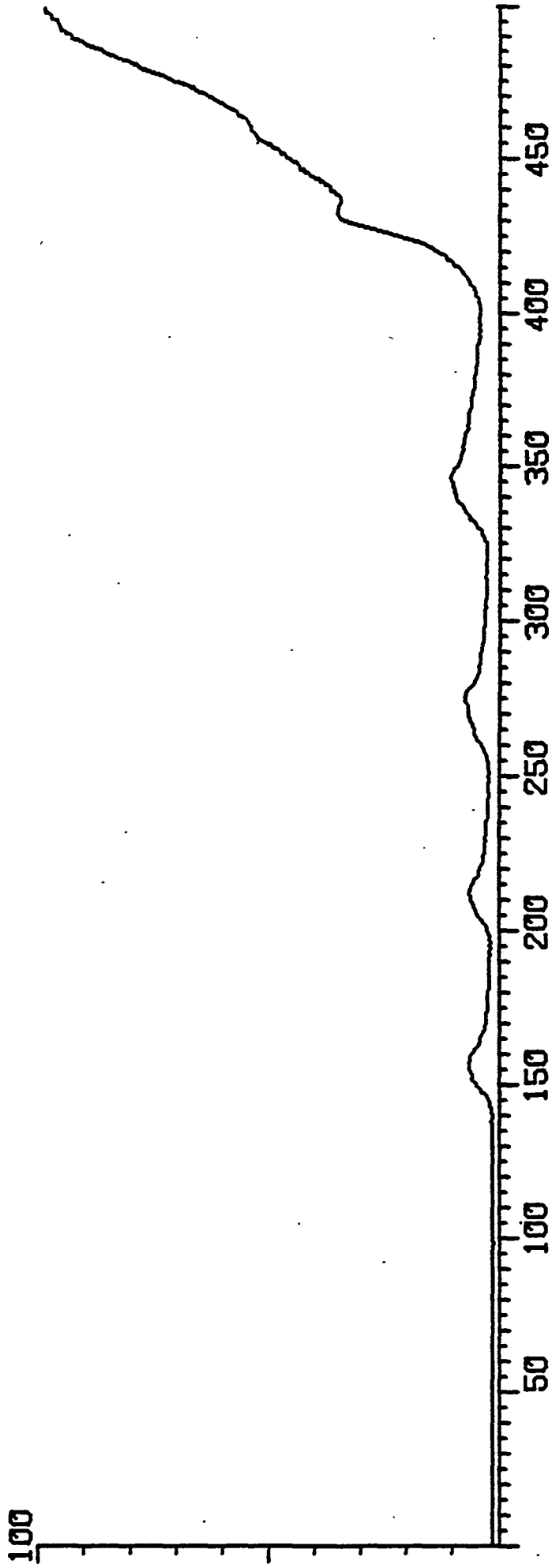
SALT SAMPLE

MASS 48 SEARCH X1   2516.3
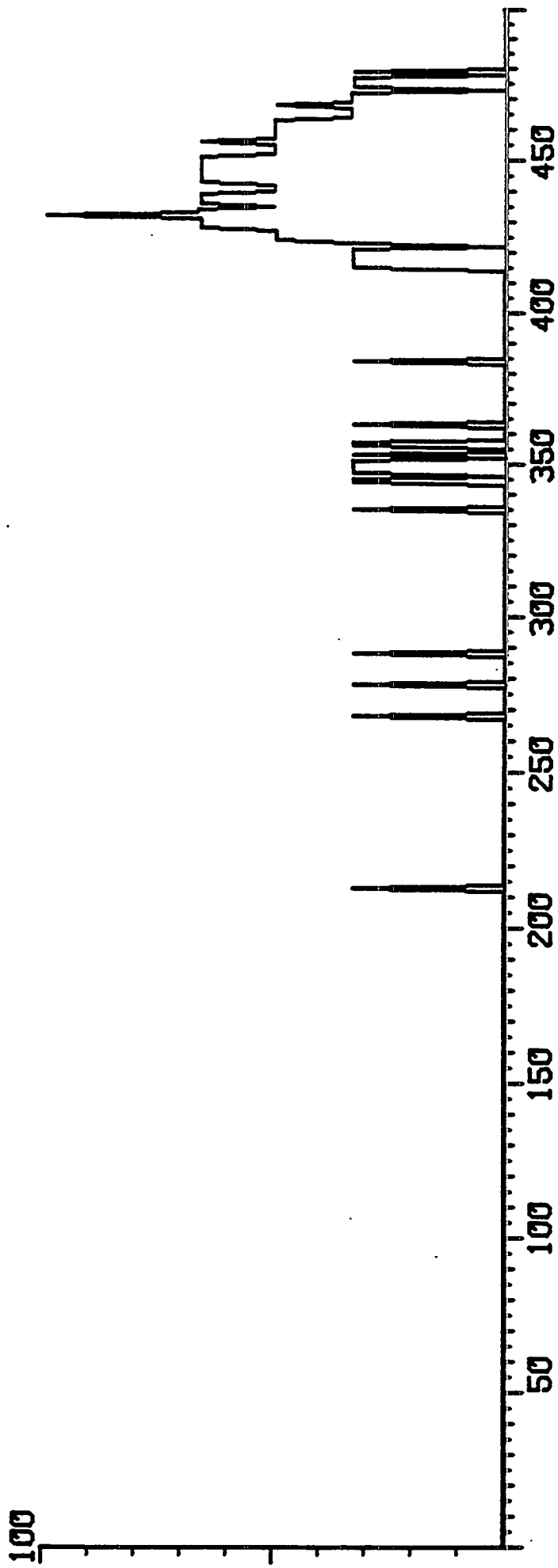
SALT SAMPLE   2658.5

TOTAL ION CHROMATOGRAM

100
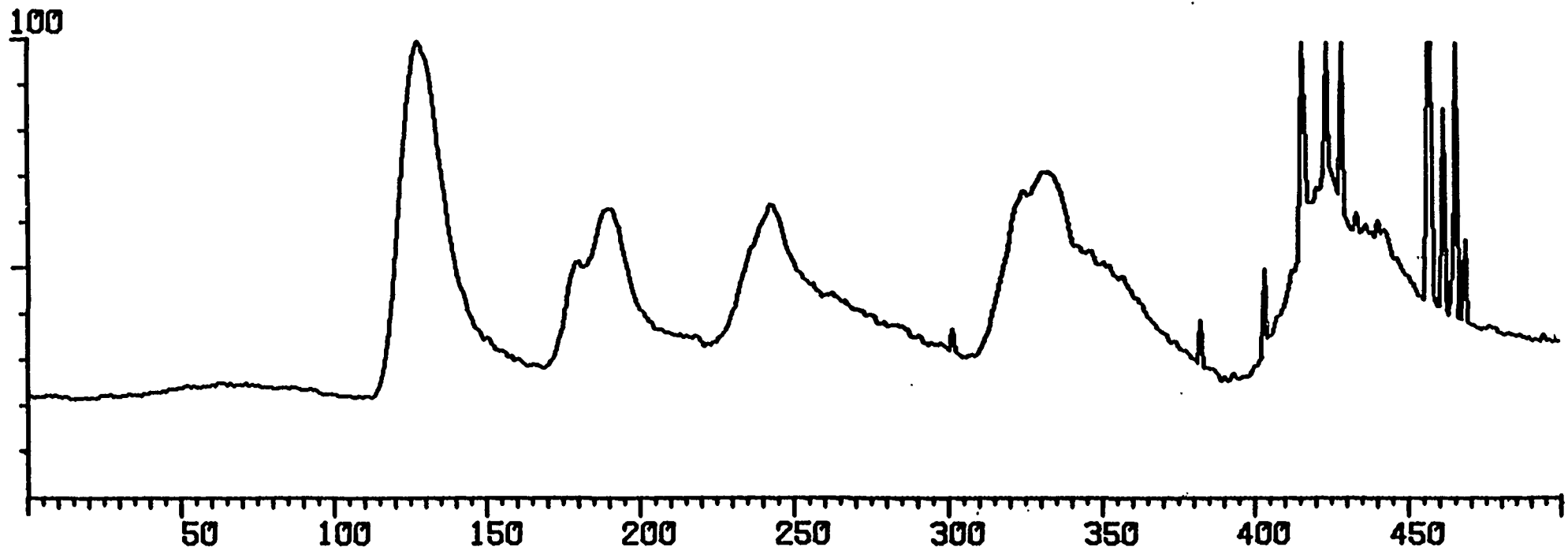
SALT SAMPLE   2658.5

MASS 14 SEARCH X1
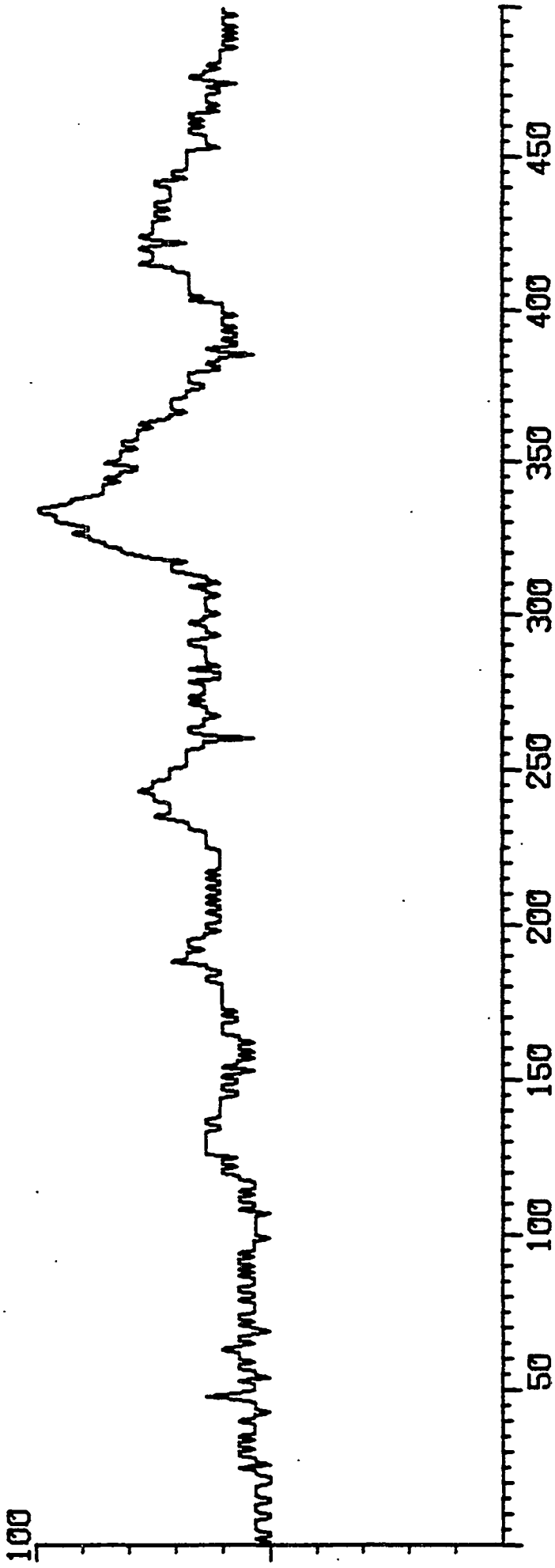
SALT SAMPLE   2658.5

MASS 18 SEARCH X4 (CH 127 = 100%)
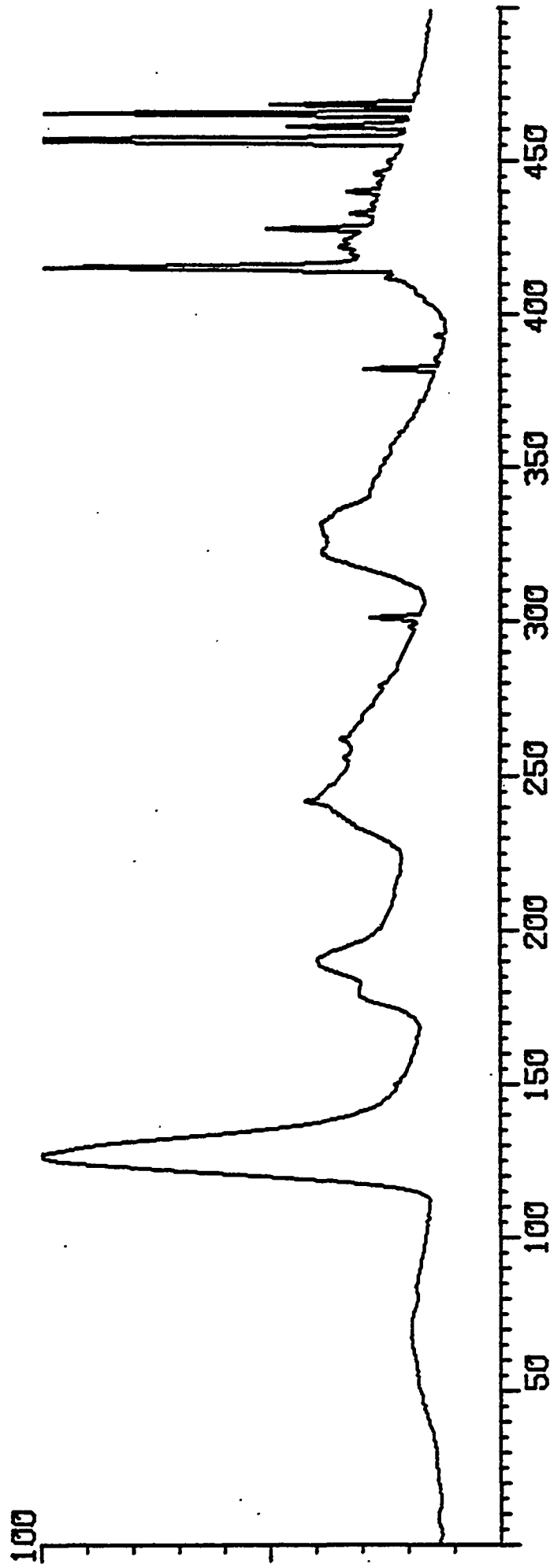
SALT SAMPLE   2658.5

MASS 28 SEARCH X3

100

50   100   150   200   250   300   350   400   450
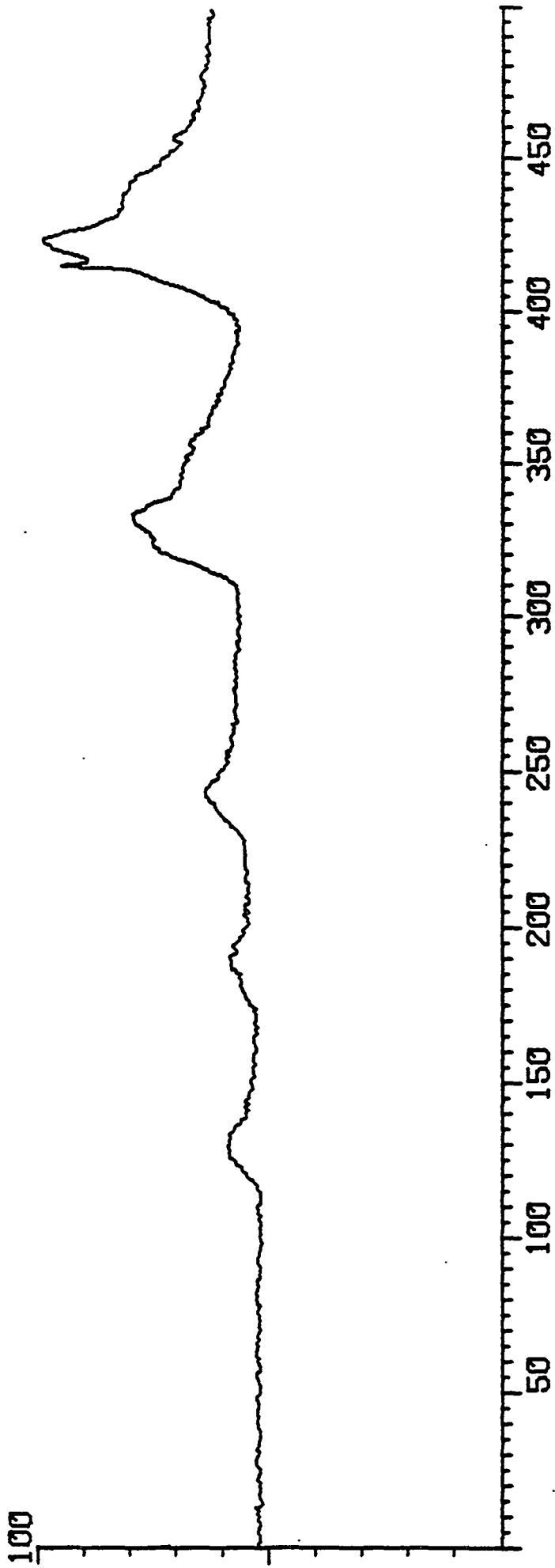
SALT SAMPLE   2658.5

MASS 32 SEARCH X1
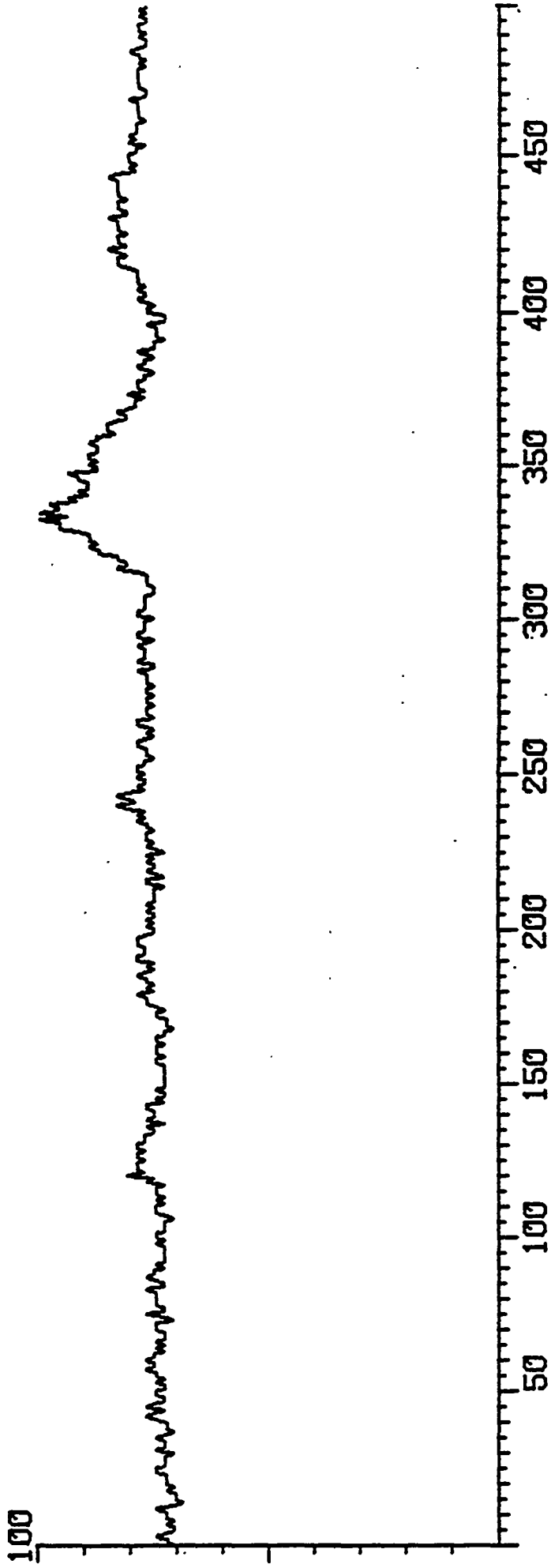
SALT SAMPLE

2658.5

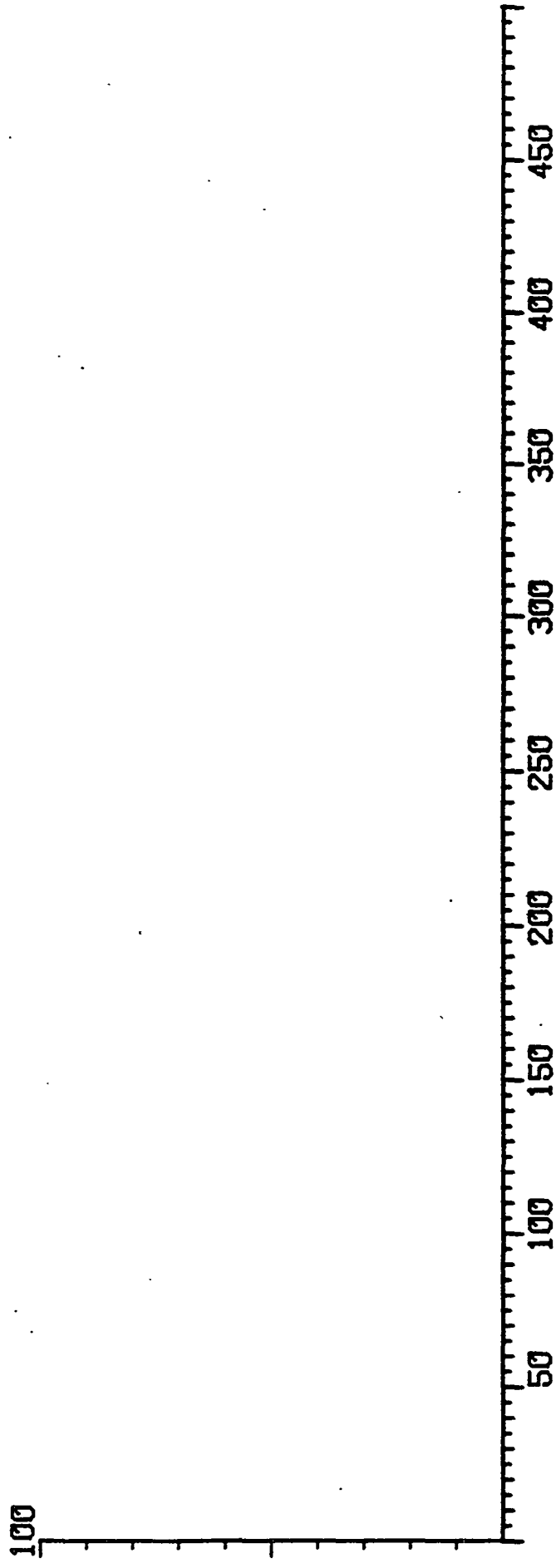MASS 36 SEARCH X2 (CH 415 = 100%)
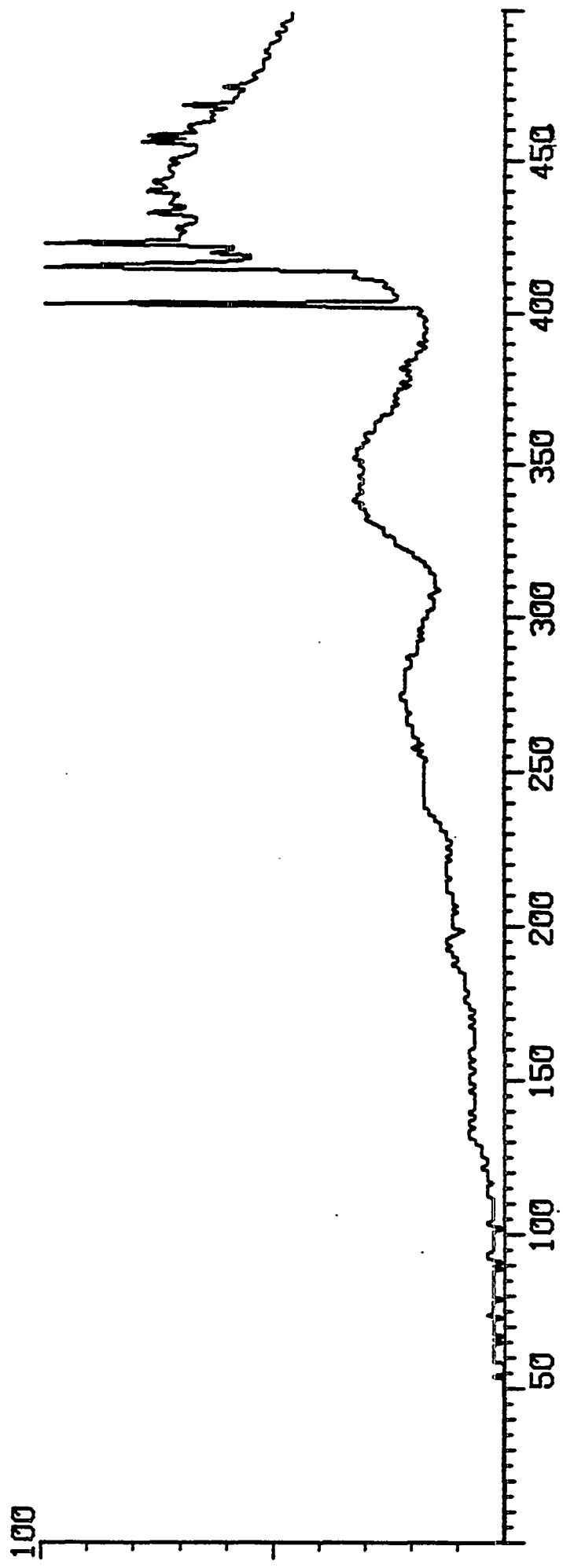
SALT SAMPLE   2658.5

MASS 44 SEARCH X2
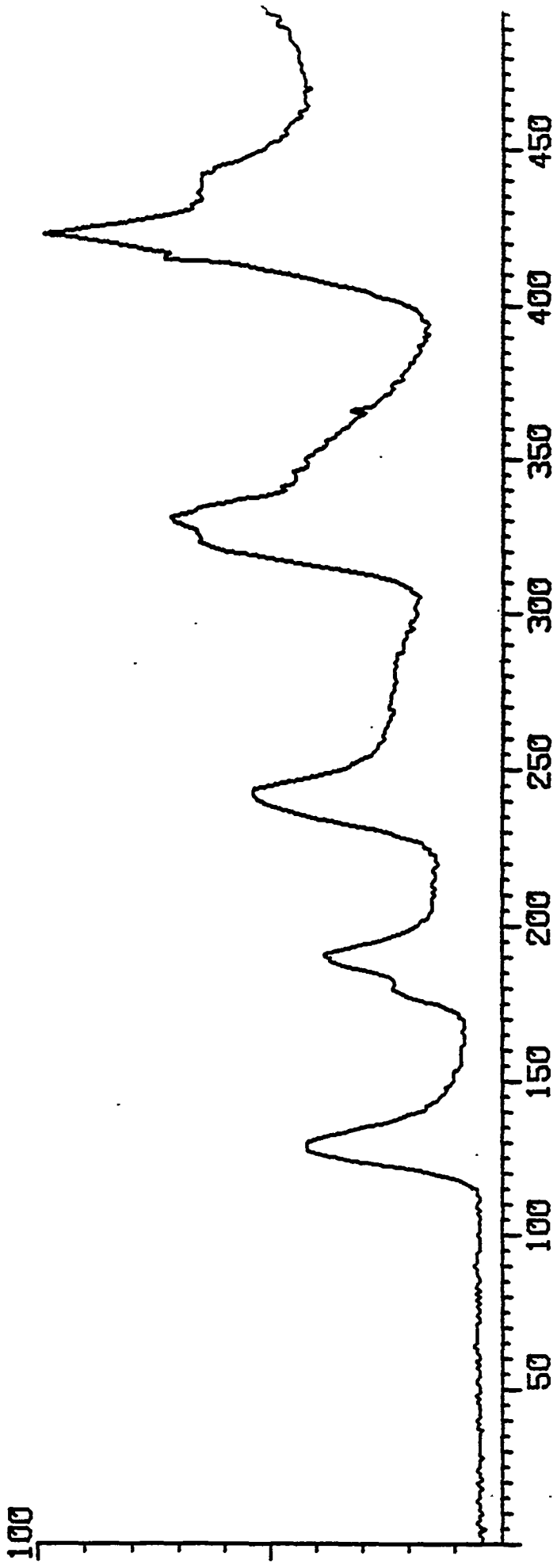
SALT SAMPLE

MASS 48 SEARCH X1   2658.5
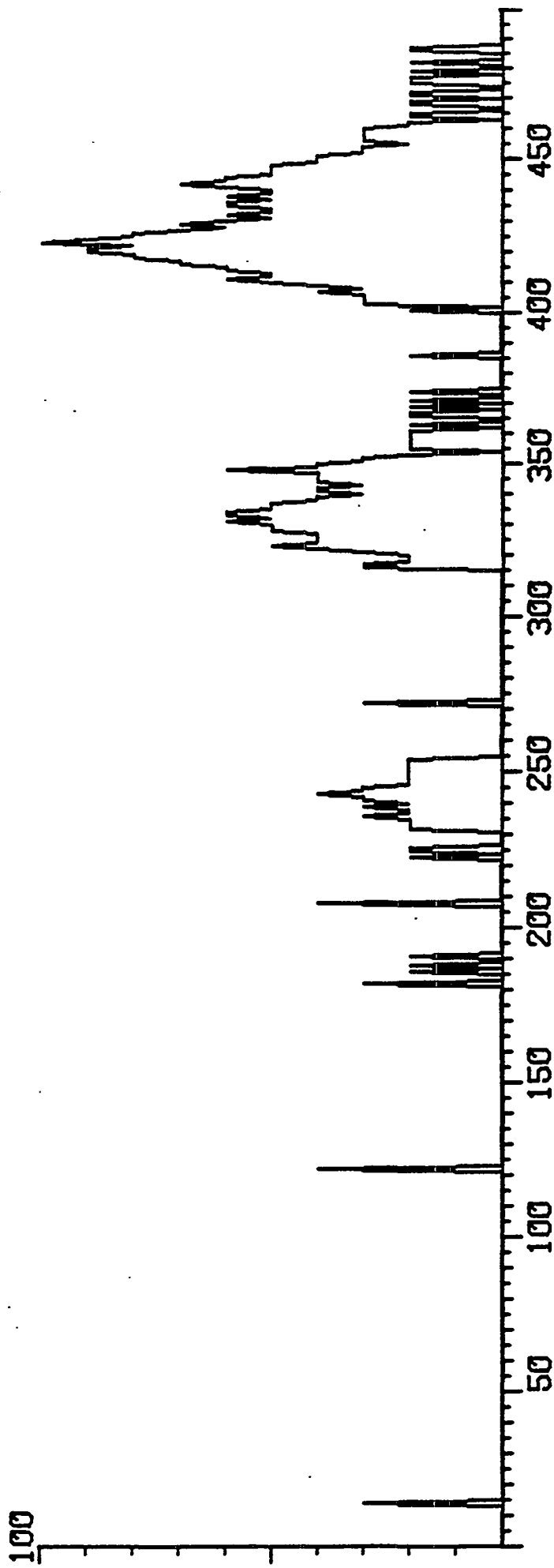
SALT SAMPLE

2786.5

TOTAL ION CHROMATOGRAM
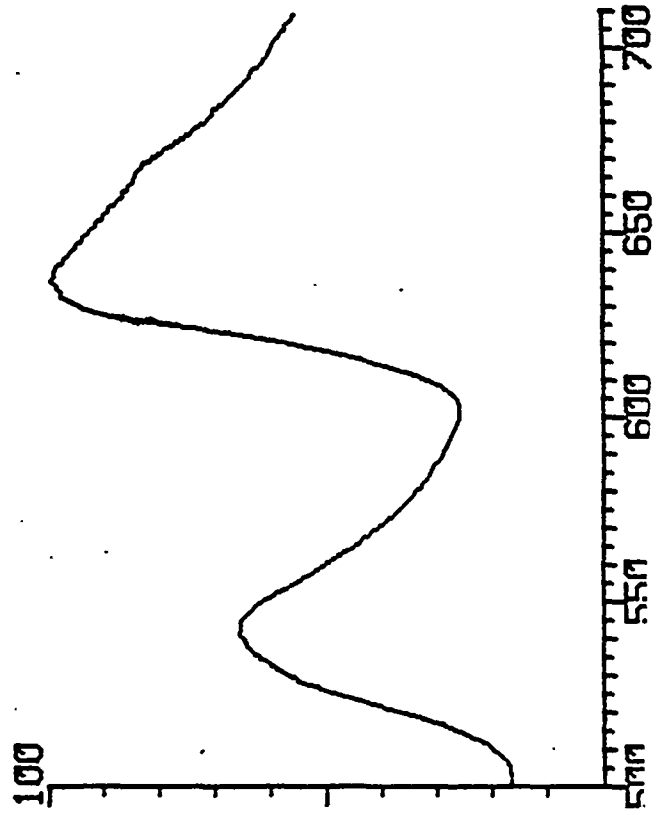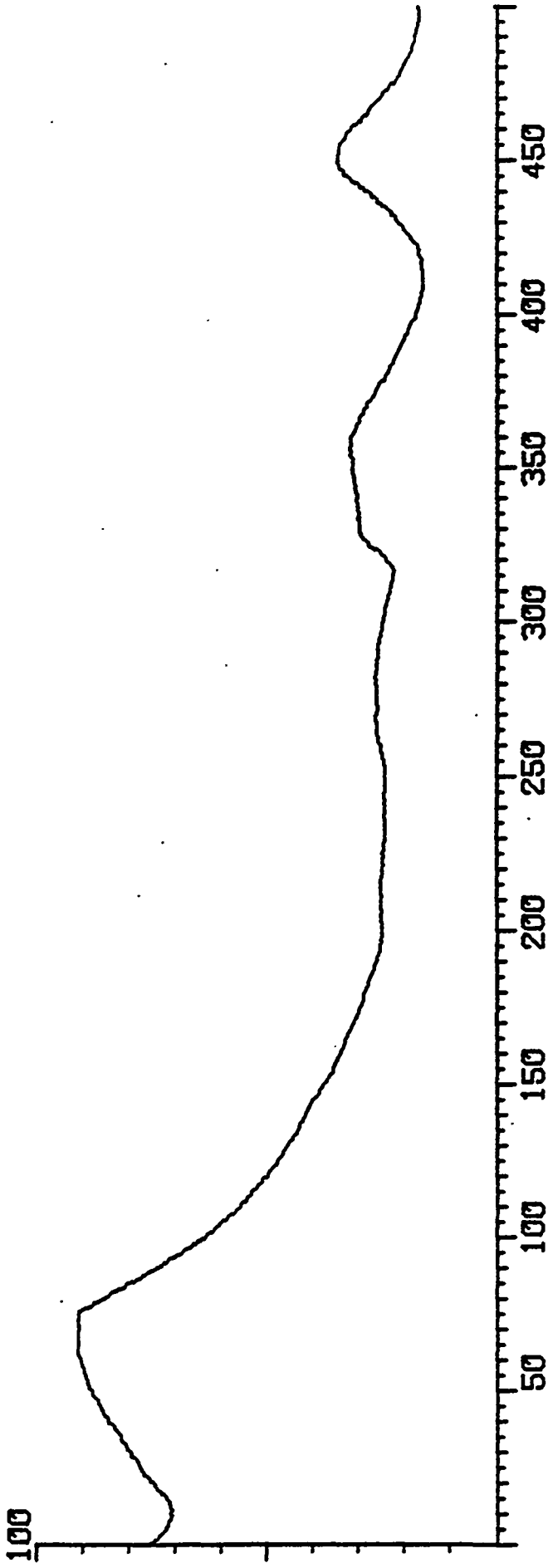
SALT SAMPLE   2786.5

MASS 14 SEARCH X1
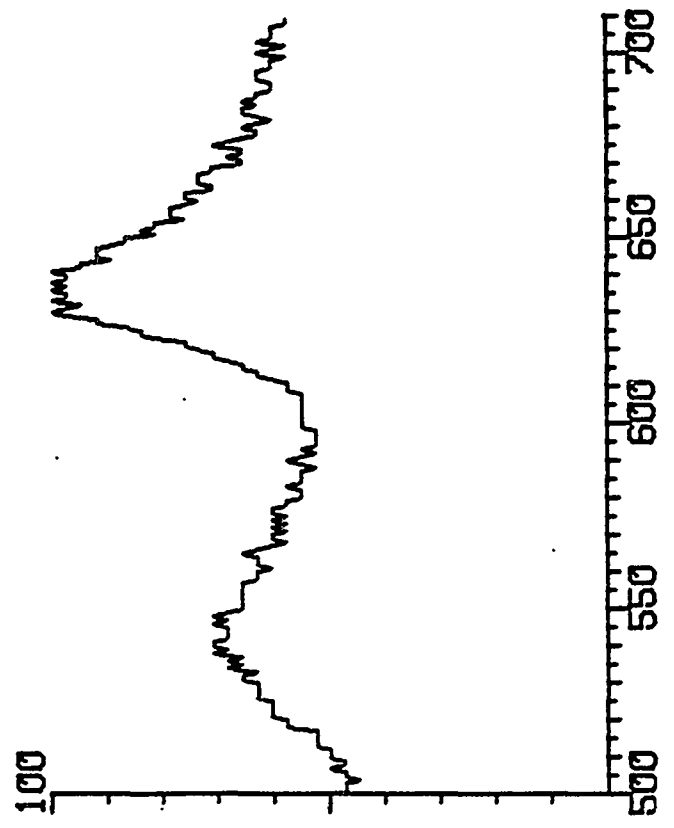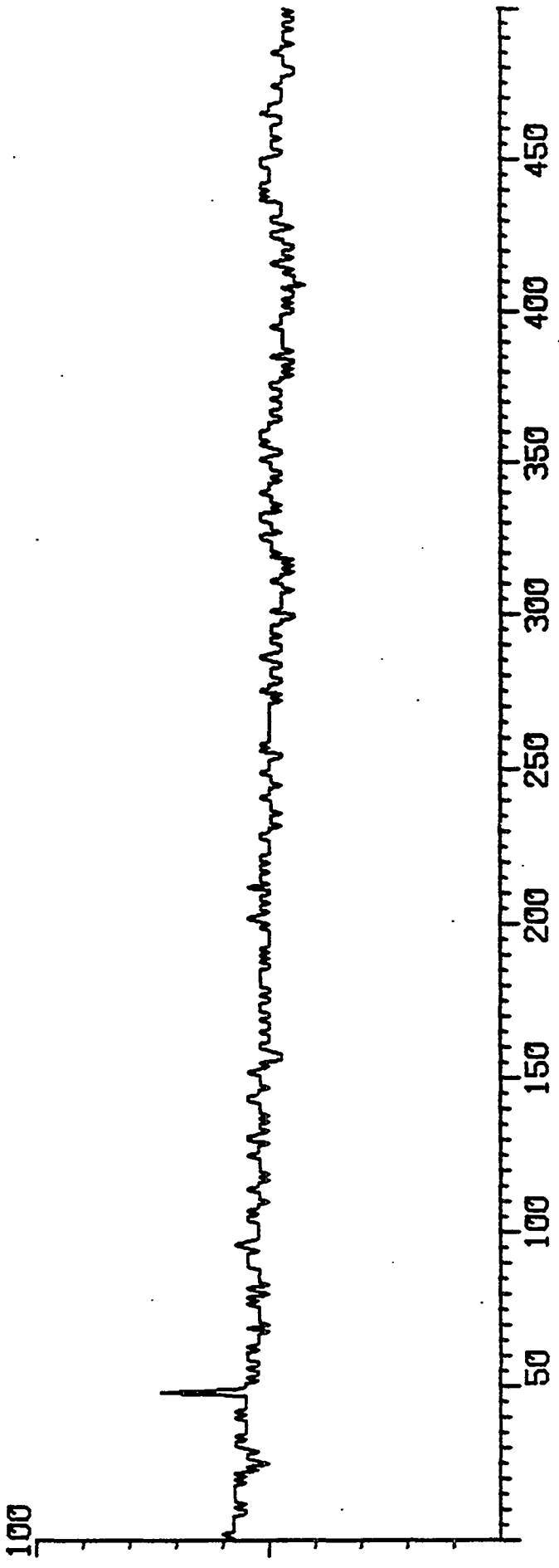
SALT SAMPLE   2786.5

MASS 18 SEARCH X4
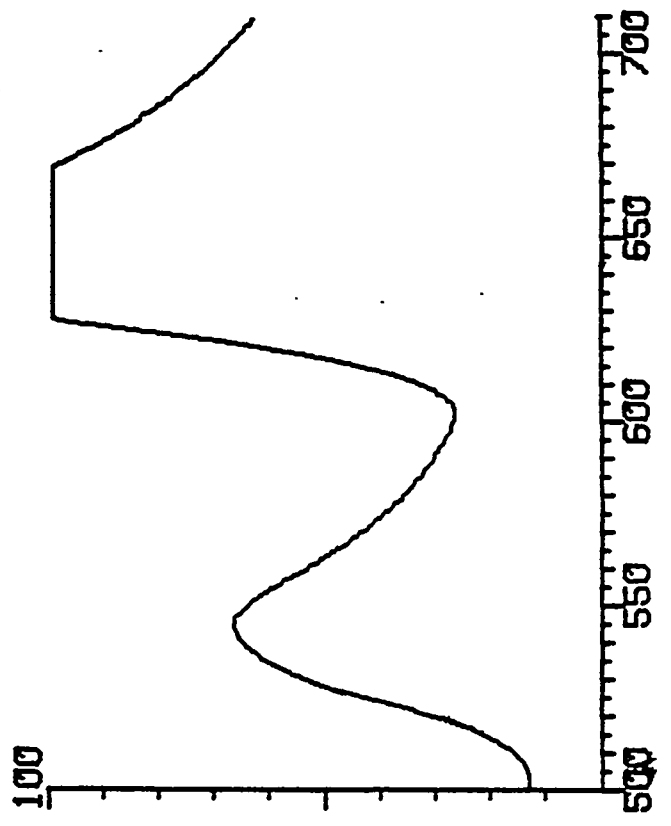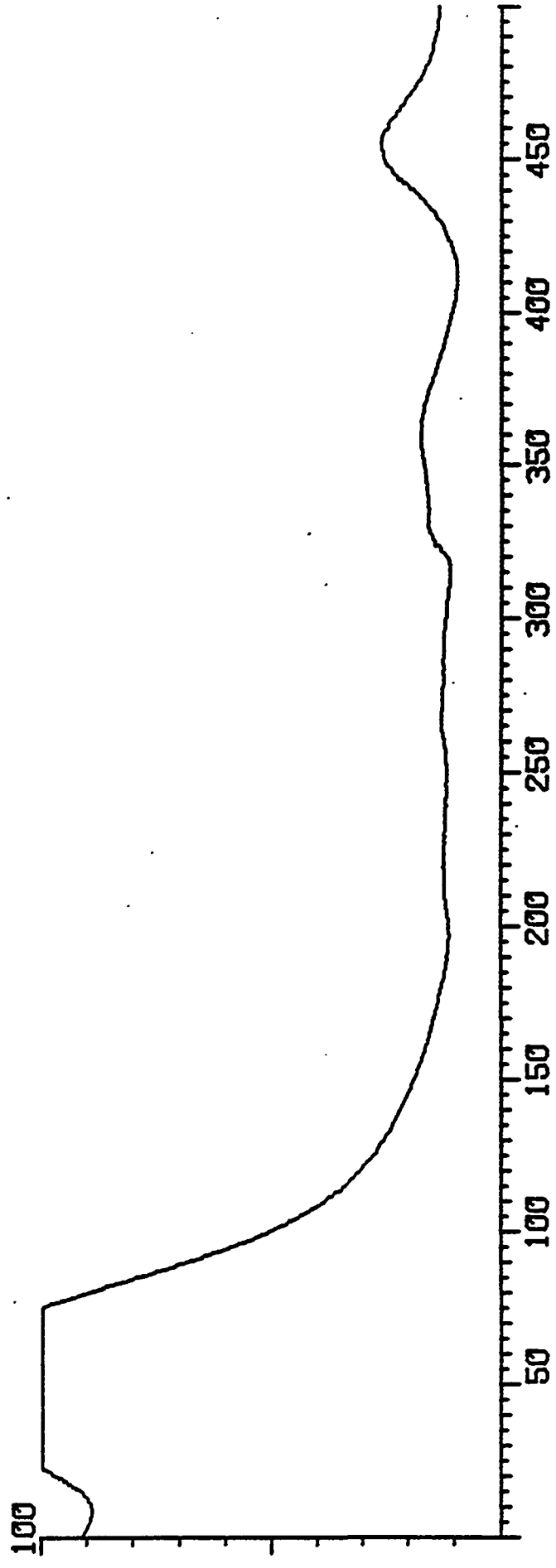
SALT SAMPLE   2786.5

MASS 19 SEARCH X1
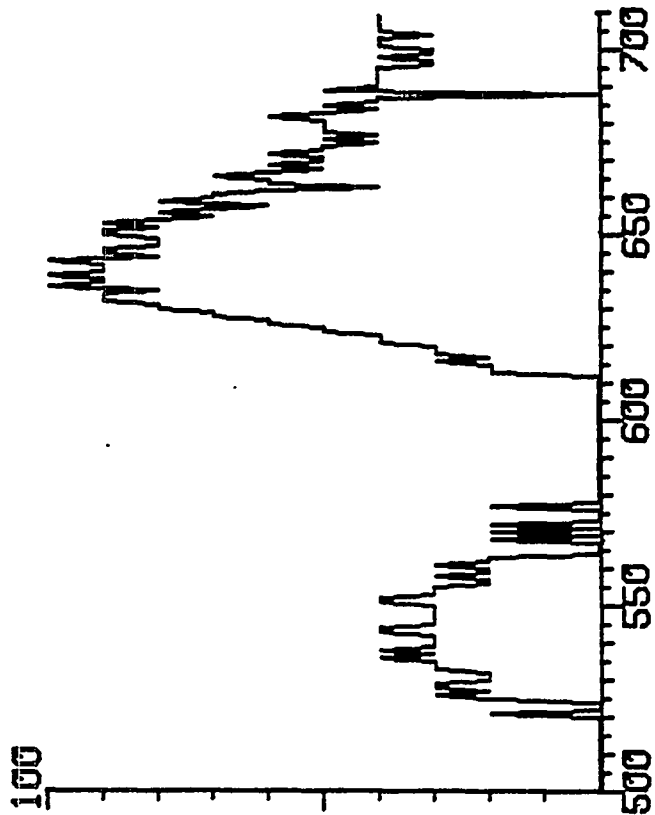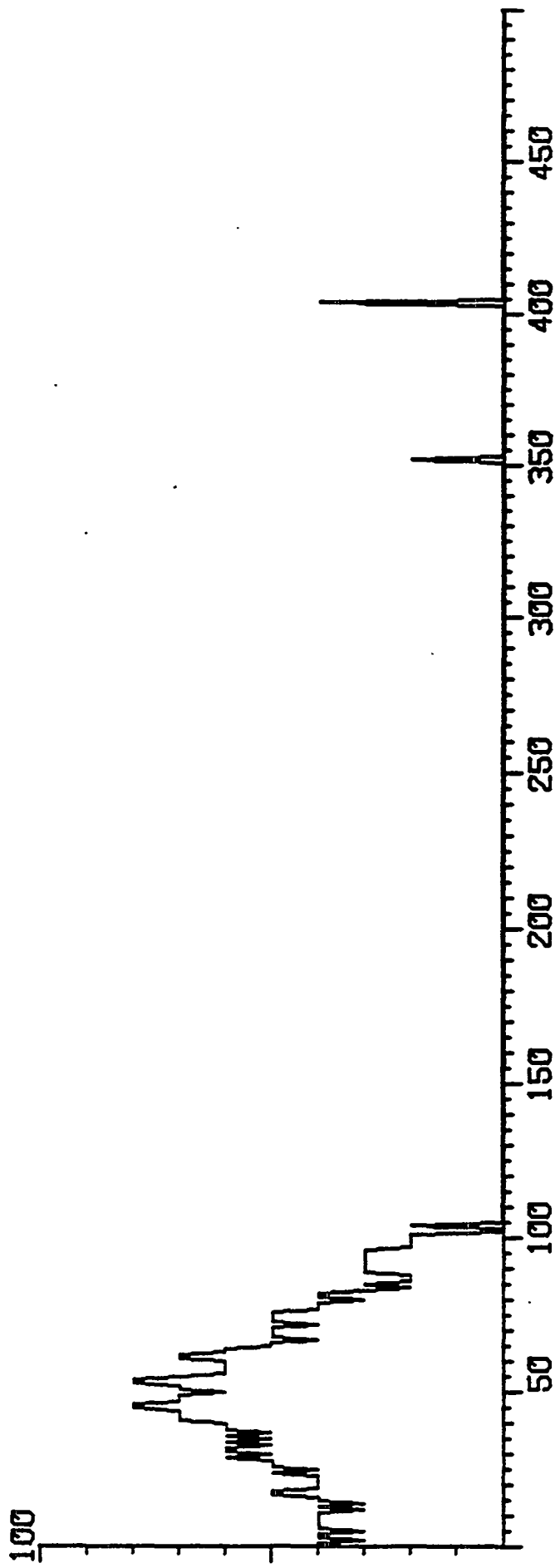
SALT SAMPLE   2786.5

MASS 28 SEARCH X3
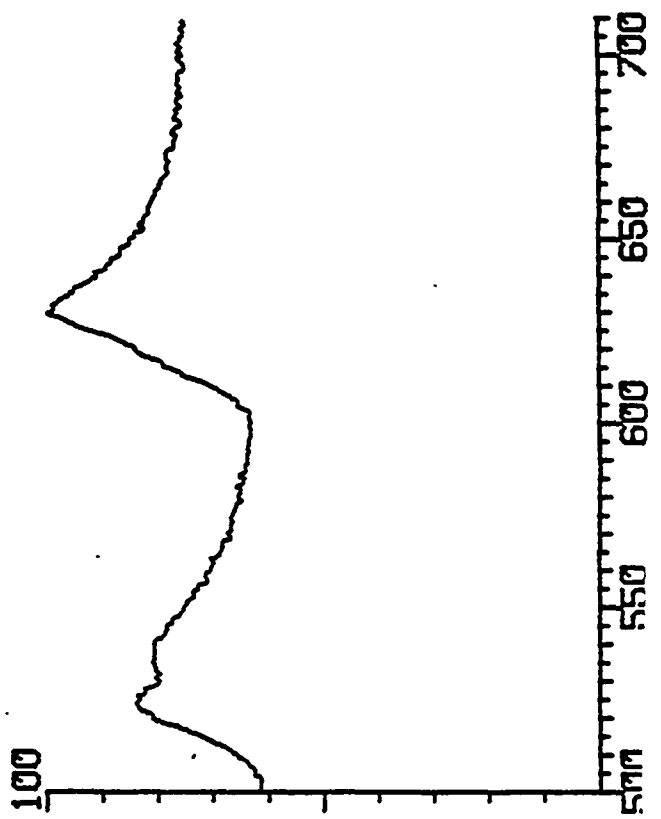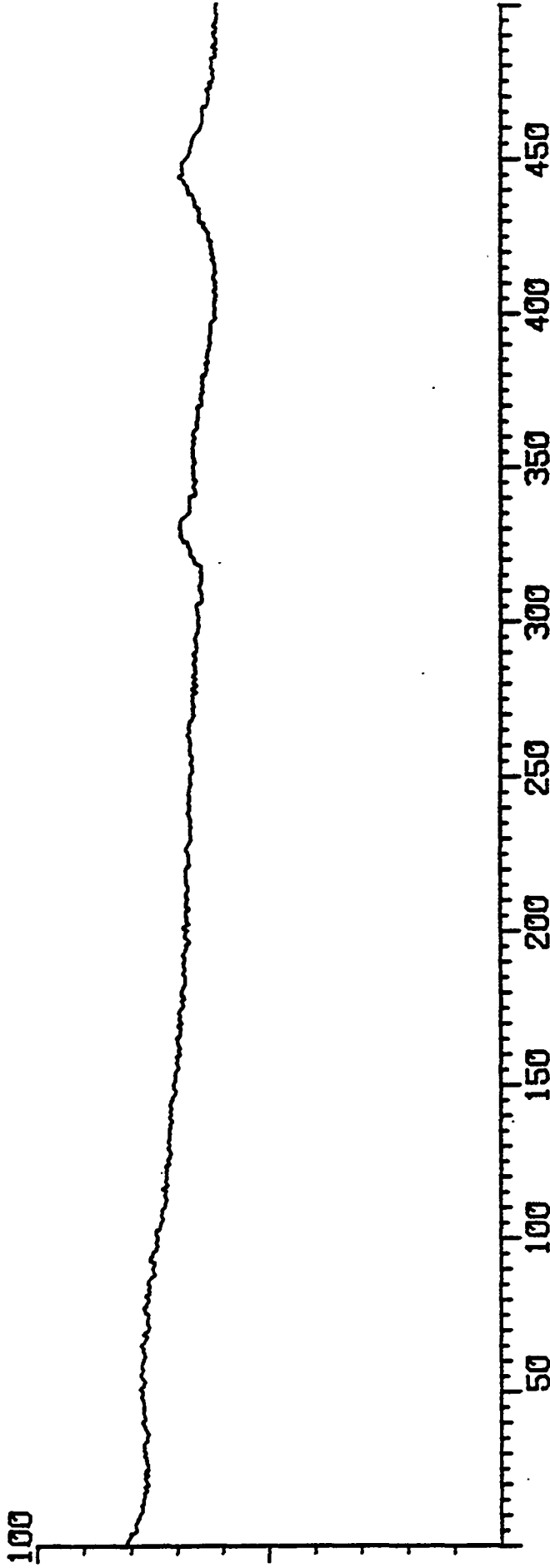
SALT SAMPLE   2786.5

MASS 32 SEARCH X1
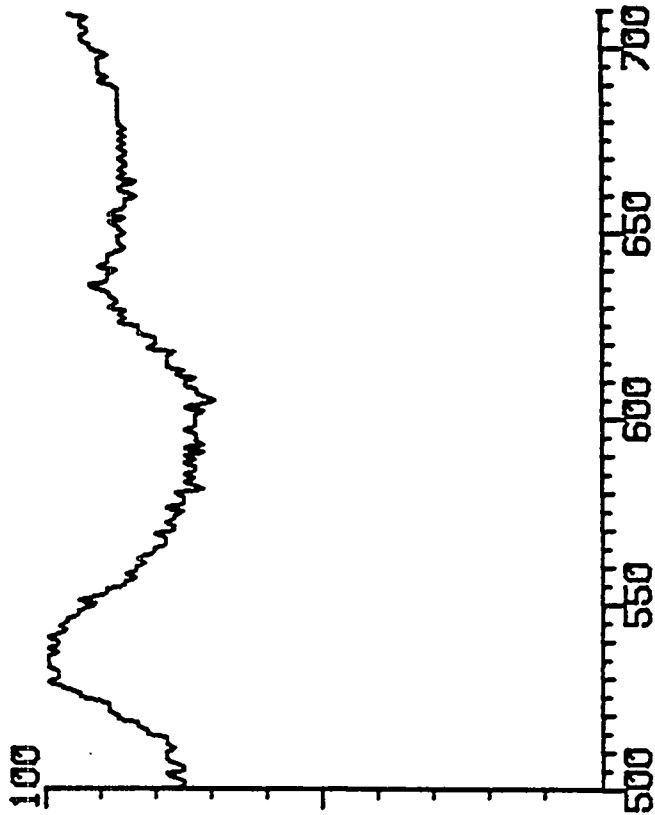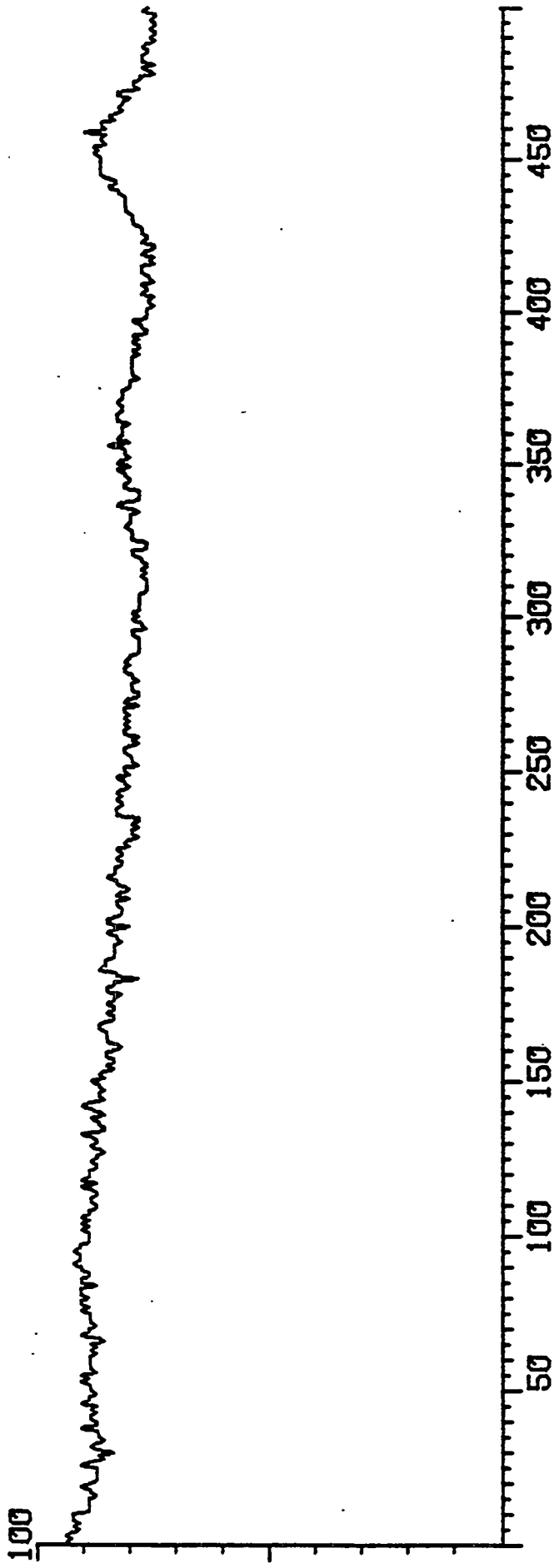
SALT SAMPLE   2786.5

MASS 36 SEARCH X2
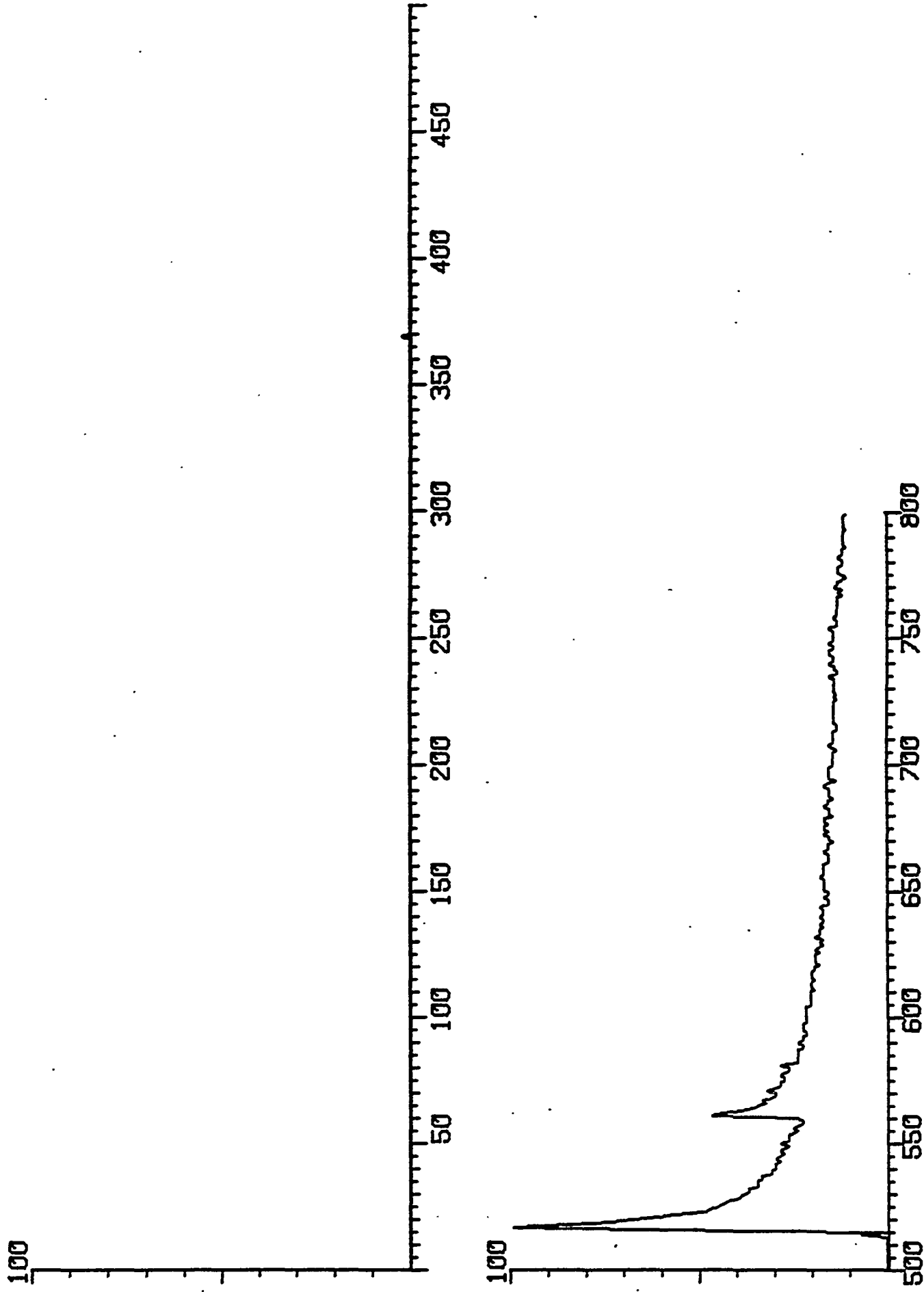
SALT SAMPLE   2786.5

MASS 44 SEARCH X2
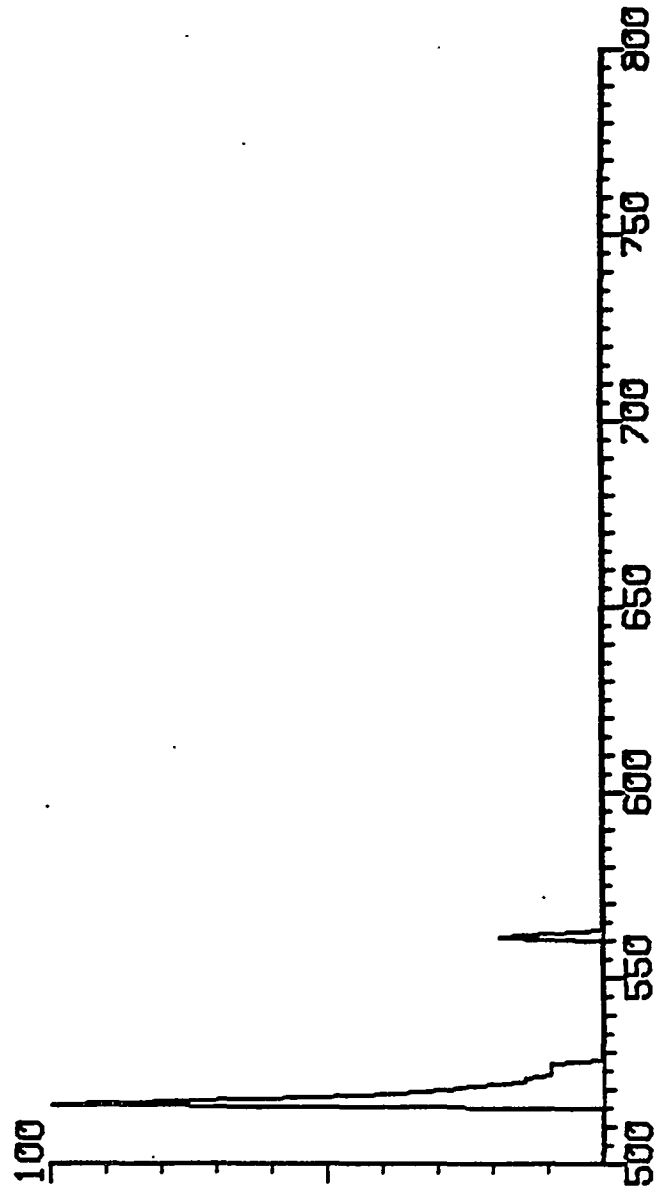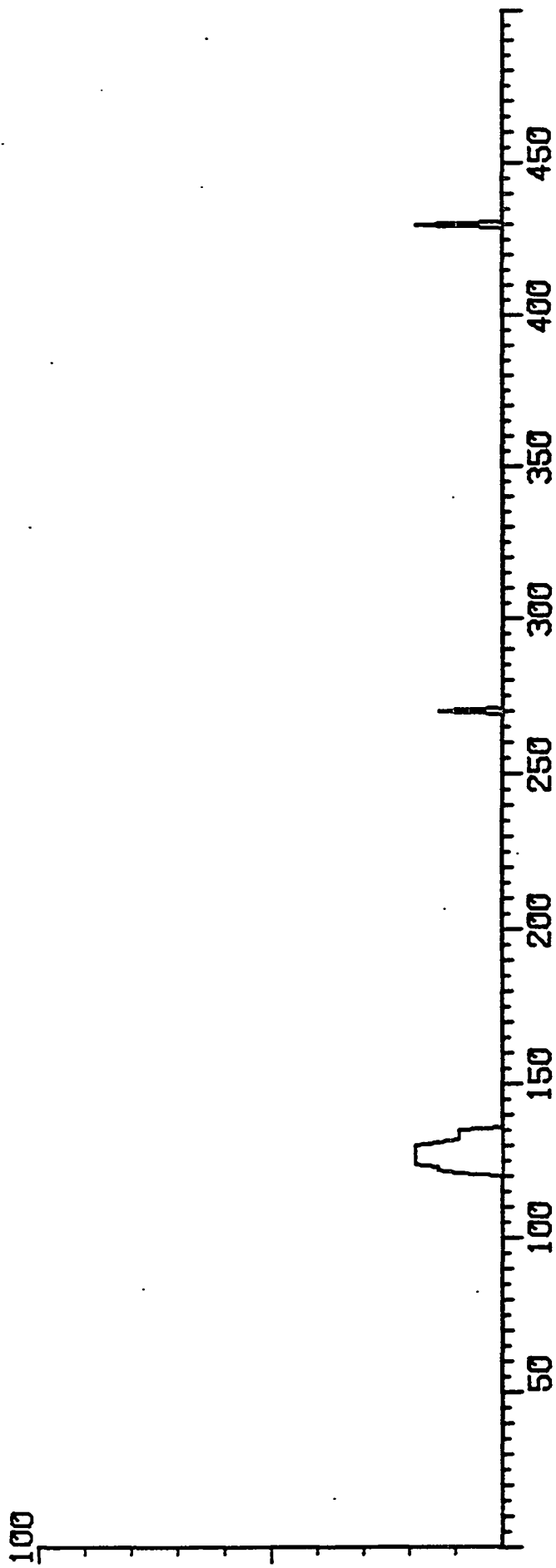
SALT SAMPLE

2786.5

MASS 48 SEARCH X1

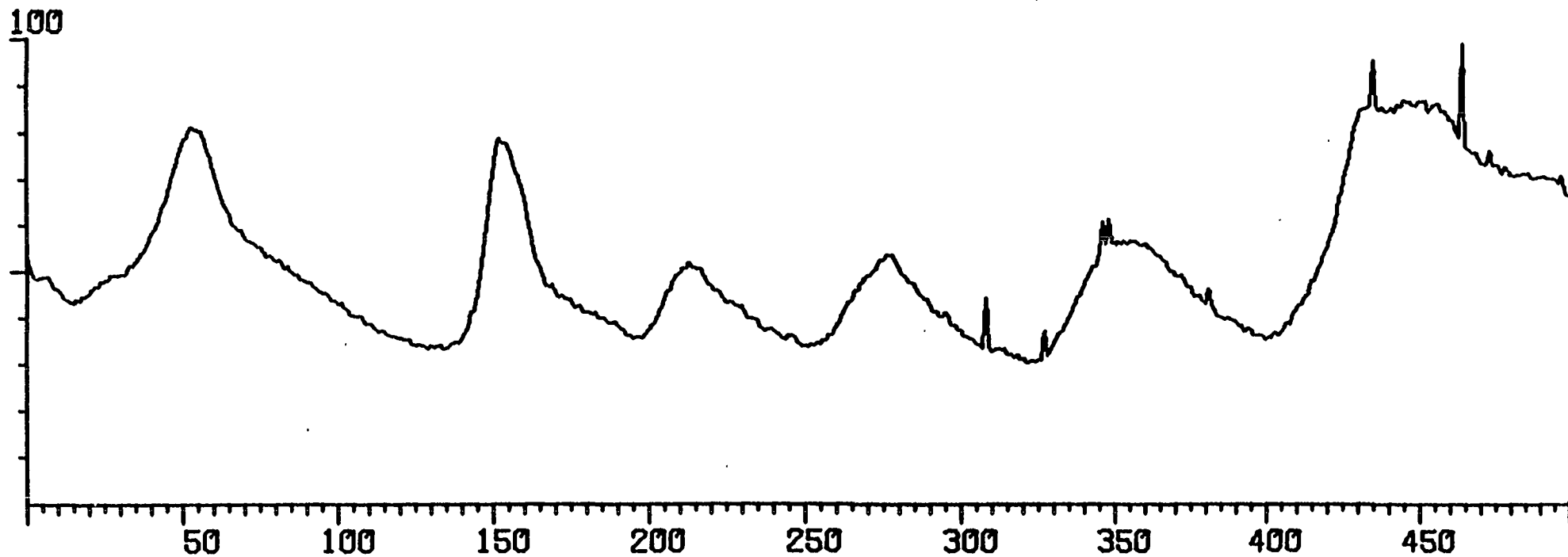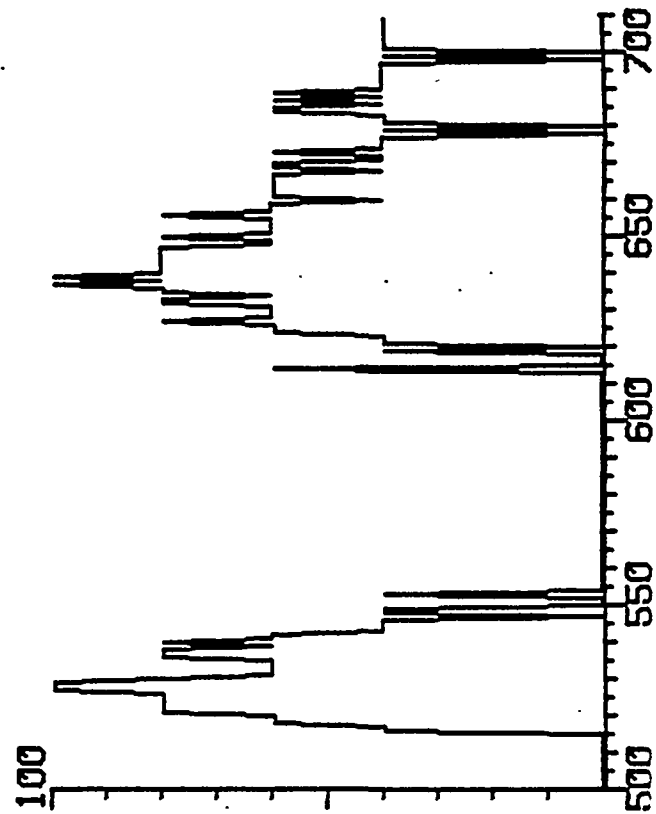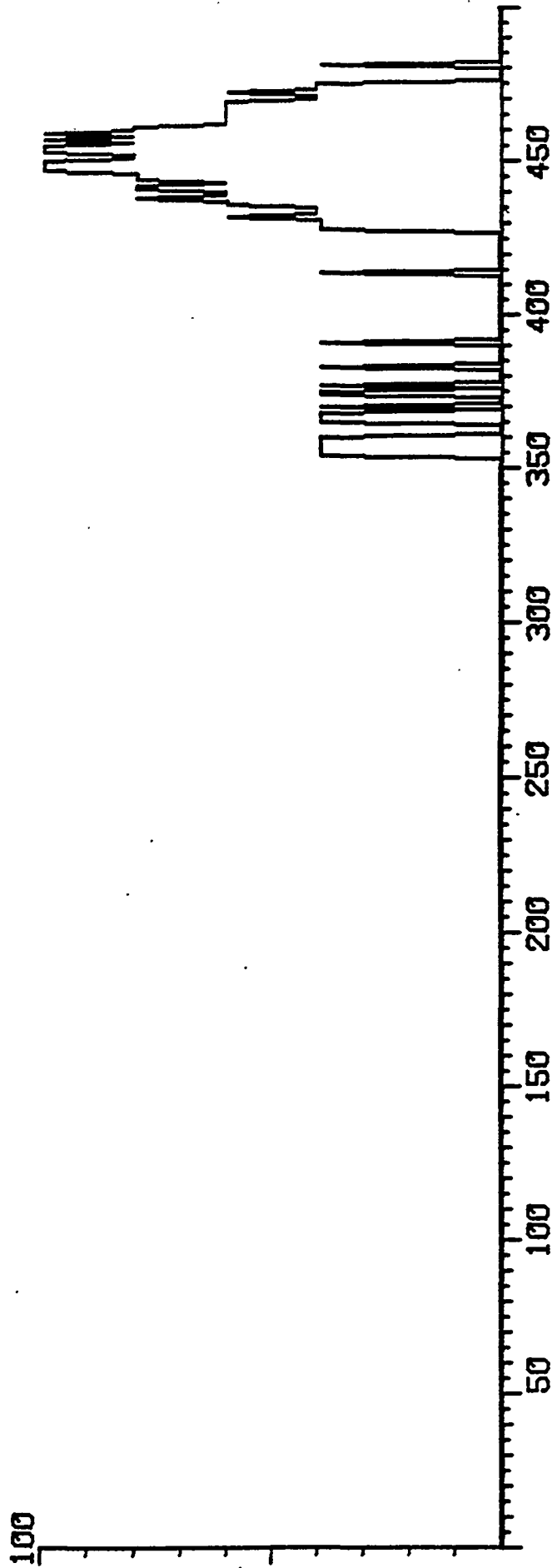SALT SAMPLE   2821.0
TOTAL ION CHROMATOGRAM
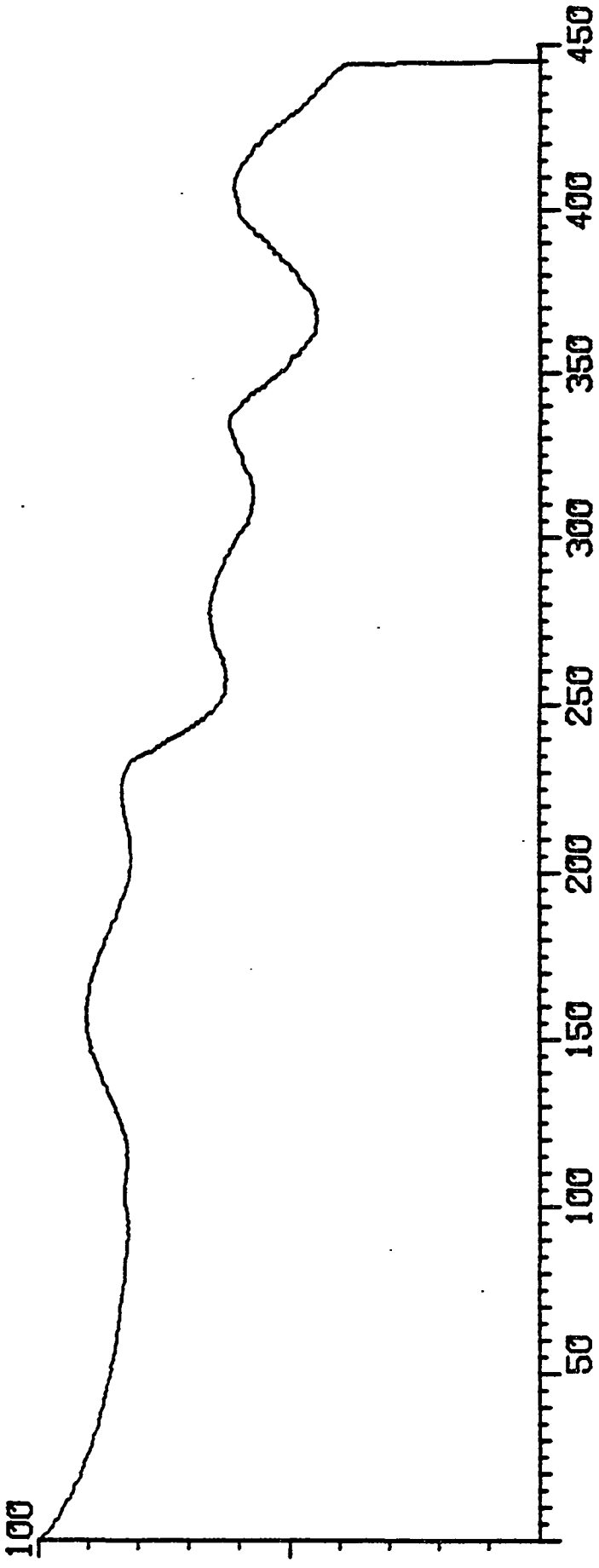
SALT SAMPLE   2821.0

MASS 14 SEARCH X3
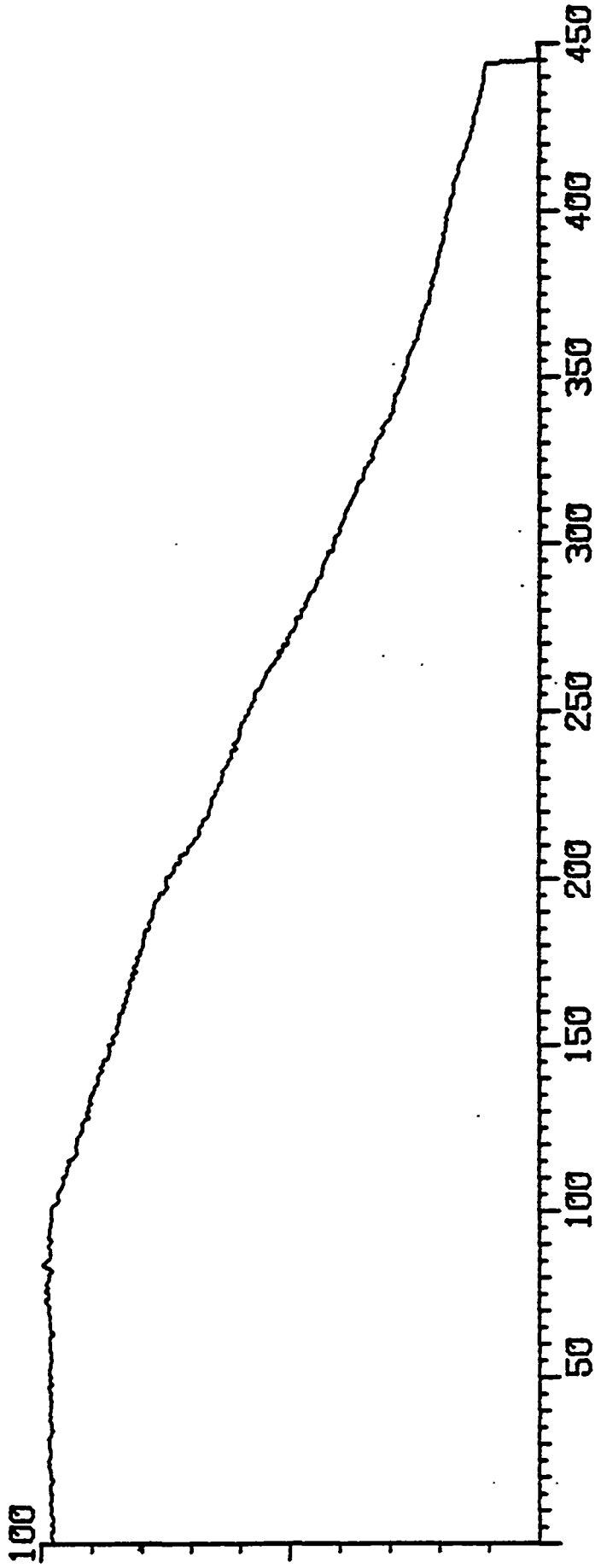
SALT SAMPLE   2821.0

MASS 18 SEARCH X4

100

50 100 150 200 250 300 350 400 450
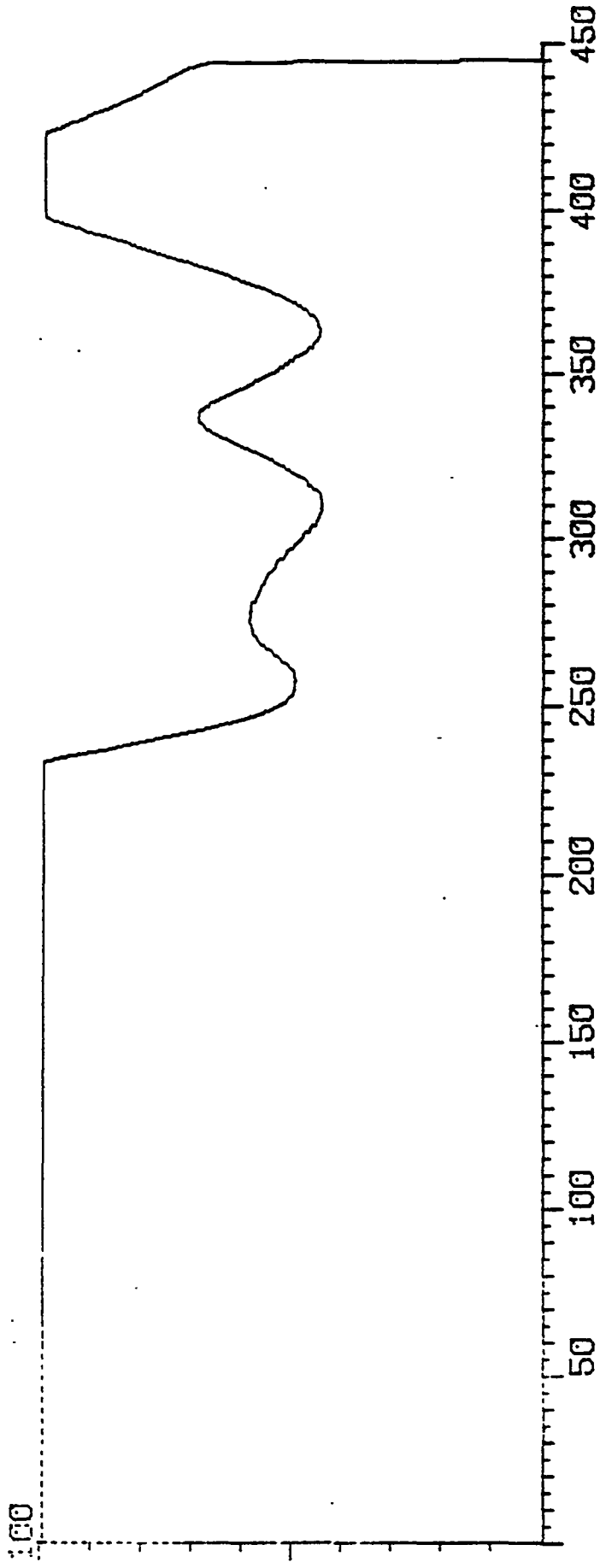
SALT SAMPLE   2821.0

MASS 28 SEARCH X4
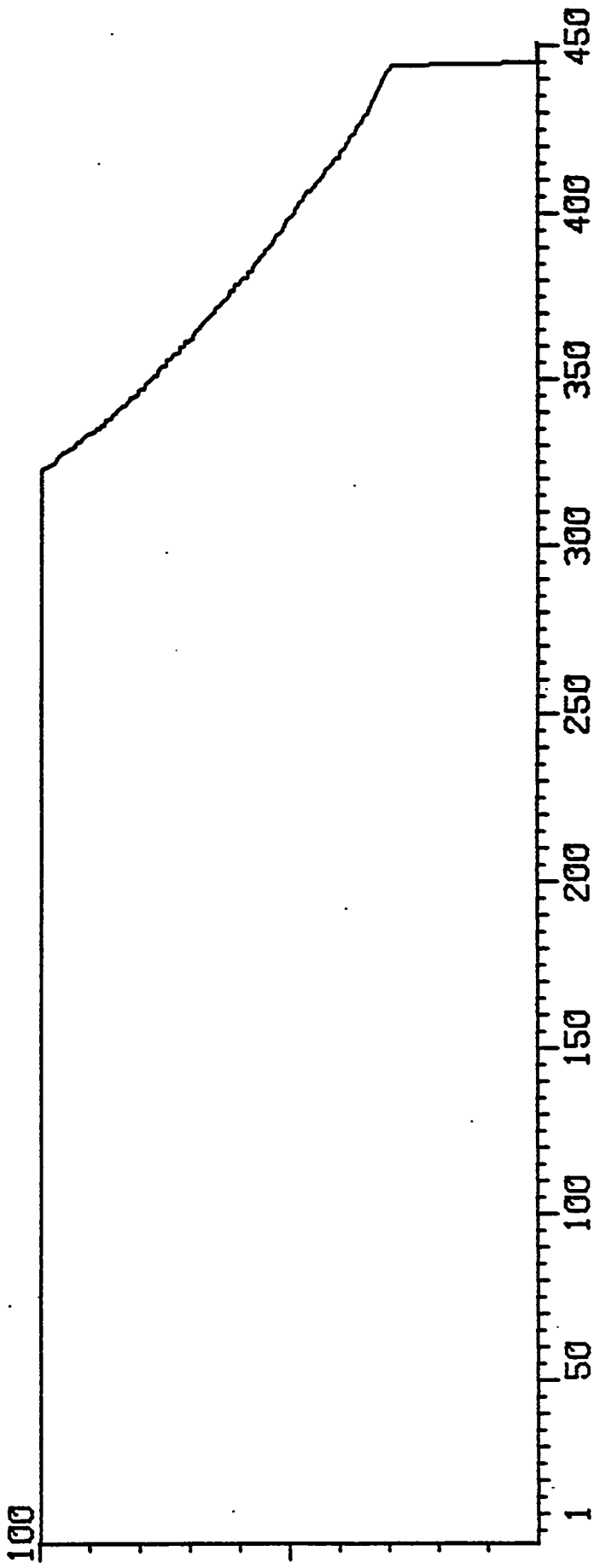
SALT SAMPLE   2821.0

MASS 32 SEARCH X4

100   50   100   150   200   250   300   350   400   450
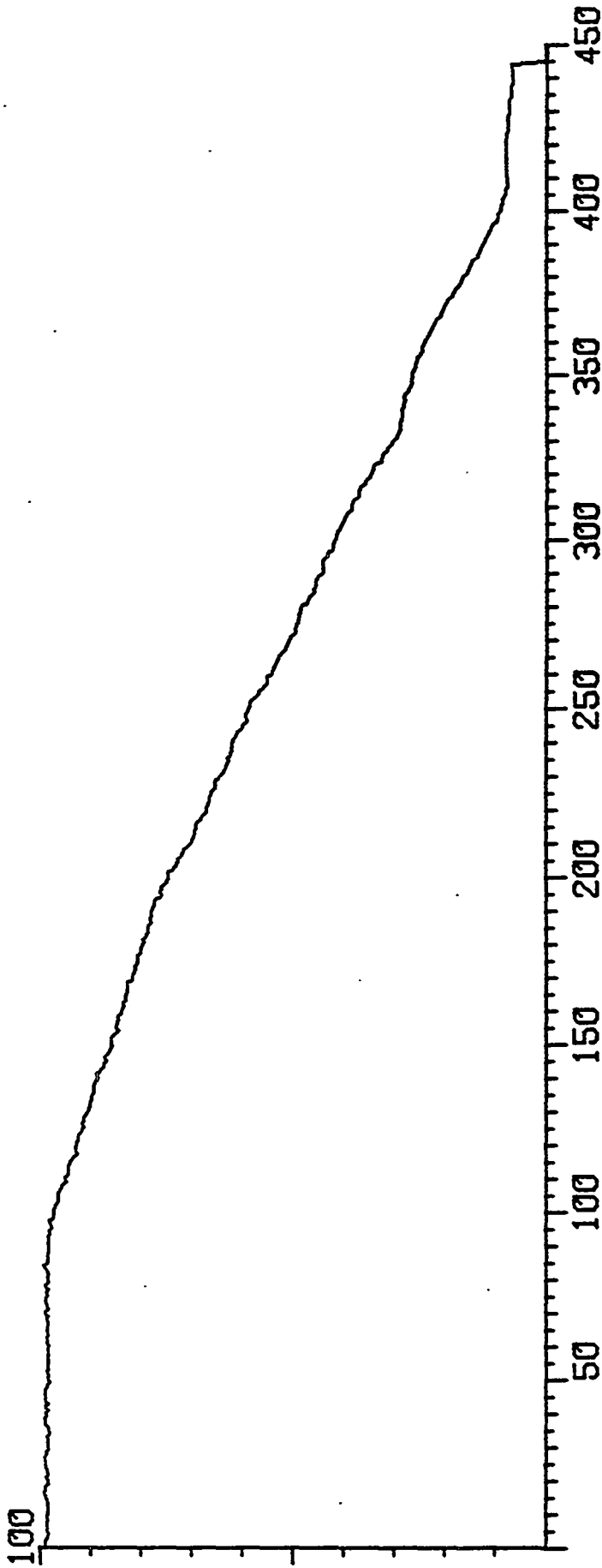
SALT SAMPLE   2821.0

MASS 36 SEARCH X2
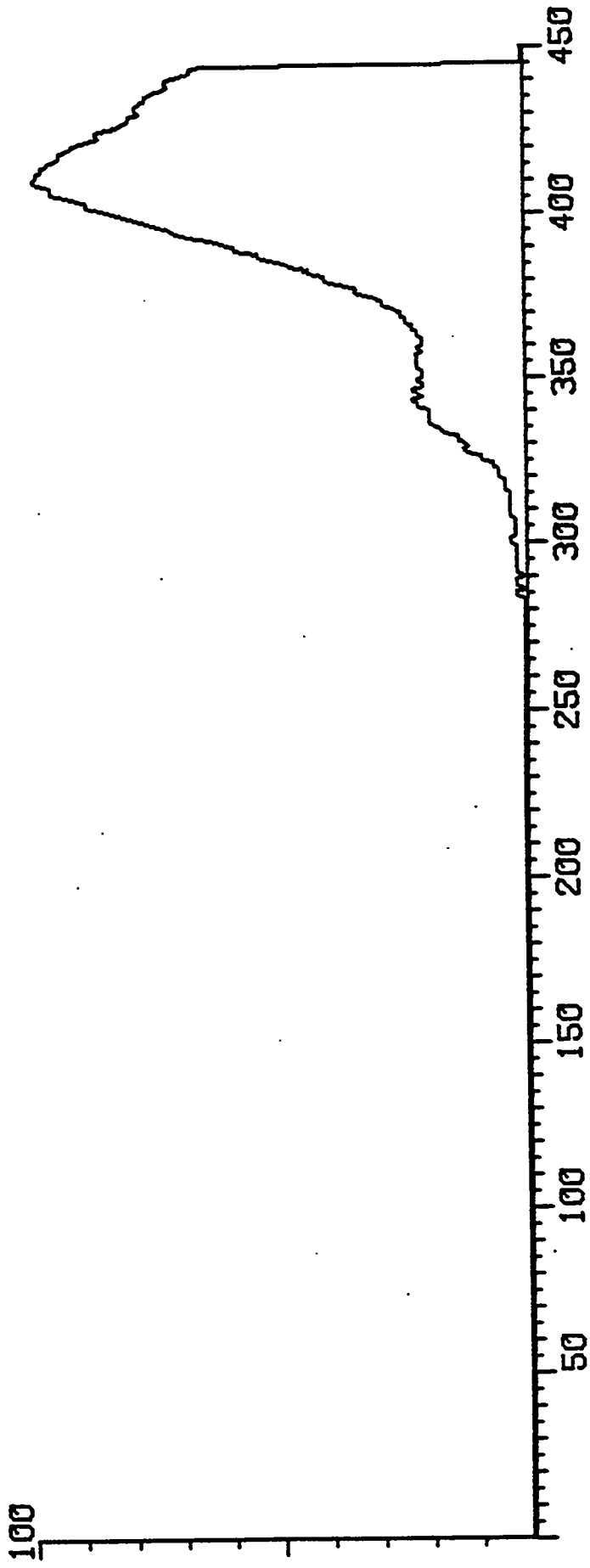
SALT SAMPLE   2821.0

MASS 44 SEARCH X2
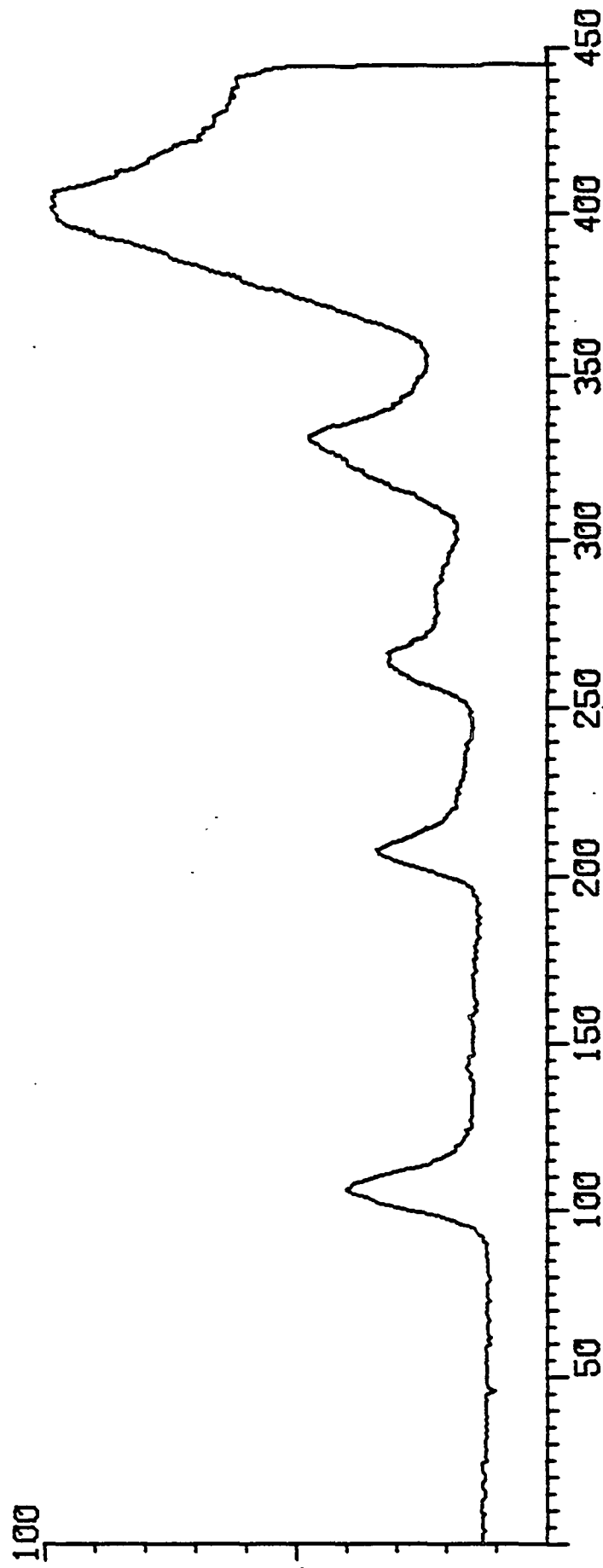
APPENDIX 7.F.   Analytical Precision.   (Ref. Sec. 7.5)

1.   General statement concerning sample sizes, weighing errors, etc.

The sample weights used in this study ranged from approximately 0.5 to 2.5 grams, but typically were from 1.5 to 2.0 grams.   The sample bottles were weighed before each new batch of samples was prepared, and both the sample bottles and the combined sample bottle and sample were weighed two times or more.   Replicate weighings errors should result in a precision of no worse than ±0.1 to 0.2 weight %.

2.   Results of triplicate analyses on selected samples.

Triplicate analyses were performed on separate splits taken from the sample vial using different initial sample weights each time.   The results are tabulated below:

Sample	Weight Losses Determined (Wt. %)			Mean to Nearest 0.1%
7-1044	0.1	0.1	0.3	0.2
7-1296	1.3	0.9	1.3	1.2
8-1794	1.2	1.4	1.2	1.3
8-1986	0.0	0.0	0.1	0.0
8-2563	2.0	2.3	1.9	2.1
8-2616	0.0	0.0	0.0	0.0

The results of these analyses indicate that most weight losses determined from replicate samples (taken from the same sample bottle) fall within ± 0.2 to 0.3 of the mean value. Because of vertical and lateral variation in mineral content typical of sedimentary rocks the range anticipated for <u>different</u> samples of the same core would be larger, but it is not possible to estimate the precision under such non-reproducible conditions. In the case of relatively uniform samples (such as some halite or anhydrite beds) the precision might be anticipated to remain fairly good. On the other hand, samples which contain varying amounts of clays or other hydrous minerals might be expected to show much larger variations in their weight losses upon heating.

APPENDIX 7.G. Weight Loss Data for Cores #7 and #8, Carlsbad, New Mexico, Including Comparisons with the Data of Section 7.3.   (Ref. Sec. 7.5)

1. Core #7.

Sample (ft)	Depth (m)	Weight Losses at 102 ± 5°C (Wt.%)	@70°C	Data from Section 7.3 To 200°C	To Above 400°C
1044	318.2	0.1	0.10	0.10	0.10
1107	337.4	1.0	0.12	0.22	1.99
1171	356.9	0.1	0.14	0.14	0.80
1221	372.2	0.2	0.30	0.44	0.51
1342	409.0	0.2	0.27	0.27	0.43
1402	427.3	0.1	0.19	0.19	0.31
1468	447.4	2.2	1.27	1.73	2.59
1533	467.3	0.1	0.22	0.23	0.47
1615	492.3	0.2	0.34	0.43	0.80
1697	517.2	3.4	0.82	0.82	0.85
1755	534.9	0.2	0.19	0.23	0.28
1952	595.0	0.0	0.14	0.14	0.58
1954	595.6	0.6	0.32	0.32	0.41
1958	596.8	0.2	0.20	0.20	0.32
1960	597.4	0.1	0.07	0.39	0.39
1967	599.5	0.1	0.20	0.20	1.13
1969	600.2	0.2	0.43	0.51	0.71
1973	601.4	0.3	0.19	0.26	0.40
1975	602.0	0.2	0.17	0.17	0.24
1978	602.9	0.8	0.36	0.40	1.67
1983	604.4	0.0	0.29	0.32	0.51
1986	605.3	0.0	0.10	0.10	0.10
1993	607.5	0.0	0.19	0.24	1.04
2702	823.6	0.0	0.24	0.27	0.39
2716	827.8	0.2	0.22	0.22	0.26
2736	833.9	0.1	0.08	0.08	0.11

APPENDIX 7.G. Weight Loss Data, Continued.

2. Core #8

Sample (ft)	Depth (m)	Weight Losses at 102 ± 5°C (Wt.%)	Data from Section 7.3		
			@70°C	To 200°C	To Above 400°C
1391	424.0	0.1	0.04	0.07	0.26
1495	455.7	0.1	0.05	0.08	0.08
1573	479.5	0.2	0.04	0.33	1.18
1652	503.5	0.1	0.09	0.09	4.52
1705	519.7	0.0	0.15	0.17	0.32
1769	539.2	0.1	0.09	0.15	0.35
1787	544.7	0.2	0.32	0.36	0.59
1794	546.8	1.4	0.44	0.71	5.41
1804	549.9	0.0	0.02	0.07	0.07
1829	557.5	0.1	0.16	0.39	0.39
1838	560.2	0.3	0.39	0.39	0.39
1857	566.0	0.1	0.07	0.07	0.10
1875	571.5	1.2	0.22	0.64	0.64
1884	574.2	0.9	0.36	0.36	0.80
1890	576.1	0.1	0.05	0.05	0.13
1894	577.3	0.4	0.30	0.30	0.30
1899	578.8	0.1	0.16	0.16	0.16
1900	579.1	0.1	0.17	0.17	0.81
1905	580.6	1.0	0.36	0.36	0.62
1911	582.5	0.2	0.06	0.06	0.10
1913	583.1	0.2	0.11	0.14	0.21
1916	584.0	0.0	0.13	0.13	0.25
1923	586.1	0.1	0.19	0.19	0.49
1930	588.3	0.4	0.05	0.05	0.47
1933	589.2	0.1	0.19	0.28	0.28
1938	590.7	0.0	0.13	0.27	0.49
1953	595.3	0.1	0.05	0.10	0.42
1967	599.5	0.5	0.28	0.32	0.52
1986	605.3	0.0	0.07	0.07	5.81

APPENDIX 7.G.   Weight Loss Data, Continued.

2.   Core #8

Sample (ft)	Depth (m)	Weight Losses at 102 ± 5°C (Wt.%)	Data from Section 7.3		
			@70°C	To 200°C	To Above 400°C
2006	611.4	0.1	0.20	0.20	0.66
2017	614.8	0.2	0.22	0.24	0.41
2039	621.5	0.1	0.21	0.26	1.02
2050	624.8	0.0	0.11	0.11	0.79
2068	630.3	0.1	0.04	0.04	0.14
2084	635.2	0.3	0.17	0.22	0.71
2130	649.2	0.0	0.11	0.18	0.28
2162	659.0	0.1	0.14	0.14	0.62
2217	675.7	0.1	0.04	0.04	0.44
2280	694.9	0.0	0.19	0.19	0.27
2326	709.0	0.1	0.11	0.14	0.70
2366	721.2	1.9	0.43	0.43	6.84
2427	739.7	0.0	0.03	0.03	0.43
2460	749.8	0.0	0.17	0.22	0.37
2519	767.8	0.0	0.08	0.08	0.14
2563	781.2	2.3	1.87	2.13	2.24
2616	797.4	0.0	0.21	0.21	0.27
2666	812.6	0.0	0.25	0.25	0.73
2707	825.1	0.6	0.16	0.16	1.66
2758	840.6	0.0	0.11	0.11	0.16
2779	847.0	0.2	0.21	0.21	0.21
2793	851.3	0.0	0.18	0.18	0.18
2803	854.4	0.0	0.10	0.12	0.14
2809	856.2	0.0	0.15	0.24	0.48
2821	859.8	0.2	0.18	0.18	0.36
2879	877.5	0.2	0.06	0.06	3.37
2948	898.6	0.1	0.20	0.22	0.26

APPENDIX 7.G. Weight Loss Data, Continued.

3. Weight losses determined at higher temperatures for selected samples from Core #8.

Sample (ft)	Depth (m)	Weight Losses 102 ± 5°C	(± 0.1 to 0.2 Weight %)	
			170 ± 5°C	300 ± 10°C
1804	549.9	0.0	0.0	0.2
1829	557.5	0.1	0.2	0.4
1875	571.5	1.2	1.8	2.2
1884	574.2	0.9	1.0	1.5
1923	586.1	0.1	0.1	0.2
1967	599.5	0.5	0.5	1.4
2050	624.8	0.0	0.0	0.7
2366	721.2	1.9	2.0	7.4
2948	898.6	0.1	0.0	0.2

Note: In this set of weight loss determinations, one split from each sample selected was heated to successively higher temperatures.

APPENDIX 7.H.   Mineralogy and Petrology of Core #7 and #8.

1.   Abbreviations used.

    <u>Minerals</u>   In the summaries which follow the approximate amounts of the minerals present are indicated by upper and lower case letters. AN + MAJOR ($>$ 25%); An + Minor (5 to 25%); an = trace ($<$ 5%. Often less than 1%)

AN	=	Anhydrite	HA	=	Halite
CAR	=	Carnallite	KAIN	=	Kainite
CEL	=	Celestite	PH	=	Polyhalite
CSSM	=	Clay and silt-sized	QTZ	=	Quartz
		minerals (often magnesitic)	SYL	=	Sylvite
FELD	=	Feldspar(s)			
GLAU	=	Glauconite			
GYP	=	Gypsum			

<u>Grain Sizes</u>

fg	=	Fine grained ($<$ 1 mm)
mg	+	medium grained (1 mm to 1 mm)
cg	=	coarse grained ($>$ 1 cm)

    With the exception of halite, which shows a wide range of grain sizes, most of the minerals observed are fine grained.

APPENDIX 7.H.   Mineralogy and Petrology, Continued.

2. Core #7

Depth (ft)	Description
1044	cg HA with An and cssm in patches and stringers. An also in isolated crystals and crystal clusters.
1107	fg to mg HA with mg gyp which is partially replaced by An. fg to mg ph in patches and stringers along with cssm.
1171	Appears macroscopically bedded. Primarily vuggy AN. Voids filled with radial ("starbursts") of ph and also with ha and cssm.
1221	cg HA. Patches and stringers filled with ph (radial in part) and an. Some evidence of ph replacing an.
1296	mg to cg HA with Cssm, ph and possibly some an in patches and stringers. Some of the Cssm appears intergranular among HA crystals. May represent subaerial deposition.
1342	mg to cg HA with ph and cssm in patches and stringers.
1402	mg HA. ph (radial in part) and an in patches and stringers and as crystal clusters.
1468	mg HA with much intergranular Cssm. Possibly represents subaerial deposition. Trace an and ph as isolated crystals and crystal clusters. Some authigenic quartz and feldspar.
1533	mg to cg HA with poorly preserved hoppers. Ph in patches and stringers, some possibly intergranular with HA. Trace Cssm associated with the Ph.
1615	mg to cg HA with hoppers. fg to mg An and ph in patches and stringers. ph appears to be replacing An, some of which may be psuedomorphic after gypsum.
1697	Appears to be macroscopically bedded. Large, nodular masses of AN (possibly pseudomorphic after gypsum nodules) with voids filled with Cssm, Ph, ha and syl. Ph associated with Cssm; syl associated with Ph.

APPENDIX 7.H.   Mineralogy and Petrology, Continued.

2.   Core #7, continued

Depth (ft)	Description
1755	mg to cg Ha with poorly preserved hoppers. ph and an in patches and stringers. ph replaces an in part. Perhaps a little syl is present.
1952	Appears macroscopically bedded. mg to cg HA with hoppers. Ph and an in patches, stringers and as isolated crystals and clusters. Ph replacing an in part.
1954	mg to cg HA with Cssm in patches and stringers. Some Cssm is intergranular with HA. May represent subaerial deposition. Some isolated crystals and clusters of ph associated with Cssm.
1958	mg to cg HA. cssm in patches and stringers. (Some cssm may be intergranular). ph and possible an in patches and stringers associated with cssm and also in isolated crystals and clusters.
1960	Possibly macroscopically bedded. fg to cg HA with hoppers. Intergranular Cssm with associated authigenic qtz and feld. May represent suberial deposition. Some isolated crystals and clusters of ph and an.
1967	mg to cg HA with poorly preserved hoppers. ph in patches and stringers shows some evidence of flow or deformation. A few isolated crystals and clusters of an.
1969	fg to cg HA with poorly preserved hoppers. Intergranular Cssm with associated authigenic qtz and feld. Isolated crystals and clusters of an and lesser ph.
1973	cg HA with very few patches and stringers of cssm, ph and even some ha crystals.
1975	cg HA with ph, cssm and an in patches and stringers. ph appears to be replacing an. ph associated with cssm.
1978	mg to cg HA with intergranular Cssm and ph. May represent subaerial deposition. Some ph in patches and stringers and as isolated crystals and clusters. Some ph is mg. Isolated crystals of an are associated with the ph.

APPENDIX 7.H. Mineralogy and Petrology, Continued.

2. Core #7, continued

Depth (ft)	Description
1983	mg to cg HA with hoppers. Ph and an in patches and stringers Ph replacing an.
1986	mg to cg HA with small amounts of ph, an and cssm in patches and stringers.
1993	cg HA with hoppers. Ph and an in patches and stringers. (Some Ph and an may be intergranular). Ph appears to replace an.
2702	mg to cg HA with An and cssm in patches and stringers.
2716	mg to cg HA with hoppers. an and cssm in patches and stringers, some possibly intergranular with HA. May represent subaerial deposition.
2736	mg to cg HA with hoppers. An and cssm in patches and stringers, some possibly intergranular with HA. May represent subaerial deposition.

APPENDIX 7.H. Mineralogy and Petrology, Continued.

3. Core #8

Depth (ft)	Description
1391	cg HA with ph and possibly some an in patches and stringers.
1495	mg to cg HA with hoppers. Ph associated with cssm in patches and stringers. Some may be intergranular. Ph shows evidence of flowage or deformation.
1573	Appears macroscopically bedded. mg to cg HA with Ph and fg to mg An in large patches. Ph appers to be replacing An.
1652	Appears macroscopically bedded. fg to mg AN with Ph. mg Ha in patches or voids. Some syl associated with Ph. Algal laminations may be present in the An.
1705	fg to cg HA with hoppers. Ph in patches and stringers; some may be intergranular. Small amount of an associated with Ph.
1769	mg to cg HA with poorly preserved hoppers. fg to mg Ph in patches and stringers and intergranular with HA. In part, Ph appears to be replacing HA. Some gyp (?) may be present in very small amounts. There also may be trace amounts of cel (?).
1787	mg to cg HA with hoppers. Ph in patches and stringers and some intergranular with HA. Some mg, acicular an crystals and mg, acicular cel (?) crystals noted. There may be a small amount of gyp (?) present in this slide.
1794	Appears macroscopically bedded. fg to mg HA with hoppers. CSSM is intergranular with HA. May represent subaerial deposition. Also noted: a few isolated ph crystals, some authigenic qtz and feld, and a trace of glau (?).
1804	fg to cg HA with poorly presrved hoppers. CSSM is intergranular with HA. May represent subaerial deposition. ph in isolated crystals and cluters.
1829	cg HA with hoppers. Cssm in patches and stringers and some intergranular. Possible subaerial deposition. Trace of ph.

APPENDIX 7.H.   Mineralogy and Petrology, Continued.

3.   Core #8, continued

Depth (ft)	Description
1838	fg to mg HA with poorly preserved hoppers. Cssm intergranular with HA. Ph and An in patches and stringers and associated wtih the Cssm. May represent subaerial deposition.
1857	cg HA with poorly preserved hoppers. ph along stringers.
1875	Apperas macroscopically bedded. fg to mg HA intergranular with CSSM. May represent subaerial deposition. Isolated crystals and clusters of ph and fg to mg an. Traces of authigenic qtz and feld.
1884	fg to mg HA with hoppers, intergranular with CSSM. May represent subaerial deposition. Some isolated crystals and clusters of fg to mg an (some may be pseudomorphic after gyp). Possible trace of syl.
1890	mg to cg HA with hoppers. ph and an in patches and stringers.
1894	mg to cg HA with poorly preserved hoppers. ph and an in patches and stringers. cssm in patches and stringers with authigenic qtz and feld.
1900	fg to cg HA with hoppers. Ph, An and cssm in patches and stringers and some intergranular with HA. May represent subaerial deposition. Some Ph appears to be deformed or to have flowed.
1905	mg to cg HA with patches and stringers and some intergranular Cssm. (May represent subaerial deposition). Scattered, isolated crystals of ph and an.
1910	mg to cg HA with poorly preserved hoppers. Ph, an and cssm intergranular with HA and in patches and stringers. Ph apperas to be replacing an.
1911	mg to cg HA with hoppers. Ph, An and cssm in patches and stringers, some intergranular with HA. (May represent subaerial deposition). Ph appears to be replacing an.

APPENDIX 7.H.   Mineralogy and Petrology, Continued.

3.   Core #8, continued

Depth (ft)	Description
1913	fg to cg HA with intergranular Cssm. Inclusions of ha in Cssm. May represent subaerial deposition. Isolated crystals of ph. A few authigenic grains of qtz and feldspar.
1916	cg HA with poorly preserved hoppers. ph and an in patches and stringers.
1923	fg to cg HA with intergranular Cssm. May represent subaerial deposition. ph and an in patches and stringers and as isolated crystals. Trace authigenic feld.
1930	mg to cg HA with poorly presrved hoppers. Ph and an in patches and stringers, some as isolated crystals. cssm in patches and stringers. Possible trace gyp (?).
1933	cg HA with hoppers. cssm, ph and an in patches and stringers. Small amounts of authigenic qtz and feld (?).
1938	cg HA with poorly preserved hoppers. Ph and an in patches and stringers.
1953	fg to mg HA with hoppers. Cssm intergranular with HA and in patches and stringers. May represent subaerial deposition. Isolated crystals and clusters of ph and an.
1967	fg to cg HA with hoppers. Cssm intergranular with HA and in patches and stringers. May represent subaerial deposition. Isolated crystals and clusters of ph and an.
1986	Appears cross-bedded. PH with mg AN. Ph appeas to be replacing AN. Some fine laminations may be algal lamination or traces of cssm seams. ha in patches or filling void places.
2006	fg to cg HA with hoppers. Ph and an in patches and stringers. Trace of syl associated with Ph.

APPENDIX 7.H. Mineralogy and Petrology, Continued.

3. Core #8, continued

Depth (ft)	Description
2017	mg to cg HA with hoppers. Ph and an in patches and stringers. Ph appears to be replacing an. cssm in patches.
2039	mg to cg HA with hoppers. Ph and an with cssm in patches and stringers. Much of the Ph is radial. Ph appears to be replacing an.
2050	mg AN with numerous inclusions. AN apperas to be replacing ha with former cubic crystal outlines preserved.
2068	fg to cg HA. Patches and stringers and intergranular An, cssm and possible ph (?). May represent subaerial deposition.
2084	fg to cg HA with much intergranular Cssm, ph and poissible an (?). May represent subaerial deposition. Some Ha crystals appear to be growing in the Cssm.
2130	fg to mg HA with intergranular An and minor cssm. Some ph (?) may be replacing An.
2162	cg HA with intergranular Cssm and Ph. May represent subaerial deposition. Trace of an associated with Ph. Trace of syl associated with Ph.
2217	cg HA with patches and stringers of Ph and an. Some Ph radial and replacing an. Possible syl associated with Ph.
2280	fg to cg HA with patches and stringers of Ph and an. POssible trace of kain (?).
2326	fg to cg HA with poorly·preserved hoppers. Cssm intergranular with HA. May represent subaerial deposition. Isolated crystals and clsuters of ph and an. Trace authigenic feld (?).
2366	Possibly macroscopically bedded. fg, radial PH with minor an. cssm scattered throughout.

APPENDIX 7.H. Mineralogy and Petrology, Continued.

3. Core #8, continued

Depth (ft)	Description
2803	fg to cg HA with hoppers. Intergranular An and cssm. Some An in patches with possible ph (?). A few large, isolated crystals of An. May represent subaerial deposition.
2809	fg to mg HA with trace evidence of hoppers. An and cssm in patches, stringers and as intergranular material. May represent subaerial deposition.
2821	mg to cg HA with hoppers. Intergranular An and cssm. Some An in patches and stringers. May represent subaerial deposition.
2879	Possible macroscopic evidence of bedding. fg to mg HA with hoppers. Patches and stringers of An and cssm. POssible trance of ph (?). An unknown minerals with lower birefringence and positive relief was observed. Also present are some large, isolated crystals of An.
2948	Possible macroscopic evidence of bedding. mg to cg HA with hoppers. Some patches and stringers of An present. Some may be nodular (?) (possibly pseudomorphic after gyp). a few isolated crystals of ph (?) were noted.

APPENDIX 8A

Analyses of Potash for Department of Energy
(then ERDA) and Industry Boreholes in the WIPP Area

Source is Table 3, John et al., 1978

Table 3 - Calculated mineral content of selected samples from potassium-bearing intervals with summation of percent K₂0 as ore mineral*

[Drill-hole no.: Drill-hole designations; P, Energy Research and Development Administration; FC, Farm Chemical Res. Dev. Corp; IMC, International Minerals and Chemical Corp; NFU, Farmers Edu. and Coop. Union of America; D, Duval Sulphur and Potash Co.. U, U.S. Potash Co., Inc. Arc, arcanite; Bs, bischofite; Bl, bloedite. C, carnallite; Gl, glaserite; Gu, glauberite; Ka, kainite; Ki, kieserite; L, langbeinite; Le, leonite; Lo, loewite; S, sylvite; Va, vanthoffite]

Drill-hole no.	Ore zone	Sample no.	Depths of interval (feet)	Thickness (feet)	Calculated minerals present (weight percent)					K₂0 as ore minerals (percent)	Weighted average K₂0 as ore mineral for all intervals in ore zone (feet and percent)
					Polyhalite	Halite	Sylvite	Langbeinite	Other minerals		
P-1	5	9	1440.47-1441.35	0.88	8	76	---	15.0	Tr/Ka[1]	3.4/L	
	5	10	1441.35-1442.30	0.95	9	86	---	4.4		1.0/L	
	5	11	1442.30-1443.50	1.20	---	79	---	---	14.0/Ka Tr/Bl[1]	---	
	5	12	1443.50-1444.35	0.85	---	95	---	2.34	---	0.53/L	
	5	13	1444.35-1445.30	0.95	1	79	---	17.07	---	3.87/L	4.83-1.67/L
P-2	10	14	1627.15-1628.35	1.20	1	39	---	39.9	1.9/Ka 5.0/Le	9.05/L	
	10	15	1628.35-1629.52	1.17	1	46	---	43.1	2.6/Ka 0.5/Le	9.78/L	2.37-9.41/L
	4	5	1802.70-1804.00	1.30	1	39	---	38.0	12.9/Ka	8.6/L	
	4	6	1804.00-1805.00	1.00	6	80	---	---	---	---	
	4	7	1805.00-1805.85	0.85	5	89	---	---	---	---	
	4	8	1805.85-1806.30	0.45	6	60	---	20.0	4.0/Ka 3.7/Le	4.54/L	3.60-3.67/L
	2	1	1833.08-1834.00	0.92	2	79	---	4.4	1.9/Ka	3.14/L	
	2	2	1834.00-1834.50	0.50	---	38	---	52.9	0.5/Ka	12.0/L	1.42-6.26/L
P-3	4	3	1596.30-1597.60	1.30	2	72	---	24.7	0.5/Ka	5.6/L	
	4	4	1597.60-1598.70	1.10	2	62	---	18.6	0.5/Ka	4.22/L	
	4	5	1598.70-1599.53	0.83	34	38	---	23.4	---	5.31/L	3.23-5.06/L
P-4	10	2	1572.60-1574.97	2.37	1	56	46.0	---	---	29.40/S	
	10	3	1574.97-1576.17	1.20	4	64	27.6	---	---	17.48/S	
	10	4	1576.17-1577.77	1.60	3	86	7.0	---	---	4.32/S	
	10	5	1577.77-1578.69	0.92	4	64	28.0	---	---	17.46/S	6.09-18.66/S
P-5	10	6	1546.69-1548.65	1.96	6	65	28.0	---	---	18.28/S	
	10	7	1548.65-1549.66	1.01	4	76	13.3	---	---	8.42/S	
	10	8	1549.66-1551.40	1.74	3	60	21.0	---	---	13.41/S	
	10	9	1551.40-1552.75	1.35	2	65	14.5	---	---	9.14/S	6.06-13.2/S
P-6	4	12	1476.00-1477.45	1.45	6	74	---	22.0	1.0/Ki	5.01/L	
	4	13	1477.45-1478.37	0.92	1	83	2.0	8.0	6.0/Ki	1.90/L 1.26/S	
	4	14	1478.37-1480.00	1.63	3	84	---	12.0	---	2.78/L	4.00-3.39/L
	2	18	1510.50-1511.32	0.82	1	37	2.0	54.0	6.0/Ki	12.31/L	
	2	19	1511.32-1512.10	0.78	---	53	---	42.0	---	9.65/L	
	2	20	1512.10-1513.05	0.95	7	79	3.0	1.0	8.6/Ka	0.19/L	2.55-6.98/L
P-7	4	2	1479.73-1481.20	1.47	2	65	1.0	29.0	---	6.53/L[4]	
	4	3	1481.20-1483.00	1.80	---	89	2.0	3.0[4]	---	0.75/L[4]	
	4	4	1483.00-1483.48	0.48	3	69	2.0	3.8	5.7/Ka 1.0/Le 1.0/Bl	3.8/L	3.75-3.41/L
P-8	10	2	1363.70-1365.00	1.30	---	52	29.0	25.0	---	18.45/S 5.62/L	
	10	3	1365.00-1366.72	1.72	1	46	3.0	45.0	4.0/Ka 2.0/Le	10.3/L 1.65/S	
	10	4	1366.72-1368.05	1.33	1	86	---	14.0	---	8.23/L	4.35-6.74/L 4.35-6.17/S mixed ore equivalent: 4.35-9.2/L

Table 3 - Calculated mineral content of selected samples
from potassium-bearing intervals with summation
of percent K₂O as ore mineral--continued

Drill-hole no.	Ore zone	Sample no.	Depths of intervals (feet)	Thickness (feet)	Calculated minerals present (weight percent)					K₂0 as ore minerals (percent)	Weighted average K₂0 as ore mineral for all intervals in ore zone (feet and percent)
					Polyhalite	Halite	Sylvite	Langbeinite	Other minerals		
P-9	10	8	1522.56-1523.41	0.85	1	42	7.0	48.0	0.67/Ka	4.73/S 10.8/L	
	10	9	1523.41-1524.07	0.66	1	93	2.0	---	3.0/Ki	0.96/S	
	10	10	1524.07-1524.70	0.63	2	17	7.0	63.37	---	4.42/S 14.37/L	
	10	11	1524.70-1526.04	1.34	3	95	---	1.10	---	0.24/L	
	10	12	1526.04-1526.74	0.70	2	65	---	31.31	---	7.1/L	4.18-5.63/L 2.14-3.48/S mixed ore equivalent: 4.18-6.34/L
	4	17	1703.65-1705.23	1.58	2	70	---	28.70	---	6.51/L	
	4	18	1705.23-1705.65	0.42	1	89	---	6.80	3.0/Ka	1.55/L	2.00-5.47/L
P-10	11	1	1650.38-1651.22	0.84	6	89	1.8	---	1.0/Ka	1.13/S	
	11	2	1651.22-1652.03	0.81	7	81	6.1	---	2.0/Ki	3.83/S	
	11	3	1652.03-1653.83	1.80	5	85	7.7	---	1.0/Ki	4.85/S	3.45-3.70/S
	11	4	1653.83-1654.58	0.75	6	94	---	---	---	---	
P-11	11	2	1601.90-1603.56	1.66	---	56	5.0	---	3.60/Ki 1.0/C	3.34/S	
	11	3	1603.56-1604.64	1.08	3	61	2.0	---	31.0/Ka 3.0/C	1.48/S	
	11	4	1604.64-1605.38	0.74	4	84	3.0	---	7.0/Ka 2.0/C	2.20/S	3.48-2.52/S
	10	7	1670.70-1671.84	1.14	1	71	19.0	8.0	1.0/Ki	12.0/S 1.82/L	
	10	8	1671.84-1673.42	1.58	2	66	10.0	18.0	1.0/Ki	6.32/S 3.98/L	
	10	9	1673.42-1674.70	1.28	3	71	16.7	---	1.0/Ki	10.53/S	4.00-9.29/S 2.72-3.07/L mixed ore equivalent: 4.00-14.51/S
	9	14	1688.72-1689.60	0.88	3	76	22.0	---	---	13.74/S	
	9	15	1689.60-1690.89	1.29	1	64	36.9	---	---	23.30/S	
	9	16	1690.89-1691.95	1.06	1	71	21.3	---	2.0/C	13.43/S	
	9	17	1691.95-1693.28	1.33	2	92	2.0	---	1.0/C	1.24/S	4.56-12.73/S
	4	19	1840.60-1842.35	1.75	1	58	---	40.0	5.0/Ki	9.14/L	
	4	20	1842.35-1843.40	1.05	4	76	5.0	4.9	---	1.11/L 2.98/S	2.80-6.0/L
	2	22	1868.67-1870.28	1.61	1	38	2.0	60.0	2.0/Ki	13.65/L	
	2	23	1870.28-1871.10	0.82	---	54	5.0	45.0	1.0/Ki	13.53/L	
	2	24	1871.10-1872.30	1.20	---	27	---	58.3	8.0/Ka₁ Tr/Bl&Lo	13.24/L	3.63-13.49/L

Table 3 - Calculated mineral content of selected samples from potassium-bearing intervals with summation of percent K$_2$O as ore mineral--continued

Drill-hole no.	Ore zone	Sample no.	Depths of interval (feet)	Thickness (feet)	Polyhalite	Halite	Sylvite	Langbeinite	Other minerals	K$_2$O as ore minerals (percent)	Weighted average K$_2$O as ore mineral for all intervals in ore zone (feet and percent)
					Calculated minerals present (weight percent)						
P-12	10	2a	1344.97-1345.27	0.3	4	36	62.3[2]	---	1.0/Ki	39.38/S	
	10	2b[4]	1345.27-1345.90	0.63	---	10	24.0[2]	---	59.0/Ki	15.08/S	
	10	3	1345.90-1346.95	1.05	1	59	18.0	---	18.0/Ki	11.39/S	
	10	4	1346.95-1348.90	1.95	3	64	18.0	---	19.0/Ki	11.36/S	
	10	5	1348.90-1349.91	1.01	7	44	20.0	---	8.6/Ki 8.7/Ka	12.63/S	
	10	6	1349.91-1350.80	0.89	3	67	16.0[3]	---	2.0/Ka	10.42/S	5.83-13.29/S
	8	14	1390.19-1390.97	0.78	4	80	15.5	---	---	9.77/S	
	8	15	1390.97-1392.66	1.69	7	88	7.0	---	---	4.12/S	
	8	16	1392.66-1394.29	1.63	4	88	10.3	---	---	6.47/S	
	8	17	1394.29-1394.90	0.61	8	51	35.5	---	---	22.42/S	4.71-8.24/S
	4	21	1520.00-1521.55	1.55	1	22	23.0	45.0	9.0/Ki	14.47/S 10.13/L	2.39-7.08/L
	4	22	1521.55-1522.39	0.84	10	48	7.0	6.0	16.0/Ka 10.0/Le	1.44/L 4.42/S	2.39-10.94/S mixed ore equivalent: 4.00-8.23/L
	3	26	1533.50-1535.05	1.55	---	40	11.0	49.0	---	7.0/S 8.59/L	
	3	27	1535.05-1535.59	0.54	34	86	.1.0	8.0	1.0/Ki	1.80/L 0.62/S	3.51-5.98/L
	3	28	1535.59-1537.01	1.42	2	47	10.0	21.0	---	4.72/L 6.32/S	3.51-5.74/S mixed ore equivalent: 3.51-8.27/L
	2	34	1549.79-1550.65	0.86	3	85	---[4]	11.0	2.42/L	0.54/L	
	2	35a	1550.65-1551.29	0.64	---	20	5.0	70.0	1.0/Ka Tr/Le[1]	15.93/L	
	2	35b	1551.29-1551.61	0.32	---	21	5.0	30.0	18.0/Ka 19.0/Le 17.0/Bl	12.48/L	1.82-8.05/L
P-13	10	29	1318.02-1319.00	0.98	1	46	49.5	---	---	31.32/S	
	10	30	1319.00-1320.22	1.22	1	62	17.0	2.0	15.0/Ki	10.92/S	
	10	31	1320.22-1320.88	0.66	3	97	---	---	---	---	
	10	32[4]	1320.88-1321.87	0.99	1	30	20.0	10.0	30.0/Ki 10.0/Ka	12.6/S 2.27/L	3.85-14.67/S
	9	36	1334.82-1336.38	1.56	2	94	2.0	---	---	1.12/S	
	9	37	1336.38-1337.32	0.94	2	62	34.8	---	---	21.99/S	
	9	38	1337.32-1338.64	1.32	---	90	3.8	---	---	2.41/S	3.82-6.7/S
	8	21	1359.65-1360.63	0.98	2	67	30.2	---	---	19.13/S	
	8	22	1360.63-1361.70	1.07	8	80	9.14	---	---	4.97/S	2.05-11.74/S
	4	2	1480.20-1481.73	1.53	2	82	2.0	9.0	3.0/Ki	2.03/L	
	4	3	1481.73-1482.78	1.05	1	63	---	33.2	0.4/Le	7.53/L	3.53-4.06/L
	4	4	1482.78-1483.73	0.95	1	64	---	7.0	7.0/Bl	1.59/L	

34

Table 3 - <u>Calculated mineral content of selected samples</u>
<u>from potassium-bearing intervals with summation</u>
<u>of percent K₂O as ore mineral</u>--continued

Drill-hole no.	Ore zone	Sample no.	Depths of interval (feet)	Thickness (feet)	Calculated minerals present (weight percent)					K₂O as ore minerals (percent)	Weighted average K₂O as ore mineral for all intervals in ore zone (feet and percent)
					Polyhalite	Halite	Sylvite	Langbeinite	Other minerals		
	3	8	1493.23-1493.88	0.65	2	86	---	7.0	---	1.59/L	
	3	9	1493.88-1494.58	0.70	---	15	---	53.0	---	12.06/L	
	3	10	1494.58-1495.50	0.92	3	86	---	10.0	---	2.21/L	2.27-5.07/L₅ 4.00-2.88/L₅
P-14	10	2	1255.24-1255.64	0.40	---	41	57.0	---	---	36.03/S	
	10	3	1255.64-1257.56	1.92	---	41	57.0	---	---	36.06/S 8.84/S	
	10	4	1257.56-1259.07	1.51	3	64	14.0	18.0	Tr/Ka[1]	3.99/L	
	10	5	1259.07-1260.15	1.08	4	74	7.0	22.0	---	4.36/S 4.88/L	
	10	6	1260.15-1261.05	0.90	2	55	12.0[6]	---	16.0/Ka	6.21/S	5.81-18.47/S 2.59-4.36/L mixed ore equivalent: 5.81-23.33/S
	5	10	1364.44-1366.11	1.67	5	74	5.0	15.0	1.0/Ka	3.35/L 3.00/S	
	5	11	1366.11-1367.86	1.75	3	83	---	19.0	Tr/Ka[1]	4.3/L	
	5	12[6]	1367.86-1369.26	1.40	1	80	---	13.0	Tr/Ka[1]	3.03/L	4.82-3.60/L 1.67-3.0/S mixed ore equivalent: 4.82-4.02/L
	4	18	1440.79-1441.98	1.19	4	46	6.0	38.5	---	8.74/L 3.99/S	
	4	19	1441.98-1442.84	0.86	5	95	---	---	---	---	
	4	20	1442.84-1443.98	1.14	16	56	4.0	23.0	Tr/Le 2.0/Ka	5.22/L 2.53/S	
	4	21	1443.98-1444.61	0.63	3	88	---	11.0	---	2.50/L	3.82-4.69/L 3.19-2.39/S
P-15	4	7	1371.94-1372.81	0.87	6	76	---	25.0	---	5.59/L	
	4	8	1372.81-1374.77	1.96	8	89	---	4.0	---	1.00/L	
	4	9	1374.77-1375.80	1.03	9	64	---	28.0	---	6.30/L	3.86-3.45/L
	2	13	1399.66-1400.38	0.72	3	64	---	32.0	4.0/Ka	7.18/L	
	2	14	1400.38-1401.51	1.13	---	78	---	17.0	3.0/Ka 3.0/Le	4.28/L	1.85-5.41/L
P-16	10	4	1301.94-1302.57	0.63	3	93	0.7	4.0	---	0.47/S 0.89/L	
	10	5	1302.57-1303.91	1.34	3	79	---	21.0	---	4.77/L	
	10	6	1303.91-1304.39	0.48	---	61	---	34.0	8.1/Le 8.0/Le Tr/Ki[1]	7.77/L	2.45-4.63/L
	4	10	1476.76-1478.40	1.64	---	36	2.0	53.0	Tr/Ka&Le[1]	12.01/L 1.26/S	
	4	11	1478.40-1478.95	0.55	2	86	---	8.7	---	1.98/L	2.19-9.49/L
	4	12	1490.12-1491.00	0.88	1	83	1.0	14.1[7]	---	4.94/L	
	4	13	1491.00-1491.56	0.56	0	39	7.0	19.7[7]	---	4.40/L 4.12/S	
	4	14	1491.56-1492.64	1.08	7	79	---	12.0	---	2.75/L	
	4	15	1492.64-1493.89	1.25	2	56	3.0	31.0	6.0/Le 2.0/Ka	7.05/L 2.09/S	3.77-4.93/L

Table 3 - Calculated mineral content of selected samples
from potassium-bearing intervals with summation
of percent K₂O as ore mineral--continued

Drill-hole no.	Ore zone	Sample no.	Depths of interval (feet)	Thickness (feet)	Calculated minerals present (weight percent)					K_2O as ore minerals (percent)	Weighted average K_2O as ore mineral for all intervals in ore zone (feet and percent)
					Polyhalite	Halite	Sylvite	Langbeinite	Other minerals		
P-16	2	19	1526.90-1528.00	1.10	1	51	1.0	42.0	2.0/Ka	9.05/L	1.10-9.60/L
P-17	10	2	1365.60-1367.20	1.6	1	27	---	68.8	---	15.61/L	
	10	3	1367.20-1368.45	1.25	3	76	---	12.6	2.0/Ka	2.87/L	
	10	4	1368.45-1369.70	1.25	3	44	---	6.64	30.0/Le 9.0/Ka	1.51/L	4.10-7.43/L
	4	8	1542.90-1543.68	0.78	---	48	---	38.0	13.0/Le Tr/Ka[1]	8.62/L	
	4	9	1543.68-1544.46	0.78	---	43	---	53.0	3.0/Le	12.03/L	1.56-10.33/L
	2	18	1591.39-1592.71	1.32	1	44	---	46.0	1.0/Ka	10.46/L	
	2	19	1592.71-1594.21	1.50	4	83	---	2.4	2.0/Ka	0.53/L	2.82-5.18/L
P-18	10	3	1728.40-1728.78	0.38	1	41	33.0	35.0	---	22.83/S 7.94/L	
	10	4	1728.78-1730.45	1.67	3	86	9.0	---	---	5.61/S	
	10	5	1730.45-1731.49	1.04	6	80	0.72	---	---	0.45/S	
	10	6	1731.49-1732.29	0.80	4	74	0.81	---	---	0.51/S	3.89-4.86/S 0.38-7.94/L mixed ore equivalent: 3.89-6.8/S
P-19	10	7	1741.80-1742.35	0.55	1	55	6.70	36.0	---	4.23/S 8.24/L	
	10	8	1742.35-1743.72	1.37	1	26	2.0	59.0	---	1.20/S 13.39/L	
	10	9	1743.72-1745.09	1.37	4	81	1.0	15.0	---	0.62/S 3.40/L	
	10	10	1745.09-1746.00	0.91	2	53	---	30.0	8.4/Le 2.0/Ka	9.21/L	4.20-8.03/L
	4	21	1925.20-1925.90	0.70	1	74	---	11.0	12.0/Ki	2.50/L	
	4	22	1925.90-1926.70	0.80	1	27	---	57.0	2.0/Ka 9.0/Ki	12.93/L	
	4	23	1926.70-1927.94	1.24	2	62	---	3.6	5.0/Ka Tr/Le[1]	0.82/L	2.74-4.79/L
	2	26	1956.40-1957.36	0.96	6	64	1.0	16.0	15.0/Ki	3.74/L	
	2	27	1957.36-1958.71	1.35	1	29	---	65.0	Tr/Ka	14.83/L	
	2	28	1958.71-1959.21	0.50	0.5	61	---	25.0	Tr/Ka[1]	5.72/L	2.81-9.42/L
P-20	10	2	1725.00-1726.15	1.15	2	72	21.2	Tr/L[4]	---	13.43/S	
	10	3	1726.15-1728.10	1.95	4	64	7.0	35.0	---	4.42/S 8.01/L	
	10	4	1728.10-1729.62	1.52	3	60	28.0[6]	---	6.0/Ka	17.69/S	1.95-8.01/L
	10	5	1729.62-1731.48	1.86	3	60	34.0	---	---	21.48/S	6.51-14.03/S mixed ore equivalent: 6.51-20.03/S
	4	10	1898.80-1900.45	1.65	5	53	1.0	37 0	5.0/Ka	8.35/L	
	4	11	1900.45-1901.77	1.32	16	85	---	1.3	---	0.30/L	
	4	12	1901.77-1903.35	1.58	10	74	---	17.7	---	4.0/L	4.55-4.5/L

36

Table 3 - Calculated mineral content of selected samples
from potassium-bearing intervals with summation
of percent K2O as ore mineral--continued

Drill-hole no.	Ore zone	Sample no.	Depths of interval (feet)	Thickness (feet)	Calculated minerals present (weight percent)					K2O as ore minerals (percent)	Weighted average K2O as ore mineral for all intervals in ore zone (feet and percent)
					Polyhalite	Halite	Sylvite	Langbeinite	Other minerals		
P-20	2	14[4]	1925.08-1926.30	1.22	3	95	---	0.88	---	0.2/L	
	2	15	1926.30-1927.75	1.45	1	61	---	35.5	---	8.05/L	2.67-4.46/L
P-21	10	2	1644.03-1644.84	0.81	4	80	17.0	---	---	10.82/S	
	10	3	1644.84-1646.00	1.16	4	81	11.8_6	---	2.0/Ki	7.46/S	
	10	4	1646.00-1646.33	0.33	1	28	20.2^6	---	42.0/Ki	12.76/S	
	10	5	1646.33-1647.20	0.87	1	41	25.5_2^6	---	18.0/Ki	16.14/S	
	10	6	1647.20-1648.22	1.02	1	62	29.5^2	---	1.0/Ki	18.66/S	
	10	7	1648.22-1649.23	1.01	3	64	31.3	---	---	19.81/S	5.20-14.37/S
	8	15	1685.17-1686.48	1.31	0	55	45.0_6	---	---	28.4/S	
	8	16	1686.48-1687.20	0.72	4	83	6.0^6	---	---	3.72/S	
	8	17	1687.20-1688.24	1.04	5	92	3.0	---	---	1.95/S	
	8	18	1688.24-1688.77	0.53	4	95	0.8	---	---	0.52/S	
	8	19	1688.77-1690.19	1.42	6	86	9.9	---	---	6.24/S	
	8	20	1690.19-1691.26	1.07	8	90	1.0	---	---	0.75/S	
	8	21	1691.26-1692.40	1.14	3	65	33.0	---	---	21.16/S	
	8	22	1692.40-1693.34	0.94	5	65	13.0	---	---	8.18/S	8.17-10.24/S
	4	24	1809.90-1811.50	1.60	0	31	3.0	64.0	2.5/Ka 3.9/Le	14.60/L	1.92-14.69/L
	4	25	1811.50-1811.82	0.32	0	18	5.0^2	54.66	9.0/Ka 10.60/Le	15.12/L	4.00-7.05/L[5]
	4	30	1815.51-1816.10	0.59	11	51	5	27.0	9.0/Ki	6.08/L	
	4	31	1816.10-1817.25	1.15	3	42	5	44.0	8.0/Ka	9.95/L	1.74-8.64/L[5] 4.00-3/76/L[5]
AEC-8	10	10	1589.10-1589.70	0.60	1	85	5	---	5/Ki 2/An	2.97/S	
	10	11[6]	1589.70-1591.70	2 00	---	43	16	---	40/Ki	10.32/S	
	10	12[6]	1591.70-1592.20	0.50	---	37	24	---	6/C 30/Ki	15.16/S	
	10	13[6]	1592.20-1594.50	2 30	---	49	32	---	9.1/An 7/C 9/Ka 9.8/An	20.31/S	
	10	14	1594.50-1594.70	0 20	---	38	4	---	51/C 9/Ka 1/Ki 9.1/An	2.34/S	
	10	15[6]	1594.70-1595.50	0.80	2	85	3	---	4/C 2/Ki 9/Ka 9.9/An	2.18/S	6.4-12.33/S
	4	2	1752.70-1753.40	0.70	---	95	---	4	---	0.86/L	
	4	3	1753.40-1754.00	0.60	1	69	2	33	3/Ka	7.39/L	
	4	4	1754.00-1755.00	1.00	---	33	2	63	2/Ka	13.90/L	
	4	5	1755.00-1756.70	1.70	---	24	---	69	3/Le	15.38/L	4-11.27/L

Table 3 - <u>Calculated mineral content of selected samples
from potassium-bearing intervals with summation
of percent K_2O as ore mineral</u>--continued

Drill-hole no.	Ore zone	Sample no.	Depths of interval (feet)	Thickness (feet)	Calculated minerals present (weight percent)					K_2O as ore minerals (percent)	Weighted average K_2O as ore mineral for all intervals in ore zone (feet and percent)
					Polyhalite	Halite	Sylvite	Langbeinite	Other minerals		
FC-70	10	2	1377.67-1379.00	1.33	2	65	11.2[6]	---	20.0/Ki	7.11/S	
	10	3	1379.00-1381.00	2.00	2	51	39.1[6]	---	1.0/Ki	24.72/S	
	10	4	1381.00-1382.00	1.00	2	64	19.4[6]	---	3.0/C 3.0/Ki	12.29/S	4.33-16.44/S
	9	6	1391.50-1393.00	1.50	1	53	28.00	---	---	17.74	1.5-17.74/S
	8	7	1415.08-1415.75	0.67	2	70	25	---	Tr/Ki[1]	16.10/S	
	8	8	1415.75-1416.50	0.75	5	89	2	---	Tr/Ki[1]	1.35/S	
	8	9	1416.50-1418.00	1.50	2	97	1	---	1.0/Ka Tr/Ki[1]	0.57/S	
	8	10	1418.00-1419.50	1.50	3	91	3	---	---	1.62/S	
	8	11	1419.50-1420.42	0.92	2	80	16	---	1.0/Ka Tr/Ki[1]	10.04/S	
	8	12	1420.42-1421.50	1.08	1	71	16	---	1.0/Ka	10.21/S	6.42-5.5/S
	5	16	1466.00-1467.58	1.58	---	72	---	19.6	---	4.43/L	
	5	17	1467.58-1469.00	1.42	1	53	---	40.7	---	9.22/L	
	5	18	1469.00-1469.67	0.67	1	70	---	24.2	---	5.49/L	3.67-6.48/L
	4	19	1529.92-1531.42	1.50	1	36	---	52.6[6]	---	11.93/L	
	4	20	1531.42-1532.42	1.00	---	45	---	33.0[6]	---	7.42/L	2.5-10.13/L
FC-81	8	7	1564.17-1564.92[8]	0.75	2	58	36.6	---	2.0/C	23.16/S	
	8	8	1564.92-1566.13	1.21	2	79	15.3	---	4.0/C	9.71/S	
	8	9	1566.13-1567.38	1.25	5	66	8.9	6.1	10.0/C	5.62/S 1.38/L	3.21-11.26/S 3.21-0.54/L mixed ore equivalent: 3.21-12.61/S
	4	10	1687.00-1688.21	1.21	---	20	---	74.0	4.0/Ka Tr/Va[1]	16.71/L	
	4	11	1688.21-1689.46	1.25	1	25	---	67.0	Tr/Va[1]	15.31/L	2.46-16.0/L
	2	15	1712.88-1714.46	1.58	1	40	---	56.0	2.2/Le	12.7/L	
	2	16	1714.46-1715.46	1.00	---	65	---	30.3	3.0/Ka Tr/Le[1]	6.9/L	
	2	17	1715.46-1716.00	0.54	4	45	---	42.8	Tr/Le[1]	9.71/L	3.12-10.4/L
FC-82	5	1	1541.42-1541.79	0.37	---	17	---	72.2	2.0/Le 6.0/C	16.34/L	
	5	2	1541.79-1542.29	0.50	---	85	7.0	7.2	---	1.63/L	
	5	3	1542.29-1543.96	1.67	2	5	---	49.8	4.0/Lo 20.9/C	11.3/L	
	5	4	1543.96-1544.50	0.54	1	59	5.0	20.0	Tr/Le[1]	4.54/L	3.08-9.37/L
	4	5	1613.42-1615.08	1.66	---	17	---	63.0	9.3/Ki Tr/Lo[1]	14.3/L	
	4	6	1615.08-1615.92	0.84	1	48	0.7	12.8	17.7/Le 12.0/Ki	2.9/L	2.5-10.52/L

38

Table 3 - <u>Calculated mineral content of selected samples from potassium-bearing intervals with summation of percent K_2O as ore mineral</u>--continued

Drill-hole no.	Ore zone	Sample no.	Depths of interval (feet)	Thickness (feet)	Calculated minerals present (weight percent)					K_2O as ore minerals (percent)	Weighted average K_2O as ore mineral for all intervals in ore zone (feet and percent)
					Polyhalite	Halite	Sylvite	Langbeinite	Other minerals		
FC-82	3	7	1624.33-1625.58	1.25	2	57	---	31.1	3.5/Bl 3.7/Ka	7.06/L	
	3	8	1625.58-1627.00	1.42	2	67	---	29.9	0.6/C Tr/Bl[1]	6.78/L	
	3	9	1627.00-1627.75	0.75	1	28	---	62.2	5.0/Gl	14.11/L	3.42-8.49/L
FC-91	4	34	1712.25-1712.66	0.42	1	18	---	50.0	11.0/Ka 7.5/Le 6.0/Ki	11.35/L	
	4	35	1712.66-1713.08	0.42	---	62	---	---	5.0/Ka 3.4/Ki	---	
	4	36	1713.08-1714.17	1.08	1	25	---	64.6	5.0/Ki	14.66/L	
	4	37	1714.17-1714.75	0.58	2	32	---	58.7	5.0/Ka 1.3/Ki	13.32	
	4	38	1715.75-1715.75	1.00	20	38	---	47.0	5.0/Ka Tr/Gu[1]	10.66	
	4	39	1715.75-1716.33	0.58	6	31	---	54.0	6.2/Ka 4.0/Gl 1.2/Ki	12.25/L	4.08-11.3/L
	4	40	1718.66-1719.42	0.75	3	81	---	8.0	3.0/Ka 9.0/Bs	1.82/L	
	4	41	1719.42-1720.75	1.33	2	37	---	59.5	---	13.5/L	
	4	42	1720.75-1722.00	1.25	---	60	---	37.08	Tr/Gu 3.4/Bs	8.41/L	
	4	43	1722.00-1722.58	0.58	---	71	---	13.5	0.4/Ka 6.0/Bs Tr/Gu[1]	3.06/L	3.91-8.08/L
	2	44	1742.75-1743.25	0.50	---	15	---	62.0	8.8/Ka Tr/Va[2]	14.07/L	
	2	45	1743.25-1744.25	1.00	---	47	---	30.5	10.0/Ki 10.0/Va	6.92/L	
	2	46	1744.25-1745.00	0.75	---	61	---	1.0	3.2/Ka 10.1/Ki 24.0/Va Tr/Gu[1]	0.73/L	2.25-6.44/L
FC-92[9]	8	5	1604.92-1606.04	1.12	1	51	47	Tr[1]	Tr/C[1]	29.0/S	
	8	6	1606.04-1606.50	0.46	---	50	49	Tr[1]	Tr/C[1]	31.0/S	
	8	7	1606.50-1606.75	0.25	---	60	29	1	5.7/C	18.5/S	1.83-28/S
	4	57	1740.66-1741.58	0.92	1	51	---	46.7	---	10.6/L	
	4	58	1741.58-1742.25	0.66	1	36	---	61.0	---	13.85/L	
	4	59	1742.25-1743.25	1.00	1	36	---	61.2	0.1/Ki	13.89/L	
	4	60	1743.25-1744.08	0.83	1	34	---	61.3	---	13.91/L	
	4	61	1744.08-1745.00	0.92	2	38	---	48.8	1.8/Ki	11.07/L	4.33-12.6/L
	2	62	1769.42-1770.08	0.66	1	42	---	55.4	3.0/Va	12.57/L	
	2	63	1770.08-1771.42	1.33	1	51	---	45.7	2.0/Va 1.0/Arc	10.37/L	
	2	64	1777.42-1772.08	0.66	---	39	---	33.0	17.0/Va 8.0/Ki 1.0/Gu	7.49/L	
	2	65	1772.08-1772.58	0.5	---	73	---	1.5	14.0/Va 1.0/Gu	0.34/L	3.16-8.64/L

39

Drill-hole no.	Ore zone	Sample no.	Depths of interval (feet)	Thickness (feet)	Calculated minerals present (weight percent)					K_2O as ore minerals (percent)	Weighted average K_2O as ore mineral for all intervals in ore zone (feet and percent)
					Polyhalite	Halite	Sylvite	Langbeinite	Other minerals		
IMC-374	4	8	1430.70-1432.10	1.40	6	86	0.7	2.0	0.7/Ki	0.46/L	
									0.3/Ka	0.44/S	
	4	9	1432.10-1433.10	1.00	13	68	1.0	6.4	1.35/Le	1.46/L	2.4-0.88/L
										0.63/S	2.4-0.51/S
IMC-375	4	7	1627.90-1629.00	1.10	2	78	---	6.6	2.0/Ka	1.50/L	
	4	8	1629.00-1630.50	1.50	4	70	2.0	13.2	2.0/Le	3.0/L	2.5-2.46/L
									1.0/Ka	1.3/S	1.5-1.3/S
IMC-376	10	2	1427.00-1427.70	0.7	---	60	38.4	---.	---	24.3/S	
	10	3	1427.70-1428.30	0.6	---	98	0.2	---	---	0.1/S	
	10	4	1428.30-1429.20	0.9	1	96	0.4	---	---	0.26/S	
	10	5	1429.20-1431.00	1.8	2	86	11.2	---	---	.7.1/S	4.0-7.52/S
	5	13	1528.00-1528.90	0.9	2	89	1.0	2.8	---	0.63/L	
	5	14	1528.90-1530.90	2.0	0	45	---	51.3	1.0/Le	11.65/L	3.7-6.5/L
	5	15	1530.90-1531.70	0.8	2	93	1.0	1.05	---	0.25/L	(4.0-6.03/L)[5]
NFU-1[10]	8		1536.25-1540.17	3.92	---	---	---	---	---	19.67/S	3.92-19.67/S
	4		1646.75-1649.08	2.33	---	---	---	---	---	11.96/L	2.33-11.96/L
NFU[10]	10		1441.08-1445.17	4.03	---	---	---	---	---	0.8/S	4.08-0.8/S
	8		1479.80-1483.80	4.00	---	---	---	---	---	9.1/S	4.0-9.1/S
	4		1598.50-1602.70	4.20	---	---	---	---	---	13.1/L	4.2-13.1/L
D-120[10]	10		1248.30-1249.80	1.50	---	---	---	---	---	31.63/S	
	10		1249.80-1251.10	1.30	---	---	---	---	---	10.4/S	
	10		1251.10-1252.50	1.40	---	---	---	---	---	7.34/S	4.2-15.3/S
	4		1419.60-1421.30	1.70	---	---	---	---	---	13.8/S	2.2-10.7/S
	4		1421.30-1421.80	0.50	---	---	---	---	---	0.5/S	2.2-7.5/L mixed ore equivalent: 2.2-29.45/S
D-48[10]	10		1236.60-1240.60	4.00	---	---	---	---	---	---	4.0-11/S 4.0-2.1/L (visual estimate)
	8		1280.52-1289.78	9.26	---	---	---	---	---	---	9.26-17.37/S
	4		1414.20-1416.20	2.00	---	---	---	---	---	---	2.0-8.8/L (visual estimate)

Table 3 - <u>Calculated mineral content of selected samples</u>
<u>from potassium-bearing intervals with summation</u>
<u>of percent K₂O as ore mineral</u>--continued

Drill-hole no.	Ore zone	Sample no.	Depths of interval (feet)	Thickness (feet)	Calculated minerals present (weight percent)					K₂O as ore minerals (percent)	Weighted average K₂O as ore mineral for all intervals in ore zone (feet and percent)
					Polyhalite	Halite	Sylvite	Langbeinite	Other minerals		
D-207	10	24	1358.60-1359.60	1.00	4	87	5	---	2/Ka	3.34/S	. .
	10	25	1359.60-1360.20	0.60	4	89	5	1	2/Ka	3.34/S	
										0.25/L	
	10	26	1360.20-1360.60	0.40	1	75	4	1	6/Ka	0.31/L	
	10	27⁴	1360.60-1361.20	0.60	1	47	6	16	5/Ka	3.79/S	
										3.70/L	
	10	28	1361.20-1361.80	0.60	2	69	2	9	2/Ka	2.04/L	
	10	29	1361.80-1362.30	0.50	7	62	5	10	7/Ka	3.34/S	
										2.31/L	
	10	30	1362.30-1363.10	0.80	6	83	4	---	1/C 3/Ka	2.66/S	4.5-2.54/S 2.7-1.8/L mixed ore equivalent: 4.5-5.24/S
	4	33	1533.10-1533.50	0.40	2	53	36	7	---	1.51/L 22.74/S	
	4	34	1533.50-1533.80	0.30	4	86	2	11	---	2.43/L	
	4	35	1533.80-1534.40	0.60	2	85	1	2	---	0.50/L	
	4	36	1534.40-1534.70	0.30	3	95	---	4	---	0.85/L	
	4	37	1534.70-1535.00	0.30	2	74	4	1	3.0/Ki	0.14/L	
	4	38	1535.00-1539.80	4.80	6	87	2	4	---	0.85/L	6.7-0.90/L 0.4-22.74/S mixed ore equivalent: 6.7-1.44/L
	3	44	1545.90-1546.30	0.40	1	66	---	32.0	0.74/Le	7.2/L	
	3	45	1546.30-1546.66	0.30	1	11	---	73.2	9.0/Ki	16.6/L	
	3	46	1546.66-1548.00	1.40	2	62	---	30.3	3.8/Le	6.89/L	
	3	47	1548.00-1548.60	0.60	1	43	---	54.7	---	12.4/L	2.7-9.24/L
	2	52	1552.20-1553.00	0.80	11	83	---	5.0	---	1.05/L	
	2	53	1553.00-1553.20	0.20	11	45	---	41.5	2.0/Le	9.41/L	
	2	54	1553.20-1553.60	0.40	4	81	---	15.8	---	3.59/L	
	2	55	1553.60-1554.00	0.40	1	47	---	49.4	1.32/Le	11.19/L	
	2	56	1554.00-1554.80	0.80	18	86	1.4	8.8	---	2.0/L 0.9/S	2.6-3.94/L Tr/S⁴
D-104¹⁰	10		1340.40-1341.70	1.30	---	---	---	---	---	---	
	10		1341.70-1343.20	1.50	---	---	---	---	---	---	
	10		1343.20-1344.00	0.80	---	---	---	---	---	---	
	10		1344.00-1344.70	0.70	---	---	---	---	---	---	
	10		1344.70-1346.40	1.70	---	---	---	---	---	---	6.0-5.5/S 3.2-4.71/L mixed ore equivalent: 6.0-11.78/S
	8		1391.10-1392.00	0.90	---	---	---	---	---	---	
	8		1392.00-1395.30	3.30	---	---	---	---	---	---	
	8		1395.30-1396.30	1.00	---	---	---	---	---	---	5.2-10.8/S
	4		1519.90-1522.80	2.90	---	---	---	---	---	---	2.9-9.4/L

41

Table 3 - <u>Calculated mineral content of selected samples from potassium-bearing intervals with summation of percent K$_2$0 as ore mineral</u>--continued

Drill-hole no.	Ore zone	Sample no.	Depths of interval (feet)	Thickness (feet)	Calculated minerals present (weight percent)					K$_2$0 as ore minerals (percent)	Weighted average K$_2$0 as ore mineral for all intervals in ore zone (feet and percent)
					Polyhalite	Halite	Sylvite	Langbeinite	Other minerals		
D-104[10]	3		1527.50-1528.90	1.40	---	---	---	---	---	---	1.4-5.0/L
	3		1528.90-1530.50	1.60	- -	---	---	---	---	---	2.9-11.4/S mixed ore equivalent: 2.9-6.66/L
	2		1539.50-1540.20	1.20	---	---	---	---	---	---	1.2-15.0/L
U-134[10]	10		1319.58-1321.25	1.69	3	---	6.0	---	2.0/Ka 0.7/C	3.79/S	
			1321.25-1322.83	1.58	2	---	---	---	12.5/Ka	17.22/S	3.27-10.28/S
	8		1361.10-1362.17	1.08	---	---	---	---	---	---	
	8		1362.17-1364.50	2.33	---	---	---	---	---	---	
	8		1364.50-1366.50	2.00	---	---	---	---	---	---	6.33-7.89/S
	8		1366.50-1367.42	0.92	---	---	---	---	---	---	(4.0-12.5/S)[5]
	5		1406.75-1409.42	2.66	---	---	---	---	---	14.44/L	
	5		1409.42-1410.00	0.58	---	---	---	---	---	8.03/L	
	5		1410.00-1411.66	1.66	---	---	---	---	---	7.05/L	4.9-11.2/L
	4		1471.66-1474.00	2.33	---	---	---	---	---	3.54/L	2.33-8.54/L
	3		1484.91-1487.33	2.42	---	---	---	---	---	3.6/L	
	3		1487.33-1490.25	2.92	---	---	---	---	---	1.86/L	
	3		1490.25-1491.33	1.08	---	---	---	---	---	8.7/L	6.42-3.7/L[3]

*Values in table for percent mineral and K$_2$0 equivalent are not consistent owing to independent rounding of assays and conversion factors by numerous authors and investigators.

[1] Trace amount; equals 0 to 2.0 percent
[2] Incomplete dissolution of sample
[3] 5.9 percent insolubles, by weight
[4] Incomplete or unreliable assay
[5] Grade adjusted to 4-foot interval
[6] High insoluble content
[7] 7.1 percent potassium assay used
[8] Outside of the ERDA area by 300 feet, included due to influence
[9] Raw data unavailable; these are company figures
[10] Company interval data; raw data unavailable; no sample numbers assigned

42